

Control performance assessment for a high pressure leaching process by means of fault database creation and simulation

by

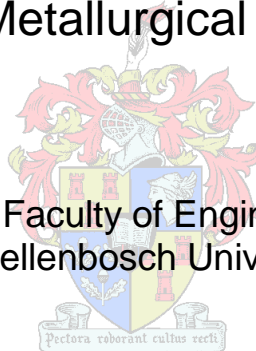
Jason John Miskin

Thesis presented in partial fulfillment
of the requirements for the Degree

of

MASTER OF ENGINEERING
(Extractive Metallurgical Engineering)

in the Faculty of Engineering
at Stellenbosch University



Supervisor:
Dr. L. Auret

Co-supervisors:
Prof. C. Dorfling
Prof. S.M. Bradshaw

March 2016

DECLARATION

By submitting this thesis electronically, I declare that the entirety of the work contained therein is my own, original work, that I am the sole author thereof (save to the extent explicitly otherwise stated), that reproduction and publication thereof by Stellenbosch University will not infringe any third party rights and that I have not previously in its entirety or in part submitted it for obtaining any qualification.

March 2016

ABSTRACT

Platinum group metal (PGM) producing companies typically extract PGMs from a nickel-copper ore through a combination of processes including comminution, flotation, smelting, converter treatment, and leaching (Dorfling, 2012; Lamy, 2007; Liddell et al., 1986). The latter processing step is a hydrometallurgical process which aims to dissolve base metals (i.e. copper and nickel sulphides) out of a converter matte and into the liquid phase by means of oxidative reaction, while limiting the dissolution of PGMs.

Dorfling (2012) developed an open-loop dynamic process model within MATLAB™ comprising the second and third stage pressure leaching system and surrounding process units of Western Platinum base metal refinery (BMR). The dynamic process model was subsequently reprogrammed into Simulink™ by Haasbroek and Lindner (2015). The developed dynamic process model is a powerful tool which can be used to investigate and possibly improve several aspects of the Western Platinum BMR operation.

This project aims to improve the dynamic process model to mimic the Western Platinum BMR operation, and to ultimately use the model to analyse the process performance during the occurrence of faults (i.e. abnormal events that potentially lead to failure or malfunction of equipment which causes significant process performance degradation). The updated dynamic process model will allow the possibility of developing and testing fault detection and diagnostic algorithms for Western Platinum BMR.

The Simulink™ dynamic process model was firstly validated using an approach developed by Sargent (2005). This approach validates the entire model on four different levels namely conceptual model validation, computerised model verification, operational validation and data validation.

A total of 34 dynamic process model issues divided into the four validation categories of Sargent (2005) were identified. It was concluded that the reaction kinetics used within the baseline dynamic process model might cause inaccurate leaching predictions. This is attributed to issues existing in both the rate expressions and the experimental data used to fit the kinetics. Most of the other issues which effect the model predictability were addressed. The dynamic process model is therefore valid for predicting general process behaviour, but invalid for exact leaching predictions. The affect which a variety of variable step-changes has on the direction of leaching behaviour is however as expected.

Several control layers which exist at Western Platinum BMR were implemented on the Simulink™ open-loop dynamic process model. This includes regulatory control, supervisory control, alarm systems and safety interlock systems. The addition of control layers ensures that the dynamic process model mimics and acts in a similar manner than the actual process.

A total of 35 sensors; 21 actuators; 30 regulatory controllers; 33 alarms systems; 37 safety interlocks; and 4 supervisory controllers was implemented into the open-loop dynamic process model. These control layers correspond to that which is used at Western Platinum BMR. The developed closed-loop dynamic process model is a useful tool which can be used to train operators and therefore assist in developing operator decision making.

A fault database was developed which contains entries of faults which commonly occur at Western Platinum BMR. Valuable fault characteristics (Himmelblau, 1978; Isermann, 2005; Patton et al., 2013) such as transition rate, frequency of occurrence, fault type and symptoms were included for each fault present in the fault database. Faults were organised based on their point of origin (Venkatasubramanian et al., 2003). Several faults were modelled which ultimately served as a tool to perturb the process so as to assess the process performance during fault occurrences.

A total of 17 faults with the necessary fault characteristics were gathered during a site visit (McCulloch et al., 2014) and composed into a fault database. This includes common faults such as valve wear, valve stiction, pump impeller wear, and controller misuse. A total of 12 faults were subsequently modelled. The fault database can serve as a means of information transfer between several Western Platinum BMR operators and personnel.

The control performance was expressed in terms of control and operational key performance indicators which were calculated at several locations within the dynamic process model. The control and operational key performance indicators (Gerry, 2005; Marlin, 1995; McCulloch et al., 2014; Zevenbergen et al., 2006) include integral absolute error, maximum deviation, time not at set-point, valve reversals, valve saturation; and throughput, extent of base metal leaching, extent of PGM leaching, spillage; respectively. The process performance during the occurrence of faults was compared to a faultless baseline run.

The control performance during the occurrence of 8 independent fault cases was investigated. The extent in which process performance degraded varied significantly between faults. Two faults namely pump impeller wear and solid build-up in cooling coils proved to be the faults which caused the largest process upset. This is attributed to significant autoclave pressure and temperature variations, and the activation of safety

interlocks. These two faults also proved to have the least localised symptoms. This is attributed to the major effect they have early in the process which results in a propagation of symptoms. Two faults namely valve wear and level sensor blockage on the other hand caused minimal deviation in process performance while also propagating through only a few of the measured key performance indicators. These faults occur in the latter part of the process which explains their localised symptoms. The extent to which the process performance was degraded by the level sensor blockage corresponds with expert knowledge (McCulloch et al., 2014); while the model underpredicts the process performance degradation caused by valve wear.

The updated closed-loop dynamic process model together with the modelled faults can be used to develop and test fault detection and diagnostic algorithms for Western Platinum BMR. Moreover, fault signatures produced in this this project could possibly be used as a baseline at Western platinum BMR in an attempt to detect and identify fault occurrences though expert interpretation.

OPSOMMING

Platinum groep metale (PGM) word tipies vanuit 'n nikkel-koper erts ontgin deur middel van 'n verskeidenheid prosesse insluitend komminusie, flotasië, smelting, mat behandeling en loging (Dorfling, 2012; Lamy, 2007; Liddell et al., 1986). Die laasgenoemde stap is 'n hidrometallurgiese proses met die doelwit om basis metale (koper en nikkel sulfiede) uit 'n mat op te los deur middel van oksidatiewe reaksies en ter selfde tyd die oplossing van PGMe te beperk.

Dorfling (2012) het 'n oop-lus dinamiese proses model in MATLAB™ ontwikkel wat die tweede en derde hoë druk logingstelsel en omliggende proseseenhede by Western Platinum basis metaal raffinadery (BMR) bevat. Die dinamiese proses model is binne Simulink™ deur Haasbroek en Lindner (2015) herprogrammeer. Die dinamiese proses model is 'n kragtige hulpmiddel wat verskeie aspekte van Western Platinum BMR se bedryf moontlik kan verbeter.

Die projek mik om eerstens die dinamiese proses model te verbeter tot 'n mate dat dit die Western Platinum BMR bedryf beter naboots. Die projek se finale uitkomst is om die prosesverrigting tydens die voorkoms van foute (d.w.s. abnormale aktiwiteite wat potensieël die mislukking of wanfunksionering van toerusting veroorsaak en lei tot beduidende prosesverrigting agteruitgang) te voorspel. Die verbeterde toe-lus dinamiese proses model sal moontlik help om fout opsporing en diagnose algoritmes te ontwikkel wat ten einde op die Western Platinum BMR toegepas kan word.

Die geldigheid van die Simulink™ dinamiese proses model is eerstens verklaar met behulp van 'n benadering getoon in Sargent (2005). Hierdie benadering kyk na die geldigheid van die hele model op vier verskillende vlakke; naamlik konseptuele model validering, gerekenariseerde model verifiëring, operasionele model validering en data validering.

'n Totaal van 34 dinamiese proses model kwessies wat in die vier validasie vlakke van Sargent (2005) verdeel is, is geïdentifiseer. Die model validasie is afgesluit deur uit te wys dat die reaksie kinetika wat in die aanvangsmeting dinamiese proses model gebruik word moontlik onakkurate loging voorspellings veroorsaak. Hierdie word toegeskryf aan kwessies wat bestaan in beide die tempo-uitdrukkings en eksperimentele data wat gebruik is om kinetika te pas. Meeste van die kwessies wat die model voorspelling affekteer is aangespreek. Die model, vir die rede, voorspel algemene proses gedrag akkuraat, maar voorspel die presiese loginggedrag onakuraat. Die rigting van loging verander egter in die verwagte rigting wanneer 'n verskeidenheid insetveranderlikes stapagtig verander word.

Verskeie beheerlae wat bestaan by Western Platinum BMR is op die Simulink™ dinamiese proses model geïmplimenteer. Hierdie sluit regulatoriese beheer, toesighoudende beheer, alarmstelsels en veiligheidsbindingstelsels in. Die addisionele beheerlae verseker dat die dinamiese proses model die werklike proses naboots.

'n Totaal van 35 sensors, 21 aandrywers, 30 regulatoriese beheerders, 33 alarmstelsels, 37 veiligheidsbindingstelsels en 4 toesighoudende beheerders is in die oop-lus dinamiese proses model geïmplimenteer. Hierdie beheerlae stem ooreen met die wat tans by Western Platinum BMR bestaan. Die ontwikkelde toe-lus dinamiese proses model is 'n nuttige hulpmiddel wat kan help om operateurs op te lei en dus help met die ontwikkeling van operateur besluitneming.

'n Fout databasis met inskrywings van algemene foute wat by Western Platinum BMR teëgekomp word, is ontwikkel. Waardevolle fouteienskappe (Himmelblau, 1978; Isermann, 2005; Patton et al., 2013) insluitend oorgangstempo, voorkomingsfrekwensie, fout tipe en simptome is in die fout databasis ingesluit. Foute is volgens die punt van oorsprong georganiseer (Venkatasubramanian et al., 2003). Verskeie foute is gemodelleer en gebruik as 'n hulpmiddel om die proses te ontstel met die einddoel om prosesverrigting te bepaal.

'n Totaal van 17 foute met die nodige fouteienskappe is tydens 'n aanlegbesoek versamel (McCulloch et al., 2014) en in 'n fout databasis saamgestel. Hierdie sluit algemene foute soos klepverwering, klepwyking, stuwerverwering, en misbruik van beheerders, in. 'n Totaal van 12 foute is hierna gemodelleer. Die fout databasis kan optree as 'n metode van inligting oordrag tussen verskeie Western Platinum BMR operateurs en personeel.

Die prosesverrigting is in terme van beheer en operasionele kern verrigting-aanwysers uitgedruk. Die kern verrigting-aanwysers is by verskeie plekke binne die dinamiese proses model bereken. Die beheer en operasionele kern verrigting-aanwysers (Gerry, 2005; Marlin, 1995; McCulloch et al., 2014; Zevenbergen et al., 2006) sluit die integraal absolute fout, maksimum afwyking, tyd nie by stel-punt, klepomkerings, klepversadiging en deurset, mate van basis metaal logging, mate van PGM logging, en morsing onderskeidelik in. Die prosesverrigting tydens verskeie fout voorkomste is vergelyk met die van 'n foutlose aanvangsmeting lopie.

Die prosesverrigting tydens die voorkoms van 8 onafhanklike foutgevalle is ondersoek. Die mate van prosesverrigting agteruitgang verskil grootliks tussen foute. Twee foute naamlik stuwerverwering en vastestof-opbou in verkoelingspoele het die grootste prosesversteuring veroorsaak. Hierdie word aan die beduidende outoklaaf druk en temperatuur versteurings wat tydens die fout voorkomste ontaard het asook die aktivering van veiligheidsbindings

toegeskryf. Hierdie foute het ook die minste gelokaliseerde simptome gehad. Hierdie word aan die beduidende groot simptome wat vroeg in die proses ontstaan het toegeskryf. Die vroeë simptome het verder deur die proses gepropageer. Twee foute naamlik klepverwering en vlak sensorverstoping het aan die ander kant minimale afwyking in prosesverrigting veroorsaak en het ook net deur net 'n paar gemete kern verrigting-aanwysers gepropageer. Die gelokaliseerde simptome word toegeken aan die foute wat plaasvind in die laaste deel van die proses. Die mate van prosesverrigting versteuring wat veroorsaak was deur vlak sensorverstoping stem ooreen met deskundige kennis (McCulloch et al., 2014); terwyl die prosesverrigting versteuring ondervoorspel word deur die model in die geval van klepverwering.

Die verbeterde toe-lus dinamiese proses model saam met die gemodelleerde foute kan help om fout opsporing en diagnose algoritmes te ontwikkel wat ten einde op die Western Platinum BMR gebruik kan word. Verder kan die fouthandtekening van die model moontlik as 'n aanvangsmeting by Western Platinum BMR gebruik word om foute deur deskundige interpretasie te identifiseer.

ACKNOWLEDGEMENTS

I would like to express my appreciation to the following people:

- My main supervisor, Dr. Lidia Auret, for her patience, guidance and significant technical contributions.
- My co-supervisors, Prof. Christie Dorfling and Prof. Steven Bradshaw, for supporting this project and sharing their valuable technical knowledge.
- Part of the Process Monitoring and Systems research group namely Dr. JP Barnard and Mr. Brian Lindner, for sharing their substantial Simulink™ and MATLAB™ knowledge.
- The rest of the Process Monitoring and Systems research group namely Mr. Johannes Rabie, Mr. Adriaan Henning, Mr. Ernst Nienaber, Mrs. Mollin Siwella and Mr. Zander Horn, for making each day at the office interesting.
- My project sponsors, SAMMRI and NRF, for making this project possible.

TABLE OF CONTENT

CHAPTER 1 : Introduction	1
1.1. Background.....	1
1.2. Project Objectives	3
1.3. Thesis Structure.....	3
CHAPTER 2 : Process Description	5
2.1. Background.....	5
2.2. Leaching Process Overview.....	7
2.2.1. 1 st atmospheric leaching stage.....	7
2.2.2. 2 nd and 3 rd pressure leaching stage.....	8
2.3. Leaching Process Chemistry	11
2.3.1. Base metals	11
2.3.2. Platinum group metals	13
2.4. Leaching Process Control Philosophy.....	14
2.4.1. Control objectives	14
2.4.2. Regulatory control.....	15
2.4.3. Supervisory control	19
2.4.4. Alarm systems	21
2.4.5. Safety interlock systems	22
CHAPTER 3 : Dynamic Process Model Description	24
3.1. Overview.....	24
3.2. Batch Experimentation.....	25
3.3. Reaction Kinetics	26
3.4. Dynamic Process Model Overview.....	28
3.5. Mass and Energy Balances	29
3.6. Constitutive Equations	30
3.7. Model Programming.....	30
3.7.1. MATLAB™ dynamic process model.....	30

3.7.2.	Simulink™ dynamic process model.....	33
3.8.	Model Assumptions.....	35
3.8.1.	Leaching chemistry and reaction mechanisms.....	35
3.8.2.	Batch experimentation.....	36
3.8.3.	Rate expression development.....	36
3.8.4.	Rate expression optimisation.....	36
3.8.5.	Dynamic process model development.....	36
CHAPTER 4 :	Literature Review.....	37
4.1.	Model Verification and Validation.....	37
4.1.1.	Participating parties.....	38
4.1.2.	V&V approaches.....	39
4.1.3.	V&V techniques.....	41
4.2.	Control Implementation.....	43
4.3.	Fault Database.....	47
4.3.1.	Fault characteristics.....	48
4.3.2.	Fault information sources.....	50
4.3.3.	Fault examples.....	51
4.4.	Control Performance Assessment.....	55
4.4.1.	Control key performance indicators.....	55
4.4.2.	Operational key performance indicators.....	58
CHAPTER 5 :	Project Objectives and Tasks.....	60
CHAPTER 6 :	Model Verification and Validation.....	62
6.1.	Overview.....	62
6.2.	Data Validation.....	66
6.2.1.	Ion concentration adjustments in batch experimental data.....	67
6.2.2.	Acid concentrations in batch experimental data.....	69
6.2.3.	Ion concentration variation in batch experimental data.....	73
6.2.4.	Physically realisable checks on plant data.....	75
6.2.5.	Mass and energy balances on plant data.....	78

6.2.6.	Data reconciliation on plant data	82
6.2.7.	Global test on plant data	86
6.2.8.	Measurement test on plant data.....	87
6.3.	Conceptual Model Validation	90
6.3.1.	Copper cementation reactions	90
6.3.2.	Ferric to ferrous ion reduction mechanism influence	92
6.3.3.	PGM leaching reaction initiation.....	93
6.3.4.	Rate expressions scaled to large process units	95
6.3.5.	Initial concentrations in a continuous process	96
6.3.6.	Dynamic process model oxygen solubility estimation.....	97
6.3.7.	Mass transfer limits digenite and covellite leaching reactions.....	98
6.3.8.	PGM-oxide shape factors with infinite size	99
6.3.9.	Data point/parameter ratio in reaction kinetic optimisation	100
6.3.10.	Objective function used in reaction kinetic optimisation	102
6.3.11.	Reaction kinetics optimisation	103
6.4.	Computerised Model Verification	111
6.4.1.	Static testing	111
6.4.2.	Dynamic testing	114
6.5.	Operational Validation.....	114
6.5.1.	Degree of freedom analysis	115
6.5.2.	Constant temperature and composition inputs	116
6.5.3.	Isothermal preparation tanks.....	123
6.5.4.	Constant mass in all autoclave compartments	124
6.5.5.	Isobaric autoclave	125
6.5.6.	Sulphuric acid and water streams entering flash recycle tank	127
6.5.7.	Ideal CSTR characteristics.....	128
6.5.8.	No reactions in auxiliary tanks	129
6.5.9.	Constant agitator work and heat loss	129
6.5.10.	Single flash recycle tank/autoclave set	130

6.5.11.	Extreme condition testing	131
6.5.12.	Face validation	132
6.5.13.	Dynamic process model predictability.....	135
6.6.	Model Update Summary	136
6.7.	Model Validity Conclusion	139
CHAPTER 7 : Control Implementation		141
7.1.	Overview.....	141
7.2.	Sensors	142
7.2.1.	Methodology	142
7.2.2.	Results and discussion	143
7.3.	Actuators	145
7.3.1.	Methodology	145
7.3.2.	Results and discussion	147
7.4.	Regulatory control.....	150
7.4.1.	Methodology	150
7.4.2.	Results and discussion	155
7.5.	Supervisory control	160
7.5.1.	Methodology	160
7.5.2.	Results and discussion	164
7.6.	Alarm systems	166
7.6.1.	Methodology	166
7.6.2.	Results and discussion	168
7.7.	Safety interlock systems	170
7.7.1.	Methodology	170
7.7.2.	Results and discussion	171
7.8.	Summary	173
CHAPTER 8 : Fault Database Creation and Simulation		174
8.1.	Overview.....	174
8.2.	Fault Database	175

8.3.	Fault Modelling	177
8.3.1.	Valve blockage – density disturbance	177
8.3.2.	Valve wear	180
8.3.3.	Valve stiction.....	185
8.3.4.	Pump impeller wear	189
8.3.5.	Solid build-up in cooling coils	192
8.3.6.	Peristaltic pump tube failure.....	194
8.3.7.	Sulphuric acid controller misuse.....	195
8.3.8.	Bubbler level sensor blockage	197
8.4.	Summary	200
CHAPTER 9 : Control Performance Assessment		201
9.1.	Overview.....	201
9.2.	Key Performance Indicator Methodology	202
9.2.1.	Control key performance indicators.....	202
9.2.2.	Operational key performance indicators.....	204
9.2.3.	Key performance indicator application	205
9.3.	Fault Scenario Run Methodology	208
9.3.1.	Fault scenarios	208
9.3.2.	Dynamic process model inputs	209
9.4.	Results and Discussion.....	211
9.4.1.	Baseline run.....	211
9.4.2.	Valve blockage – density disturbance	214
9.4.3.	Valve wear	220
9.4.4.	Valve stiction.....	222
9.4.5.	Pump impeller wear	226
9.4.6.	Solid build-up in cooling coils	235
9.4.7.	Peristaltic pump tube failure.....	241
9.4.8.	Sulphuric acid controller misuse.....	246
9.4.9.	Bubbler level sensor blockage	250

9.5. Summary	254
CHAPTER 10 : Conclusions and Recommendations	257
10.1. Model Verification and Validation	257
10.2. Control Implementation	257
10.3. Fault Database Creation and Simulation	258
10.4. Control Performance Assessment	258
10.5. Recommendations	259
CHAPTER 11 : Future Work	260
11.1. Model Predictability	260
11.2. Fault Detection and Diagnosis.....	261
Appendix A : Nomenclature.....	272
Appendix B : Data	279
Appendix C : Sample Calculations	281
Appendix D : Equations and Procedures.....	283
Appendix E : Flow Diagrams	297
Appendix F : Results	302

LIST OF FIGURES

Figure 1.1: Flow diagram of project objectives	3
Figure 2.1: Typical PGM processing steps (Redrawn from Lamya (2007) and Liddell et al. (1986)).....	6
Figure 2.2: PFD of 1 st leaching stage: Western Platinum BMR (Redrawn from Dorfling (2012)).....	7
Figure 2.3: PFD of 2 nd and 3 rd leaching stages: Western Platinum BMR	10
Figure 2.4: Autoclave compartment 1 and flash recycle tank P&ID.....	18
Figure 2.5: On/off (left) and continuous (right) operator controllers.....	20
Figure 3.1: Representation of information flow between process units within the dynamic model	31
Figure 3.2: MATLAB™ dynamic process model structure	32
Figure 3.3: Simulink™ dynamic process model hierarchy	33
Figure 3.4: Generic MATLAB™ function block used inside the second stage slurry preparation tank reference model	34
Figure 3.5: Simulink™ dynamic process model structure	35
Figure 4.1: Simple Verification and Validation Approach (Redrawn from Sargent (2005))	40
Figure 4.2: Different layers used to control for safety (Marlin, 1995).....	44
Figure 4.3: Single-loop feedback control block diagram (Redrawn from Lipták (2006))	45
Figure 4.4: Control hierarchy in plantwide industrial control architecture (Romagnoli & Palazoglu, 2012)	46
Figure 4.5: Area of faults occurrences within a process (Venkatasubramanian et al., 2003)	48
Figure 4.6: Rate of fault transition: (a) abrupt; (b) incipient; (c) intermittent (Redrawn from Isermann (2005)).....	49
Figure 4.7: Basic models of faults: (a) additive (b) multiplicative	50
Figure 5.1: Project objectives divided into tasks	61
Figure 6.1: Effect of significant sample sizes on the volume and area of a batch reactor	68
Figure 6.2: Model predicted acid concentration for high (left) and low initial acid concentrations (right)	71
Figure 6.3: Approaches to PGM oxidation state issue.....	72
Figure 6.4: Physically realisable check results for several tags.....	76
Figure 6.5: Online measurement reliability (McCulloch et al., 2014)	77
Figure 6.6: Mass balance results: Second stage slurry preparation tank.....	79
Figure 6.7: Manually measurement reliability (McCulloch et al., 2014)	80
Figure 6.8: Mass balance results: Flash recycle tank of autoclave 300	81
Figure 6.9: Mass balance results: Flash recycle tank of autoclave 200	82
Figure 6.10: Data reconciliation results: Second stage slurry preparation tank	84
Figure 6.11: Data reconciliation results: Flash recycle tank of autoclave 300.....	85
Figure 6.12: Global test results	87
Figure 6.13: Measurement test results: Significant ζ outputs	89

Figure 6.14: Several cupric ion concentration trends in batch experimentation conducted by Dorfling (2012)	91
Figure 6.15: Epsilon insensitive objective function	103
Figure 6.16: Reaction kinetic optimisation methodology	104
Figure 6.17: Excel optimisation worksheet reproduced in MATLAB™ (results for experiment 2a)	107
Figure 6.18: Cupric ion concentration of first four experiments with optimised fits.....	110
Figure 6.19: Mass balance consistency checks.....	114
Figure 6.20: Random walk generator developed in Simulink™	117
Figure 6.21: Second stage slurry preparation tank temperature profile compared to a random walk	118
Figure 6.22: Frequency diagrams for first stage residue compositions	119
Figure 6.23: First stage leach residue composition random walk generation.....	120
Figure 6.24: Frequency diagrams for formic filtrate liquid concentrations	121
Figure 6.25: Formic filtrate liquid concentration and composition random walk generation	122
Figure 6.26: Autoclave compartment level profiles	124
Figure 6.27: Autoclave pressure profile	126
Figure 6.28: Autoclave vapour temperature estimated using compartment temperatures and volumes	127
Figure 6.29: Typical FIC-0202 operation	128
Figure 7.1: Control layer implementation sequence	141
Figure 7.2: Simple sensor operation (Redrawn from Webster (2014)).....	142
Figure 7.3: Block interface (top left), block mask (top right) and mechanism (bottom) of sensor modelled in Simulink™	143
Figure 7.4: Sensor noise for TIC-3001 generated by the sensor block in Simulink™	144
Figure 7.5: Typical actuator structure (Bartys & de las Heras, 2003)	145
Figure 7.6: Valve flow characteristics (Redrawn from Marlin (1995)).....	145
Figure 7.7: Block interface (top left), block mask (top right) and mechanism (bottom) of actuator modelled in Simulink™	147
Figure 7.8: Actuator time constant estimation using FIC-0201	148
Figure 7.9: K_v relationship for FCV-1102	150
Figure 7.10: Mechanism of PID controller implemented in Simulink™	151
Figure 7.11: Block interface (left) and block mask (right) of PID controller modelled in Simulink™	151
Figure 7.12: Process parameter estimation using reaction curves.....	154
Figure 7.13: LIC-0101 cascade control modelled in Simulink™	155
Figure 7.14: Step-test: LIC-0101 (left) cascaded with FIC-0106 (right).....	156
Figure 7.15: PIC-3001 cascade and ratio control modelled in Simulink™	157
Figure 7.16: Step-test: PIC-3001 (left) cascaded with FIC-3001A/B/C (right).....	157
Figure 7.17: TIC-3001 cascade control modelled in Simulink™	158
Figure 7.18: Step-test: TIC-3001 (left) cascaded with FIC-0205 (middle) causally related through LIC-0201 (right).....	158
Figure 7.19: Feedforward solid percentage control modelled in Simulink™	159

Figure 7.20: Step-test: Solid percentage control (left) that feed forwards to FIC-0101 and FIC-1102 (right).....	159
Figure 7.21: Mechanism of normal operation block showing gain-scheduling	161
Figure 7.22: Mechanism of gain-scheduling modelled in Simulink™	162
Figure 7.23: Block interface (top left), block mask (top right) and mechanism (bottom) of on/off operator controller modelled in Simulink™	163
Figure 7.24: Block interface (top left), block mask (top right) and mechanism (bottom) of continuous operator controller modelled in Simulink™	163
Figure 7.25: Supervisory control test: Gain-scheduling used within FIC-1102.....	164
Figure 7.26: Supervisory control test: Continuous operator control - acid concentration in TK-150 ..	165
Figure 7.27: Supervisory control test: On/off operator control – acid concentration exiting the flash recycle tank	166
Figure 7.28: Block interface (top left), block mask (top right) and mechanism (bottom) of alarm modelled in Simulink™	167
Figure 7.29: Functioning of alarm hysteresis.....	168
Figure 7.30: LIC-0101 control with alarm system modelled in Simulink™	169
Figure 7.31: Alarm test: LIC-0101 with high and high-high alarms.....	169
Figure 7.32: Alarm hysteresis test: Artificial level connected with LIC-0101 alarm system.....	170
Figure 7.33: Block interface (top left), block mask (top right) and mechanism (bottom) of interlock modelled in Simulink™	171
Figure 7.34: LIC-0101 control with safety interlock system modelled in Simulink™	172
Figure 7.35: Safety interlock test: LIC-0101 with high-high alarm interlock.....	173
Figure 8.1: Location of fault 1: Density disturbance.....	178
Figure 8.2: Block interface (top left), block mask (top right) and mechanism (bottom) of density disturbance modelled in Simulink™	179
Figure 8.3: Quantification of density spikes in first stage leach residue stream using real-time data	179
Figure 8.4: Linear valve (left) and quick-opening valve (right) prior to and after valve wear	180
Figure 8.5: Location of fault 2: Valve wear.....	181
Figure 8.6: Actual and worn valve position relation at different extents of degradation	182
Figure 8.7: Block interface (top left), block mask (top right) and mechanism (bottom) of valve wear modelled in Simulink™	183
Figure 8.8: Quantification of fourth compartment valve degradation over time using real-time data .	183
Figure 8.9: Quantification of rate of fourth compartment valve degradation using real-time data.....	184
Figure 8.10: Behaviour of the valve wear fault for an artificial sinusoidal valve position	185
Figure 8.11: Location of fault 3: Valve stiction	186
Figure 8.12: Input-output behaviour of valve stiction (redrawn from Choudhury et al. (2005))	186
Figure 8.13: Block interface (top left), block mask (top right) and mechanism (bottom) of valve stiction modelled in Simulink™	187
Figure 8.14: Quantification of valve stiction parameters using real-time data	188
Figure 8.15: Behaviour of the valve stiction fault for an artificial sinusoidal valve position set-point..	189

Figure 8.16: Location of fault 4: Pump impeller wear	190
Figure 8.17: Block interface (top left), block mask (top right) and mechanism (bottom) of impeller wear modelled in Simulink™	190
Figure 8.18: Behaviour of the pump impeller wear fault for an artificial sinusoidal valve position set-point.....	191
Figure 8.19: Location of fault 5: Solid build-up in cooling coils	192
Figure 8.20: Block interface (top left), block mask (top right) and mechanism (bottom) of solid build-up modelled in Simulink™	193
Figure 8.21: Behaviour of the solid build-up fault for an artificial sinusoidal valve position set-point.	193
Figure 8.22: Location of fault 6: Peristaltic pump tube failure	194
Figure 8.23: Block interface (top left), block mask (top right) and mechanism (bottom) of peristaltic pump tube failure modelled in Simulink™	195
Figure 8.24: Behaviour of the peristaltic pump tube failure fault for an artificial sinusoidal flow rate	195
Figure 8.25: Location of fault 7: Sulphuric acid controller misuse	196
Figure 8.26: Sulphuric acid flow rate set-point provided by an operator	197
Figure 8.27: Bubbler level sensor measurement mechanism (redrawn from ITA (2009)).....	197
Figure 8.28: Location of fault 15: Bubbler level sensor blockage	198
Figure 8.29: Block interface (top left), block mask (top right) and mechanism (bottom) of level sensor blockage modelled in Simulink™	198
Figure 8.30: Behaviour of the level sensor blockage fault for an artificial sinusoidal level.....	199
Figure 9.1: Hierarchy for mitigating control performance issues (McCulloch et al., 2014)	203
Figure 9.2: Summary of modelled fault locations which were used within control performance assessment	210
Figure 9.3: General approach used to describe KPI deviation from the baseline	211
Figure 9.4: Operational KPIs of baseline run: PGMs in liquid and BMs in solid	213
Figure 9.5: Verification of fault 1 occurrence: solid fraction of stream 1	214
Figure 9.6: Fault 1 occurrence: first stage leach residue flow rate	217
Figure 9.7: PGMs in liquid and BMs in solid for fault 1 – density disturbance.....	218
Figure 9.8: PGMs present in the first compartment liquid phase over time during fault 1 – density disturbance.....	219
Figure 9.9: Verification of fault 2 occurrence: Compartment 4 outlet flow control valve (left) and flow rate (right).....	220
Figure 9.10: Valve characteristics at 0 and 0.73 extents of degradation	221
Figure 9.11: Verification of fault 3 occurrence: Spent electrolyte flow controller valve position over time for baseline (left) and fault (right)	222
Figure 9.12: Travel distance of the spent electrolyte flow control valve over time during fault 3 - valve stiction	224
Figure 9.13: Density of second stage slurry preparation tank during fault 3 – valve stiction.....	225
Figure 9.14: PGMs in liquid and BMs in solid for fault 3 – valve stiction	226

Figure 9.15: Verification of fault 4 occurrence: Flash recycle tank outlet flow control valve (left) and corresponding flow rate (right)	227
Figure 9.16: Temperature (left) and outlet flow rate (right) of compartment 1 during fault 4 – Pump impeller wear	229
Figure 9.17: Level of flash recycle tank (left) and outlet flow rate of second stage slurry preparation tank (right) during fault 4 – Pump impeller wear	230
Figure 9.18: Level of compartment 1 during fault 4 – Pump impeller wear	231
Figure 9.19: Level of second stage slurry preparation tank (left) and cascaded flow rate of first stage leach residue (right) during fault 4 – Pump impeller wear	232
Figure 9.20: Density of second stage slurry preparation tank during fault 4 – Pump impeller wear ..	233
Figure 9.21: Solid fraction of feed to compartment 4 during fault 4 – Pump impeller wear	234
Figure 9.22: PGMs in liquid and BMs in solid for fault 4 – pump impeller wear	234
Figure 9.23: Verification of fault 5 occurrence: Compartment 2 temperature control valve (left) and flow rate (right)	236
Figure 9.24: Temperature in compartment 2 (left) and compartment 1 (right) during fault 5 – solid build-up in cooling coils	237
Figure 9.25: Temperature in compartment 3 (left) and compartment 4 (right) during fault 5 – solid build-up in cooling coils	239
Figure 9.26: PGMs in liquid and BMs in solid for fault 5 – solid build-up in cooling coils	240
Figure 9.27: Verification of fault 6 occurrence: First stage leach residue flow rate	241
Figure 9.28: Level of second stage slurry preparation tank during fault 6 – Peristaltic pump tube failure	242
Figure 9.29: Density of second stage slurry preparation tank during fault 6 – Peristaltic pump tube failure.....	243
Figure 9.30: Solid fraction of compartment 1 (left), 2 (middle) and 3 (right) during fault 6 – Peristaltic pump tube failure	244
Figure 9.31: Solid fraction of compartment 4 during fault 6 – Peristaltic pump tube failure	245
Figure 9.32: PGMs in liquid and BMs in solid for fault 6 – Peristaltic pump tube failure	246
Figure 9.33: Verification of fault 7 occurrence: Flash recycle tank acid concentration (left) and acid flow rate (right)	247
Figure 9.34: Temperature in compartment 1 (left) and compartment 2 (right) during fault 7 – H ₂ SO ₄ controller misuse	248
Figure 9.35: Autoclave pressure during fault 7 – H ₂ SO ₄ controller misuse	249
Figure 9.36: PGMs in liquid and BMs in solid for fault 7 – H ₂ SO ₄ controller misuse	250
Figure 9.37: Verification of fault 15 occurrence: Compartment 3 level for the baseline (left) and fault (right)	251
Figure 9.38: PGMs in liquid and BMs in solid for fault 15 – Level sensor blockage	253
Figure 9.39: Hierarchy of faults based on performance impact (left) and least localised (right)	254
Figure D.1: Mechanism of the travel distance KPI implemented in Simulink™	288
Figure D.2: Behaviour of the travel distance KPI for an artificial sinusoidal temperature	288

Figure D.3: Mechanism of the integral absolute error KPI implemented in Simulink™	289
Figure D.4: Behaviour of the integral absolute error KPI for an artificial sinusoidal temperature	289
Figure D.5: Mechanism of the maximum deviation KPI implemented in Simulink™	290
Figure D.6: Behaviour of the maximum deviation KPI for an artificial random number generator input	290
Figure D.7: Mechanism of the time not at set-point KPI implemented in Simulink™	291
Figure D.8: Behaviour of the time not at set-point KPI for an artificial sinusoidal variable	291
Figure D.9: Mechanism of the standard deviation KPI implemented in Simulink™	292
Figure D.10: Behaviour of the standard deviation KPI	292
Figure D.11: Mechanism of the valve at a limit KPI implemented in Simulink™	293
Figure D.12: Behaviour of the valve at a limit KPI for an artificial signal	294
Figure D.13: Mechanism of the valve reversal KPI implemented in Simulink™	294
Figure D.14: Behaviour of the valve reversal KPI for an artificial sinusoidal signal	295
Figure E.1: P&ID of Leaching Process: Western Platinum Ltd. BMR autoclave 300	297
Figure E.2: P&ID of Leaching Process: Western Platinum Ltd. BMR autoclave 200	298
Figure E.3: Baseline Simulink™ model flow diagram of Leaching Process: Western Platinum Ltd. BMR	299
Figure E.4: Flow diagram to determine steady-state operating conditions	300
Figure E.5: Flow diagram to determine steady-state extent of reactions	301
Figure F.1: Data reconciliation results: FIC-0101 (left) and FIC-1102 (right)	313
Figure F.2: Data reconciliation results: FIC-0103 (left) and FIC-0106 (right)	313
Figure F.3: Data reconciliation results: FIC-0201 (left) and FIC-0202 (right)	313
Figure F.4: Data reconciliation results: FIC-0205 (left) and FIC-0203 (right)	314
Figure F.5: Data reconciliation results: FIC-2202 (left) and FIC-2203 (right)	314
Figure F.6: Data reconciliation results: FIC-2204	314
Figure F.7: Measurement test results: FIC-0106, FIC-0101, FIC-1102 and FIC-0103	315
Figure F.8: Measurement test results: FIC-0201, FIC-0203, FIC-0202 and FIC-0205	315
Figure F.9: Measurement test results: FIC-2204, FIC-2203 and FIC-2202	316
Figure F.10: K_v relationship for FCV-0106	319
Figure F.11: K_v relationship for FCV-0101	319
Figure F.12: K_v relationship for FCV-1102	319
Figure F.13: K_v relationship for FCV-0201	320
Figure F.14: K_v relationship for FCV-0202	320
Figure F.15: K_v relationship for FCV-0203	320
Figure F.16: K_v relationship for FCV-0205	321
Figure F.17: K_v relationship for FCV-3001A	321
Figure F.18: K_v relationship for FCV-3001B	321
Figure F.19: K_v relationship for FCV-3001C	322
Figure F.20: K_v relationship for FCV-3002	322
Figure F.21: K_v relationship for FCV-0150-3	322

Figure F.22: K_v relationship for FCV-0150-4.....	323
Figure F.23: K_v relationship for FCV-0150-5.....	323
Figure F.24: K_v relationship for FCV-0150-9.....	323
Figure F.25: K_v relationship for FCV-3003.....	324

LIST OF TABLES

Table 2.1: Composition of material from Western Platinum BMR (Dorfling, 2012; McCulloch et al., 2014)	9
Table 2.2: Operating conditions: Western Platinum BMR (van der Merwe & Mrubata, 2014)	11
Table 2.3: Regulatory control loops: Western Platinum BMR (van der Merwe, 2014)	16
Table 2.4: Supervisory control: Western Platinum BMR (McCulloch et al., 2014)	20
Table 2.5: Alarm systems: Western Platinum BMR (McCulloch et al., 2014).....	22
Table 2.6: Safety interlocks systems: Western Platinum BMR (Steenekamp et al., 2009)	23
Table 3.1: Experimental run conditions (Dorfling, 2012).....	25
Table 3.2: Main constitutive equations used by Dorfling (2012) in dynamic process model	30
Table 3.3: Dynamic process model inputs (Dorfling, 2012)	31
Table 4.1: Examples of possible symptoms (Himmelblau, 1978)	50
Table 4.2: Faults simulated in MODEX2 examination (Venkatasubramanian & Rich, 1988).....	51
Table 4.3: Faults throughout a variety of processes (Himmelblau, 1978)	52
Table 4.4: Pump faults within offshore oil and gas facility (Raza & Liyanage, 2009)	52
Table 4.5: Centrifugal pump faults (Himmelblau, 1978)	53
Table 4.6: Instrumentation faults (Lees, 1976)	53
Table 4.7: Actuator faults used in DAMADICS benchmark study (Koscielny & Bartys, 2000)	53
Table 4.8: Control valve faults (Anyakora, 1971).....	54
Table 4.9: Faults within a reactor and separator process (Downs & Vogel, 1993).....	54
Table 6.1: Model verification and validation reference index.....	64
Table 6.2: Available historian tag data sets	65
Table 6.3: Available manually measured data sets	66
Table 6.4: Error induced by sample adjustments.....	69
Table 6.5: Standard deviations and averages of time-zero samples (Dorfling, 2012).....	74
Table 6.6: Ratio test: Experimental data points per reaction kinetic parameters	101
Table 6.7: Excel optimisation worksheet reproduced in independent worksheet	107
Table 6.8: Objective function outputs for several sets of MATLAB™ global optimised reaction kinetics	108
Table 6.9: Errors noticed and corrected during a structured walk-through.....	112
Table 6.10: Degree of freedom analyses for respective process units.....	115
Table 6.11: Extreme conditions testing for baseline model	131
Table 6.12: Face validation of step response dynamics for volumetric flow rate step increases in an open-loop model	133
Table 6.13: Baseline dynamic process model composition predictions	135
Table 6.14: Model verification and validation reference index summarising model updates	137
Table 6.15: Model verification and validation reference index summarising model issues and future work.....	138

Table 6.16: Model verification and validation reference index summarising issues that affect model validity	139
Table 7.1: Sensor variance estimation: Western Platinum BMR	144
Table 7.2: K_v relationships developed for valves	149
Table 7.3: Controller parameter estimation (Merrick & Ponton, 1995)	154
Table 7.4: Supervisory control: Dynamic process model (McCulloch et al., 2014)	160
Table 8.1: Section of fault database (McCulloch et al., 2014)	176
Table 9.1: Control loop performances considered during control performance assessment	205
Table 9.2: Valve performances considered during control performance assessment.....	206
Table 9.3: Operational performances considered during control performance assessment	206
Table 9.4: List of fault scenarios used in control performance assessment	208
Table 9.5: Baseline travel distances related to sensor variances.....	212
Table 9.6: Baseline travel distances per valve reversals	213
Table 9.7: Significant KPIs for fault 1: density disturbance.....	215
Table 9.8: Significant KPIs for fault 2: valve wear	221
Table 9.9: Significant KPIs for fault 3: Valve stiction	223
Table 9.10: Significant KPIs for fault 4: Pump impeller wear.....	228
Table 9.11: Significant KPIs for fault 5: Solid build-up in cooling coils	237
Table 9.12: Significant KPIs for fault 6: Peristaltic pump tube failure	242
Table 9.13: Significant KPIs for fault 7: Sulphuric acid controller misuse.....	247
Table 9.14: Significant KPIs for fault 15: Level sensor blockage.....	252
Table B.1: Dynamic process model input data (Dorfling, 2012)	279
Table B.2: Western Platinum BMR controller data obtained during a site visit (McCulloch et al., 2014)	280
Table D.1: Rate expressions for Reaction 1 to Reaction 21 developed by Dorfling (2012)	283
Table F.1: Face validation by model input step increases.....	302
Table F.2: KPIs at the end of simulation: Baseline	303
Table F.3: Equivalence of baseline KPIs and fault 1 KPIs at $t = 50$ hours	304
Table F.4: KPIs at the end of simulation: Fault 1 – Valve blockage	305
Table F.5: KPIs at the end of simulation: Fault 2 – Valve wear	306
Table F.6: KPIs at the end of simulation: Fault 3 – Valve stiction.....	307
Table F.7: KPIs at the end of simulation: Fault 4 – Pump impeller wear	308
Table F.8: KPIs at the end of simulation: Fault 5 – Solid build-up in cooling coils	309
Table F.9: KPIs at the end of simulation: Fault 6 – Peristaltic pump tube failure	310
Table F.10: KPIs at the end of simulation: Fault 15 – Level sensor blockage.....	311
Table F.11: Fault database (McCulloch et al., 2014).....	312
Table F.12: Reaction kinetic optimisation results: Parameters for GS and GS with PS.....	317
Table F.13: Reaction kinetic optimisation results: Parameters for GA and GA with PS.....	318

CHAPTER 1: INTRODUCTION

This chapter serves to inform the reader on the relevance of the project by considering the project background and the development of applicable project objectives. A thesis structure is also provided to show how the thesis is divided.

1.1. Background

Platinum Group Metals (PGMs) by definition are a group of closely related metals similar to that of platinum. These similarities include their low natural abundance and related physical and chemical properties (Vermaak, 1995). PGMs, occasionally referred to as Platinum Group Elements (PGEs), include ruthenium (Ru), rhodium (Rh), palladium (Pd), osmium (Os), iridium (Ir) and platinum (Pt). Beneficial physical and chemical properties of PGMs include electrical conductivity, high melting point and catalytic activity (Xiao & Laplante, 2004). These properties are commonly utilised by using PGMs within catalytic converters for air pollution reduction, jewellery production, hydrogen fuel cells, catalysts for certain chemical and petroleum processes, and many more (Glaister & Mudd, 2010; Bernardis et al., 2005).

South African PGM production has made a significant contribution to the national economy (DMR, 2009). It is important for the South African mining industry to continue to dominate PGM production in an efficient and effective manner.

The largest PGM reserve in the world covers the North West, Gauteng, Limpopo and Mpumalanga provinces in South Africa. This reserve is known as the Bushveld complex, covering an area of approximately 66 000 km² (Von Gruenewaldt, 1977). Several companies including Anglo American Platinum, Impala Platinum and Lonmin, among others, mine the Bushveld Complex (Johnson Matthey, 2008; Dzvinamurungu, 2012).

These companies typically extract PGMs from a nickel-copper ore through a combination of processes including comminution, flotation, smelting, converter treatment, and leaching (Lamya, 2007; Liddell et al., 1986; Dorfling, 2012). The latter processing step is a hydrometallurgical process which attempts to dissolve base metals (i.e. copper and nickel sulphides) out of a converter matte and into the liquid phase by means of oxidative reaction,

while limiting the dissolution of PGMs. This process, typically forming part of a base metal refinery (BMR), removes base metals from the solid phase in order to produce a high-grade PGM solid residue which is treated further in a PGM refinery. The BMR leaching process generally consist of two separate steps used to remove the majority of nickel (i.e. first leaching stage) and copper (i.e. second and third leaching stage) from the solid phase through atmospheric and high pressure leaching, respectively.

The second and third stage leaching processes are operated in a non-optimal manner due to the inability to fundamentally understand and control extents of base metal and PGM leaching (Dorfling, 2012). Dorfling (2012) for this reason investigated the reaction mechanisms occurring in second and third stage leaching process, and subsequently developed an open-loop dynamic process model within MATLAB™ comprising the second and third stage pressure leaching system and surrounding process units of Western Platinum Ltd. BMR (a subsidiary of Lonmin PLC). This was done in an attempt to produce a tool which can be used to assist with autoclave (i.e. high pressure, high temperature reactor where leaching occurs) behaviour predictions. Matzopoulos (2011) lists several additional uses of dynamic process models:

1. Analysis and design of regulatory control schemes
2. Optimisation of operating procedures and conditions
3. Analysis of process safety
4. Reconciliation of plant data
5. Design of online soft-sensing
6. Training of operators

The dynamic process model developed by Dorfling (2012) is a powerful tool which can be used to investigate and possibly improve several aspects of the Western Platinum BMR operation.

Literature indicates that as many as 60 % of all mineral- and chemical process controllers have performance problems (Bialkowski, 1993; Desborough & Miller, 2002; Ender, 1993; Jelali, 2006). This significantly high figure is partially attributed to the occurrence of underlying faults which affect process controllability and ultimately reduces process effectiveness and profit. Faults are defined as events which could potentially lead to failure or malfunction of equipment and therefore cause significant process abnormality (Isermann, 2005). Expert knowledge from Western Platinum BMR also report of reduced process controllability during the occurrence of faults (McCulloch et al., 2014). The disadvantageous effects caused by fault occurrences could be limited if the occurrences could be detected at an early stage.

This project aims to improve and update the dynamic process model to mimic the Western Platinum BMR operation, and to ultimately use the model to analyse the process performance during the occurrence of faults. The updated dynamic process model will allow the possibility of developing and testing fault detection and diagnostic algorithms for Western Platinum BMR.

1.2. Project Objectives

The main outcome of this project was to predict what effects abnormal events have on the control performance of Western Platinum BMR using the developed dynamic model. Three preceding objectives had to be met in order to reach the final project outcome. Refer to the project objective flow diagram below.

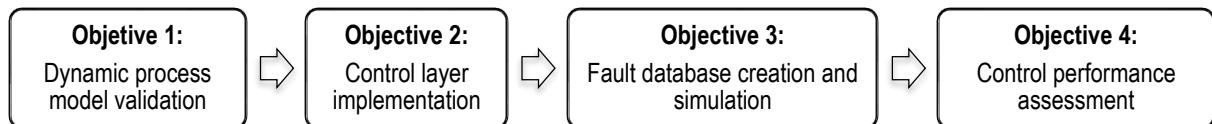


Figure 1.1: Flow diagram of project objectives

The first project objective was to validate the dynamic process model in a structured manner and implement necessary improvements which fall within the project scope. Control layers had to be implemented on the open-loop dynamic model in order to allow actuation and control of applicable variables. The implementation of control layers will ensure that the faults symptoms are dealt with in a similar way as that of the actual process. A database containing a collection of actual Western Platinum BMR faults and associated information had to be developed by using several information sources from a site visit. Faults from the database had to be modelled and subsequently used to mimic Western Platinum BMR fault scenarios. The fault scenarios had to be used to perturb the dynamic process model in order to assess the performance of the current control strategy.

1.3. Thesis Structure

Chapter 2 provides background on the generic processing steps used to produce valuable metals (i.e. PGMs and base metals) from Bushveld Complex ores. This chapter continues to provide an in-depth description of a specific processing step which is relevant in this project, namely the base metal leaching operation at Western Platinum BMR. The focus then moves

to the chemistry and control philosophy associated with this leaching process, specifically the second and third stage leaching steps at Western Platinum BMR.

Chapter 3 describes the methodology used by Dorfling (2012) to develop the second and third stage leach dynamic process model from batch experiments. Several assumptions and issues related to the development of the dynamic process model are highlighted and summarised in this chapter. This is done in an attempt to familiarise one with the model development and related issues prior to the first objective, namely model validation.

Chapter 4 investigates relevant literature which can be used to address the project objectives.

Chapter 5 reiterates the project objectives and uses relevant literature to divide the objectives into several tasks.

The first project objective namely model validation is addressed in Chapter 6. Several dynamic process model assumptions and aspects highlighted during the model description chapter are investigated and validated within this chapter. Several model improvements are made and a final conclusion on the validity of the dynamic process model is given.

Chapter 7 continues to second project objective namely control implementation. Several control layers are implemented onto the dynamic process model in accordance with what is seen at Western Platinum BMR.

Chapter 8 addresses the third project objective namely fault database creation and simulation. A list of faults seen at Western Platinum BMR in the form of a fault database is firstly provided. This chapter also discusses the methodologies used to subsequently model some of these faults and the resulting fault behaviour.

Chapter 9 addresses the final project objective in which the dynamic process model is used to predict the control and operational performance during the occurrence of several fault scenarios.

Chapter 10 summarises the project conclusions and provides several recommendations, while novel future work is listed in Chapter 11.

The appendices contain the project nomenclature (Appendix A), Western Platinum BMR controller data and dynamic process model input data (Appendix B), sample calculations (Appendix C), constitutive equations and rate expressions used in the dynamic process model (Appendix D), flow diagrams including Western Platinum BMR piping and instrumentation diagrams (Appendix E), and project results (Appendix F).

CHAPTER 2: PROCESS DESCRIPTION

This chapter aims to describe in detail the physical operation on which this project is based. It starts with an overview of the overall processing steps used to convert mine ore to separated PGMs and base metals, and continues with an in-depth description of the operation, chemistry and control philosophy of the BMR at Western Platinum Ltd.

At the end of this chapter the scope of the process within this project should be clear. The operation and control philosophy for this process should also be well understood. This will pave the way forward for Chapter 3, where a dynamic model for this process will be discussed.

2.1. Background

A number of different processing steps are required to produce concentrated PGMs from the initial ore. These processes generally consist of steps seen in Figure 2.1.

Ore containing PGMs with concentrations ranging from 3-10 g/tonne within the Bushveld complex (Vermaak, 1995; Bernardis et al., 2005; Cramer, 2001) enters a comminution stage where the particle size is reduced in order to liberate valuable minerals from gangue (refer to Figure 2.1). Typical methods of comminution include crushing, ball-, rod- and autogenous milling (Cramer, 2001; Liddell et al., 1986). Recent studies indicate that stirred milling have become increasingly applied within the PGM extraction industry (Rule, 2011).

The particles are classified below approximately 60 % passing 74-300 micrometers by typically using a hydrocyclone. The acceptable sized particles thereafter report to a flotation circuit (Mainza et al., 2005; Cramer, 2001). Particles larger than the allowable size are recycled for further comminution. Flotation circuits are used to separate gangue from valuable minerals, in this case base metal sulphides encapsulating PGMs in several mineral forms. This is done by selectively manipulating the hydrophobicity of minerals by adding collectors, frothers, activators, depressants and adjusting the pH of the slurry. Air bubbles are typically added from the bottom of the flotation cell where highly hydrophobic minerals, usually the valuable minerals, attach to the bubbles which can then be collected at the top.

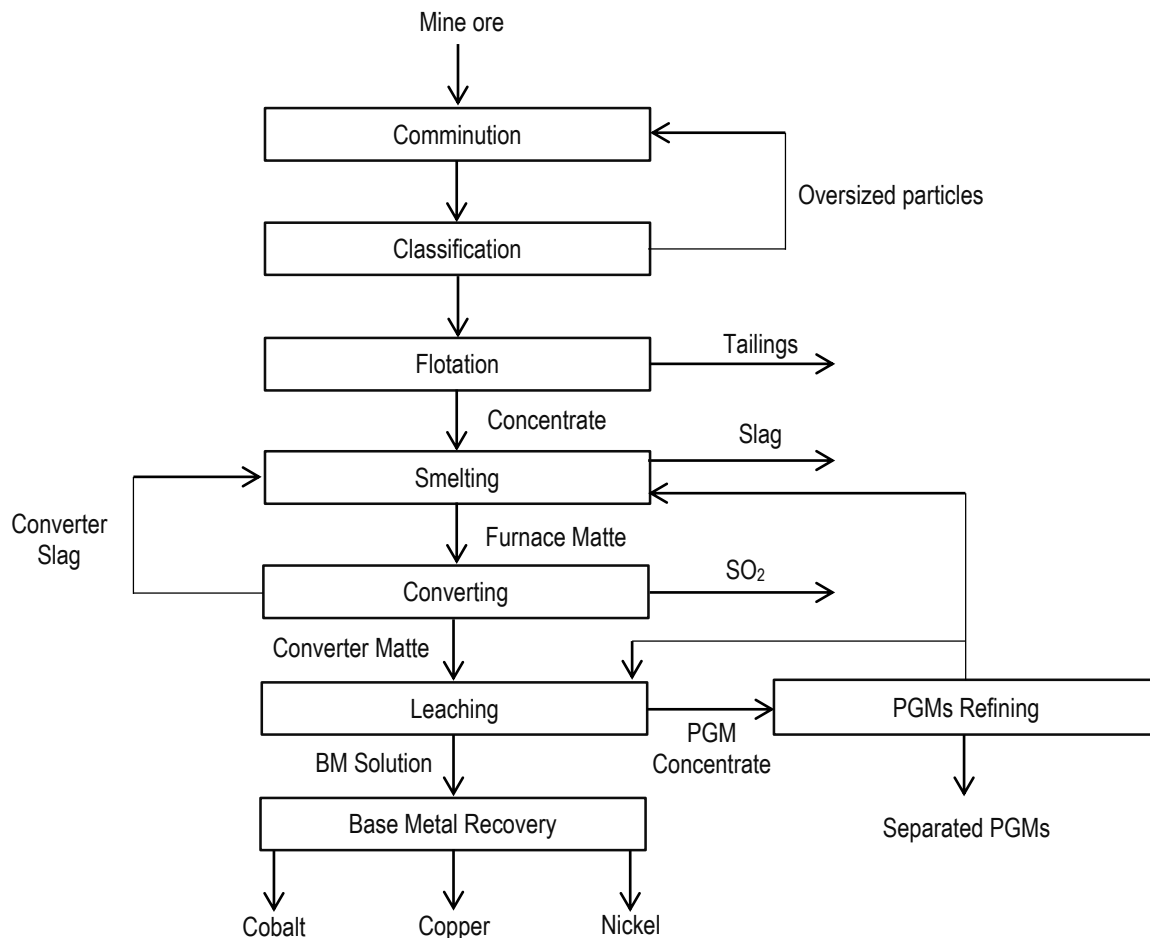


Figure 2.1: Typical PGM processing steps (Redrawn from Lamya (2007) and Liddell et al. (1986))

Gravity separation was also used in the past as a primary PGM recovery technique which bypassed the smelting and converting stages (Mainza et al., 2005).

The concentrate, containing low levels of recovered base metal sulphides encapsulating PGMs together with oxides such as silica (SiO_2), magnesia (MgO), iron(II) oxide (FeO) and lower amounts of quicklime (CaO), alumina (Al_2O_3) and chromium(III) oxide (Cr_2O_3), report to a smelting stage. Blast furnaces and, more recently, electric submerged arc furnaces are two smelting methods used in the industry (Cramer, 2001). The smelting stage is used to melt and react the concentrate in order to separate an immiscible lower density liquid slag containing predominantly gangue from a valuable matte phase containing most of the base metals and PGMs.

The PGMs and base metal concentrate is further upgraded in the converter stage typically using Peirce Smith converters. Silica, converter reverts and oxygen is added in order to remove sulphur and iron through oxidation of the matte phase. A metal-rich matte containing base metal and PGM alloy phases, often referred to as converter matte, is produced

(Lamya, 2007). Refer to Lindsay (1988) for more information on the smelting and converting process of silicates, sulphides and PGMs.

The converter matte reports to the leaching stage for further processing. The leaching section forms part of the project scope and will be discussed separately in the subsequent section.

2.2. Leaching Process Overview

2.2.1. 1st atmospheric leaching stage

Methods of separation at this stage start to differ quite significantly amongst the various PGM producers (Lamya, 2007). Leaching methods applied by Western Platinum BMR which is applicable to this project will be considered from now on. Refer to Lamya (2007) for more information on the different leaching methods applied by different operations within South Africa.

The term leaching refers to the dissolution of a component into an ion state by means of reaction. The first stage leaching process is primarily used to leach nickel sulphides and impurities from the PGM containing converter matte in order to produce two valuable product streams: solid residue containing PGMs and predominantly copper sulphide solids, and pregnant nickel leach solutions with trace amounts of dissolved PGMs.

The converter matte is firstly sent to a ball mill with a hydrocyclone classification step prior to entering the first leaching stage (refer to Figure 2.2). The particle size is reduced to approximately 9-12 % > 75 micrometers (Dorfling, 2012).

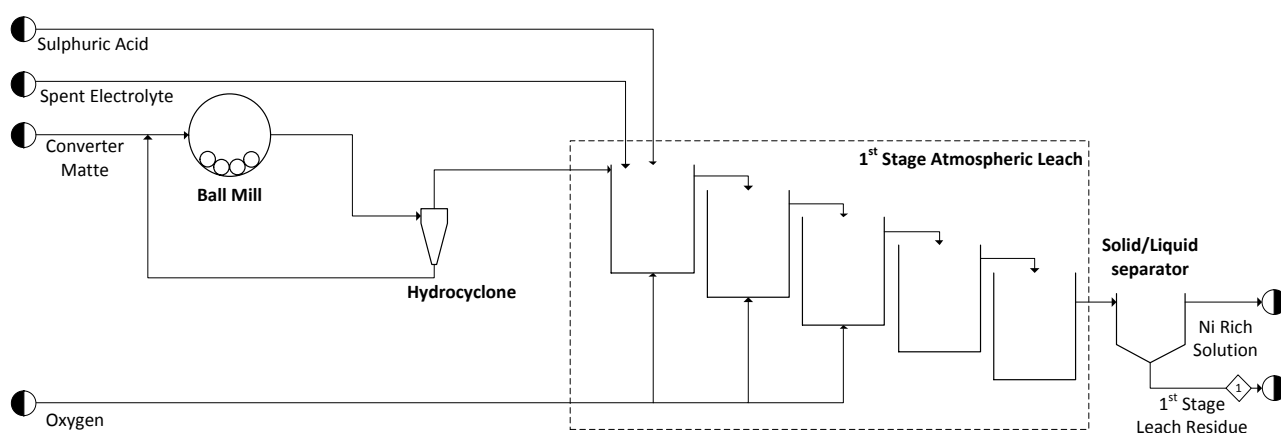


Figure 2.2: PFD of 1st leaching stage: Western Platinum BMR (Redrawn from Dorfling (2012))

The adequately sized matte particles report to the first of a series of five leaching tanks. Both spent electrolyte (refer to Table 2.1 for compositional data), obtained from a downstream electrowinning section, and fresh sulphuric acid act as a leaching solution and is fed into the first tank. All leaching tanks are agitated. The first three tanks are aerated in order to selectively benefit acid leaching reactions. The latter three non-oxidative tanks provide residence time used to remove copper from solution via cementation reactions (van Schalkwyk, 2011). The first leaching stage operates at 85 °C to 95 °C and under atmospheric conditions. Approximately 50 % to 70 % of the initial nickel mass in the matte residue is leached in this stage while cupric and PGM ions in solution are precipitated (Dorfling, 2012; Lamy, 2007). The slurry then enters a solid-liquid separator where a nickel rich solution is removed and sent to nickel sulphate crystallisers. The first stage leach residue is processed further in the second and third pressure leaching stages.

2.2.2. 2nd and 3rd pressure leaching stage

This project is based on a process scope that includes the second and third pressure leaching stages or, more specifically, the process scope considered by Dorfling (2012). Numerous references will be made to work conducted by Dorfling (2012) in an attempt to familiarise one with methodologies and assumptions used by Dorfling (2012) to produce a dynamic process model. The dynamic process model forms the basis for this project; and the first project objective is to validate it.

The main purpose of the second and third pressure leaching stage is to leach the remaining solid base metal sulphides while simultaneously precipitating PGM ions from solution. Two valuable products are therefore produced: a solid residue consisting predominantly of PGMs and a pregnant copper leach solution.

First stage leach residue, spent electrolyte and formic acid leach filtrate (recycled from a downstream process) enters a second stage slurry preparation tank in order to prepare the correct slurry mix for the leaching process (refer to Figure 2.3). Typical compositions for these streams are given in Table 2.1. The first stage leach residue consist mostly of copper sulphide and nickel sulphide in the form of digenite ($\text{Cu}_{1.8}\text{S}$) and millerite (NiS), respectively.

The spent electrolyte contains base metal ions and traces of PGM ions. This stream also contains sulphuric acid, which is re-used as an acid source within the second and third stage leaching process. The formic filtrate composition is not listed in Table 2.1 since it reportedly consists mostly of water (Dorfling, 2012). Refer to Table B.1 in Appendix B for a mineralogical composition of the first stage leach residue.

Table 2.1: Composition of material from Western Platinum BMR (Dorfling, 2012; McCulloch et al., 2014)

Species	First stage leach residue (wt%)	Second stage leach residue (wt%)	Third stage leach residue (wt%)	Spent electrolyte (mg/l)
Ni	13	5.7	2.5	22800
Cu	50	19.4	4.9	25300
S	26	16.3	7	-
Co	0.13	0.09	0.08	261
Fe	0.42	3.3	7.2	856
Ir	0.03	0.93	1.4	33.6
Rh	0.088	2.5	3.4	56.1
Ru	0.2	4.4	5.4	193
Pd	0.18	6.4	10.6	5.3
Pt	0.39	14.1	21.8	8
SO ₄ ²⁻	-		-	113700

Note that Western Platinum BMR operates two separate flash recycle tanks and autoclaves in parallel which is not indicated in Figure 2.3. This project will only focus on a single set of process units.

The mixed slurry reports to a flash recycle tank. Concentrated sulphuric acid and water are occasionally added to the flash recycle tank if the correct slurry mix was not obtained in the upstream preparation tank. The mixed slurry continues into the first compartment of the second leaching stage via stream 7. Note that the first three compartments and the fourth compartment of the autoclave make up the second and third leaching stages, respectively. The fourth compartment is connected to the other compartments only by a vapour space which prevents any slurry transfer. The main benefit for dividing the autoclave into two leaching stages is to allow for more precise solid composition control within the third stage by mixing the solid residue with a new liquid stream (Steenekamp et al., 2009).

Stream 9 is used to recycle a fraction of the slurry in the first compartment. The recycling of slurry from a high pressure tank to an atmospheric tank causes liquid to flash, which aids in temperature control in the first compartment.

Stream 8 act as a gas bleed which prevents a build-up of inert gasses. The inert gasses together with flashed water vapour exits the flash recycle tank via stream 6.

Oxygen is added to the second, third and fourth compartment via stream 10, 11 and 12, respectively. Cooling water serve as heat sinks within the second and third compartment, while steam addition via stream 13 serve as a heating source for the fourth compartment.

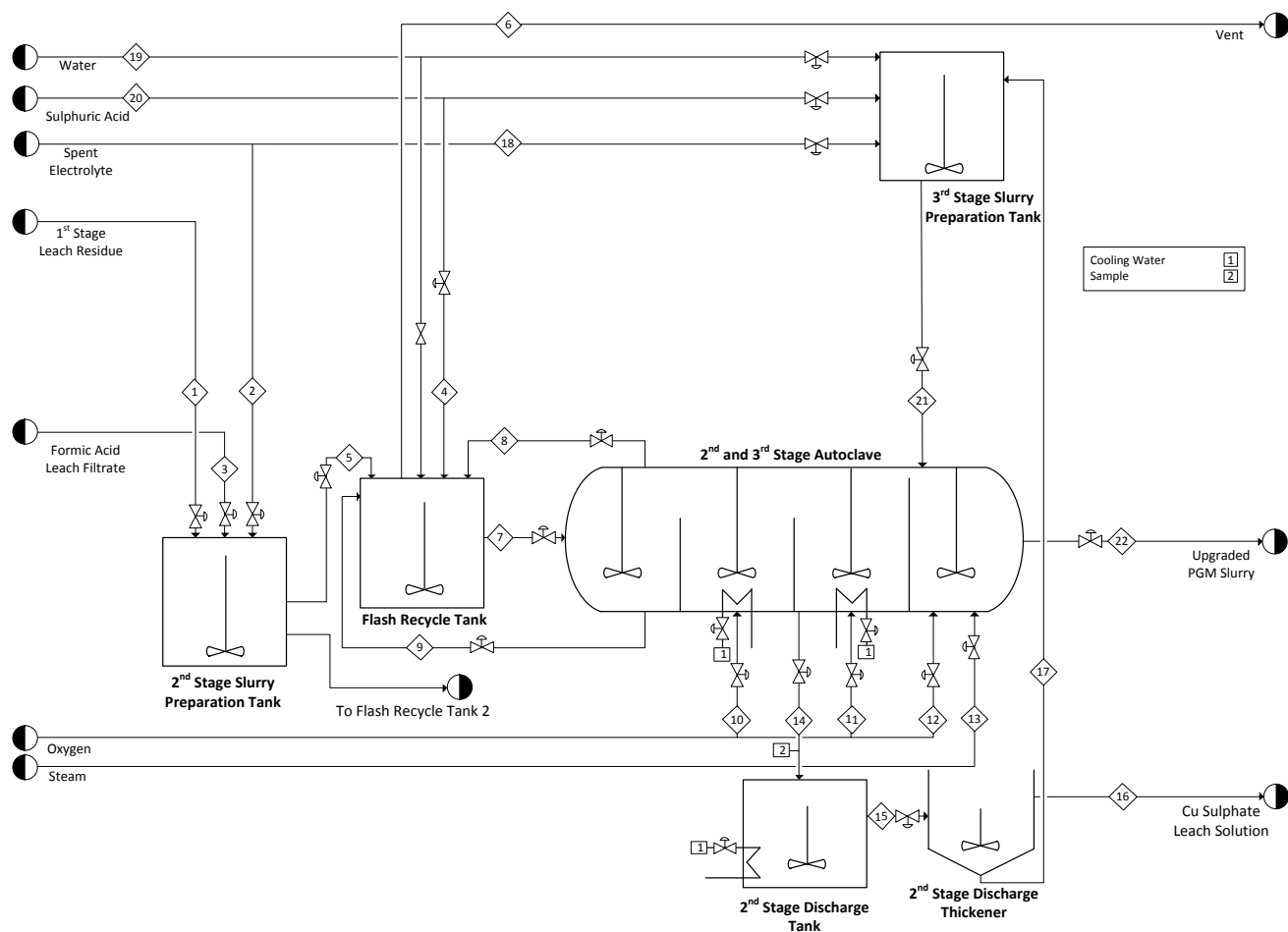


Figure 2.3: PFD of 2nd and 3rd leaching stages: Western Platinum BMR

The copper in the solid residue is ideally reduced to less than 18 wt% when exiting the second leaching stage (refer to Table 2.1).

The second stage discharge thickener increases the solid content of the PGM concentrate by removing copper sulphate leach solution. The leach solution is treated in selenium (Se)/tellurium (Te) reactors prior to copper electrowinning. The solid residue leaving the discharge thickener via stream 17 is mixed with fresh water, sulphuric acid and spent electrolyte which is then pumped into the third and final leaching stage. The upgraded PGM solid residue exiting the fourth compartment ideally contains less than 3 wt% copper with PGMs upgraded to compositions above 40 wt% (predominantly platinum – refer to Table 2.1). This PGM slurry is sent for further processing in order to recover individual PGMs.

Note that only the leaching process section corresponding to that in Figure 2.3 will be considered further in this project.

Reported operating conditions within the second and third leaching stage are shown in Table 2.2.

Table 2.2: Operating conditions: Western Platinum BMR (van der Merwe & Mrubata, 2014)

Compartment 1		Value
Temperature (°C)		130
Acid concentration (g/l)		18 - 25
Redox potential (mV)		350 - 380
Compartment 2		
Temperature (°C)		130
Acid concentration (g/l)		15 - 20
Compartment 3		
Temperature (°C)		125
Level (%)		70
Redox potential (mV)		450 - 480
Compartment 4		
Temperature (°C)		140
Acid concentration (g/l)		35 - 45
Level (%)		80
Redox potential (mV)		520 - 550

Dorfling (2012) reports autoclave pressures around 600-700 kPa, while a pressure of 550 kPa was noted during a recent site visit (McCulloch et al., 2014). In addition, temperatures ranging between 125-140 °C were noted inside the second leaching stage during the site visit, while Dorfling (2012) reports temperatures between 115-145 °C. Typical input stream compositions can be found in Table B.1.

2.3. Leaching Process Chemistry

Only the reactions assumed by Dorfling (2012) to describe the second and third stage leaching process will be mentioned in this section. Reactions will be written in net ionic form. Note that spectator ions are present within the electrolyte but will not feature in reactions.

2.3.1. Base metals

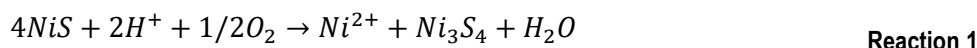
Lamya, Lorenzen (2006) and Knuutila et al. (1997) studied the atmospheric leaching mechanism of a nickel-copper matte in an acidic-copper leach solution. The main minerals found in the matte in both cases were predominantly heazlewoodite (Ni_3S_2), chalcocite (Cu_2S), djurleite ($\text{Cu}_{1.96}\text{S}$) and nickel-copper alloys. The main mineral phases found within the inlet to the second leaching stage are similar to that of the atmospheric leaching stage. However, nickel-sulphide minerals are present in lower nickel to sulphide ratios.

Rademan (1995) studied the leaching mechanisms of a nickel-copper matte in a high pressure and acidic environment. Rademan (1995) divided the leaching mechanism into roughly three periods:

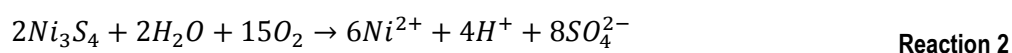
- Period I – Copper cementation via nickel leaching from alloy and heazlewoodite phases
- Period II – Selective nickel leaching to form a reduced Ni/S-ratio Ni-S mineral phase, while simultaneously leaching and cementing of copper into different Cu-S mineral phases.
- Period III – Simultaneous leaching of copper and nickel.

The mineralogical composition of the first stage leach residue of Western Platinum BMR corresponds well with that of the third period of Rademan (1995). Reactions occurring in the first two periods were therefore excluded in the dynamic process model developed by Dorfling (2012). Reduction in copper ion concentrations within experimentation conducted by Dorfling (2012) was attributed to variations in feed material and not to copper cementation.

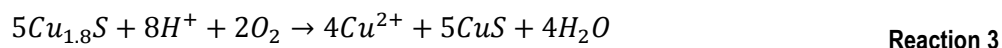
Millerite (NiS) is leached during period II and III to produce polydymite (Ni₃S₄) through Reaction 1:



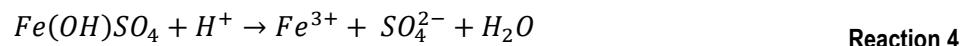
Nickel in the form of polydymite is leached by means of Reaction 2 as soon as all of the heazlewoodite has been removed:



The leaching of copper proceeds via Reaction 3 during Period III after the majority of chalcocite and djurleite has been transformed to digenite (Cu_{1.8}S) and covellite (CuS):



The previously mentioned copper-sulphide and nickel-sulphide oxidation reactions occur to almost a complete extent in the second leaching stage. Steenekamp and Dunn (1999) categorised reactions occurring in the third leaching stage into two groups. The first group comprises the leaching of hydrolysis products from the first leaching stage via Reaction 4:

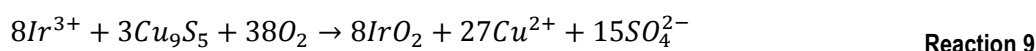
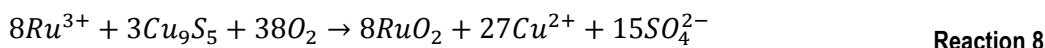
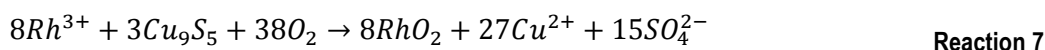


The second group comprises oxidation of nickel- and copper sulphide minerals via Reaction 5 and Reaction 6, respectively.

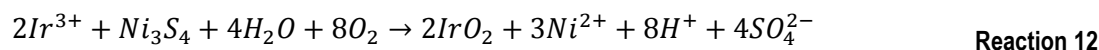
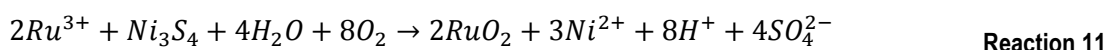
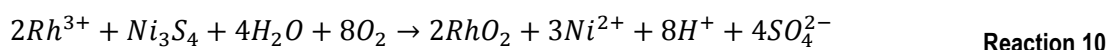


2.3.2. Platinum group metals

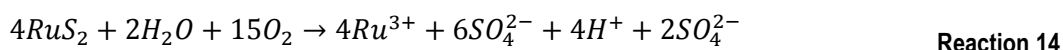
Dorfling (2012) researched the behaviour and properties of PGMs within an acidic solution and oxidative environment. It was concluded that Other Precious Metals (OPMs) comprising Rh, Ru and Ir, are the PGMs which undergo the largest extent of dissolution during the leaching process. Dorfling (2012) further determined that OPM cementation reactions will produce OPM-oxide mineral products as indicated in Reaction 7 to Reaction 12.



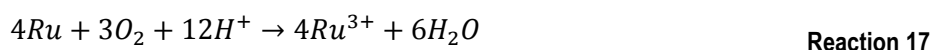
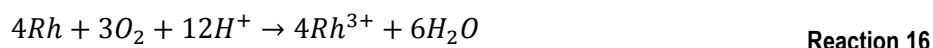
Reaction 7, Reaction 8 and Reaction 9 represents the OPM cementation reactions for rhodium, ruthenium and iridium, respectively. Similar cementation reactions occur with nickel being the mineral that is leached:



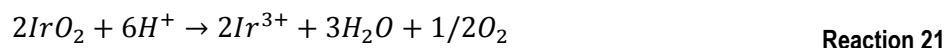
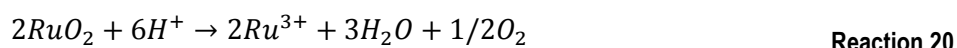
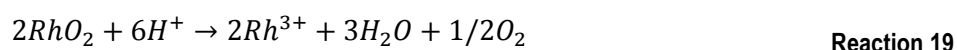
OPM-sulphide minerals are oxidised according to Reaction 13 to Reaction 15 to produce PGM ions in solution:



OPM-alloys are leached according to Reaction 16 to Reaction 18:



OPM-oxides, products of Reaction 10 to Reaction 12, are once again leached according to Reaction 19 to Reaction 21:



2.4. Leaching Process Control Philosophy

2.4.1. Control objectives

Marlin (1995) lists a number of important control objectives in hierarchical form, which is applicable to all industrial processes:

1. Safety

2. Environmental protection
3. Equipment protection
4. Smooth plant operation and production rate
5. Product quality
6. Optimisation of profit
7. Monitoring and diagnosis

The control objectives listed above are self-explanatory. Strategies used to satisfy the control objectives at Western Platinum BMR will be discussed throughout the subsequent control layer sections.

2.4.2. Regulatory control

Regulatory control loops currently implemented at Western Platinum BMR is given in Table 2.3. Refer to the Piping and Instrumentation Diagram (P&ID) in Figure E.1 to correlate process unit tags to their generally used names, and to identify controller tags. Refer to Table B.2 for controller set-point values. Note that the BMR is not always operated using the control loops shown in Table 2.3. Operators often operate control loops in a manual configuration whereby controller set-points are changes manually (McCulloch et al., 2014).

Regulatory control at Western Platinum BMR ensures both smooth plant operation and production rate. Smooth production rates are obtained by constant fourth autoclave compartment (FIC-0150-5) and flash recycle tank (FIC-0201) feed flow rates. Other regulatory controllers attempt to obtain smooth plant operation by keeping controlled variables at their corresponding set-points. The previous statement is less applicable to level controllers which often mitigate flow rate surges by allowing slight level changes.

Flow control

Seventeen flow control loops are present on the BMR. Eleven of these flow controllers are secondary inner loops to a cascade; with level, density or temperature controllers being the primary outer loop. A site visit (McCulloch et al., 2014) indicated that all flow controllers have proportional-integral (PI) control algorithms except for FIC-3001C, which is proportional-integral-derivative (PID). The reason for using a PID algorithm on a fast acting flow control loop is uncertain.

Level control

A site visit indicated all applicable process units have cascade level controllers as primary loop which governs a flow controller in a secondary loop. Either PI or PID control algorithms are used within these loops.

Table 2.3: Regulatory control loops: Western Platinum BMR (van der Merwe, 2014)

Controller tag	CV	MV	Control algorithm
Flow control			
FIC-0106	Flow (Stream 1)	Valve (Stream 1)	PI
FIC-0101	Flow (Stream 2)	Valve (Stream 2)	PI
FIC-1102 ¹	Flow (Stream 3)	Valve (Stream 3)	PI
FIC-0202	Flow (Stream 4)	Valve (Stream 4)	PI
FIC-0201	Flow (Stream 5)	Valve (Stream 5)	PI
FIC-0203	Flow (Stream 7)	Valve (Stream 7)	PI
FIC-0205	Flow (Stream 9)	Valve (Stream 9)	PI
FIC-3001A	Flow (Stream 10)	Valve (Stream 10)	PI
FIC-3001B	Flow (Stream 11)	Valve (Stream 11)	PI
FIC-3001C	Flow (Stream 12)	Valve (Stream 12)	PID
FIC-3002	Flow (Stream 14)	Valve (Stream 14)	PI
FIC-0401	Flow (Stream 15)	Valve (Stream 15)	PI
FIC-0150-3	Flow (Stream 21)	Valve (Stream 21)	PI
FIC-0150-4	Flow (Stream 20)	Valve (Stream 20)	PI
FIC-0150-5	Flow (Stream 18)	Valve (Stream 18)	PI
FIC-0150-9	Flow (Stream 19)	Valve (Stream 19)	PI
FIC-3003	Flow (Stream 22)	Valve (Stream 22)	PI
Level control			
LIC-0101	Level (TK-10)	Flow (FIC-0106)	Cascade PI
LIC-0201	Level (TK-20)	Flow (FIC-0203)	Cascade PI
LIC-0401	Level (TK-40)	Flow (FIC-0401)	Cascade PID
LIC-151	Level (TK-150)	Flow (FIC-0150-9)	Cascade PID
LIC-3002	Level (compartment 3)	Flow (FIC-3002)	Cascade PI
LIC-3003	Level (compartment 4)	Flow (FIC-3003)	Cascade PI
Density control			
-	Density (Stream 5)	Flow (FIC-0101)	Feedforward
Temperature control			
TIC-3001	Temperature (compartment 1)	Flow (FIC-0205)	Cascade PI
TIC-3003	Temperature (compartment 2)	Valve (CW in AC2)	PID
TIC-3004	Temperature (compartment 3)	Valve (CW in AC3)	PI
TIC-0401	Temperature (TK-40)	Valve (CW in TK-40)	PI
TIC-3005	Temperature (compartment 4)	Valve (Stream 13)	PI
Pressure control			
PIC-3001	Pressure (Autoclave)	Flow (Stream 10+11+12)	Cascade PI
Other control			
-	Flow ratio	Flow (Stream 2, 3)	Feedforward
-	Flow ratio	Flow (Stream 18, 20)	Feedforward
-	Flow ratio	Flow (Stream 10, 11, 12)	Feedforward

Each flow controller is situated on the outlet of their respective tank except for the first stage leach residue flow controller (FIC-0106) on the second stage slurry preparation tank (TK-10) and the water flow controller on the second stage slurry preparation tank (TK-150), which is located on an inlet stream. All levels are controlled between 45 % and 80 %.

¹ FIC-1102 makes use of gain-scheduling, refer to Supervisory control.

Density control

Density control prior to the inlet of the autoclave is important since large density changes would result in varying base metal sulphide solid concentrations, which affects the amount of heat released within the autoclave and also the product quality. Excessive amounts of heat released could result in the inability to control temperatures within respective autoclave compartments due to manipulated variable (MV) saturation.

The density of the stream exiting the second stage slurry preparation tank (stream 5) is controlled between 1.22 kg/l and 1.25 kg/l by using a feedforward algorithm. The algorithm uses the flow rate of stream 1 (FIC-0106) with corresponding density measurements in a mass balance. The mass balance provides set-points to the spent electrolyte (FIC-0101) and formic filtrate (FIC-1102) flow controllers in order to reach a certain user defined solid percentage. The feedforward algorithm is given in Equation 2.1.

$$\dot{V}_{0101_{SP}} = \frac{\dot{V}_{0106} \left(\frac{\frac{1}{\rho_{0106}} - \frac{1}{\rho_{0106,L}}}{\frac{1}{\rho_{0106,S}} - \frac{1}{\rho_{0106,L}}} \right) \times 100 - \text{solid}\% \dot{V}_{0106} \rho_{0106}}{\text{solid}\% \left(\rho_{0101} + \left(\frac{100}{\text{spent}\%} - 1 \right) \rho_{1102} \right)} \quad \text{Equation 2.1}$$

The densities seen in Equation 2.1 are measured hourly. A typical solid percentage set-point of 4.5 is used at Western Platinum BMR. The spent percentage is a user-defined ratio which relates set-points of FIC-0101 and FIC-1102 (refer to Other control section). Refer to Appendix C for the derivation of Equation 2.1.

Temperature control

The copper-sulphide and nickel-sulphide leaching reactions mentioned in Section 2.3.1 each are highly exothermic. These reactions occur in bulk (up to 95 wt% conversion) within the second stage leach, which necessitates some form of cooling to keep temperatures at an acceptable level (Steenekamp et al., 2009). Temperatures in the second and third compartment are controlled between 125 °C and 130 °C by directly adjusting a valve which manipulates cooling water flow. No cascade control therefore exists (i.e. flow rates are not measured). Knoblauch (2012) reports similar findings. The temperature inside the first compartment is controlled at 130 °C using a difference approach. The temperature control mechanism for this compartment is depicted in Figure 2.4.

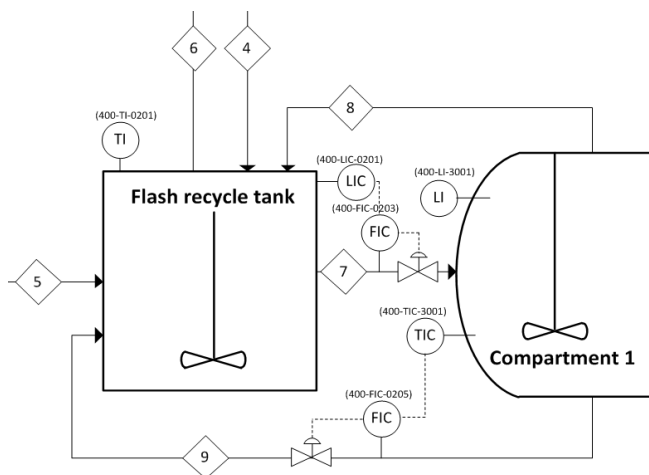


Figure 2.4: Autoclave compartment 1 and flash recycle tank P&ID

Slurry from the first compartment is recycled to a flash recycle tank via stream 9. The flash recycle tank operates at atmospheric pressure while the autoclave is operated under high pressure. The pressure decrease in stream 9 results in the vaporisation of water, which leaves via a vent (stream 6). The water vaporisation cools this slurry stream to its boiling point at atmospheric pressure. The cooled slurry serves as a heat sink when it returns to the first compartment via stream 7. The temperature controller in the first compartment (TIC-3001) is therefore cascaded with the flash recycle flow controller (FIC-0205). The temperature controller and flash recycle flow controller has no causal relationship unless proper level control is applied to the flash recycle tank. The level controller on the flash recycle tank (LIC-0201) ensures that changes in the level, possibly caused by first compartment temperature controller actions via FIC-0205, are mitigated by varying the flow rate of stream 7. The first compartment temperature control method is interesting and complicated. This method of temperature control is dependent on its interaction with the flash recycle tank level controller.

The temperature in the first compartment is occasionally controlled using model predictive control (MPC). Operators have the option of running the first compartment temperature controller in a cascade or MPC setup. They switch to cascade control as a fall-back when MPC is not performing well. Only the cascade control will be considered within this project due to a lack of information regarding the MPC algorithm.

The fourth and final compartment requires heating since operating temperatures around 140 °C cannot be maintained by the remaining base metals in the solid phase. The addition of energy inside the fourth and final compartment is accomplished by directly injecting steam into the slurry. The temperature is controlled using a PI control algorithm which directly controls the steam valve.

Pressure control

Dissolved oxygen availability is a major factor influencing the dissolution of base metals and PGMs (Dorfling, 2012). The partial pressure of oxygen within the autoclave strongly affects the oxygen solubility. The total pressure in the autoclave is controlled at 5.5 bar by using a cascade pressure controller which manipulates the total oxygen flow rate into the autoclave in an attempt to ensure an adequate oxygen partial pressure.

Other control

The formic filtrate flow controller (FIC-1102) set-point is determined by a calculation which involves a user-defined ratio and the spent electrolyte flow controller (FIC-0101) set-point. The relation is shown in Equation 2.2 (McCulloch et al., 2014).

$$\frac{\dot{V}_{1102_{SP}}}{\dot{V}_{0101_{SP}}} = \left(\frac{100}{\text{spent}\%} - 1 \right) \quad \text{Equation 2.2}$$

The spent percentage set-point is generally kept at 35 %. Ratio control is applied in a similar manner to streams entering the third stage slurry preparation tank. The set-point of a different spent electrolyte flow controller (FIC-0150-5) is determined by multiplying the set-point of a sulphuric acid flow control loop (FIC-0150-4) with a spent/sulphuric acid ratio defined by an operator.

The total oxygen flow rate set-point (the autoclave pressure controller output) is multiplied by an operator defined ratio and act as set-point inputs to the second, third and fourth compartment oxygen flow controllers FIC-3001A, FIC-3001B and FIC-3001C, respectively. These ratios are generally identical. Oxygen is not sparged into the first compartment. The impellers within the first compartment are designed to mix available oxygen from the vapour space into the liquid phase.

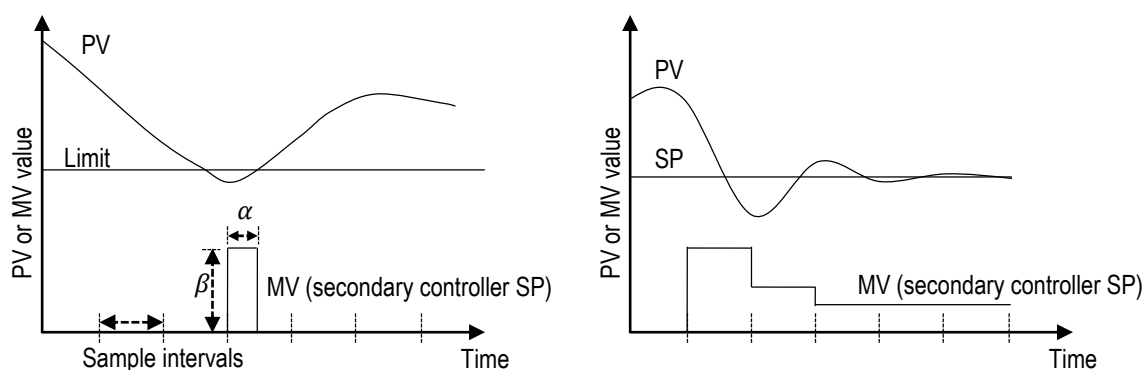
2.4.3. Supervisory control

Several supervisory control strategies used at Western Platinum BMR are captured in Table 2.4.

Table 2.4: Supervisory control: Western Platinum BMR (McCulloch et al., 2014)

CV	MV	Control method
Manual		
Acid concentration (Stream 7)	Flow SP (FIC-0202)	On/off operator control
Acid concentration (Stream 7)	Spent% SP	Continuous operator control
Density (Stream 7)	Flow SP (FIC-0201)	Continuous operator control
Total metal concentration in solution (Stream 14)	Solid% SP	Continuous operator control
Acid concentration (Stream 21)	Flow SP (FIC-0150-4)	Continuous operator control
Total metal concentration in solution (Stream 21)	Flow SP (FIC-0150-9)	On/off operator control
Residence time (Compartment 4)	Flow SP (FIC-0150-5)	Continuous operator control
Base metal concentration in residue (Stream 14) Base metal concentration in residue (Stream 22) PGMs in solution (Stream 14) PGMs in solution (Stream 22) Redox potential (Stream 14) Redox potential (Stream 22)	Temperature SP (Compartment 1) Temperature SP (Compartment 2) Temperature SP (Compartment 3) Temperature SP (Compartment 4) Pressure (Autoclave) Acid concentration (Stream 7) Residence time (Compartment 4)	Continuous operator control
Automated		
Flow (FIC-1102)	Valve (Stream 3)	Gain-scheduling

A manual form of supervisory control frequently used at Western Platinum BMR is the adjustment of control loop set-points by operators. These control strategies will be referred to as operator controllers from now on. These control strategies form a critical part of the leaching process since they control for variables which are manually measured. An operator controller can be viewed as a cascade with the operator being the primary loop. Two secondary loop set-point adjustment practices were noticed during a recent site visit (McCulloch et al., 2014), and is defined here as an on/off and continuous operator controller. The operation of these two practices is captured in Figure 2.5.

**Figure 2.5: On/off (left) and continuous (right) operator controllers**

The on/off operator controller ensures that a manually measured variable (i.e. PV) stays above or below a limit. This is done by introducing steps to a manipulated variable (MV) with a certain size (β) which are kept for a specific holding time (α), before the secondary controller set-point is once again dropped to zero. The acid concentration exiting the flash

recycle tank (stream 7) and the total metals in solution in the stream exiting the third stage slurry preparation tank (stream 21) at Western Platinum BMR are kept above 20 g/l and below 100 g/l, respectively, using this control approach (McCulloch et al., 2014; Steenekamp et al., 2009).

The continuous operator controller simply varies a manipulated variable to ensure that a manually measured variable meets a set-point. Several continuous operator adjustments are made to control for numerous manually measured variables at Western Platinum BMR (McCulloch et al., 2014; Steenekamp et al., 2009). The density exiting the flash recycle tank is controlled at 1.28 kg/l by adjusting the inlet flow rate to this vessel. Varying the spent percentage serves as another way to control the acid concentration in stream 7. The acid concentration entering the fourth compartment is controlled between 35 g/l and 45 g/l by manipulating a concentrated sulphuric acid flow rate set-point (FIC-0150-4). The residence time in the fourth autoclave compartment is controlled by adjusting its inlet flow rate set-point (FIC-0150-5). The residence time affects the extent to which compounds leach, which serves as a way to control product compositions. A variety of methods exists in which operators at Western Platinum BMR control the base metals in the residue and PGMs in solution. This includes varying autoclave temperatures and pressures (refer to Table 2.4). The redox potential serves as a rapid way of estimating the product compositions in order to make necessary adjustments to manipulated variables in a timely manner. The redox potentials are typically controlled between 350 mV to 550 mV within the autoclave compartments. The acid concentration set-point, which is already a supervisory control, is in certain cases also adjusted to ensure on specification product compositions (van der Merwe & Mrubata, 2014; Steenekamp et al., 2009).

A non-linear control algorithm namely gain-scheduling is one form of automatic supervisory control used at Western Platinum BMR. Gain-scheduling adjusts controller parameters based on real-time measurements in order to compensate for process nonlinearities (Marlin, 1995). The formic filtrate flow controller (FIC-1102) at Western Platinum BMR makes use of gain-scheduling.

2.4.4. Alarm systems

Alarm systems used at Western Platinum BMR are captured in Table 2.5.

Table 2.5: Alarm systems: Western Platinum BMR (McCulloch et al., 2014)

Tags	Units	HH	H	L	LL
FIC-0106	m ³ /h	100	85	30	0
FIC-1102	m ³ /h	5	5	0	0
LIC-0101	%	100	85	30	0
TI-0101	°C	100	95	0	0
FIC-0101	m ³ /h	200	95	3	1
FIC-0201	m ³ /h	100	95	0	0
FIC-0202	l/min	100	95	0	0
TI-0201	°C	100	95	5	0
FIC-0203	m ³ /h	100	95	3	1
LIC-0201	%	100	95	0	0
LI-3001	%	105	95	5	0
TI-3002	°C	100	95	5	0
FIC-0205	m ³ /h	100	95	0	0
TIC-3001	°C	150	147	0	0
TIC-3003	°C	150	140	130	0
TIC-3004	°C	150	135	125	0
TIC-3005	°C	150	145	90	0
FIC-3001A	Nm ³ /h	200	95	3	1
FIC-3001B	Nm ³ /h	200	95	3	1
FIC-3001C	Nm ³ /h	200	95	3	1
LIC-3003	%	100	95	0	0
LIC-3002	%	100	90	50	0
FIC-3002	m ³ /h	100	95	0	0
TIC-0401	°C	100	90	70	0
LIC-0401	%	100	70	50	0
FIC-0401	m ³ /h	100	95	0	0
FIC-0150-09	m ³ /h	18	15	5	0
LIC-151	%	100	95	0	0
FIC0150-4	l/h	1.5	1	3	1
FIC-0150-5	m ³ /h	18	15	5	0
FIC-0150-3	m ³ /h	100	95	0	0
FIC-3003	m ³ /h	100	95	0	0
PIC-3001	kPa	1000	780	520	0

The majority of alarms captured in Table 2.5 seem to have default values. Most alarms have values of 100, 95, 0 and 0 for high-high, high, low and low-low, respectively. This is evident irrespective of the type of controller. The sulphuric acid flow rate (FIC-0150-4) has a low alarm which is larger than its high alarm. This alarm configuration is unrealisable.

Most of the alarms captured in Table 2.5 are expected to be disabled as they fail at their intended purpose of notifying operators of abnormal behaviour. Reasonable alarm values do however exist on variables which significantly contribute to the safety of the personnel; integrity of equipment; and quality of product. These variables include the autoclave temperature (TIC-3001, TIC-3003, TIC-3004 and TIC-3005) and pressure (PIC-3001).

2.4.5. Safety interlock systems

Safety interlocks implemented at Western Platinum BMR is given in Table 2.6.

Table 2.6: Safety interlocks systems: Western Platinum BMR (Steenekamp et al., 2009)

Valve tag	Open-interlock	Close-interlock
FCV-0106	-	TK-10 level (HH)
FCV-0101	-	TK-10 level (HH)
FCV-1102	-	TK-10 level (HH)
FCV-0202	-	TK-20 level (HH)
FCV-0201	-	TK-10 level (LL); TK-20 (HH)
FCV-0203	-	TK-20 level (L); Compartment 3 level (HH)
FCV-0205	Compartment 1 temperature (H)	Compartment 1 level (LL)
FCV-3001A	-	Autoclave pressure (HH); Compartment 1,2,3,4 temperature (HH)
FCV-3001B	-	Autoclave pressure (HH); Compartment 1,2,3,4 temperature (HH)
FCV-3001C	-	Autoclave pressure (HH); Compartment 1,2,3,4 temperature (HH)
FCV-3002	-	Compartment 3 level (LL); TK-40 level (HH)
FCV-0401	-	TK-40 level (L)
FCV-0150-3	-	TK-150 level (L); Compartment 4 level (HH)
FCV-0150-4	-	TK-150 level (HH)
FCV-0150-5	-	TK-150 level (HH)
FCV-0150-9	-	TK-150 level (HH)
FCV-3003	-	Compartment 4 level (L)
TCV-3003	Compartment 2 temperature (H)	-
TCV-3004	Compartment 3 temperature (H)	-
TCV-0401	-	-
TCV-3005	-	Compartment 4 temperature (H)

High alarm level interlocks are used to prevent overflowing of vessels to avoid spillage, while low alarm level interlocks are used to prevent vessels from running dry so as to protect pumps. Safety interlocks which act on vessel agitators exist at Western Platinum BMR (not shown in Table 2.6). These interlocks stop agitation inside vessels when the levels are low, in order to protect agitators.

The autoclave at Western Platinum BMR has a temperature design limit of 155 °C (Steenekamp et al., 2009). The oxygen to the autoclave is stopped at 150 °C in an attempt to prevent equipment damage. Pressure safety interlocks are used to prevent excessively high pressures which could endanger personnel.

CHAPTER 3: DYNAMIC PROCESS MODEL DESCRIPTION

Chapter 2 described the process operation and control philosophy of Western Platinum BMR in detail. Literature on expected chemistry and reaction mechanisms were also discussed.

This chapter aims to describe the background and fundamental development of a BMR open-loop dynamic model derived by Dorfling (2012). It starts off with background on batch experimentation conducted so as to develop reaction kinetics. This is followed by description of reaction kinetics, mass and energy balances, constitutive equations and model programming. A summary of assumptions made during the development is also provided. This chapter will form a core part in executing one of the project objectives – model validation.

At the end of this chapter the mathematical framework of the dynamic model should be well understood. The procedure used by Dorfling (2012) to program the mathematical framework into a computerised model should be clear. Some key assumptions used to develop the model should also be understood.

3.1. Overview

An open-loop dynamic process model was developed by Dorfling (2012) which mimics the operation of Western Platinum BMR. The dynamic process model forms the basis for this project; and the first project objective is to validate it. Numerous references will therefore be made to work conducted by Dorfling (2012) in an attempt to familiarise one with methodologies and assumptions used by Dorfling (2012) to produce the dynamic process model. The assumptions made by Dorfling (2012) are summarised in the final section in this chapter. All assumptions and observations will be investigated in the model validation process discussed in Chapter 6.

This chapter is divided into several sections that follow a chronological order in which the dynamic process model was developed by Dorfling (2012). Section 3.4 provides interim information which allows a better understanding of the dynamic process model.

3.2. Batch Experimentation

Dorfling (2012) conducted experiments within a batch reactor in order to investigate the reaction kinetics of base metals and PGMs under a variety of conditions typically seen at Western Platinum BMR. Dorfling (2012) conducted a full factorial with temperature, pressure, initial acid concentration and solid content as factors. The full factorial included two levels for each factor with upper and lower values seen in Table 3.1.

Table 3.1: Experimental run conditions (Dorfling, 2012)

Variable	Value
Temperature (°C)	116-130
Pressure (kPa)	700-900
Experimental run time (h)	7
Live reactor volume (m ³)	0.002
Oxygen flow rate (g/(h . l solution))	7.5-78
Initial acid concentration (g/l)	140-165
Solid content (g/l)	80-130

The initial acid concentrations used by Dorfling (2012) in the batch experiments were determined by firstly assuming the occurrence of certain reactions and an extent of leaching, and thereafter calculating the required acid to produce a final acid concentration of 35 grams per litre.

The concentrations of base metal ions namely Fe³⁺, Ni²⁺, and Cu²⁺ were measured using inductively coupled plasma optical emission spectrometry (ICP-OES). No distinction was made between ferric (Fe³⁺) and ferrous (Fe²⁺) ions during sample measurements. The concentrations of PGMs namely Rh³⁺, Ru³⁺, Ir³⁺, Os³⁺, Pt³⁺ and Pd³⁺ were measured using inductively coupled plasma mass spectrometry (ICP-MS). The solid composition and pH were not measured during the leaching experiments. An initial slurry volume of 1 l was used by Dorfling (2012) in each run. Dorfling (2012) removed approximately 12 ml of slurry during each sample, with a total of 13 samples per run. A significant portion of the slurry was lost due to sampling. The resulting ion concentrations were therefore adjusted by Dorfling (2012) to account for the sampling sizes. It was also noticed that initial ion sample concentrations showed large variation even though they were taken from the same liquid source.

The batch experiments were conducted in order to use resulting concentrations over time within a mole balance that contains a rate of reaction term:

$$\frac{dC_i}{dt} = \sum_j v_{i,j} \times r_j \quad \text{Equation 3.1}$$

where C_i and $v_{i,j}$ represents the molar concentration of component i and the stoichiometric coefficient of component i in reaction j , respectively. The rate of reaction (r_j) is expressed through a mathematical model which is often a function of reactant concentrations, temperature, and more. Equation 3.1 serves as a way to link experimental data and mathematical models. Dorfling (2012) continued to developed rate expressions for all 21 chemical reactions (see Section 2.3). The development of these rate expressions will be discussed in the subsequent section.

3.3. Reaction Kinetics

The final set of reactions used by Dorfling (2012), assumed to describe the behaviour of the leaching process, is given in Section 2.3. Dorfling (2012) aimed to develop rate expressions for these reactions which describe at what rate they occur and what they are dependent of.

A typical rate expression is presented in Equation 3.2:

$$r_j = \frac{Ak_j \prod C_{i,j}^{\alpha_{i,j}}}{V} \quad \text{Equation 3.2}$$

Parameters α , k and A refer to the order of reactant, rate expression constant, and surface area of solids, respectively. Dorfling (2012) produced rate expressions for reactions listed in Section 2.3 by firstly assuming either zero, first or second order dependence on the concentration of all reactants. Assuming a zero order dependence of a reactant produces a rate expression that is independent of that reactant. The dissolved oxygen concentration in the liquid was also replaced with the dissolved oxygen concentration at equilibrium based on finding by Provis et al (2003). This assumes that the oxygen concentration within the liquid is at all times equal to the maximum oxygen solubility limit. The surface area of a solid was estimated with an equation derived by Salmi et al. (2010):

$$A = \sigma \times M_w \times n_0^{1/f_{sh}} \times n^{1-1/f_{sh}} \quad \text{Equation 3.3}$$

The molecular weight and mole amount of the solid is represented by M_w and n , respectively. Subscript 0 in Equation 3.3 represents the initial value (i.e. value at time zero). The original specific surface area (σ) is defined as follows:

$$\sigma = \frac{A_0}{m_0} \quad \text{Equation 3.4}$$

A_0 and m_0 represent the initial particle surface area and mass, respectively. The shape factor (f_{sh}) is a ratio of initial volume, area and length of particles:

$$f_{sh} = \frac{A_0 \times L_0}{V_0} \quad \text{Equation 3.5}$$

Dorfling (2012) subsequently combined equations above; used the Arrhenius equation; and agglomerated all constants to produce the following generic rate expression:

$$r_j = \left(k_{0,j} e^{-\frac{E_{a,j}}{RT}} \right) \prod C_{i,j}^{\alpha_{i,j}} \left(n_0^{f_{sh}} \times n^{1-\frac{1}{f_{sh}}} \right)_{solid} \quad \text{Equation 3.6a}$$

Dorfling (2012) developed rate expressions for Reaction 1 to Reaction 21 which is summarised in Table D.1. The functional forms of the rate expressions used by Dorfling (2012) for the 21 chemical reactions varies slightly from that of Equation 3.6a, and will be discussed in Chapter 6.

Mole balances were subsequently performed by Dorfling (2012) for all species present in reactions. This was done by substituting rate expressions in Table D.1 into Equation 3.1. The resulting differential equations were numerically integrated using the 4th order Runge-Kutta method with a time step of 0.2 minutes. The calculated differential equations were subsequently optimised in Microsoft[®] Excel using the Solver function. The batch experimental data was fitted by varying parameters which included 21 pre-exponential factors; 21 activation energies; and 13 shape factors. Values for these parameters were varied to minimise a single objective sum of square concentration error for 16 experimental runs containing 6 ion concentrations measured 13 times over 420 minutes:

$$ObjFunc = \sum_{i=1}^{i=6} \sum_{r=1}^{r=16} \sum_{t_0}^{t_f} (C_{M,i} - C_{E,i})_{t,r}^2 \quad \text{Equation 3.7a}$$

where C_M and C_E represents the model predicted concentration; and the experimentally determined concentration, respectively.

The batch experimentation was conducted in an attempt to mimic the leaching behaviour seen at Western Platinum BMR. The rate expressions developed by Dorfling (2012) describe the leaching behaviour within batch experimentation after the optimisation of reaction kinetic parameters (shape factors, activation energies and pre-exponential factors). The developed rate expressions were subsequently used by Dorfling (2012) to develop a dynamic process model, which aims to reflect the actual continuous Western Platinum BMR process. The development of the dynamic process model will be discussed in the subsequent section.

3.4. Dynamic Process Model Overview

The goal of the process model is to dynamically predict the behaviour of the Western Platinum BMR under a range of conditions and circumstances. The dynamic process model developed by Dorfling (2012) aims not only to describe the leaching behaviour within the autoclave at Western Platinum BMR, but also the flow of material and energy throughout the process.

The dynamic process model incorporates all process units shown in the Western Platinum BMR PFD (refer to Figure 2.3):

1. Second stage slurry preparation tank
2. Flash recycle tank
3. First autoclave compartment
4. Second autoclave compartment
5. Third autoclave compartment
6. Second stage discharge tank
7. Second stage discharge thickener
8. Third stage slurry preparation tank
9. Fourth autoclave compartment

Dorfling (2012) modelled all process units listed above as continuous stirred tank reactors (CSTR). The majority of inputs to the process model are listed in Table 3.3, which comprises

information on all streams entering the PFD (see Figure 2.3). Additional inputs include starting conditions for all differential equation, which will be discussed in Section 3.7. Outputs of the process model include flow rate; temperature; solid composition; solid fraction; and liquid composition for all streams found on the PFD.

Dorfling (2012) developed mass and energy balances used to model each process unit. The development of these equations will be discussed in the subsequent section.

3.5. Mass and Energy Balances

Dorfling (2012) conducted mass balances across a generalised process unit which produced the following equation:

$$\frac{dm_i}{dt} = \sum_{in} \dot{m}_{i,k} - \sum_{out} \dot{m}_{i,k} + V \sum v_{i,j} \times r_j \times M_{w,i} \quad \text{Equation 3.8a}$$

where $\dot{m}_{i,k}$ represents the mass flow rate of component i in stream k . Equation 3.8a can be applied to either the solid, liquid or gas phase. Dorfling (2012) used a mass fraction differential version of Equation 3.8a within the process model:

$$\frac{dx_i}{dt} = \frac{\sum_{in} \dot{m}_{i,k} - \sum_{out} \dot{m}_{i,k} + V \sum v_{i,j} \times r_j \times M_{w,i}}{m_{tot}} \quad \text{Equation 3.8b}$$

Note that the equation above assumes a constant mass within the generalised process unit. This issue is addressed in Chapter 6.

Dorfling (2012) conducted energy balances across a generalised process unit which produced the following equation:

$$\frac{d(m_{tot}\hat{H})}{dt} = \dot{Q} - \dot{W}_{shaft} + \sum_{in} \dot{m}_{i,k} \hat{H}_{i,k} - \sum_{out} \dot{m}_{i,k} \hat{H}_{i,k} - V \sum r_j \Delta \hat{H}_{rxn,j}^o \quad \text{Equation 3.9a}$$

where \dot{Q} and \dot{W}_{shaft} represent the rate at which heat is added to the system and work is done by the system, respectively. The standard heat of reaction and specific enthalpy are notated as $\Delta \hat{H}_{rxn,j}^o$ and $\hat{H}_{i,k}$, respectively. Shaft work and standard heat of reactions were assumed by Dorfling (2012) to have constant values. Dorfling (2012) calculated the standard

heats of reactions by using HSC Chemistry[®] which manipulates standard heats of formations. Dorfling (2012) used Equation 3.9a for all autoclave compartments. The heat of reaction term in Equation 3.9a was excluded when used within the flash recycle tank. Dorfling (2012) assumed isothermal preparation tanks.

Dorfling (2012) determined several terms within mass balances; energy balances; and rate expressions using constitutive equations.

3.6. Constitutive Equations

A summary of the main constitutive equations used by Dorfling (2012) to quantify certain parameters within mass balances; energy balances; and rate expressions is provided in Table 3.2.

Table 3.2: Main constitutive equations used by Dorfling (2012) in dynamic process model

Parameter	Formula reference	Equation
c_p	Kopp's law for estimating specific heat capacities	Equation D.1
\hat{H}_k	Standard method of calculating specific enthalpy	Equation D.2
\dot{Q}	Empirical correlation developed by Incropera and De Witt (1996)	Equation D.3
$C'_{O_2,eq}$	Thermodynamic equation developed by Tromans (1998)	Equation D.5

Refer to Appendix D for a detailed description of how these constitutive equations were used in the process model.

3.7. Model Programming

Dorfling (2012) developed a dynamic BMR process model inside MATLAB[™]. This model was later rebuilt into Simulink[™] by Haasbroek and Lindner (2015). These models will be discussed separately.

3.7.1. MATLAB[™] dynamic process model

A flow diagram is shown in Figure 3.1 which represents the flow of information between process units within the dynamic model. The dashed line in Figure 3.1 indicates information flow that was removed in the updated model, and will be discussed in Chapter 6.

The autoclave was divided into four process units with each compartment being a subsystem. Five other subsystems exist in the dynamic process model each representing a

process unit. Seven liquid component mass balances; fourteen solid component mass balances; and a single energy balance were applied together with necessary constitutive equations and rate expressions to each subsystem within the BMR. Dorfling (2012) assumed that reactions only occur in the autoclave.

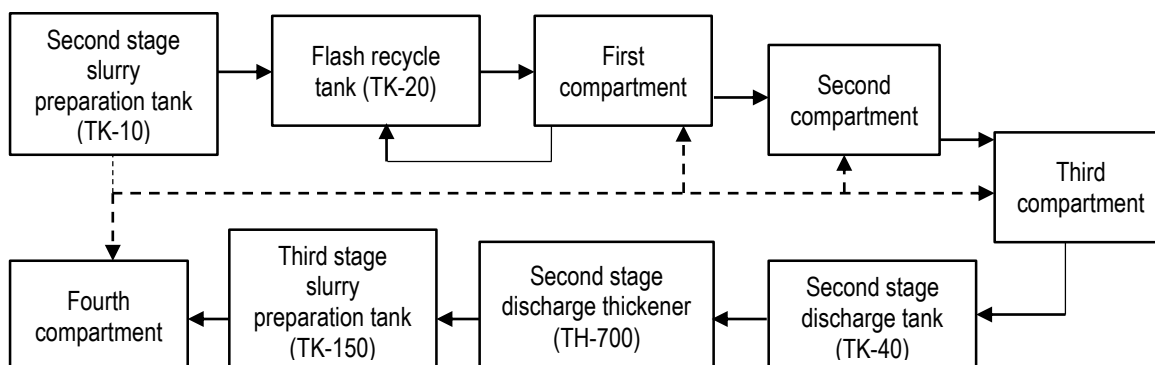


Figure 3.1: Representation of information flow between process units within the dynamic model

Rate expressions listed in Table D.1 are therefore only present in the autoclave compartment mass and energy balances. Dorfling (2012) assumed isothermal preparation tanks (TK-10, TK-40, TH-700 and TK-150). Energy balances for all preparation tanks were therefore ignored by Dorfling (2012). It was furthermore assumed that the mass inside autoclave compartment 1 is constant, simplifying Equation 3.8b for this subsystem. Equation 3.8b was also used in the modelling of the flash recycle tank. The amount of water flashed within this vessel was determined by an additional energy balance which takes into account the temperature of the inlet recycle stream.

Inputs to the dynamic model are listed in Table 3.3.

Table 3.3: Dynamic process model inputs (Dorfling, 2012)

Stream Number	Variable
1-4	Flow rate, composition, temperature
18-20	Flow rate, composition, temperature
9	Flow rate
5	Temperature
21	Temperature
13	Flow rate, composition, temperature
10-12	Flow rate, composition, temperature
Autoclave	Pressure

Dorfling (2012) assumed all inputs listed in Table 3.3 are constant. The flow rate of the flash recycle stream (Stream 9) used to control the temperature of the first autoclave compartment was specified to be a fixed value during the model development as the model was open-loop.

Sets of mass and energy balances; rate expressions; constitutive equations; and operating conditions listed in Table 3.3 were then used by Dorfling (2012) to determine steady-state conditions in a sequential modular manner. A tear stream was required to solve steady-state conditions for the flash recycle tank due to the recycle stream (also depicted in Figure 3.1). A flow diagram is presented in Figure E.4 which is used to briefly describe the steady-state calculation methodology. Extent of reactions within all autoclave compartments were calculated by Dorfling (2012) according to a methodology presented in Figure E.5. This involves the calculation of oxygen solubility, reaction rates, consumption rates and thereafter determining the limiting reagents.

The steady-state conditions were used by Dorfling (2012) as a starting point to solve ordinary differential equations (ODE) for the dynamic model. The overall MATLAB™ model contains approximately 8600 lines of code within seven functions. A simplified representation of the dynamic process model structure is given in Figure 3.1.

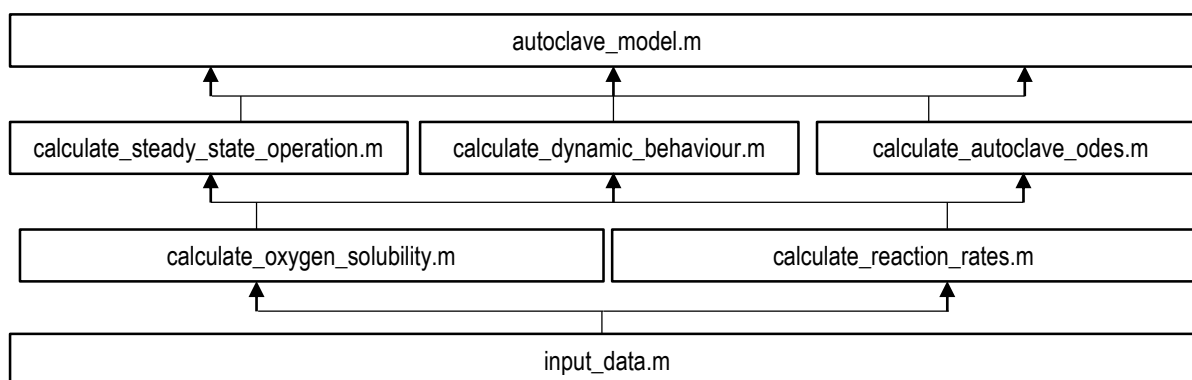


Figure 3.2: MATLAB™ dynamic process model structure

The MATLAB™ function named `input_data.m` (refer to Figure 3.2) contains the data listed in Table 3.3 and all the parameters required to solve constitutive equations; mass balances; energy balances; and rate expressions. The functions `calculate_steady_state_operation.m`; `calculate_autoclave_odes.m`; and `calculate_dynamic_behaviour.m`; each contain mass balances, energy balances, and constitutive equations to solve all process units in the BMR. The only difference between the latter two functions is their outputs (i.e. the type of results they produce).

Functions listed in Figure 3.2 contain numerous lines of copied static code² which is challenging to edit. Knoblauch (2014) attempted to implement control strategies in the

² This refers to code that has been written for a specific purpose, which has been copied and pasted in several functions. When changes are made within one piece of code, the piece of code needs to be traced to all the other places it had been pasted, which makes editing challenging

MATLAB™ model which proved to be difficult. Moreover, the MATLAB™-coded model is difficult to interpret and comprehend due to its large size.

3.7.2. Simulink™ dynamic process model

The MATLAB™ process model proved to be difficult to interpret and edit. The model was consequently rebuilt into Simulink™ by Haasbroek and Lindner (2015) to overcome these issues. Simulink™ is a high level programming language with a built-in library containing useful tools such as PID controller blocks, integrator blocks, and more. Simulink™ also has valuable capabilities such as zero-crossing detection which allows accurate integration close discontinuities; custom model references to allow the re-use of models; and custom libraries which allow changes to a block within the library to be pushed to everywhere the block is used. The rebuilt Simulink™ model therefore allowed easier implementation of model improvements, control strategies, and model upkeep within this project.

A hierarchy of the rebuilt Simulink™ BMR process model is shown below.

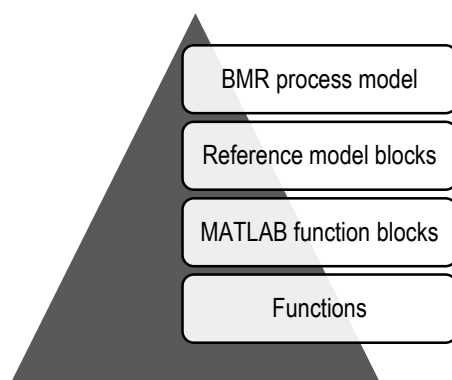


Figure 3.3: Simulink™ dynamic process model hierarchy

The BMR process model contains nine reference model blocks, each representing a process unit. Each reference model block contains information regarding the specific process unit including vessel volume, initial conditions and more. A generic MATLAB™ function block exists within each model reference block. The MATLAB™ function block has several inputs to which the specific process unit information reports. Generic mass balances; energy balances; rate expressions; and constitutive equations are found within these MATLAB™ function blocks. Three generic MATLAB™ function blocks exist in a library: an autoclave compartment, a preparation tank and a flash recycle tank. Two generic MATLAB™ function blocks exist in order to distinguish between vessels in which reactions are occurring and are not occurring.

Simulink™ transfers information through signals. The simplest signal contains at least a time series and corresponding variable values. The majority of signals within the process model are busses, which is a composite of smaller simpler signals. The main bus type used within the Simulink™ model, namely the stream bus, contains six simpler signal entries namely temperature; mass flow rate; liquid composition with seven components; solid composition with fourteen components; solid fraction and liquid fraction. Stream busses are used to share information in between reference model blocks. A MATLAB™ function block within the second stage slurry preparation tank reference model block is shown below.

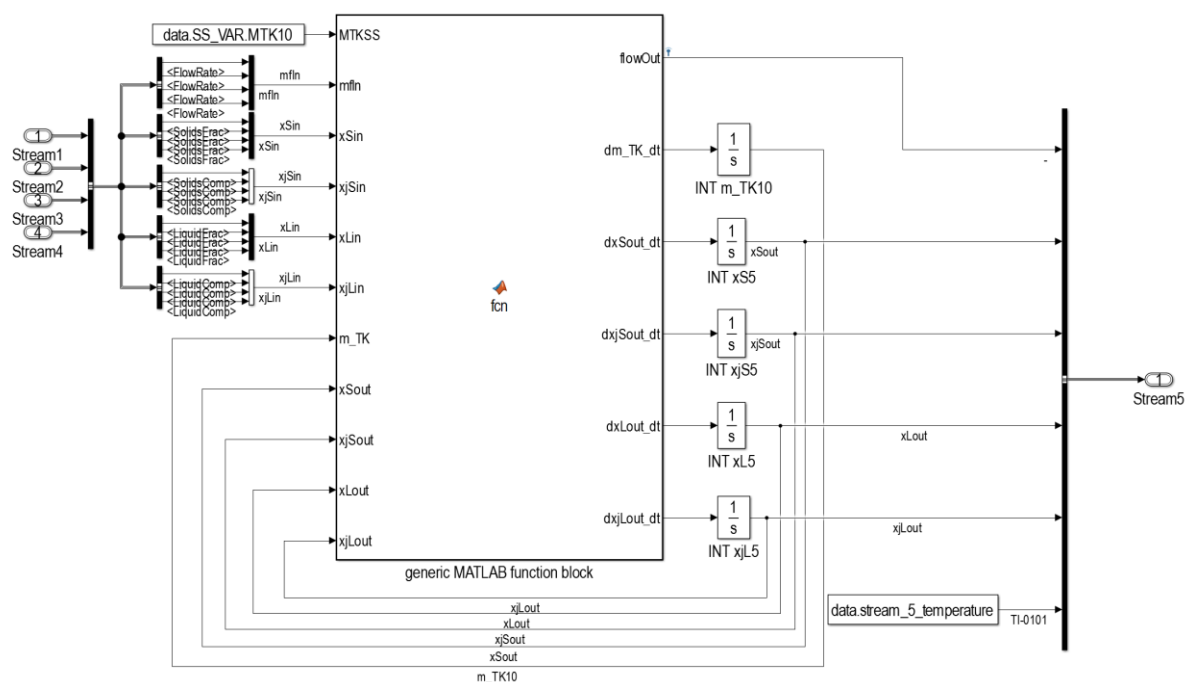


Figure 3.4: Generic MATLAB™ function block used inside the second stage slurry preparation tank reference model

Variable time-step integrator blocks are used to integrate MATLAB™ function block outputs (i.e. all mass and energy balance ODEs). The temperature is not integrated in this demonstration since Dorfling (2012) assumed isothermal preparation tanks. Refer to Figure E.3 for a flow diagram of the Simulink™ process model showing all the reference models.

Figure 3.5 show inner model structure of a generic MATLAB™ function block.

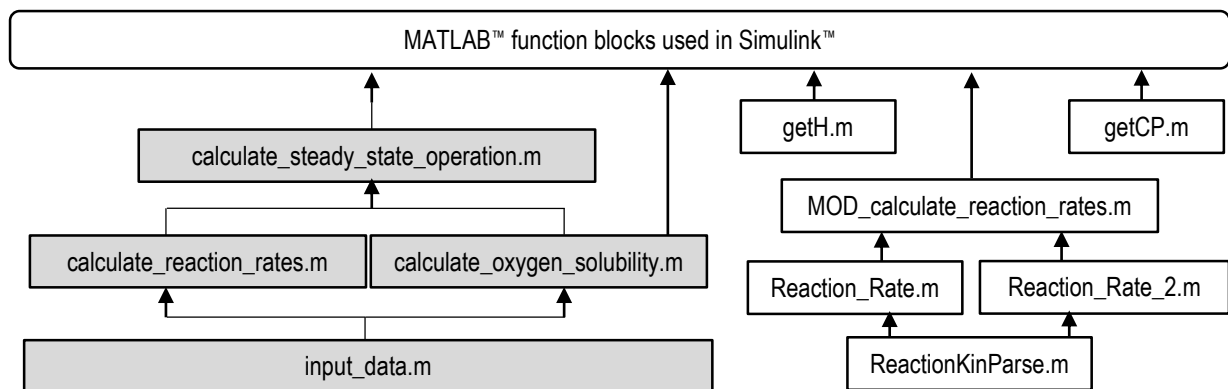


Figure 3.5: Simulink™ dynamic process model structure

The Simulink™ model still uses the same MATLAB™ code developed by Dorfling (2012) to calculate steady-state conditions (re-used code is highlighted in Figure 3.5). Several other functions were written by Haasbroek and Lindner (2015) which mimics portions of code within the bulk MATLAB™ code developed by Dorfling (2012). These functions include the calculation of enthalpies, specific heat capacities and reaction rates. Generic mass balances; energy balances; rate expressions; and constitutive equations are present inside the MATLAB™ function blocks, as previously mentioned. No additional functions are therefore called to solve these equations.

The rebuilt Simulink™ model shows good reproducibility in areas close to steady-state conditions (Haasbroek & Lindner, 2015). The Simulink™ model forms the baseline of this project and will for this reason be validated within Chapter 6.

3.8. Model Assumptions

A list of assumptions made and methodologies used by Dorfling (2012) during the BMR model development are summarised and divided into five sections below. These assumptions will form a core part in the model validation and verification chapter.

3.8.1. Leaching chemistry and reaction mechanisms

- A1. Copper cementation reactions were assumed to be negligible.
- A2. All iron ions were assumed to be ferric, and the reduction mechanism of ferric to ferrous ions was excluded.
- A3. Initiation of PGM leaching reactions were assumed to occur only when 99 % of digenite entering the second stage slurry preparation tank was leached.

3.8.2. Batch experimentation

- A4. Sampling affects the rate of reactions.
- A5. Batch experiment acid concentrations were similar to that of the actual process.

3.8.3. Rate expression development

- A6. Rate expressions were assumed to be directly scalable to larger process units (i.e. rate expressions have intensive properties).
- A7. Rate expressions were assumed to be directly transferable to a continuous process (i.e. initial concentrations in batch reactor kinetics are undefined in a continuous process).
- A8. Oxygen concentration within the liquid was assumed to be equal to the maximum oxygen solubility limit.
- A9. Digenite and covellite leaching reactions were assumed to be mass transfer limited.
- A10. PGM-oxide shape factors were assumed to be infinite (i.e. very large surface area to volume ratios).

3.8.4. Rate expression optimisation

- A11. The amount of experimental data points was assumed sufficient in determining the amount of parameters.
- A12. Sum of square concentration error objective function was assumed to be sufficient for the optimisation problem.

3.8.5. Dynamic process model development

- A13. The dynamic model was assumed to have zero degrees of freedom.
- A14. Temperature and composition of input stream 1, 2, 3, 4, 18, 19 and 20 were assumed to stay constant.
- A15. All preparation tanks were assumed to be isothermal.
- A16. The total mass inside all autoclave compartments were assumed to stay constant.
- A17. The autoclave was assumed to be isobaric.
- A18. Addition of water and sulphuric acid directly to the flash recycle tank was excluded.
- A19. All process units were assumed to have ideal CSTR characteristics.
- A20. It was assumed that no reactions are occurring inside auxiliary units.
- A21. A constant shaft work and heat loss was assumed for process units.
- A22. A single flash recycle tank and autoclave set was assumed to describe the leaching process.

CHAPTER 4: LITERATURE REVIEW

Chapter 3 described how Dorfling (2012) conducted batch experiments in order to fit developed rate expressions, and how the optimised rate expressions were then used together with mass balances; energy balances; constitutive equations in a dynamic model which describes Western Platinum BMR.

This chapter aims to provide an in-depth literature review on all project objectives:

- 1. Validation and verification of the BMR dynamic process model*
- 2. Modelling and implementation of critical control layers on the dynamic process model*
- 3. Fault gathering; fault database development; and fault simulation*
- 4. Assessing the ability of the control to mitigate fault scenarios*

The chapter starts off with literature on model verification and validation and proceeds to review literature on control architecture and safety layers. Fault characteristics and possible information sources are investigated for the third objective. Examples of a wide variety of faults from literature are listed. Control performance assessment is then investigated by considering both operation- and control key performance indicators.

At the end of this chapter several methods of addressing the project objectives should be clear. This will pave the way forward for the development of a structured approach of addressing objectives.

4.1. Model Verification and Validation

The Western Platinum BMR open-loop dynamic process model developed by Dorfling (2012) and improved by Haasbroek and Lindner (2015) was introduced in Chapter 3. The dynamic process model has not yet been validated for its intended purpose. The validation of the process models is the first objective within this project. This section aims to obtain a

comprehensive approach to model validation from literature which can be applied to the dynamic process model.

Models are typically used to compare or predict the future performance of a modified system, new system or an existing system under new conditions. When models are used for comparison, it is normally made to an existing baseline model, a concept model or to real-time system data. In each case it is required to know the accuracy of the model (Carson, 2002). Any type of developed model therefore requires validation and verification (V&V) to some extent. The degree of V&V depends on the model's specific purpose; may it be designing, prediction or simulation. It is often costly, dangerous or even impossible to absolutely validate and verify a developed model (i.e. operating the actual process near dangerous conditions so as to compare it to model predicted results). The ultimate goal of V&V would therefore be to assess if the issue which motivated the modelling exercise could be solved using the developed model (Ljung, 2009).

Distinction can be made between verification and validation of a model. A more formal definition of model verification and model validation would respectively be “ensuring that the computer program of the computerised model and its implementation are correct” and “substantiation that a computerised model within its domain of applicability possesses a satisfactory range of accuracy consistent with the intended application of the model” (Sargent, 2005; Schlesinger et al., 1979). Slight variation of these definitions exist (Carson, 2002). The former definitions are accepted within this project.

4.1.1. Participating parties

It is important to firstly define who will be taking part and conclude in the final validity of the model. Model credibility would increase if for instance it was concluded that the model is valid by competent end-users. Carson (2002) suggests the primary person responsible for model accuracy and to correct deficiencies as they are found is the model developer. Sargent (2005) mentioned four different parties which could take part in the V&V process.

The first party, one which is often used according to Sargent (2005), would be for the team who developed the model. This approach might cause subjective rationalisation of model results and selective testing. Similar finding have been reported by Balci (1997). In the industrial sector examples of personnel on a modelling team would be model developers, engineers, process owners, operators, supervisors, decision makers, vendors, designers and system integrators (Carson, 2002).

The second party makes use of the heavily involved model users during the validation process. The focus moves, compared to the first party, from the model developers to the end-users. More objective model result rationalisation is expected in this case, since the aim of the end-users would be to acquire a rigorous and healthy model. However, it is expected that the model user would have less of a comprehensive understanding of the model compared to the developer, since the user was absent during the fundamental development of the model. This approach does aid model credibility if the user is satisfied (Sargent, 2005).

Another possibility would be to make use of an independent third party such as simulation consulting groups. This method is often used when the application of model outputs is associated with high costs. It is also used when model developers find the V&V process difficult because a change in mind-set and attitude is required, compared to that of the model development stage (Carson, 2002). The third party approach is conducted either concurrently or after model development. Carson (2002) suggests having all key personnel involved from the beginning of model development.

The fourth and final party mentioned in Sargent (2005) is to use a computer to quantitatively score a model. Weights and constraints for different aspects of the model are defined by the person performing V&V, and used as an objective function to score a model. Pseudo-random inputs can be used to run and score a model under different conditions. The final model output score is then compared to the minimum defined score. This approach is seldom used, as a model might receive a passing score even though it has a defect which requires modification.

4.1.2. V&V approaches

Numerous publications (Buranathiti et al., 2006; Ljung, 2009; Mayer & Butler, 1993) approach model V&V by solely comparing model outputs to the modelled system outputs. Several techniques are used which include graphical comparisons, statistical tests, deviance measures and more. These tests are essential in model V&V, but provide only feedback on the upper level of the model – its operation. Moreover, this validation approach is limited to the operational area considered.

Sargent (2005) approaches model V&V from a fundamental point of view, considering not only the model outputs, but all aspects of the model. Sargent (2005) defines two common approaches, namely the simple and complex approach. Banks et al. (1987) used both approaches during a review and concluded that the simple approach is much more clearly defined. This simple model V&V approach is presented in Figure 4.1.

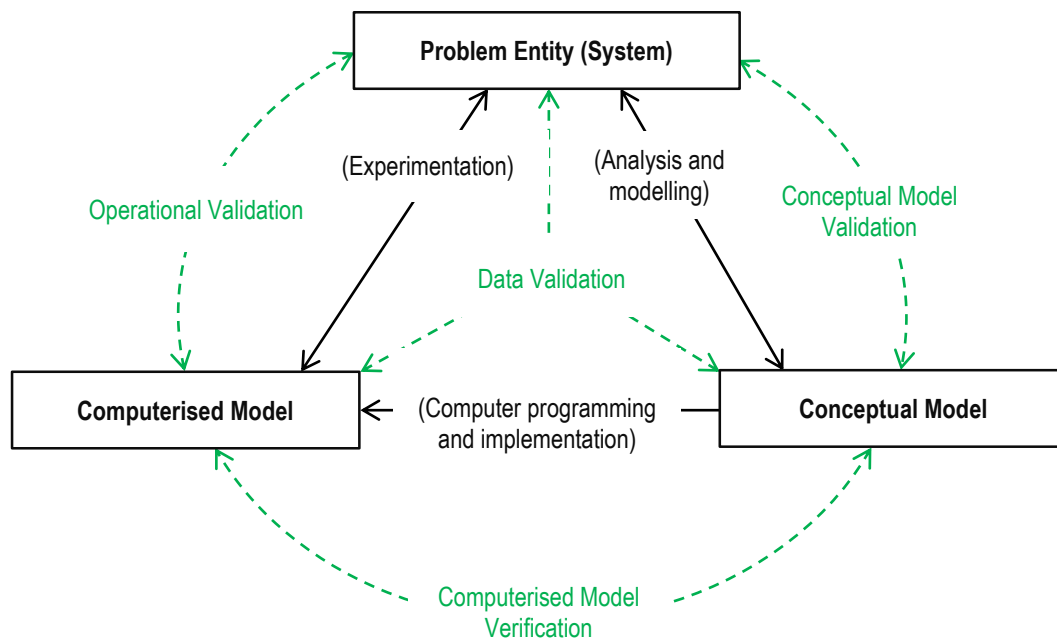


Figure 4.1: Simple Verification and Validation Approach (Redrawn from Sargent (2005))

The problem entity refers to the problem, system, idea or phenomenon to be modelled. The conceptual model refers to the logical or mathematical representations used to express the problem entity through certain analysis and modelling. The computerised model is the conceptual model implemented into a computer program.

Sargent (2005) divided model V&V into four categories which can be used to assess the overall validity of a model. These categories tie different sections of the modelling procedure together, and are indicated by dashed lines in Figure 4.1.

Conceptual model validation is used to confirm that theories, mathematics and underlying assumptions are sufficiently correct, and that the model represents the problem entity realistically enough for the intended purpose. Computerised model verification ensures the computer programming and implementation of the conceptual model is correct. Data validation ensures the data used within model development, assessment and testing are correct and adequate. Operational validation determines if the model's output behaviour corresponds to the problem entity for its intended purpose and also within the model's intended domain of applicability. The operation of the model needs to be validated over a range of conditions in order to obtain high confidence in a model (Sargent, 2005). Any deficiencies arising from the operational validation section are in general caused by problems from other sections. Operational validation is often considered to be the ultimate criterion in determining the validity of a model (Landry et al., 1983). However, the validity of a model cannot solely be dependent on operational validation.

Carson (2002) also suggests a similar holistic approach to model validation, where modelling errors are categorised into four groups:

- Project management errors
- Data and data modelling errors
- Logic modelling errors
- Experimentation errors

Project management errors are related to miscommunication issues between the modelling team (Carson, 2002). This is applicable in the service and industrial sectors. Data and data model errors are defined in a similar way as Sargent's (2005) data validation category. Data errors include incorrect or incomplete input data, whereas data modelling errors refer to the inappropriate use of data within a model. Logic modelling errors is the incorrect implementation of model specifications within a simulation language. It therefore corresponds with computerised model verification defined by Sargent (2005). Experimentation errors relate to operational validation. This includes any errors made during the experimentation, sampling and analysis of the problem entity.

4.1.3. V&V techniques

Balci (1997) lumps all V&V techniques into four groups, namely: informal, formal, static and dynamic. Most of the techniques listed throughout this section can be applied in either a formal or informal manner. Subjective applications include graphical analysis such as histograms; box and whisker plots; time-series plots; and behaviour graphs using scatter plots. Objective applications include statistical analysis such as confidence intervals, hypothesis tests and residual analysis.

Conceptual model validation

Sargent (2005) states that the conceptual model is validated after considering two areas: the theories and assumptions underlying the model is correct; and the model's structure, logic, mathematical relationships, and causal relationships are rational. Mathematical analysis and statistical methods could be used on problem entity data to test assumptions such as linearity and independence of data (Sargent, 2005). However, a wide range of theories and assumptions exist and problem entity data is not always available. Theories and assumptions could be evaluated qualitatively to determine if they are reasonable for the intended purpose of the model. A literature survey on respective assumptions together with logic reasoning could be used to arrive at conclusions. Knowledgeable people in the specified field could also be used to rationalise assumptions and test theories.

Computerised model verification

A major factor which determine techniques used in computerised model verification is whether a simulation language³ or a high level programming language⁴ has been used. The use of a simulation language will in general result in fewer errors when compared to using a high level program. Computerised model verification, in the case of a simulation language, is primarily concerned with the proper programming of the conceptual model. A high level programming language, in addition to proper programming, requires the correct use of functions to be validated. Fairley (1976) described two basic methods for testing a program:

- Static testing – program is analysed without being run.
- Dynamic testing – program is analysed during and after it is run.

Static testing techniques include structured walk-throughs, correctness proofs, reviews, inspections and examining the correctness of the program's structure properties (Balci, 1997). Dynamic testing techniques include traces, input-output relation investigations, internal consistency checks and reprogramming of critical components so see if the same outputs are obtained (Sargent, 2005). Carson (2002) reports using similar techniques.

Operational validation

The operational validation category is where most of the validation and testing occurs if other categories proved valid. Techniques used to validate model operation include (Sargent, 2005; Landry et al., 1983; Cramer, 2001):

- Model comparison - comparing different model outputs for the same problem entity.
- Event validation - comparing certain problem entity occurrences to the model predicted outputs.
- Extreme condition testing - testing the model operation under extreme conditions.
- Face validation - using the opinion of knowledgeable people to qualitatively verify the rationality and accuracy of model responses.
- Historical data validation – using a series of past data to determine if the model behaves as the problem entity did.
- Sensitivity analysis - changing model inputs and investigating its effects on the output behaviour.
- Predictive validation – using the model to predict the problem entity behaviour and conducting field tests or experiments to validate it.

³ ExtendSim, VisSim, Simulink.

⁴ FORTRAN, C++, MATLAB.

- Turing test - verifying that knowledgeable people cannot distinguish between system outputs and model outputs.
- Spectral analysis - evaluating if the model and system outputs are similar inside the frequency domain.

Event validation is similar to predictive validation since model outputs are in both cases compared to problem entity outputs. However, model outputs precede problem entity outputs in predictive validation, whereas the opposite is true for event validation. Predictive validation can be used when change is allowed to the problem entity, allowing tests to be conducted as pleased. Historical data validation can be used to compare several system outputs between long periods of time to ensure that the system is not drifting.

Techniques such as face validation and Turing tests are qualitative and based on opinion, therefore informal or subjective. These techniques do however provide initial confirmation that the model might be valid, and can easily indicate if the model is drastically inconsistent.

Data validation

Typical techniques used for data validation are mass balances, energy balances and physically realisable checks (Sargent, 2005). Data reconciliation can be used to improve data if measurement noise is a severe issue (Kuehn & Davidson, 1961). Many authors suggest the use of global tests to prove if a gross error is statistically significant (Almasy & Szatno, 1975; Madron & Veverka, 1977; Ripps, 1965). Mah and Tamhane (1982) suggest the use of measurement tests to statistically identify which measurements are likely causing gross errors by utilising data reconciliation outputs.

4.2. Control Implementation

A Western Platinum BMR dynamic process model has been developed by Dorfling (2012) and improved by Haasbroek and Lindner (2015). However, no control exists on the dynamic process model. Control needs to be implemented on the model if fault occurrences are to be mitigated during the assessment of control performance (i.e. for the latter two project objectives). This section aims to identify common control mechanisms used within industrial processes in order to develop a generic and comprehensive control implementation approach. The control implementation approach can then be applied to the dynamic process model using Western Platinum BMR control strategies.

Marlin (1995) structures control mechanisms into fall-back safety layers, and will firstly be considered within this section. A different approach to control partitioning described by Romagnoli and Palazoglu (2012) will also be investigated.

Marlin (1995) divides control mechanisms used for safety into five fall-back layers. The five fall-back layers, presented in Figure 4.2, provide a sequence in which control mechanisms act in order to ensure safe process operation.

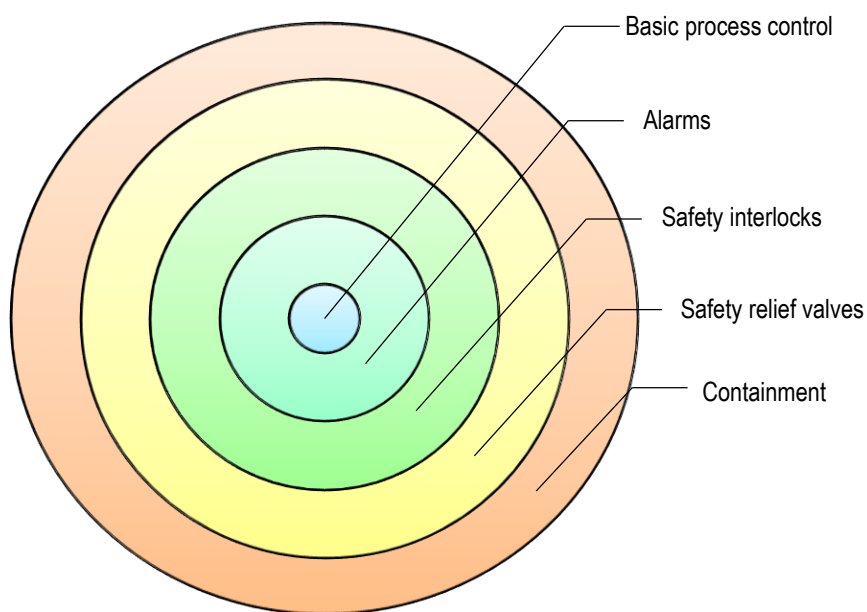


Figure 4.2: Different layers used to control for safety (Marlin, 1995)

The first layer in Marlin (1995) involves the use of basic process control strategies (BPCS). BPCS can be divided into two groups: regulatory control and supervisory control. Regulatory control maintains controlled variables in a safe state by means of adjusting causally related manipulated variables. Supervisory control can be considered as the manipulation of regulatory control loops in an attempt to improve the current state of control objectives. Supervisory control includes automated actions such as gain scheduling, and manual human interventions such as control loop switching and SP adjustments (Sheridan, 1992; Hespanha, 2015). The most common form of regulatory control used in the industry is a single-loop feedback controller. Several components which features in a single-loop feedback controller is presented in Figure 4.3.

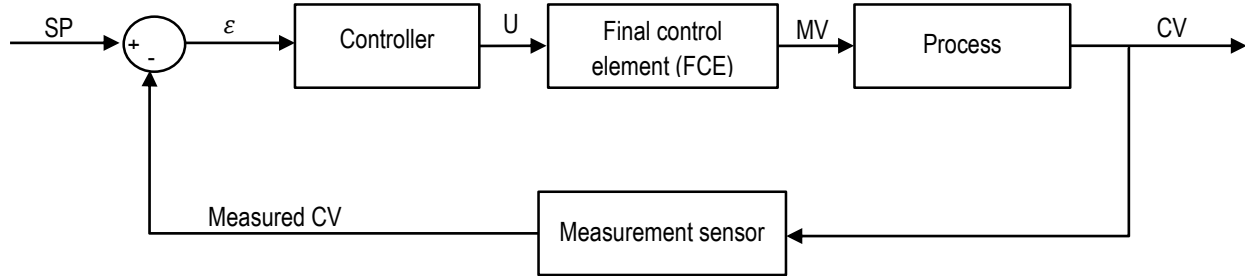


Figure 4.3: Single-loop feedback control block diagram (Redrawn from Lipták (2006))

Feedback control comprises any control strategy which returns controlled variable (CV) information to a controller in order to make necessary adjustments to a manipulated variable (MV) via a FCE, which ultimately affects the controlled variable through the process block (refer to Figure 4.3). Feedback control often attempts to keep the controlled variable at a set-point (SP).

A sensor is used to measure a controlled variable. The measured controlled variable is subtracted from a set-point to produce an error term ($\varepsilon(t)$). The error term reports to a mathematical controller which gives instructions to a final control element, typically an actuator in single-loop controls. The controller's instruction to change the manipulated variable is an attempt to reduce the error term. Enhancements to these controllers often include cascade control, feedforward control, inferential control, ratio control, relation control, and more (Marlin, 1995; Ahmad, 2008). Elements such as signal transmissions, sensors, computers, and more, fail occasionally. This not only becomes a safety hazard, but often impacts profitability. Feedback control is therefore in most cases insufficient in single-handedly controlling industrial processes.

Alarms are the second layer used to control for safety. Alarms do not automatically initiate action, but simply draws attention through sounds within the control room and flashing displays on an operator user-interface when certain variables exceed specified limits. Necessary actions and precautions can be taken by operators when they are notified by alarms. Alarms are often arranged into three levels of priority: high, medium and low (Marlin, 1995). This classification of alarms is required since operators become overwhelmed when too many alarms are urgently sounding, and tend to simply ignore them.

Safety interlock systems instantaneously override BPCS by directly manipulating the FCE to a totally open or closed state in an attempt to prevent certain variables from reaching dangerous limits. These limits are often close to equipment design limits and could cause injury to personnel, damage to equipment or the environment if exceeded.

A fourth layer used in the industry is safety relief valves. Equipment which could possibly reach dangerous pressures are often fitted with safety relief valves which open mechanically at a designed pressure. This ensures that dangerous pressures are never reached within vessels even if safety interlocks were to fail.

Containment is the final layer, and is important if all else fails. Containment is simply different approaches used to contain dangerous liquids and gasses if they should be released when all other layers fail. The containment layer is a design consideration and is addressed during the process design stage.

Romagnoli and Palazoglu (2012) divide a typical plant-wide industrial control strategy into several levels as well. The goal of partitioning a control strategy is to manage the inherent complexity of plantwide industrial control architecture (Romagnoli & Palazoglu, 2012). The levels in Figure 4.4 are indicative of the hierarchy in which control is applied. The first level is the foundation of the plantwide control, and is utilised from the plant start-up onward. The second level is implemented only after the plant is in operation. The third level is aimed at handling abnormal operational conditions.

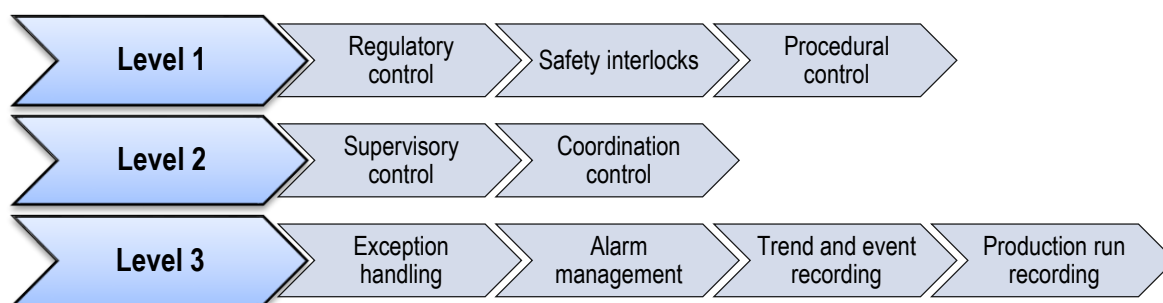


Figure 4.4: Control hierarchy in plantwide industrial control architecture (Romagnoli & Palazoglu, 2012)

Romagnoli and Palazoglu (2012) states that the decomposition of control levels is arbitrary, and activities amongst different levels may be superimposed for a particular application. However, it is further stated that the hierarchical decomposition into levels provide a step-by-step procedure in building plantwide control.

The first entry of the first and second level in Figure 4.4 corresponds to the first safety layer in Figure 4.2. The fact that supervisory control is present in the first layer of safety but present in the second level in control architecture suggests that it is a secondary form of control, but vital for safety.

Alarms do not automatically take action but require human intervention. Alarms therefore do not directly contribute to the controllability of the process. This would be a reason why

Romagnoli and Palazoglu (2012) classifies it as “alarm management”, and places it in the third level, in contrast to being the second layer of safety.

Safety interlock systems are listed in the first level of Romagnoli and Palazoglu’s (2012) control architecture as opposed to the third layer of safety control. This suggests that these interlocks are active from the start of operation and are not dependent on higher levels of control, such as supervisory actions.

Both safety relief valves and containment control layers are not listed in the Romagnoli and Palazoglu’s (2012) control architecture as they inherently form part of the process design procedures.

Exception handling is an important control level not mentioned in Figure 4.2. Exception handling refers to the management of actions taken for failure and recovery of a process during and after the occurrence of an abnormal event. Trend recording and event recording is often used when conducting a post-mortem on the process after the occurrence an abnormal event. Information derived from this could be used to improve maintenance strategies, or even used to create fault databases which could later be utilised in early fault detection and diagnosis.

4.3. Fault Database

Different industrial process control mechanisms have been investigated in Section 4.2, and will be implemented into the dynamic process model. Several of these control mechanisms are used to keep a process in safe operation during the occurrences of abnormal events (referred to as faults). This sections aims to investigate different faults seen in industrial processes. It also aims to characterise faults and determine different sources where fault information can be obtained. The goal of this section is to obtain a structured way of obtaining and characterising faults in order to build a fault database. The fault database will be used to produce different fault scenarios within the process model in order to assess the extent of control performance degradation.

A fault database, in general, is an organised collection of information regarding different faults. In an industrial process environment, a fault database holds information on system states which could potentially lead to failure or malfunction of equipment which would cause significant process abnormality (Isermann, 2005). Fault databases could serve as a tool in early fault detection, isolation and diagnosis.

4.3.1. Fault characteristics

A fault characteristic is a quality or feature that belongs and describes a fault. Several fault characteristics will now be considered.

Classification

Venkatasubramanian et al. (2003) classifies faults into five categories based on their point of origin. These categories include controller malfunction; process disturbances; sensor failures; structural failures and actuator failures. The location where faults can originate within a process is illustrated in Figure 4.5.

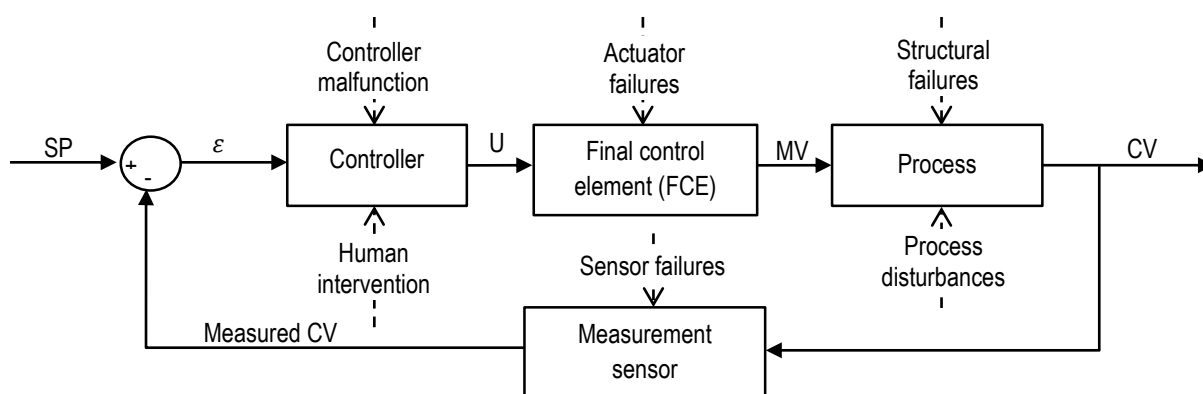


Figure 4.5: Area of faults occurrences within a process (Venkatasubramanian et al., 2003)

Process disturbances include any variation of inputs which cannot be adequately attenuated. Structural failures are changes occurring in the process equipment itself. These failures are often hard equipment failures, for example a pump failure. Actuator failures and sensor failures are common within processes, and are classified separately from structural failures. Human intervention is not included in the five categories listed by Venkatasubramanian et al. (2003), but occurs often (Bainbridge, 1983; Buchanan & Bessant, 1985; Haight & Kecojevic, 2005). Human intervention was therefore added as an additional fault category.

Transition rate

Another characteristic of faults would be the rate at which they transition into full size. Isermann (2005) distinguishes between three different transition rates: abrupt faults, incipient faults and intermittent faults. These rates are captured in the figure below.

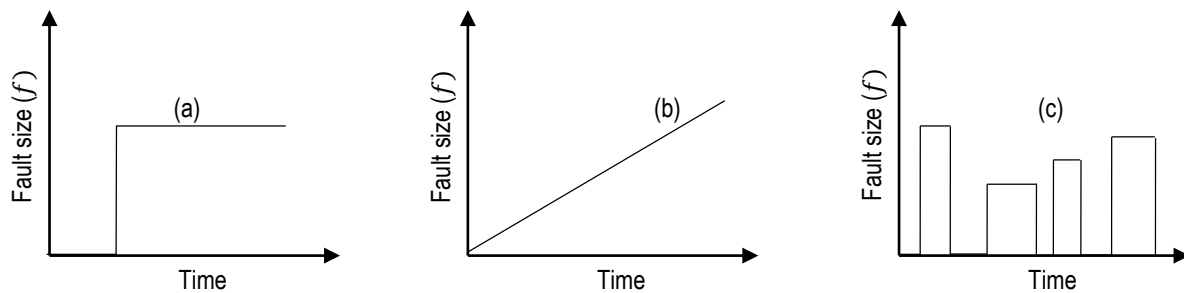


Figure 4.6: Rate of fault transition: (a) abrupt; (b) incipient; (c) intermittent (Redrawn from Isermann (2005))

An abrupt fault would occur instantaneously in full size until the fault is rectified, for example a power failure. Abrupt faults are easier to detect due to their sudden appearance. Incipient faults occur incrementally with time, for example continuous fouling inside heat exchangers. Incipient faults which occur slowly with time tend to become difficult to detect due to control strategies mitigating their effect. Intermittent faults occur abruptly in varying sizes and for varying time intervals.

Frequency of occurrence

An important fault characteristic would be the frequency of the fault occurrence. This information can be used as a baseline to determine when faults are occurring more frequently, which could possibly be indicative of the occurrence of another issue. Lees (1976) reports on instrumentation faults occurring on three separate chemical plants and includes information on the number of instruments on site and the number of faults per year. Himmelblau (1978) also mentions the usefulness of having failure frequency data.

Priority for mitigation

Priority for mitigating faults and their frequency of occurrence can be used to analyse the fault risk in terms of safety issues and effects on profitability. High priority faults that occur frequently would be considered the highest risk.

Type

Isermann (2005) further characterises faults into being either additive or multiplicative (refer to Figure 4.7).

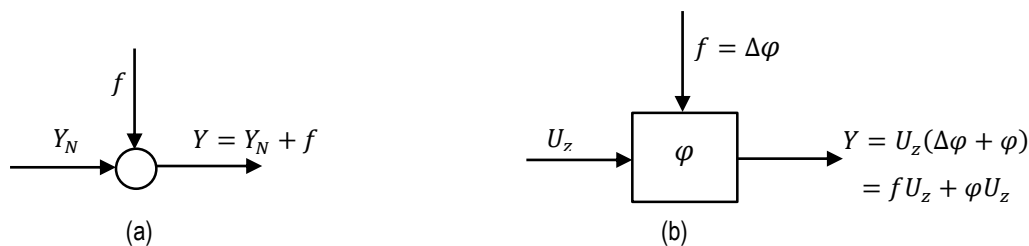


Figure 4.7: Basic models of faults: (a) additive (b) multiplicative

An additive fault results in an output (Y) having an offset of fault size (f). A multiplicative fault results in an output change which is dependent on the input size (U_z) due to the change in a process parameter (φ) with a certain size ($\Delta\varphi$).

Symptoms

A fault symptom can be defined as a feature caused by a certain process abnormality serving as evidence of it. Himmelblau (1978) divided symptoms into two types: frequently measured and qualitative symptoms.

Table 4.1: Examples of possible symptoms (Himmelblau, 1978)

Frequently measured	Qualitative	
Pressure deviations	Corrosion	Loading
Temperature deviations	Erosion	Expansion
Flow deviations	Fouling	Contraction
Level deviations	Cavitation	Fluid properties
Excessive vibration	Fluid hammer	Catalyst activity

Frequently measured symptoms are measured online, and are therefore noticed easier. Qualitative symptoms such as erosion, corrosion and fouling, are obtained observations made during equipment inspection (Patton et al., 2013). These symptoms are infrequently noticed since information is typically obtained only during scheduled maintenance.

4.3.2. Fault information sources

A range of sources are available which can provide necessary fault information:

- Expert knowledge
- Process hazard analysis
- Plant records
- Historian tag data
- Model predicted data

Expert knowledge includes information from process operators, plant engineers, maintenance personnel and many more. Raza and Liyanage (2009) used expert interpretation and perception to develop a variety of process faults. Koscielny and Bartys (2000) also used experts' heuristic knowledge to develop a range of actuator faults.

Process hazard analyses (PHA) comprises hazard and operability (HAZOP) studies; checklists; what-if analyses; failure modes and effects analyses (FMEA); and fault tree analyses (FTA) (Center for Chemical Process Safety, 1992). The importance of performing a comprehensive PHA is illustrated by (Kletz, 1986; Kletz, 1988; Kletz, 1991) describing major industrial accidents which could have been prevented. The use of PHA studies should therefore provide a wide range of possible fault information.

Plant records include operator logbooks, maintenance records and any other physical source of information. Notes are often made by personnel during the occurrence of abnormal events, and act as a source of information. Anyakora (1971) used plant records to produce a list of valve and actuator failures.

Historian tag data includes all online measured plant tag data. Himmelblau (1978) report plant data collections are useful as they capture frequently measured fault symptoms. However, historian tag data does not always indicate the occurrence of a fault (i.e. some faults symptoms are not measured online). Companies typically keep historian tag data for some time, and this could serve as a major source of information. Koscielny and Bartys (2000) mentioned the use of plant data in obtaining fault features.

Certain fault information can be deduced from model predicted information. Koscielny and Bartys (2000) mentioned the use of analytical models, but concluded that a lot of manpower is required and have high associated costs.

4.3.3. Fault examples

Venkatasubramanian and Rich (1988) simulated different faults in an attempt to examine the diagnostic abilities of an expert system called MODEX2 (Model Oriented Diagnostic Expert).

Table 4.2: Faults simulated in MODEX2 examination (Venkatasubramanian & Rich, 1988)

Incorrect SP	Valve stick
Sensor bias	Loss of signal from sensor to controller
Loss of control air to valve	Pipe blockage
Low tank level	Reactor leak

Faults listed in Table 4.2 are associated with a CSTR heat exchanger setup, and is

contained in a knowledge base which is connected to an inference engine which compares current operation with fault symptoms using MODEX2.

Himmelblau (1978) listed a number of faults found in a wide range of processes.

Table 4.3: Faults throughout a variety of processes (Himmelblau, 1978)

Poor distribution	Failure to follow operating procedure
Improper mixing	Stress on bearings and shafts
Hot spots	Materials decomposition
Overheating	Defects in construction
Resonance	Improper lubrication
Blockage	Vortex generation
Sedimentation	Improper design
Adhesion	Catalyst poisoning
Surging	Instrument failure
Syphoning	Sticking valves
Leakage	Contaminants
Spillage	Human error
Power failure	Climate effects

Table 4.3 shows possible faults for a variety of processes, and may differ significantly from process to process.

Raza and Liyanage (2009) mention different critical pump faults found in an offshore oil gas production facility.

Table 4.4: Pump faults within offshore oil and gas facility (Raza & Liyanage, 2009)

Cavitation	Leakage
Defective bearings	Seal failure
System head > design head	SG too high
Viscosity too high	Internal wear
Misalignment	Deviation from best efficient point

Faults listed in Table 4.4 could cause improper pump operation and even lead to equipment damage. Three months of data were used by Raza and Liyanage (2009) in attempt to identify occurrences of these faults using fault identification techniques. Note that cavitation in this case is identified as a fault compared to being a symptom in Table 4.1. If the symptom itself causes abnormal unwanted process deviation it could be considered as a fault. For example, impeller cavitation in a cooling water pump could result in inadequate cooling which causes a runaway reaction.

Himmelblau (1978) listed a further 89 faults found within centrifugal pumps. A few of these faults are listed in Table 4.5.

Table 4.5: Centrifugal pump faults (Himmelblau, 1978)

Air entering pump during operation	Insufficient speed
Incorrect rotation direction	Available NPSH too low
Leakage	Viscosity too high
Casing partially clogged	Impeller damaged
Impeller incorrectly assembled in casing	Obstruction in suction and/or discharge piping
Foot valve clogged	Incorrect layout of suction and/or discharge piping
Oversized impeller	Misalignment of pump and driver
Mechanical seal improperly installed	Bent shaft
Rotating elements not balanced	Improper lubrication of bearings
Worn bearings	Gland too tight

Lees (1976) provided a substantial amount of information regarding instrumentation faults on three different chemical plants. A condensed version is given in Table 4.6.

Table 4.6: Instrumentation faults (Lees, 1976)

Control valves		Thermocouples
Leakage	Failure to shut off power	Element faults
Not opening/Not closing	Glands repacked/Tightened	Pocket faults
Blockage	Diaphragm faults	
Valve greased	Sticking/Seized	

Koscielny and Bartys (2000) listed a wide variety of actuator faults which were used within the Development and Application of Methods for Actuator Diagnosis in Industrial Controls Systems (DAMADICS) Fault Detection and Isolation (FDI) benchmark study (Bartys et al., 2006).

Table 4.7: Actuator faults used in DAMADICS benchmark study (Koscielny & Bartys, 2000)

Valve clogging	Valve or valve seat sedimentation
Valve or valve seat erosion	Increase of valve friction
External leakage	Internal leakage
Liquid evaporation or critical flow	Twisted servo-meter stem
Driving force housing or terminal tightness	Driving force diaphragm perforation
Driving force spring fault	Electro-pneumatic transducer fault
Step displacement sensor fault	Air supply pressure sensor fault
Positioner spring fault	Positioner supply pressure drop
Unexpected pressure change across valve	Fully or partly opened bypass valves
Flow rate sensor fault	Pressure sensor fault

Anyakora (1971) created a list of actuator and valve faults using plant record data.

Table 4.8: Control valve faults (Anyakora, 1971)

PTFE chevron rings too tight in gland	Diaphragm failure
Blockage in body	Blockage in valve
Poor fit of plug and seat	Seat joint fracture
Vibration and hydraulic hammering	Internal corrosion
Packing worn out	PTFE material wedged under valve seat

Several faults are reported by Downs and Vogel (1993) in the well-known Tennessee Eastman reactor and separator process.

Table 4.9: Faults within a reactor and separator process (Downs & Vogel, 1993)

Feed compositions	Feed temperatures
Reactor cooling water inlet temperature	Condenser cooling water inlet temperature
Feed loss	Reaction kinetic drift
Reactor cooling water valve sticking	Condenser cooling water valve sticking

Several events listed in Table 4.9 could be considered as minor disturbances if they were to occur in other processes due to expected negligible effect they would have on process performance.

Finch et al. (1990) used a CSTR setup with numerous faults in order to test a fault diagnostic system namely MIDAS (model-integrated diagnostic analysis system). A program was written to simulate 109 different malfunctions which included blockages, leaks, heat transfer faults, reaction faults, valve malfunctions, controller malfunctions, variation at process boundaries, and sensor failures. The rapidity and extent of faults were tuneable parameters, and were specified with random values.

It becomes evident from literature that numerous faults occur in industrial processes (Himmelblau, 1978; Koscielny & Bartys, 2000; Finch et al., 1990). This is not limited to large and complex processes, for instance, Himmelblau (1978) listed 89 faults only within centrifugal pumps and Koscielny and Bartys (2000) listed over 20 actuator faults. Certain faults seem to be present over a wide range of processes – not being limited to a certain industry. Some of the faults listed previous are therefore expected to occur at Western Platinum BMR.

A fault database could serve as a way to capture and summarise all the fault characteristics. The fault database could then assist in manual fault diagnosis, and possibly automated fault diagnosis and detection. A fault detection and diagnostic system could serve as a tool which notifies personnel in the early stages of a fault, which allows the timely recovery of a process.

4.4. Control Performance Assessment

Zevenbergen et al. (2006) discussed several case studies where control performance assessment (CPA) techniques were implemented in industrial processes. The CPA techniques uncovered and diagnosed several faults. Corrective actions resulted in major process profitability increases. This section's goal is to obtain several ways to quantify the extent of control performance degradation during the occurrence of faults.

Jelali (2006) defines CPA as an evaluation of a variety of statistics that reflect process performance over a specific period of time, and is often used in the industry to evaluate control loops in order to maintain efficient operation of automated systems. Poor control performance could be caused by inadequate controller tuning; inappropriate control; lack of maintenance, equipment malfunction, or poor design which results in faults.

Statistics often used in CPA are divided into two variations of key performance indicators (KPI) namely control KPIs and operational KPIs. Control KPIs include a wide range of measures which indicate different controlled variable characteristics. Operational KPIs are plant specific measures which are not controlled in a loop, but need to be constrained or manually controlled in order to ensure effective operation.

4.4.1. Control key performance indicators

Marlin (1995) groups control KPIs into disturbances and set-point changes. Disturbance control KPIs are the measures of a controller's ability to cope and keep a controlled variable at a set-point during unaccounted changes in the process. Set-point change control KPIs are the measures of a controller's ability to adjust a controlled variable to a new user-defined value. The project scope includes assessing control performance during the occurrence of a variety of faults and disturbances. Control performance measures based on set-point changes will therefore not be discussed further. Refer to Marlin (1995) for more information regarding this topic.

It is crucial for control systems to compensate for disturbances in order to avoid significant controlled variable variation. Control KPIs for disturbances include (Marlin, 1995; Seborg et al., 2004; Gerry, 2005; Thornhill et al., 2003; Zevenbergen et al., 2006):

1. Integral error measures
2. Maximum controlled variable deviation
3. Mean of controller error; standard deviation of controller error
4. Mean of controller output; standard deviation of controller output

5. Time in normal
6. Harris index
7. Noise band
8. Oscillation index
9. Valve at a limit
10. Travel distance
11. Valve reversals
12. Time not at set-point

Integral error measures are quantitative methods of describing the cumulative deviation of the controlled variable from its set-point during unsteady-state conditions. Several versions of integral error measures exist, namely integral absolute error (IAE), integral of square error (ISE), integral of product of time (ITAE), and integral error (IE):

$$IAE = \sum_t |SP(t) - CV(t)| \Delta t \quad \text{Equation 4.1}$$

$$ISE = \sum_t (SP(t) - CV(t))^2 \Delta t \quad \text{Equation 4.2}$$

$$ITAE = \sum_t t \times |SP(t) - CV(t)| \Delta t \quad \text{Equation 4.3}$$

$$IE = \sum_t (SP(t) - CV(t)) \Delta t \quad \text{Equation 4.4}$$

IAE is a quantitative measure which is easy to interpret as it is a sum of all the areas above and below the set-point. ISE is often used when large deviations cause much larger process degradation. ITAE penalises errors that endure for long times. IE is not normally used as a KPI since the positive and negative errors cancel.

Maximum controlled variable deviation shows how far the controlled variable moves away from its set-point due to the occurrence of a disturbance. This performance indicator is sensitive to dead time between the manipulated- and controlled variable.

Seborg et al. (2004) and Gerry (2005) reports the use of both the mean and standard deviation for control error and controller output.

$$\overline{MV} = \frac{1}{N} \sum_t MV(t) \quad \text{Equation 4.5}$$

$$s = \sqrt{\frac{1}{(N-1)} \sum_t (\overline{MV} - MV(t))^2} \quad \text{Equation 4.6}$$

Equation 4.5 and Equation 4.6 represents the controller output mean and standard deviation, respectively. These equations can also be applied to controller error by simply replacing the manipulated variable with the difference between the controlled variable measurement and set-point.

Seborg et al. (2004) and Gerry (2005) defines time in normal as the fraction of time the controller is operated in its intended mode. Operators often operate cascade controllers in a manual configuration (McCulloch et al., 2014). Low time in normal indicates that the normal controller outputs are unsatisfactory and requires attention.

The Harris index is defined as the ratio between control error variance divided by a minimum variance controller (i.e. theoretically best achievable variance in a feedback controller (Harris, 1989)). Harris index values vary between one and infinity, with one being perfect control with minimum variance. The index rises as the loop performance decreases.

Gerry (2005) defines noise band as the standard deviation of a controlled variable during the quietest time. These variations are often associated with electrical interference, magnetic fields, flow turbulence loops, waves in a tank in level loops and more. Larger noise bands generally lead to poorer control performance.

An oscillation index analyses the error signal for recurring patterns in an attempt to determine if oscillations are present (Gerry, 2005). Control loops that are oscillating typically result in either high energy costs, quality problems, or an unstable process (Zevenbergen et al., 2006).

Valve at a limit is defined as the total time, maximum time, or number of times at which the valve is saturated. Large values indicate that the current control configuration is inadequate for the control problem at hand.

Valve travel distance indicates the total distance a valve has travelled within a certain time. Large valve travel values might indicate aggressive control which could lead to valve degradation. Travel distance could also be used as a controlled variable KPI since it can

identify ineffective controllers unable to keep a variable at its set-point. The valve reversal control KPI is a count of how many times a valve changed direction. This is also an indication of control aggression. High valve reversals tend to be unwanted, and could be indicative of high static friction within the valve internals resulting in valve sticking and jumping behaviour (i.e. valve stiction).

4.4.2. Operational key performance indicators

Gerry (2005) reports the use of thresholds and economic significance in CPA, which can be classified under operational KPIs. Thresholds are typically bounds which should not be surpassed in order to avoid possible hazardous or unwanted operating conditions. These thresholds are process specific and could include temperature, pressure, concentration, level or density bounds. Downs and Vogel (1993) report having temperature, pressure and level thresholds for a reactor in the Tennessee Eastman process.

Economic significance is used in the industry when monetary and control correlations can be drawn. However, these correlations require in-depth process knowledge and tend to be difficult to establish (Bauer & Craig, 2008). Bauer and Craig (2008) conducted a web survey on the economic significance of improved process control which included 60 industrial expert cases. Main profit contributors are given below. Zevenbergen et al. (2006) report similar operational KPIs.

1. Throughput increase
2. Process stability improvement
3. Energy and utility usage reduction
4. Increase in yield
5. Quality giveaways reduction
6. Downtime reduction
7. Better use of raw materials
8. Reprocessing reduction
9. Responsiveness increase
10. Safety increase
11. Operating manpower reduction

Improving throughput would be beneficial if the additional quantities can be sold at the same price as normal throughput. Process stability improvement ensures product consistency and that it meets customer requirements. Energy consumption in many industrial applications is a large expense; reducing the energy consumption would therefore be beneficial. Increase in yield and reducing quality giveaway ensures an increase in valuable products to be sold.

Reducing downtime will in essence ensure a larger throughput. It is reported that improved use of raw materials and the reduction of reprocessing under the correct circumstances could lead to profit increases. It is further reported that increasing responsiveness and safety of personnel while reducing operating manpower could be economically beneficial.

It is expected that Western Platinum BMR would have similar operational KPIs as what is reported by Bauer and Craig's (2008), as they improve the economic position of the company if implemented correctly.

CHAPTER 5: PROJECT OBJECTIVES AND TASKS

Chapter 4 provided literature on each of the project objectives with the aim of obtaining usable tools to address them.

This chapter aims to refresh and elaborate on project objectives introduced in Chapter 1. Each project objective is structured with several tasks which need to be met. Tasks will make reference to tools obtained from the literature review.

At the end of this chapter the project aims and objectives should be clearly defined. The use of the literature review in addressing project objectives should be clear. This will pave the way forward for developing structured research methodologies within upcoming chapters.

Formal definitions of project objectives are given as follow:

1. Validate and verify the open-loop second and third stage pressure leach Simulink™ baseline model using approaches defined by Sargent (2005).
2. Model and implement several critical control layers namely regulatory control, alarm systems, safety interlock systems and supervisory control.
3. Develop and simulate a fault database which includes a variety of fault characteristics obtained from several information sources.
4. Assess the control performance on its ability to mitigate a variety of fault scenarios using important control KPIs and operational KPIs.

Figure 5.1 shows how project objectives are divided into tasks.

Several techniques listed in the literature review will be used in model validation. Validation of batch experimental data will act as a first assessment of reaction kinetics currently implemented before considering the rate expressions. The validity of process data will also be investigated before operational validation can commence. The accuracy of the baseline model cannot be evaluated if the process itself produces incorrect data. Necessary model improvements will be made and a summary of problem areas will be used to conclude on the overall model validity.

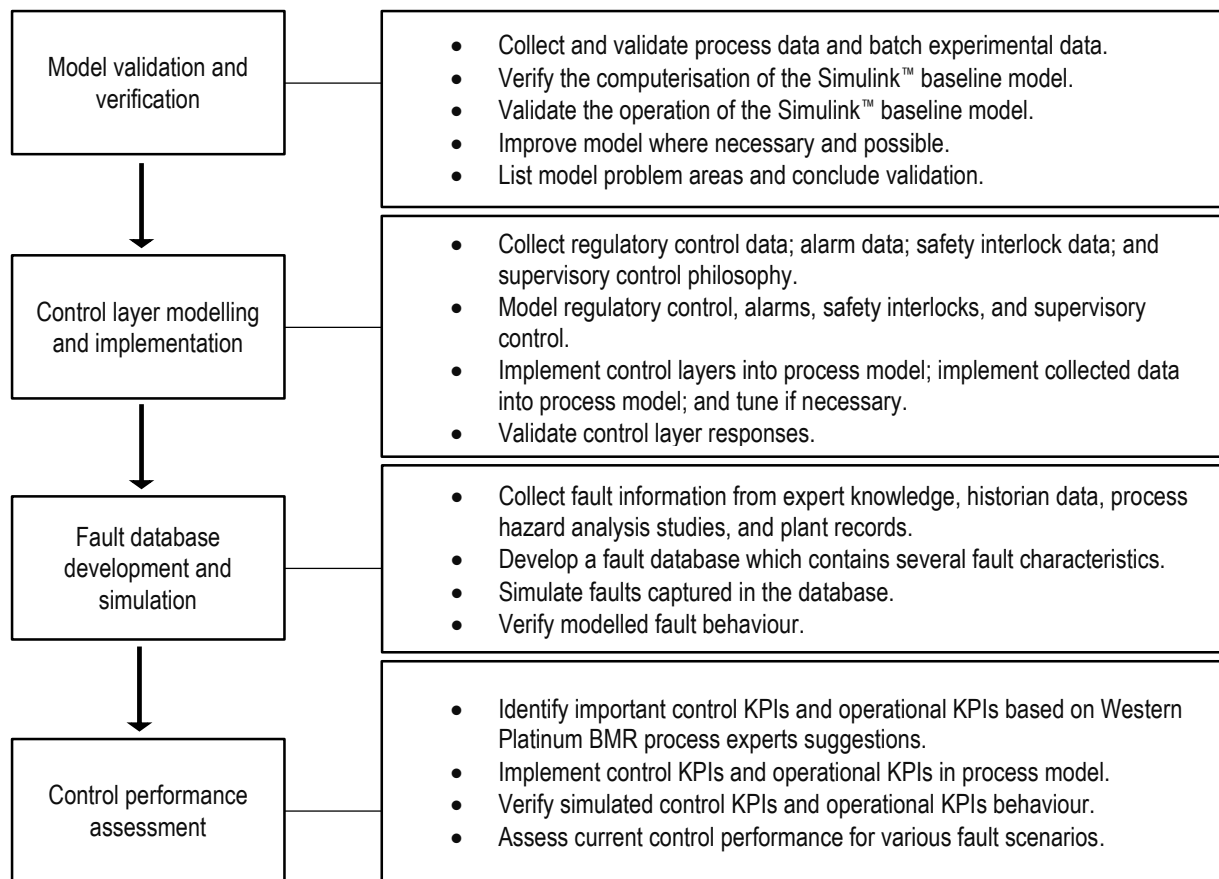


Figure 5.1: Project objectives divided into tasks

Control layers illustrated by Marlin (1995) will be modelled and implemented into the Simulink™ model in conjunction with Western Platinum BMR control information. Tuning of feedback and supervisory controllers might be required.

A fault database with a comprehensive list of fault characteristics revealed in the literature review will be developed. Information will be obtained from expert knowledge, historian tag data, process hazard analysis studies, and plant records. Faults will be modelled if they fit within the current model resolution. The fault dynamics will be validated.

Expert knowledge will be used to identify critical control- and operational KPIs. These KPIs will be implemented in the Simulink™ model. All simulated faults will be used to individually perturb the process model and values for critical KPIs will be reported.

The objectives will be undertaken in the sequence indicated in Figure 5.1. Subsequent chapters cover an individual project objective.

CHAPTER 6: MODEL VERIFICATION AND VALIDATION

Chapter 5 formally defined all project objectives and divided them into several tasks.

This chapter reports on the validity of the Simulink™ dynamic process model. The validation and verification approach developed by Sargent (2005) is used. This approach reviews the validity of several aspects of the model, namely: data validity, conceptual validity, computerised veridicality and operational validity.

Model validity conclusions were made after considering 34 dynamic process model issues. It was concluded that the reaction kinetics used within the baseline dynamic process model might cause inaccurate leaching predictions due to issues existing in batch experimental data. Most of the other issues which affect the model predictability were addressed in this project. The dynamic process model is valid for predicting general process behaviour, but invalid for extent of leaching predictions.

6.1. Overview

The validation of the dynamic process model developed by Dorfling (2012) and subsequently improved by Haasbroek and Linder (2015) is required in order to build trust in the model predictability. The validation process will also provide an indication of necessary dynamic process model improvements that are required.

The dynamic process model was intended to be used as a basic tool in assisting the prediction of autoclave behaviour. This will form the basis on which it is validated. The Simulink™ dynamic process model (Haasbroek & Lindner, 2015) forms the baseline for the verification and validation procedure. All categories in Sargent's (2005) validation approach are applicable in this model, and will be used in the validation process.

The final section of the Dynamic Model Description chapter summarises assumptions made by Dorfling (2012) during the development of the dynamic model. The validation of all of these assumptions is considered in this chapter, and is listed once again:

A1. Copper cementation reactions were assumed to be negligible.

- A2. All iron ions were assumed to be ferric, and the reduction mechanism of ferric to ferrous ions was excluded.
- A3. Initiation of PGM leaching reactions were assumed to occur only when 99 % of digenite entering the second stage slurry preparation tank was leached.
- A4. Sampling affects the rate of reactions.
- A5. Batch experiment acid concentrations were similar to that of the actual process.
- A6. Rate expressions were assumed to be directly scalable to larger process units (i.e. rate expressions have intensive properties).
- A7. Rate expressions were assumed to be directly transferable to a continuous process (i.e. initial concentrations in batch reactor kinetics are undefined in a continuous process).
- A8. Oxygen concentration within the liquid was assumed to be equal to the maximum oxygen solubility limit.
- A9. Digenite and covellite leaching reactions were assumed to be mass transfer limited.
- A10. PGM-oxide shape factors were assumed to be infinite (i.e. very large surface area to volume ratios).
- A11. The amount of experimental data points was assumed sufficient in determining the amount of parameters.
- A12. Sum of square concentration error objective function was assumed to be sufficient for the optimisation problem.
- A13. The dynamic model was assumed to have zero degrees of freedom.
- A14. Temperature and composition of input stream 1, 2, 3, 4, 18, 19 and 20 were assumed to stay constant.
- A15. All preparation tanks were assumed to be isothermal.
- A16. The total mass inside all autoclave compartments were assumed to stay constant.
- A17. The autoclave was assumed to be isobaric.
- A18. Addition of water and sulphuric acid directly to the flash recycle tank was excluded.
- A19. All process units were assumed to have ideal CSTR characteristics.
- A20. It was assumed that no reactions are occurring inside auxiliary units.
- A21. A constant shaft work and heat loss was assumed for process units.
- A22. A single flash recycle tank and autoclave set was assumed to describe the leaching process.

A reference index is provided in the table below. This table can be used to associate a subsection heading with an assumption number. The reference index is useful since not all subsections within the model validation chapter deals with explicit assumptions.

Table 6.1: Model verification and validation reference index

Validation and verification category	Subsection	Assumption
Data validation	6.2.1. Ion concentration adjustments in batch experimental data ♣	A4
	6.2.2. Acid concentrations in batch experimental data ♣	A5
	6.2.3. Ion concentration variation in batch experimental data♣	-
	6.2.4. Physically realisable checks on plant data ♣	-
	6.2.5. Mass and energy balances on plant data ♣	-
	6.2.6. Data reconciliation on plant data ♣	-
	6.2.7. Global test on plant data ♣	-
	6.2.8. Measurement test on plant data ♣	-
Conceptual model validation	6.3.1. Copper cementation reactions ♦	A1
	6.3.2. Ferric to ferrous ion reduction mechanism influence ♦	A2
	6.3.3. PGM leaching reaction initiation ♦	A3
	6.3.4. Rate expressions scaled to large process units ♦	A6
	6.3.5. Initial concentrations in a continuous process ♦	A7
	6.3.6. Dynamic process model oxygen solubility estimation ♦	A8
	6.3.7. Mass transfer limits digenite and covellite leaching reactions ♦	A9
	6.3.8. PGM-oxide shape factors with infinite size♦	A10
	6.3.9. Data point/parameter ratio in reaction kinetic optimisation ♦	A11
	6.3.10. Objective function used in reaction kinetic optimisation ♦	A12
	6.3.11. Reaction kinetics optimisation ♦	-
Computerised model verification	6.4.1. Static testing ♦	-
	6.4.2. Dynamic testing ♦	-
Operational validation	6.5.1. Degree of freedom analysis ♦	A13
	6.5.2. Constant temperature and composition inputs ♦	A14
	0. The natural change in model inputs via random walks	A15
	6.5.4. Constant mass in all autoclave compartments ♦	A16
	6.5.5. Isobaric autoclave ♦	A17
	6.5.6. Sulphuric acid and water streams entering flash recycle tank ♦	A18
	6.5.7. Ideal CSTR characteristics ♦	A19
	6.5.8. No reactions in auxiliary tanks♦	A20
	6.5.9. Constant agitator work and heat loss ♦	A21
	6.5.10. Single flash recycle tank/autoclave set ♦	A22
	6.5.11. Extreme condition testing ♦	-
	6.5.12. Face validation ♦	-
	6.5.13. Dynamic process model predictability♦	-

Legend			
Validation of:	♣ Plant data	♠ Batch experimental data	♦ Dynamic process model feature
Validation using:	Plant data	Batch experimental data	Literature

The type of validation and the information used in the validation process is also shown for each subsection.

The batch experimental data in Table 6.1 refers to that used by Dorfling (2012) in the fitting of reaction kinetics. Many of the subsections listed in Table 6.1 required plant data for validation purposes. Several sets of Western Platinum BMR historian data were obtained during a recent site visit (McCulloch et al., 2014). A summary of the historian data sets are captured in Table 6.2.

Table 6.2: Available historian tag data sets

Data set	Start date	End date	Time length (days)	Interval size (min)
<i>Low resolution, High timespan</i>				
1	01-Oct-13	28-Sep-14	362	25
2	01-Oct-12	01-Aug-13	304	25
3	01-Oct-11	28-Sep-12	363	25
4	01-Nov-10	01-Sep-11	304	25
<i>Medium resolution, Medium timespan</i>				
5	01-Oct-14	24-Oct-14	23	5
6	01-Oct-12	31-Oct-12	30	5
<i>High resolution, Low timespan</i>				
7	06-Jan-14	07-Jan-14	1	1
8	03-Feb-14	04-Feb-14	1	1
9	06-Mar-14	07-Mar-14	1	1
10	19-Apr-14	20-Apr-14	1	1
11	11-May-14	12-May-14	1	1
12	07-Jun-14	08-Jun-14	1	1
13	30-Jul-14	31-Jul-14	1	1
14	10-Aug-14	11-Aug-14	1	1
15	06-Sep-14	07-Sep-14	1	1
16	07-Oct-14	08-Oct-14	1	1
17	13-Jan-13	14-Jan-13	1	1
18	18-Feb-13	19-Feb-13	1	1
19	28-Mar-13	29-Mar-13	1	1
20	15-Apr-13	16-Apr-13	1	1
21	09-May-13	10-May-13	1	1
22	19-Jun-13	20-Jun-13	1	1
23	28-Jul-13	29-Jul-13	1	1
24	02-Aug-13	03-Aug-13	1	1
25	19-Sep-13	20-Sep-13	1	1
26	04-Oct-13	05-Oct-13	1	1
27	28-Nov-13	29-Nov-13	1	1
28	19-Dec-13	20-Dec-13	1	1

Each data set in Table 6.2 contains data for 338 tags, including all tags found on P&ID's for both autoclave 200 and autoclave 300 in Appendix E. Data sets contain controller set-points; sensor present-values; and controller outputs. A variety of time resolutions; time lengths; and

dates were recorded for different uses and purposes. Manually measured data were also obtained (refer to Table 6.3).

Table 6.3: Available manually measured data sets

Start date	End date	Time length (days)	Interval size (min)
<i>Compositions</i>			
10-Oct-13	28-Sep-14	353	480
01-Oct-12	01-Oct-13	365	480
01-Oct-11	02-Aug-12	306	480
01-Nov-10	04-Oct-11	337	480
<i>Densities</i>			
01-Oct-14	24-Oct-14	23	60
01-Oct-12	01-Nov-12	31	60

Compositional data for each entry in Table 6.3 include the first stage leach residue; second stage leach residue; second stage leach filtrate; third stage leach residue; and third stage leach filtrate. Density data include that of the first stage slurry preparation tank outlet; the flash recycle tank outlet; and the third stage slurry preparation tank outlet.

The validation process in accordance with Table 6.1 will now be followed.

6.2. Data Validation

Sargent (2005) states that data are required for three purposes: to build a conceptual model, to validate a model, to perform experiments with the validated model. The validity of data used for the former two purposes are addressed in this section:

1. Validation of batch experimental data used by Dorfling (2012) to produce the reaction kinetics which appear in the dynamic process model.
2. Validation of BMR plant data which is ultimately used to verify dynamic model outputs.

The validation of batch experimental data is firstly considered by addressing a few assumptions. This is followed by the validation of BMR plant data by using several techniques.

6.2.1. Ion concentration adjustments in batch experimental data

Problem statement and methodology

Data obtained from experimentation often requires transformation before it is in a usable form. Sargent (2005) states that the techniques used to transform data should also be validated. The ion concentration adjustments made by Dorfling (2012) on batch experimental data is one such case.

Dorfling (2012) used the following equation to adjust all experimentally determined ion concentration measurements to compensate for sampling sizes:

$$C_{i,j}^* = \frac{(V - \sum_{b=1}^{j-1} V_{sample,b}) \times C_{i,j} + \sum_{b=1}^{j-1} (V_{sample,b} \times C_{i,b})}{V} \quad \text{Equation 6.1}$$

where $C_{i,j}^*$ refers to an adjusted concentration of species i for sample number j . V and $V_{sample,b}$ represent the initial solution volume and sample b volume, respectively.

Issues associated with the validity of Equation 6.1 are investigated, and an alternative solution is provided.

Results and discussion

A mole balance is present in the numerator of Equation 6.1. The first term in the numerator is used to calculate the mole amount of component i in the autoclave at sample number j . The second term in the numerator is used to calculate the mole amount of component i which is removed from the autoclave due to the sum of samples. The mole balance is divided by the total volume to produce an adjusted concentration $C_{i,j}^*$. Equation 6.1 is invalid since the second term in the numerator adds static mole amounts of samples which do not take part in further reactions.

The effect that sampling has on reaction kinetics is investigated in order to determine if sample adjustments are in fact required. Consider the initial mole balance across a batch reactor which is used in the derivation of Equation 3.1:

$$\frac{dn_k}{dt} = \sum_j v_{k,j} A k_j \prod C_{i,j}^{\alpha_{i,j}} - C_k \dot{V}_{sample} \quad \text{Equation 6.2a}$$

where \dot{V}_{sample} represents the volumetric flow rate of a sample. The generic rate expression was substituted into Equation 6.2a for the purpose of clarifying upcoming statements. Equation 6.2a can be converted to Equation 6.2b by applying a product rule after substituting the mole amount with a reactor volume and concentration:

$$\frac{dC_k}{dt} = \frac{\sum_j v_{k,j} A k_j \prod C_{i,j}^{\alpha_{i,j}}}{V} - \frac{C_k}{V} \dot{V}_{sample} - \frac{C_k}{V} \frac{dV}{dt} \quad \text{Equation 6.2b}$$

The third term in Equation 6.2b cancels out with the second term since they have the exact same size with opposite signs (i.e. the sample volumetric flow rate and the batch reactor volume differential has an equal size but opposite sign). The first term in Equation 6.2a therefore describes the change in component concentration, irrespective of reactor volume size. The effect that significant sample sizes have on variables within the first term of Equation 6.2b is captured in Figure 6.1.

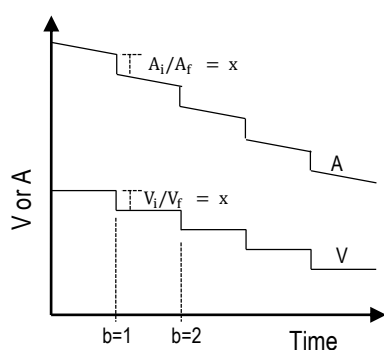


Figure 6.1: Effect of significant sample sizes on the volume and area of a batch reactor

All samples taken during experiments are assumed to be homogenous. Equal extents of total surface area and volume change are therefore expected when samples are taken (refer to the equal ratios of volume and surface area change in Figure 6.1). Equation 6.2b is therefore independent of sampling as it is not affected by varying volume. Note that Figure 6.1 shows a decrease in total surface area as time progresses; however, similar conclusions can be made for increasing surface areas. Choo et al. (2006) developed concentration adjustments to take into account sampling volumes, but did not consider total solid surface area changes.

The errors induced after adjusting batch experimental concentrations are summarised in Table 6.4. The error is defined as the absolute percentage change between the adjusted

and unadjusted concentration (the percentage change is in this case relative to the unadjusted concentration).

Table 6.4: Error induced by sample adjustments

	Fe ³⁺	Ni ²⁺	Cu ²⁺	Ru ³⁺	Rh ³⁺	Ir ³⁺
Average error (%)	1.40	2.09	2.17	3.95	7.86	3.59
Maximum error (%)	2.98	3.58	9.29	11.53	242.53	9.53

The average percentage error is relatively low for all species. There are however situations where the adjustments did induce large errors, for example the maximum error of Rh³⁺. This extremely large error occurred due to the cementation behaviour of Rh³⁺ in the initial stages of an experiment. Free Rh³⁺ ions which enter in the electrolyte are initially cemented via Reaction 7 and Reaction 10. The large error occurred when a sample was taken which still contained a large amount of Rh³⁺ ions, and subsequently added to an autoclave liquid via Equation 6.1 containing almost no Rh³⁺ ions.

Proposed model updates

Ion concentration adjustments in batch experimentation are related to the dynamic process model through the quality of the reaction kinetic fit. Re-fitting of reaction kinetics is therefore required in order to improve the current state of the dynamic process model. Unchanged concentrations were used in the optimisation of several versions of reaction kinetics, which is considered in Section 6.3.11.

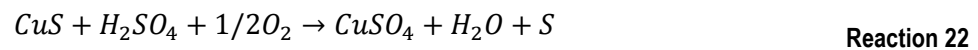
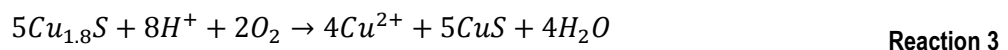
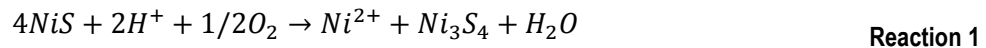
6.2.2. Acid concentrations in batch experimental data

Problem statement and methodology

One concern that is highlighted by Sargent (2005) when considering the requirements of data is the appropriateness of the collected data. The collected data, when used to build a conceptual model, should correspond with the problem entity. A discrepancy issue between batch experimental data and Western Platinum BMR operation is addressed here.

A typical sulphuric acid concentration of 35 g/l is used in the autoclaves at Western Platinum BMR. Dorfling (2012) had to conduct batch experiments in the same acid concentration regions in order to reproduce the autoclave conditions. Dorfling (2012) theoretically calculated the necessary initial acid concentrations so as to produce a final acid concentration around 35 g/l. Dorfling (2012) made the following assumptions in order to calculate the theoretical amount:

- All the nickel present in the first stage leach residue is in the form of millerite, and leaches according to Reaction 1.
- All the copper present in the first stage leach residue is in the form of digenite, and leaches according to Reaction 3.
- Covellite produced in Reaction 3 leaches according to Reaction 22.



Reaction 22 represents a covellite leaching mechanism in which both oxygen and sulphuric acid are consumed. Dorfling (2012) reasoned that covellite could leach simultaneously according to Reaction 22 and Reaction 6 at high sulphuric acid concentrations. However, Reaction 22 was excluded from Dorfling's (2012) final reaction kinetics since Western Platinum BMR does not operate under high acid concentrations. Reaction 6 was therefore the only covellite leaching mechanism within the reaction kinetics developed by Dorfling (2012). However, Dorfling (2012) incorrectly used Reaction 22 instead of Reaction 6 in initial acid concentration calculations, which resulted in a much higher initial acid concentration than intended. The high initial acid concentrations were used by Dorfling (2012) within batch experimentation, which affects the consistency between the conditions used in batch experimentation compared to that of Western Platinum BMR operation.

The rate expressions developed by Dorfling (2012) are captured in Appendix D. These rate expressions were reproduced in MATLAB™ (refer to Section 6.3.11 for reproducibility) and used within 21 component mole balance ODEs (see Equation 3.1). The reproduced MATLAB™ model allows one to predict concentration trends for all 21 components after providing the necessary initial conditions including temperature, solid loading, liquid composition and solid composition.

The initial conditions of Dorfling's (2012) batch experiments is used in the MATLAB™ model to determine expected acid concentration trends using the ODE45 solver in MATLAB™. Discrepancies between the intended acid concentrations and the model-predicted acid

concentrations are reported. The issues associated with using highly acidic batch experimental conditions to determine Western Platinum BMR leaching kinetics is discussed.

Results and discussion

The actual acid concentrations were not measured by Dorfling (2012) during batch experimentation. The model-predicted acid concentrations for all the experiments conducted by Dorfling (2012) are given below.

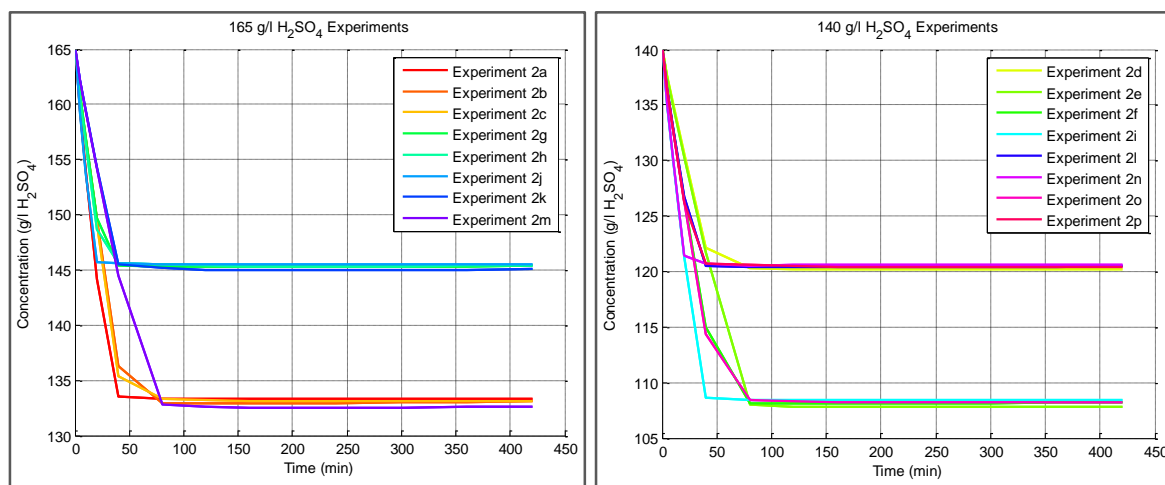


Figure 6.2: Model predicted acid concentration for high (left) and low initial acid concentrations (right)

Note that the H₂SO₄ concentration shown in Figure 6.2 is in actual fact the remaining H⁺ concentration expressed as H₂SO₄. The acid concentration was conveyed in this way since the BMR quantifies it in this manner (McCulloch et al., 2014).

The grouping of acid concentration trends seen in both the left and right side of Figure 6.2 is attributed to the initial solid loading of the slurry. The initial solid loading directly affects the extent of acid consumption since it determines the amount of copper and nickel sulphide present in the experiment. The important characteristic that should be noted from Figure 6.2 is the high final acid concentrations. The lowest acid concentration predicted by Dorfling's (2012) final set of reaction kinetics, using the intended covellite leaching Reaction 6, is approximately 107 g/l. This concentration is much higher than the intended final 35 g/l. It is therefore expected that experiments proceeded at acid concentrations of 100 g/l and up.

Rard (1985) reports that the oxidation state of ruthenium moves from 3 to 4 when sulphuric acid concentrations reach values below 49 g/l. Significantly less Ru(IV) compounds are therefore expected under high acid concentrations (i.e. conditions used in batch experimentation), and vice versa (i.e. conditions used at Western Platinum BMR). A definite error therefore exists when attempting to describe the Western Platinum BMR PGM leaching

reactions by using the batch experimental data without including a redox couple between the two oxidation states (distinction between oxidation states were not made during experimentation conducted by Dorfling (2012), which limits the inclusion of redox couples). The errors are illustrated in Figure 6.3.

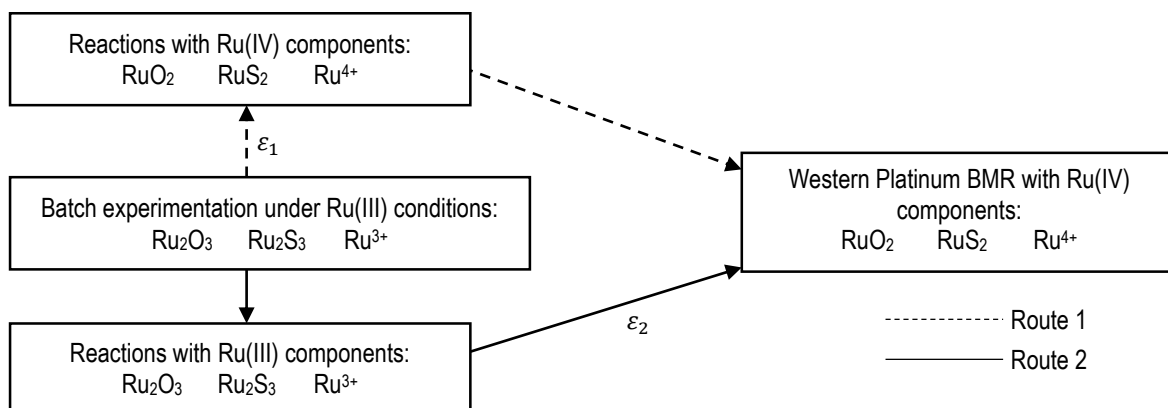


Figure 6.3: Approaches to PGM oxidation state issue

Two separate approaches exist in attempting to solve the ruthenium oxidation state issue without conducting new experiments. Each route will induce an error (ε) to the PGM leaching predictability since the acid concentration in batch experimentation is in fact inconsistent with that of Western Platinum BMR. The first route attempts to use reactions which incorporates Ru(IV) components to predict experimental data where Ru(III) components exist, which results in an error (ε_1). The second route uses different ruthenium reactions which correspond to what is expected in batch experiment results, but attempts to predict the Western Platinum BMR operation, causing an error (ε_2). Similar oxidation state issues could exist for other applicable OPMs and possibly other species as well. An entire underlying speciation model is required to describe the interchange of oxidation states and ionic charges. Both the benefits and possibility of modelling such a system requires further investigation. The issue captured in Figure 6.3 is faced if such a speciation model is excluded.

It is difficult to estimate the error sizes caused by following each approach mentioned in Figure 6.3 as it is dependent on the quality in which the reactions are fitted to the experimental data. It is expected that, if the kinetics were to fit experimental data well in both approaches, the first approach would result in a reduced accuracy for the Ru(IV) reaction set kinetic parameters since the reaction set is inconsistent with the reaction mechanisms occurring in batch experimental data (i.e. stoichiometry of components in reactions and atomic ratios within compounds). The second approach would result in more accurate kinetic parameters for the Ru(III) reaction set. However, the fall-back for using the second approach

would be that it would have a reduced Western Platinum BMR leaching predictability due to the inconsistency between the reaction mechanism model and what is occurring in the actual process.

Kanome et al. (1987) report that high sulphuric acid concentrations results in the formation of elemental sulphur via Reaction 22. This in turn reduces the extent and rate of copper and nickel leaching due to a sulphur layer forming over particles which inhibits mass transfer. Dorfling (2012) experienced a low extent of copper leaching during experiments, and attributed it solely to a reduction in oxygen solubility (refer to the nature of Equation D.5 to Equation D.8). The low extent in which copper was leached during the batch experimentation conducted by Dorfling (2012) could possibly be attributed to a sulphur layer formation. Another possibility would be the fact that high acid concentrations suppress oxygen solubility within the liquid phase, which ultimately limits the oxidation of base metals. This is expected to translate to underpredicted base metal leaching when the operation of the dynamic process model is considered.

Proposed model updates

The ruthenium oxidation state issue was addressed by suggestion two different approaches which do not require additional experimentation. The ruthenium predictability error sizes for the two approaches relative to one another are unknown. The extent to which the ruthenium oxidation state issue affects other areas of the dynamic process model (i.e. base metal leaching; autoclave temperatures etc.) is expected to be low, since ruthenium reactions occur significantly less than base metal leaching reactions. Reactions were therefore kept as is.

Batch experimental runs might have to be repeated in order to avoid the suppression of base metal leaching caused by the high sulphuric acid concentrations. The dynamic process model concentration predictability is considered in Section 6.5.13.

6.2.3. Ion concentration variation in batch experimental data

Problem statement and methodology

Dorfling (2012) measured six ion concentrations namely Fe^{3+} , Ni^{2+} , Cu^{2+} , Ru^{3+} , Rh^{3+} and Ir^{3+} prior to the start of 16 batch experiments. The ion concentrations prior to batch experiments indicate great variation even though they were taken from the same source.

The concentration variation within samples was quantified using a standard deviation calculation. The standard deviation of concentrations is compared to the average

concentrations in order to highlight the variation. The effect that the calculated concentration variation could have on the reaction kinetic fit to batch experimental is discussed.

Results and discussion

The standard deviations and averages of 6 ions calculated from 16 time-zero samples are presented in Table 6.5.

Table 6.5: Standard deviations and averages of time-zero samples (Dorfling, 2012)

	Fe ³⁺ (mg/l)	Ni ²⁺ (g/l)	Cu ²⁺ (g/l)	Ru ³⁺ (mg/l)	Rh ³⁺ (mg/l)	Ir ³⁺ (mg/l)
σ	107.49	1.45	3.12	11.70	3.91	1.68
\bar{x}	1117.25	20.94	32.43	153.47	10.10	27.91

Major sample deviations exist for most components when compared to their averages. The sample measurements also deviate more than what is reported in literature for the corresponding measurement techniques (AEG, 2015). These deviations are likely caused by a combination of measurement and sampling errors, and are expected to have occurred consistently throughout the batch experimentation conducted by Dorfling (2012).

Such variations in concentration are detrimental when fitting reaction kinetics, not only because the measurements are slightly inaccurate, but because common optimisation objective functions try to force a fit to all experimental data points equally, irrespective of the expected concentration variation. The latter issue can be countered by using an epsilon insensitive objective function (Zisserman, 2015; Scholkopf, 2015) during reaction kinetic optimisation, in contrast to a standard quadratic objective function as shown in Equation 3.7a. The epsilon insensitive objective function ensures a fit error of zero at a certain data point when the uncertainty of that measurement (i.e. the variation) overpowers the quality of its fit. Refer to Section 6.3.10 for a detailed description of an epsilon insensitive objective function.

Proposed model updates

The ion concentration variations is expected to affect the quality of the reaction kinetic fit developed by Dorfling (2012) as the variation was not taken into account in the objective function prior to the optimisation. Re-fitting of reaction kinetics to batch experimental is therefore required by making use of an epsilon insensitive objective function. The epsilon insensitive objective function is considered in Section 6.3.10 prior to the fitting of several reaction kinetic sets.

6.2.4. Physically realisable checks on plant data

Problem statement and methodology

The operation of a developed model can be validated by comparing its outputs to the behaviour of the problem entity. That is the second purpose of data mentioned by Sargent (2005), during model validation. The quality and accuracy of Western Platinum BMR data is examined in order to see if it is even possible to validate the dynamic process model.

Physically realisable checks as described in Sargent (2005) were applied to process data as a first step to plant data validation. This included checking for negative and unrealisable values. Several important process tags are considered which included at least one of each measured variable type. Data set 3 from Table 6.2 was used in these checks since it is the longest data set in which the autoclave under consideration was in operation. Sections of data were removed where the autoclave was clearly out of operation (evident from ambient temperatures and pressures within the autoclave). Limits for unrealisable values were estimated using controller set-point limits; high-high alarms; low-low alarms; valve characteristics and unrealisable constraints (for example, negative flow rates and slurry densities below 1 kg/l). Additional leeway was added to the previously mentioned limits to accommodate for realisable but infrequent values.

Results and discussion

The quality of plant data points were inspected by using physically realisable checks. This included checking if relevant data tags had values abnormally low or high. Missing values were also noticed during the inspection, and was added as a realisable check. The physically realisable check results are shown in the Figure 6.4.

The x-axes of graphs within Figure 6.4 show the total number of data points (14123 data points were available in this data set and used in physically realisable checks), while the y-axes show the different physically realisable checks that were considered. The number of data points failing the three separate checks for several tags are shown in each graph.

The first compartment temperature tag, TIC-3001, indicates the lowest total errors. All other temperature tags within the autoclave show similar results. The flash recycle tank level tag, LIC-0201, has the highest number of errors with unavailable entries dominating the total. It is speculated that this could have been caused by sensor malfunction or a historian reporting error. Other level tags show more issues related to values below and exceeding 0 % and 100 %, respectively. This is however only a small fraction of the total data points.

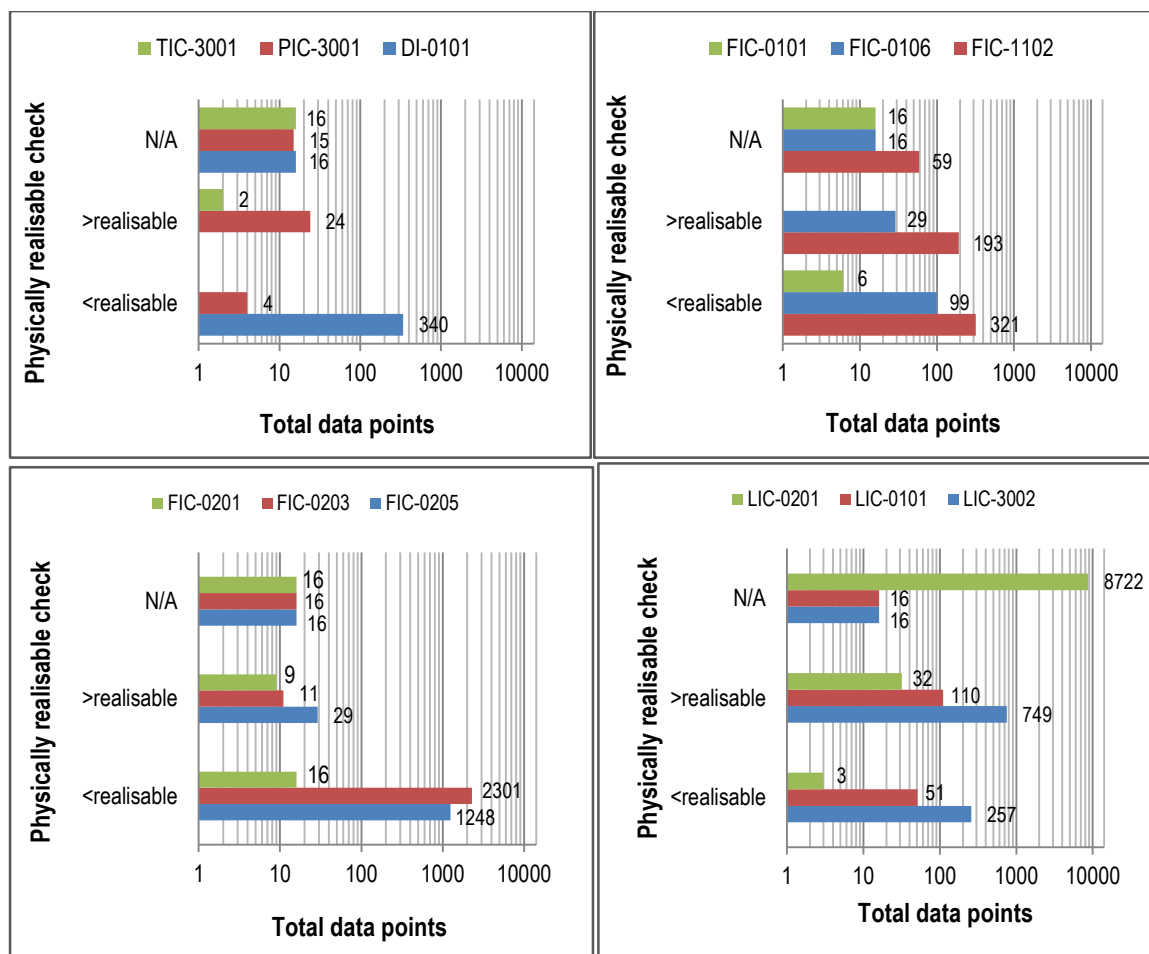


Figure 6.4: Physically realisable check results for several tags

The majority of flow tag errors consist of negative values. This serves as a red flag in conducting mass balances. Certain flow tags indicate much better data point quality than others, for instance, flow measurements surrounding the second stage slurry preparation tank (FIC-0101 and FIC-0201) compared to flow measurements between the flash recycle tank and first compartment (FIC-0203 and FIC-0205). The reduced quality of the latter two measurements could be caused by the fact that they generally have significantly higher mass flow rates together with a substantial solid loading, which causes increased sensor wear. McCulloch et al. (2014) attributes poor FIC-0205 data point quality to air pockets which form in this recycle stream. Most tags show consistently 16 unavailable data points. This could have been caused by a failure for the historian to capture 16 consecutive data points for all tags.

The quality of temperature and pressure data points within the autoclave seems to be very good. This is understandable since these variables should be precisely controlled to ensure the safety of personnel; protection of equipment; and consistent as well as on specification

product quality. Flow controllers show a wide range of measurement qualities with FIC-0101 and FIC-0203 representing the highest and lowest qualities, respectively.

Expert knowledge at Western Platinum BMR was used to create a hierarchy which describes the reliability of online measurements. The hierarchy is captured in the figure below (McCulloch et al., 2014). Variable measurements at the top of the triangle represent high reliability and vice versa.

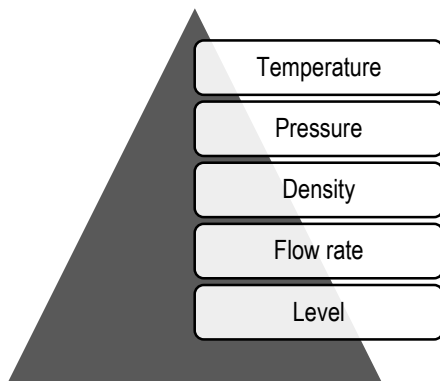


Figure 6.5: Online measurement reliability (McCulloch et al., 2014)

The reliability of online measurements according to expert knowledge at Western Platinum BMR corresponds with the quality of data points noticed from physically realisable checks. However, the quality of certain flow rate measurements seen in Figure 6.4 is worse than certain level measurements (for example, FIC-0203 compared to LIC-0101).

Note that no proposed model update section exists since the physically realisable checks simply attempts to determine the validity of Western Platinum BMR plant data. Valid plant data should ultimately be used to validate the dynamic process model behaviour. The quality of liquid and solid composition measurements at Western Platinum BMR should be further investigated in order to ensure accurate data when compositional predictions of the dynamic process model are validated.

Physically realisable checks highlighted the low quality of several flow rate measurements. These low quality flow measurements are expected to result in unsatisfied mass and energy balances which would classify the data as invalid. Mass and energy balances are considered in the subsequent section.

6.2.5. Mass and energy balances on plant data

Problem statement and methodology

Mass and energy balances within plant data should be consistent if the data is to be used as inputs to the dynamic process model when attempting to validate its predictions.

The following equation is a numerically integrated (i.e. trapezoidal integration) mass balance across a generic BMR process unit:

$$\sum_{t=t_0}^{t=t_f} 0.5 \times \left(\left[\left(\sum_{k=1}^n \dot{m}_k \right)_{in} - \left(\sum_{k=1}^m \dot{m}_k \right)_{out} \right]_t + \left[\left(\sum_{k=1}^n \dot{m}_k \right)_{in} - \left(\sum_{k=1}^m \dot{m}_k \right)_{out} \right]_{t+\Delta t} \right) \Delta t = [(\rho V)_{t_f} - (\rho V)_{t_0}] \quad \text{Equation 3.8c}$$

where the mass flow rate (\dot{m}_k) is calculated by simply multiplying the volumetric flow rate with the stream density. Equation 3.8c is numerically integrated from the initial time (t_0) to the final time (t_f) in time steps of size delta time (Δt), and is generalised for n and m streams flowing in and out of the process unit, respectively. The integration of Equation 3.8c was conducted over a long period of time where the vessel levels stayed approximately constant. This calculation resulted in large amount of unaccounted mass in the left hand side of Equation 3.8c. The unaccounted mass was significantly larger than the effects that a slight density change had on the right hand side of Equation 3.8c (also taking into account the negligible vessel volume change as previously mentioned). The right hand side of Equation 3.8c was therefore negligible. Equation 3.8c was arranged in order to express a residual in terms of a mass percentage error defined as follows:

$$\text{Mass error \%} = \frac{\sum_{t=t_0}^{t=t_f} 0.5 \times [(\sum_{k=1}^n \dot{m}_k)_t + (\sum_{k=1}^m \dot{m}_k)_{t+\Delta t}]_{in} - [(\sum_{k=1}^n \dot{m}_k)_t + (\sum_{k=1}^m \dot{m}_k)_{t+\Delta t}]_{out}}{\sum_{t=t_0}^{t=t_f} 0.5 \times [(\sum_{k=1}^n \dot{m}_k)_t + (\sum_{k=1}^m \dot{m}_k)_{t+\Delta t}]_{in}} \quad \text{Equation 6.3}$$

The error is defined as the total mass entering minus the total mass exiting, as seen in the numerator, over the total mass entering. A section of data set 5 was used in which the active vessel volume (V), derived from level sensor data, was approximately equal at the start and end. Equation 6.3 was applied across the first stage leach residue vessel and both flash recycle tanks. Volumetric flow rates were obtained from data set 5 and corresponding densities from Table 6.3. Densities are only measured hourly, and were extrapolated in a held-forward manner across other time intervals. The vapour stream mass flow rates exiting the flash recycle tanks are not measured, and were approximated by using the temperature of the first compartment and the corresponding flash recycle stream flow rate in an energy balance so as to produce a saturated liquid recycle stream at 100 °C. The effect of the

vapour stream estimations on mass balance errors are highlighted during the discussion. An instantaneous mass balance error simply compares the total flow rate in and out derived using a similar approach as Equation 6.3, and is included in the results.

The following equation is a numerically integrated energy balance across a generic BMR process unit:

$$\sum_{t=t_0}^{t=t_f} 0.5 \left(\left[\left(\sum_{k=1}^n \dot{m}_k \hat{H}_k \right)_{in} - \left(\sum_{k=1}^m \dot{m}_k \hat{H}_k \right)_{out} + E \right]_{t+\Delta t} + \left[\left(\sum_{k=1}^n \dot{m}_k \hat{H}_k \right)_{in} - \left(\sum_{k=1}^m \dot{m}_k \hat{H}_k \right)_{out} + E \right]_{t} \right) \times \Delta t = [\rho V \hat{H}_{vessel}]_{t_f} - [\rho V \hat{H}_{vessel}]_{t_0} \quad \text{Equation 3.9b}$$

$$E = \dot{Q} - \dot{W}_{shaft} - V \sum r_j \times \Delta \hat{H}_{rxn,j}^o \quad \text{Equation 6.4}$$

Not all applicable temperatures featuring in the calculation of stream enthalpies are measured at Western Platinum BMR. Energy balances were therefore excluded from plant data validation due to a lack of information.

Results and discussion

The first mass balance was conducted over the second stage slurry preparation tank (shown in Figure 6.6).

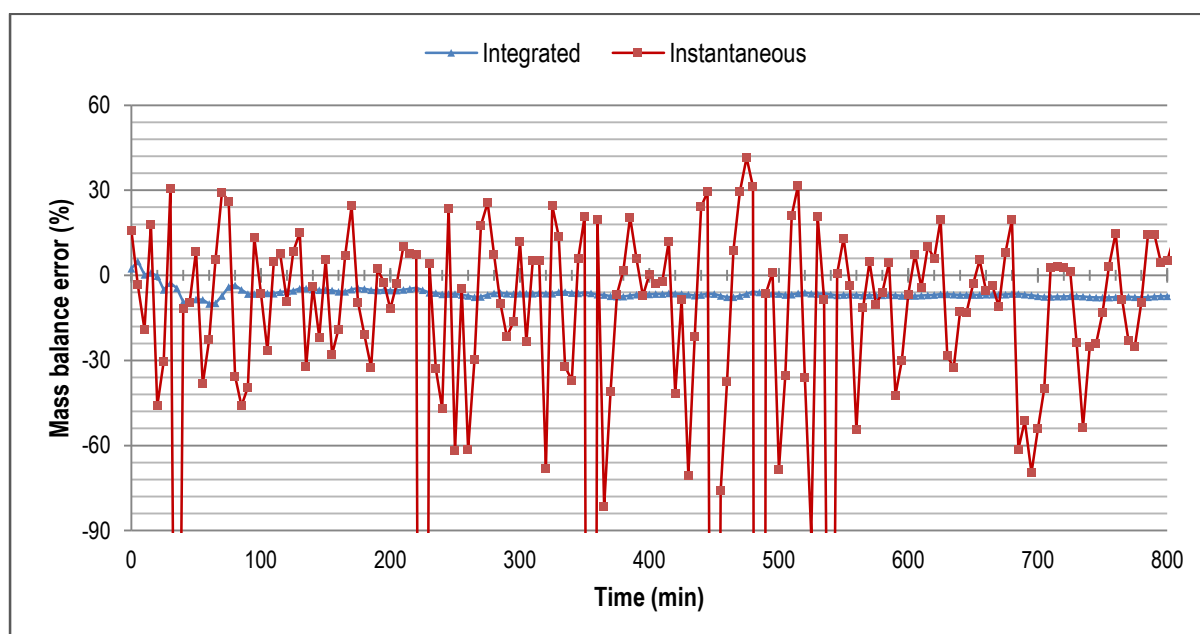


Figure 6.6: Mass balance results: Second stage slurry preparation tank

The instantaneous mass balance for second stage slurry preparation tank shows great variation. Note that it was shown in Figure 6.4 that flow measurements surrounding the

second stage slurry preparation tank had relatively low unrealisable values. These two statements do not necessarily contradict one another. The variation seen in the instantaneous mass balance from Figure 6.6 could possibly be an indication that the instantaneous inlet and outlet flow rates are not always equal to one another due to slight level variations (level variation causes an temporary accumulation of mass), in contrast to the ideal case. The integrated mass balance shows an average error of -6.3 % with low variation. The flat line suggests that the accumulated mass term in Figure 6.3 increases/decreases as a steady rate. The negative bias suggests that either the flow rate measurement into the vessel is too low or the flow rate out is too high (i.e. the accumulated mass that enters and exits the vessel increase at different rates). Another possibility could be erroneous density measurements used within the mass balance error calculations. Consider the overall manual measurement reliability at Western Platinum BMR according to expert knowledge (McCulloch et al., 2014).

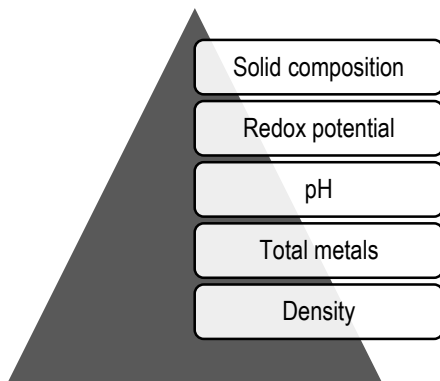


Figure 6.7: Manually measurement reliability (McCulloch et al., 2014)

The most accurate manual measurement is that of solid composition while density measurement is the least accurate. Figure 6.7 highlights the low reliability of manual density measurements. McCulloch et al. (2014) attributes the unreliability of manual measured densities and total metals to the irregular method by which samples are taken.

The second mass balance was conducted over the flash recycle tank of autoclave 300. The result is captured in the Figure 6.8.

A lower variation in instantaneous mass balance error is noticed around the flash recycle tank when compared to that of the second stage slurry preparation tank. The reduced variation could be attributed to a lower level variation in the flash recycle tank which ultimately reduces the temporary accumulation of mass. A lower level variation in the flash recycle tank makes sense, since aggressive level control is required in this vessel in order to

realise the temperature control action of the first compartment (refer to Section 2.4.2 for the first compartment temperature control mechanism).

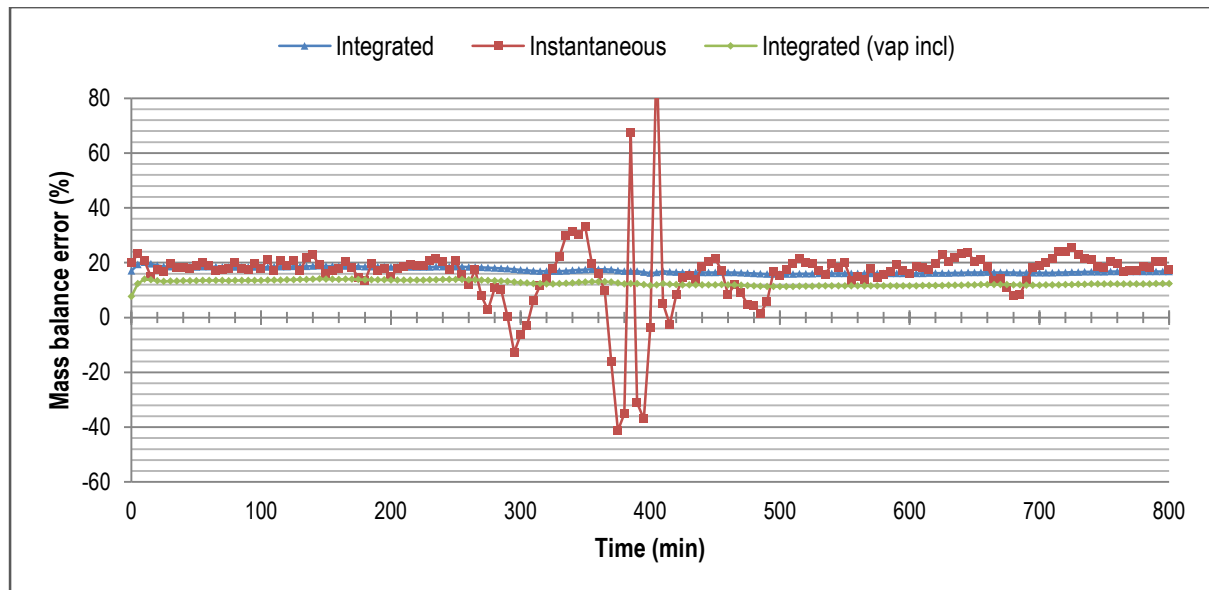


Figure 6.8: Mass balance results: Flash recycle tank of autoclave 300

The integrated mass balance once again shows a constant bias, with an average error of 17.2 %. This average is reduced to 12.5 % when the vapour estimation stream is incorporated in the mass balance. The addition of the vapour stream in the mass balance improves the mass balance error, as expected. However, a bias is still present. The positive bias suggests that either the flow rate into the vessel is too high or the flow rate out is too low. Notice that a negative mass balance error bias is evident around the second stage slurry preparation tank, while a positive mass balance error bias is evident around the flash recycle tank. This could suggest that the flow rate in between these two vessels is too high. However, the flow measurement between these two vessels (FIC-0201) indicated high flow measurement quality during physically realisable checks. A calibration issue in FIC-0201 could explain a high measurement quality with a bias. The mass balance error in Figure 6.8 cannot solely be attributed to the FIC-0201 measurement, if at all; due to the fact that this mass balance error is much higher when compared to that of the second stage slurry preparation tank (i.e. the flash recycle tank mass balance error cannot be justified solely by an error in FIC-0201, since this would result in a positive bias in the second stage slurry preparation tank mass balance error). Physically realisable checks indicated that certain flow measurements surrounding the flash recycle tank (i.e. FIC-0203 and FIC-0205) have many values lower than possible (i.e. negative flow rates). The fact that so many data points for these two flow controllers are erroneous already indicates their contribution to the mass

balance error. The extent to which they contribute to the positive mass balance error bias is yet uncertain.

A similar mass balance was applied to the flash recycle tank which operates with autoclave 200. Refer to the figure below.

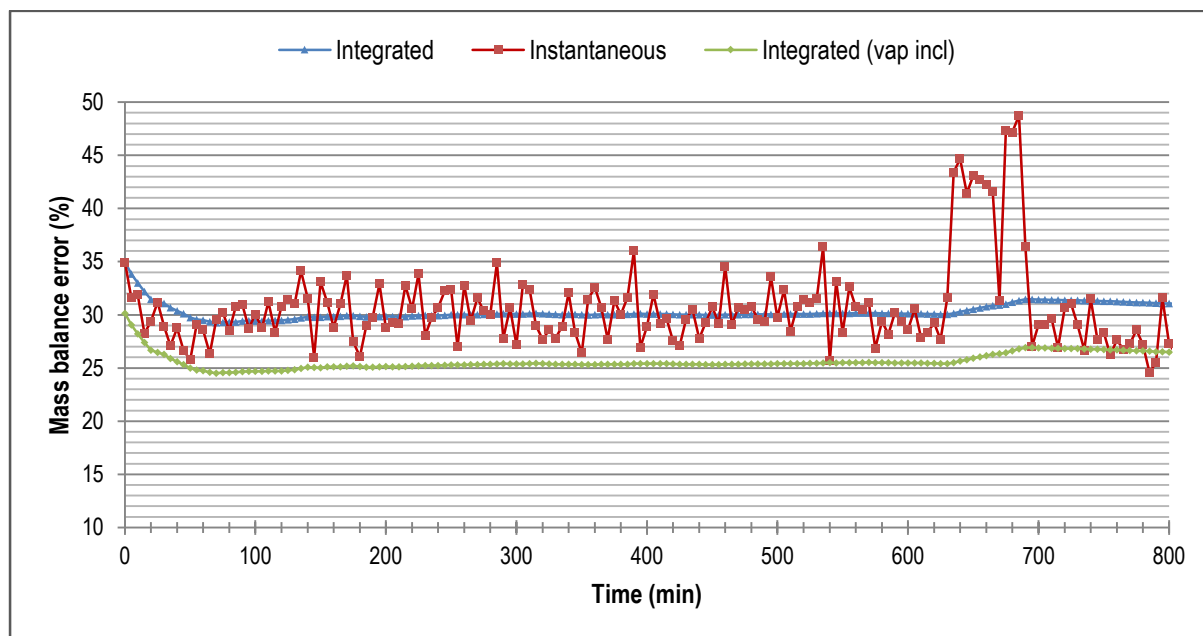


Figure 6.9: Mass balance results: Flash recycle tank of autoclave 200

A positive bias is once again reported with an average error of 30.3 % and 25.6 % for the integrated mass balance which excludes and includes the vapour stream, respectively.

Biases seem to exist within all mass balances that were conducted within this section. The existence of these biases, or gross errors, can be statically proven using gross error detection techniques such as global tests and measurement tests. Data reconciliation can be used to adjust data points in an attempt to get a better estimation of true variable states, assuming the measurement error is normally distributed.

6.2.6. Data reconciliation on plant data

Problem statement and methodology

Measurements of temperature, flow rate, concentration, and more, are often made within chemical plant operations for the purpose of process control and performance evaluation (Tamhane & Mah, 1985). These measurements, in the ideal case, are expected to satisfy mass and energy balances. However, sensor measurements are often unreliable due to an inability to precisely and accurately report variable states. Sensor measurement inaccuracies

can therefore cause mass and energy balance inconsistencies when these balances applied to process data. Consider Equation 6.5 which relates the measurement of a variable to the actual variable state (Karlsson, 2004):

$$y = \hat{y} + \delta + e \quad \text{Equation 6.5}$$

where y , \hat{y} , δ and e represent the measured variable, true variable state, gross error, and random noise. Measurement errors can therefore be caused by a combination of gross error and random noise. The random noise is normally distributed with an expected mean of zero. Random noise therefore adds variability to the data without affecting averages. Gross errors tend to be consistently negative or positive which is often caused by measurement device failures, calibration issues, and more (NCSA, 2003). Data reconciliation is a technique which is used to adjust measurements in a way so that the conservation equations (i.e. mass balances in this case) are satisfied, in an attempt to produce more accurate estimations of the true variable state. In order to do this, data reconciliation assumes the measurement error is solely caused by random noise (Bagajewicz, 1996; NCSA, 2003). Data reconciliation is done by minimising a least-squared objective function determined from constraints (i.e. a mass balance). The constraints contain variable measurements that are weighted by an estimation of their sensor variances. The following data reconciliation equation is valid for a steady-state linear process with no unmeasured variables (Tamhane & Mah, 1985):

$$x = y - \Sigma_y A^T (A \Sigma_y A^T)^{-1} A y \quad \text{Equation 6.6}$$

where y , x , Σ_y and A represent the measured variable vector; adjusted variable vector; sensor covariance matrix; and the adjacency matrix for a mass balance, respectively.

Data reconciliation was used to rectify inconsistent mass balances across the second stage slurry preparation tank and both flash recycle tanks using the same data from Section 6.2.5. All three mass balances were reconciled simultaneously in order to ensure that flow rates between dependent vessels are consistently approximated. The sensor covariance matrix was assumed to be diagonal with its entries estimated using sensor data where flow controller set-points and outputs were approximately constant. Only small sets of data were available for sensor covariance matrix approximation since flow controllers were rarely stationary.

Results and discussion

Only flow rate measurements which are relevant to this project are displayed. All the data reconciliation outputs can be found in Appendix F.

The following figures show the reconciled mass flow rate data (x) compared to the measured mass flow rate data (y) over time. The mass flow rate data points are also plotted against a straight line with no errors in order to determine the validity of the no gross error assumption (data reconciliation assumes that the measurement error is solely caused by random noise).

Figure 6.10 captures the results of tags that surrounding the second stage slurry preparation tank.

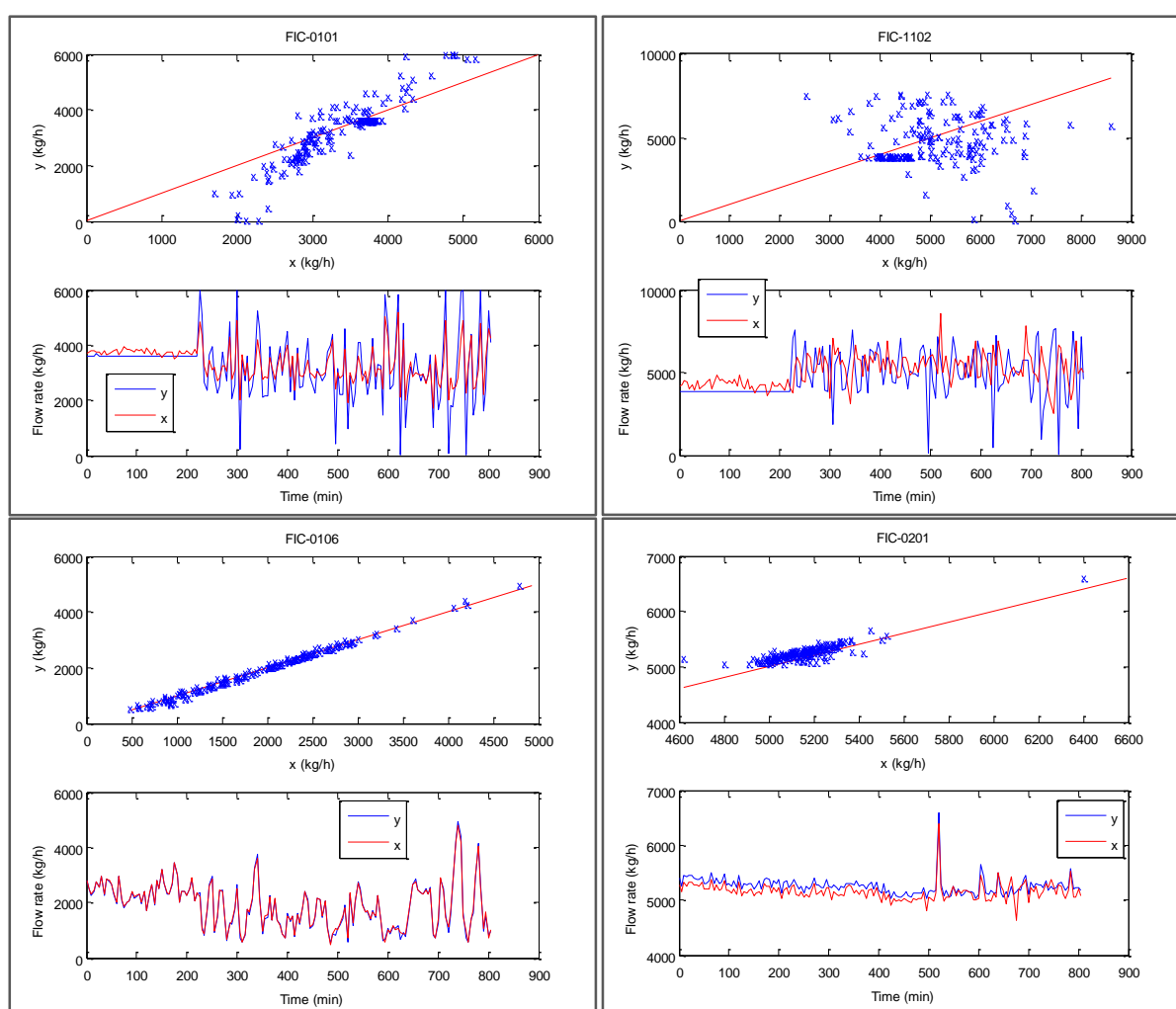


Figure 6.10: Data reconciliation results: Second stage slurry preparation tank

The first stage leach slurry flow measurements (FIC-0106) show little to no adjustments. Similar results are noticed for the flow rate measurements of the stream that exits the second stage slurry preparation tank (FIC-0201). Data for this tag is, however, slightly

adjusted so as to reduce the flow rate with a seemingly constant bias. This statement corresponds with deductions made from mass balance errors seen in Figure 6.6. The flow out of the second stage slurry preparation tank is reduced to compensate for both the second stage slurry preparation tank negative mass balance error bias and the flash recycle tank positive bias. Note that this seemingly bias reconciled data disregards the no gross error assumption, and could therefore be an invalid approximation of the true variable state (gross error detection is discussed in subsequent sections). Spent electrolyte (FIC-0101) and formic filtrate (FIC-1102) flow measurements are scattered across the linear line. No clear bias exists for these measurements. It is however noticed that the flow measurements of FIC-0101 is not normally distributed across the straight line, which disregards the normally distributed error assumption inherent within data reconciliation.

The following figures show data reconciliation results for tags surrounding the flash recycle tank of autoclave 300.

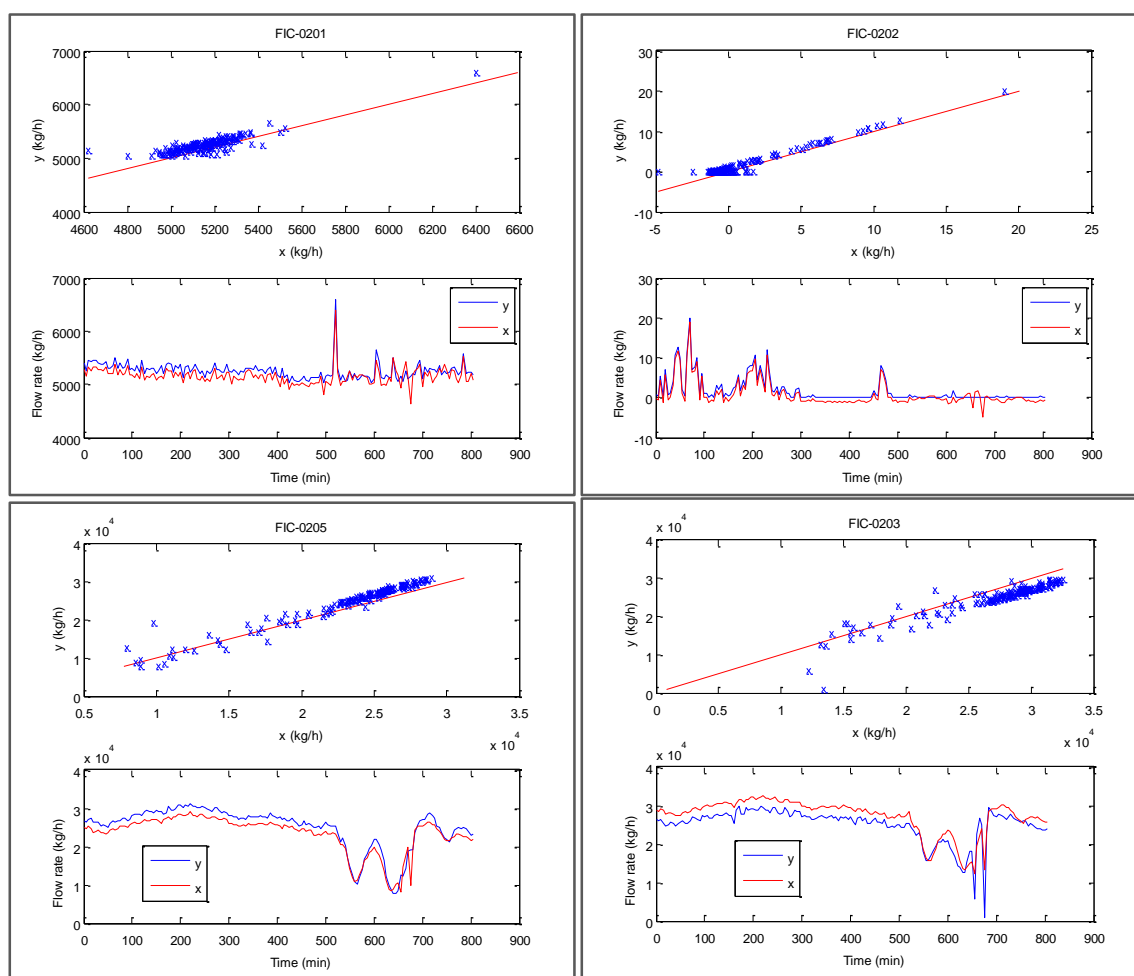


Figure 6.11: Data reconciliation results: Flash recycle tank of autoclave 300

Small, seemingly constant biases are noticed for all flow rate measurements around the flash recycle tank. Note that data is adjusted by increasing and decreasing the flow rates leaving (FIC-0203) and entering (FIC-0202, FIC0205 and FIC-0201) the flash recycle tank, respectively. This corresponds with deductions made from mass balance errors in Figure 6.8. The flow rates are adjusted in a manner so as to reduce the positive mass balance error bias for the flash recycle tank. Major adjustments are noticed in the stream leaving the autoclave 200 flash recycle tank (FIC-2204) in order to compensate for large mass balance error biases in Figure 6.9 (refer to Figure F.6).

Several adjusted flow rate measurements that were previously discussed seems to be indicative of gross error. This disregards the normally distributed error assumption of data reconciliation. It is necessary to statistically determine if these gross errors are in fact present in flow rate measurements. This can be done by using techniques that detect gross errors with a certain statistical significance.

6.2.7. Global test on plant data

Problem statement and methodology

Gross error, as previously mentioned, is a type of measurement error that contributes generally in a positive or negative bias (refer to Equation 6.5). Many authors suggest the use of global tests to statistically prove the existence of gross errors within conservation balance residuals (Almasy & Szatno, 1975; Madron & Veverka, 1977; Ripps, 1965). Global tests assess null hypotheses (H_0) which state that no gross errors exist. The residuals are firstly calculated:

$$\mathbf{r} = \mathbf{A}\mathbf{y} \quad \text{Equation 6.7}$$

where \mathbf{r} represents a residual vector which contains the conservation equation errors (i.e. mass balance errors, therefore an accumulation of measurement errors). A global test statistic (γ) is calculated (Karlsson, 2004):

$$\gamma = \mathbf{r}^T (\mathbf{A}\Sigma_y \mathbf{A}^T)^{-1} \mathbf{r} \quad \text{Equation 6.8}$$

The global test statistic is used in a chi-squared test. The null hypothesis is rejected if the global test statistic exceeds a χ^2 distribution value at a specified level of significance (α_{GT}) with a degree of freedom equal to the rank of \mathbf{A} .

The measured variable data from Section 6.2.5 was once again used in this gross error detection technique. The global test was applied to mass balance residuals at each time step within the previously mentioned data set.

Results and discussion

Mass balance error biases were noticed in Section 6.2.5. These biases transpired into the reconciled data results in the form of gross errors. The statistical significance of these gross errors is captured in Figure 6.12.

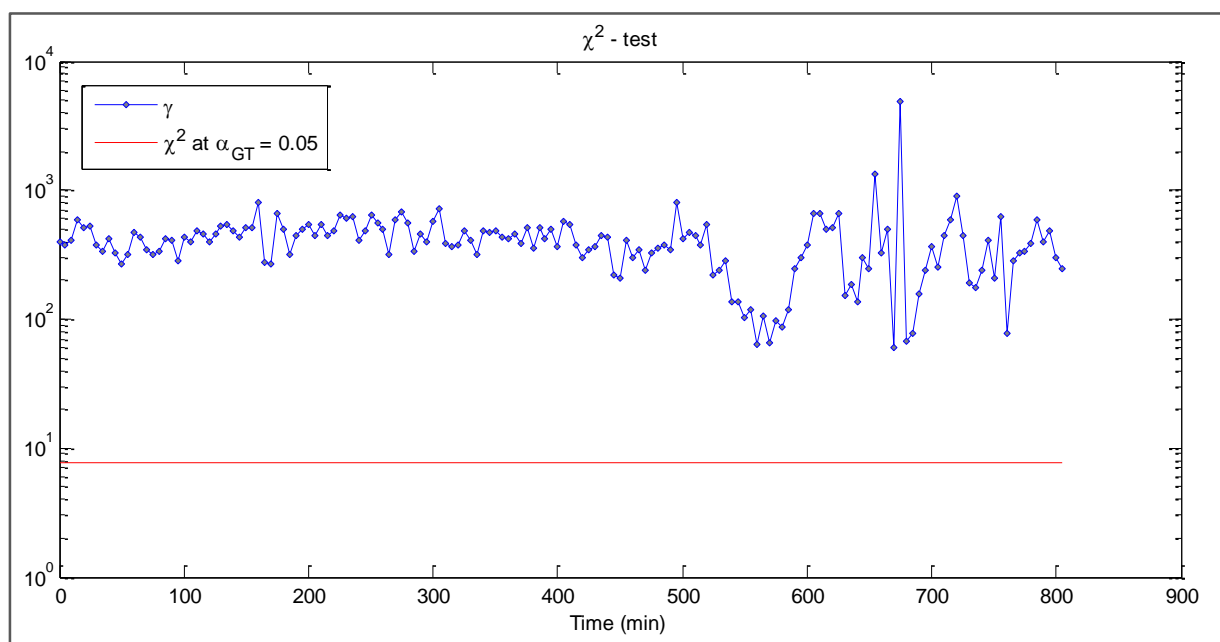


Figure 6.12: Global test results

All the mass balance residuals are indicative of gross error with at least 95 % significance. Some fluctuation of the global test statistic is noticed, which could be caused by the instantaneous steady-state assumption which is temporarily unsatisfied due to small level variation.

It is statistically evident that gross errors exist within mass balance residuals. Another statistical technique, namely measurement test, can be used to identify the origin of the gross error with a certain level of confidence.

6.2.8. Measurement test on plant data

Problem statement and methodology

A measurement test can be used to relate gross errors to specific variable measurements (i.e. sensors) with certain confidence, in the case of statistically significant gross error (Mah

& Tamhane, 1982). This allows one to identify erroneous sensors that are responsible for gross errors. A normalised residual (r^*) is firstly calculated by using data reconciliation outputs. A measurement test statistic (ζ_k) is then calculated, which is used in hypotheses testing (Tamhane & Mah, 1985):

$$r^* = \Sigma_y^{-1}(x - y) \quad \text{Equation 6.9}$$

$$\zeta_k = \frac{r_k^*}{\sqrt{\text{cov}(r_k^*)}} \quad \text{Equation 6.10}$$

A null hypothesis for the k^{th} sensor is rejected if ζ_k falls outside two-tailed standard normal distribution significance boundaries (α_{MT}^*):

$$|\zeta_k| > \alpha_{MT}^* \quad \text{Equation 6.11}$$

where the significance used is an adjustment using a Bonferroni correction:

$$\alpha_{MT}^* = \frac{1}{2} \left(1 - (1 - \alpha_{MT})^{\frac{1}{n}} \right) \quad \text{Equation 6.12}$$

The correction factor n is the size of all the sensor measurements k .

Measurement tests were applied to all reconciled data from Section 6.2.6 in order to determine if the occurrence of gross errors can be related to any of the sensors.

Results and discussion

Only meaningful measurement test results are plotted in Figure 6.13. All results can be found in Appendix F.

A gross error exists within FIC-2204 measurements with 95 % certainty. A measurement issue within FIC-2204 is therefore expected. Fortunately this flow sensor is not present in the process scope within this project; it was merely included in the investigation since it exists within the mass balance across the second stage slurry preparation tank.

Several data points within flow measurements FIC-1102, FIC-0203 and FIC-0205 have gross errors with certainty close to 95 %. These variations in confidence correspond with fluctuations in mass balance errors, which were previously attributed to steady-state issues

caused by slight level variations. The measurement test statistics of FIC-0203 and FIC-0205 during proper steady-state time zones are approximately -1.011 and 0.798, respectively.

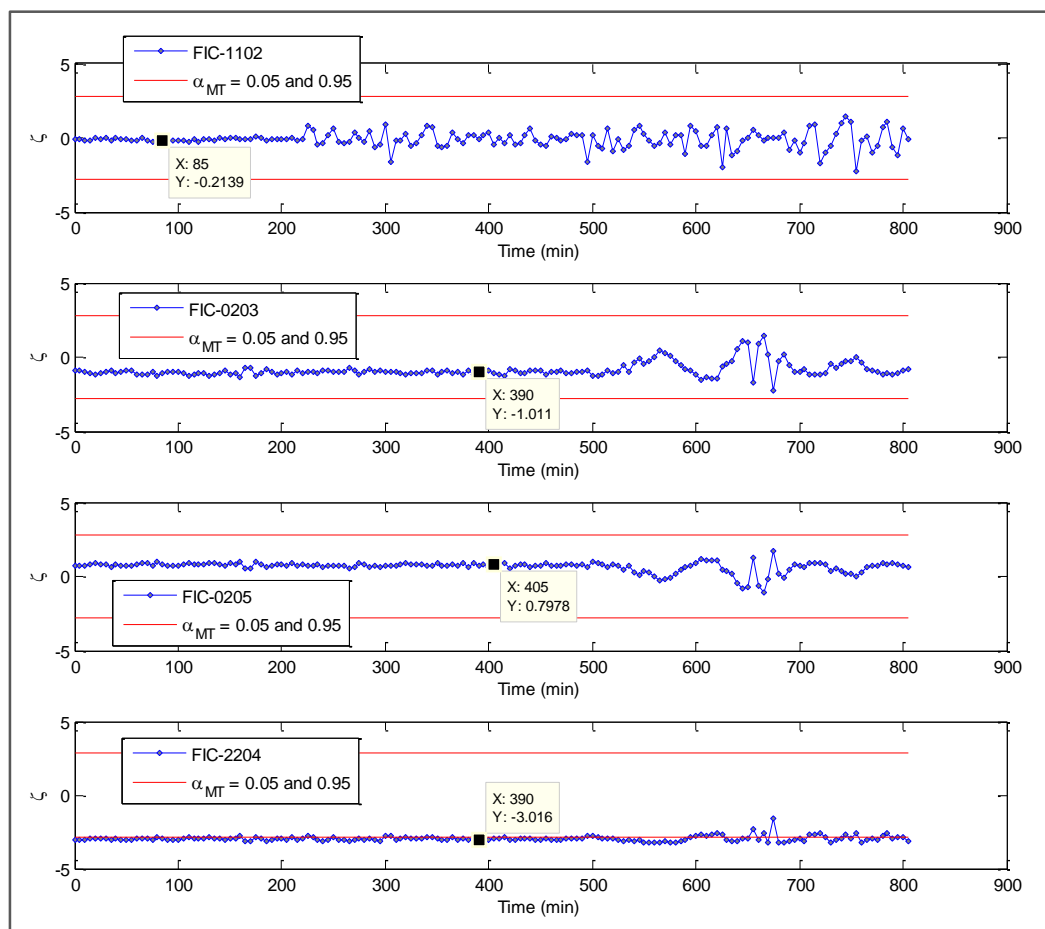


Figure 6.13: Measurement test results: Significant ζ outputs

These measurement test statistics translate to gross error confidences of 76 % and 71 %, respectively. Physically realisable checks indicated that these two flow measurements had the poorest quality of all flow measurements. Moreover, these two flow measurements were the most indicative of biases during graphical inspection in data reconciliation.

Mass balances across several process units at Western Platinum BMR proved to be inconsistent. An attempt at improving the data quality via data reconciliation proved to be somewhat useful. However, certain relevant flow measurements were indicative of gross errors. It therefore becomes difficult to use process data as inputs to the dynamic process model (for the purpose of model behaviour validation), even if data reconciliation is applied, due to the uncertainty of flow rates associated with biases. Note that the validity of statistical tests performed is expected to change when using data sets at other historian times, due to possible sensor degradation and replacement.

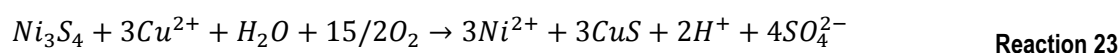
6.3. Conceptual Model Validation

This section considers the validity of the mathematical basis on which the Simulink™ model (Haasbroek & Lindner, 2015) was developed, and includes validating several assumptions made to produce the dynamic process model.

6.3.1. Copper cementation reactions

Problem statement and methodology

The occurrence of copper cementation reactions are widely described in literature (Rademan, 1995; Lamy & Lorenzen, 2006; Rademan et al., 1999). Copper cementation reactions comprise copper precipitation in the form of a copper sulphide, via nickel sulphide leaching (Rademan et al., 1999):



Reaction 23 can occur via leaching of several different nickel-sulphide ratio compounds. The cementation mechanism via the leaching of polydymite is of interest, since polydymite is present in the first stage leach residue of Western Platinum BMR.

Copper cementation reactions were assumed to be negligible by Dorfling (2012) since initial experimentation indicated no reduction in cupric ion concentrations. Dorfling (2012) therefore excluded copper cementation from the final set of reactions which were ultimately used in the development of reaction kinetics.

The possibility that copper cementation reactions occurred during batch experimentation conducted by Dorfling (2012) is investigated. Cupric ion trends from the batch experiments are used in the procedure.

Results and discussion

Cupric ion trends from batch experimentation conducted by Dorfling (2012) are shown in Figure 6.14.

Error bars were introduced in a single set of data points, applicable to all other points, in order to show the extent of error possibly induced by measurement errors (sample variation from Table 6.5). Two standard deviations of measurement error were used. A decrease in cupric ion concentrations is evident from Figure 6.14 even when measurement errors are included.

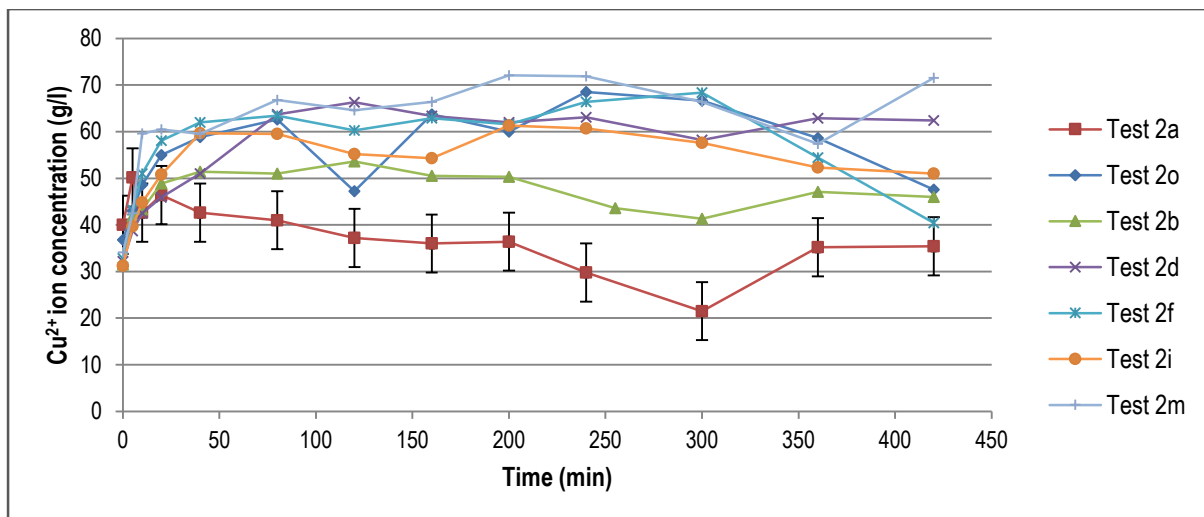


Figure 6.14: Several cupric ion concentration trends in batch experimentation conducted by Dorfling (2012)

Note that copper cementation could occur even if decreases in cupric ions are not evident; it might only suggest that copper leaching occurs at a faster rate than copper cementation. The reduction in cupric ion concentrations in batch experimentation could be attributed to copper cementation via Reaction 23. However, a corresponding increase in nickel ion concentration is expected at the same time, which is not clearly evident. Another contributing factor could be the cupric ion solubility limit which is exceeded when samples were drawn which results in an upper limit and a plateau in cupric concentrations (i.e. crystallisation of cupric ions in the form of copper(II)sulphate in samples). Crystallisation of material within samples did occur but the crystal composition was never measured (Dorfling & Miskin, 2015). The slight plateau decline could be attributed to the increasing sulphate ions caused by direct nickel leaching which ultimately reduces the cupric ion solubility limit.

The reaction kinetics currently used cannot describe a decrease in cupric ion concentration, which has a major impact on the quality of the reaction kinetic fit to experimental data. The reaction kinetics fit the decreasing cupric ion trends seen in Figure 6.14 poorly. The copper leaching rate constants are currently underestimated. This statement follows from the countering copper cementation which is not present in the reaction kinetics (if copper cementation does in fact occur) and the cupric ion concentration is suppressed by exceeded solubility limits.

Proposed model updates

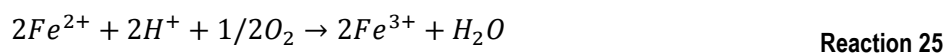
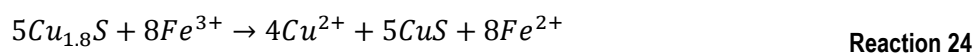
The origin of the cupric ion concentration decreases needs to be further investigated. Adding the additional cementation reaction to the current leaching kinetics should provide the required cupric ion decrease dynamics, which is expected to be beneficial for the quality of the fit and therefore the predictability of the dynamic process model (not taking into account

the issues discussed in Section 6.2.2). This statement is only valid if the concentration decrease is in fact ascribed to cementation. The experimental work needs to be repeated under lower cupric concentrations and solid loadings if the cupric ion concentration solubility limits were reached. This would allow a more accurate re-estimation of the copper leaching kinetic parameters. The proposed model updates require significant additional work which falls outside the scope of this project.

6.3.2. Ferric to ferrous ion reduction mechanism influence

Problem statement and methodology

An additional pathway exists by which copper sulphide leaches, where ferric ions act as an oxidising agent. Reaction 24 represents the mechanism where ferric ions contribute to the leaching of digenite. Reaction 25 indicates how ferrous ions are oxidised back to the ferric state (Rademan et al., 1999).



Hofirek and Kerfoot (1992) also states that iron can act as an electron carrier during copper sulphide leaching. Dorfling (2012) could not distinguish between ferric and ferrous ions during experimentation. The ferric to ferrous ion reduction mechanism and its contribution to digenite leaching was therefore excluded by Dorfling (2012).

The occurrence of digenite leaching via iron ions as electron carrier is verified using reference to literature. The effect of excluding the contribution this leaching mechanism is addressed. The possibility of model updates is also considered.

Results and discussion

Richmond (2004) and Wilmot et al. (2004) found that the pathway for copper sulphide leaching via Reaction 24 plays a significant role within pressure leaching operations. As it stands, batch experimentation results produced by Dorfling (2012) cannot be used to differentiate between oxidation states of ions since ICP-MS and ICP-OES analysis techniques were used. All forms of analytes are converted to positive charged atomic ions in the plasma during ICP measurements. A separation technique such as ion chromatography is required prior to the ICP stage (Chen et al., 2007).

Note that Reaction 3 is produced by combining Reaction 24 and Reaction 25. The extent to which the dynamic process model copper predictability is affected therefore depends on the nature of the additional reaction mechanism under varying conditions – varying behaviour of digenite leaching possibly exists which is not captured in the current mechanism (i.e. the current digenite leaching prediction could be constrained). This could occur if the iron electron carrying mechanism is susceptible to varying conditions.

Proposed model updates

The current digenite leaching rate expression (i.e. kinetic parameters) carries the contribution of Reaction 24. The exclusion of the iron ion as an electron carrier for digenite leaching is expected to cause an overestimation of the current digenite leaching mechanism rate constant (Reaction 3). However, the current digenite leaching fit might be sufficient in this sense if the iron electron carrying mechanism is unaffected by varying operating conditions. The effect of varying conditions on the rate of digenite leaching needs further investigation. Dynamic process model improvements cannot be made without conducting additional batch experimentation. Sample analyses will need to include chromatography so as to distinguish between ion states. The proposed model updates relate back to the lack of an underlying speciation model described in Section 6.2.2. The proposed model updates require significant work which falls outside the scope of this project.

6.3.3. PGM leaching reaction initiation

Problem statement and methodology

The initiation of PGM leaching reactions was approximated by Dorfling (2012) to commence when 99 % of the time zero digenite was leached, during the development of kinetics from batch experimentation. Dorfling (2012) implemented the same principle to the continuous dynamic process model by initiating PGM leaching reactions in all autoclave compartments with reference to the digenite present in an inlet stream.

The origin of the PGM leaching commencement approximation is firstly considered, followed by its validity within batch reactors. The validity of using a reference stream to implement the same principal in a continuous process is considered by simply making use of a thought experiment. Model improvements are made, which ensures a more realisable PGM leaching commencement.

Results and discussion

All reactions that contribute to leaching process are of electrochemical nature (Dorfling, 2012; Nicol, 2014). The redox potential can therefore serve as a measurement to estimate

the commencement of reactions (not considering available particle surface area). Dorfling (2012) described the difficulty of obtaining reliable redox potential measurements during batch experimentation, and did not incorporate a reduction-oxidation cell potential model within the reaction kinetics (i.e. dynamic process model). Dorfling (2012) therefore estimated the commencement of PGM leaching reactions to occur when 99 % of the time zero digenite was leached, which is an approximation based on batch experimentation observations. This estimation could be valid for batch processes if conditions do not change significantly so as to affect the point at which PGM leaching commences. Dorfling (2012) applied the same approach to a continuous process and used the inlet to the flash recycle tank as a reference point for PGM leaching commencement in all autoclave compartments.

$$(\dot{n}_{out,comp\ i})_{Cu_9S_5} \leq 0.01 \times (\dot{n}_5)_{Cu_9S_5} \quad \text{Equation 6.13}$$

Equation 6.13 governs the commencement of PGM leaching reactions for compartment i in the autoclave. Consider reducing digenite flow rate in stream 5 to zero in a step action. PGM leaching reactions would instantaneously stop since Equation 6.13 is unsatisfied, irrespective of the composition within the compartment. Equation 6.13 in this case requires that no digenite be present in the compartment outlet before PGM leaching commences. Using an extent of reaction to govern commencement of other reactions simply does not work in continuous processes due to the difficulties of defining a reference point and the implications thereof.

Model updates

The ideal solution to this issue would be to use redox potentials to define the commencement, but the inclusion of a reduction-oxidation cell potential model and possibly even additional experimentation would be required. A specific digenite concentration within autoclave compartments would serve as a better commencement point for PGM leaching reactions since it does not fall prone to the previously mentioned inlet step-test issues. The digenite concentration is approximated as the digenite concentration in batch experimentation when 99 % of it is leached, and is used as a substitution to the previous method.

6.3.4. Rate expressions scaled to large process units

Problem statement and methodology

Dorfling (2012) assumed that the developed rate expressions are directly scalable to the Western Platinum BMR operation. This assumption is partially validated by specifically considering the effects that the physical reactor size increase (from a bench scale to an industrial scale) has on the extensive (i.e. being dependent on the system size) rate expressions. An alternative solution to rate expression formulation is included in the model updates which ensure intensive reaction kinetic properties, allowing first approximation scalability.

Results and discussion

Reconsider the generic rate expression developed by Dorfling (2012):

$$r_j = \left(k_{0,j} e^{\frac{-E_{a,j}}{RT}} \right) \prod C_{i,j}^{\alpha_{i,j}} \left(n_0^{\frac{1}{f_{sh}}} \times n^{1-\frac{1}{f_{sh}}} \right)_{solid} \quad \text{Equation 3.6a}$$

The reaction-specific rate expressions are summarised in Table D.1. Equation 3.6a contains molar amount terms which have extensive properties (i.e. being dependent on the system size). An increase or decrease in operating volume will proportionally increase the molar amounts in rate expressions developed by Dorfling (2012). The rate expressions therefore also exhibit extensive properties, which is invalid when considering scaling requirements from a 2 l batch reactor to a 14 m³ CSTR (i.e. the rate expressions should exhibit intensive properties). The extensive property of the generic rate expression exist because the rate expression constant ($k_{0,j}$) contains an agglomeration of different parameters including the vessel volume (V), among others. However, the volume term should not be included in the agglomerated rate constant as it is not constant in the continuous process. The agglomerated rate constant can be disassembled in order to eject the volume term. The generic rate expression can be rewritten as follows:

$$r_j = \left(k'_{0,j} e^{\frac{-E_{a,j}}{RT}} \right) \prod C_{i,j}^{\alpha_{i,j}} \left(C_0^{\frac{1}{f_{sh}}} \times C^{1-\frac{1}{f_{sh}}} \right)_{solid} \quad \text{Equation 3.6b}$$

The adjusted rate expression constant ($k'_{0,j}$) is an agglomeration of constants similar to that of the rate expression constant ($k_{0,j}$), excluding the volume term as shown in Equation 3.2.

Equation 3.6b is preliminarily scalable to reactor sizes used at Western Platinum BMR as it contains no terms with extensive properties.

Model updates

The methodology used to update the generic rate expression in order for it to exhibit intensive behaviour is applied to all rate expressions seen in Table D.1. The new rate expressions are implemented in the dynamic process model.

6.3.5. Initial concentrations in a continuous process

Problem statement and methodology

The new rate expression developed in Section 6.3.4 is still a function of an initial concentration. The initial concentration has a clear definition in a batch reactor – the concentration of a component at the start of experimentation. This definition is however unclear for a continuous process (i.e. Western Platinum BMR) since no “start of experimentation” exists.

The approach Dorfling (2012) used to define the initial concentration terms in the dynamic process model (i.e. a continuous process) is investigated. A simple thought experiment is used to test the current definition. The origin of the initial concentration terms within the rate expressions are obtained from literature, and is used in the final validation of this definition.

Results and discussion

Dorfling (2012) defined the initial concentration for all rate expressions within the dynamic process model as the concentration of reactant flowing into the autoclave. Consider the following dynamic process model behaviour when applying this definition: a step increase in the reactant concentration entering the autoclave will, according to Equation 3.6b, have an equal effect on reaction rates irrespective of the flow rate size. The current definition of initial concentration in Equation 3.6b also implies that reaction rates will instantaneously stop if the concentration entering the autoclave is reduced to zero in a step action, irrespective of the amount of reactants available in the autoclave at that time.

The origin of the initial concentration in the rate expressions comes from a derivation of the total available reactant surface area by Salmi et al. (2010). The initial concentration in rate expressions is used as a reference point to approximate the change in particle volume, therefore the available particle surface area, as the reactions continue. Using the autoclave inlet concentration to represent the C_0 term in Equation 3.6b is therefore nonsensical, since

the inlet stream particle surface area is expected to be significantly different to what is present in autoclave compartments.

Proposed model updates

The dynamic process model currently cannot quantify available particle surface area since it contains no particle size distribution estimations or particle population balances, which would have been the ideal solution to this issue. Another solution would be to approximate the initial concentration as a constant during reaction kinetics optimisation, and subsequently in the dynamic process model. This approximation would serve as a reasonable solution if the dynamic process model does not vary significantly from the batch experimental baseline. The initial concentration term can be lumped into the rate expression constants:

$$r_j = \left(k''_{0,j} e^{\frac{-E_{a,j}}{RT}} \right) \prod C_{i,j}^{\alpha_{i,j}} \left(C^{1-\frac{1}{f_{sh}}} \right)_{solid} \quad \text{Equation 3.6c}$$

The initial concentrations of all rate expressions are lumped into the pre-exponential constant. The new set of rate expressions forms one of the reaction kinetic versions which is optimised in this project, and is discussed in Section 6.3.11. The rate expression version is labelled as “initial concentration lumping”.

The optimisation of different reaction kinetic versions serves to address rate expression and related batch experimental data issues in an attempt to improve the current dynamic process model leaching predictability. Note that the suggested reaction kinetics is not implemented into the dynamic process model prior to discussing the quality of the new reaction kinetic fit.

6.3.6. Dynamic process model oxygen solubility estimation

Problem statement and methodology

Dorfling (2012) assumed that the oxygen concentration in the liquid phase at any given stage of the dynamic process model operation to be equal to the maximum oxygen solubility at equilibrium. Dorfling (2012) took into account effects of temperature, oxygen partial pressure and solute concentrations according to methods described by Tromans (1998). However, the rate of oxygen consumption from and addition to the liquid phase was not taken into account.

This assumption is validated by considering normal Western Platinum BMR operation. The implication that this assumption has on the dynamic process model operation in the

occurrence of faults (i.e. for the purpose of this project) is also considered. The difficulty of implementing an oxygen mass balance around the liquid phase is also mentioned.

Results and discussion

The assumption is expected to be valid if the stirring rate (ensures oxygen transfer to the liquid phase) and oxygen feed (supplies oxygen) is adequate. Western Platinum BMR seldom operates autoclave compartments at extreme conditions at which the oxygen supply is lower than the combined effect of oxygen consumption through reactions and the liquid's ability to absorb oxygen. Oxygen is sparged in excess through the liquid of autoclave compartments to ensure high extents of base metal sulphide leaching.

The objectives for this project include operating the dynamic process model under extreme conditions (i.e. during the occurrence of process faults). One such condition might entail the depletion of oxygen within the autoclave.

Proposed model updates

One would require more information regarding gas-to-liquid mass transfer within autoclave compartments in order to conduct a dissolved oxygen mass balance. This includes mass transfer coefficients and effective mass transfer areas which are not available or easily estimated. The availability of oxygen within the autoclave should be taken into account through its causal relationship with the partial pressure term in Equation D.5 within the updated model (assumption which is addressed in Section 6.5.5).

6.3.7. Mass transfer limits digenite and covellite leaching reactions

Problem statement and methodology

Dorfling (2012) obtained low activation energies for the two copper sulphide leaching reactions (Reaction 3 and Reaction 6) after following an optimisation procedure. The low activation energies suggest that these reactions are not chemically controlled since temperature changes have negligible effect on their rates (Burkin, 2001). Dorfling (2012) therefore assumed that the two copper sulphide leaching reactions are oxygen mass transfer limited. Shape factor terms within the digenite and covellite leaching rate expressions were therefore excluded by Dorfling (2012), since the mass transfer limitation insists that the reactions are independent of the available reaction surface area.

A method is provided which avoids the copper sulphide rate limiting assumption. The solution forms a new set of reaction kinetic parameters that is optimised.

Results and discussion

The oxygen mass transfer limitation assumption can be avoided by including the shape factor terms within the copper sulphide leaching reactions. An optimisation solution exists where the reaction kinetic parameter values suggest the reaction is independent of available surface area. The two rate expressions under consideration could be considered independent of available surface area if the two shape factors are close to one.

Proposed model updates

New rate expressions are developed for the two copper sulphide reactions comprising the addition of shape factors terms. The change in rate expressions is used within a new reaction kinetic set that is optimised in Section 6.3.11, labelled as “shape factor changes”.

6.3.8. PGM-oxide shape factors with infinite size

Problem statement and methodology

Dorfling (2012) determined that there is no PGM-oxides present in the initial first stage leach residue used in batch experimentation. This has implications on the operability of PGM-oxide rate expressions since PGM-oxide initial concentrations feature in their corresponding rate expressions. Consider the PGM-oxide rate expressions:

$$r_{19} = \left(k_{0,19} e^{\frac{-E_{a,19}}{RT}} \right) \left(C_0^{\frac{1}{f_{sh}}} \times C^{1-\frac{1}{f_{sh}}} \right)_{RhO_2} \quad \text{Rate expression 19}$$

$$r_{20} = \left(k_{0,20} e^{\frac{-E_{a,20}}{RT}} \right) \left(C_0^{\frac{1}{f_{sh}}} \times C^{1-\frac{1}{f_{sh}}} \right)_{RuO_2} \quad \text{Rate expression 20}$$

$$r_{21} = \left(k_{0,21} e^{\frac{-E_{a,21}}{RT}} \right) \left(C_0^{\frac{1}{f_{sh}}} \times C^{1-\frac{1}{f_{sh}}} \right)_{IrO_2} \quad \text{Rate expression 21}$$

Substituting zero into C_0 causes the PGM-oxide rate expressions to be inoperative. Dorfling (2012) reasoned that PGM-oxide shape factors can be approximated as being infinite due to small inclusions of this material forming large surface area to volume ratios. Zero to the power of zero was then taken as one, which allowed the PGM-oxide rate expressions to have realisable values.

The origin of the initial concentration term in Equation 3.6b is reviewed and used to develop a different definition for initial concentrations that not only effects PGM-oxide leaching reactions, but all PGM leaching reactions. The methodology used by Dorfling (2012) to

estimate the PGM-oxide shape factors is avoided when the different, more suitable, initial concentration definition is applied. Model updates are suggested, and is included in a reaction kinetic set which is optimised in Section 6.3.11.

Results and discussion

It was previously mentioned that PGM leaching reactions only occur when 99 % of all covellite is leached. When taking into account that the initial concentration is used as a reference point to approximate the change in particle volume, it becomes clear that all initial concentrations of PGM containing minerals should be redefined to be at the time when these reactions start; thus when 99 % of all covellite is leached. This is a more logical definition and it avoids assuming infinite shape factors for all PGM-oxide minerals.

Proposed model updates

The updated definition of initial concentration applies to all PGM leaching reactions. The new PGM leaching rate expressions, which simply have different initial concentration definitions, are incorporated in the “shape factor changes” reaction kinetic version discussed in Section 6.3.7 (these changes are also associated with available surface area approximation). The optimisation process is discussed in Section 6.3.11.

6.3.9. Data point/parameter ratio in reaction kinetic optimisation

Problem statement and methodology

A total of 16 experimental runs were conducted by Dorfling (2012) in which 6 ion concentrations were measured 13 times over 420 minutes. Dorfling (2012) subsequently used these concentration trends to optimise a set of reaction kinetics. In doing so, Dorfling (2012) assumed that there were enough experimental data points to adequately fit the reaction kinetic parameters.

The ratio between the number of data points and reaction kinetic parameters is calculated and compared to literature heuristics in order to determine the validity of this assumption. Additional issues are mentioned which cannot be addressed using this simple ratio test.

Results and discussion

The number of reaction kinetic parameters, data points, and ratios are summarised in Table 6.6.

Several versions of reaction kinetics are considered in Table 6.6. The first set represents the reaction kinetic version used by Dorfling (2012). The additional three reaction kinetic

versions incorporate changes which were made within this project, which require similar validation.

Table 6.6: Ratio test: Experimental data points per reaction kinetic parameters

Parameters	No updates	Shape factor changes	Initial concentration lumping	All updates
$k_{0,j}$	21	21	21	21
$E_{a,j}$	21	21	21	21
$f_{sh,j}$	10	15	10	15
<i>Total</i>	52	57	52	57
Available data points	1146	1146	1146	1146
Data points per parameter	22	20	22	20

A data point-parameter ratio of one would, for a simple algebraic system, yield a single solution of parameters since a zero degree of freedom exists (e.g. a polynomial with three parameters a , b , c , fitted to three data points). The slightest data point inaccuracy in such a case would have major effects on the quality of the model. A ratio of lower than one would yield an infinite number of parameter solutions that depicts an incomplete model. The same principle could be applied to a complex ODE system such as reaction kinetics.

Data point-parameter ratios of at least 20 are used within all reaction kinetic versions listed in Table 6.6. This seems to be sufficient as a first approximation⁵. This simple test does not take into account the distribution of data points and its implication on data and parameter relations. For instance, experiments were conducted at only two different temperatures which in essence results in a single solution of activation energies via the Arrhenius equation. The relations between data points and other parameters are more complicated. The test also does not consider the sample interval resolution requirements (e.g. the amount of data points that would sufficiently define a concentration curve). Dorfling (2012) used adequate sample intervals that seem to capture the necessary and expected leaching behaviour.

Proposed model updates

A high data point-parameter ratio is evident. No model updates are therefore proposed.

⁵Consider 40 data points used to fit a straight line. This corresponds with 20 data points per parameter.

6.3.10. Objective function used in reaction kinetic optimisation

Problem statement and methodology

The objective function which was used by Dorfling (2012) during reaction kinetic optimisation is presented again.

$$ObjFunc = \sum_{i=1}^{i=6} \sum_{r=1}^{r=16} \sum_{t_0}^{t_f} (C_{M,i} - C_{E,i})_{t,r}^2 \quad \text{Equation 3.7a}$$

Two issues exist when using Equation 3.7a as an objective function: the objective function's sensitivity to measurement errors; and adding concentrations which differ with several orders. The molarity of Ru^{3+} , Rh^{3+} and Ir^{3+} varies between the order of 10^{-6} and 10^{-2} , while the molarity of Cu^{2+} and Ni^{2+} varies between the order of 10^{-1} to 10^1 . The molarity of Fe^{3+} falls inbetween these extremes. It is clear that the objective function in Equation 3.7 will be governed by errors solely induced through Cu^{2+} and Ni^{2+} concentrations. The PGM ion fit will therefore suffer under this objective function. A different objective function is proposed which counters the previously mentioned issues. The new objective function is used in the optimisation of different reaction kinetic sets within this project.

Results and discussion

Major concentration measurement errors were evident in the batch experimental runs conducted by Dorfling (2012) (refer to Table 6.5). The objective function used by Dorfling (2012) does not take into account measurement errors. This causes the objective function to report the existence of an error in cases where the error should be negligible due to high uncertainty of the actual sample concentration. Measurement deviations need to be taken into account in the objective function. This will ensure that the optimisation algorithm does not focus on improving errors which is dominated by measurement noise. A newly proposed objective function is given in Equation 3.7b.

$$ObjFunc = \sum_{i=1}^{i=6} \sum_{r=1}^{r=16} \sum_{t_0}^{t_f} \left(\frac{f(\sigma_{m,i}, C_{M,i,t,r}, C_{E,i,t,r})}{C_{E,i,r}^{Max}} \right)^2 \quad \text{Equation 3.7b}$$

where $C_{E,i,r}^{Max}$ and $\sigma_{m,i}$ represents the maximum concentration of component i for run r ; and the standard deviation of measurements due to error for component i , respectively. Note that the new objective function normalises the component concentrations to produce a comparable error term. This addresses and counters the second objective function related

issue – adding concentration errors which differ with several orders. The function (f) in Equation 3.7b is defined as follows:

$$f(\sigma_{m,i}, C_{M,i,t,r}, C_{E,i,t,r}) = \begin{cases} 0, & |C_{M,i} - C_{E,i}|_{t,r} < 2\sigma_{m,i} \\ (|C_{M,i} - C_{E,i}|_{t,r} - 2\sigma_{m,i}) & |C_{M,i} - C_{E,i}|_{t,r} \geq 2\sigma_{m,i} \end{cases} \quad \text{Equation 6.14}$$

The new objective function is known as epsilon insensitive. A schematic presentation of an epsilon insensitive objective function output is given below.

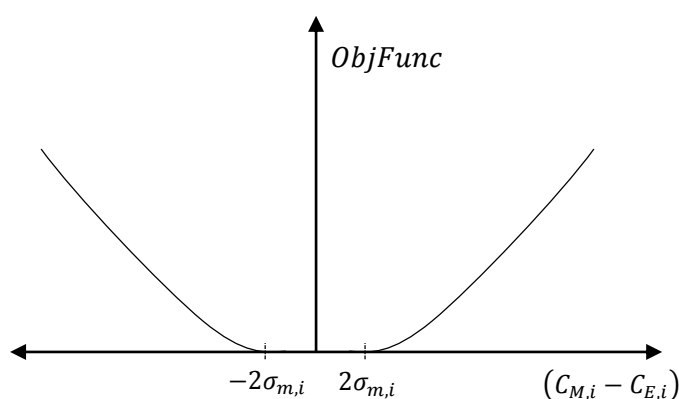


Figure 6.15: Epsilon insensitive objective function

The improved objective function uses an epsilon insensitive action to ensure that errors smaller than two standard deviations are zero. More information on epsilon insensitive objective functions is listed (Zisserman, 2015; Scholkopf, 2015).

Proposed model updates

The epsilon insensitive objective function is used in the optimisation of different reaction kinetic versions in an attempt to improve the fit to batch experimental data.

6.3.11. Reaction kinetics optimisation

Problem statement and methodology

Several issues related to the reaction kinetics developed by Dorfling (2012) have been addressed. Some of the proposed solutions require reaction kinetic adjustments, and therefore the subsequent refitting to batch experimental data. The necessary reaction kinetic adjustments are listed below:

1. Initial concentrations in a continuous process (Section 6.3.5)
2. Mass transfer limits digenite and covellite leaching reactions (Section 6.3.7)

3. PGM-oxide shape factors with infinite size (Section 6.3.8)

The first rate expression adjustments listed above formed a single reaction kinetic version (i.e. initial concentration lumping). The second and third rate expression adjustments were combined into one reaction kinetic version (i.e. shape factor changes). Other changes which were included in the new optimisation problem are listed below:

1. Ion concentration adjustments in batch experimental data (Section 6.2.1)
2. Objective function used in reaction kinetic optimisation (Section 6.3.10)

Dorfling's (2012) standard batch experimental data was used in the optimisation problem. The epsilon insensitive objective function was used to ensure that the optimisation algorithm does not focus on improving errors which are dominated by measurement noise, and that all ion species carry similar weight.

The optimisation methodology which was used is captured in Figure 6.16.

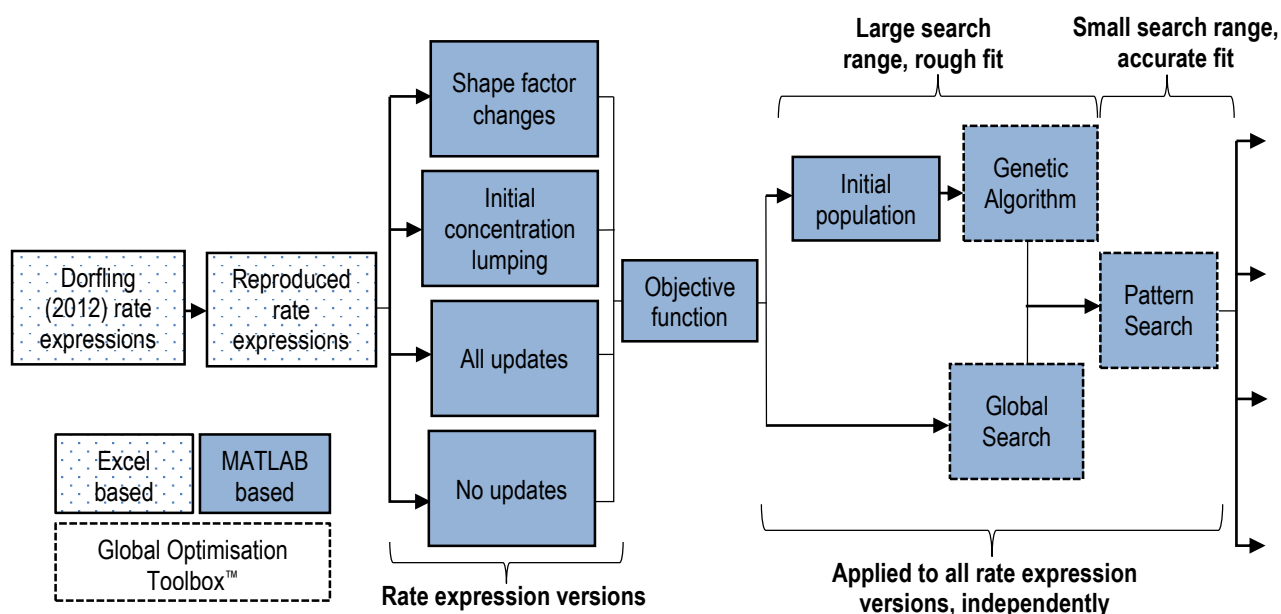


Figure 6.16: Reaction kinetic optimisation methodology

The optimisation problem considered by Dorfling (2012) inside Microsoft® Excel was firstly reproduced in an independent workbook. The Microsoft® Excel workbook optimisation problem comprises 4th order Runge-Kutta numerical integration for all species concentrations using a constant step size of 0.2 minutes over 420 minutes, repeated for all 16 experiments. All cells containing concentration calculations referenced to a single set of kinetic parameters. An objective function uses the kinetic predicted ion concentrations at the batch experimental time steps in order to calculate an objective function value. The objective

function is changed by varying the set of kinetic parameters. The subsequent optimisation of 55 parameters using the Microsoft® Excel Solver function to minimise the objective function failed to converge at a realisable solution.

The optimisation problem was reproduced in MATLAB™. The MATLAB™ optimisation problem comprises separate functions containing ODEs; an objective function; nonlinear constraints; and an overarching optimisation algorithm and function caller. Benefits of using a MATLAB™ environment for optimisation include ODE variable step solver capabilities and the availability of several highly versatile optimisation algorithms. Variable step integration uses changing time step sizes in order to reduce the numerical integration error. The Global Optimisation Toolbox™ within MATLAB™ provides several algorithm possibilities for objective optimisation. Five single objective global optimisation algorithms exist in the Global Optimisation Toolbox™ for MATLAB™ 2014a (MathWorks, 2015):

1. Genetic algorithm – mimics the process of natural selection by using a random population of sets of parameters to create children with improved objective functions.
2. Global search – uses scattered starting points to calculate basins of attraction and subsequently attempts to enter certain basins by using gradient-based techniques.
3. Multi start – uses uniformly produced starting points to calculate basins of attraction and subsequently attempts to enter all basins by using gradient-based techniques.
4. Pattern search – calculates the objective function in a uniform mesh of parameters and moves in the direction of the decreasing objective function.
5. Simulate annealing – mimics the process of heating material and lowering the temperature to decrease defects.

MathWorks (2015) suggest the use of pattern search (PS) and genetic algorithm (GA) for high-dimensional non-smooth problems. PS is proven to converge to the local optimum, while GA has no convergence proof due to its randomised approach. The use of global search (GS) is suggested if the problem is smooth and a single global solution is required. Simulate annealing is not recommended as it is extremely slow. Multi start is useful to obtain a set of local minima and is typically slower than GS since it continues to analyse all starting points (MathWorks, 2015).

Four versions of rate expressions were optimised: a version for each separate group of updates; a version with all of the updates; and a version with no updates. The optimisation problems at hand had single objectives; was highly dimensional; and was smooth. GA and GS were selected to search a wide parameter range in order to investigate both randomised and gradient-based technique results. It was decided to refine the GA and GS outputs using the PS algorithm. Values derived by Dorfling (2012) for rate expression constants,

activation energies and shape factors were used as a starting point for GS. Starting points were automatically generated for GA. Upper and lower bounds were defined for both GA and GS. Bounds for shape factors were estimated using physical constraints. Bounds for rate expression constants and activation energies were approximated from results of Dorfling (2012). A non-linear constraint was used to avoid a combination of rate expression constants and activation energies which produce unrealisable rate of reactions:

$$k_{j,high} < k_{0,j} e^{\frac{-E_{a,j}}{RT}} < k_{j,low} \quad \text{Equation 6.15}$$

Values for $k_{j,high}$ and $k_{j,low}$ were estimated by calculating maximum and minimum possible reaction rates for reaction j , respectively, by using extreme concentration gradients from batch experimental data. This constraint was necessary since certain combinations of rate expression constants and activation energies resulted in unrealisable objective function values (i.e. NaN and Inf), which interrupted the algorithms.

The number of starting points for GS and initial population size for GA were increased due to the high dimensionality of the optimisation problem. ODE113 is a variable order Adams-Bashforth-Moulton differential equation solver in MATLAB™. ODE113 has a low to high order of accuracy and is often used to solve computationally intensive problems (MathWorks, 2015). It was therefore used within both the GA and GS optimisation problems. The GA and GS outputs were intended to be rough estimation of an optimal zone. ODE45 is based on an explicit 4th and 5th order Runge-Kutta formula, and is typically used to solve differential equations with medium accuracy. ODE45 was used in the subsequent PS optimisation problem in an attempt to provide a more accurate final set of parameters.

Results and discussion

The Microsoft® Excel reproducibility of Dorfling's (2012) standard reaction kinetics is expressed in concentration percentage errors. Refer to the table below.

Table 6.7: Excel optimisation worksheet reproduced in independent worksheet

Experiment	Maximum percentage error (%)	Experiment	Maximum percentage error (%)
2a	0.11	2i	0.17
2b	0.27	2j	3.41
2c	0.19	2k	0.30
2d	0.72	2l	0.12
2e	1.49	2m	0.10
2f	0.13	2n	0.06
2g	0.16	2o	0.18
2h	27.62	2p	0.10

Values reported in Table 6.7 are percentage differences between Dorfling's (2012) Excel worksheet and the reproduced version. These values are the maximum percentage differences for respective experiments noticed over all components and for all 0.2 minute time steps. Minor differences are reported for all experiments, except for experiment 2h. This large error was caused by Dorfling (2012) not using the measured Ni^{2+} concentration at time zero for experiment 2h, but rather an average of the time zero Ni^{2+} concentration. The replaced Ni^{2+} concentration was lower than subsequent Ni^{2+} concentration data points, which is unrealisable.

The standard reaction kinetics was then reproduced in MATLAB™. The reproducibility of a single experiment is shown below.

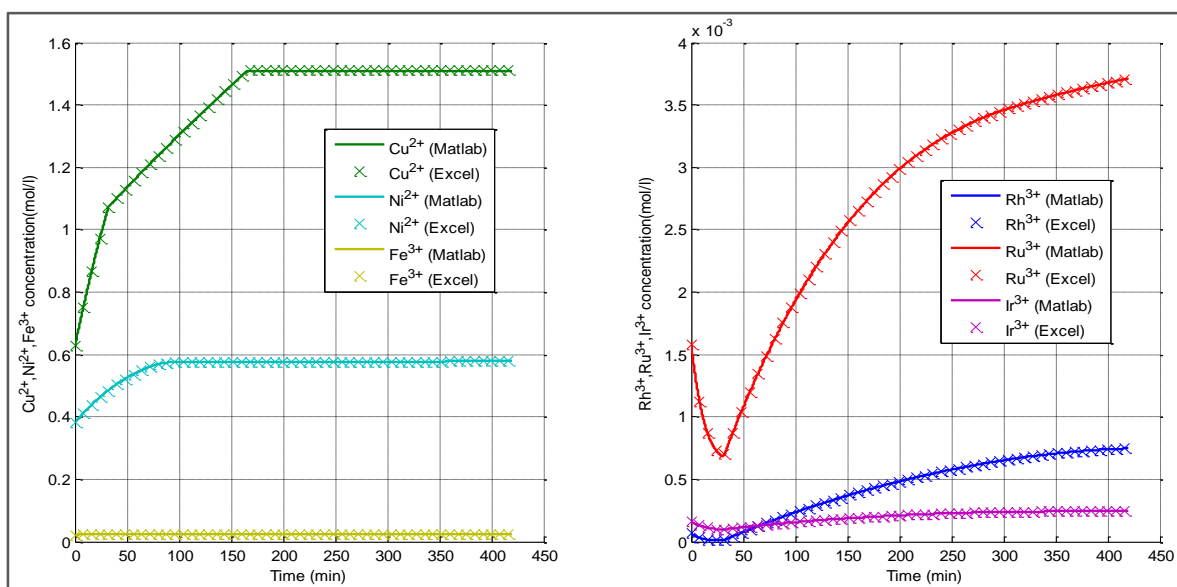


Figure 6.17: Excel optimisation worksheet reproduced in MATLAB™ (results for experiment 2a)

Dorfling's (2012) Excel worksheet is almost perfectly reproduced in MATLAB™. Similar correlations are obtained for other experimental runs.

The other three reaction kinetic versions were implemented in MATLAB™. All four versions were then optimised according to Figure 6.16 and by using the improved objective function. The optimisation results are captured in Table 6.8. The reaction kinetic parameters for each solution are provided in Appendix F.

The standard fit in Table 6.8 represents the improved objective function calculated for standard kinetics and parameters presented by Dorfling (2012). Both genetic algorithm (GA) and global search (GS) produced an improved fit for the standard kinetics, when compared to the standard fit. These outputs were further improved when given to separate pattern searches (PS).

Table 6.8: Objective function outputs for several sets of MATLAB™ global optimised reaction kinetics

	No updates	Shape factor changes	Initial condition lumping	All updates
GS	10.99	11.45	84.63	84.29
GS with PS	10.91	11.31	33.07	35.92
GA	19.69	130.93	130.92	123.78
GA with PS	17.90	119.21	118.01	119.25
Standard fit	27.62			

In terms of improved reaction kinetic sets, only the shape factor changes after GS optimisation; and GS with PS optimisation; respectively, indicates an improved fit. Other reaction kinetic versions have large objective function values. It is speculated that this was caused by the inability to provide other reaction kinetic versions with similar quality parameter starting points. It is furthermore expected that the solvers had difficulty navigating through these high dimensionality problems.

The lack of convergence proof for GA is evident in Table 6.8, where a good fit is only seen for the standard kinetics. The difficulty for GA to obtain consistent quality fits is partially attributed to the high dimensionality of the optimisation problem (up to 57 dimensions – see Table 6.6) and the associated difficulty to produce improved objective function children. GS, a gradient-based algorithm, produced a much better fit irrespective of reaction kinetic version. The gradient-based technique moved pragmatically towards an improved objective function at several starting points. It is therefore clear that the gradient-based technique is superior within this optimisation problem. The gradient-based technique can exploit the smoothness of the objective function plane, while GA relies on interpolating between different population values in a discrete manner (expected to be superior within non-smooth optimisation problems). The PS algorithm managed to improve the fit in all reaction kinetic sets. The extent to which it improved differs significantly. PS is proven to converge to local minima. It can therefore be deduced that a local minima has been reached by algorithms in

cases where PS did not show a significant improvement. This statement is evident for the GS algorithm in both no updates and shape factor changes reaction kinetic versions, and is substantiated by the closely related kinetic parameters. The same principle can be applied to the GA and the subsequent GA and PS solutions. The latter three reaction kinetic version fittings in the GA and GA with PS are rather suboptimal. It is expected that the combined GA and PS solutions for these three cases were far away from an adequate solution, therefore in a region where expected changes had insignificant effects on the objective function. This statement is substantiated by the remote kinetic parameters for these solutions, and the closely related values between respective GA and PS solutions.

A comprehensive search for the global minima is challenging due to the high dimensionality of the optimisation problem, and requires a great deal of time and computational capacity. The optimisation effort within this project also showed the necessity for adequate initial conditions and limited bounds, especially in such high dimensionality optimisation problems. GA, GS and PS contain additional settings which can be adjusted to improve the robustness of the search which is expected to improve the search for a global minimum. This, however, will notably increase the optimisation time and computational capacity requirements which were limited for this section of the project.

The majority of objective function error for kinetics with a reasonable fit are attributed to the copper ion concentrations. The cupric ion concentration for the first four batch experiments together with the fitted reaction kinetic predictions are shown below. Refer to Dorfling (2012) for the experimental conditions.

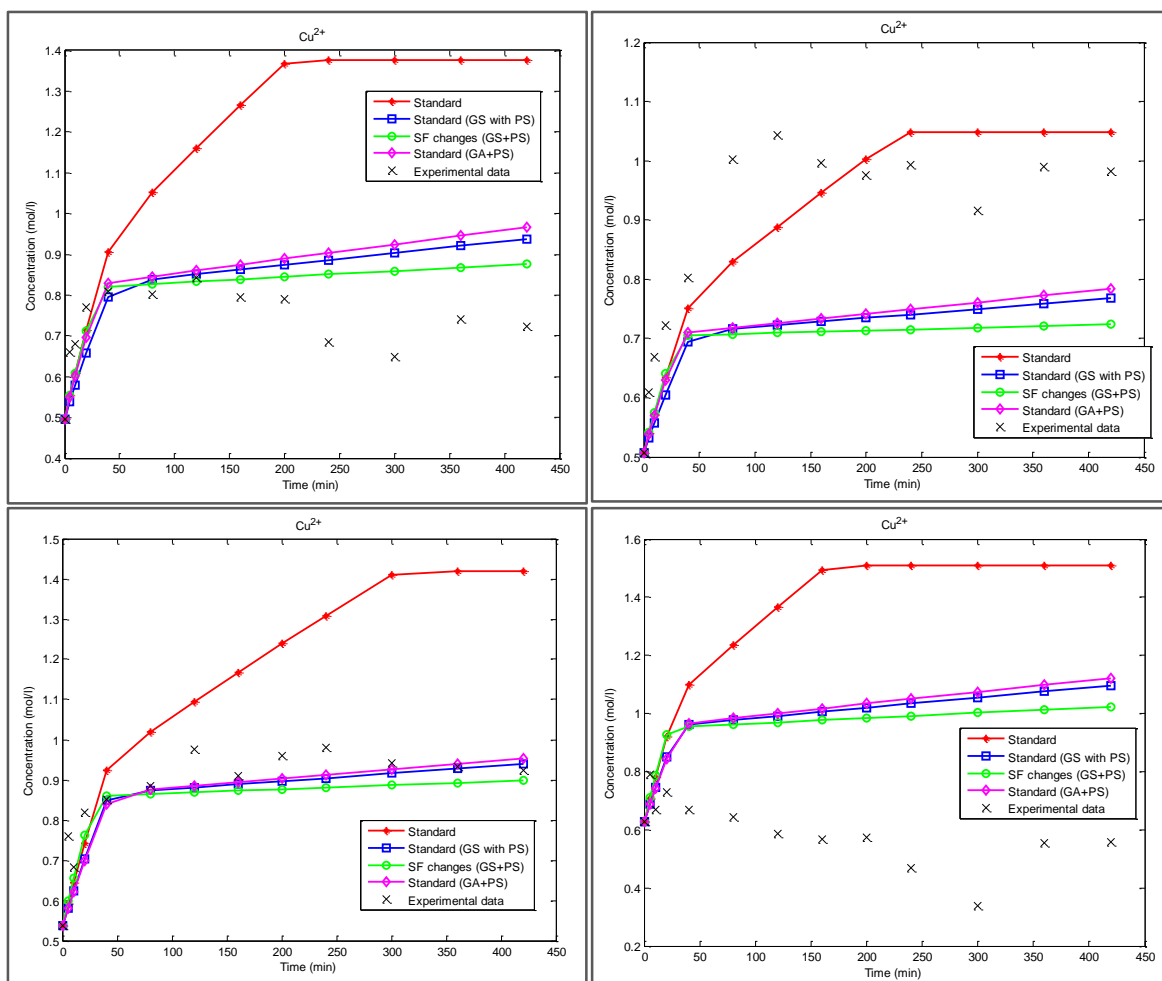


Figure 6.18: Cupric ion concentration of first four experiments with optimised fits

The overall fit (i.e. objective function) of each optimised reaction kinetic version shown in Figure 6.18 improved when compared to the standard case. However, none of these optimised kinetics fit well when visually inspected. This is caused by cupric ion concentration decreases which is currently not described by any reaction in the final set used by Dorfling (2012). The optimisation algorithms attended to these unrealisable errors within the objective function which ultimately caused a reduced fit in other realisable areas (refer to the top right graph in Figure 6.18). The reduction in cupric concentrations were possibly caused by cementation reactions, which is considered in Section 6.3.1.

Note how the modelled cupric ion concentration trends are constrained to linear dynamics with a few abrupt gradient changes, whereas the batch experimental data indicate more movement (the contribution of measurement variance to these dynamics are unknown). The constrained modelled dynamics is attributed to the copper leaching rate expressions that are only dependent on available oxygen and acid concentrations. The sudden gradient changes reflect the stop of reactions due to the depletion of a reactant. The additional copper leaching mechanism (i.e. via ferric ion oxidation, discussed in Section 6.3.2) might contribute

in capturing additional cupric ion data point movement by relating the copper sulphide leaching to other variables.

The fit of other cupric ion experimental data looks similar to that in Figure 6.18. Other ion species concentrations indicate much better fits. However, copper reactions are of prime concern since they dominate the leaching process.

Proposed model updates

The improved and refitted reaction kinetics indicated a significant decrease in the objective function value. However, this improvement is negligible when the copper ion concentration trends and model predictions are visually compared. The improvement of the objective function is still small compared to the objective function value itself. The source of the large objective function value comes from the inability of the current reaction kinetics to describe a decrease in cupric ion concentrations. This issue needs to be addressed first. No dynamic process model updates were therefore made.

6.4. Computerised Model Verification

The programming and implementation of the mathematical basis into the Simulink™ dynamic process model is verified in this section. No explicit assumptions require validation.

The baseline model is a hybrid of high level programming and simulation language due to the MATLAB™ code which exists within the Simulink™ model. Verification of both proper equation implementation and use of correct functions are therefore required (Sargent, 2005).

6.4.1. Static testing

Problem statement and methodology

Static testing was done specifically on the Simulink™ baseline model (Haasbroek & Lindner, 2015) by using structured walk-throughs on model areas listed in Figure 3.5 in an attempt to address computerised issues that exist within the dynamic process model. The structured walk-through for each model area comprised four separate checks:

1. Correct implementation of equations.
2. Correct use and transformation of units.
3. Correct use of functions and model blocks.
4. Correct use of constants.

The checks listed above were applied to 9 functions and 9 function blocks that make up the Simulink™ dynamic process model.

Results and discussion

Several problems surfaced within a range of functions and reference models during static testing. Refer to the table below.

Table 6.9: Errors noticed and corrected during a structured walk-through

MATLAB functions					
	Implementation of equations	Use of units	Use of functions or model blocks	Use of constants	Total
getH.m	0	0	0	0	0
getCP.m	0	0	4	0	4
MOD_calculate_reaction_rates.m	0	0	0	0	0
Reaction_Rate.m	0	0	0	1	1
Reaction_Rate_2.m	0	0	0	1	1
fraction2conc.m	1	0	0	0	1
calculate_oxygen_solubility.m	0	0	0	0	0
ReactionKinParse.m	0	0	0	0	0
input_data.m	0	0	0	5	5
Simulink reference models					
Second stage slurry prep tank	0	0	0	1	1
Flash recycle tank	2	0	1	1	4
Compartment 1	0	2	0	0	2
Compartment 2	0	2	0	0	2
Compartment 3	0	2	0	0	2
Compartment 4	0	2	0	1	3
Second stage discharge tank	0	0	0	1	1
Thickener	0	0	0	1	1
Third stage slurry prep tank	0	0	0	1	1
<i>Total</i>	3	8	5	13	29

A total of 29 problems are listed in Table 6.9. Most of these problems exist within Simulink™ reference models. These problems are briefly discussed.

The use of mass flow rates in Equation D.10 (featuring in fraction2conc.m) was unnecessary. Avoiding this allows the removal of for-loops within autoclave compartment MATLAB™ function blocks, since the calculation used to determine the autoclave compartment concentration becomes independent of the compartment outlet flow rate (the outlet flow rate is a function of oxygen consumption which relates it to concentrations via rate expressions). The updated Equation D.10 is also realisable when mass flow rates are zero.

A simplified version of a generic energy balance (Equation 3.9a) was previously implemented in the flash recycle tank which did not take vessel mass changes into account:

$$\frac{dT}{dt} = \frac{\dot{Q} - \dot{W}_{shaft} + \sum_{in} \dot{m}_{i,k} \hat{H}_{i,k} - \sum_{out} \dot{m}_{i,k} \hat{H}_{i,k} - V \sum r_j \Delta \hat{H}_{rxn,j}^o}{m_{tot} C_p} \quad \text{Equation 3.9c}$$

An improved version is given in Equation 3.9d:

$$\frac{dT}{dt} = \frac{\left(\frac{\dot{Q} - \dot{W}_{shaft} + \sum_{in} \dot{m}_{i,k} \hat{H}_{i,k} - \sum_{out} \dot{m}_{i,k} \hat{H}_{i,k} - V \sum r_j \Delta \hat{H}_{rxn,j}^o}{C_p} - (T - T_{ref}) \times \frac{dm_{tot}}{dt} \right)}{m_{tot}} \quad \text{Equation 3.9d}$$

Equation 3.9d takes into account change in vessel mass.

Discrepancies existed between heat capacities; heat of water vaporisation; and other energy balance units within autoclave compartments. The units were simply converted so as to be consistent.

Compartment temperatures were used in the getCP.m function to calculate the specific heat capacities for inlet streams to all four compartments. This was simply corrected by using inlet stream temperatures in these calculations.

Autoclave volumes featuring in both Reaction_Rate.m and Reaction_Rate_2.m were constant which caused incorrect heat release and concentration predictions when volumes changed, among others. This problem is countered by making volumes vary with varying compartment levels.

All five preparation vessel volumes within input_data.m were incorrect (all vessel volume were 1 m³). This caused lowered disturbance attenuation effects and reduced tank holdup. Correct vessel volumes were obtained from Knoblauch (2014) and implemented in the dynamic process model.

An incorrect vessel length was used in the calculation of heat lost to the environment for the fourth compartment (see Equation D.3). The correct length was subsequently implemented.

Model updates

The model updates were mentioned throughout the results and discussion section in order to ease the readability.

6.4.2. Dynamic testing

Problem statement and methodology

Dynamic testing was done by verifying mass balance consistencies around all process units in the dynamic process model.

Results and discussion

The results of mass balance consistency checks for all process units within the dynamic process model are shown below.

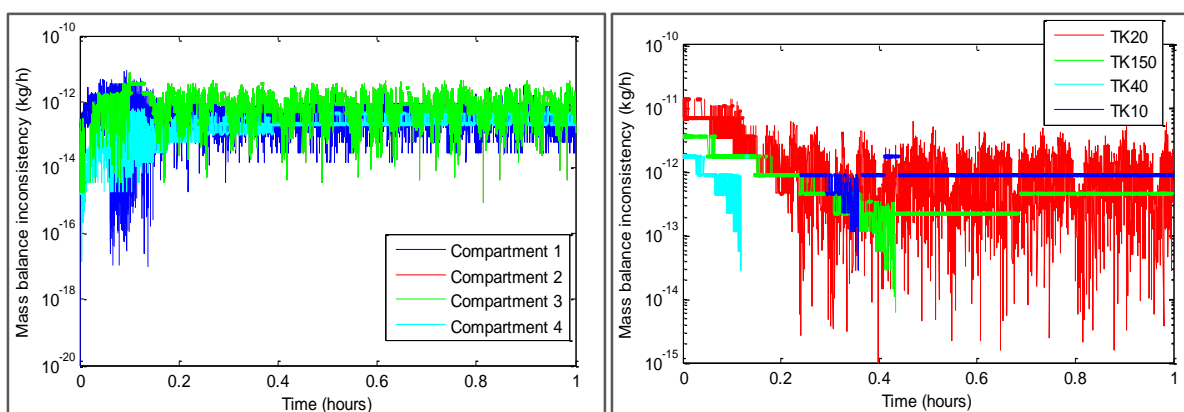


Figure 6.19: Mass balance consistency checks

The y-axes of plots given in Figure 6.19 are logarithmic to show a large range of mass flow rates. The mass balance inconsistencies are negligible when Figure 6.19 is considered. These inconsistencies are caused by Simulink™ computational error tolerances.

Proposed model updates

No dynamic process model updates are required.

6.5. Operational Validation

This section describes the validation of model operation when compared to the actual Western Platinum BMR outputs.

6.5.1. Degree of freedom analysis

Problem statement and methodology

A zero degree of freedom (DOF) is required over the entire dynamic process model to ensure that the model is not over-specified or under-specified. The DOF over a process unit can be calculated using Equation 6.16.

$$N_{DOF} = N_{Eq} - (N_V + N_{DV}) \quad \text{Equation 6.16}$$

where N_{Eq} , N_V and N_{DV} represents the number of equations, variables, and variables defined with values, respectively. All unknowns are firstly classified as variables, and thereafter classified as variables with defined values if it is in fact a constant parameter. Equations listed in Appendix F from Dorfling (2012) which describe the dynamic process model mathematically were used in the DOF analyses. The DOF numbers were counted for process units in the following order: TK-10; TK-20; Compartment 1; Compartment 2; Compartment 3; TK-40; TH-700; TK-150; Compartment 4.

Results and discussion

Results for degree of freedom (DOF) analyses for respective process units are provided in the following table.

Table 6.10: Degree of freedom analyses for respective process units

Vessel	Equations	New variables	Variables defined with values	DOF
TK-10	52	101	49	0
TK-20	35	77	16	-26
Compartment 1	136	331	221	26
Compartment 2	34	44	10	0
Compartment 3	34	42	8	0
TK-40	28	29	1	0
TH-700	21	22	1	0
TK-150	33	66	33	0
Compartment 4	35	47	12	0
<i>Total</i>	<i>408</i>	<i>759</i>	<i>351</i>	<i>0</i>

An overall DOF of zero is obtained. This was only evident after additional equations not listed in Appendix F of Dorfling (2012) were added. These equations link reaction kinetics; oxygen consumption rates; and mass balances within the process model.

A negative DOF discrepancy exists in TK-20, and is subsequently equalised in the first compartment. This is expected since recycle stream variables are not available when conducting a DOF analysis over TK-20, prior to taking the first compartment into account.

The first compartment shows far more equations and variables compared to the others. This is caused by numerous generic parameters from rate expressions and applicable constitutive equations being defined in the first compartment. The fourth compartment shows one additional equation when compared to the second and third compartment. This is caused by the direct steam injection stream only present in the fourth compartment. Preparation tank equations vary slightly due to the amount of streams entering and exiting.

Proposed model updates

The DOF analyses balanced. The dynamic process model is therefore correctly specified. No model updates were required.

6.5.2. Constant temperature and composition inputs

Problem statement and methodology

Dorfling (2012) assumed constant temperature and composition inputs to the dynamic process model (refer to Table 3.3). Historian tag data and manually measured data provided temperature and compositional profiles which were used to check the validity of this assumption. The assumption did not hold for certain temperatures and compositions, and therefore required the simulation of natural change in variables. A one-dimensional random walk was built in Simulink™ to produce this natural change in input variable values which were previously assumed to be constant (Nordlund, 2006; Lawler & Vlada, 2010):

$$s_i = \begin{cases} +l, & x_i < 0.5 \\ -l, & x_i \geq 0.5 \end{cases} \quad \text{Equation 6.17}$$

where l represents an expected time related gradient for variable v . Variable x assumes a pseudorandom and uniform generated value between 0 and 1 for every time step i . This produces a random combination of variable gradients s_i , which is numerically integrated:

$$v = \sum_{i=1}^N s_i \Delta t + v_0 \quad \text{Equation 6.18}$$

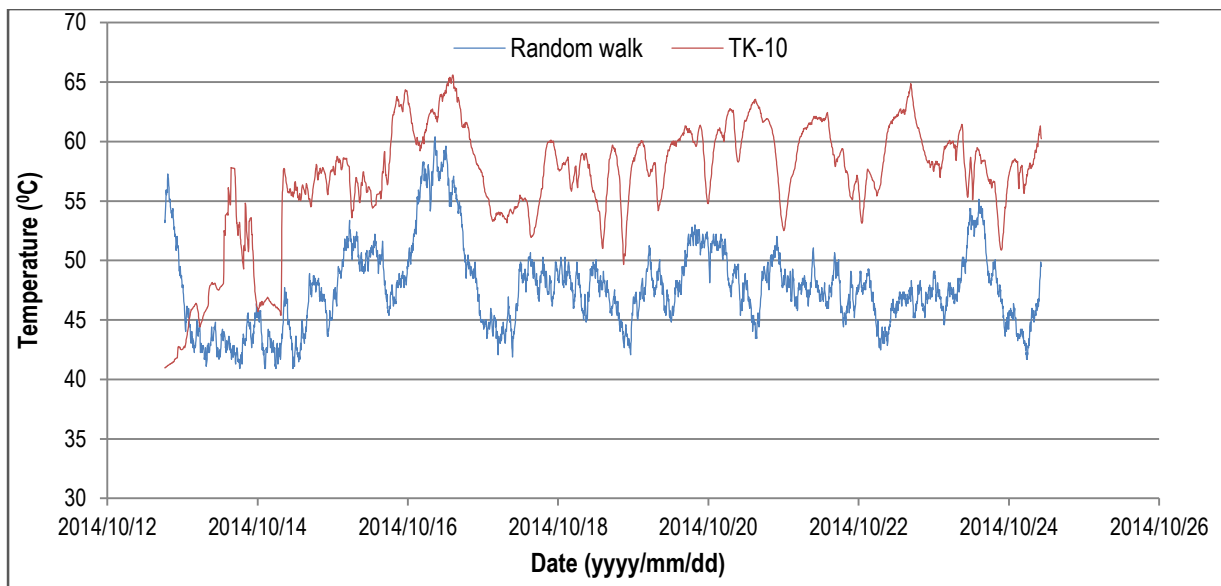


Figure 6.21: Second stage slurry preparation tank temperature profile compared to a random walk

The temperature inside the vessel is clearly not constant or close to ambient conditions. The generated random walk should not predict the temperature profile exactly, but merely move in a similar manner over time. The random walk generator was applied to temperatures of stream 1, 2 and 3 with similar variable gradients and variable starting points but with different starting seeds. Stream 18 has the same source as stream 2 and was therefore given the same seed. Stream 4 is a fresh feed of sulphuric acid, and is not expected to follow the trend seen in Figure 6.21. A sine wave was used to predict the temperature profile of stream 4 with the amplitude, bias and frequency determined from ambient temperature profiles of Marikana.

A similar methodology can be applied to the third stage slurry preparation tank. However, temperature profiles for the third stage slurry preparation tank or its inlet streams are unavailable. These stream temperatures are not expected to follow trends seen in Figure 6.21 since they are fresh feeds. A temperature profile similar to that of stream 4 was applied to these streams.

The frequency diagrams captured in Figure 6.22 illustrates the first stage leach residue composition movement over four years. Compositional data is only available for stream 3 and the solid phase of stream 1. All compositional data sets in Table 6.3 are used.

It is clear that the composition in the first stage leach residue is not constant. High reproducibility in frequencies is noticed for iron and nickel over the four years. Copper concentrations seem to have increased after 2012. Change in one species composition affects all other compositions, which is not clear for components in Figure 6.22.

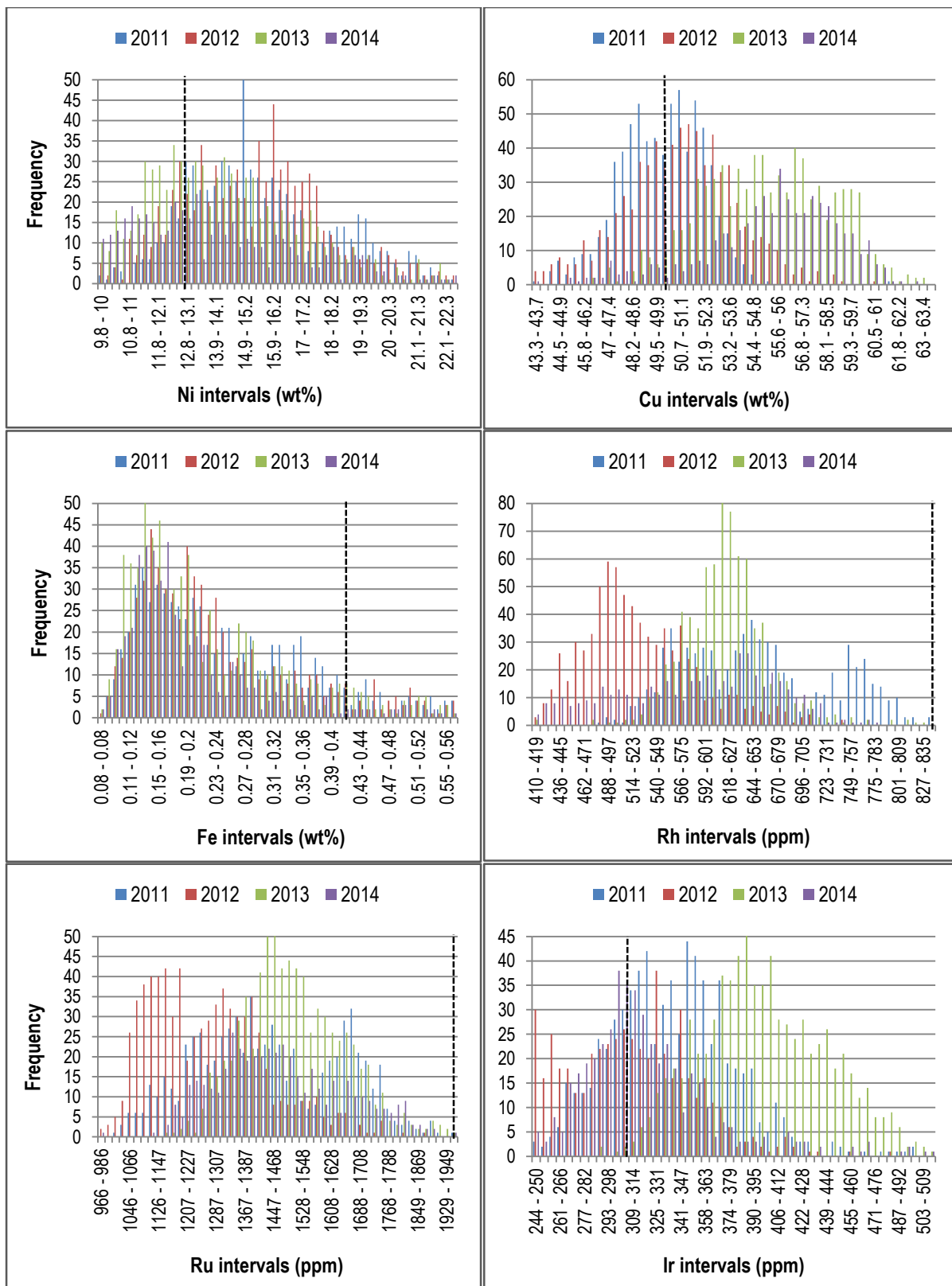


Figure 6.22: Frequency diagrams for first stage residue compositions

PGMs show large frequency changes over the four years. This movement seems to correlate slightly between PGMs. The dashed line indicates where Dorfling (2012) assumed

a constant input value for the model. The model values seem to correspond with the highest nickel, copper and iridium composition frequencies for 2011 and 2012. This is at the time Dorfling (2012) obtained residue samples. The same conclusion cannot be made for iron, rhodium and ruthenium compositions.

It would be difficult if not impossible to simulate the movement of compositions as several years pass by. This is however not required since the model will not be operated over such long periods. Compositions within the latest year were used to produce random walks for all species in Figure 6.22. Random walk results are shown in Figure 6.23.

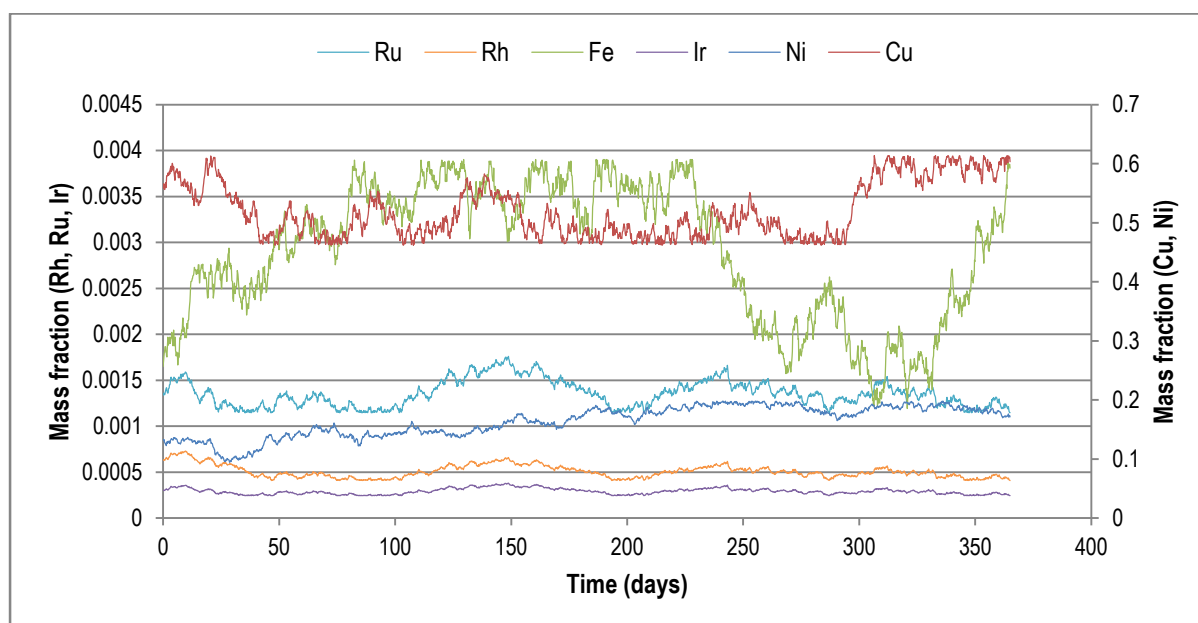


Figure 6.23: First stage leach residue composition random walk generation

Random walks in Figure 6.23 show similar range of movement over one year when compared to data in Figure 6.22. The random walk starting points are also an improvement when compared to the previously assumed constant values.

A similar methodology is applied to the formic filtrate liquid stream. Dorfling (2012) assumed the liquid stream consist only of water and a small fraction of sulphuric acid. Frequency diagrams shown in Figure 6.24 illustrate the formic filtrate liquid concentration movement over four years.

Large frequencies are noticed for all PGMs at the lowest concentration interval. Most of these measurements are reported only to be smaller than 0.001. A variety of other PGM concentrations are seen, but low concentrations dominate the frequency graph. Note that frequencies seen in Figure 6.24 for each year are incomplete – numerous data points are missing, which corresponds to the low total reported frequency in Figure 6.24.

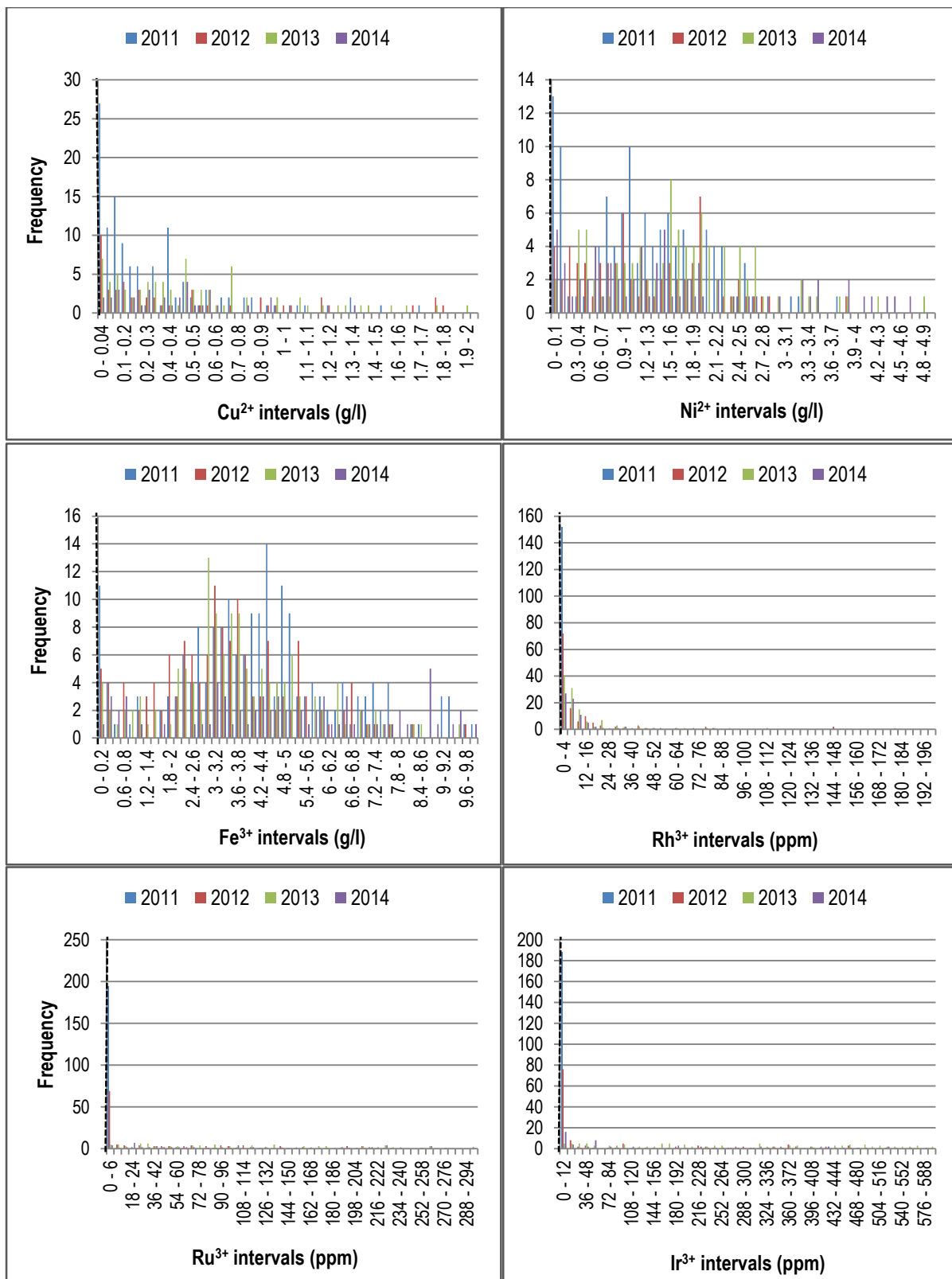


Figure 6.24: Frequency diagrams for formic filtrate liquid concentrations

Nickel and ferric concentrations show a wide range of concentrations for each year, while cupric ion concentrations show lower variance.

Compositions within the latest year were once again used to produce random walks for all species in Figure 6.24. Random walk results are shown in the figure below.

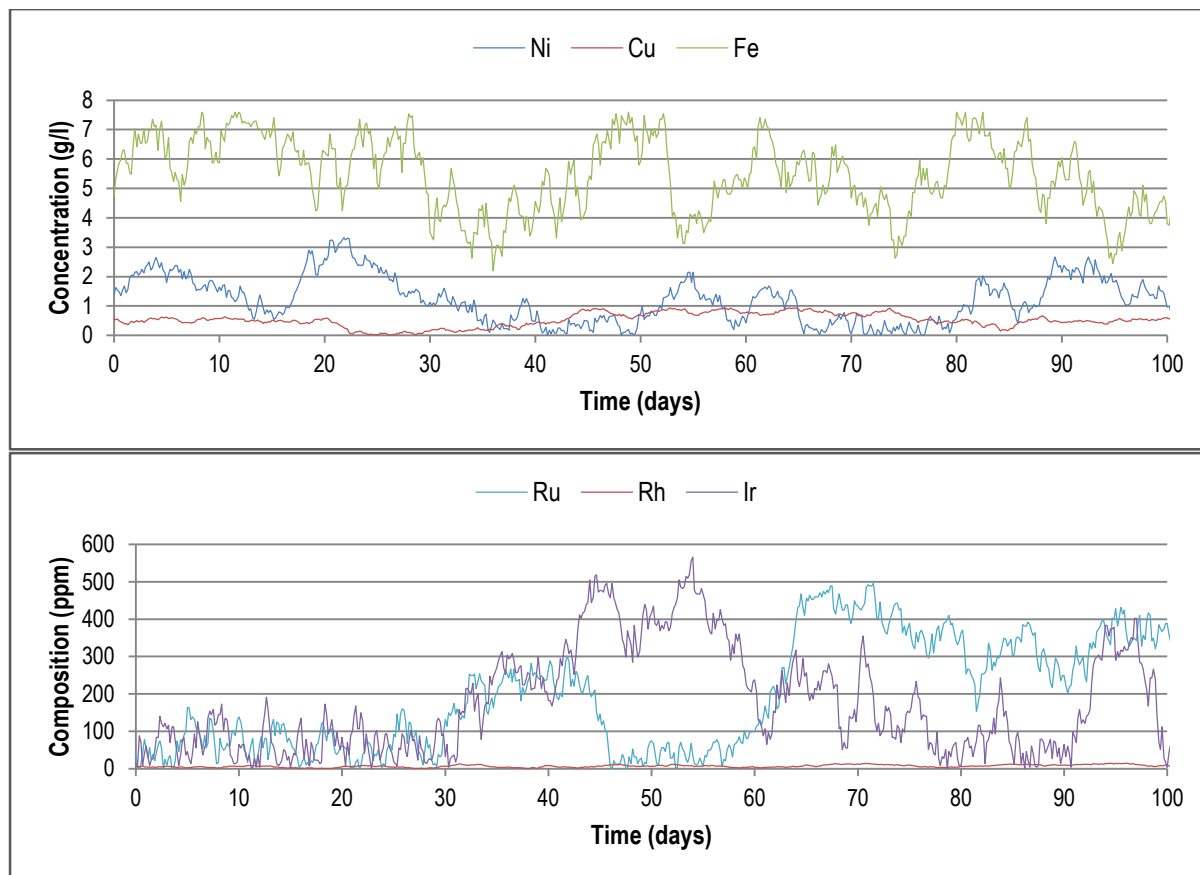


Figure 6.25: Formic filtrate liquid concentration and composition random walk generation

Ferric and nickel ion concentrations move more rapidly and over a bigger concentration range when compared to the cupric ion concentrations. This corresponds to the actual plant data when the frequency diagrams are considered. The same conclusion is drawn for ruthenium and iridium when compared to rhodium. The iridium and ruthenium trends seem to have major movement. This expected since similar movements are noted in compositional data over a short span of time.

Compositional variance of spent electrolyte input streams are also expected. However, no spent electrolyte compositional data is available so as to produce random walks.

Model updates

Model updates are discussed throughout the previous section in order to ease the readability.

The natural change in model inputs via random walks ensures that control strategies are continuously active and compensating for expected changes.

6.5.3. Isothermal preparation tanks

Problem statement and methodology

The assumption of constant temperature inputs to the dynamic model was proven to be invalid (discussed in Section 6.5.2). All streams entering the second stage slurry preparation tank are model inputs and therefore have constant input temperatures. This allowed Dorfling (2012) to assume that the second stage slurry preparation tank is isothermal at an ambient temperature, since all the other energy balance terms (shaft work and heat loss) are expected to have insignificant contribution to the temperature changes. Dorfling (2012) used the same isothermal assumption for all other auxiliary tanks (i.e. for the three consecutive process units following the third compartment: second stage discharge tank, second stage discharge thickener, third stage slurry preparation tank). Dorfling (2012) used the third compartment steady-state temperature as the outlet temperature for these auxiliary tanks. The validity of assuming isothermal preparation tanks are addressed using results from the previous section.

Results and discussion

It was previously shown that the second stage slurry preparation tank temperature is not constant or close to ambient. An energy balance in the second stage slurry preparation tank is therefore required.

The P&ID's of Western Platinum BMR indicate that cooling water is used in the second stage discharge tank to control the vessel temperature (the set-point temperature of the second stage discharge tank and the third compartment are dissimilar). Moreover, a thickened slurry stream with a typically low flow rate is mixed with streams of dissimilar temperatures within the third stage slurry preparation tank. These three consecutive auxiliary tanks are therefore expected to have varying temperatures which are dissimilar to the third compartment steady-state temperature. The necessity of energy balances in auxiliary tanks become more evident when considering the purpose of the dynamic process model in this project. Certain faults are expected to upset temperature profiles within vessels. These upsets need to propagate properly through downstream process units.

Model updates

Energy balances as shown in Equation 3.9d were implemented in all auxiliary tanks found in the dynamic process model to ensure proper temperature estimations and energy propagation.

6.5.4. Constant mass in all autoclave compartments

Problem statement and methodology

Dorfling (2012) assumed that the mass in all autoclave compartments stay constant. This assumption is validated by using operable plant data from data set 5.

Results and discussion

The Western Platinum BMR autoclave compartment level profiles are considered over a few days.

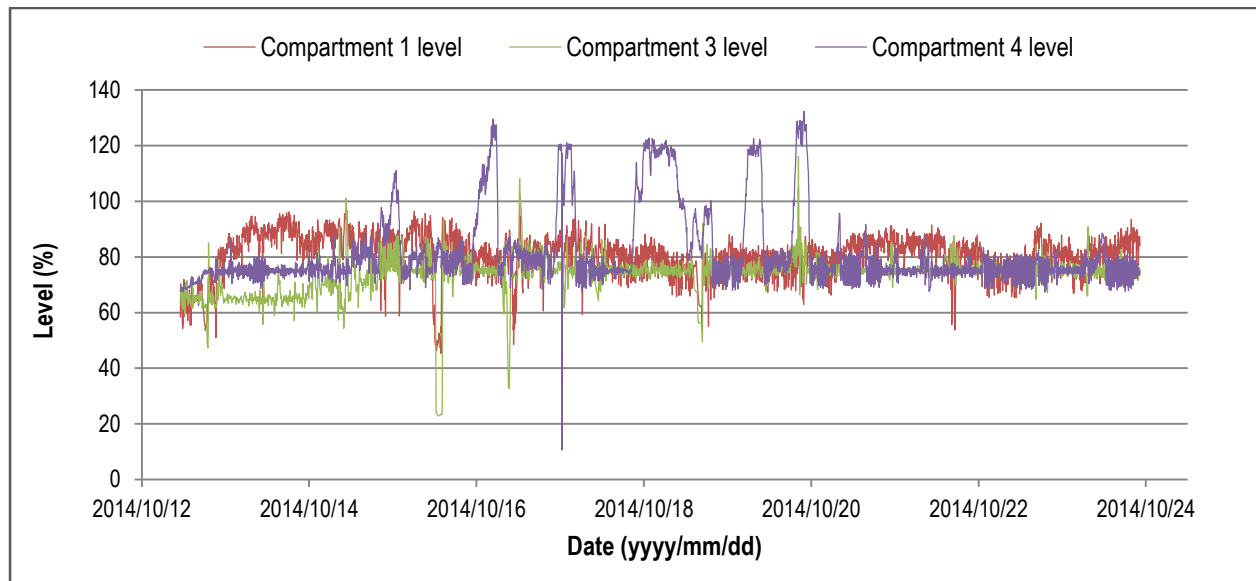


Figure 6.26: Autoclave compartment level profiles

The level in the first compartment varies over time reaching values as low as 50 %. The level in the third varies more significantly and reaches extreme values (i.e. 20 % and above 100 %). Similar trends are noticed for the fourth compartment. Levels above 100 % are possibly caused by sensor bias or level leeway incorporated during level calibration. Notice that the second compartment is not shown in Figure 6.27. This compartment does not have a level indicator since it is purely an overflow vessel. The mass inside this compartment might change due to density changes, but not significantly. The constant mass assumption is therefore valid for the second compartment.

The level changes in the plant data are significant, as expected; disturbances often cause levels to vary from their set-points. The variation in compartment levels affects the residence time and therefore the extent of leaching. In addition, this project considers the occurrence of faults in the dynamic process model which could result in abnormal process behaviour. Level changes are required in the dynamic process model to ensure that the model is realistically

perturbed when safety interlocks on level controllers activate. In addition, the overflow occurring in the first compartment and its perturbation in the occurrence of a level disturbance could also be realised.

Model updates

Mass balance ODEs (Equation 3.8a) were implemented in the first, third and fourth compartment for all material phases.

6.5.5. Isobaric autoclave

Problem statement and methodology

Dorfling (2012) assumed a constant autoclave pressure in the dynamic process model. This assumption was reconsidered after reviewing Western Platinum BMR autoclave pressure profiles using operable data in data set 5. Improvements were made as follows. The water vapour pressure in the autoclave was calculated using Antoine's equation (refer to Equation D.13). The temperature of the autoclave vapour, expected to be significantly dependent on liquid temperature, was estimated using a weighted compartment temperature average relative to the respective liquid surface areas:

$$T_{vap} = \frac{1}{A_{liq,tot}} \times \sum_{i=1}^{N=4} A_{liq,i} \times T_i \quad \text{Equation 6.19}$$

Each compartment liquid surface area is approximately proportional to their respective volumes, which are known. This estimation will be validated by applying it to plant data. The autoclave total pressure is simply the sum of the partial pressures:

$$P_{tot} = P_{O_2} + P_{H_2O} \quad \text{Equation 6.20}$$

The oxygen partial pressure was calculated using the ideal gas law:

$$P_{O_2} = \frac{n_{O_2}RT_{vap}}{V_{vap}} \quad \text{Equation 6.21}$$

The vapour space was calculated from a design sheet and added to additional space unoccupied by slurry at a specific time. An oxygen mole balance was conducted around the autoclave and integrated in order to predict the oxygen mole amount in the vapour space at a specific point in time:

$$\frac{dn_{O_2}}{dt} = \sum_{i=1}^{N=3} \dot{n}_{O_2,in,i} - \sum_{i=1}^{N=4} \dot{n}_{O_2,consumed,i} - \dot{n}_{O_2,out} \quad \text{Equation 6.22}$$

Oxygen is consumed in each of the four compartments. There are three areas where oxygen enters and only one point of exit. The molar flow rate exiting the autoclave was modelled as a function of the autoclave pressure.

Note that using the ideal gas law does not reduce the accuracy of the oxygen partial pressure prediction. It simply provides a means of relating oxygen flow rates to the total pressure via Equation 6.22.

Results and discussion

The autoclave pressure profile is considered below.

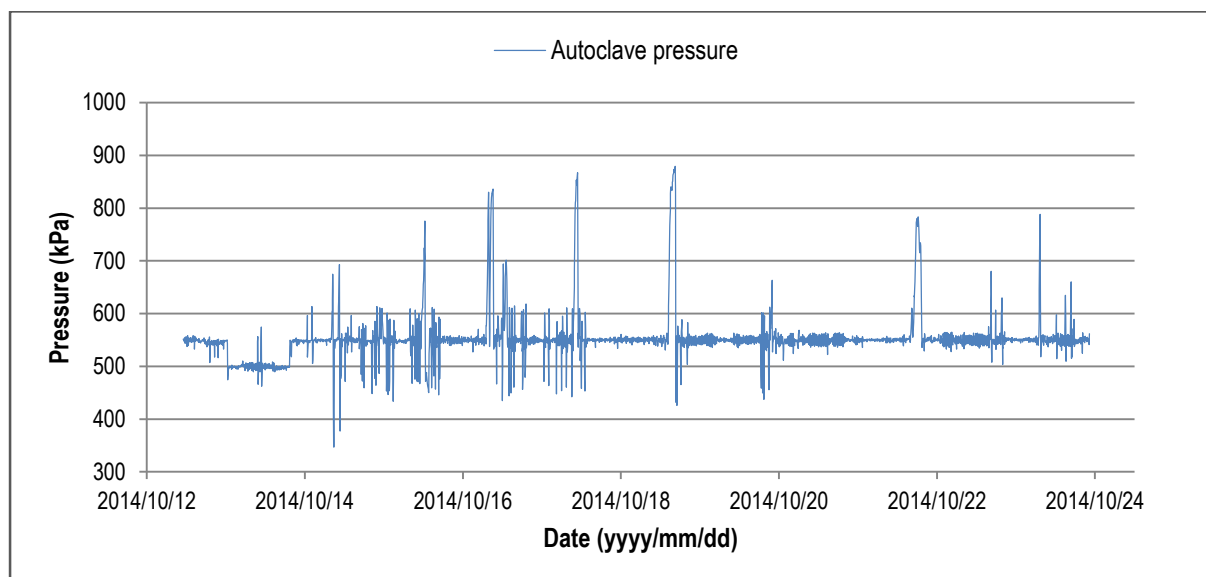


Figure 6.27: Autoclave pressure profile

The pressure seems to be controlled well at 550 kPa. There are a few instances where pressure exceeds 700 kPa and drop below 500 kPa. The fact that the oxygen mass flow rate has no effect on the autoclave pressure in the baseline dynamic process model is inadequate under faulty and extreme conditions.

The vapour temperature estimation (Equation 6.19) is applied to plant data to verify its validity. Note that Equation 6.19 is applied to autoclave 200 since the vapour temperature indicator in autoclave 300 was malfunctioning. Vapour temperature estimation results are shown in Figure 6.28.

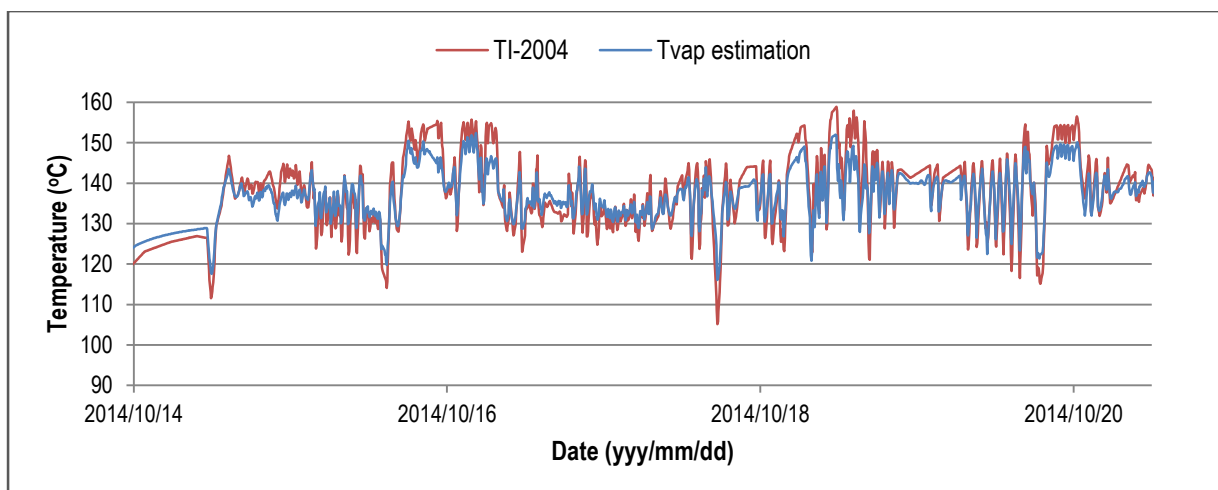


Figure 6.28: Autoclave vapour temperature estimated using compartment temperatures and volumes

The vapour temperature seems to be estimated relatively well via Equation 6.19. It is therefore an adequate approximation which can be used in oxygen partial pressure calculations.

Model updates

Pressure change was included in the updated dynamic process model. The compartment liquid temperatures; oxygen flow rate; and available vapour space now affects the total pressure in the updated model. The interactions between the different autoclave compartments via the vapour space are therefore also realised.

6.5.6. Sulphuric acid and water streams entering flash recycle tank

Problem statement and methodology

Western Platinum BMR P&ID's and the associated Delta-V™ user-interface reports two additional streams which enter the flash recycle tank which was not described by Dorfling (2012) or included in the dynamic process model. These two streams are used by operators as supervisory control mechanisms. Plant data is used to validate the operation of one of the streams.

Results and discussion

A concentrated sulphuric acid stream (FIC-0202) entering the flash recycle tank is excluded in the baseline model. Typical operation of this stream is shown in Figure 6.29. Data set 15 is used.

The sulphuric acid stream is not operated consistently, with low flow rates for short periods of time.

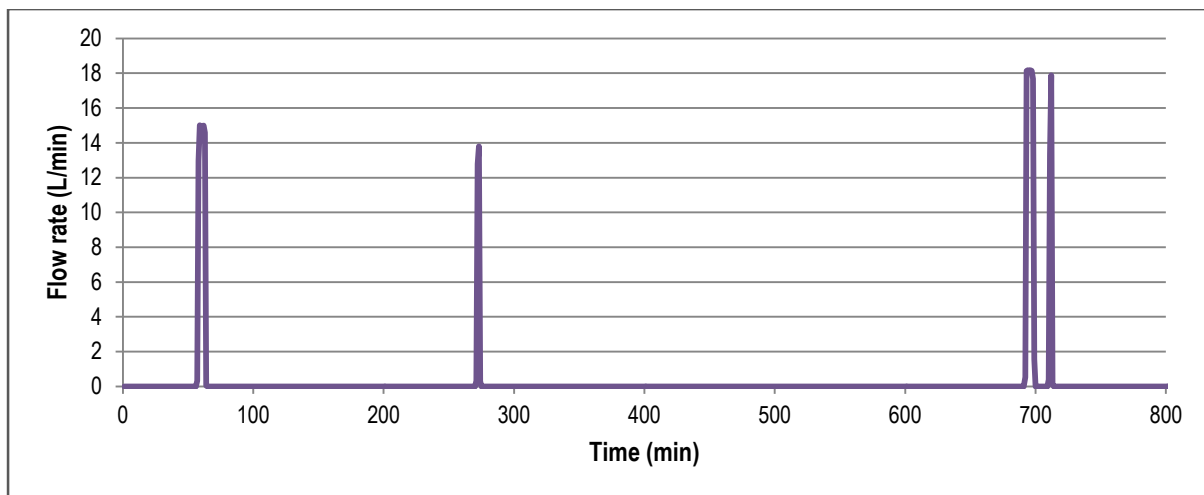


Figure 6.29: Typical FIC-0202 operation

Western Platinum BMR P&ID's and expert knowledge also showed that a manually controlled water stream exists which is occasionally utilised (McCulloch et al., 2014). The water stream is used only in abnormal situations, and has no only measurements as it is manually controlled.

Model updates

The sulphuric acid stream forms an important mechanism of acid concentration control in the flash recycle tank, making it part of the control philosophy used at Western Platinum BMR. One outcome of this project is to implement different layers of control onto the model. The sulphuric acid stream was therefore included in the updated model. The mechanism by which this flow controller is utilised to control acid concentrations is discussed in Chapter 7.

The water stream was also added to the updated model since it forms a part of abnormal process operation. The usage of the water stream is however limited as an abnormal event.

6.5.7. Ideal CSTR characteristics

Problem statement

Dorfling (2012) assumed all process units found in the dynamic process model exhibits ideal CSTR characteristics. The validity and possible issues related to this assumption are discussed. The possibility of model updates is mentioned.

Results and discussion

The validity of approximating process units as ideal CSTRs was inconclusive as insufficient plant information is available on this topic.

The ideal CSTR characteristics at Western Platinum BMR, if at all present, comes from aggressive mixing which ensures homogeneous reactor concentrations. Western Platinum BMR has several safety interlocks that stop agitation when levels are low in vessels. The ideal CSTR assumption is expected to be flawed under these circumstances. Limited agitation would result in a heterogeneous vessel. The dynamic process model predictability would at this point decrease significantly as the reaction mechanisms and rate expressions are expected to change under these conditions.

Proposed model updates

No dynamic process model changes were made since tremendous model adaption would be required to produce heterogeneous process units with low anticipated model predictability improvements. However, model predictability issues are expected when no agitation are evident within vessels, but would require additional modelling (i.e. sedimentation of particles, population balances etc.)

6.5.8. No reactions in auxiliary tanks

Problem statement

Dorfling (2012) assumed that no reactions occur in auxiliary tanks. This assumption is briefly discussed.

Results and discussion

The validity of this assumption was inconclusive as insufficient plant information is available on this topic. Reactions could easily be included in all auxiliary tanks found in dynamic process model. However, the current set of reactions is applicable for high temperature and high pressure operation, and should not be extrapolated into a low temperature low pressure region. Different reaction mechanisms are also expected if reactions are in fact occurring in these process units.

Proposed model updates

No dynamic process model updates were included.

6.5.9. Constant agitator work and heat loss

Problem statement

Dorfling (2012) approximated the heat lost to the surroundings for each autoclave compartment as a constant value by solving Equation D.3 at steady-state conditions. The

agitator work was also assumed to be constant with a value around standard operation. These estimations are briefly considered by referring to the expected autoclave conditions. The requirements for excluding these assumptions are also discussed.

Results and discussion

Dorfling (2012) roughly estimated the outer temperature of each compartment to be a constant 50 °C. The outer temperature is expected to vary with varying inner temperatures. There is no apparent method of fundamental calculating the outer surface temperature using known process variables such as inner temperatures, without requiring extensive information on autoclave materials; degree of slurry agitation; and slurry material properties such as viscosity. The constant heat loss assumption is therefore the best current approximation. The constant shaft work assumption holds for the same reason. A fundamental approximation of shaft work is improbable due to unknowns including slurry viscosity and impeller information. An empirical estimation would be possible, but the shaft work does not feature in data sets listed in Table 6.2.

Proposed model updates

No dynamic process model updates were included.

6.5.10. Single flash recycle tank/autoclave set

Problem statement

Western Platinum BMR operates two autoclaves and flash recycle tanks in parallel. Only one autoclave and flash recycle tank set was used by Dorfling (2012) in the dynamic process model. The use of two recycle tank/autoclave sets at Western Platinum BMR is discussed. The effect of excluding the second set is considered thereafter.

Results and discussion

The parallel operation of autoclave 300 and autoclave 200 with their respective flash recycle tanks serves to continue processing raw materials while one set undergoes maintenance. They are however operated simultaneously when possible. These two sets have exactly the same operating procedure and control strategies. For the extent of current model predictability, validation of one set would suggest the validity of the joint operation.

Proposed model updates

No dynamic process model updates were included.

6.5.11. Extreme condition testing

Problem statement and methodology

Extreme condition testing is a technique used to validate model behaviour under severe operating conditions. This test was applied to the dynamic process model. The tests conducted comprise stopping preparation tank feeds; stopping preparation tank outlets; stopping autoclave oxygen feeds; and closing autoclave cooling water.

Results and discussion

Extreme condition testing results are captured in the table below.

Table 6.11: Extreme conditions testing for baseline model

Action	Result	Reason
Stopping TK-10 feed	Failed	Complex numbers in AC2
Stopping stream 9	Passed	Expected dynamics obtained
Stopping stream 7	Failed	Negative flow rate for AC1 equal to the size of stream 9 flow rate
Stopping autoclave oxygen feed	Failed	No effect on anything
Stopping TK-10 outlet	Failed	Mass increases without limit
Stopping compartment 2 heat removal	Passed	Temperature increases as expected

Complex numbers are produced in the downstream second compartment when the feed to TK-10 is stopped. This happens even though saturation limits are defined for integrator blocks (refer to Figure 3.4) of the first compartment. This phenomenon is caused by a Simulink™ capability called zero-crossing detection. In order to accurately determine the time of the zero crossing (i.e. the time at which some component is depleted i.e. $x_{4,L,i} = 0$) during a minor step, the saturation's ranges are temporarily disabled so that the corner can be found exactly. Essentially the solver bounces around the saturation point until the point is found exactly. In doing so, negative concentration values are evident during the minor steps. These negative values do not form part of the final output since they only serve an interim purpose. They do however become a problem when unavoidable math operations such as square roots are applied during these interim values (i.e. causing complex numbers). The usefulness of zero-crossing detection is evident; it ensures that dynamics at critical points in time are accurately predicted; and was for this reason left as is. Guards that moderate and change negative values to zero were added before susceptible math operations within all process units. This ensures the prevention of unrealisable outputs such as complex numbers at these interim calculations.

The first compartment overflow assumes a negative value equal to the size of the recycle stream when the feed to the autoclave is stopped. This is caused by the first compartment not being able to handle situations where no overflow exists. In addition, the recycle stream flow rate is a constant input to the first compartment MATLAB™ function block, and is in no way being warned of mass balance inconsistencies. This was corrected by adding an if-statement which ensures the overflow within the mass balance is set to zero when the current occupied volume is smaller than the total compartment volume. Vessel outlet flow rates were also set to zero when the mass in the vessel is approximately zero.

No changes are noticed when the oxygen feed to the autoclave is stopped. This issue was addressed in Section 6.5.5. In the updated model the partial pressure of oxygen moves towards zero if no oxygen is fed while oxygen is continuously consumed. The reduced partial pressure in turn affects the reaction kinetics via oxygen solubility calculations (Equation D.5).

The second stage slurry preparation tank (TK-10) mass increases without limit when its outlet flow rate is stopped. This occurs for all other baseline process units with no inherent overflow. This issue was countered by defining an overflow stream which obtains a value when the current occupied volume is larger than the vessel volume (i.e. a spillage term). An additional 20 % vessel volume was added above the reported vessel volume which acts as a volume leeway before spillage occurs (this added leeway was introduced after considering the vessel levels reported in Figure 6.26). Another solution to mass increase issue would be to add upper saturation limits to integrators. However, the size of the overflow streams would in this case be unknown and were therefore not used (not taking into account spillage sizes will cause mass balance inconsistencies during the occurrence of spillage).

Model updates

Model updates are discussed throughout the previous section in order to ease the readability.

6.5.12. Face validation

Problem statement and methodology

Face validation is a technique which uses the opinion of knowledgeable people to qualitatively verify the rationality and accuracy of model responses. Face validation was used to validate the updated open-loop dynamic model's response to input changes. Current knowledge of the model internals were used to explain certain aspects of the model output behaviour. Certain model behaviour can easily be verified, as it is trivial. However, certain

behaviour following input changes (specifically referring to effects on extent of reactions and compositions) require the validation from expert knowledge at Western Platinum BMR.

Results and discussion

A total of 18 individual step increases were made while all other inputs were kept constant. These steps included different stream volumetric flow rates; temperatures and solid content. A total of 29 model outputs were used to report the effects of the step-changes. The model outputs include different stream and vessel solid content; levels; pressures; temperatures and extent of leaching. Only a fraction of the results is discussed. All results are reported in Table F.1.

Refer to Table 6.12 for variable step responses in the case where volumetric flow rate step increases were made in the open-loop dynamic process model.

Table 6.12: Face validation of step response dynamics for volumetric flow rate step increases in an open-loop model

Step increase	Step response									
	Solid content		Level				Pressure	Temperature		
<i>Volumetric Flow</i>	<i>Stream 5</i>	<i>Stream 9</i>	<i>TK-10</i>	<i>TK-20</i>	<i>TK-40</i>	<i>AC3</i>	<i>Autoclave</i>	<i>Stream 5</i>	<i>Stream 7</i>	<i>Stream 9</i>
Stream 1	↑FO	↑FO	↑R	↓R	-	↑R	↑FO	↓nO	↓FO	↑FO
Stream 2	↓FO	↓FO	↑R	↑R	-	↓R	↓FO	↓nO	↑FO	↓FO
Stream 3	↓FO	↓FO	↑R	↑R	-	↓R	↓FO	↓FO	↑FO	↓FO
Stream 4	-	↑nO	-	↑R	-	↓R	↑nO	-	↑nO	↓nO
Stream 5	-	↑FO	↓R	↑R	-	↑R	↑FO	-	↓FO	↑FO

Legend	
FO	First order response
nO	N th order response
R	Ramp response

There are numerous contributing factors which govern step response dynamics, especially in the autoclave and flash recycle tank setup which have very intricate interaction pathways. Some of these contributing factors are discussed.

A step increase in the flow rate of stream 1 results in an increase in the solid content for both stream 5 and 9. This response is expected since stream 1 has a higher density than all the other streams which are added to the second stage slurry preparation tank and flash recycle tank (stream 2, 3 and 4). Coinciding results are obtained when steps are made in these lower density stream flow rates, except for that of stream 4. An increase in density is obtained in stream 9 for a step increase in stream 4 flow rate. This could be attributed to the fact that stream 4 is a concentrated sulphuric acid stream; a small step increase of reasonable size relative to normal operation is made, which does not significantly contribute

to density changes through its physical mixing. The step increase in sulphuric acid flow rate increases the acid concentration in the autoclave. This increase suppresses the oxygen solubility and therefore limiting the rate at which solids are leached, and subsequently results in an increase in the recycled stream 9 density.

Step increases in stream 1, 2 and 3 results in ramp responses within the second stage slurry preparation tank (TK-10), as expected. Volumetric flow rates entering and exiting TK-10 is at steady-state prior to flow rate step increases. An offset in this steady-state will result in a ramp response in the vessel level, which represents either the draining or filling up of the vessel.

Step increases in stream 1, 2 and 3 have no effect on the second stage discharge tank (TK-40) level, which is expected. The volumetric flow rate leaving the third autoclave compartment (AC3) is constant, which means the level in TK-40 should be left unaffected. These step increases do however affect the flash recycle tank (TK-20) and the AC3. The TK-20 response can be attributed to the change in AC1 reaction rates which ultimately results in a variation in stream 9 temperature. The change in stream 9 temperature affects the rate at which water is vaporised out of TK-20, which results in a TK-20 net volumetric flow rate offset, causing a ramp response. The directions of TK-20 ramps correspond inversely with the temperature response directions of stream 9 for steps under consideration, which supports the TK-20 ramp response theory.

The AC3 level ramp response to step increases in stream 1, 2 and 3 could also be attributed to the change in reaction rates, specifically the combined effect of the change in the rate at which oxygen is consumed and the rate at which water is vaporised in AC3. The temperature response direction of AC3 (refer to stream 21 in Table F.1) directly corresponds with the AC3 level ramp direction. A direction change in stream 21 temperature demands a similar direction change in base metal sulphide oxidation; therefore oxygen consumption rate. This suggests that the rate of oxygen consumption dominates the combined effect, since a direction change in oxygen consumption rate seen in Table 6.12 changes the net volumetric flow rate in the same direction. Note that the ramp responses in levels following the previously described mechanisms are very slow relative to a level ramp response caused by directly changing an inlet or outlet volumetric flow rate.

The pressure in the autoclave changes in the same direction as the first compartment temperature, except once again for the stream 4 flow rate step change. The former case can be attributed to an increase in liquid temperature which increases the water vapour pressure. The latter case, which is the stream 4 step-change phenomenon, can be attributed to the

increase in acid concentration in the autoclave, which causes a decrease in oxygen consumption; more oxygen in the gas phase is therefore present.

Note that the pressure within the autoclave and the level in compartment 3 are affected when step increases are made. No variation in these two measurements was evident in the baseline dynamic process model. These variations are attributed to changes which were made to the baseline dynamic process model necessary to improve its behaviour. The same applies to the varying temperature of stream 5 and 21; and the level of compartment 1 and compartment 4 (refer to Table F.1).

6.5.13. Dynamic process model predictability

Problem statement and methodology

A lot of reaction kinetics issues have been highlighted within previous sections. The composition predictability of the dynamic process model is investigated in this section in order to determine if the previously mentioned issues (or possibly issues that exist which have not been highlighted) effect model accuracy.

Operating conditions close to that of Western Platinum BMR are implemented onto the baseline dynamic process model. The steady-state dynamic process model compositions for both the second and third stage leach residues are compared to that of the actual process.

Results and discussion

The baseline dynamic process model second and third stage leach residue composition predictions at steady-state are captured in Table 6.13.

Table 6.13: Baseline dynamic process model composition predictions

Species	First stage leach residue (wt%)	Second stage leach residue (wt%)	Third stage leach residue (wt%)
Ni	12.92	9.97	9.94
Cu	49.76	37.47	28.77
Fe	0.10	0.00	0.00
S	25.11	20.07	18.61
Rh	0.09	0.28	0.38
Ru	0.20	0.72	1.02
Ir	0.03	0.12	0.17

Values in Table 6.13 can be compared to compositions normally seen at Western Platinum BMR (refer to Table 2.1). Both nickel and copper, in the form of sulphide minerals, are under-leached within the baseline model predictions. This occurs in both the second and third stage of the process. The high copper/sulphur and nickel/sulphur ratios predicted by the

model suggest that a lack of higher ratio mineral leaching occurs. This is expected in under-predicting circumstances since higher base metal/sulphur ratio minerals tend to leach faster as they are more susceptible to oxidation. The PGM compositions are under-predicted, attributed mostly to the effects of low base metal leaching.

Note that the reaction kinetic model developed by Dorfling (2012) overestimates cupric ion trends in most cases. It would therefore be expected, assuming the batch experimental data is adequate, that the dynamic process model overestimates the extent of copper leaching. This is, however, not the case. The fact that the dynamic process model still under-predicts the extent of copper leaching points to the inability of batch experiments to characterise the actual process. This is expected to be caused by the high acid concentration in batch experiments which suppress oxygen solubility, therefore base metal leaching.

Proposed model updates

The low base metal leaching predictions could possibly be caused by reaction kinetics that have been developed and fitted to highly acidic batch experimental data. Kanome et al. (1987) report that high sulphuric acid concentrations results in the formation of elemental sulphur, causing a layer around particles which limits diffusion. Another possibility could be the fact that high acid concentrations suppress oxygen solubility within the liquid phase, which ultimately limits the oxidation of base metals.

6.6. Model Update Summary

Many dynamic process model issues have been identified in the previous sections. Solutions have been developed for several of these issues. Problems that have been addressed which resulted in dynamic process model updates are summarised in Table 6.14.

All of the dynamic process model updates that were made are related to specific dynamic process model features. Both plant data and literature were used in the validation and update process. Each update is briefly discussed.

The point at which PGMs start to leach was redefined using a more appropriate reference point. Leaching of PGMs initiate when specific concentration of digenite within compartments are attained, as opposed to initialisation when the available digenite in the compartment is lower than 99 % of that in the autoclave inlet stream.

Rate expressions were changed to exhibit intensive properties. The intensive nature of reaction kinetics allows the ability to scale to varying reactor sizes.

Table 6.14: Model verification and validation reference index summarising model updates

Validation and verification category	Subsection
Conceptual model validation	6.3.3. PGM leaching reaction initiation♦
	6.3.4. Rate expressions scaled to large process units♦
Computerised model verification	6.4.1. Static testing♦
Operational validation	6.5.2. Constant temperature and composition inputs♦
	0. The natural change in model inputs via random walks ensures
	6.5.4. Constant mass in all autoclave compartments♦
	6.5.5. Isobaric autoclave♦
	6.5.6. Sulphuric acid and water streams entering flash recycle tank♦
	6.5.11. Extreme condition testing♦

Legend			
Validation of:	♣ Plant data	♠ Batch experimental data	♦ Dynamic process model feature
Validation using:	Plant data	Batch experimental data	Literature

Temperatures and compositions of input data were adjusted from constants to variables by implementing random walks that ensure natural input variation.

Static tests were used to identify several issues within the programmed dynamic process model including the use of incorrect units, equations, constants and functions.

All process units were proven to vary in temperature; energy balances were therefore added to isothermal vessels. The mass inside the first, third and fourth compartments vary since they contain level-independent outlet flows. Varying mass within these compartments were therefore taken into account by using appropriate mass and energy balances.

A varying pressure within the autoclave was implemented into the dynamic process model. This ensured that oxygen flow rates into the autoclave affected the partial pressure of oxygen and therefore the reaction kinetics.

The sulphuric acid and water streams which enter the flash recycle tank were added to the dynamic process model since these streams are used in a supervisory control mechanism and as an abnormal event, respectively.

Extreme condition testing identified several issues including negative flow rates in the first compartment, unlimited integration of mass within all vessels, and complex numbers caused by taking the square root of a negative number. These issues were resolved by limiting the overflow of the first compartment to situations where sufficient slurry volume is available within the vessel; limiting the amount of slurry that can be present in a vessel and adding a

spillage flow rate; adding guards that prevent negative and unrealisable values during interim steps; respectively.

Several issues have not been rectified, and require further investigation. These issues are summarised in Table 6.16.

Table 6.15: Model verification and validation reference index summarising model issues and future work

Validation and verification category	Subsection
Data validity	6.2.2. Acid concentrations in batch experimental data♣
	6.2.6. Data reconciliation on plant data♣
Conceptual model validation	6.3.1. Copper cementation reactions♦
	6.3.2. Ferric to ferrous ion reduction mechanism influence♦
	6.3.3. PGM leaching reaction initiation♦
	6.3.5. Initial concentrations in a continuous process♦
Operational validation	6.5.9. Constant agitator work and heat loss♦
	6.5.12. Face validation♦
	6.5.13. Dynamic process model predictability♦

Legend			
Validation of:	♣ Plant data	♠ Batch experimental data	♦ Dynamic process model feature
Validation using:	Plant data	Batch experimental data	Literature

The model leaching predictability, when compared to data from Western Platinum BMR, suggests the necessity of adjusted reaction kinetics. The inability to predict correct extents of leaching is expected to be caused by acid concentrations in batch experimental data that were much higher than intended. The ideal and fundamental solution to this issue would be to re-do batch experiments and thereafter refit the kinetics. This is one of the major recommendations made within my project. Another solution would be to fit the dynamic process model to plant data – a possibility which was considered. However, composition samples at the BMR are taken only every 8 hours – a resolution which will not capture the necessary dynamics needed to fit several rate expressions (to give scope – (Dorfling, 2012) used 7 hours as a total experimental time). Moreover, the online plant data has proven to be inconsistent. It would therefore be difficult to mimic the operation of the process using the plant data as inputs to the model.

Including a copper cementation reaction and a ferric to ferrous reduction mechanism for digenite leaching could possibly improve the reaction kinetic fit to batch experimental data. The implementation of the latter reaction would require quantification of ferric and ferrous ions, which necessitates additional experimentation.

Available reactant surface area needs to be quantified in order to replace the initial concentration terms within rate expressions. Additional batch experimentation would be required for this. The implementation of a particle population balance would also be required within the dynamic process model.

A temporarily solution was provided in which the initiation of PGM leaching reactions are determined. A more fundamental approach of PGM leaching initiation is required. Quantification of redox potentials can be used to more accurately determine the initiation of PGM leaching reactions.

Data reconciliation of plant data exhibited significant biases. A more in-depth investigation, possibly utilising dynamic data reconciliation, could produce consistent and accurate plant data which can ultimately be used to confidently validate the dynamic process model behaviour.

6.7. Model Validity Conclusion

The issues that are expected to affect the validity of the baseline dynamic process model is summarised in Table 6.16.

Table 6.16: Model verification and validation reference index summarising issues that affect model validity

Validation and verification category	Subsection	Solved in updated model?
Data validity	6.2.2. Acid concentrations in batch experimental data♣	No
Conceptual model validation	6.3.1. Copper cementation reactions♦	No
	6.3.2. Ferric to ferrous ion reduction mechanism influence♦	No
	6.3.3. PGM leaching reaction initiation♦	No
	6.3.4. Rate expressions scaled to large process units♦	Yes
	6.3.5. Initial concentrations in a continuous process♦	No
	6.3.8. PGM-oxide shape factors with infinite size♦	No
Computerised model verification	6.4.1. Static testing♦	Yes
Operational validation	6.5.2. Constant temperature and composition inputs♦	Yes
	0. The natural change in model inputs via random	Yes
	6.5.4. Constant mass in all autoclave compartments♦	Yes
	6.5.5. Isobaric autoclave♦	Yes
	6.5.11. Extreme condition testing♦	Yes
	6.5.13. Dynamic process model predictability♦	No

Legend			
Validation of:	♣	♠	♦
Validation using:	Plant data	Batch experimental data	Literature

Several issues that are shown in Table 6.16 render sections of the baseline dynamic process model as invalid. The baseline dynamic process model concentration predictions are incorrect (substantiated by Section 6.5.13) possibly due to the associated reaction kinetic issues, which relate back to batch experimental data problems. The baseline dynamic process model also fails to operate in a realisable way when exposed to extreme conditions. The baseline dynamic process model does however predict correct mass flow between vessels close to standard conditions.

Table 6.16 specifies if the issues that render sections of the baseline dynamic process model invalid were corrected in the updated dynamic process model. All the issues listed in Table 6.16 that have not been improved in the updated dynamic process model are associated with reaction kinetics. The inability for the updated dynamic process model to accurately predict liquid and solid concentrations still exist. The updated dynamic process model is however more robust at handling abnormal situations. The updated model also incorporates important variable dependencies including the effect of oxygen flow rate on autoclave oxygen partial pressure, and the effect of compartment temperatures on the partial pressure of water in the autoclave.

Face validation showed that the directional changes of variables are as expected. A reasonable approximation of fault effects on operational performance can still be made. The updated model is valid for the purpose of the rest of the project.

CHAPTER 7: CONTROL IMPLEMENTATION

Chapter 6 validated the Simulink™ dynamic process model using an approach developed by Sargent (2005). The final validity of the model was also concluded at the end of the chapter.

This chapter reports on the goal to simulate critical control layers and implement them on the Simulink™ dynamic process model. Critical control layers include regulatory control, alarm systems, safety interlock systems and supervisory control. The implementation of these control layers firstly requires the simulation of sensors and actuators to ensure data sampling and actuation, which is also covered in this chapter.

The behaviour of simulated control layers was firstly validated. A total of 35 sensors; 21 actuators; 30 regulatory controllers; 33 alarms systems; 37 safety interlocks; and 4 supervisory controllers were then implemented into the open-loop dynamic process model. These control layers correspond to that which is used at Western Platinum BMR to ensure the model operation mimics the actual process.

7.1. Overview

The final outcome of this project is to use the available dynamic process model to assess control performance degradation during the occurrence of fault scenarios. Control strategies within the dynamic process model are therefore required. Moreover, control strategies similar to that of Western Platinum BMR is required in order to mimic the actual operation.

The baseline Simulink™ dynamic process model has no control implemented on it. Several control layers mentioned in the literature review were simulated and implemented into the dynamic process model in an order shown in Figure 7.1.

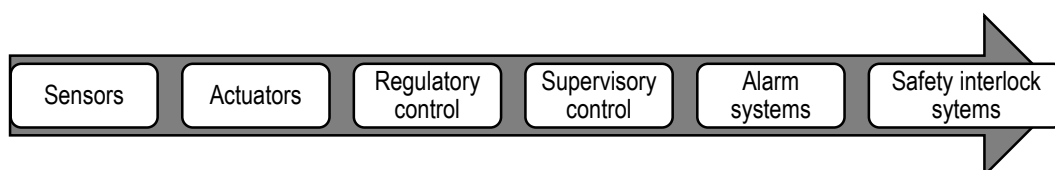


Figure 7.1: Control layer implementation sequence

Data sampling and variable actuation are required before any form of control can be applied. Sensors and actuators were therefore also simulated and implemented.

Each entry in Figure 7.1 will be discussed in a separate section. Each section contains a methodology and a results and discussion subsection.

7.2. Sensors

7.2.1. Methodology

A sensor is a device which responds to a changing phenomenon. Common physical variables which are measured by sensors are force, length, temperature, velocity, pressure, among others. Changing phenomenon which are used to quantify these physical variables include voltage, displacement, current, force, pressure, light, and more (Webster et al., 2014). A simplified representation of a sensor operation is given below.

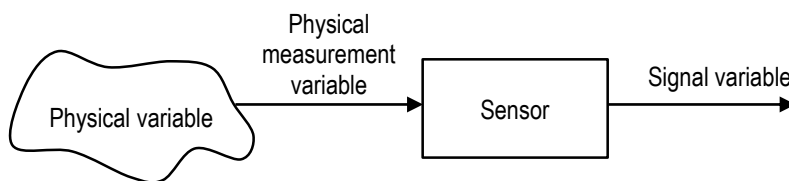


Figure 7.2: Simple sensor operation (Redrawn from Webster (2014))

The quantification process, occurring in the sensor block in Figure 7.2, include in some cases amplification of analogue signals and analogue-to-digital conversions, depending on the type of sensor. Systematic and random errors could creep in throughout the measurement process (Webster et al., 2014).

A generic sensor was modelled for the Western Platinum BMR model which includes sampling of a physical measurement variable at a specific rate (present-value (PV) in Figure 7.3), with the addition of random noise. A perfect transfer from actual PV to measured PV was used, which assumes ideal measurements with negligible transmission times. More in-depth modelling would be redundant when considering the model accuracy and its intended purpose.

The sensor noise was approximated in a similar way as the data reconciliation covariance matrix in Section 6.2.6. Different seeds were provided to sensors. Sensor sampling rates used at Western Platinum BMR are unknown.

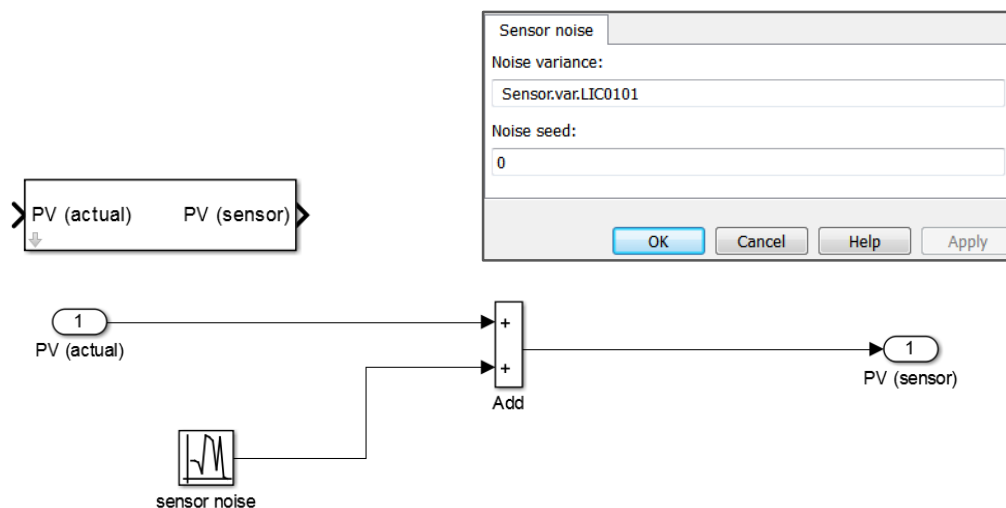


Figure 7.3: Block interface (top left), block mask (top right) and mechanism (bottom) of sensor modelled in Simulink™

Lipták (2006) states four to ten samples should be taken in each transient response period. If the sampling rate is too slow, fast-occurring disturbances might be undetected which could cause an upset. An increase in computational demand without substantial improvement will result if the sampling rate is too fast. The sampling rate was assumed to be one second, which is fast for a mineral processing operation with slow transient behaviour (Tano, 2005). DCS sampling rates between 1 and 5 seconds is reported at the BMR (McCulloch et al., 2014), which often corresponds with the sensor sampling rate. A mask was created which allows easy accessibility of values inside the block from the MATLAB™ base workspace.

7.2.2. Results and discussion

35 sensors exist at the Western Platinum BMR section under consideration. A sensor block was added in the model for each sensor with corresponding variances captured in Table 7.1.

Variances for both FIC-0150-9 and TI-0501 were taken as zero since estimates could not be established. No non-zero data exists for the flow controller. Usable data for FIC-0150-9 should be available when considering it forms the secondary loop in a level control cascade (van der Merwe, 2014). The lack of usable data for FIC-0150-9, in an attempt to calculate a sensor variance, could have been caused by operators removing this flow controller out of the level cascade. No data exists for the temperature indicator, TI-0501. It is speculated that this indicator has been out of operation for a while.

Table 7.1: Sensor variance estimation: Western Platinum BMR

Tags	Tag unit	Variance	Tags	Tag unit	Variance
FIC-0106	m ³ /h	0.0035	LIC-0201	%	0.099
FIC-0101	m ³ /h	0.014	LIC-0401	%	0.00871
FIC-1102	m ³ /h	0.042	LIC-151	%	0.0083
FIC-0202	l/min	1.27E-05	LI-3001	%	9.21E-04
FIC-0201	m ³ /h	0.0018	LIC-3002	%	0.0073
FIC-0203	m ³ /h	0.049	LIC-3003	%	0.11
FIC-0205	m ³ /h	0.019	DI-0101	kg/l	2.45E-05
FIC-3001A	Nm ³ /h	1.69E-06	TI-0101	°C	0.039
FIC-3001B	Nm ³ /h	5.60E-06	TI-0201	°C	6.98E-04
FIC-3001C	Nm ³ /h	1.34E-04	TIC-3001	°C	5.00E-04
FIC-3002	m ³ /h	0.023	TI-3002	°C	0.044
FIC-0401	m ³ /h	0.0020	TIC-3003	°C	6.78E-05
FIC-0150-3	m ³ /h	6.51E-04	TIC-3004	°C	1.11E-04
FIC0150-4	l/h	0.023	TIC-3005	°C	3.62E-04
FIC-0150-5	m ³ /h	0.0015	TIC-0401	°C	0.021
FIC-0150-9	m ³ /h	0	TI-0501	°C	0
FIC-3003	m ³ /h	0.030	PIC-3001	kPa	3.29E-07
LIC-0101	%	0.038			

The behaviour of the sensor block implemented in Simulink™ is considered. The first compartment temperature within the dynamic process model is used as an example. Results are captured in Figure 7.4.

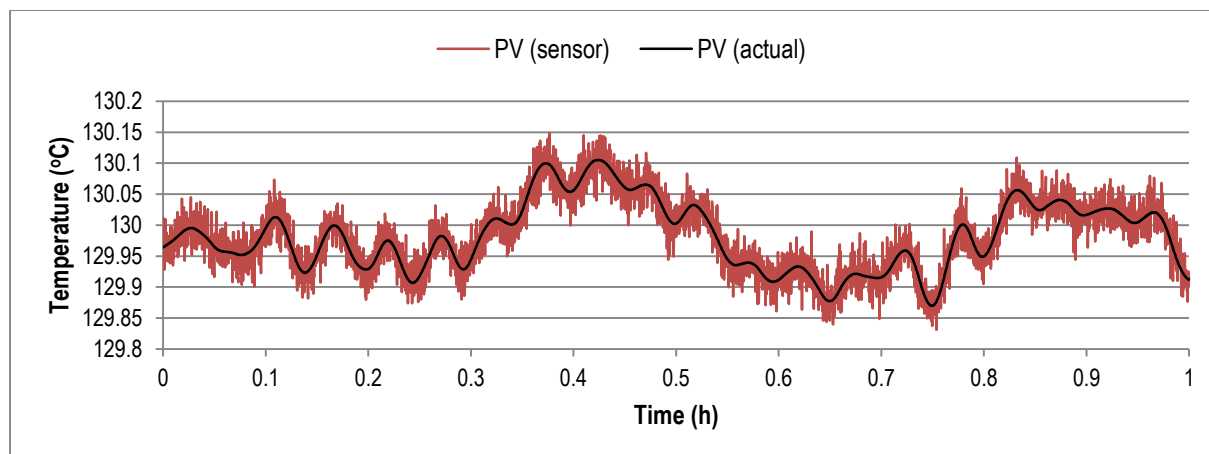


Figure 7.4: Sensor noise for TIC-3001 generated by the sensor block in Simulink™

Low noise variation which is normally distributed across the actual value exists for the temperature indicator, as expected. The change in the present-value (PV) is caused by on-going controller actuation.

7.3. Actuators

7.3.1. Methodology

An actuator, specifically one which adjusts a valve position, consists of roughly three main structures (refer to Figure 7.5).

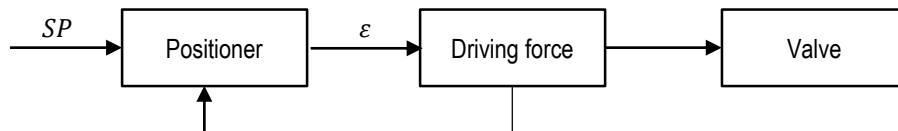


Figure 7.5: Typical actuator structure (Bartys & de las Heras, 2003)

The positioner is typically a proportional controller that measures and controls the stem position at a set-point obtained from the output of a primary controller. The positioner incorporates additional elements such as low pass filters and certain transducers, depending on the type of actuator. The positioner output reports to a driving force. The driving force moves the valve position which ultimately regulates the flow rate. Numerous types of valves exist in the industry for a variety of different applications. Standard valves exhibit quick-opening; linear; or equal-percentage characteristics (refer to Figure 7.6). These characteristics are determined by the shape and size of the valve housing, ports, and the restrictor (Bartelt, 2007).

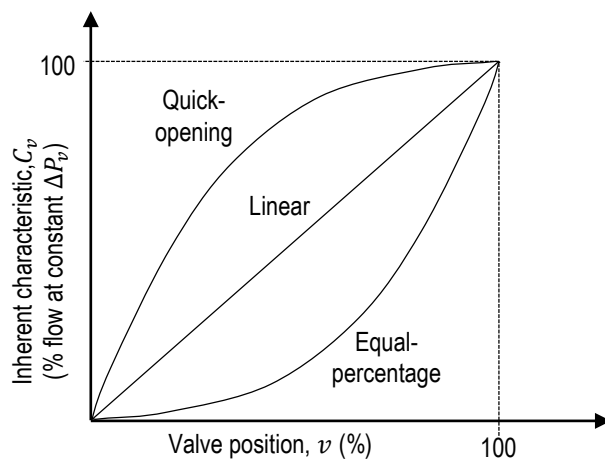


Figure 7.6: Valve flow characteristics (Redrawn from Marlin (1995))

A valve characteristic can be transformed into a flow rate using a flow through restriction calculation (Hutchinson, 1992):

$$F = F_{max} \times \frac{C_v(v)}{100} \times \sqrt{\frac{\Delta P_v}{\rho}} \quad \text{Equation 7.1a}$$

where C_v , ΔP_v and F_{max} represents the valve characteristic, pressure drop across the valve, and the maximum volumetric flow rate through the valve. A generic actuator was modelled for the Western Platinum BMR dynamic process model. The positioner control loop was excluded since no positioner controller information is available. Most of the actuator driving forces identified on plant P&ID's are pneumatic. These driving forces are expected to contribute to the actuator dynamics due to its relatively slow mechanical stem movement and air compression requirements.

Bartys and de las Heras (2003) modelled a pneumatic driving force by conducting a force balance around the stem and a mass balance across the pneumatic chamber. Results of stem travel in Bartys and de las Heras (2003) can be approximated as a first order transfer function. Lipták (2006) reports stroke times between 2 seconds and 1 minute for pneumatic valves. Marlin (1995) reports final control element time constants between one and four seconds. Whether these time constants have a noticeable effect on dynamics depends on its size relative to the primary loop (Lipták, 2006).

A flow controller set-point step-test was used to approximate a time constant of an actuator, since corresponding flow dynamics resulting from this step-test is expected to be predominantly caused by the actuator (i.e. negligible pipe dead-time etc.). The produced actuator dynamics were applied to all other actuators. The approximation of the time constant will be discussed later.

The valve pressure drop in Equation 7.1a cannot be estimated with available information, and the sampling interval of available density data is too slow when compared to the expected valve speeds. The pressure drop and density terms were therefore lumped into the valve characteristic term:

$$F = K_v(v) \quad \text{Equation 7.1b}$$

All applicable valve characteristics at Western Platinum BMR were approximated using Equation 7.1b. Available flow rate data were fitted against valve positions (i.e. valve percentages) using empirical equations. The choice of empirical equation was decided based on the valve flow characteristics as depicted in Figure 7.6. Valve characteristics were also constrained to zero flow rate when the valve is fully closed, irrespective of what plant

data points suggest. Linear equations suited most of the valve characteristics. Some valves exhibited quick-opening behaviour, where a logarithmic equation was more appropriate. An exponential equation was used to describe one valve, which exhibited equal-percentage behaviour. There were several valves (mostly valves used to regulate gas flow rates) that showed a specific linear behaviour in a certain valve position region, which abruptly changed into a different linear behaviour when the valve position region changed. This behaviour was captured by using two linear equations that interchange in a continuous manner when that specific valve position point is passed. These results will be discussed later.

A Simulink™ general expression block was used for the valve characteristics in which a custom equation can be defined. The modelled actuator is shown below.

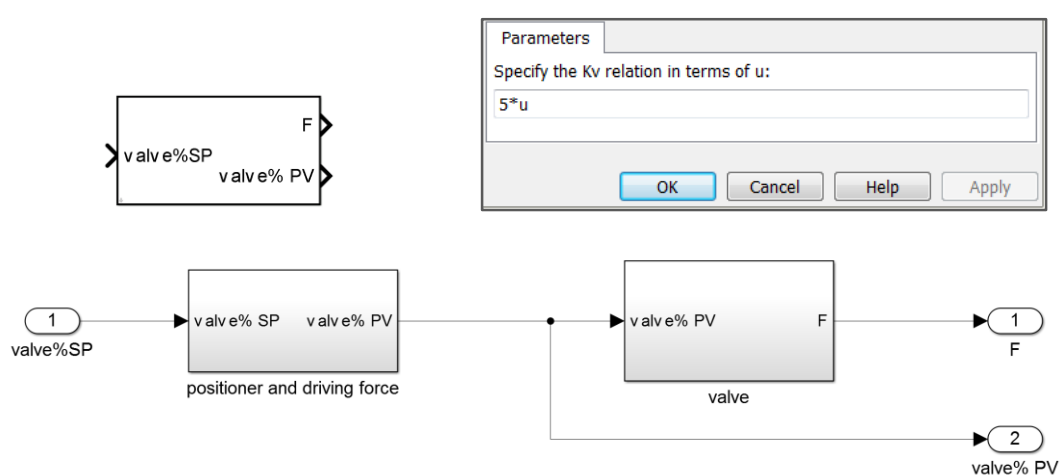


Figure 7.7: Block interface (top left), block mask (top right) and mechanism (bottom) of actuator modelled in Simulink™

A block mask was designed which allows one to change the K_v relation easily. The first order transfer function can be found in the positioner and driving force subsystem, while the valve characteristic expression block can be found in the valve subsystem.

7.3.2. Results and discussion

FIC-0201 was used to approximate an actuator time constant (refer to Figure 7.8) since this flow controller is not subjected to a cascade loop; operator step-changes were therefore available. In addition, FIC-0201 has also proven to have the lowest flow sensor noise, which makes it the best candidate.

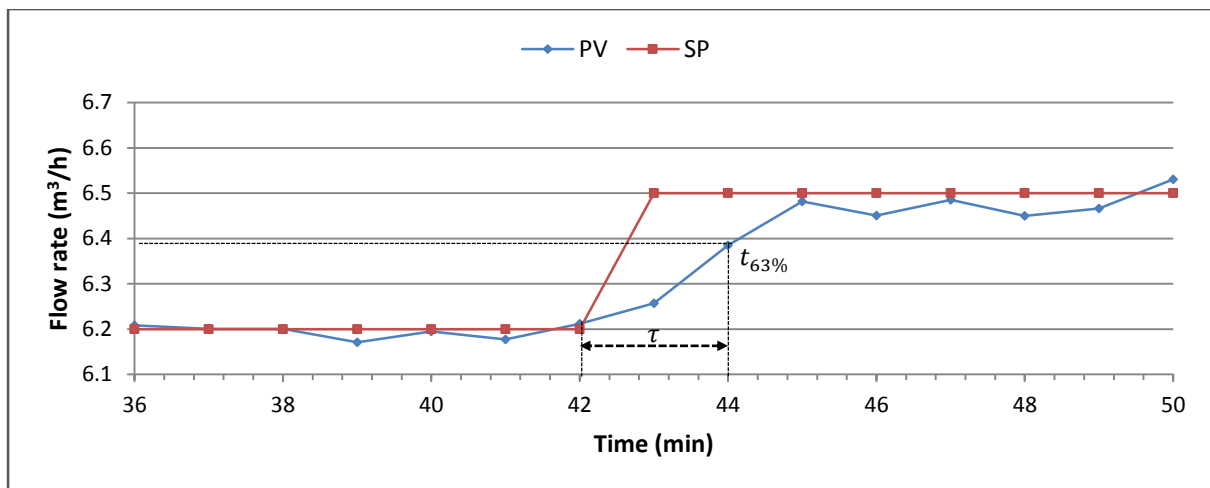


Figure 7.8: Actuator time constant estimation using FIC-0201

Data set 25 was used as it provides the most recent, high-resolution data. An actuator time constant of 2 minutes is derived. This value is not far from discussed literature (Lipták, 2006). Variation in actuator dynamics is expected across the BMR, but insufficient data is available to produce individual time constants. The derived time constant therefore serves as an approximation for all 21 actuators in the model.

Valve characteristics were derived for 16 actuators across Western Platinum BMR. The derived valve characteristics are captured in Table 7.2. Most of the relationships in Table 7.2 were derived using data from data set 5. The small time range of data set 5 ensures that the valve dynamics represents the valve at a specific state in time, and is not affected by long-term faults such as valve wear.

The valve position for FCV-0401 was not available in the data sets. The K_v relationship for this valve was obtained from Henning (2014). Most K_v relationships indicate good R^2 -values. However, data for FCV-0106, FIC-0203 and FCV-0150-3 had simply no correlation. This could possibly be attributed to the quality of flow measurements. Physically realisable checks proved that FCV-0203 produced poor quality flow measurements for data set 3 (refer to Section 6.2.4). The data produced from FCV-0106 had reasonable quality (i.e. reasonable amount of realisable values). However, the data point quality conclusions from physically realisable checks do not address realisable data point accuracy and consistency (i.e. it merely checks if data points are realisable as a first step to determine data point quality). Linear K_v characteristics were assumed for these three valves. The gradients were simply determined by using the maximum expected flow rate and a zero flow rate which represents a fully opened and fully closed valve, respectively.

Several derived flow control valves have nonlinear relationships.

Table 7.2: K_v relationships developed for valves

Valve tag	$K_v(u)$ relation	R^2
FCV-0106	$0.214u$	0.101
FCV-0101	$0.0941u$	0.908
FCV-1102	$1.95 \times \ln(u + 1)$	0.858
FCV-0202	$5.6 \left(\frac{60}{1000} \right) \times \ln(u + 1)$	0.888
FCV-0201	$((0.0933u - 2.09) \times (u \geq 64.6) + (0.0619u) \times (u < 64.6))$	0.939
FCV-0203	$0.316u$	0.0946
FCV-0205	$0.530u$	0.633
FCV-3001A	$((1.72u - 53.6) \times (u \geq 33.5) + (0.117u) \times (u < 33.5))$	0.894
FCV-3001B	$((1.53u - 14.2) \times (u \geq 15.2) + (0.598u) \times (u < 15.2))$	0.809
FCV-3001C	$((1.53u - 24.4) \times (u \geq 20) + (0.316u) \times (u < 20))$	0.871
FCV-3002	$0.118u$	0.739
FCV-0401	$0.4u$	-
FCV-0150-3	$0.033u$	0.000166
FCV-0150-4	$\frac{1}{1000} \times (0.946u - 29.502) \times (u \geq 32.8)$	0.965
FCV-0150-5	$1.24 \times e^{(0.0158u)} - 1.24$	0.762
FCV-0150-9	$0.0343u$	0.575
FCV-3003	$0.068u$	0.840
TCV-3003	$0.0051u$	-
TCV-3004	$0.00714u$	-
TCV-0401	$0.2414u$	-
TCV-3005	$0.871u$	-

This could be caused by valve design characteristics, varying pressure drop, or even faults such as valve wear. Both FCV-1102 and FCV-0202 exhibit quick-opening valve characteristics, which is described by the logarithmic K_v relationships. Note that a value of one was added to all valve positions within logarithmic functional equations. This was done in order to realise a flow rate when the valve position is zero (i.e. adding one produces a flow rate of zero at a valve position of zero).

Only FCV-0150-5 showed equal percentage valve characteristics. An exponential functional form described this relation well. All three oxygen flow control valves (FCV-3001A/B/C) consistently formed two straight lines, with an increase in gradient as the valve size increased. These valve characteristics are unlikely to be caused by measurement issues when taking into account the quality of the flow measurement trends.

FCV-0202 and FCV-0150-4 have units of litres per minute and litres per hour, respectively. These units are converted in order to correspond with dynamic process model units, which clarify the additional multiplication of terms.

The latter four valves in Table 7.2 receive commands directly from a temperature controller with no secondary flow controller. The K_v relationships for these valves could therefore not be derived from plant data, since flow rate data was unavailable. These K_v relationships were assumed to be linear, and were scaled so as to exhibit a 70 % valve position at standard operating conditions (i.e. valve positions of 70 % are evident when the process operates under normal conditions).

An example of a K_v relationship and the corresponding fit is given in Figure 7.9.

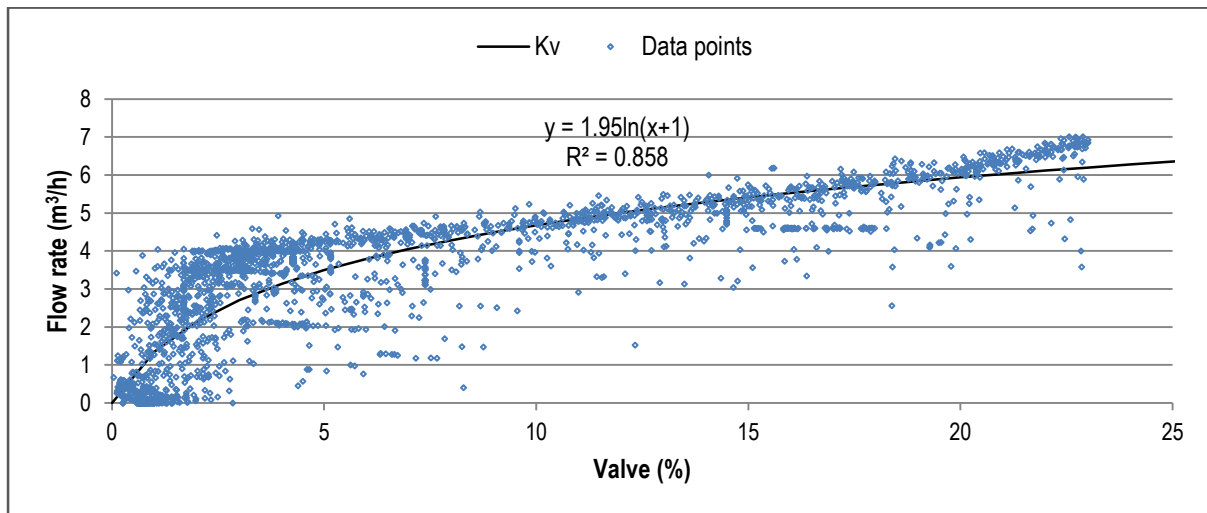


Figure 7.9: K_v relationship for FCV-1102

The logarithmic functional form captures the FCV-1102 valve characteristic, substantiated by the high R^2 -value. FCV-1102 rarely exceeds a valve position higher than approximately 23 %. The flow rate at this opening is high when compared to the flow rates of other streams. Find all other K_v relation graphs in Appendix F.

7.4. Regulatory control

7.4.1. Methodology

A regulatory controller attempts to maintain a controlled variable at a specific place by means of adjusting a causally related manipulated variable. The main type of regulatory control used at Western Platinum BMR is feedback control in the form of a PID control algorithm. Refer to Section 2.4.2 for an in-depth discussion on regulatory control used at Western Platinum BMR.

A PID controller block exists in the default Simulink™ library, and was used in the implementation of a controller. The PID controller block can be found in the normal operation

block seen in Figure 7.10. An if-block was used to switch between normal PID control operation and safety interlock situations.

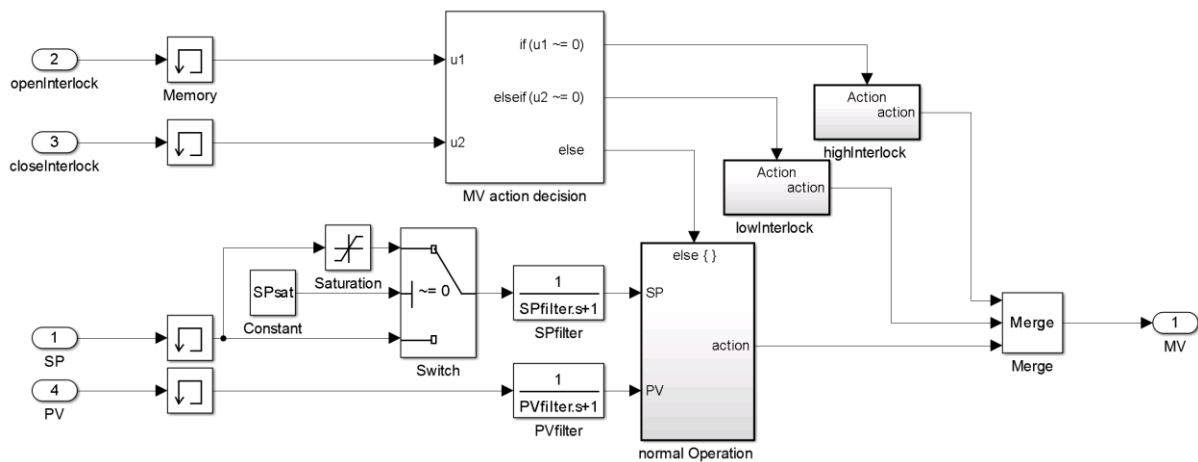


Figure 7.10: Mechanism of PID controller implemented in Simulink™

A safety interlock signal assumes a Boolean value at each time step which indicates if the interlock is on or off. Two safety interlock signals exist, namely open and close. These two signals represent the action to be taken by the manipulated variable. The open and closed state of the manipulated variable is determined by its upper and lower set-point limit, respectively. The controller output assumes a value from either one of the three signals prior to the merge block (the merge block combines signals into a single output), depending on the variable state. Another control feature which is common in the industry and used by Western Platinum BMR is set-point saturation. Set-point saturation limits the controller instruction to a specified value. This feature was included in the model, and can be switched on and off in the controller block mask shown below.

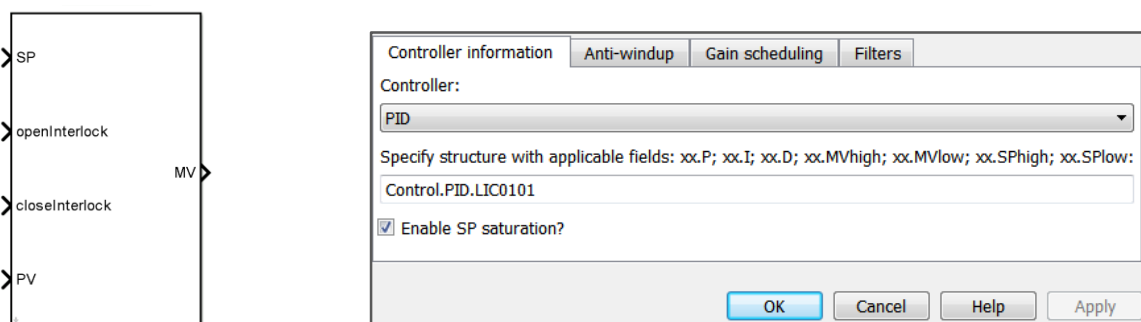


Figure 7.11: Block interface (left) and block mask (right) of PID controller modelled in Simulink™

Sensor noise can influence PID controller outputs since the noise moves through the algorithms via the present-value term. A present-value low-pass filter is often used to remove the measurement noise prior to entering the controller. A set-point filter, on the other

hand, is often used to provide a controller with a smooth set-point change to counter for cases where abrupt set-point changes are made (i.e. to counter abrupt step-changes made by operators). Several controllers at Western Platinum BMR have first order filters for present-values and set-points. Present-value and set-point filter time constants can be defined in the filters tab (see the block mask in Figure 7.11).

The controller type (PID, PI, PD or P) can be selected by using a drop-down list. A structure defined in the workspace which contains the controller gains; manipulated variable limits; and set-point limits were used to carry information over to the Simulink™ PID controllers. The manipulated variable limits were used to restrict the Simulink™ PID controller output and safety interlock situations.

The PID feedback control algorithm used in Simulink™ is given in Equation 7.8 (MathWorks, 2015):

$$U(s) = P \left(1 + \frac{I}{s} + D \times \frac{N}{\left(1 + \frac{N}{s}\right)} \right) \times \varepsilon(s) \quad \text{Equation 7.2}$$

where P , I and D refer to the proportional, integral and derivative gain parameters. The filter coefficient (N) sets the location of the pole in the derivative filter (MathWorks, 2015). The integrator term in Equation 7.2 contributes to the controller output in the form of an integrated error term. This ensures that no steady-state offset exists, as long the final element has the ability to be adjusted. An offset can exist if the valve cannot be adjusted further due to it being fully opened or closed. The integrator term in the case of saturation will unknowingly continue to integrate the error (i.e. the offset which cannot be compensated for) which will lead to large controller outputs. This large controller output reduces the controller's ability to recover when returning out of a saturation state. The integrator term should for this reason be limited in the case of valve saturation. This phenomenon is called windup, and was prevented in the controller blocks by using a clamping method available in the Simulink™ PID controller. This feature is readily used at Western Platinum BMR, which is operated by delta-V™ distributed control system software.

Western Platinum BMR controller information was obtained from the delta-V™ system during a recent site visit, and is captured in Table B.2. The same control parameters from Western Platinum BMR were introduced into the dynamic process model. The parameters were firstly converted since the control algorithms used at Western Platinum BMR differs from that of Simulink™. The standard PID algorithm used in the delta-V™ control system is given in Equation 7.3 (PID Function Block, 2012; Beall, n.d.):

$$U(s) = P' \left(1 + \frac{1}{T_r s} + \frac{T_d s}{\alpha T_d s + 1} \right) \times \varepsilon(s) + F(s) \quad \text{Equation 7.3}$$

where T_r , T_d , α and $F(s)$ represent the reset time, derivative time, derivative filter factor and feedforward contribution. No feedforward contribution is used in applicable controllers at Western Platinum BMR. The controller information from Western Platinum BMR was transformed into a usable form by equating Equation 7.2 and Equation 7.3. The resulting equations are given as follows:

$$P = P' \quad \text{Equation 7.4}$$

$$I = \frac{3600}{T_r} \quad \text{Equation 7.5}$$

$$D = \frac{T_d}{3600} \quad \text{Equation 7.6}$$

$$N = \frac{3600}{\alpha T_d} \quad \text{Equation 7.7}$$

Time constants were also converted from seconds to hours, which is the unit used in the dynamic process model.

Control parameters were re-estimated for the dynamic process model after the transformed parameters proved to be inadequate. Parameters for each control loop captured in Table 2.3 were approximated using correlations. The process steady-state gains (K_p), dead times (θ) and time constants (τ) were firstly estimated using process reaction curves produced from input step-changes using an open-loop model. Refer to Figure 7.12 (Marlin, 1995).

The reaction curves were assumed to be close to first-order-with-dead-time models. Note that the process in this case refers to controller input-output relation, and not the overall BMR process. Controller parameters were then approximated using Ciancone, Lopez and Ziegler-Nichols correlations.

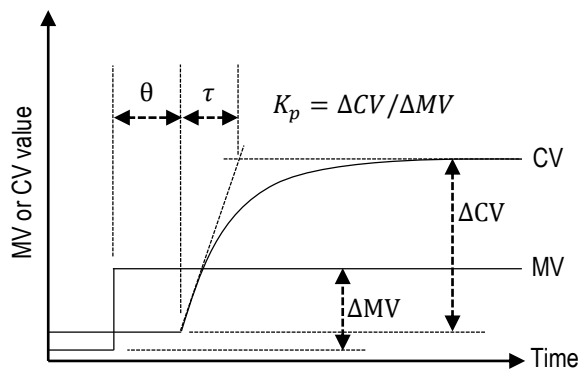


Figure 7.12: Process parameter estimation using reaction curves

Dimensionless numbers in Table 7.3 are defined as follows:

$$P = \frac{\mu'}{K_p} \quad \text{Equation 7.8}$$

$$I = \frac{1}{P \times \tau' \times (\theta + \tau)} \quad \text{Equation 7.9}$$

Table 7.3: Controller parameter estimation (Merrick & Ponton, 1995)

$\frac{\theta}{(\theta + \tau)}$	Ciancone		Lopez		ZN (open)	
	μ'	τ'	μ'	τ'	μ'	τ'
0	1.1	0.23	5.8	0.4	-	-
0.1	1.1	0.23	5.8	0.5	8.1	0.33
0.2	1.8	0.23	3.1	0.6	3.6	0.66
0.3	1.1	0.72	2.1	0.7	2.1	1
0.4	1	0.72	1.7	0.8	1.35	1.32
0.5	0.8	0.7	0.91	0.9	0.9	1.65
0.6	0.59	0.67	-	-	0.67	1.98
0.7	0.42	0.6	-	-	0.43	2.31
0.8	0.32	0.53	-	-	0.25	2.6

Controller parameters calculated from the Ciancone correlation were used in the dynamic process model. These parameters were detuned where multivariate interaction occurred and also fine-tuned using the PID tuner function in Simulink™. This function linearizes the plant and dynamically estimates control responses when controller parameters are varied.

Control parameter estimations mentioned above cannot be used for integrator processes like levels, since step-tests result in ramping outputs. Methods in Marlin (1995) were used to approximate level controller parameters:

$$P = -0.736 \times \frac{\Delta F_{max}}{\Delta L_{max}} \quad \text{Equation 7.10}$$

$$I = -\frac{1}{4\zeta^2 \times A} \quad \text{Equation 7.11}$$

where ΔF_{max} , ΔL_{max} , ζ and A represents the maximum expected flow rate disturbance; maximum level deviation; damping factor and vessel surface area.

7.4.2. Results and discussion

30 regulatory controllers exist at the Western Platinum BMR section under consideration (refer to Table 2.3). Regulatory controllers were added to the BMR model in a modular manner; starting at the second stage slurry preparation tank and moving downstream. Set-point step-tests were conducted for every controller type to validate behaviour.

The second stage slurry preparation tank level cascade is used as an example to demonstrate level control behaviour within the dynamic process model. Consider the cascade control below.

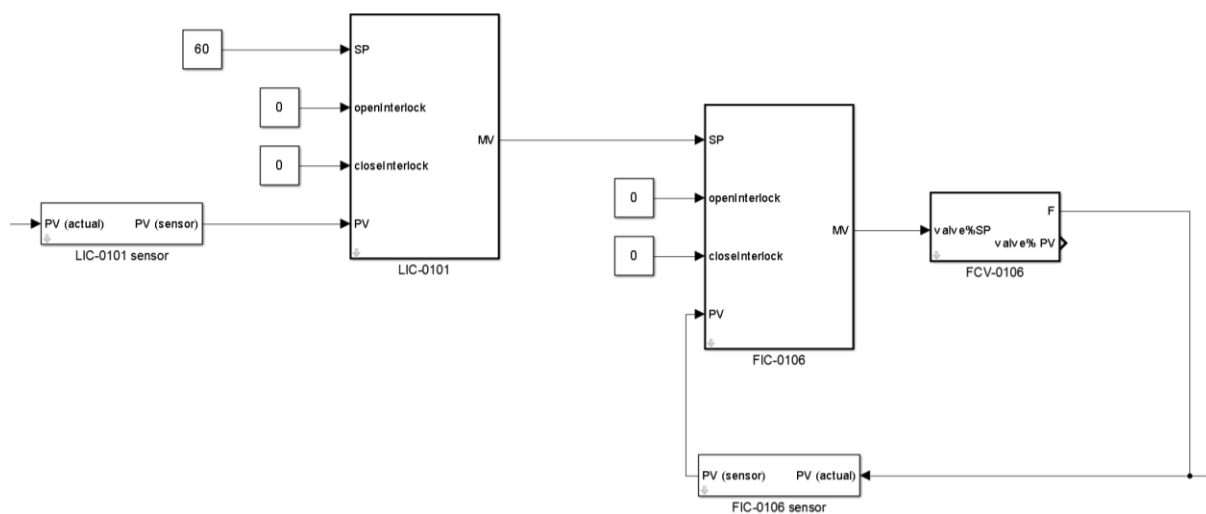


Figure 7.13: LIC-0101 cascade control modelled in Simulink™

The actual present-value for the level comes from the TK-10 MATLAB™ function block, which is not included in Figure 7.13. The constant set-point is replaced with a step-change from 60 % to 50 % at 20 hours. Results are captured in Figure 7.14.

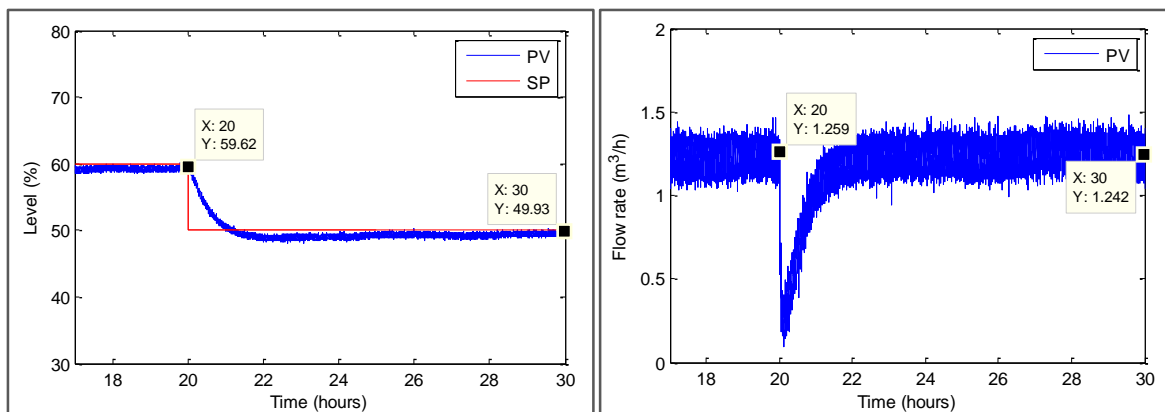


Figure 7.14: Step-test: LIC-0101 (left) cascaded with FIC-0106 (right)

LIC-0101 successfully meets its reduced set-point by lowering the first stage leach slurry flow rate entering the vessel, namely FIC-0106. The flow controller moves towards its previous operating zone after the new level is obtained. This makes sense since level systems are integrator processes. The reduction in the first stage leach slurry flow rate does not affect the density leaving the vessel since a ratio control ensures that the lower density streams entering this vessel reduce in a similar manner. The level decrease occurs over the span of around 2 hours. Note that the present-value does not meet the set-point exactly over the span of time indicated in Figure 7.14. This is caused by the level controller's relatively small integral parameter. Controlling levels aggressively at an exact set-point is in most cases unnecessary and often unwanted. Slow level control tends to attenuate surges such as flow rates by allowing variation in the level.

The autoclave pressure controller is used as an example to demonstrate pressure control behaviour within the dynamic process model (the only pressure controller present). Consider the cascade control shown in Figure 7.15.

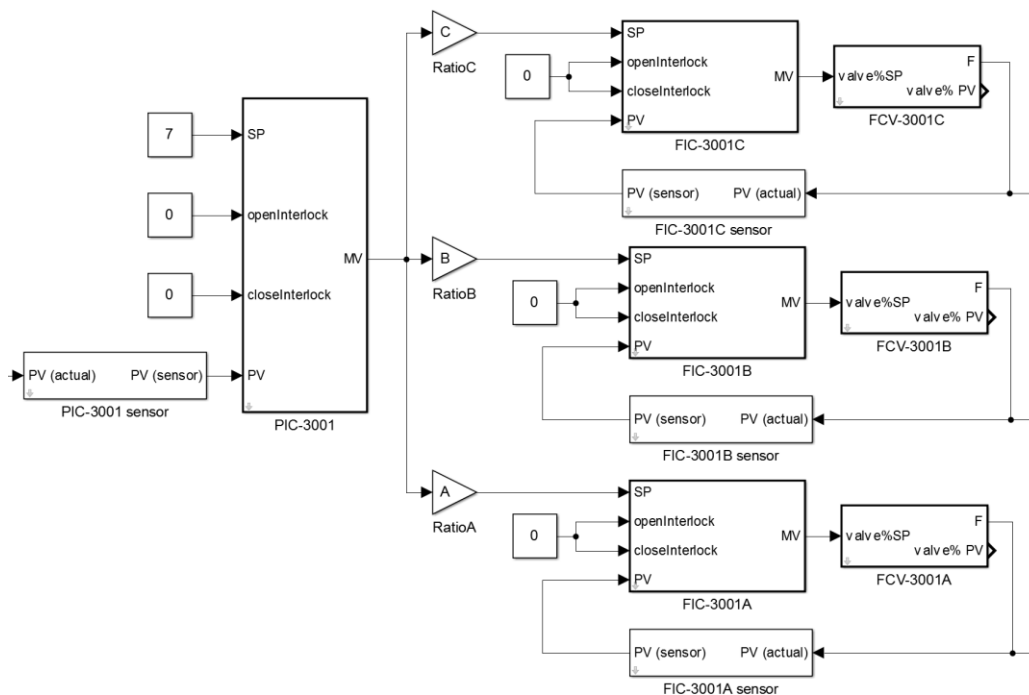


Figure 7.15: PIC-3001 cascade and ratio control modelled in Simulink™

The secondary loop in the cascade consists of three oxygen flow controllers which are managed with ratios.

A pressure step-change is made from 5.5 to 6 bar. Results are captured in Figure 7.16.

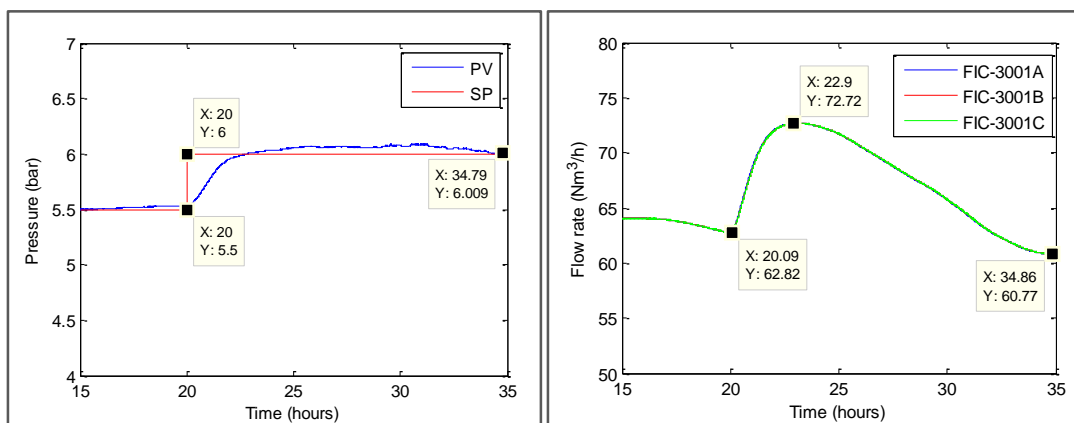


Figure 7.16: Step-test: PIC-3001 (left) cascaded with FIC-3001A/B/C (right)

The pressure present-value moves to the new set-point by increasing the oxygen inlet flow rates. All three oxygen flow controllers receive the same set-point since the pressure controller output is divided into equal portions (i.e. similar ratios exist for flow controllers). Notice that the oxygen flow rates are different at the start and end of this demonstration. This is attributed to the fact that the pressure of the autoclave affects the rate of oxygen consumption through reaction rate expressions, and therefore the necessary oxygen flow

rate. Note that the dynamic process model had not yet reached equilibrium before the implementation of the step-change. This explains the unexpected overall reduction in oxygen flow rate.

The first compartment temperature controller is used as an example to demonstrate temperature control behaviour within the dynamic process model. Consider the cascade control below.

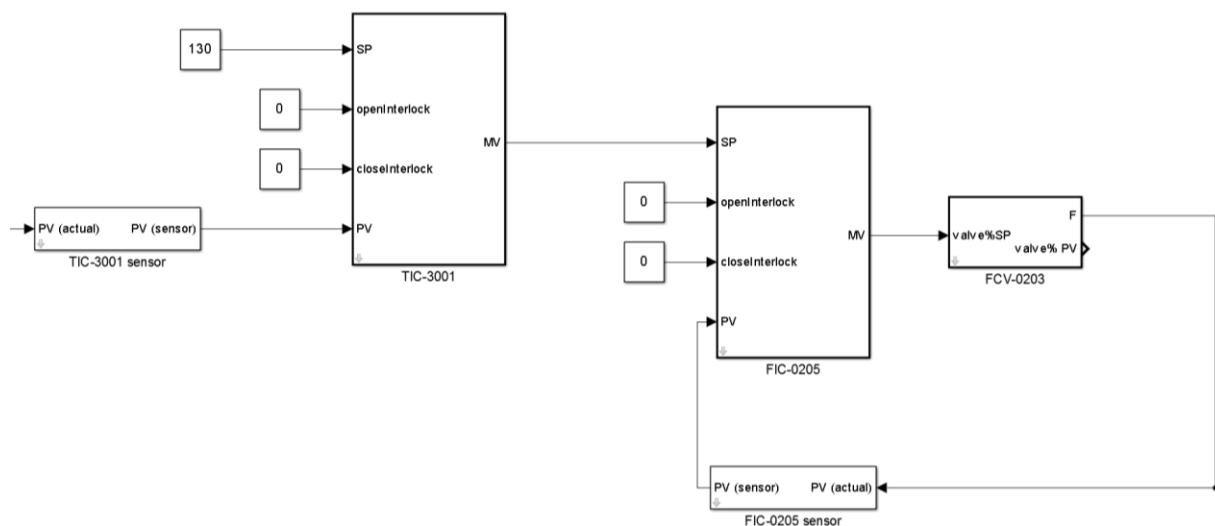


Figure 7.17: TIC-3001 cascade control modelled in Simulink™

The temperature controller manipulates the flow rate of an outlet slurry stream. This slurry stream is cooled by water vaporisation and returned to the first compartment via the flash recycle tank.

A temperature step-change is made from 130 °C to 135 °C at 20 hours. Results are shown below.

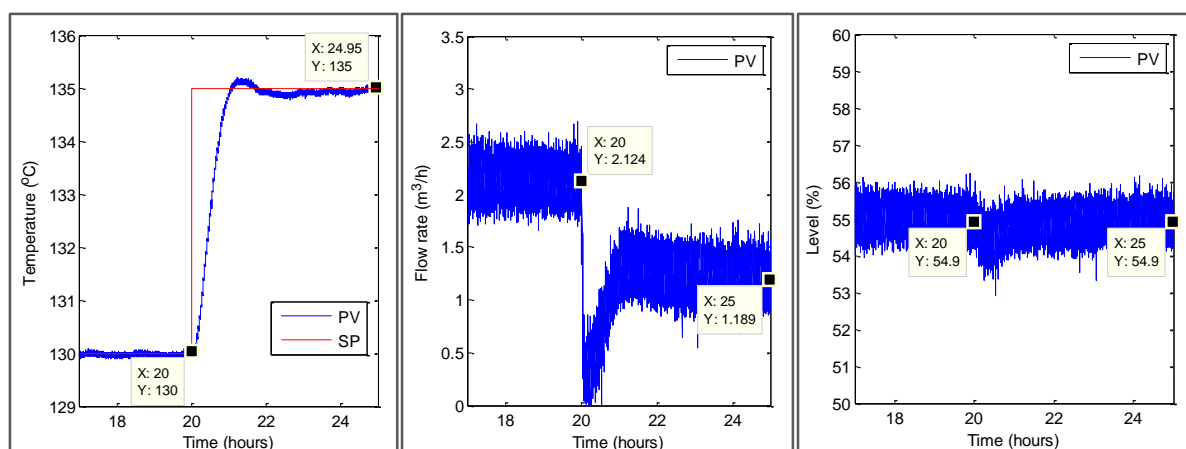


Figure 7.18: Step-test: TIC-3001 (left) cascaded with FIC-0205 (middle) causally related through LIC-0201 (right)

The complex technique used to control temperature in the first compartment temperature at Western Platinum BMR works within the dynamic process model. The first compartment temperature controller (TIC-3001) is able to increase the temperature by reducing the flash recycle flow rate (FIC-0205). The flash recycle flow rate and first compartment temperature are causally related through the flash recycle level controller. The decrease in the flash recycle flow rate affects the level in the flash recycle tank (LIC-0201). The relatively aggressive flash recycle tank level controller compensates for this by reducing its outlet flow rate which ultimately increases the temperature in the first compartment (remember that the flash recycle stream is colder than the slurry within the first compartment due to the vaporisation of water during flashing). The aggressiveness of the flash recycle tank level control is intended in this case as it ensures faster first compartment temperature control.

The final controller behaviour to be considered is the second stage slurry preparation tank outlet solid percentage feedforward controller.

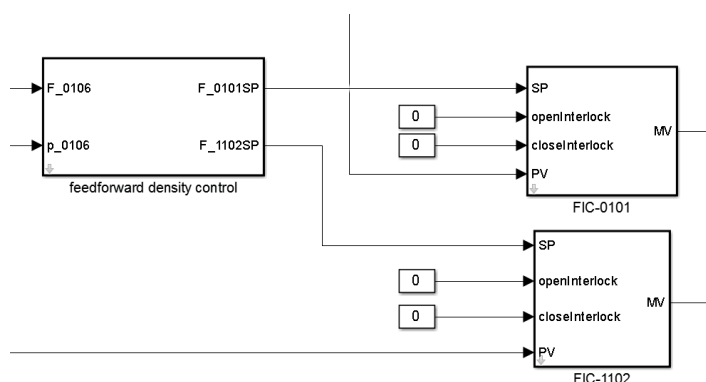


Figure 7.19: Feedforward solid percentage control modelled in Simulink™

A solid mass percentage step is made from 14.2 % to 18 % at 10 hours. Results are shown below.

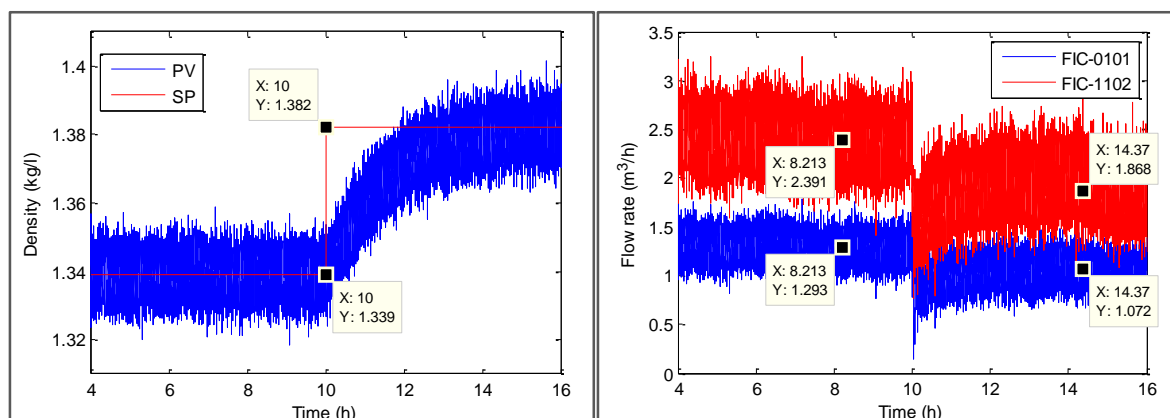


Figure 7.20: Step-test: Solid percentage control (left) that feed forwards to FIC-0101 and FIC-1102 (right)

The solid percentage set-points are translated into density set-points using the following equation:

$$x_s = \frac{\left(\frac{1}{\rho_m} - \frac{1}{\rho_L}\right)}{\left(\frac{1}{\rho_s} - \frac{1}{\rho_L}\right)} \quad \text{Equation 7.12}$$

The feedforward controller manages to attain the new increased set-point by reducing the spent electrolyte (FIC-0101) and formic filtrate (FIC-1102) flow rate as described by Equation 2.1 and Equation 2.2. The reduction in spent electrolyte and formic filtrate flow rates make sense, since lowering these flow rates allows the higher density slurry stream to increase the density within the vessel. These flow rates are also reduced according to a specified ratio, namely spent percentage.

7.5. Supervisory control

7.5.1. Methodology

Supervisory control was previously defined as the manipulation of regulatory control loops in an attempt to improve the current process state. Numerous supervisory control strategies are used at Western Platinum BMR. Refer to Section 2.4.3 for an in-depth discussion on supervisory control used at Western Platinum BMR.

Western Platinum BMR supervisory controllers which were implemented in the dynamic process model are captured in Table 7.4.

Table 7.4: Supervisory control: Dynamic process model (McCulloch et al., 2014)

CV	MV	Control method
Manual		
Acid concentration (Stream 7)	Flow SP (FIC-0202)	On/off operator control
Acid concentration (Stream 21)	Flow SP (FIC-0150-4)	Continuous operator control
Total metal concentration in solution (Stream 21)	Flow SP (FIC-0150-9)	On/off operator control
Automated		
Flow (FIC-1102)	Valve (Stream 3)	Gain-scheduling

The supervisory controllers listed in Table 7.4 are realisable within the dynamic process model, irrespective of the unreliable extent of leaching predictions. These controllers have set-points or limits (i.e. for continuous and on/off operator control, respectively) which are attainable with the available manipulated variables. Some supervisory controllers listed in

Table 2.4 were not included in the dynamic process model since unrealisable set-points or limits exist due to the model-plant mismatch. This includes the control of density of stream 7, the base metal concentration in residues, and the PGMs in solution. Furthermore, many of these unrealisable supervisory controllers require multivariate control knowledge and a weighted approach of adjusting manipulated variables which differs between operators. Redox potentials are also controlled at Western Platinum BMR, but not controlled in the model since it is currently unquantifiable.

The procedures used to model the three supervisory control methods are discussed next.

Gain-scheduling

Gain-scheduling adjusts controller parameters based on real-time measurements in order to compensate for process nonlinearities (Marlin, 1995). Delta-V™ allows one to use gain-scheduling in reference to a present-value, controller output or an auxiliary present-value. A present-value gain-scheduling mechanism was modelled in Simulink™, since it is used at Western Platinum BMR. The mechanism of the normal operation block from Figure 7.10 is depicted in the figure below.

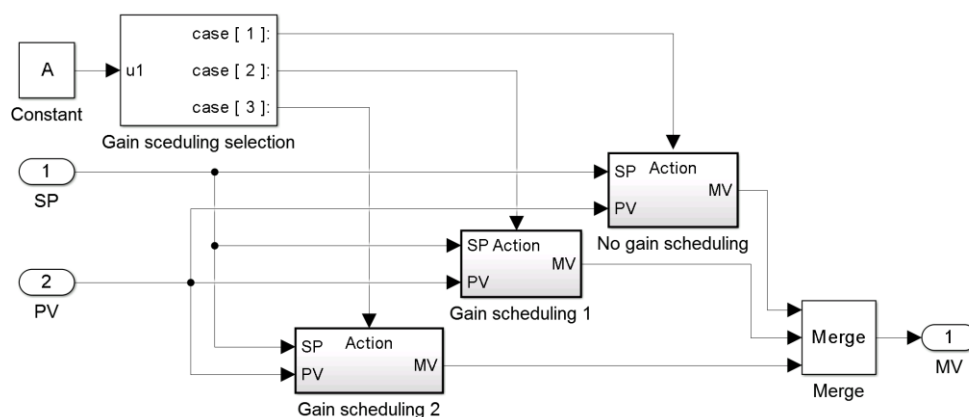


Figure 7.21: Mechanism of normal operation block showing gain-scheduling

The designed algorithm automatically detects and implements the number of defined control regimes (currently at a maximum of three) via a constant input, A, which is determined in the initialization command within the mask. Figure 7.22 shows the mechanism of the gain-scheduling 2 block from Figure 7.21. Gain-scheduling logic is required in order to allow the switching of controllers. The gain-scheduling logic is determined in the initialisation command within the block mask by using user-defined control information which specifies at which PV points controllers switch.

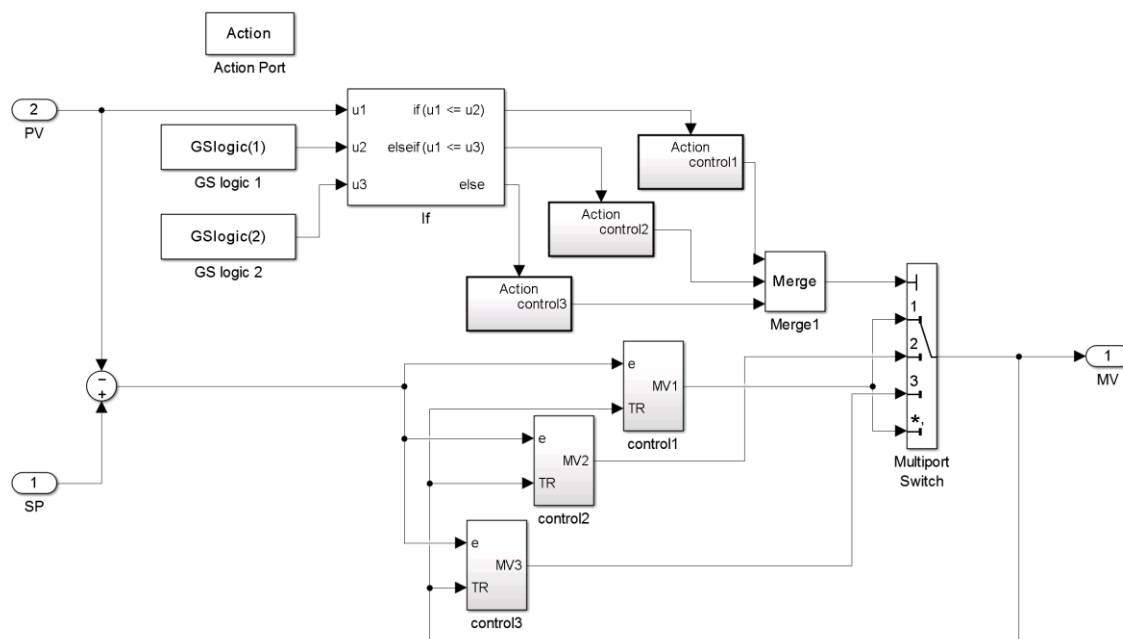


Figure 7.22: Mechanism of gain-scheduling modelled in Simulink™

Each control block in Figure 7.22 contains a PID controller defined with applicable parameters. The tracking ability developed by Simulink™ allows controllers to track a manipulated variable in order to ensure bumpless transfer when controllers are switched.

On/off operator control

The on/off operator control was modelled using a repeating sequence stair (refer to Figure 7.23).

A constant holding time is defined in the on/off controller block mask, which is used in a repeating sequence stair to produce the MV dynamics seen in the left schematic of Figure 2.5. The sample time of the sequence stair is equal to holding time. The first sample of the sequence stair is one, which is subsequently multiplied by a controller gain and an error. Controller action therefore adjusts proportionally to an error size, and only occurs when a defined PV value limit with a specified relational operator is satisfied. The holding-time was approximated using plant data, while the controller gain was manually tuned to provide acceptable responses from normal dynamic process model operation.

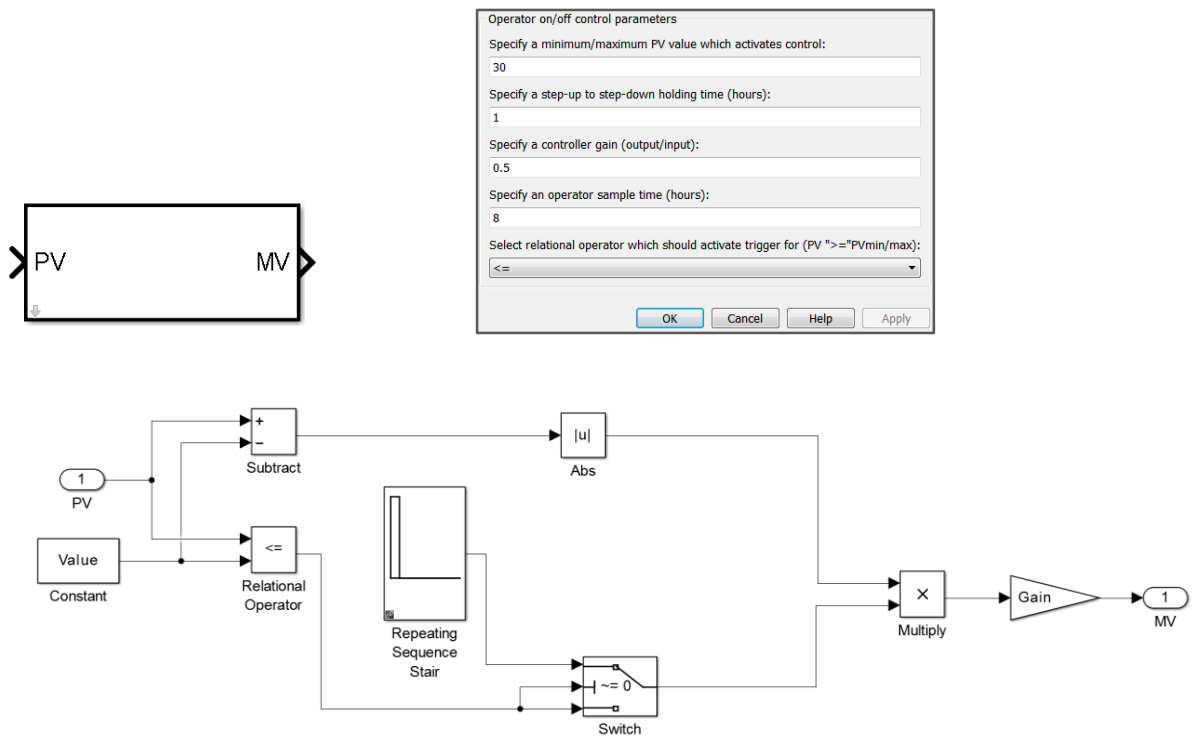


Figure 7.23: Block interface (top left), block mask (top right) and mechanism (bottom) of on/off operator controller modelled in Simulink™

Continuous operator control

The continuous operator control was modelled using a PI controller, and is shown below.

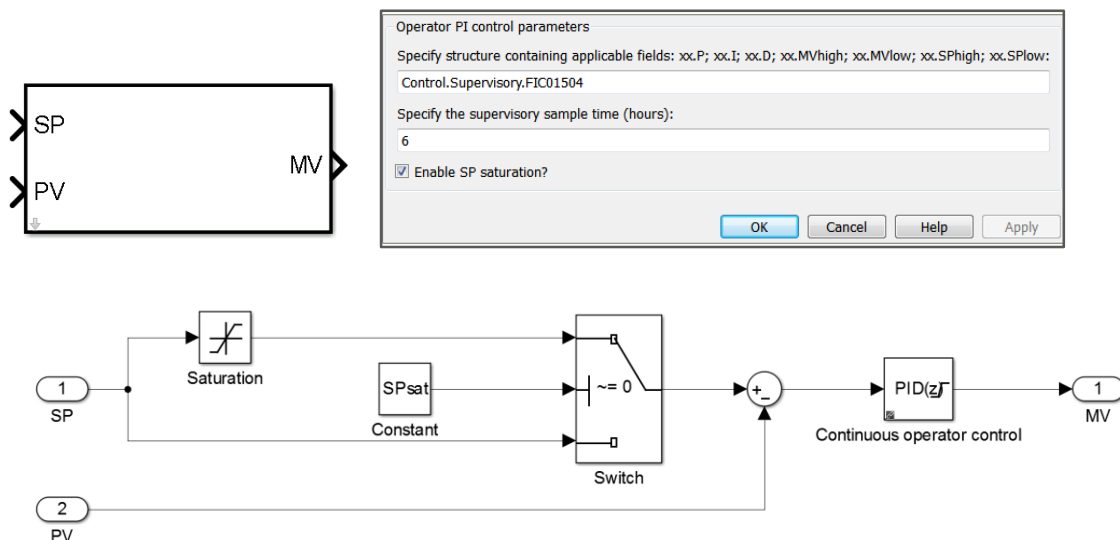


Figure 7.24: Block interface (top left), block mask (top right) and mechanism (bottom) of continuous operator controller modelled in Simulink™

The discrete operator controller in Figure 7.24 only makes adjustments at every user-defined sample time. Controller information is kept in a structure similar to the normal PID controller seen in Figure 7.11.

7.5.2. Results and discussion

Three types of supervisory control were discussed in the methodology: gain-scheduling, continuous operator control, and on/off operator control. All of these supervisory control methods are used at Western Platinum BMR. Those that were implemented in the dynamic process model are captured in Table 7.4. The behaviour of each supervisory control method will now be validated.

Gain-scheduling

Gain-scheduling is used in the formic filtrate flow rate controller (FIC-1102). This could be attributed to its associated valve showing quick-opening characteristics. The aggressiveness of the controller increases as the valve position increases in order to counter the quick-opening valve characteristics. The controller parameters are scheduled at two discrete present-values: 0.8 m³/h and 3 m³/h. The figure below shows the gain-scheduling behaviour for an induced set-point oscillation. The oscillation is used to highlight the flow behaviour attributed to gain-scheduling. The flow controller is equipped with the actual gain-scheduling parameters used at Western Platinum BMR.

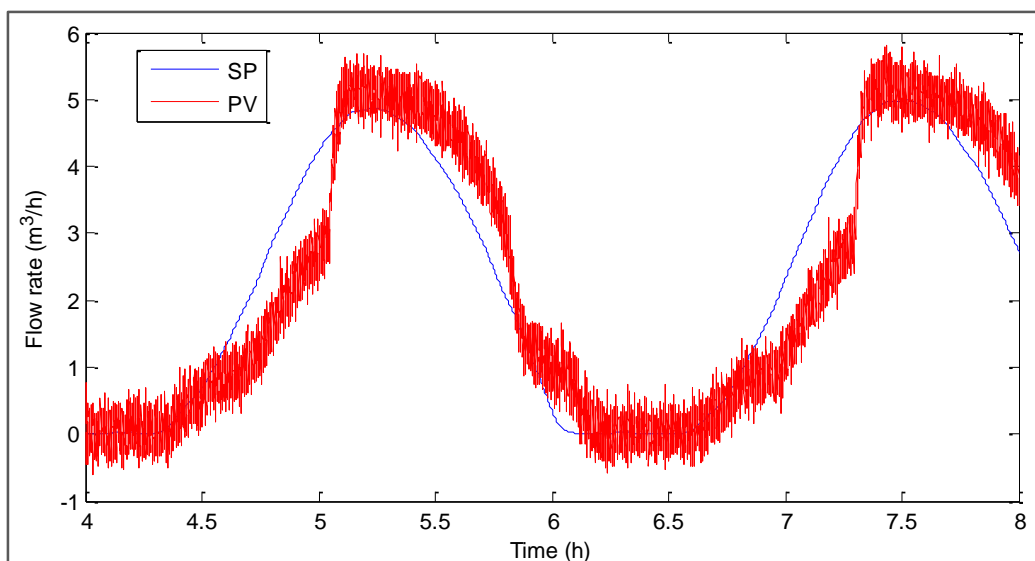


Figure 7.25: Supervisory control test: Gain-scheduling used within FIC-1102

Notice the sudden increase in control aggressiveness when the flow rate increases above 3 m³/h. An increase in controller aggressiveness is required, since the valve characteristic flattens as the valve position increases. The gain-scheduling effects are not as evident when the flow rate crosses 0.8 m³/h, which is possibly due to the smaller relative controller gain change from the first controller state to the second. Note that a negative flow rate is evident in Figure 7.25. This is merely attributed to the sensor noise.

Continuous operator control

Western Platinum BMR uses continuous operator control to regulate the acid concentration entering the fourth compartment between 30 g/l and 45 g/l. Acid concentration samples are taken every two hours for this vessel. The set-point of the concentrated sulphuric acid flow rate is used as a manipulated variable. This control mechanism is used as an example to show the behaviour of the continuous operator controller modelled in Simulink™. Figure 7.26 captures the results.

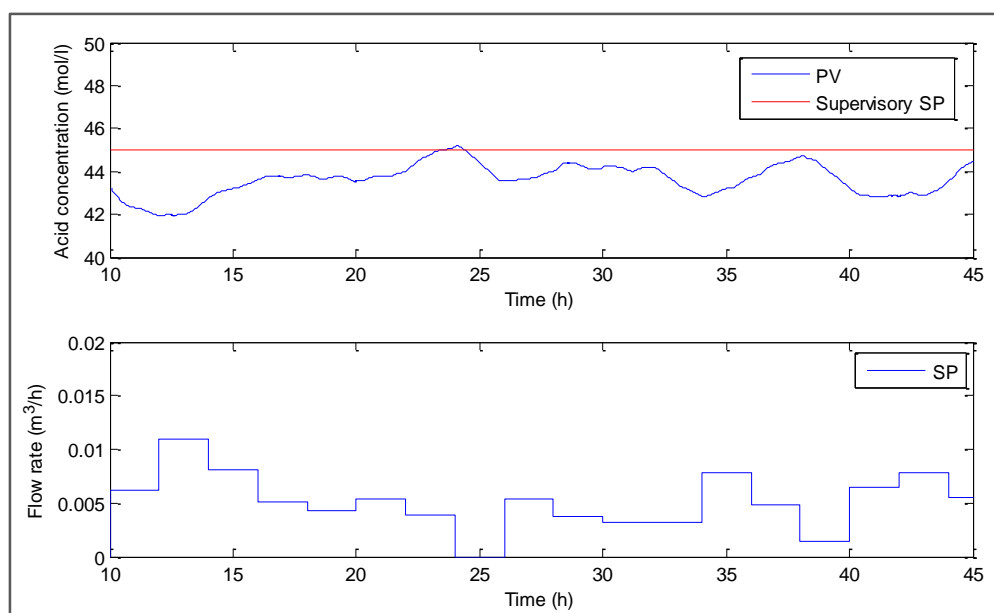


Figure 7.26: Supervisory control test: Continuous operator control - acid concentration in TK-150

Operators make necessary adjustments to the sulphuric acid flow controller set-point to compensate for any offset after each sample is taken. The continuous operator controller succeeds in controlling the acid concentration within the required range.

On/off operator control

Two on/off operator control methods used at Western Platinum BMR were implemented into the dynamic process model. On/off operator control is used to keep the total metals in the liquid phase leaving the third compartment slurry preparation tank below 100 g/l. This is done by varying the water flow controller (FIC-0150-9) set-point, in addition to the level control cascade. Unwanted precipitation could occur in pipelines when dissolved metals increase above 100 g/l. Operators also keep the acid concentration exiting the flash recycle tank above 20 g/l by using the on/off control strategy. This is done by varying the sulphuric acid flow controller (FIC-0202) set-point. Improper leaching occurs in the autoclave when the acid concentrations decrease below 20 g/l. Samples within both cases are taken every two hours. These operator actions are mimicked in an on/off operator control block. Results of

only one of these controllers are considered in order to validate the behaviour of the developed supervisory block. The latter on/off operator control action is used to consider the supervisory controller behaviour. Dynamic process model outputs for the flash recycle tank acid concentration regulated by an on/off operator control using FIC-0202 is captured in Figure 7.27.

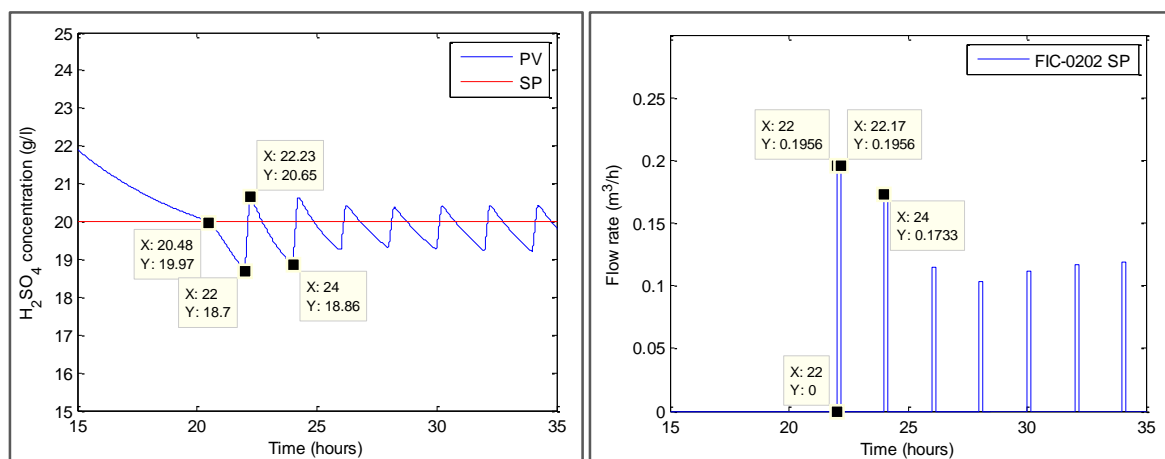


Figure 7.27: Supervisory control test: On/off operator control – acid concentration exiting the flash recycle tank

No operator action is noticed when the acid concentration drops below 20 g/l for the first time. This is due to acid concentration samples that are taken in multiples of 2 hours. The acid concentration drops below 20 g/l only after the 20th hour sample. The next acid concentration sample is lower than the limit which results in operator action. The sample following this one is also lower which shows yet again operator action. However, the second operator action is smaller than the first due to the acid concentration being closer to the 20 g/l limit.

7.6. Alarm systems

7.6.1. Methodology

An alarm system is used to notify operators of unwanted or possibly dangerous variable conditions. Two types of alarms can be defined in Delta-V™: deviation alarms that sound when the measured variable deviates too far from the set-point; and limit alarms that sound when the measured variable moves above or below user-defined limits. However, deviation alarms are not used at Western Platinum BMR. Refer to Section 2.4.4 for a discussion on limit alarms available in the Delta-V™ system used Western Platinum BMR.

A limit alarm was designed in Simulink™ which compares the sensor measurement to user-defined limits. Four different limits exist, namely high; high-high; low; or low-low. Alarm information is contained in a structure form described in Figure 7.28. The block was designed so that each alarm can be switched on or off. The alarm block interface was created to show all the alarms which are switched on. Alarm signals are assigned with Boolean values, with false representing off.

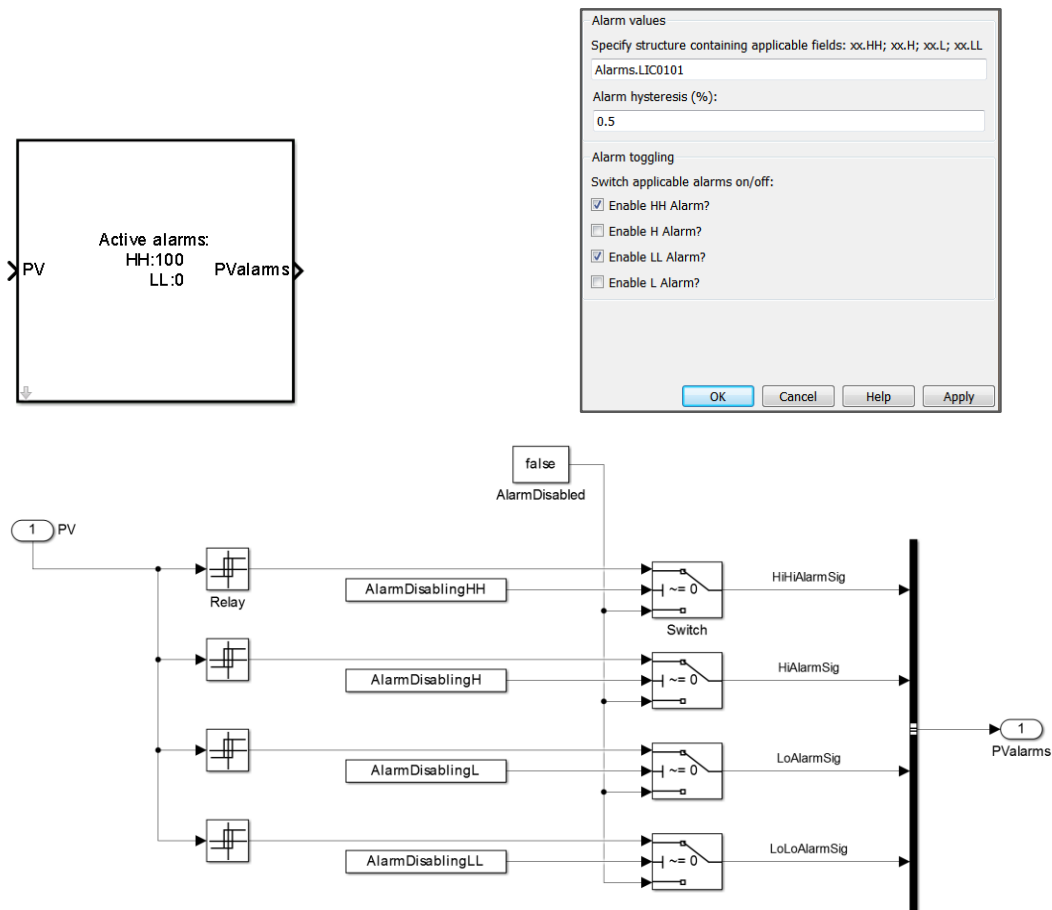


Figure 7.28: Block interface (top left), block mask (top right) and mechanism (bottom) of alarm modelled in Simulink™

Alarms in Delta-V™ do not switch off directly after the present-value reaches the value at the point it switched on (refer to Figure 7.29).

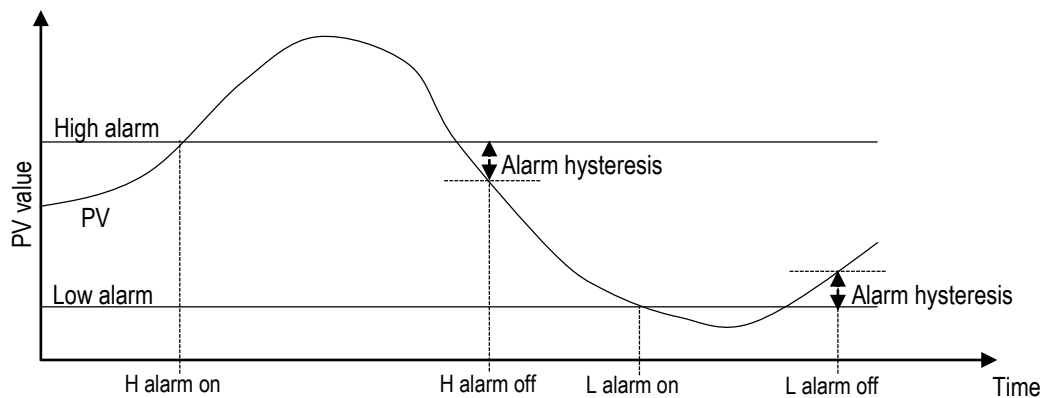


Figure 7.29: Functioning of alarm hysteresis

This phenomenon is called alarm hysteresis, and is defined as a percentage of the present-value scale in $\Delta-V^{\text{TM}}$ (PID Function Block, 2012). Relay blocks were used to incorporate the alarm hysteresis into the alarm triggering mechanism. Alarm hysteresis is expected to be particularly useful for safety interlocks, as it prevents excessive on-off toggling of interlocks which could damage actuators. Alarm hysteresis values of 0.5 % are used in all alarms at Western Platinum BMR. Similar alarm hysteresis values were used within the dynamic process model. The present-value scale was determined to be the difference between high-high and low-low alarms. The alarm values report to the relay blocks through the alarm structure that is specified in the block mask.

7.6.2. Results and discussion

A total of 33 alarm systems comprising 132 limit alarms exist at the Western Platinum BMR section under consideration (refer to Table 2.5). Many of these alarms have nonsensical values (i.e. the alarm values do not correspond with reasonable variable values). All alarms were added to the model, while only the critical alarms were activated. These critical alarms include the levels of all vessels, and the temperatures and pressure in the autoclave.

An alarm system within the second stage slurry preparation tank setup is shown in Figure 7.30.

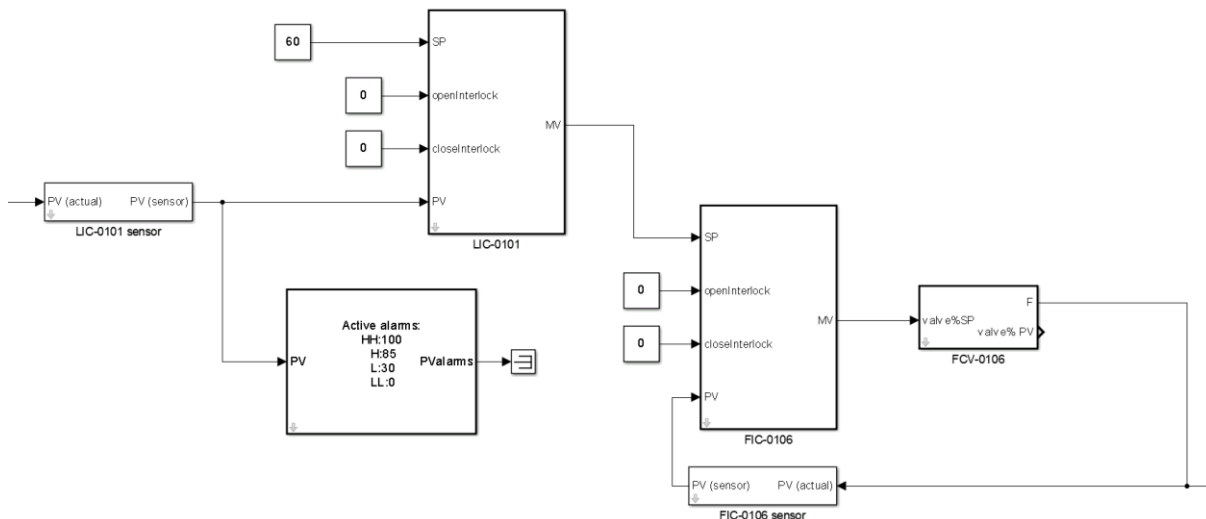


Figure 7.30: LIC-0101 control with alarm system modelled in Simulink™

All four alarms for LIC-0101 are activated in the following scenario. FIC-0106 is removed from the cascade loop at 20 simulation hours and a step increase is made to this flow rate's set-point. The results are shown below.

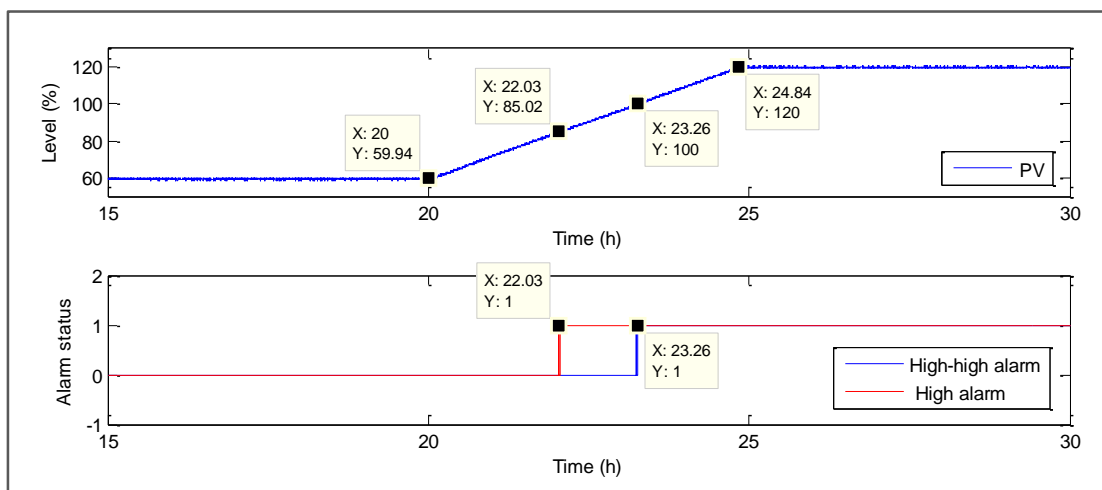


Figure 7.31: Alarm test: LIC-0101 with high and high-high alarms

The level increases since a step increase is made an inlet flow rate. The high alarm switches on at a level of 85 % while the high-high alarm switches on at 100 %. This corresponds with the alarm values seen in Figure 7.30. The plateau noticed after 24.84 hours is caused by vessel overflow (no interlocks are present in the results thus far). Note that the plateau occurs at a vessel level of 120 %, which is the point at which the vessel overflows (refer to Section 6.5.11).

The effect of alarm hysteresis is easily illustrated using an artificial sine wave which in this demonstration represents a level (refer to the figure below).

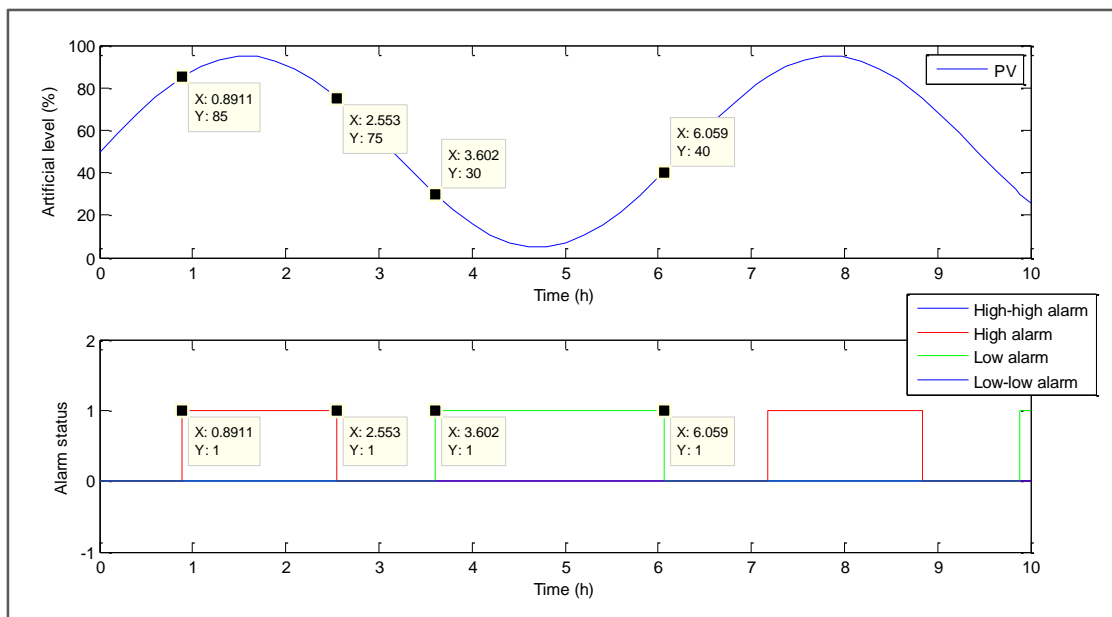


Figure 7.32: Alarm hysteresis test: Artificial level connected with LIC-0101 alarm system

The alarm system of LIC-0101 is used with an artificial level. The alarm hysteresis is increased to 10 % in order to easily convey its effect. The high alarm switches on at 85 % once again. However, it switches off at 75 %. A similar result can be noticed for the low alarm. The low alarm switches on at 30 % and switches off at 40 %.

7.7. Safety interlock systems

7.7.1. Methodology

A safety interlock system substitutes regulatory control in typically dangerous conditions. The safety interlock acts upon a user-specified alarm, and orders a final element to instantaneously move into an extreme condition (fully open or closed) in an attempt to suppress dangerous conditions.

A safety interlock system was designed which is used as an input to a final element controller (see Figure 7.11). The modelled safety interlock system is shown in Figure 7.33. Two separate interlocks were modelled: one which fully opens the final element and the other that fully closes the final element. The interlock mask allows one to choose which interlock state should act on which alarm. This is modelled by using an index vector to switch to the user-specified alarm.

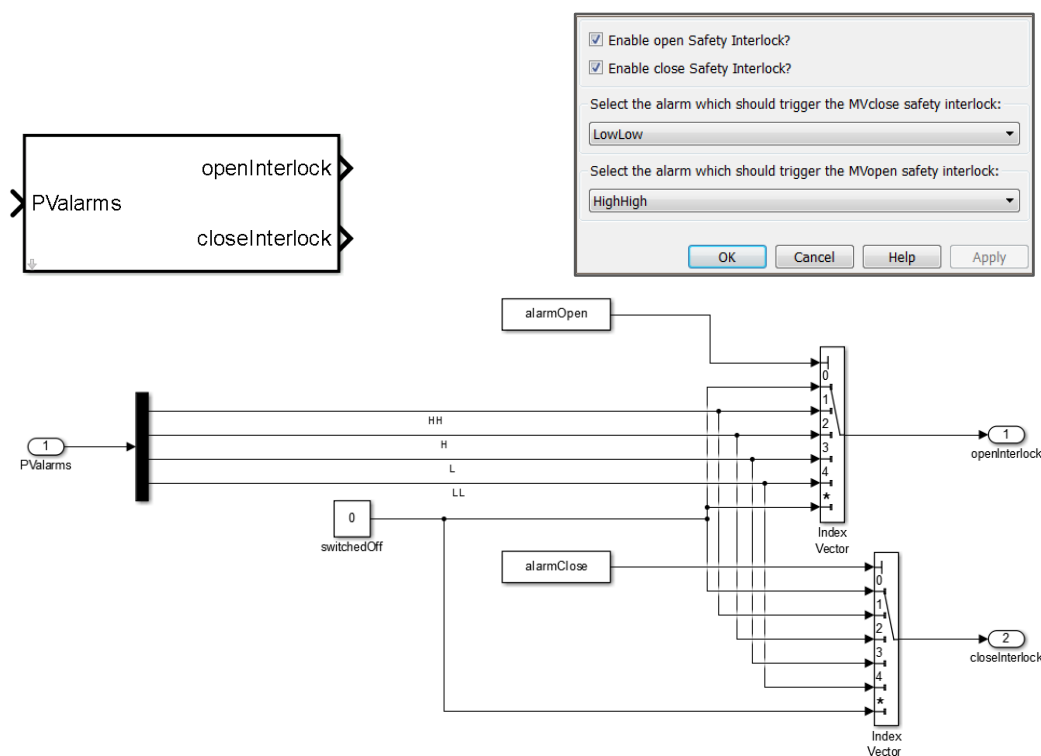


Figure 7.33: Block interface (top left), block mask (top right) and mechanism (bottom) of interlock modelled in Simulink™

Note that no additional aspects were added to the simulation of safety interlocks, as these electronic calculations and transmissions can be approximated as instantaneous.

7.7.2. Results and discussion

A total of 37 safety interlocks are known to exist at the Western Platinum BMR (refer to Table 2.6). All the safety interlock systems are implemented in the dynamic process model to ensure an interlock resemblance to the actual process. Safety interlocks which stop agitation within vessels were excluded from the dynamic process model since the ideal CSTR assumption would become invalid if agitators were to be switched off. The dynamic process model currently cannot describe a situation where no agitation occurs.

The second stage slurry preparation tank level cascade is used to demonstrate the behaviour of a safety interlock system. Refer to Figure 7.34.

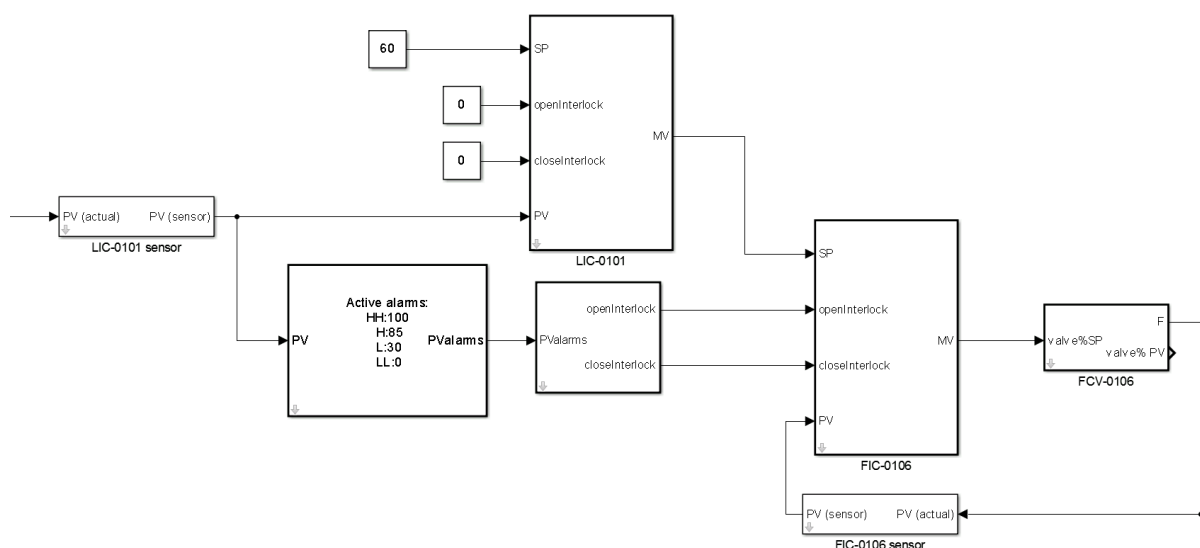


Figure 7.34: LIC-0101 control with safety interlock system modelled in Simulink™

Note that the interlock signal reports to the flow controller and not the level controller. The interlock signal is in this way bypassing the flow controller algorithm; therefore directly acting onto the actuator (i.e. if the interlock signal reports to the level controller, it would merely bypass the level control algorithm and not the flow control algorithm as well). The speed of the interlock action is in this case solely dependent on the actuator speed. The close-interlock is paired with the high-high alarm, while the open-interlock is paired with the low-low alarm. The interlock signals report to all inlet flow controllers to ensure that the interlock is effective.

The FIC-0106 flow controller is in this demonstration switched and operated in manual at 20 simulation hours in order to obtain extreme level conditions (i.e. the level controller is excluded). The vessel outlet flow rate is reduced to 0.5 m³/h in this demonstration (the outlet flow rate is operated lower than the inlet). Closing this stream fully would result in a trivial situation where the level stays constant at the high-high alarm level minus the alarm hysteresis value, with no flow entering or leaving. The alarm hysteresis is increased to 5 % for the time being to reveal the effect of the interlock. Results are shown below.

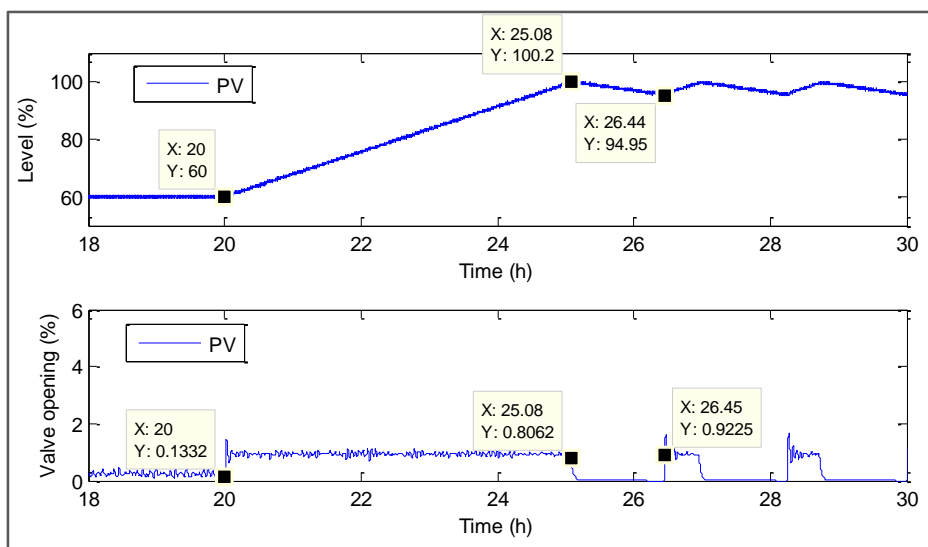


Figure 7.35: Safety interlock test: LIC-0101 with high-high alarm interlock

The ramp increase in level is caused by the switch from automated level controller to manual inlet flow control. The interlock switches on at 100 % level, at which point it stops all flow entering the vessel. This can be seen by the sudden decrease in the valve position of the inlet flow controller. The low valve position is caused by the lowered flow rate conditions previously mentioned. The level reduces to 95 % before the safety interlock switches off due to the 5 % alarm hysteresis. The flow controller attempts once again to reach its set-point since it is free from the interlock intervention. This causes the level to increase once again to the 100 % limit.

7.8. Summary

Western Platinum BMR uses several layers of control in order to operate an efficient, smooth, safe and profitable process. These control layers include regulatory control, supervisory control, alarm systems and safety interlock systems. This chapter reports on Western Platinum BMR control layers and its implementation onto the dynamic process model in an attempt to replicate the control philosophy. The behaviour of individual control layers was considered using a range of control scenarios. A closed-loop dynamic process was one of the major outcomes of this chapter.

CHAPTER 8: FAULT DATABASE CREATION AND SIMULATION

Chapter 7 describes the implementation of several control layers into the dynamic process model in order to prepare the model to mitigate occurrences of faults.

This chapter reports on the work of fault information gathering; fault database packaging; fault modelling; fault simulation in Simulink™; and fault behaviour verification. The simulated faults are to be used to assess the mitigation abilities of a control strategy in Chapter 9.

A total of 17 faults were gathered during a recent site visit and composed into a fault database (McCulloch et al., 2014). A total of 12 of faults were subsequently modelled.

8.1. Overview

The final outcome of this project is to use the available dynamic process model to assess control performance degradation during fault scenarios. This chapter discusses several faults obtained from a recent Western Platinum BMR site visit (McCulloch et al., 2014); the modelling thereof; and the behaviour after simulation.

Several information sources were identified in the literature review and used in the gathering of faults information during the site visit. The most useful source of information was expert knowledge together with historian tag data. A summary of fault characteristics from the literature review section is given:

- Classification
- Symptom identification method
- Symptom dynamics
- Fault location
- Fault type
- Rate of fault transition
- Frequency of fault occurrence
- Priority for fault mitigation

Characteristics listed above were obtained for faults seen at Western Platinum BMR. The faults were entered into a fault database and arranged according to fault classifications made by Venkatasubramanian (2003).

The database and its entries will be discussed in Section 8.2. The fault modelling and fault behaviour will be discussed individually in Section 8.3. Note that the quantitative symptoms and issues resulting from fault occurrences within the dynamic process model will not be discussed in this chapter, but rather in Chapter 9 during control performance assessment. Artificial inputs will simply be used within this chapter to demonstrate the fault behaviour.

8.2. Fault Database

A total of 17 faults were obtained from Western Platinum BMR and are captured in Table 8.1. Refer to Table F.11 for the entire fault database with all fault characteristics.

The classification of faults in certain cases could be reasoned into several categories. The most logical category is chosen for each fault.

The majority of faults are process disturbances associated with plant personnel disturbing the process by incorrect (fault 12); excessive (fault 9 and 11) or abrupt (fault 13) addition of material to vessels. Operator intervention faults are quite similar to these process disturbances, but are distinguishable since operator interventions are associated with the misuse of automated controllers (fault 7 and 8). Other common faults are actuator failures related with valve issues (fault 1 to 3). Structural failures listed in Table 8.1 are associated with the degradation of structures within the process and include centrifugal pump impeller wear (fault 4); cooling coil solid build-up (fault 5); and peristaltic pump tube failure (fault 6). Distinction is made between structural failures and sensor and actuator failures. The latter failures are common in the industry, and could therefore form separate categories.

The possibility of modelling each fault is captured in Table 8.1. All faults would be possible to model given enough resources. The possibilities captured in Table 8.1 are based on the ability to integrate faults into the current dynamic process model resolution; the model boundaries; and the available fault knowledge. A total of 12 faults were modelled. Certain faults occur outside the dynamic process model scope (i.e. fault 11, 12, 14 and 17), and were therefore not modelled. Fault 10 occurs within the scope of the dynamic process model. However, the crystallisation of metals out of the liquid phase falls outside the dynamic process model resolution.

Table 8.1: Section of fault database (McCulloch et al., 2014)

#	Classification	Fault name	Priority for fault mitigation	Possibility of fault modelling
1	Actuator failure	Valve blockage	High	Yes
2	Actuator failure	Valve wear	High	Yes
3	Actuator failure	Valve stiction	Medium	Yes
4	Structural failure	Pump impeller wear	High	Yes
5	Structural failure	Solid build-up in cooling coils	High	Yes
6	Structural failure	Peristaltic pump tube failure	High	Yes
7	Operator intervention	Sulphuric acid controller misuse	Medium	Yes
8	Operator intervention	Excessive steam addition by bypassing control valve	High	Yes
9	Process disturbance	Excessive water addition using manual valve	Medium	Yes
10	Process disturbance	Crystallisation of metals due to high total metals in solution combined with a cold day	High	No
11	Process disturbance	Excess amounts of flocculent addition	High	No
12	Process disturbance	Addition of wrong flocculent	High	No
13	Process disturbance	Sudden addition of caustic leach slurry into formic filtrate tank	High	Yes
14	Sensor failure	Flow sensor scaling due to inadequate flushing of the line	Low	No
15	Sensor failure	Bubbler level sensor blockage	Medium	Yes
16	Controller malfunction	Incorrect valve sizing	Medium	Yes
17	Controller malfunction	Excess vibration results in malfunctioning of on/off valve control	Low	No

Legend
Modelled and used in control performance assessment
Modelled but not used in control performance assessment
Not modelled

The dynamic process model contains no formulae which take into account phase transition caused by exceeding saturation limits. The dynamic process model should therefore be operated away from operating conditions which arrive at crystallisation.

Fault 8 and 9 were modelled but require preceding abnormal conditions before these faults occur. Excessive steam is added to the fourth autoclave compartment by bypassing the automated control valve when the automated temperature controller is inadequate at attaining the required temperature (fault 8). Water is added to the flash recycle tank using a manual valve when the temperature in the first compartment exceeds its set-point while its temperature controller's output is saturated (fault 9). These two faults require preceding abnormal conditions in order to realise its occurrence, and were therefore excluded from the control performance assessment investigation.

Expert knowledge (McCulloch et al., 2014) suggests that symptoms of fault 13 are similar to that of fault 1 (i.e. density spikes leaving the second stage slurry preparation tank which upsets temperature control in the first compartment). The control performance during the occurrence of fault 1 was investigated. The control performance during the occurrence of fault 13 was excluded since it was expected that similar results would be produced. The valve characteristic of an incorrectly sized valve (fault 16) is unknown, and could therefore not be used in control performance assessment.

Faults which were modelled either have a high or medium priority for mitigation. The mitigation of these faults is of importance at Western Platinum BMR. The modelling of these faults are beneficial since they could be used as a tool in the closed-loop dynamic process model to test early fault detection and diagnosis mechanisms, which could ultimately be implemented at Western Platinum BMR.

8.3. Fault Modelling

Several faults with corresponding characteristics were obtained during a site visit, and are discussed in Section 8.2. The fault modelling procedure and fault behaviour are discussed individually in the subsequent sections. Modelled faults in a mineral processing environment are not widely available in literature (let alone dynamic processes). The nature of several faults was modelled using the knowledge of experts at Western Platinum BMR where modelling procedures from literature did not exist.

8.3.1. Valve blockage – density disturbance

Methodology

A valve situated upstream of the Western Platinum BMR boundaries under consideration occasionally blocks. This blockage results in sedimentation of particles in an upstream vessel, causing density disturbances into the second stage slurry preparation tank. Figure 8.1 shows the location where the fault disturbs the process.

The valve blockage causes major density disturbances in the first stage leach residue stream. The fault was modelled as a density disturbance in this stream, since the actual fault occurs upstream of the model scope. Online density measurements are available for the first stage leach residue stream during the occurrence of the density disturbance.

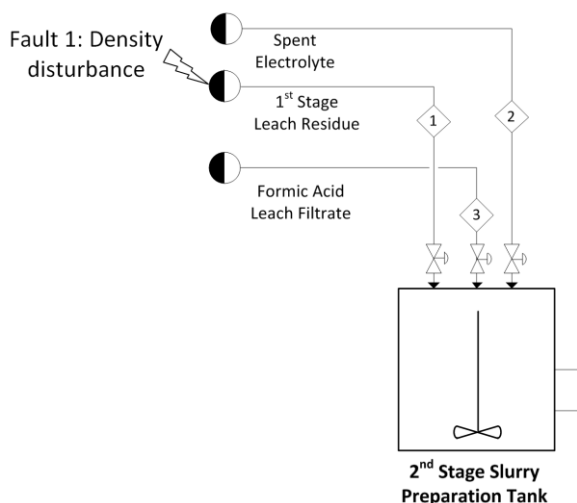


Figure 8.1: Location of fault 1: Density disturbance

The online density measurements were converted into solid mass fractions using Equation 7.12 in order to be used as an input to the dynamic process model.

Equation 7.12 is an arranged version of an average density calculation, where ρ_m represents the measured density. The liquid (ρ_L) and solid (ρ_S) densities are approximated with values used in the dynamic process model (i.e. 1200 kg/m³ and 4450 kg/m³, respectively). The solid fraction deviation from time zero is calculated:

$$x'_s = x_s - x_{s,t_0} \quad \text{Equation 8.1}$$

The solid fraction deviation time series is added to the first stage leach residue stream solid fraction in the dynamic process model. This approach is used instead of simply replacing the first stage leach residue stream solid fraction with results from Equation 7.12 in order to avoid any solid fraction discontinuities prior and subsequent to the fault occurrence.

The data produced from Equation 8.1 was imported into the dynamic process model using the Simulink™ Signal Builder (refer to the mechanism in Figure 8.2).

A delay was used to start the fault implementation at the correct time (discussed in Chapter 9). Block masks were created to manage the fault occurrences and their information from the MATLAB™ base workspace. The block interface intercepts the solid fraction signal in which the fault occurs and adds the disturbance when the fault is enabled.

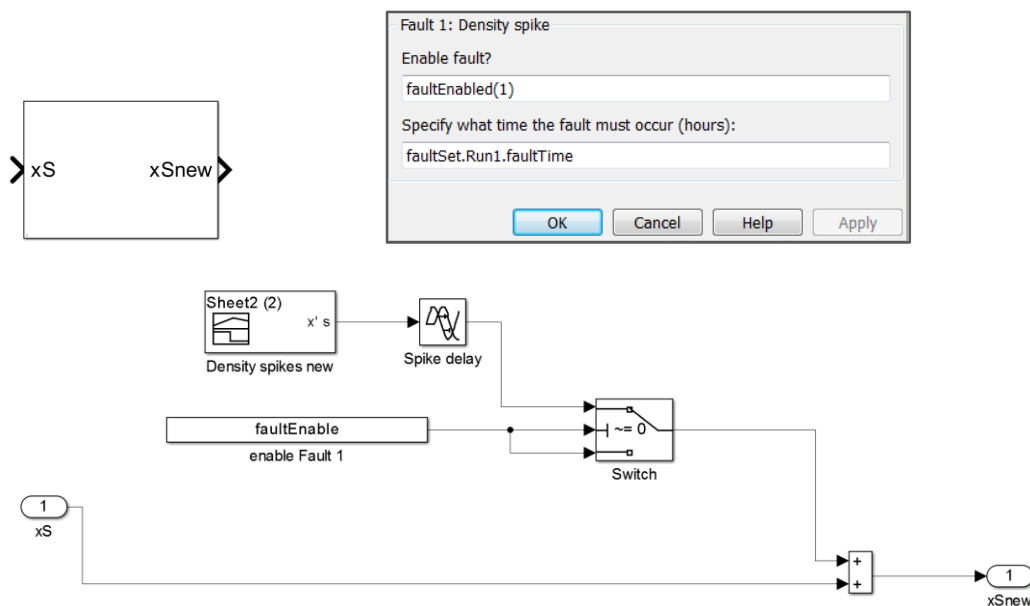


Figure 8.2: Block interface (top left), block mask (top right) and mechanism (bottom) of density disturbance modelled in Simulink™

Results and discussion

The following figure shows the solid mass fraction deviation calculated by applying Equation 8.1 to Western Platinum BMR density data during the occurrence of the disturbance.

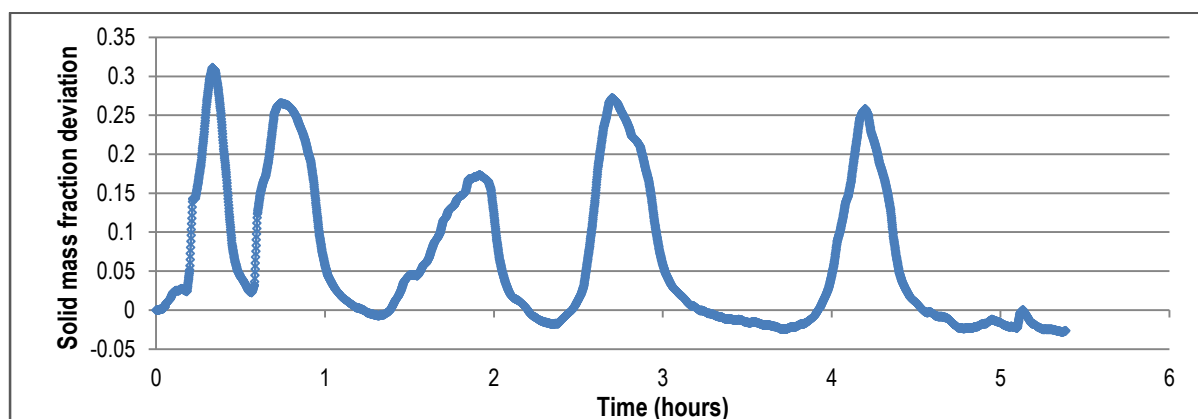


Figure 8.3: Quantification of density spikes in first stage leach residue stream using real-time data

Five solid fraction spikes are present, each representing the valve that is temporary unblocking. The unblocking of the valve causes excessive amounts of solid sediment to pass through the first stage leach residue stream. Solid fractions within the first stage leach residue increases up to around 0.6 when the first stage leach residue model solid fraction is added to that in Figure 8.3. Note that the final solid fraction deviation is not equal to zero. A steady increase toward a zero solid fraction deviation is used to ensure that the fault does not end abruptly.

8.3.2. Valve wear

Methodology

Valve wear is known to change valve characteristics due to destructive material that erodes the valve regulation pattern (i.e. affecting the flow rate-valve position relationship - see Equation 7.1a). The mechanism of valve wear is captured in the following figure.

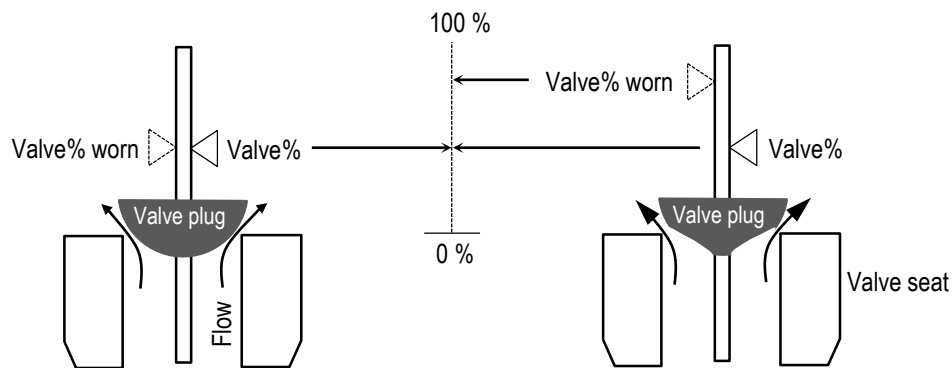


Figure 8.4: Linear valve (left) and quick-opening valve (right) prior to and after valve wear

Quick-opening valve characteristics are evident after extensive valve wear. This is attributed to the abrasive slurry that erodes the valve plug which ultimately causes more material to pass between the valve plug and seat at a specific valve position. A worn valve position is used in the modelling of this fault, and is defined as the standard unworn valve position which would produce the volumetric flow rate at the current valve state. The worn valve position increases over time at a specific valve position due to the increased volumetric flow rate evident from the worn valve, as seen in Figure 8.4.

Valve wear is a common issue when valves are subjected to an abrasive environment (Anyakora, 1971; Koscielny & Bartys, 2000). Western Platinum BMR has several valves exposed to abrasive slurry streams, and are therefore subjected to valve wear (McCulloch et al., 2014). Figure 8.5 shows the location of the fault.

The valve present on the fourth compartment outlet stream, considered within this project, is one of the many valves that are subject to abrasive conditions at Western Platinum BMR (McCulloch et al., 2014).

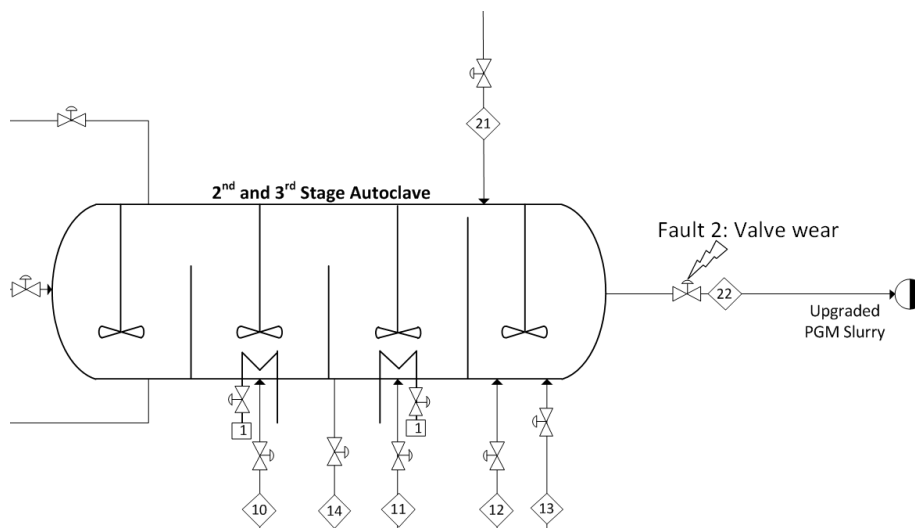


Figure 8.5: Location of fault 2: Valve wear

In-depth knowledge of slurry properties, valve shapes, valve materials, and more, would be required to model valve wear fundamentally. This would also be too extensive when compared to the current model resolution. The valve wear was therefore modelled using an empirical data-driven equation which describes the noticeable change in valve characteristics over time.

$$valve\%_{worn} = 100 \times \left(\frac{valve\%}{100} \right)^{1-\alpha(t)} \quad \text{Equation 8.2}$$

Equation 8.2 relates the actual valve position (i.e. the present-value) to a worn position. The worn position reports directly and only to the valve characteristic general expression block, which transfers a valve position to a flow rate. The extent of degradation (α) assumes a value between 0 and 1, with the former being an ideal case. The extent of degradation is also a function of time (i.e. increasing over time). Equation 8.2 was developed after considering several constraints:

1. $0 \% \leq valve\%_{worn} \leq 100 \%$
2. $valve\%_{worn} = 0 \%$ when $valve\% = 0 \%$
3. $valve\%_{worn} = 100 \%$ when $valve\% = 100 \%$
4. The function is at all times continuous

The relation between the actual valve position and the worn valve position is demonstrated in Figure 8.6. Notice that all constraints listed above are satisfied when Equation 8.2 is used.

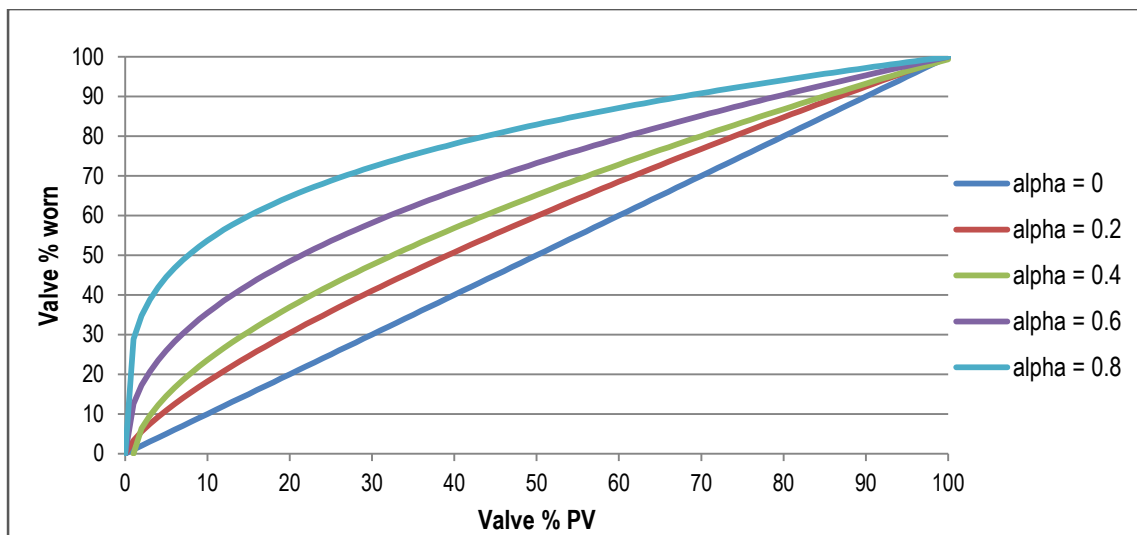


Figure 8.6: Actual and worn valve position relation at different extents of degradation

The quick-opening symptoms of valve wear are captured in trends seen in Figure 8.6. The extent of degradation starts off at zero where a linear correlation is evident, and increases over time. The extent of degradation term was related to time by using fourth compartment outlet flow rate data around several dates.

Valve wear was simulated in Simulink™. The results are captured in Figure 8.7. The actuator block comprises the transfer of a valve position to a flow rate by using specific valve characteristics (refer to Figure 7.7). The valve wear fault was therefore included in the actuator transfer block since it directly affects the valve characteristics. The valve wear fault intercepts the valve position present-value and changes it to a worn percentage as described by Equation 8.2. The worn valve position is directly and only fed to the valve characteristic general expression block. The extent of valve degradation increases linearly from a value of zero to a certain extent over a transition period all specified in the block mask. The extent of degradation is approximated using Western Platinum BMR plant data.

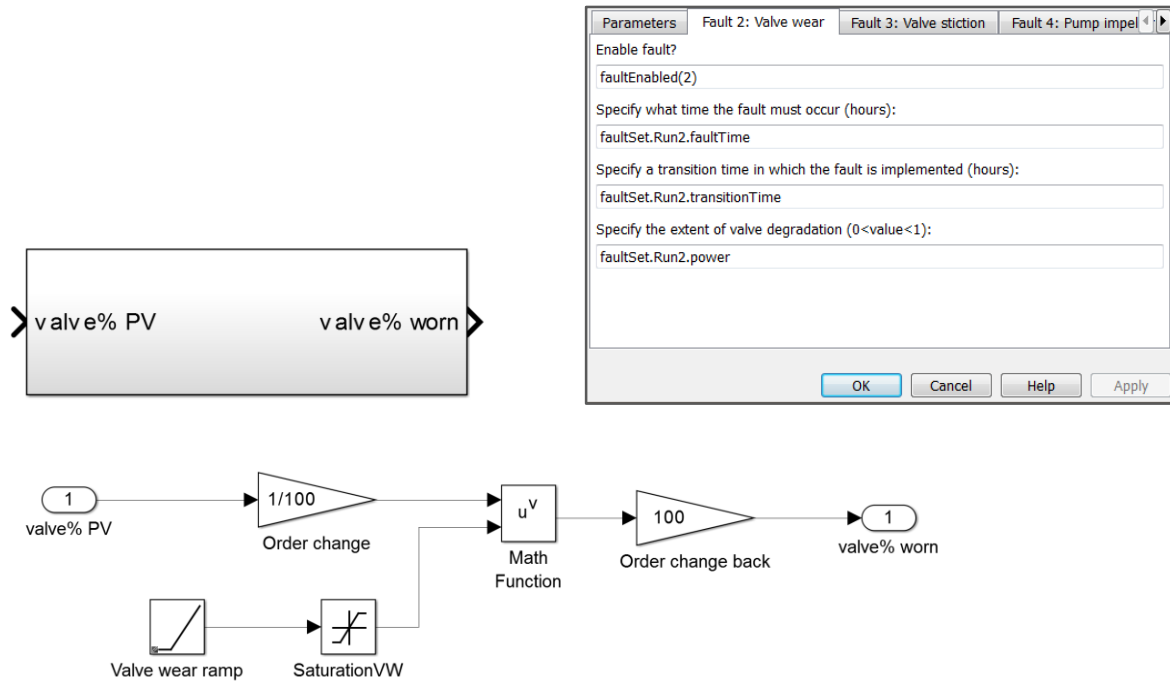


Figure 8.7: Block interface (top left), block mask (top right) and mechanism (bottom) of valve wear modelled in Simulink™

Results and discussion

Figure 8.8 shows fourth compartment flow rate and valve data around three different dates. Equation 8.2 is fitted individually to the three data sets.

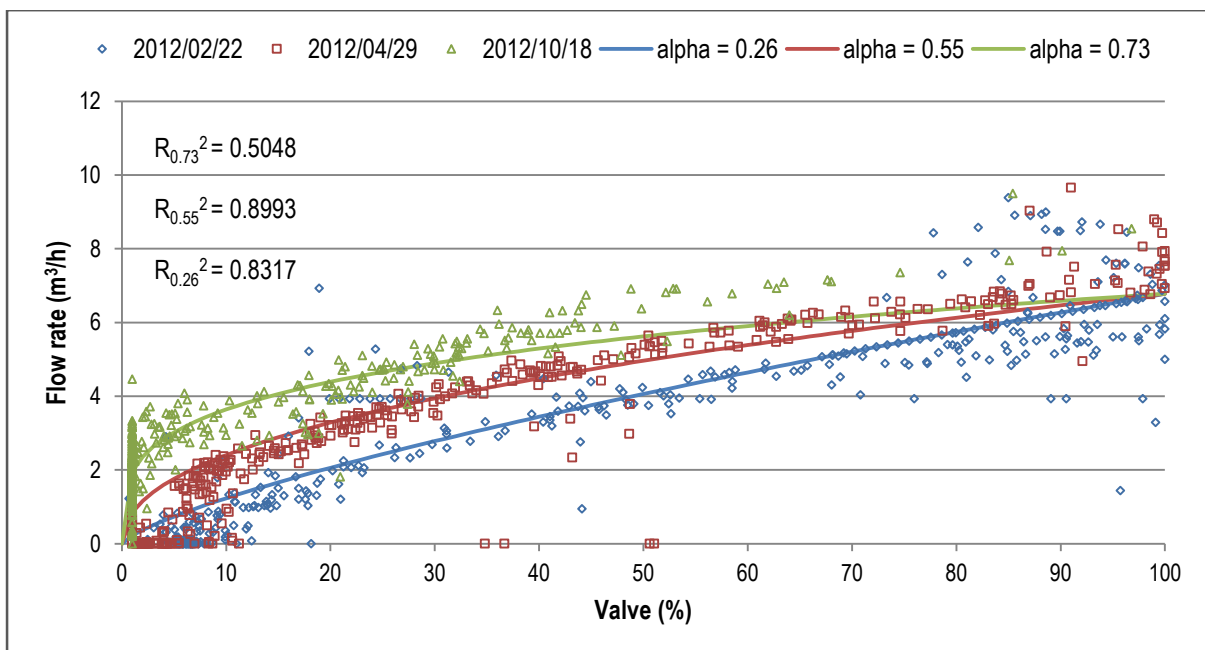


Figure 8.8: Quantification of fourth compartment valve degradation over time using real-time data

The empirical equation fits well to plant data with R^2 -values of 0.5048, 0.8893, and 0.8317 for alpha values of 0.73, 0.55, and 0.26, respectively. The highest extent of degradation only shows an adequate fit, which is attributed to the different flow rates evident at a valve position around 1 %. The valve characteristics clearly change over the span of several months. The valve characteristics change to quick-opening, as expected. The extent of degradation is now plotted against the date and correlated with a linear trend line.

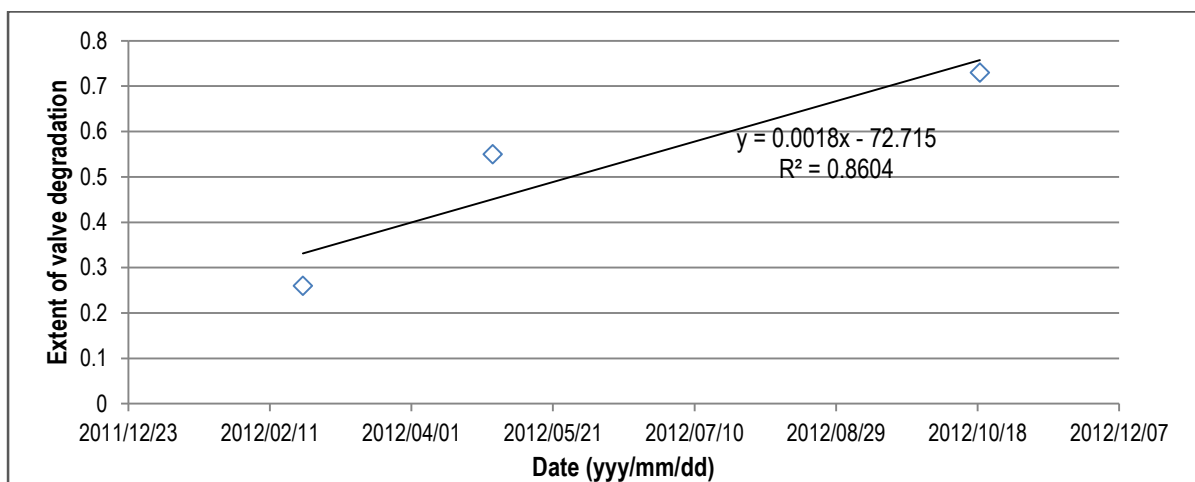


Figure 8.9: Quantification of rate of fourth compartment valve degradation using real-time data

The high R^2 -value is insignificant since only three data points are present. Another trend line might fit the data points more accurately. More data points are necessary to support the previous statement. A linear increase in valve degradation over time is adequate for the purpose of this project. The fault database (refer to Table F.11) shows that the third compartment outlet valve is replaced approximately every nine months. The final extent of valve degradation before replacement was estimated using the rate at which the valve degrades in Figure 8.9, together with the valve replacement interval. A final extent of 0.502 was evident after assuming the valve starts off with an alpha value of zero. Note that this value is smaller than extents of degradation seen in Figure 8.8. This could possibly be attributed to either an incorrect estimated rate at which valves are replaced (McCulloch et al., 2014) or the method used to extrapolate to a final extent of valve degradation. A 0.73 extent of valve degradation, evident from plant data, was used within control performance assessment. Refer to Appendix C for the extent of degradation sample calculation.

The behaviour of the valve wear fault is considered by applying an artificial sinusoidal valve set-point input to the actuator transfer block (refer to Figure 7.7). This sinusoidal wave has a low frequency so as to produce a matching valve present-value.

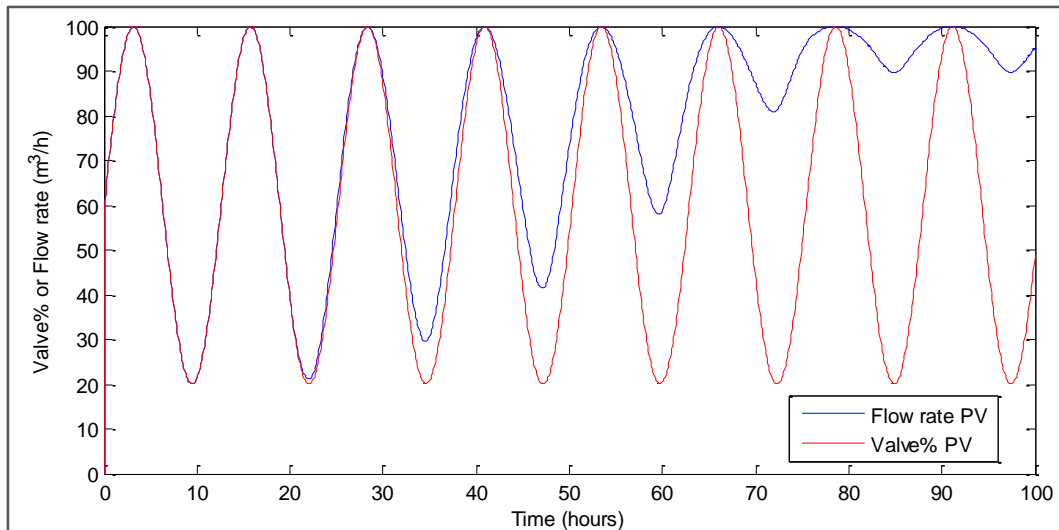


Figure 8.10: Behaviour of the valve wear fault for an artificial sinusoidal valve position

The valve characteristic for this scenario is simply taken as $1 \times u$ (i.e. a flow rate equal to the valve position present-value at a specific point in time is expected - refer to Equation 7.1b). The results are plotted below. The fault starts at 20 hours and is implemented over 60 hours (i.e. fully implemented at 80 hours). Note that this fault and most of the other faults to be discussed do not occur in a matter of hours, but over several months. The high fault transition rates are merely used to illustrate the fault behaviour.

The flow rate attained for a specific valve position increases over time, assuming the pump performance is unaffected by the abrasive material. The increased flow rate over time is expected since valve wear results in quick-opening dynamics. Note that the maximum flow rate at a valve position of 100 % does not increase over time, since valve wear changes the shape of the valve and not the flow rate capacity (this is the first and third constraint which was used to develop Equation 8.2).

8.3.3. Valve stiction

Methodology

Valve stiction can be defined as the resistance exhibited by a valve to start moving as a result of large static friction. Several literature sources report the existence of valve stiction within operations, and has been said to be the most common valve fault within the process industry (Venkatasubramanian & Rich, 1988; Himmelblau, 1978; Lees, 1976; Koscielny & Bartys, 2000; Downs & Vogel, 1993). This fault commonly occurs at Western Platinum BMR (McCulloch et al., 2014). Refer to Figure 8.11.

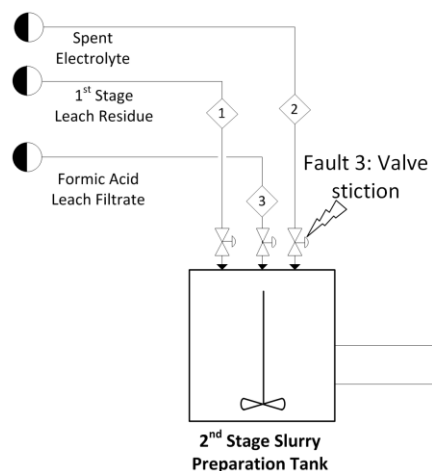


Figure 8.11: Location of fault 3: Valve stiction

The valve present on the spent electrolyte stream entering the second stage slurry preparation tank is known to exhibit valve stiction behaviour (McCulloch et al., 2014).

The dynamics of valve stiction was modelled using an empirical data-driven model described in Choudhury et al. (2005). Valve stiction behaviour is captured in Figure 8.12.

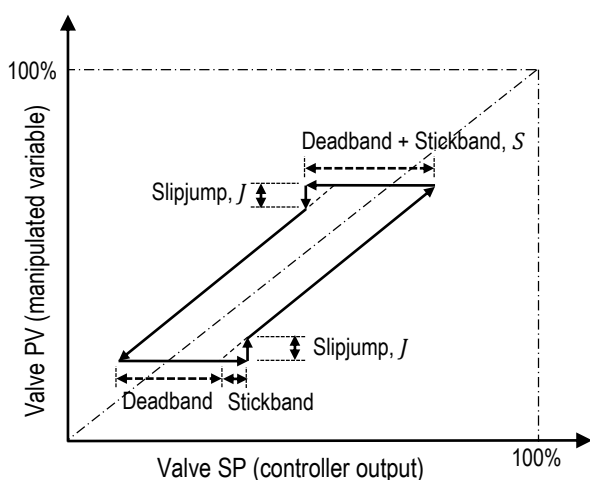


Figure 8.12: Input-output behaviour of valve stiction (redrawn from Choudhury et al. (2005))

The deadband and stickband together is the size in which the valve set-point varies with no significant change in valve present-value, upon a valve reversal. This only occurs at a valve reversal, and represents the static friction which is larger than the valve driving force when the valve speed is zero (i.e. at the time the valve changes direction). The slipjump is the size by which the valve present-value jumps after slipping out of the static position, and represents the abrupt release of potential energy stored in the valve driving force due to the high countering static friction.

Valve stiction was simulated in Simulink™. The results are captured in Figure 8.13.

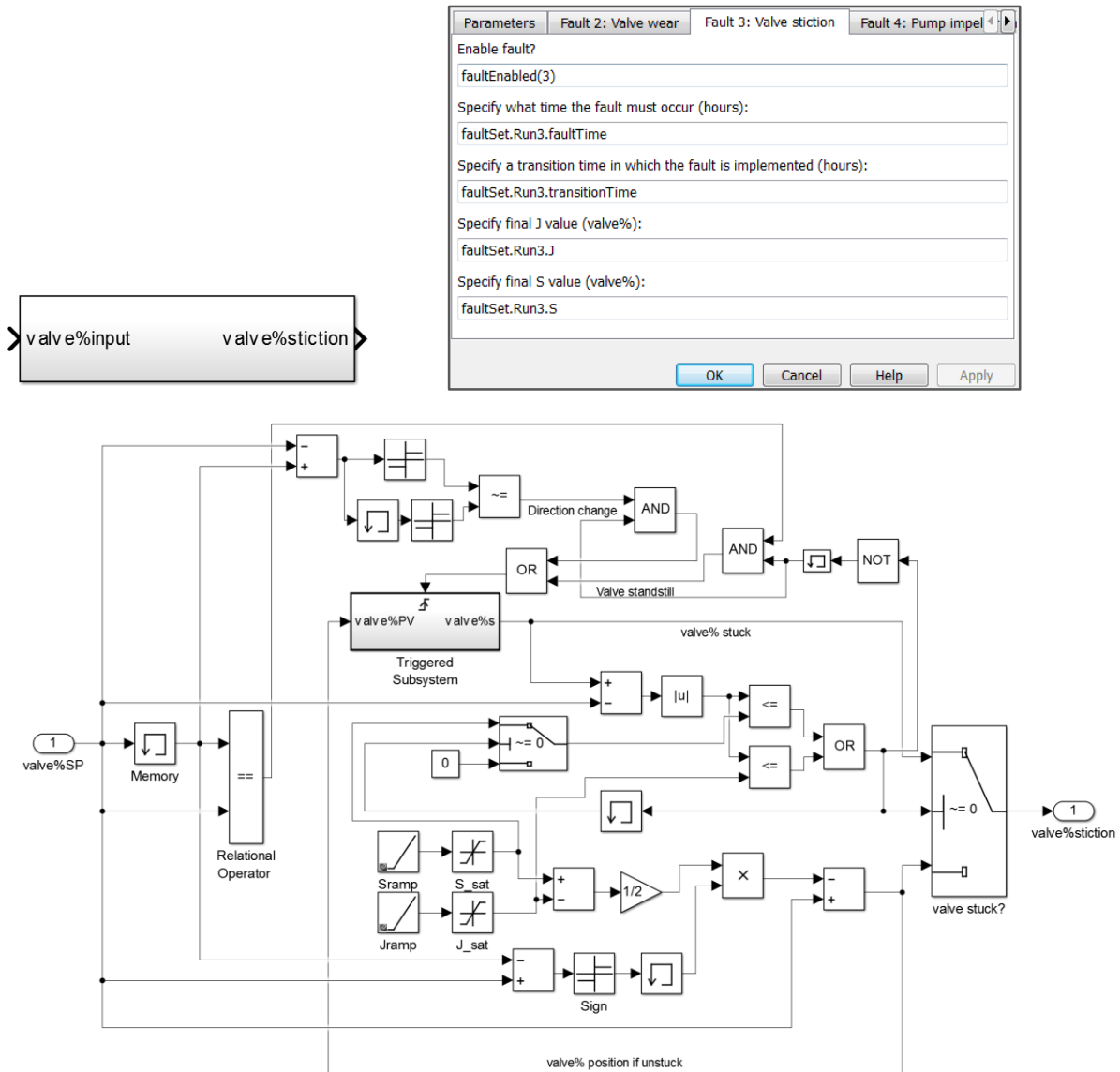


Figure 8.13: Block interface (top left), block mask (top right) and mechanism (bottom) of valve stiction modelled in Simulink™

A modelling methodology similar to Choudhury et al. (2005) was followed so as to produce the valve stiction model captured in the mechanism depicted in Figure 8.13. A valve set-point is subtracted from its preceding value. The sign of this difference is compared to its preceding sign in order to establish if the valve set-point changed direction (the valve present-value attempts to change direction when it is instructed to do so by its set-point). A triggered subsystem is activated when the valve either changes direction or does not move (excluding the time in which it is stuck). The triggered subsystem passes through a single valve position at that point in time and holds it (i.e. the valve is stuck at this position). This valve position is held until either the slipjump (S) or deadband and stickband (J) is smaller than the absolute difference between the stuck position and its set-point. The unstuck valve position is constantly calculated by adding the difference between S and J to the valve set-

point. This difference is added in a similar direction in which the valve set-point is moving. This is done so that the valve jumps in the correct direction when it starts to move. The calculations incorporating stickband, deadband and slipjump determines if the valve undershoots or overshoots its set-point when it jumps (refer to Figure 8.12). An in-depth description of valve stiction modelling can be found in Choudhury et al. (2005).

The valve stiction fault was added to the actuator block since it directly affects the valve position. The valve stiction fault adjusts the valve position according to calculations in the mechanism. The slipjump, deadband and stickband parameters increase linearly over the fault implementation transition time. Valve stiction parameters seen in Figure 8.12 were estimated using Western Platinum BMR plant data.

Results and discussion

The following figure attempts to capture the spent electrolyte valve behaviour.

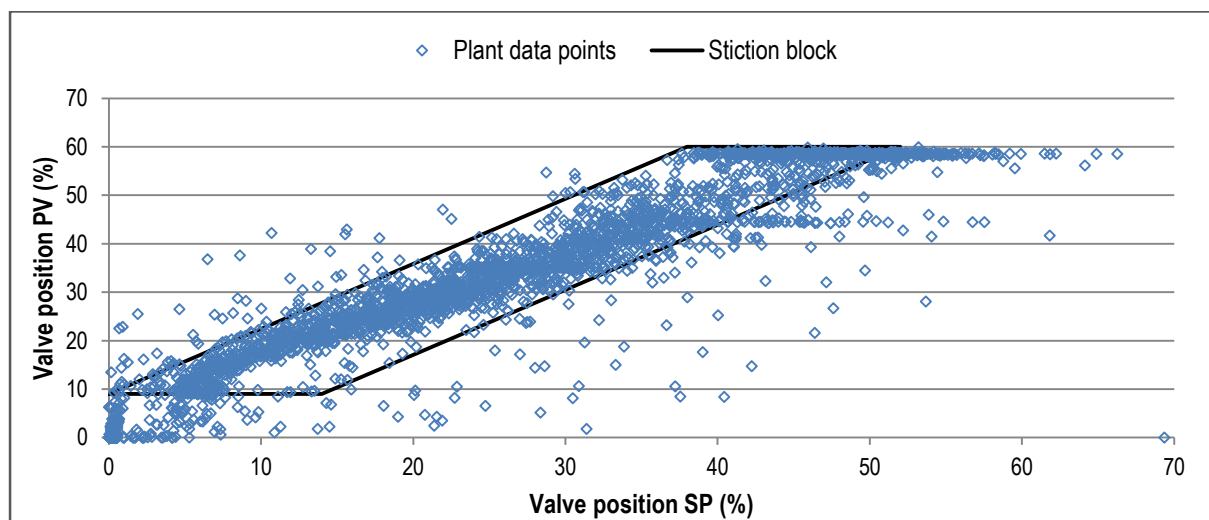


Figure 8.14: Quantification of valve stiction parameters using real-time data

The valve present-value was approximated by using normalised flow rates. No high resolution (i.e. many data point spanning over a short time) step-test data was available to decouple the effects of valve stiction from other measurement issues. The valve stiction parameters for the worst-case scenario were therefore estimated by using a wide range of data points over a span of time. A deadband and stickband of 14 % is evident when the width of the stiction block in Figure 8.14 is considered. It is expected that this value is overestimated due to the use of extensive data and inadequate resolution data which contain other measurement issues. No conclusive estimation of the slipjump can be obtained from Figure 8.14. A slipjump equal to that of the deadband and stickband is taken. This means that there will be no offset once the valve present-value jumps towards the valve set-

point. A proper estimation of valve stiction parameters should be obtained from high resolution step-test data. Incremental step-tests should reveal to what extent a valve set-point and present-value should differ before the valve jumps (i.e. the deadband and stickband). The extent to which the valve present-value misses its set-point when it jumps should reveal the slipjump size.

The behaviour of the valve stiction fault is considered by applying an artificial sinusoidal valve set-point input to the actuator transfer block. Deadband and stickband; and slipjump values of 20 % and 10 %, respectively, are used in this scenario. A slipjump value unequal to the deadband and stickband value is used in order to show the offset ability of the modelled fault. Results are plotted in Figure 8.15.

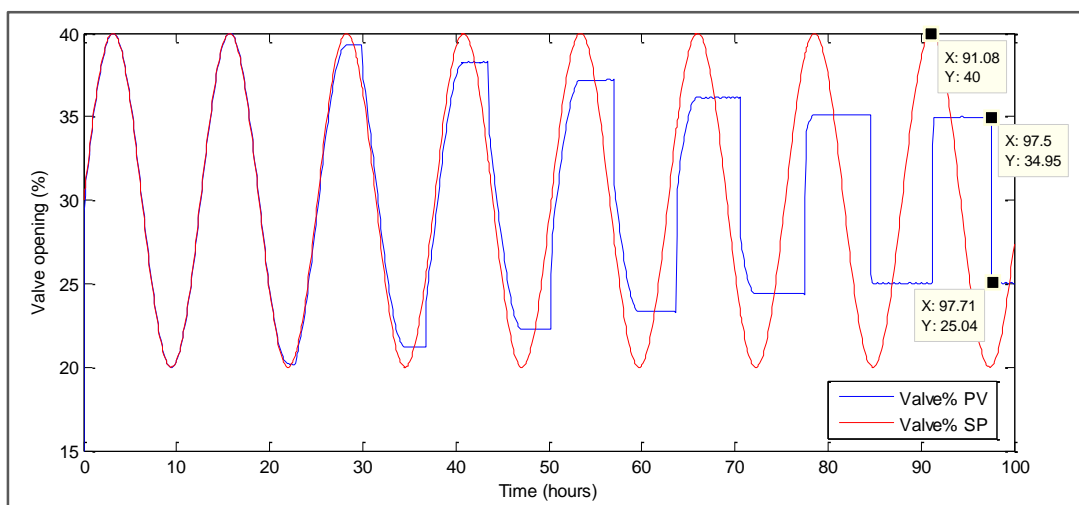


Figure 8.15: Behaviour of the valve stiction fault for an artificial sinusoidal valve position set-point

The fault starts at 20 hours and is implemented over 60 hours. The valve sticks each time it changes direction. The stiction persists until the difference between the valve set-point and present-value exceeds the deadband and stickband. The slipjump is smaller than the deadband and stickband, which causes the valve's jump to undershoot. The valve set-point range is equal to the deadband and stickband when the fault is fully implemented in this demonstration (i.e. at 80 hours). This causes the valve to jump and proceed with a turn, where it once again sticks.

8.3.4. Pump impeller wear

Methodology

Moving abrasive materials using centrifugal pumps can cause impeller wear (Himmelblau, 1978). Similar findings were seen at Western Platinum BMR. Refer to Figure 8.16.

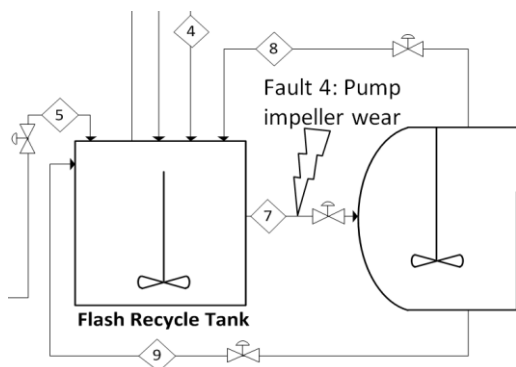


Figure 8.16: Location of fault 4: Pump impeller wear

Expert knowledge at Western Platinum BMR reports the impeller on the flash recycle tank outlet pump is often degraded by abrasive slurries (McCulloch et al., 2014).

The complex nature of impeller wear once again exceeds the resolution of the current BMR model, and was therefore modelled empirically. It is known that impeller wear reduces pump pressure head and flow rate over time (Burt & Feist, 2012). The reduction in maximum flow rate acts on the valve characteristic calculations (see Equation 7.1a), and was therefore included in the valve transfer function. Impeller wear was modelled by assuming a constant rate of impeller degradation with time. The simulated fault is shown in the figure below.

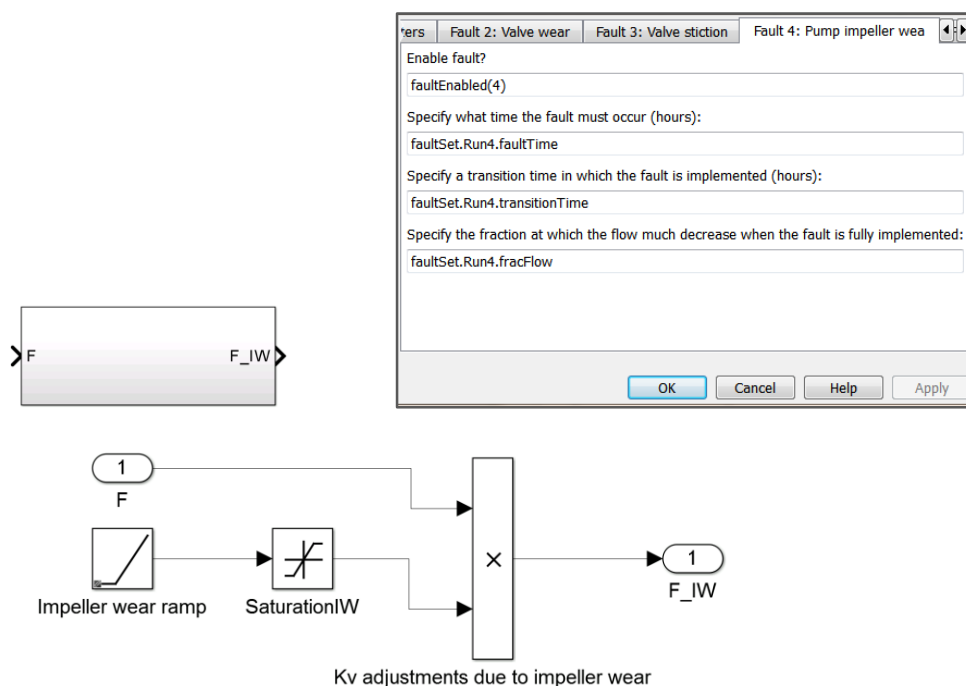


Figure 8.17: Block interface (top left), block mask (top right) and mechanism (bottom) of impeller wear modelled in Simulink™

The valve wear fault degrades the flow rate linearly up to a certain final flow rate fraction over a specified transition time; all defined in the mask by a user. The final flow rate fraction

is the fraction by which the maximum flow rate decreases when the fault is implemented fully (i.e. the extent in which the pump impeller is effectively worn).

Results and discussion

Expert knowledge at Western Platinum BMR reports the flash recycle tank outlet pump flow rate capacity reduces to such an extent that the flash recycle tank level controller valve saturates in an attempt to keep the level in check (McCulloch et al., 2014). A final flash recycle tank outlet flow rate fraction of 0.0316 in the dynamic process model causes flash recycle tank level control saturation. The low final fraction is attributed to the low flow rates used to control the first compartment temperature (i.e. the first compartment does not use its manipulated variable excessively due to the reduced extent of base metal leaching therefore heat releasing predictions).

The behaviour of the pump impeller wear fault is considered by introducing an artificial sinusoidal valve set-point to the actuator transfer block. A 0.5 extent of flow rate reduction is used in this demonstration. The valve characteristic for this scenario is once again taken as $1 \times u$. Consider the results plotted in Figure 8.18.

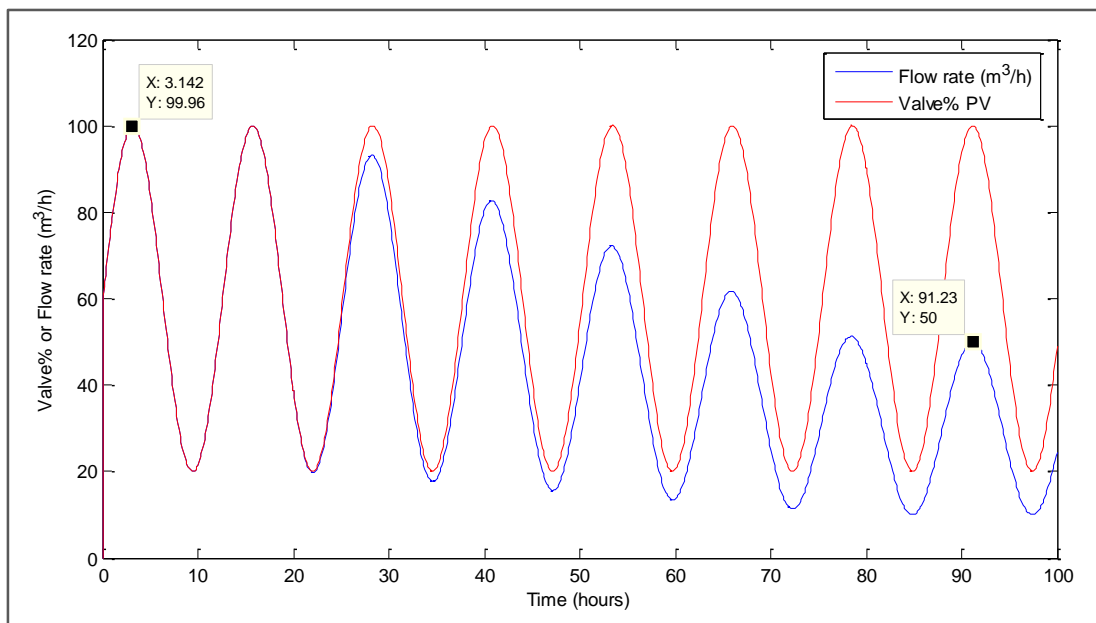


Figure 8.18: Behaviour of the pump impeller wear fault for an artificial sinusoidal valve position set-point

The fault starts at 20 hours and is implemented over 60 hours. The effectiveness of the centrifugal pump decreases as time progresses. A 50 % pumping capacity decrease is evident after the fault has been fully implemented.

8.3.5. Solid build-up in cooling coils

Methodology

Minerals often build up in cooling coils when hard water is used. This fault occurs within several autoclave compartments at Western Platinum BMR. The location of the fault considered within this project is highlighted in Figure 8.19.

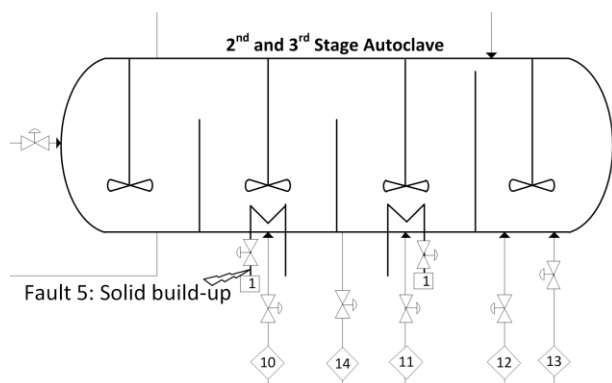


Figure 8.19: Location of fault 5: Solid build-up in cooling coils

Solid build-up occasionally occurs in the second compartment cooling coils. A total blockage could occur if this fault is left unattended or neglected (McCulloch et al., 2014).

Cooling coil solid build-up was modelled in the same way impeller wear was modelled, since it also acts on the valve characteristic calculations. A total blockage was used in the modelling of the solids build-up, reducing the maximum flow rate to zero over a specified time. Consider the solid build-up Simulink™ in Figure 8.20. The solid build-up fault degrades the flow rate linearly over a specified transition time, which is defined in the mask by a user.

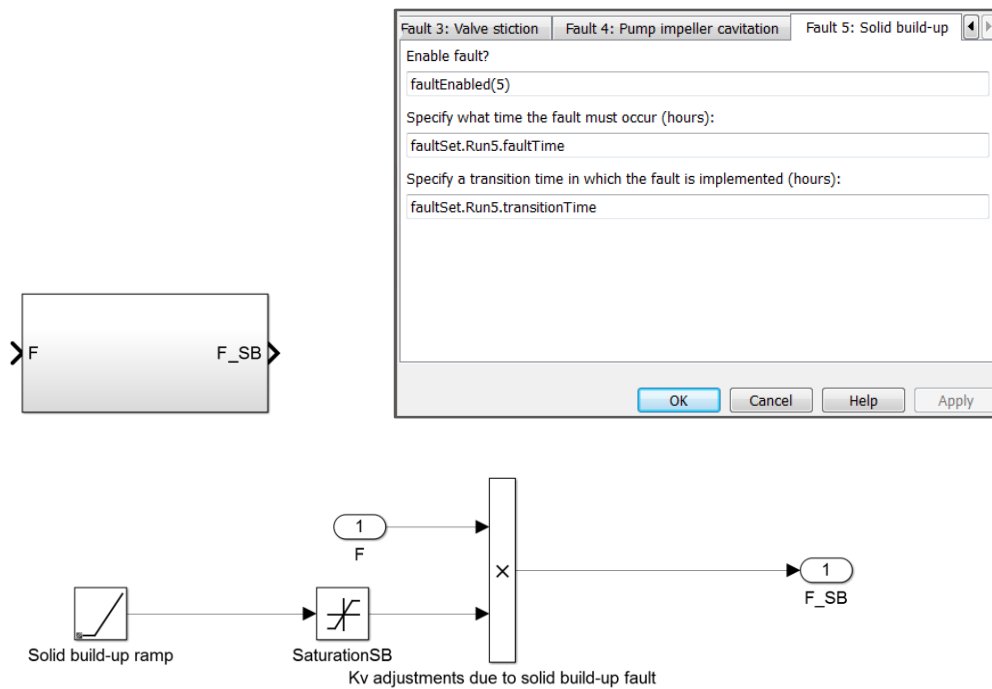


Figure 8.20: Block interface (top left), block mask (top right) and mechanism (bottom) of solid build-up modelled in Simulink™

Results and discussion

The behaviour of the solid build-up fault is considered by introducing an artificial sinusoidal valve set-point into the actuator transfer block. The valve characteristic for this demonstration is once again taken as $1 \times u$. Refer to Figure 8.21.

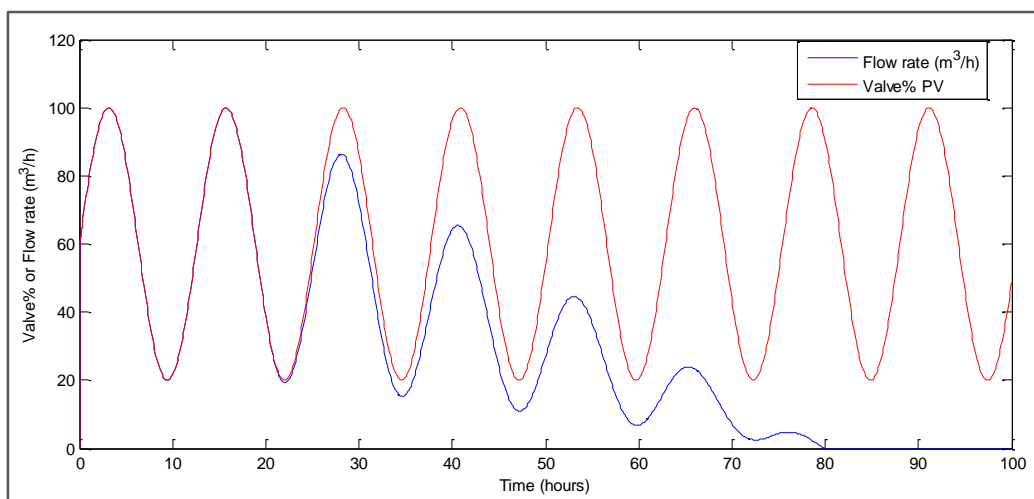


Figure 8.21: Behaviour of the solid build-up fault for an artificial sinusoidal valve position set-point

The fault starts at 20 hours and is implemented over 60 hours. The pipeline is fully blocked at 80 hours, substantiated by the zero flow rate attained at a variety of valve positions.

8.3.6. Peristaltic pump tube failure

Methodology

A peristaltic pump is used upstream of the process scope. The tube used within this pump often fails which causes leakage, particle sedimentation and ultimately blockage in an upstream pipeline. The pipeline becomes fully blocked if the flow is stopped for more than five minutes (McCulloch et al., 2014). The location at which this fault enters the process is shown in Figure 8.22.

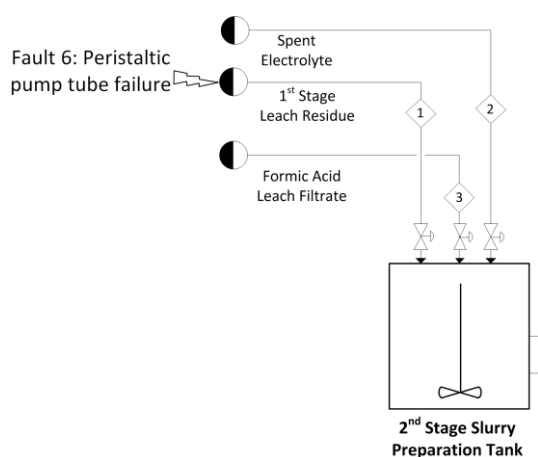


Figure 8.22: Location of fault 6: Peristaltic pump tube failure

The peristaltic pump is located upstream of the first stage leach residue stream. The peristaltic pump tube failure causes a hold-up in the upstream vessel which results in a ceased flow rate within the first stage leach residue stream.

The tube failure was modelled as an abrupt stop in the applicable stream. Consider the Simulink™ model in Figure 8.23.

The fault shown in Figure 8.23 intercepts the flow rate signal and abruptly changes it to zero at a user-defined time. Note that this fault should only be applied to input streams. Mass balances will be unsatisfied if the fault is implemented on a process unit output signal.

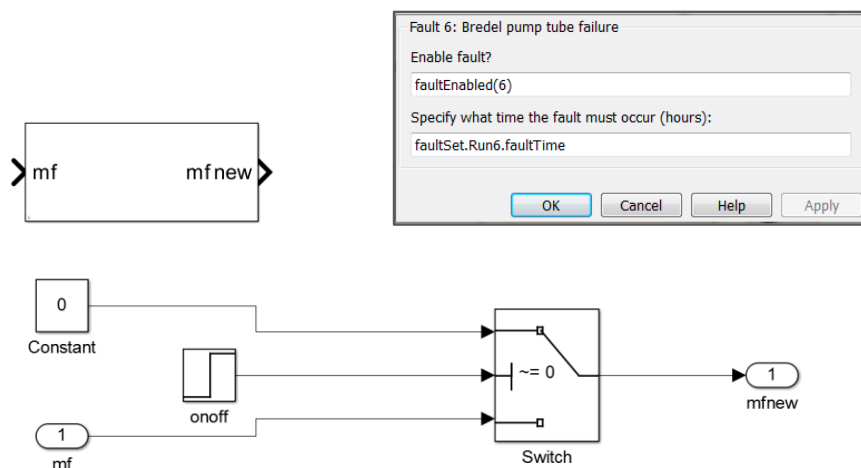


Figure 8.23: Block interface (top left), block mask (top right) and mechanism (bottom) of peristaltic pump tube failure modelled in Simulink™

Results and discussion

The behaviour of the peristaltic pump tube failure fault is considered by introducing an artificial sinusoidal signal into the fault block which represents a flow rate.

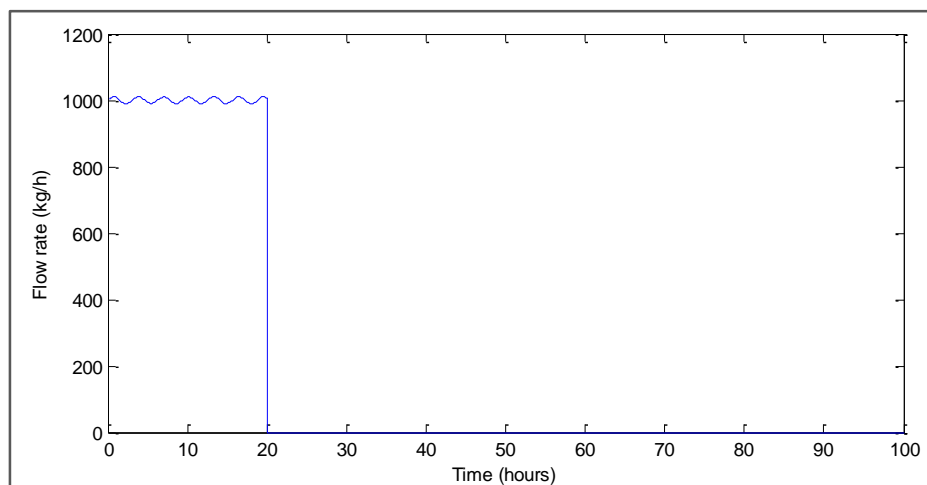


Figure 8.24: Behaviour of the peristaltic pump tube failure fault for an artificial sinusoidal flow rate

The fault is introduced at 20 hours. The flow rate instantaneously decreases to zero, representing the hold-up in the first stage leach residue stream.

8.3.7. Sulphuric acid controller misuse

Methodology

Operators keep the sulphuric acid concentration exiting the flash recycle tank above 20 g/l by manipulating the set-point of a sulphuric acid flow controller (discussed in Section 7.5).

Operator actions are however not always as consistent as the modelled supervisory controller seen in Figure 7.27. One fault often seen at Western Platinum BMR is excessive addition of acid to the flash recycle tank due to operator negligence. Refer to the figure below.

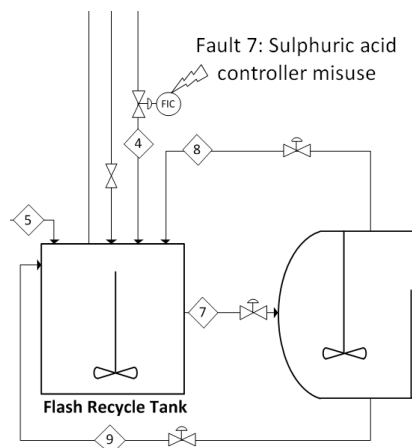


Figure 8.25: Location of fault 7: Sulphuric acid controller misuse

Operators often switch the stream 4 flow controller on and forget to switch it off timeously. The fault was therefore modelled as an on/off operator controller with an extended step-up to step-down holding time (refer to Figure 7.23). The fault holding time was estimated using a medium resolution data set with a time length which corresponds with the frequency of the fault occurrence. The longest holding time was 2.58 hours, which is longer than the manual acid sampling rate of two hours. This suggests that the acid flow controller is in certain cases left unattended until the following acid sample is taken. Moreover, operator actions are not always made exactly after every two hours.

Results and discussion

Figure 8.26 is used to compare the normal operator control action to an incorrect and negligent operator action with similar inputs. The input to the supervisory controller is defined so that the operator action only occurs at 2 hours.

The set-point of the sulphuric acid flow controller is switched off timeously during normal operation. A similar flow rate set-point is noticed during the occurrence of the fault since the operator's set-point decision should be similar in both cases. The issue with the fault is that the set-point is left unattended, which results in excessive acid concentrations inside the flash recycle tank.

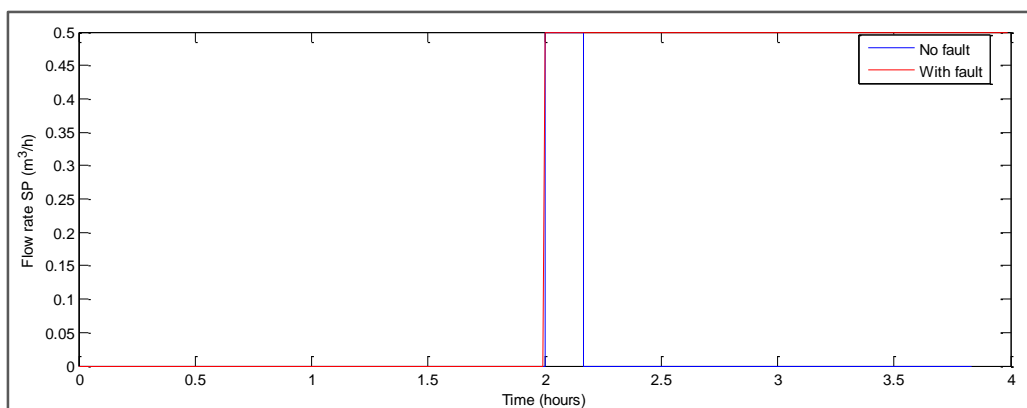


Figure 8.26: Sulphuric acid flow rate set-point provided by an operator

8.3.8. Bubbler level sensor blockage

Methodology

Most of the level sensors used at Western Platinum BMR are air bubbler systems. The figure below shows the bubbler level sensor measurement mechanism.

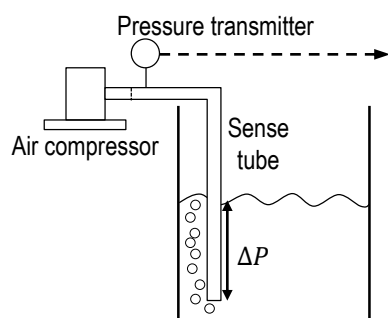


Figure 8.27: Bubbler level sensor measurement mechanism (redrawn from ITA (2009))

An air compressor is used to bubble air through a liquid. A pressure transmitter estimates the level inside the vessel by considering the pressure change in the sense tube. Figure 8.28 shows the location of a bubbler level sensor at Western Platinum BMR which occasionally blocks.

Solid particles occasionally get stuck in bubbler level sense tubes at Western Platinum BMR which increases the pressure drop and results in a positive biased level measurement. The third compartment contains one such level sensor.

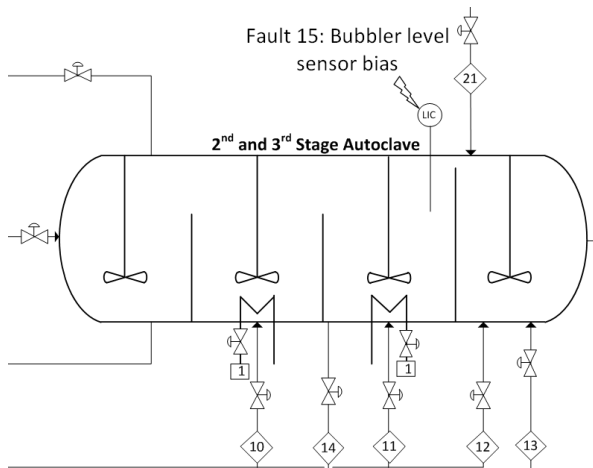


Figure 8.28: Location of fault 15: Bubbler level sensor blockage

The level sensor blockage was simulated in Simulink™. The results are captured in Figure 8.29.

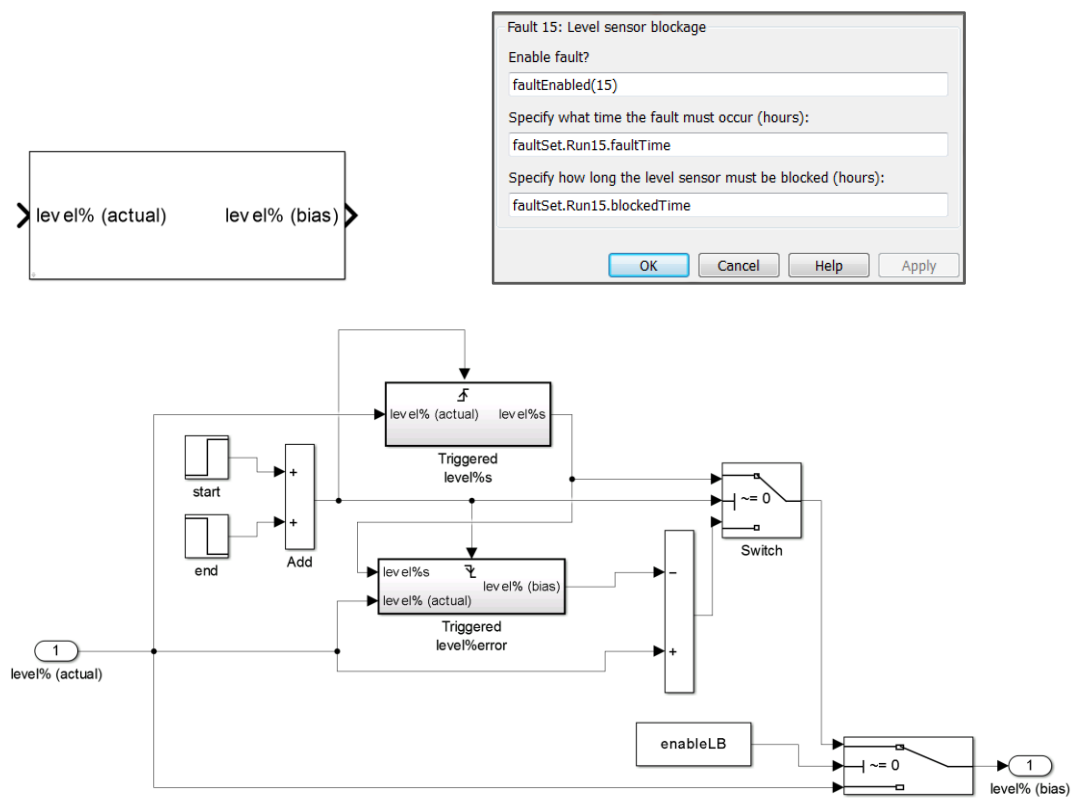


Figure 8.29: Block interface (top left), block mask (top right) and mechanism (bottom) of level sensor blockage modelled in Simulink™

The fault start time and blockage time, defined in the mask, is used in step blocks (stepping from 0 to 1 and 1 to 0, respectively) to trigger rising and falling subsystems at the respective times (the latter block steps at the combined start and blockage time). The rising and falling triggered subsystems are used to capture a blockage level and a level bias, respectively. A

switch ensures that the blockage level reports to the final output at the time the fault is initialised. This level output is evident until the blockage time is over and represents a static particle that is blocking the level measurement. This bias size is equal to the difference in the actual level at the start and at the end of the blocking time, and represents a static particle transitioning into a moving particle. A step decrease triggers a falling subsystem which reports the level bias at that point in time. The switch changes at this point to output the actual varying level with the added bias. The added bias is attributed to the moving particle which is still present in the sense tube.

Results and discussion

Level sensors within the first, third and fourth autoclave compartments at Western Platinum BMR reportedly experience level sensor blockages (McCulloch et al., 2014). Figure 8.30 shows the results of a level sensor blockage for an artificial sinusoidal level.

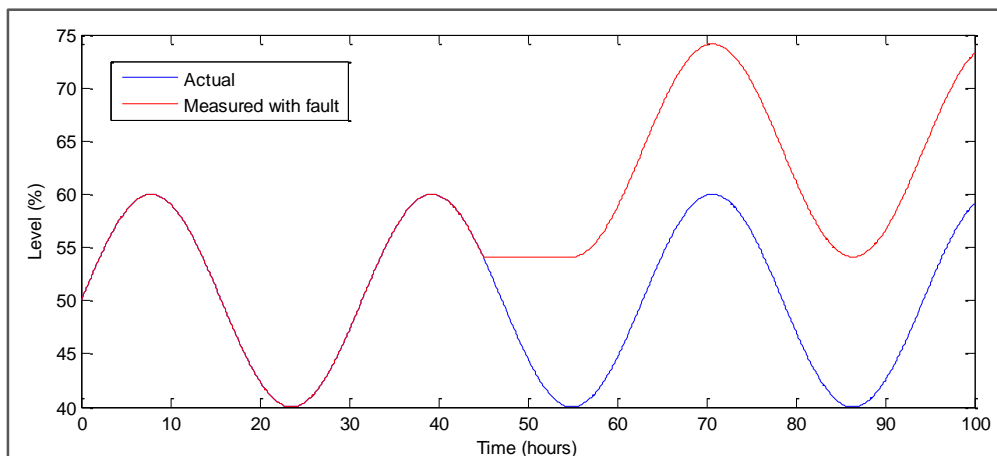


Figure 8.30: Behaviour of the level sensor blockage fault for an artificial sinusoidal level

The fault occurs at 45 hours within this scenario. The particle blocking the sense tube is then static for 10 hours. The particle starts to move, which causes the level measurement to vary. The particle is still present in the sense tube, which represents the constant bias evident in Figure 8.30. Notice that the difference in maximum and minimum levels in both measurement cases is the same. The fault merely causes a bias in the level measurement.

Expert knowledge at Western Platinum BMR could not quantify a level sensor blockage time. A blockage time of 10 hours was used.

8.4. Summary

A wide range of Western Platinum BMR faults with corresponding characteristics were obtained during a site visit. These faults include actuator failures, structural failures, operator intervention, process disturbances, sensor failures and controller malfunctions. The modelling methodologies of many of these faults were considered within this chapter. The behaviour of the modelled faults was also investigated. A fault database summarising distinguishable fault characteristics and a set of simulated faults which exhibit expected behaviour were two major outcomes within this chapter.

CHAPTER 9: CONTROL PERFORMANCE ASSESSMENT

Chapter 8 describes the modelling procedure used to simulate several faults encountered at Western Platinum BMR.

This chapter reports on the work of utilising and implementing modelled faults into the dynamic process model so as to determine the extent in which control and operational performances are degraded. The hypothesis that faults have an effect on control performance was investigated. The propagation of fault symptoms were identified and described in this chapter. Also, the ability to determine if a fault occurs based on key performance indicators was explored. This was done in a way which can easily be implemented at the BMR. The modelled output effects were thereafter compared to what is seen at the BMR.

Eight independent fault cases were investigated. The subsequent control performance of each fault was compared to a faultless baseline run. The extent in which control performance degraded varied significantly between faults. The pump impeller wear and solid build-up in cooling coil proved to be the faults which caused the largest process upset. This is attributed to significant autoclave pressure and temperature variations, and the activation of safety interlocks. The density disturbance and valve wear on the other hand proved to be the faults with the lowest effect on process performance. A correlation between fault impact size and fault symptom localisation was noticed.

9.1. Overview

Several faults that occur at Western Platinum BMR have been identified and modelled in Chapter 8. The modelled faults can now be used as a tool to perturb the dynamic process model in order to assess the effect of faults on control performance.

Control performance assessment is a procedure in which a variety of statistics that reflect the process performance over a specific time period is evaluated. The hypothesis is that fault occurrences degrade control performance. Control performance assessment would therefore

serve as a way to characterise the effects of faults on a control strategy under the hypothesis.

Key performance indicators (KPI) are often used as a way to quantify control performance. Two variations of KPIs exist, namely control KPIs and operational KPIs. Control KPIs include a wide range of measures which indicate different controlled variable characteristics. Operational KPIs are plant specific measures which are not controlled in a loop, but need to be constrained or manually controlled in order to ensure effective operation.

KPIs used in this control performance assessment are discussed in Section 9.2. This is followed by a list of locations where these KPIs were used to evaluate the modelled BMR performance. Section 9.3 summarises fault scenario runs and associated dynamic process model information. This includes when and where faults were implemented in the dynamic process model and what the dynamic process model inputs were. The faultless baseline KPI outputs is introduced and discussed in the first subsection of Section 9.4. This is followed by subsections containing a discussion of KPI results for individual faults.

9.2. Key Performance Indicator Methodology

9.2.1. Control key performance indicators

A standard control loop consists of a controlled variable that is kept at a set-point by adjusting a causally related final control element such as a valve (refer to Figure 4.3). Low variation is therefore expected in a controlled variable which comes at the expense of variation in the valve position. The measures of controlled variable performances and valve performances differ to some extent for this reason. Control KPIs can be divided into controlled variable KPIs and valve KPIs.

Controlled variables

McCulloch et al. (2014) described a hierarchy which establishes the priority for mitigating control related issues at Western Platinum BMR (refer to Figure 9.1). The mitigation priority increases when moving upward in the pyramid.

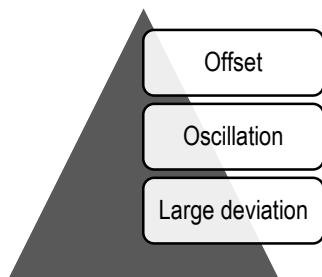


Figure 9.1: Hierarchy for mitigating control performance issues (McCulloch et al., 2014)

An offset is evident when a controlled variable moves and remains away from its set-point, as opposed to a large deviation where the former occurs but the controlled variable manages to return to its set-point. Preventing issues listed in Figure 9.1 for pressure and temperatures inside the autoclave is of particular importance, since these controlled variables have a significant effect on the quality of product; safety of the personnel; and protection of costly equipment. Issues shown in Figure 9.1 are expected to emerge during the occurrence of several modelled faults. KPIs that quantify issues listed in Figure 9.1 were incorporated in the control performance assessment of the dynamic process model.

The following controlled variable KPIs were used to quantify controlled variable performance:

1. Travel distance (TD)
2. Integral absolute error (IAE)
3. Average absolute error (AE)
4. Maximum absolute deviation (MD)
5. Time not at set-point (TNASP)
6. Standard deviation (SD)

The KPIs listed above can to a certain extent be used to identify and quantify characteristics of issues seen in Figure 9.1. For example, a small travel distance with a large integral absolute error and time not at set-point would be indicative of an offset. Oscillatory behaviour is distinguishable from offset by an expected large travel distance. A large deviation would emerge particularly in the maximum deviation KPI, but also in other KPIs.

Appendix D contains a description of methods used to implement controlled variable KPIs into Simulink™ and the validation of their behaviour.

Valves

The following valve KPIs were used to quantify valve performance:

1. Valve travel distance (TD)

2. Average absolute error (AE)
3. Integral absolute error (IAE)
4. Time not at valve set-point (TNASP)
5. Standard deviation (SD)
6. Valve at a limit (TS, LTS, CS)
7. Valve reversals (VR)

The travel distance, average error, integral absolute error, time not at set-point and standard deviation are controlled variable KPIs which are also used as valve KPIs since they produce valuable valve performance information. For example, the travel distance of a valve should not be too excessive since it could lead to quicker valve degradation. A very small valve travel could also be indicative of valve saturation, incompetent controller tuning, or high valve stiction. The valve KPIs listed above are expected to change during the occurrence of modelled faults, particularly valve wear and valve stiction. The valve at a limit KPI is divided into total time (TS), longest time (LTS), and number of times (CS) the valve is saturated at 100 %. This partitioning allows the extraction of more knowledge in the case of saturation occurrences.

Appendix D contains a description of methods used to implement valve KPIs into Simulink™ and the validation of their behaviour.

9.2.2. Operational key performance indicators

Certain factors at Western Platinum BMR are not necessarily continuously measured and automatically controlled or constrained, but contribute to the performance of the operation. The following operational KPIs were identified at Western Platinum BMR and used to quantify operational performance (McCulloch et al., 2014):

1. Extent of base metal leaching
2. Extent of PGM leaching
3. Utility usage
4. Throughput
5. Spillage

The operational KPIs shown above are quantities which significantly affect the profit of the process. These operational KPIs are consistent with that identified during the literature review. It was mentioned that the main objective of the second and third stage leaching process is to maximise the leaching of base metals while limiting the dissolution of PGMs (Dorfling, 2012). Obtaining the correct extents of leaching would improve the PGM-rich

residue composition and minimise the amount of dissolved PGMs. This will ultimately increase profit by both reducing material reprocessing and minimising the amount of dissolved PGMs lost when recycled. Reducing the usage of utilities such as cooling water, steam and sulphuric acid would reduce operating costs which ultimately increases the net profit. The throughput is in fact automatically controlled at Western Platinum BMR by varying both the second and third stage slurry preparation tank outlet flow rates. However, abnormal events could limit the process throughput via process downtime or safety interlock situations. This could ultimately lead to reduced production rates and therefore a reduced profit. Spillage of material into sump areas in the case of undesired vessel overflow is also a concern at Western Platinum BMR. The updated dynamic process model supports vessel overflow, and was therefore included in the operational KPIs.

It would be ideal to link all the operational KPIs into a single monetary value. However, the BMR is an interim process (i.e. process preceding the separation of PGMs where product value can be identified) which makes the monetary quantification of interim products difficult. In addition, the extent in which materials are lost upon recycling is unknown (the model does not contain all the necessary process units).

Appendix D contains a description of methods used to implement operational KPIs into Simulink™.

9.2.3. Key performance indicator application

Most of the controlled variable, valve and operational KPIs discussed in previous sections need to be applied to Western Platinum BMR dynamic process model measurements in order to produce valuable information.

The performance of all control loops listed in Table 9.1 was investigated. This was done by applying controlled variable KPIs to their measurements.

Table 9.1: Control loop performances considered during control performance assessment

Tag	Control loop	Tag	Control loop
PIC-3001	Autoclave pressure control	LIC-0201	Flash recycle tank level control
TIC-3001	Compartment 1 temperature control	LIC-3002	Compartment 3 level control
TIC-3003	Compartment 2 temperature control	LIC-3003	Compartment 4 level control
TIC-3004	Compartment 3 temperature control	FIC-0101	Spent electrolyte flow control
TIC-3005	Compartment 4 temperature control	FIC-0203	Flash recycle tank outlet flow control
LIC-0101	Second stage slurry preparation tank level control	FIC-3002	Compartment 3 outlet flow control
DI-0101	Second stage slurry preparation tank density	FIC-3003	Compartment 4 outlet flow control

The process P&ID (Figure E.1) can be used to relate the controller tags to their location. Important controlled variables such as autoclave temperatures, levels and pressure were included in the list of control loops. The performance of these control loops are of utmost importance. Flow controllers that surround the location of certain fault occurrences (i.e. FIC-0101 and valve stiction, FIC-0203 and pump impeller wear, FIC-3002 level sensor blockage, FIC-3003 and valve wear) were also included in order to quantify the effect that faults have on their controllability. Note that the controlled variable KPIs were calculated from sensor measurement data (i.e. the sensor present-values as shown in Figure 7.3). This ensures that the dynamic process model KPI values are affected by sensor noise in a similar way as expected when applied to plant data.

The performance of all valves listed in Table 9.2 was investigated. This was done by applying valve KPIs to their measurements.

Table 9.2: Valve performances considered during control performance assessment

Tag	Valve
TCV-3003	Compartment 2 temperature control valve
TCV-3004	Compartment 3 temperature control valve
TCV-3005	Compartment 4 temperature control valve
FCV-0101	Spent electrolyte flow control valve
FCV-0203	Flash recycle tank outlet flow control valve
FCV-0205	Compartment 1 outlet flow control valve
FCV-3002	Compartment 3 outlet flow control valve
FCV-3003	Compartment 4 outlet flow control valve

Control valves listed in Table 9.2 were expected to be directly affected by fault occurrences or form part of important control loops.

The operational KPIs were related to the Western Platinum BMR by means of operational performances listed in Table 9.3.

Table 9.3: Operational performances considered during control performance assessment

Total PGMs in liquid (compartment 1)	Total BMs in solid (compartment 1)
Total PGMs in liquid (compartment 2)	Total BMs in solid (compartment 2)
Total PGMs in liquid (compartment 3)	Total BMs in solid (compartment 3)
Total PGMs in liquid (compartment 4)	Total BMs in solid (compartment 4)
Total solid throughput	Total steam usage
Total oxygen usage	Total CW usage (compartment 2)
Total CW usage (compartment 3)	Total spillage (second stage slurry preparation tank)
Total spillage (flash recycle tank)	Total spillage (third stage slurry preparation tank)
Total BM input	Total PGM input

The extent of base metal and PGM leaching was calculated after each autoclave compartment. Three quantifiable utilities are used at Western Platinum BMR namely steam, cooling water (CW), and oxygen. The total usage of each utility was calculated during the assessment of control performance. The spillages of individual vessels were also of interest. Note that an additional set of operational KPIs namely total BM input and total PGM input were also calculated. These additional KPIs simply quantify the mass of base metals and PGMs which enter the process, which makes them in actual fact manipulated variables. However, the total BM input and total PGM input ultimately affects the throughput and extent of leaching variations and its interpretation thereof.

KPIs listed in Table 9.1, Table 9.2 and Table 9.3 were calculated for a variety of fault runs. However, some of these KPI values are arbitrary and needs to be related to baseline KPIs (i.e. standard KPIs) in order to allow insightful deductions. KPIs were therefore expressed in terms of a percentage relative to a faultless baseline run:

$$KPI_{\%} = \frac{KPI_{run\ i} - KPI_{baseline}}{KPI_{baseline}} \times 100 \quad \text{Equation 9.1}$$

All KPIs used in the assessment of control performance accumulate the effect of faults over time. It is for this reason sufficient to only report the KPI values at the end of each simulation. An increase in controlled variable and valve KPIs calculated using Equation 9.1 would indicate a decrease in control performance relative to the baseline. A similar conclusion can be made when operational KPIs such as total utility usage, vessel spillage, base metals in the solid phase and PGMs in the liquid phase increase. However, an increase in total solid throughput, total base metal input and total PGM input would be considered as an improvement in operational performance (not taking into account the quality of product yet). The following equation will therefore be used to express these three operational KPIs:

$$KPI_{\%} = \frac{KPI_{baseline} - KPI_{run\ i}}{KPI_{baseline}} \times 100 \quad \text{Equation 9.2}$$

Equation 9.2 expresses these operational KPIs as a decrease relative to the baseline. The total solid throughput, total base metal input and total PGM input KPIs will therefore be expressed as a decrease in total solid throughput, decrease in total base metal input and decrease in total PGM input, respectively, when compared to the baseline.

9.3. Fault Scenario Run Methodology

9.3.1. Fault scenarios

A list of fault scenarios and corresponding fault details are given in Table 9.4. The faults listed in Table 9.4 were used in the assessment of control performance.

Figure 9.2 shows the location where these faults originate within the process. Each fault scenario shown in Table 9.4 was introduced in a separate run. Faults do however occur simultaneously. The interaction between a variety of faults falls outside the scope of this work.

The fault sizes correspond with what is seen at the BMR. However, the actual frequency of faults and transition time of the faults were not taken into account (a single occurrence of a fault was considered, and the transition time for each fault, where necessary, was taken as a constant value). The mimicking of fault frequencies and transition times from the fault database would require extensive modelling run-times (several months for a few of the faults), which was not plausible. A shortened transition was therefore used.

KPI calculations and fault occurrences were started at 40 hours and 50 hours, respectively. A fault transition period of 50 hours was used for faults that transpire to full size over time. Note that the density disturbance occurs intermittently. The intermittent density disturbance data seen in Figure 8.3 was implemented abruptly.

Table 9.4: List of fault scenarios used in control performance assessment

Fault #	Fault name	Fault transition (hours)	Simulation end (hours)	Fault specifics
1	Density disturbance	50, Abrupt	180	-
2	Valve wear	50 - 100	180	Extent degradation: 0.73
3	Valve stiction	50 - 100	180	Deadband and stickband: 14% Slipjump: 14%
4	Impeller wear	50 - 100	180	Final flow fraction: 0.0316
5	Solid build-up	50 - 100	180	-
6	Peristaltic pump tube failure	50, Abrupt	180	-
7	H ₂ SO ₄ controller misuse	50, Abrupt	180	Operator hold time: 2 hours
15	Level sensor blockage	50, Abrupt	180	Blocked time: 10 hours

A total simulation time of 180 hours was used which allows at least 80 hours (more than the expected residence time in all simulated process units) for fully implemented faults to perturb and move through the process. The fault specifics captured in Table 9.4 were discussed throughout Section 8.3.

9.3.2. Dynamic process model inputs

Random walks were used on several dynamic process model temperature and composition inputs, as described in Section 6.5.2. These random walks contain constant seeds which ensure the baseline run and fault runs have exactly the same inputs. The sensor noise also has constant seeds for a similar reason. Control loop set-points similar to that of Western Platinum BMR were used within the dynamic process model during control performance assessment, except for the sulphuric acid and the second stage slurry preparation tank outlet flow controllers (refer to Table B.2). The sulphuric acid flow controllers (FIC-0202 and FIC-0150-9) were used as secondary loops cascaded with operator controllers. The second stage slurry preparation tank outlet flow controller set-point was decreased to 3 m³/h in order to increase the amount of heat released within the first compartment (i.e. through the reduction in first compartment residence time). The increase in heat released allowed the temperature within the first compartment to reach values above 130 °C and thereby activating the first compartment temperature control mechanism.

9.4. Results and Discussion

The KPI outputs from the faultless baseline run are discussed in Section 9.4.1. Each section from 9.4.2 to 9.4.9 describes the performance degradation during the occurrence of an individual fault (i.e. each of the eight faults shown in Table 9.4). The KPI variations are in certain cases difficult to comprehend if the propagation of the fault is not considered. KPI variations in the case of fault occurrences are therefore explained in a general order as shown in Figure 9.3.

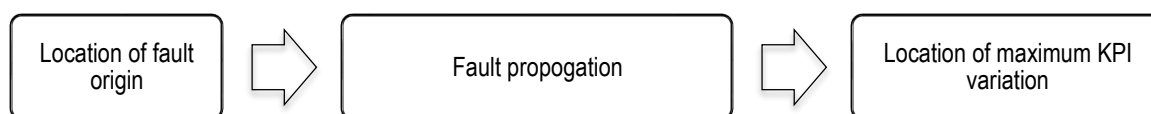


Figure 9.3: General approach used to describe KPI deviation from the baseline

The location where the fault originated is identified. The propagation of the fault from its origin to the location of largest KPI variation is described and substantiated using variable profiles.

Note that the supervisory control present on the dynamic process model is limited to that which is described in Section 7.5. This excludes any operator intervention in the case of abnormal events. The simulated faults discussed in the following subsections might for this reason not occur to the extent which has been modelled.

9.4.1. Baseline run

The KPI values at the end of the baseline run are captured in Table F.2. The travel distance of controlled variable present-values are relatively large when taking into account the total KPI recording time of 140 hours. This is predominantly caused by the fact that the KPI cannot distinguish between sensor noise and actual variable travel. The reported travel distance therefore includes travel caused by sensor noise. The contribution of sensor noise to variable travel distances is highlighted in Table 9.5.

Table 9.5: Baseline travel distances related to sensor variances

Controller	TD (variable units)	Sensor variance (variable units ²)
Autoclave pressure control (bar)	333	3.29E-07
Compartment 1 temperature control (°C)	12857	5.00E-04
Compartment 2 temperature control (°C)	4806	6.78E-05
Compartment 3 temperature control (°C)	6137	1.11E-04
Compartment 4 temperature control (°C)	10952	3.62E-04
Second stage slurry preparation tank level control (%)	110409	0.038
Flash recycle tank level control (%)	178789	0.099
Compartment 3 level control (%)	48739	0.0073
Compartment 4 level control (%)	187406	0.11
Second stage slurry preparation tank density (kg/l)	2817	2.45E-05
Spent electrolyte flow control (m ³ /h)	67927	0.014
Flash recycle tank outlet flow control (m ³ /h)	125516	0.049
Compartment 3 outlet flow control (m ³ /h)	86491	0.023
Compartment 4 outlet flow control (m ³ /h)	98467	0.03

The travel distances and sensor variances are independently scaled with colours. The significant contribution of sensor noise to variable travel distances is evident when considering the clear correlation which exists between the variable travel distances and corresponding sensor variances obtained from Table 7.1. Any deviation from this correlation would suggest that the actual variable travel contributes significantly to the travel distance. This statement is substantiated by noting that the maximum deviation of controllers seen in Table F.2 is predominantly within a four standard deviation KPI range. In addition, the standard deviation KPIs corresponds well with sensor noise standard deviations. Filters would be able to reduce the effect that sensor noise has on the travel distance. Filters were however not included in this study.

Note that the average error KPI for controllers is not equal to zero. This does not contradict the low actual variable travel theory or the non-zero averages expected from sensor noise. Remember that the average error KPI was calculated as an absolute average.

Notice that the majority of time not at set-point KPIs are zero. This is attributed to the NASP value for each controller which gives leeway to its set-point-measurement difference before registering it as being away from its set-point (NASP values considered during the discussion of the time not at set-point simulation procedure - refer to Appendix D). Also note that the time not at set-point KPI cannot be expressed as a percentage relative to the baseline (i.e. by using Equation 9.1) since the baseline time not at set-point KPI values are zero. The time not at set-point KPIs was therefore be expressed as an absolute value in the subsequent sections. The count saturated, time saturated, longest time saturated and spillage KPIs was also expressed as absolute values for similar reasons. These KPIs are

expected to have values of zero in the baseline case since spillage and valve saturation is not expected to occur during normal process operation.

A variety of valve travel distances and valve reversals are evident in Table F.2. The average valve travel distances per valve reversals and the average amount of valve reversals per time unit are captured in Table 9.6.

Table 9.6: Baseline travel distances per valve reversals

Valves	TD/VR	VR (reversals per second)
Compartment 2 temperature control valve (%)	0.00139	0.14
Compartment 3 temperature control valve (%)	0.00106	0.18
Compartment 4 temperature control valve (%)	0.0123	0.20
Spent electrolyte flow control valve (%)	0.0212	0.20
Flash recycle tank outlet flow control valve (%)	0.0524	0.13
Compartment 1 outlet flow control valve (%)	0.0044	0.20
Compartment 3 outlet flow control valve (%)	0.0235	0.19
Compartment 4 outlet flow control valve (%)	0.0525	0.21

Table 9.6 shows that the valves travel on average between 0.00106 % and 0.0525 % before changing direction. These values are low, and are expected to be caused by the low actuation required during normal operation. The controller output varies on a small scale and ultimately causes the valve to change direction after moving a very small distance. However, valve reversals between 0.14 and 0.2 per second are evident, which is realisable.

Figure 9.4 shows two operational KPIs that quantify the extent in which the inlet base metals and PGMs are leached. Refer to Equation D.14 and Equation D.15 in Appendix D for the extent of leaching definition.

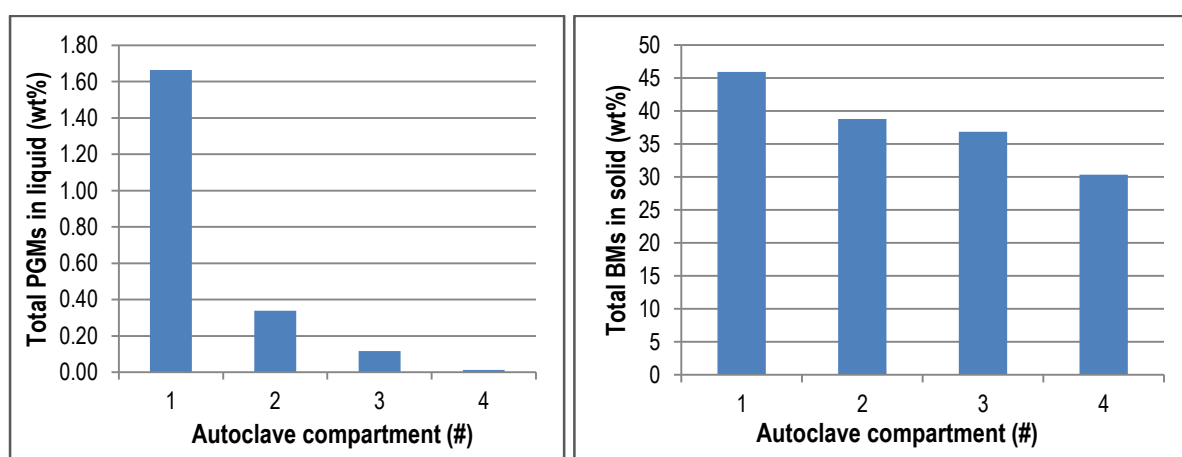


Figure 9.4: Operational KPIs of baseline run: PGMs in liquid and BMs in solid

Low amount of PGMs in liquid phase and base metals in solid phase are beneficial since it ensures that the high-grade PGM residue product stream contains less base metals and that

low amount of PGMs are lost to the liquid phase. A clear decrease in PGMs in the liquid phase is seen for an increase in autoclave compartment number. This is attributed to PGM cementation reactions that solidify PGM ions present in the liquid via base metal leaching. A similar decrease is noticed for the base metals present in the solid phase, as expected. Approximately 55 % of the base metals are leached within the first compartment while 30 % of the inlet base metals exit in the high grade PGM residue. The extent of base metal leaching is much lower when compared to Western Platinum BMR operation (refer to Table 2.1). The origin of the low predictability is discussed in Chapter 6.

The majority of KPIs at the end of each fault run will be compared to that of the baseline run by using both Equation 9.1 and Equation 9.2. In order for a valid comparison it is required that the fault runs and baseline run are complete replicates prior to the implementation of faults. This ensures that the KPI variations are solely caused by the occurrence of the fault. KPIs for the baseline run and the first fault run are compared in Table F.3 a few time steps prior to the fault implementation time of 50 hours by using the MATLAB™ equality function. The results reported in Table F.3 show that all KPIs under consideration at the time step prior to the fault occurrence are equal to that of the baseline run. This result is evident not only for the first fault run, but all other fault runs.

9.4.2. Valve blockage – density disturbance

Figure 9.5 shows the solid fraction of stream 1 for both the baseline and fault runs.

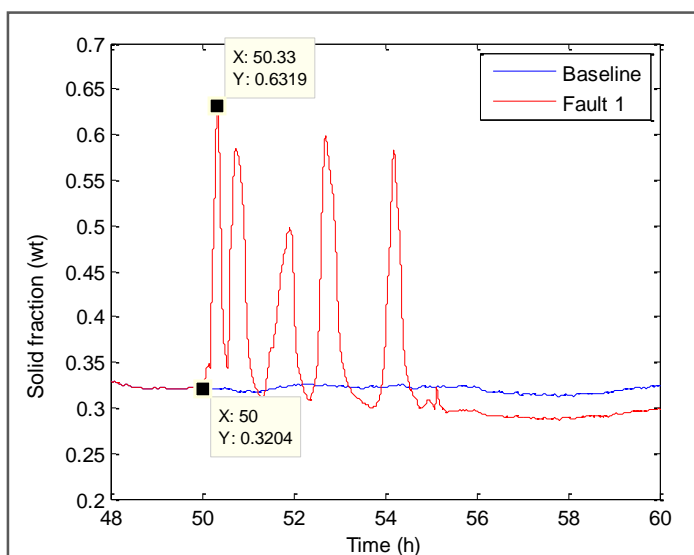


Figure 9.5: Verification of fault 1 occurrence: solid fraction of stream 1

Five spikes are noticed in Figure 9.5 with values that correspond with solid fraction deviations shown in Figure 8.3. Figure 9.5 therefore verifies the occurrence of the density disturbance within this simulation run.

Table 9.7 captures final KPI values that show significant variation from the baseline. Refer to Appendix F for the full set of unrounded KPIs. Note that the KPI deviations captured in these tables are those that varied the most during that fault run. These tables do not necessarily show detrimental KPI variations. Any positive KPI percentage is indicative of a decrease in process performance relative to the baseline case, and vice versa. The KPIs reported in Table 9.7 were for this reason scaled with colours, where red and green represents a decrease and increase in process performance, respectively. Note that the time not at set-point and valve saturation KPIs are not scaled with colour since these KPIs cannot be directly related to other KPIs as they are not in a percentage relative to the baseline. All KPIs that are in an absolute form will not be scaled with colours.

Table 9.7: Significant KPIs for fault 1: density disturbance

Controllers	TD (%)	AE (%)	MD (%)	TNASP (h)	SD (%)
Autoclave pressure control (bar)	0.00	32.74	123.6	0.00	47.11
Compartment 1 temperature control (°C)	0.00	2.19	0.41	0.00	1.90
Compartment 2 temperature control (°C)	0.00	13.34	44.92	0.00	18.36
Compartment 3 temperature control (°C)	0.00	0.48	-3.96	0.00	0.29
Compartment 4 temperature control (°C)	0.00	-0.14	-0.04	0.00	-0.13
Second stage slurry preparation tank level control (%)	0.00	49.48	180.1	0.00	75.77
Compartment 3 level control (%)	0.00	-0.35	-2.44	0.00	-0.33
Second stage slurry preparation tank density (kg/l)	0.00	4.18	58.15	0.00	14.39

Valves	TD (%)	AE (%)	TNASP (h)	VR (%)	CS (#)	TS (h)	LTS (h)
Compartment 2 temperature control valve (%)	2.79	2.86	0.00	-2.86	0	0.00	0.00

Operational KPIs	Compartment 1	Compartment 2	Compartment 3	Compartment 4
Total PGMs in liquid (%)	0.35	0.05	-0.21	-1.34
Total BMs in solid (%)	0.25	0.03	0.06	0.14

Operational KPIs	
Decrease in total BM input (%)	-0.55
Decrease in total PGM input (%)	-0.64
Decrease in total solid throughput (%)	-0.61

The largest KPI change relative to the baseline is the maximum deviation of the second stage slurry preparation tank level. This large maximum deviation in level is attributed to the feedforward controller surrounding this vessel which controls its outlet solid percentage. The first stage leach residue density spikes disturb the density in the second stage slurry preparation tank, substantiated by its maximum deviation of 58.15 %. The solid percentage

feedforward controller subsequently increases both the inlet spent electrolyte and formic filtrate flow rates (i.e. the lower density streams) in an attempt to once again decrease the solid percentage exiting this vessel. These inlet flow rate increases affect the second stage slurry preparation tank level which ultimately describes the increase in maximum level deviation. Note that deviations in the level KPIs are desirable as opposed to deviations in the density KPIs. A variation in solid percentage in the second stage slurry preparation tank has a significant effect on the autoclave temperature and pressure control performance.

The maximum level deviation increase of 180.1 % translates to approximately 3.3 % level deviation when the baseline value is considered. The 3.3 % level deviation is smaller than the NASP value defined for this level controller, which explains its time not at set-point KPI value of zero.

Notice that the travel distance for this level controller and all other controllers did not change significantly. This is attributed to the fact that the sensor noise dominates the travel distance KPI and causes actual variable travel to be concealed. Notice that integral absolute error and average error show the same deviation from the baseline (refer to Table F.4). This is understandable since the average error is simply the integral absolute error divided by the KPI recording time (the KPI recording time is similar for the fault and baseline run). The integral absolute error was for this reason omitted from Table 9.7.

The first compartment temperature profile predicted by the dynamic process model does not oscillate and vary as much as what is reported at Western Platinum BMR during the occurrence of the density disturbance (McCulloch et al., 2014). This could be partially attributed to the second stage slurry preparation tank level controller which attenuates the modelled density disturbance by lowering the set-point of its secondary loop (i.e. the first stage leach residue flow rate, which is at the origin of the fault). The profile of the first stage leach residue flow rate is given in the figure below.

The bulk of the density disturbance occurs between 50 hours and 55 hours, as shown in Figure 9.5. This corresponds with the timeframe in which the first stage leach residue flow rate is reduced, as shown in Figure 9.6. The increase in spent electrolyte and formic filtrate flow rates causes an increase in the level of the second stage slurry preparation tank, as previously mentioned. The level of this vessel is controlled by reducing the set-point of its secondary loop, which is the flow rate of the first stage leach residue.

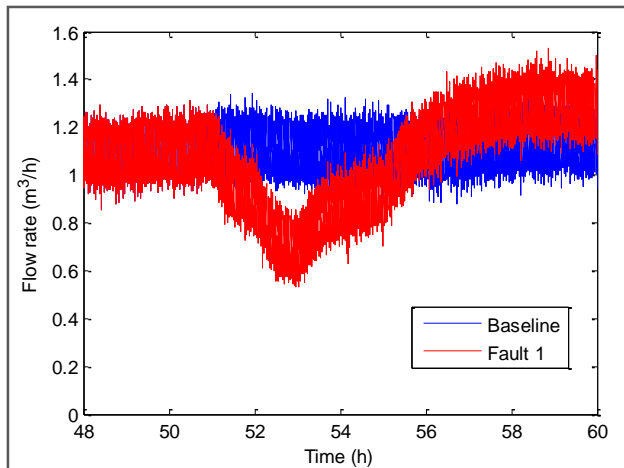


Figure 9.6: Fault 1 occurrence: first stage leach residue flow rate

The reduction in the first stage leach residue flow rate decreases the impact of the density disturbance since it causes fewer solids to enter the second stage slurry preparation tank during the 5 hour occurrence of the fault. This attenuation mechanism is expected to be ineffective in the actual process. The density disturbance is expected to shift onward in time when the flow rate of the first stage leach residue is decreased, since the solids in this stream would build up instead of disappearing (i.e. the flow rate and solid fraction of this stream is interdependent). The issue is therefore the density disturbance which was merely modelled as a change in the solid fraction of the first stage leach residue stream without accounting for variations in the corresponding flow rate. Modelling of an additional vessel upstream of the first stage leach residue stream would be required to solve this issue, which falls outside the scope of this work. Note that the fault still occurs to a reasonable extent as the first stage leach residue flow rate decreases only to a minimum of half of its standard operation. The dynamic process model's under prediction of the extent of base metal leaching is yet another contributing factor which causes the density disturbance to only have a small effect on the first compartment temperature. More than 95 wt% of the base metals which enter the first compartment at Western Platinum BMR are leached out (Steenekamp et al., 2009), compared to 55 wt% predicted by the dynamic process model (refer to Figure 9.4). A significant increase in heat is expected to be released in the first compartment during the density disturbance, since more than 95 wt% of the additional base metal solids are expected to be leached. This is not the case in the dynamic process model. The base metal solids that exit the first compartment increases by 0.25 % for a 0.55 % increase in total base metals into the process (these values are small since the fault occurred over the span of 5 hours and the simulation continued for another 125 hours).

The size of the performance degradation caused by the density disturbance is expected to decrease as one continues downstream of the first autoclave compartment, since the density

disturbance decreases in size. Notice that the second compartment temperature has a larger decrease in control performance than that of the first compartment relative to the baseline. This could be attributed to the rigorous fine-tuning of the first compartment temperature control mechanism in order for its proper cooperation with the flash recycle tank level controller. In contrast, the conservative Ciancone tuning method was used for the second compartment temperature controller. Note however that the 44.92 % increase in maximum deviation of the second compartment temperature translates to a mere 0.55 °C deviation when compared to the baseline, which is insignificant. The effects of the density disturbance decreases after the second compartment, as expected.

Table 9.7 shows a decrease in the autoclave pressure control performance notably through the increase in the maximum deviation. The density disturbance causes an increase in solids fed to the autoclave and ultimately results in an increase in heat released and oxygen consumed, since more base metals are present and leached per unit of compartment volume. The variation in autoclave pressure could be attributed to both the increase in oxygen consumption which affects the oxygen availability in the gas phase (i.e. the partial pressure of oxygen – refer to Equation 6.21 and Equation 6.22), and the variation in compartment temperatures which affect the autoclave pressure via the vapour temperature and partial pressure of water (refer to Equation 6.19).

Figure 9.7 shows the total PGMs in the liquid and total base metals in the solid phase relative to the baseline.

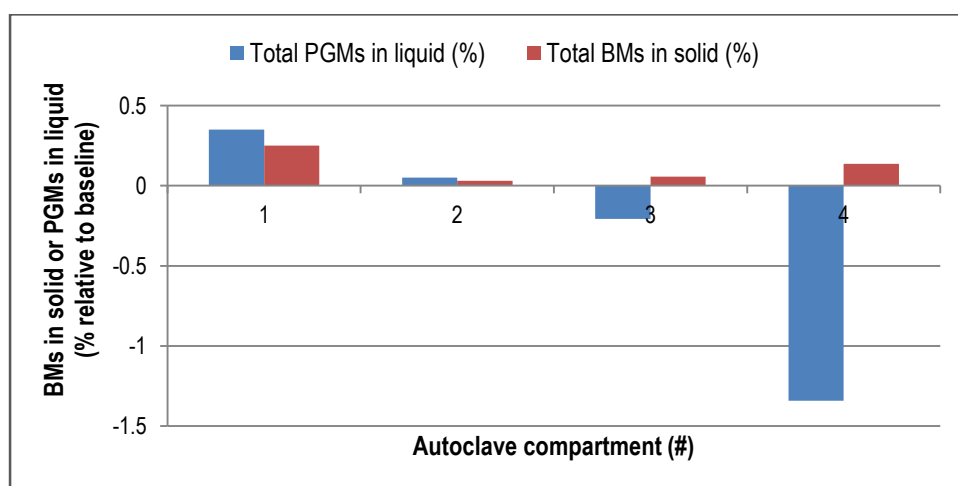


Figure 9.7: PGMs in liquid and BMs in solid for fault 1 – density disturbance

An increase in base metals is noticed in the solid phase for all autoclave compartments, as expected. This is caused by the increase in total base metals into the process as shown in Table 9.7. The PGMs present in the liquid phase decrease as the compartment number

increases, as expected. More base metal solids results in an increase in available surface area which benefits the PGM precipitation reactions (these reactions are a function of the available surface area of the base metals - refer to Reaction 7 to Reaction 12 and the corresponding rate expressions captured in Table D.1). The slight increase in PGMs present in the liquid after the first compartment is unexpected. The fact that more base metals are available in the first compartment should benefit the extent of PGM precipitation. The precipitation of PGMs is however countered by the leaching of PGMs via Reaction 13 to Reaction 21. The PGM leaching reactions are dependent on the available surface area of the corresponding PGM mineral (refer to corresponding rate expressions captured in Table D.1) which also increases when the solid loading in the first compartment increases. Figure 9.8 shows the profile of the PGMs present in the first compartment liquid phase relative to the baseline. The value at 180 hours corresponds with the value seen in Figure 9.7.

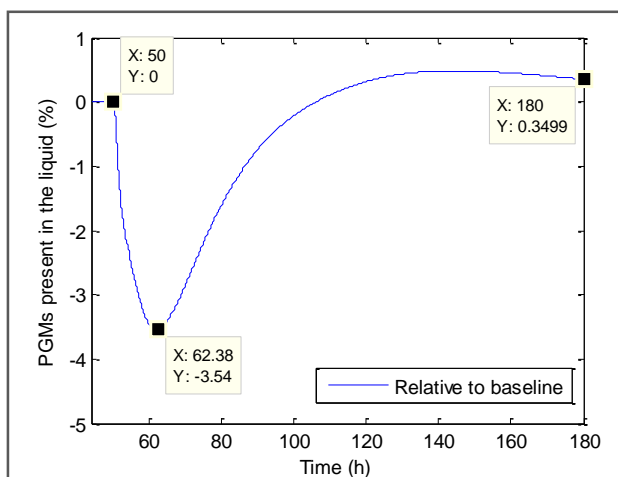


Figure 9.8: PGMs present in the first compartment liquid phase over time during fault 1 – density disturbance

Notice the initial decrease in liquid PGMs. It is speculated that the PGM leaching reactions are terminated at this point due to the increase in digenite concentration (remember that the initiation of PGM leaching is dependent on the digenite concentration in the compartment). The decrease represents the dominance of PGM precipitation via base metal leaching. The subsequent increase after 62.38 hours is caused the initiation of the PGM leaching reactions which occur at a faster rate than the corresponding precipitation rates. This is due to both the increased PGM mineral concentration caused by preceding PGM precipitation (benefitting PGM leaching as previously mentioned) and the decrease in PGMs present in the liquid phase (inhibiting PGM precipitation).

It has been shown that the control performance of the process does not decrease significantly during the density disturbance. However, the fault database states that this fault

occurs on average once a day. The cumulative effects of this disturbance if it were to be implemented every 24 hours might show a significant increase in process degradation.

9.4.3. Valve wear

Figure 9.9 shows the fourth compartment outlet flow rate and the corresponding valve position for both the baseline and fault runs.

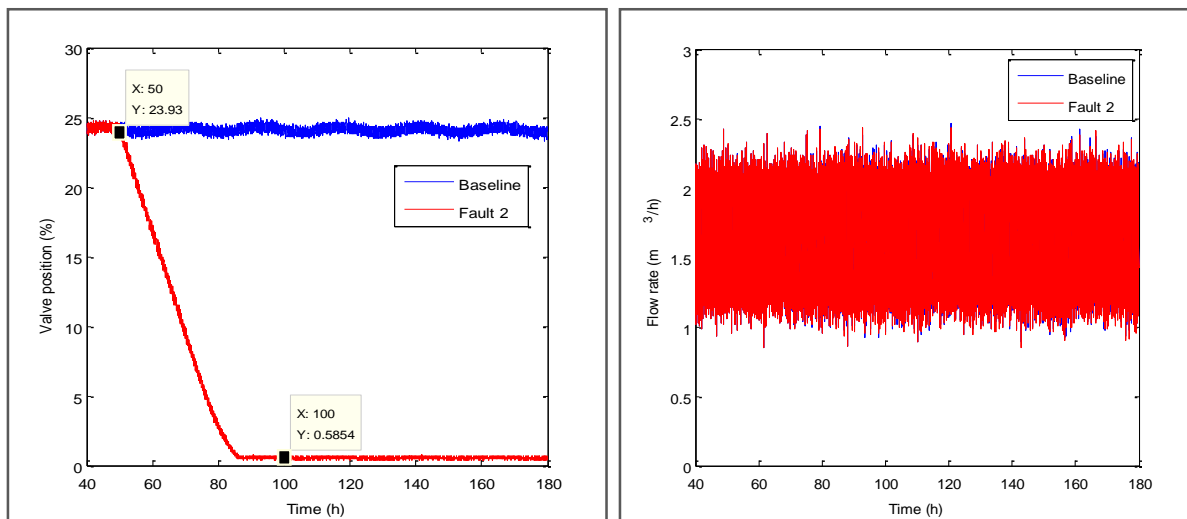


Figure 9.9: Verification of fault 2 occurrence: Compartment 4 outlet flow control valve (left) and flow rate (right)

The fourth compartment outlet flow controller reduces the valve position in the case of the fault occurrence in order to keep the flow rate at its set-point. The reduction in valve position is attributed to the valve wear which alters a linear valve to exhibit quick-opening valve characteristics. A lower valve position is required to produce a specific flow rate after valve wear since a worn valve allows more material to pass at a certain valve position (refer to Figure 8.4). A final valve position of 0.5854 % is evident after the valve wear is fully implemented. A worn valve position of approximately 23.93 % is obtained when substituting 0.5854 % into Equation 8.2 with a 0.73 extent of valve degradation. This valve position corresponds with the faultless valve position as expected for a relatively constant flow rate. Figure 9.9 verifies the occurrence of valve wear within this simulation run.

Table 9.8 captures final KPI values that show significant variation from the baseline.

Table 9.8: Significant KPIs for fault 2: valve wear

Controllers	TD (%)	AE (%)	MD (%)	TNASP (h)	SD (%)
Autoclave pressure control (bar)	0.00	0.28	1.99	0.00	0.25
Compartment 4 level control (%)	0.00	0.34	1.27	0.00	0.31
Compartment 4 outlet flow control (m ³ /h)	0.02	2.92	6.84	0.20	1.47

Valves	TD (%)	AE (%)	TNASP (h)	VR (%)	CS (#)	TS (h)	LTS (h)
Compartment 4 outlet flow control valve (%)	-35.17	-35.24	0.32	-10.60	0	0.00	0.00

The largest KPI variation can be seen around the fourth compartment outlet flow control valve, which is at the origin of the fault. The travel distance of the fourth compartment outlet flow control valve decreased with 35.17 % when compared to the baseline. This decrease can be explained when considering the valve characteristics prior to the fault occurrence and after the fault has been fully implemented. Refer to Figure 9.10.

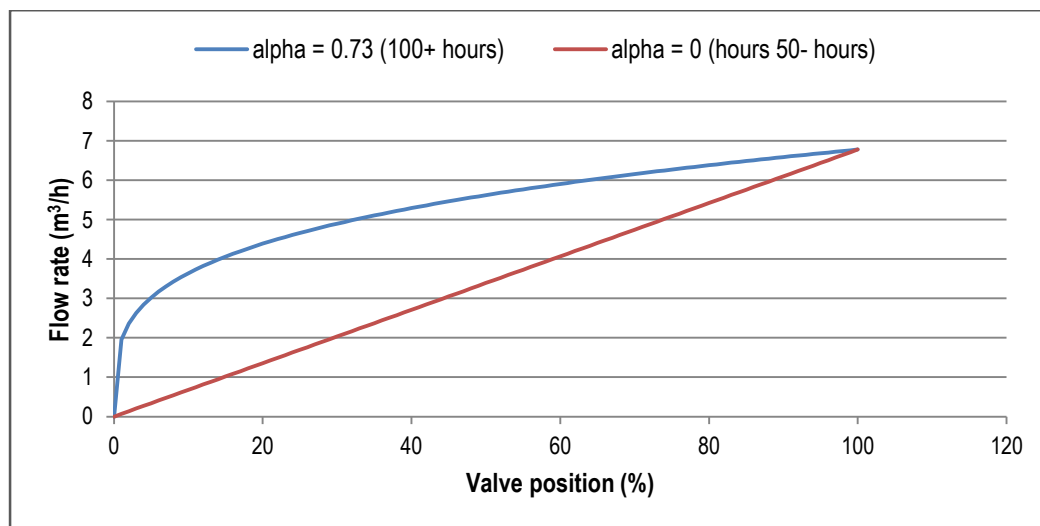


Figure 9.10: Valve characteristics at 0 and 0.73 extents of degradation

Notice that the valve characteristic gradient of the fully degraded valve⁶ is larger than that of the linear valve below a valve position of 17 % and smaller above a valve position of 17 %. The fully degraded valve will therefore travel less than the linear valve in the case of a flow rate step-change at any valve position below 17 %, and vice versa. A valve position around 0.5854 % is evident after the fault is fully implemented (refer to Figure 9.9), which falls below 17 %. The worn valve will for this reason travel less than the faultless linear valve. The reduction in valve travel reduces the valve present-value and set-point mismatch and therefore the average error and integral absolute error.

⁶ An extent of valve degradation equal to 0.73

An increase in average error, maximum deviation and standard deviation is seen for the fourth compartment outlet flow controller. This is expected to be caused by the tuning of the fourth compartment outlet flow controller which is unsuitable for the changed valve characteristics. The flow controller makes valve set-point changes as usual for a specific flow error. However, these valve set-points changes result in significantly different flow rate changes for a worn valve due to the quick-opening valve characteristics. The flow controller effectively becomes more aggressive since it is not tuned for a quick-opening valve. The extents to which the flow controller and cascaded level controller performance are affected are minimal. This could be attributed to both the low actuation required to mitigate the variation in dynamic process model inputs, and the conservative tuning method used to tune the dynamic process model controllers.

It would seem the fault occurrence improved the overall process performance when KPIs in Table 9.8 are analysed, since the valve travels significantly less while the performance of controllers are only slightly reduced. This is however not the case. The fourth compartment outlet flow controller and level controller in the case of a fully worn valve have not dealt with significant disturbances. It is expected that the flow controller will experience difficulty in attempting to mitigate disturbances or even meet significant set-point changes effectively. The inability to mitigate disturbances would be attributed to the flow controller which is tuned for a linear valve and not a valve which shows significant quick-opening behaviour.

9.4.4. Valve stiction

Figure 9.11 shows the stream 2 spent electrolyte flow controller valve position profile for both the baseline and fault runs.

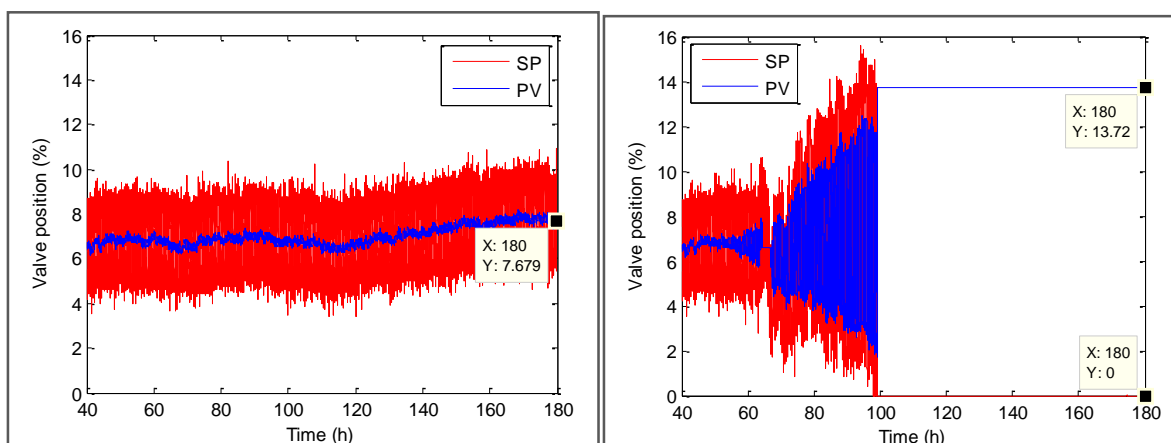


Figure 9.11: Verification of fault 3 occurrence: Spent electrolyte flow controller valve position over time for baseline (left) and fault (right)

The present-value of the valve position in the case of the fault clearly transitions into oscillatory behaviour from the point the fault was implemented (i.e. at 50 simulation hours). This is caused by the cascaded flow controller that cannot get the valve to its intended set-point due to the sticking and jumping behaviour of the valve. The flow controller output consequently starts to oscillate around the intended valve set-point. A point in time is reached where the valve gets stuck at 13.72 % whereafter the valve set-point moves down to zero. The valve set-point cannot overcome the 14 % deadband and stickband parameter at this point (the valve stiction parameter shown in Table 9.4). The valve present-value therefore remains stuck at the 13.72 % position. Figure 9.11 verifies the occurrence of valve stiction within this simulation run.

Table 9.9 captures final KPI values that show significant variation from the baseline.

Table 9.9: Significant KPIs for fault 3: Valve stiction

Controllers	TD (%)	AE (%)	MD (%)	TNASP (h)	SD (%)
Autoclave pressure control (bar)	0.05	204.0	600.0	0.00	314.4
Compartment 1 temperature control (°C)	0.00	22.91	89.86	0.00	50.36
Compartment 2 temperature control (°C)	0.00	-4.34	112.7	0.00	26.80
Second stage slurry preparation tank level control (%)	0.00	7.41	99.86	0.00	21.55
Second stage slurry preparation tank density (kg/l)	0.00	436.2	155.2	14.98	276.2
Spent electrolyte flow control (m ³ /h)	0.01	422.5	132.7	79.66	183.8

Valves	TD (%)	AE (%)	TNASP (h)	VR (%)	CS (#)	TS (h)
Spent electrolyte flow control valve (%)	125.7	1437	89.66	-88.76	0	0.00

Operational KPIs	Compartment 1	Compartment 2	Compartment 3	Compartment 4
Total PGMs in liquid (%)	48.31	82.95	122.40	63.86
Total BMs in solid (%)	-11.15	-9.05	-9.78	-9.26

Operational KPIs	
Decrease in total BM input (%)	10.45
Decrease in total PGM input (%)	8.35
Decrease in total solid throughput (%)	16.37
Total oxygen usage (%)	-7.81
Total steam usage (%)	3.28
Compartment 2 CW usage (%)	-38.71

A significant amount of KPIs varied from the baseline during the occurrence of valve stiction. The spent electrolyte flow control valve KPIs in Table 9.9 show the largest variation from the baseline. The fault in this run originated at the spent electrolyte flow control valve. A significant increase in average error for this valve is noticed. This is expected since the cascaded flow controller cannot get the valve to its intended set-point due to the sticking and

jumping behaviour of the valve, as previously mentioned. This is substantiated by the high time not at set-point of 89.66 hours. The number of valve reversals decreased and is attributed to the fact that the valve spends most of its time in a locked position which limits the valve movement and therefore the number of reversals. The travel distance of the valve increased and is explained by the oscillatory behaviour of the valve present-value shown in Figure 9.11. Notice that this valve did not travel any further after approximately 100 simulation hours. A decrease in travel distance relative to the baseline is therefore expected after this point in time. Figure 9.12 shows the spent electrolyte flow control valve travel distance over time.

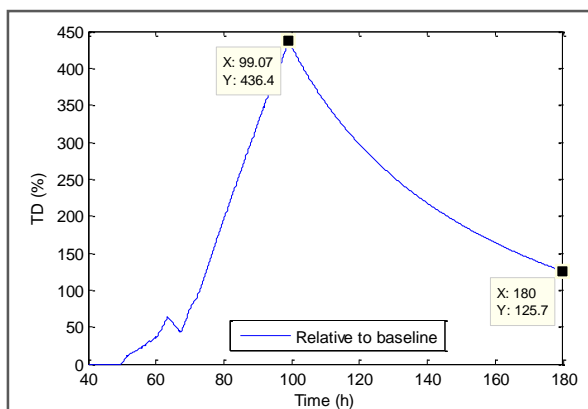


Figure 9.12: Travel distance of the spent electrolyte flow control valve over time during fault 3 - valve stiction

The decrease in travel distance relative to the baseline is evident after 99.07 hours, as expected. This decrease continues up until reaching a final percentage of 125.7 % which corresponds with the final travel distance reported in Table 9.9.

The fact that the spent electrolyte flow control valve is unable to meet its set-point and ultimately sticks at a valve position of 13.72 % explains the reduction in both the spent electrolyte flow controller and second stage slurry preparation tank density controller performance. Remember that the spent electrolyte flow controller receives a set-point from a feedforward controller which attempts to keep the second stage slurry preparation tank outlet solid percentage (i.e. the slurry density) at a user-defined value. Consider the second stage slurry preparation tank outlet density during the occurrence of valve stiction.

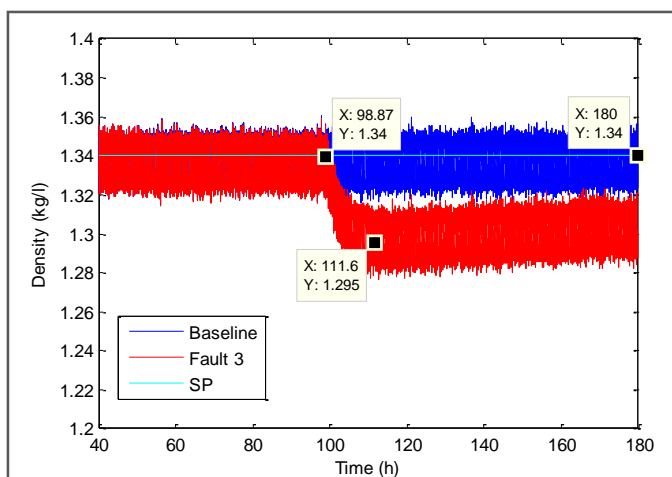


Figure 9.13: Density of second stage slurry preparation tank during fault 3 – valve stiction

A decrease in second stage slurry preparation tank outlet density is seen after 99.07 simulation hours. This is the point at which the spent electrolyte flow control valve sticks at a valve position of 13.72 %. The feedforward controller fails to reduce the spent electrolyte flow rate to its intended set-point which causes a density offset. The change in second stage slurry preparation tank density affects the both the pressure and temperatures within the autoclave. The reduction in solid percentage reduces the amount of heat released per unit of volume within the first compartment. The temperature within the first compartment shows an increase in maximum deviation for this reason. The first compartment temperature disturbance carries over into the second compartment which also indicates a deviation in temperature. The variation in compartment temperatures affects the autoclave vapour temperature and ultimately disturbs the autoclave pressure. The autoclave temperatures and pressure show large maximum deviations coupled with the low times not at set-point and average errors, which suggest that the fault caused a deviation in these controlled variables but the deviation was mitigated and no offset ultimately existed.

The total mass of base metals and PGMs that entered the process through stream 5 decreased with 10.45 % and 8.35 %, respectively. Note that this stream has a constant volumetric flow rate set-point of 3 m³/h. The decrease in total mass of base metals and PGMs is attributed to reduction in solids in stream 5 and its substitution with a combination of spent electrolyte and formic filtrate which inherently contain less base metals and PGMs per unit of mass. The decrease in solid loading is also a major contributor to the reduced solid throughput. The reduced solid loading in autoclave compartments result in lowered oxygen consumption since less solid base metals are available for oxidation. A reduction in cooling water requirements and an increase in steam requirements are evident for this same reason. Figure 9.14 shows the total PGMs in the liquid and total base metals in the solid phase relative to the baseline.

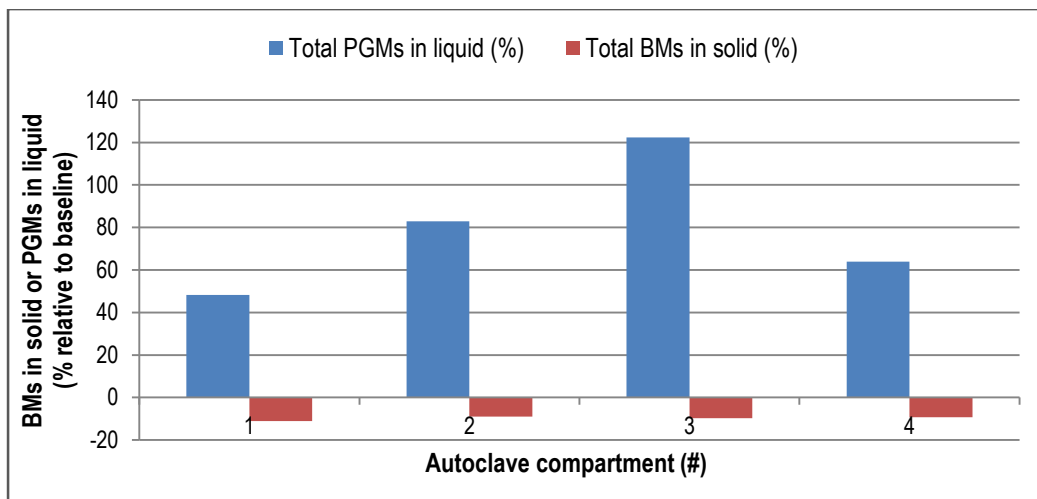


Figure 9.14: PGMs in liquid and BMs in solid for fault 3 – valve stiction

The total mass of PGMs present in the first compartment liquid phase is 48.31 % higher than that of the baseline. An increase in this value is expected since more PGMs is present in the liquid phase prior to entering the first compartment due to the displacement of solids with PGM containing spent electrolyte. The fact that the total PGMs in the liquid phase increases with the autoclave compartment number suggests that either the effectiveness of cementing PGMs via base metal leaching reduced, or the rate at which PGMs are leached increased. The latter case can be substantiated by the fact that the reduced base metals present in the solid phase would cause PGMs to leach at an earlier point in time. The increase of PGMs in the liquid phase is undesirable since this liquid stream is recycled to the first stage leach section, among others, where un-cemented PGMs are possibly lost to the nickel recovery process.

9.4.5. Pump impeller wear

Figure 9.15 shows the profiles of the flash recycle tank outlet flow control valve and its corresponding flow rate.

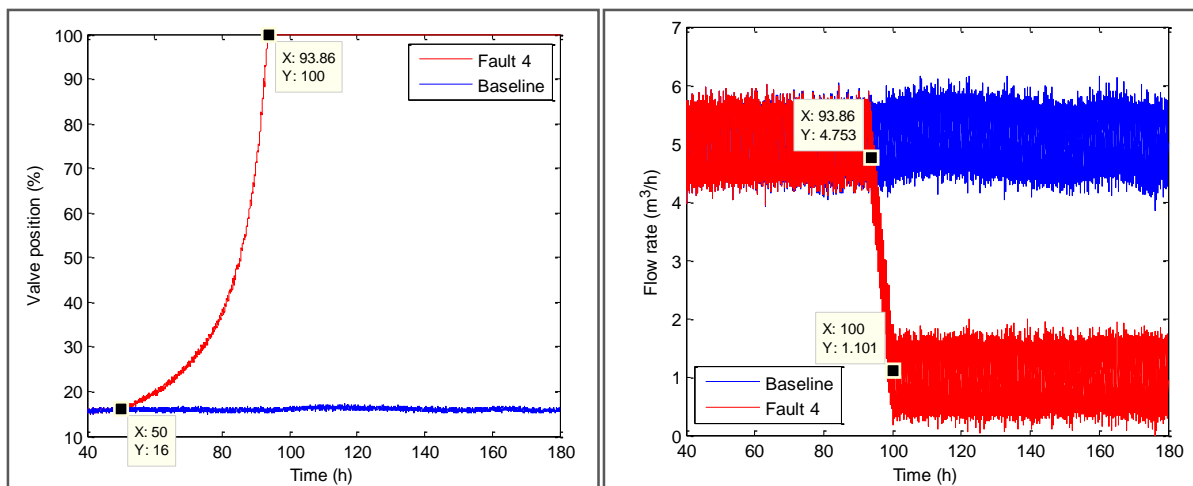


Figure 9.15: Verification of fault 4 occurrence: Flash recycle tank outlet flow control valve (left) and corresponding flow rate (right)

The position of the flash recycle tank outlet flow control valve starts to gradually deviate from the baseline at 50 hours and onward. This gradual increase in valve position exists in order to counter the pump impeller wear which causes a reduced flow rate at a specific valve position. The effect that pump impeller wear has on the flash recycle tank outlet flow rate is concealed until the point at which the valve becomes saturated (i.e. around 93.86 hours). A rapid decrease in flash recycle tank outlet flow rate is noticed at this point. This rapid decrease is attributed to the inability of the saturated flow control valve to continue to counter the pump impeller wear effects. Figure 9.15 verifies the occurrence of pump impeller wear within this simulation run.

Table 9.10 captures final KPI values that show significant variation from the baseline.

A significant amount of KPIs varied from the baseline during the occurrence of pump impeller wear. The third compartment level control KPIs in Table 9.10 show the largest variation from the baseline. The third compartment level controller is however not at the location of fault origin. The fault propagation needs to be considered in order to understand the effects on the third compartment level controller.

Table 9.10: Significant KPIs for fault 4: Pump impeller wear

Controllers	TD (%)	AE (%)	MD (%)	TNASP (h)	SD (%)
Autoclave pressure control (bar)	0.41	3607	8830	42.87	4771
Compartment 1 temperature control (°C)	0.04	6847	8328	68.84	8215
Compartment 2 temperature control (°C)	0.00	206.3	1525	2.96	726.0
Compartment 3 temperature control (°C)	0.00	85.18	912.7	0.00	365.4
Compartment 4 temperature control (°C)	0.00	13500	7734	63.65	13210
Second stage slurry preparation tank level control (%)	0.00	2628	1711	75.35	2233
Flash recycle tank level control (%)	0.00	12250	4489	84.84	8046
Compartment 3 level control (%)	0.00	20770	10520	84.18	17730
Second stage slurry preparation tank density (kg/l)	0.00	462.6	227.6	41.46	361.0
Flash recycle tank outlet flow control (m ³ /h)	0.00	7338	2082	86.20	709.0

Valves	TD (%)	AE (%)	TNASP (h)	VR (%)	CS (#)	TS (h)	LTS (h)
Compartment 4 temperature control valve (%)	-46.42	-49.46	0.00	-51.88	1	71.06	71.06
Spent electrolyte flow control valve (%)	-16.75	-17.13	0.00	-1.92	0	0.00	0.00
Flash recycle tank outlet flow control valve (%)	-61.33	-61.60	0.00	-61.78	1	86.37	86.37
Compartment 3 outlet flow control valve (%)	-28.91	-28.83	0.00	-2.35	0	0.00	0.00

Operational KPIs	Compartment 1	Compartment 2	Compartment 3	Compartment 4
Total PGMs in liquid (%)	-7.61	-7.36	-7.40	2792
Total BMs in solid (%)	-9.85	-9.44	-9.12	-1.23

Operational KPIs	
Decrease in total BM input (%)	56.37
Decrease in total PGM input (%)	57.01
Decrease in total solid throughput (%)	56.68
Total oxygen usage (%)	-41.71
Total steam usage (%)	23.24
Compartment 2 CW usage (%)	-59.92
Compartment 3 CW usage (%)	-58.67
Flash recycle tank spillage (kg)	10820

The first compartment temperature and outlet flow rate profiles are captured in Figure 9.16.

The first compartment temperature increases rapidly at 93.86 hours, which is the point in time where the flash recycle tank outlet flow control valve saturates (refer to Figure 9.15). This makes sense since the flash recycle tank at this point loses the ability to control its level and subsequently to obtain the necessary outlet flow rate in order to keep the first compartment temperature in check (refer to Section 2.4.2 for the first compartment temperature control mechanism).

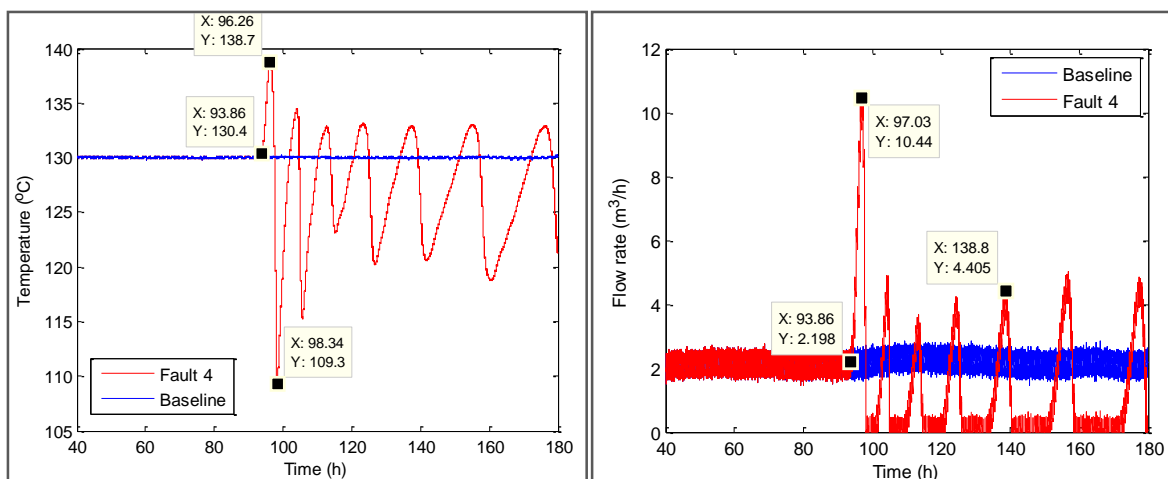


Figure 9.16: Temperature (left) and outlet flow rate (right) of compartment 1 during fault 4 – Pump impeller wear

The first compartment temperature controller increases the set-point of its secondary loop (i.e. the first compartment outlet flow rate) in an attempt to once again reach its 130 °C set-point, as seen in Figure 9.16. This flow rate increase cannot be matched by the flash recycle tank outlet pump due to the worn impeller. This ultimately causes an increase in the flash recycle tank level and the activation of a safety interlock. The profile of the flash recycle tank level is given in Figure 9.17. The profile of the second stage slurry preparation tank outlet flow rate, the stream feeding fresh material to the flash recycle tank, is also shown.

Notice that the level in the flash recycle tank reaches a value of 120 %. Remember that the level of vessels with no inherent overflow mechanism can increase to 120 % prior to overflowing. The flash recycle tank overflows at 139.3 hours which explains the non-zero spillage evident in Table 9.10 for this vessel. It is expected that the process would enter an unexpected maintenance at this point time, if not already during the major first compartment level and temperature variations. The supervisory actions and reasoning used to shut the process down has not been incorporated in this project, as previously mentioned. The fault symptoms shown within this chapter and the extent of process degradation caused by these faults are therefore a representation of what would happen if faults are left unattended.

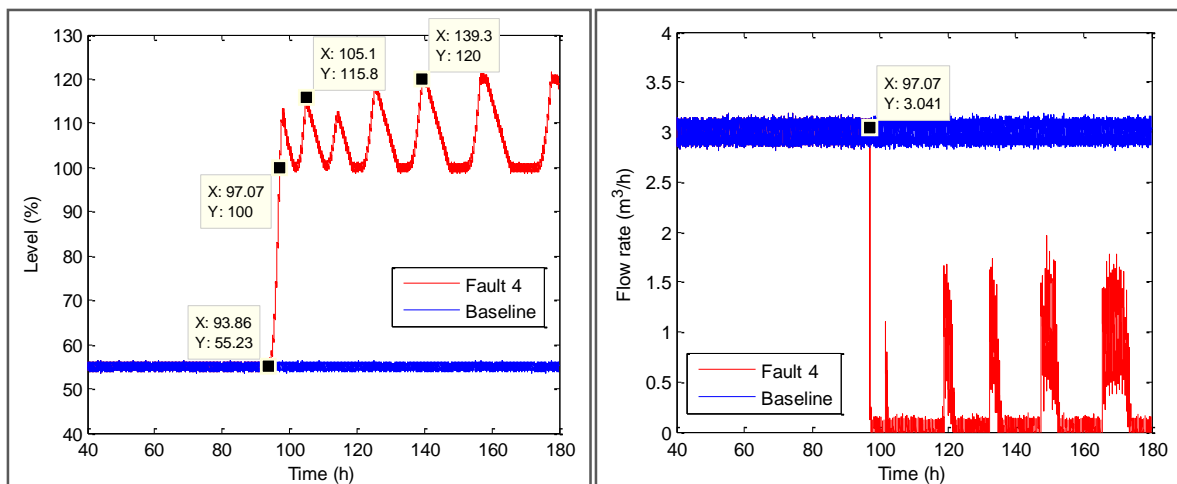


Figure 9.17: Level of flash recycle tank (left) and outlet flow rate of second stage slurry preparation tank (right) during fault 4 – Pump impeller wear

The flash recycle tank level increases rapidly at 93.86 hours since it is receiving an increased feed from the first compartment while its ability to pump the flashed material out into the first compartment via stream 7 is reduced (substantiated by the 86.2 hours the flash recycle tank outlet flow controller is not at its set-point). This explains the reduction in the flash recycle tank level control performance (i.e. the average error, maximum deviation and time not at set-point). The level interlock on the flash recycle tank activates at 97.07 hours, which is at the time the level reaches 100 %. The flash recycle tank level interlock acts by stopping the second stage slurry preparation tank outlet flow rate as seen in Figure 9.17 (refer to Section 2.4.5 for a list of safety interlocks implemented at Western Platinum BMR). However, the flash recycle tank level interlock does not act on the first compartment outlet flow rate. An increase in the flash recycle tank level is therefore still evident after the activation of the level interlock. The subsequent decrease in flash recycle tank level is caused by the first compartment temperature which lowers the set-point of its secondary control loop due to a decrease in first compartment temperature. The decrease in first compartment temperature is attributed to the lower mass present in this compartment which reduces the amount of heat released per unit of volume. Figure 9.18 shows the level in the first compartment.

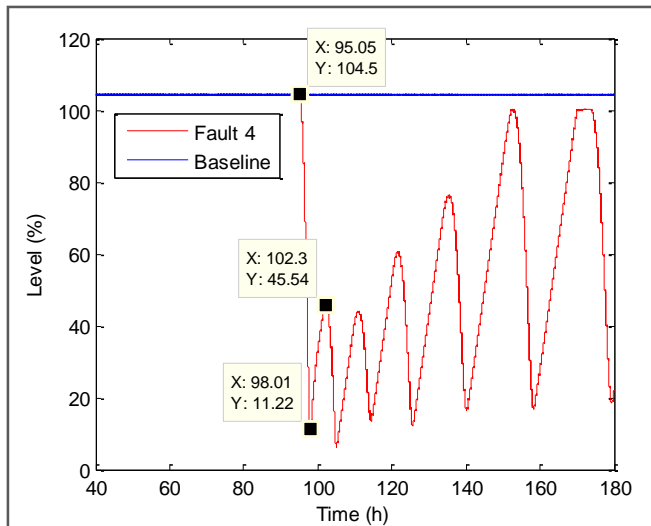


Figure 9.18: Level of compartment 1 during fault 4 – Pump impeller wear

The first compartment level decreases rapidly after 95.05 hours due to the combination of the increase in first compartment outlet flow rate and decrease in inlet flow rate. The temperature in the first compartment decreases at this point since the mass of high temperature slurry present in the first compartment reduces significantly, which ultimately requires significantly less flashed inlet flow to reduce its temperature. Also, a reduced amount of heat is released through base metal leaching due to the reduction in slurry volume. The level in both the first compartment and flash recycle tank continues to vary as the temperature controller attempts to obtain the 130 °C set-point. This mechanism of first compartment temperature control is highly undesirable. The significant variation in slurry volume affects the extent of leaching and therefore the product quality and consistency. In addition, the temperature controller is unable to get the variable to its intended set-point. The significant variation in first compartment temperature and volume also disturbs the autoclave pressure via its effect on the vapour temperature and vapour volume (refer to Equation 6.19 to Equation 6.21), which explains the reduction in pressure control performance. The first compartment level drops below 100 % several times, which stops the overflow into the subsequent autoclave compartments. This explains the reduction in the third compartment level control performance. The reduction in the second, third and fourth compartment temperature control performances are attributed to both the variation in slurry overflow compositions and autoclave pressure.

The flash recycle tank level safety interlock stops the second stage slurry preparation tank outlet flow rate, as previously mentioned. The second stage slurry preparation tank subsequently reduces its cascaded first stage leach residue flow rate to zero to counter the downstream hold-up. This action is captured in Figure 9.19.

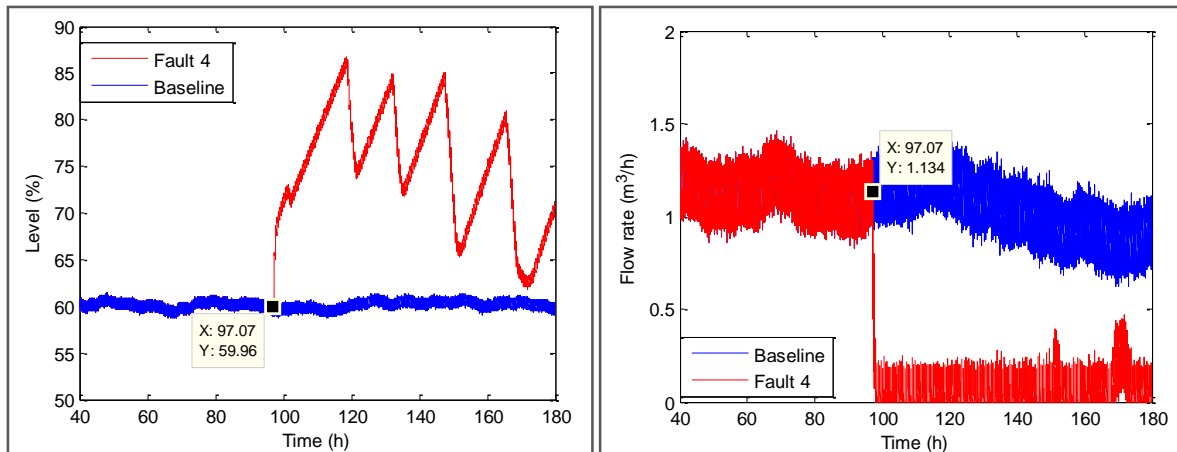


Figure 9.19: Level of second stage slurry preparation tank (left) and cascaded flow rate of first stage leach residue (right) during fault 4 – Pump impeller wear

Note that the level continues to increase even after the first stage leach residue flow rate reduces to zero, which is unexpected. Remember that the flow rates of the spent electrolyte and formic filtrate streams (the only additional streams that enter the second stage slurry preparation tank) are controlled using a feedforward controller. The set-points of these flow controllers are obtained from the first stage leach residue flow rate (refer to Section 2.4.2 for the feedforward control mechanism). All flow into the second stage slurry preparation tank should therefore stop when the first stage leach residue flow rate is zero. This should then result in a constant second stage slurry preparation tank level during the occurrence of the downstream level interlock. The increase in level noticed after the first stage leach residue flow rate reduces to zero is attributed to the noise of this flow measurement and its contribution to the spent electrolyte and formic filtrate flow rate set-points. The first stage leach residue flow measurements are non-zero even though the actual flow rate is zero. This non-zero measurement is used to determine the set-points for both the spent electrolyte and formic filtrate flow controllers (described by Equation 2.1 and Equation 2.2 in Section 2.4.2). The subsequent non-zero flow into the vessel while having an outlet flow rate of zero causes the increase in level shown in Figure 9.19. This explains the reduction in both the second stage slurry preparation tank level and density control performance seen in Table 9.10. Figure 9.20 shows the second stage slurry preparation tank density over time.

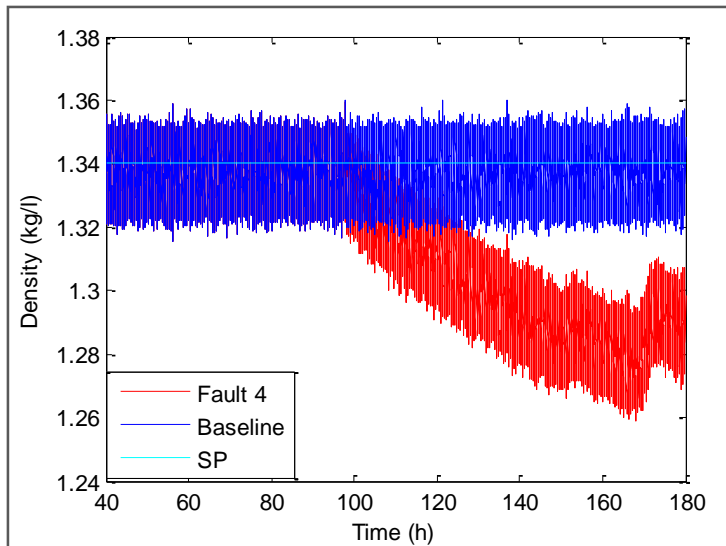


Figure 9.20: Density of second stage slurry preparation tank during fault 4 – Pump impeller wear

The second stage slurry preparation tank density reduces and moves away from its set-point since the flow rates of the lower density streams are non-zero. The feedforward controller which controls the solid percentage (i.e. density) of the second stage slurry preparation tank cannot account for this offset since it does not verify this outlet density.

A reduction in the travel distance and average error is seen for both the spent electrolyte and third compartment outlet flow control valves. Reduced actuation is evident for both these valves since they are closed for a portion of the time for reasons previously described. The significant reduction in the travel distance, average error and number of valve reversals for both the fourth compartment temperature and flash recycle tank outlet flow control valves are attributed to valve saturation. The cause of saturation for the latter valve has been mentioned several times. The saturation of the fourth compartment temperature control valve (i.e. the steam control valve) is caused by a significant reduction in heat released via base metal leaching in this compartment. The reduced pumping capacity on the outlet of the flash recycle tank causes a reduction in the flow rate leaving the third compartment. Fewer solids therefore enter the third stage slurry preparation tank after reporting to the thickener. The flow rate leaving the third stage slurry preparation tank (i.e. entering the fourth compartment) is left unaffected since this flow controller has a constant set-point of 1.42 m³/h. The discrepancy between the lower solid inlet flow and constant outlet flow is compensated by an increase in the inlet water flow rate used to control the third stage slurry preparation tank level. Figure 9.21 shows the solid fraction of the stream entering the fourth and final autoclave compartment.

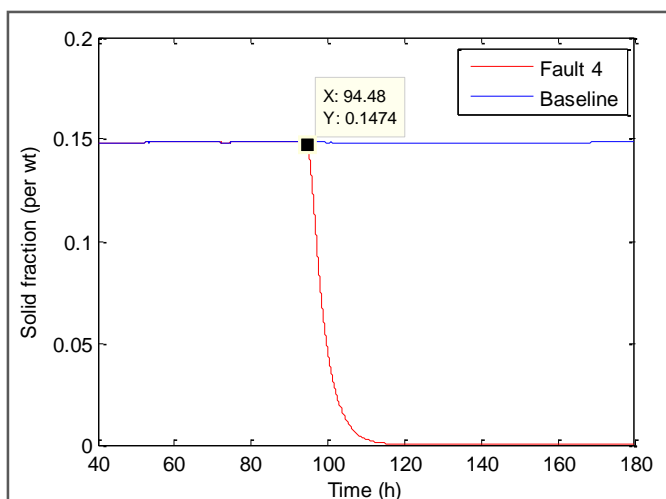


Figure 9.21: Solid fraction of feed to compartment 4 during fault 4 – Pump impeller wear

The reduction in the solid fraction shown in Figure 9.21 is a result of the excessive addition of water. The subsequent reduction in fourth compartment solid loading reduces the amount of heat released per unit of volume via base metal leaching. In addition, high temperature solids are substituted with water at ambient temperature which increases the heating requirements. This ultimately causes the steam control valve (i.e. temperature control valve) to increase and saturate.

Figure 9.22 shows the total PGMs in the liquid and total base metals in the solid phase relative to the baseline.

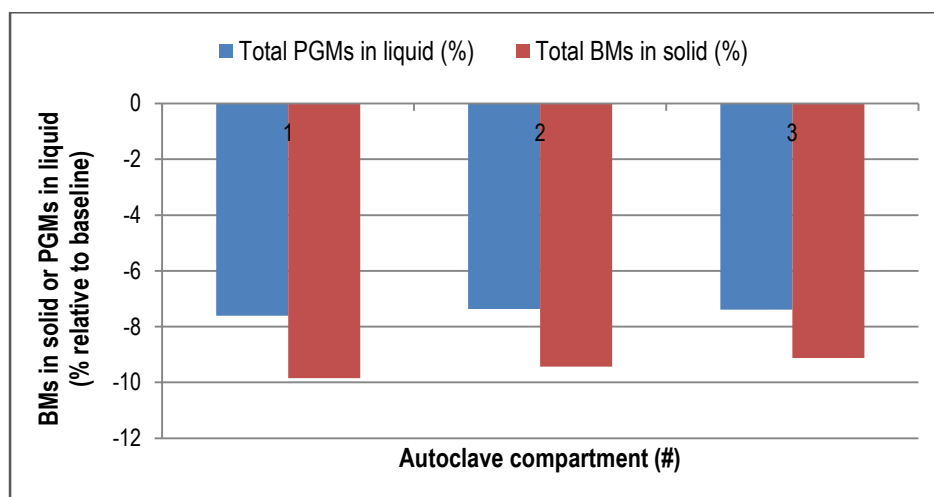


Figure 9.22: PGMs in liquid and BMs in solid for fault 4 – pump impeller wear

A decrease in both the PGMs in the liquid phase and base metals in the solid phase for the first, second and third autoclave compartments is noticed. This is attributed to an increase in residence time within these compartments due to the decrease in upstream pumping capacity. The increased residence time allows further extent of base metal leaching and

PGM precipitation to occur. These reductions would seem beneficial at first (not taking into account the major instability in the process), since more base metals are leached to produce a high grade PGM product while less PGMs are lost through the liquid phase during spent electrolyte recycling. It has been made clear that the operating conditions during the occurrence of this fault are unwanted. However, an improvement in operating conditions seems to transpire from the increased residence time caused by this fault. The increase in residence time can be mimicked by reducing the feed to the process, which should produce trends similar to that shown in Figure 9.22. However, the disadvantage of operating with an increased residence time is the significant reduction in solid throughput. The solid throughput is reduced by 56.68 % during the fault due to the lowered pumping capacity (i.e. processing capacity – notice the reduction in PGMs and base metals input to the process). In addition, a final decrease of only 1.23 % is obtained in base metals present in the fourth compartment solids. This means that an increase in extent of base metal leaching is evident in the first three compartments, but the final solids produced in the fourth compartment ultimately reaches close to the same extent of base metal leaching.

A significant increase in PGMs present in the fourth compartment liquid phase is shown in Table 9.10, and was not included in Figure 9.22 as it would conceal the trends in the first three compartments. This major increase is attributed to a combination of the increase in spent electrolyte (i.e. liquid containing PGM ions) fed to the third stage slurry preparation tank and subsequently the fourth compartment, and the lowered amount of base metal solids present to precipitate these PGM ions.

A significant reduction in the second and third compartment cooling water requirements is seen in Table 9.10. This is expected since a significant decrease in base metals are fed to the process which reduces the amount of heat generated. A similar explanation is used to substantiate the reduction in oxygen usage. An increase in steam is used, which is expected and is explained by a similar reason why the steam valve saturated.

9.4.6. Solid build-up in cooling coils

Figure 9.23 shows the profiles of the second compartment temperature control valve position and its corresponding cooling water flow rate. Note that this cooling water flow rate is not measured at Western Platinum BMR. It is only used in this case to verify the fault occurrence.

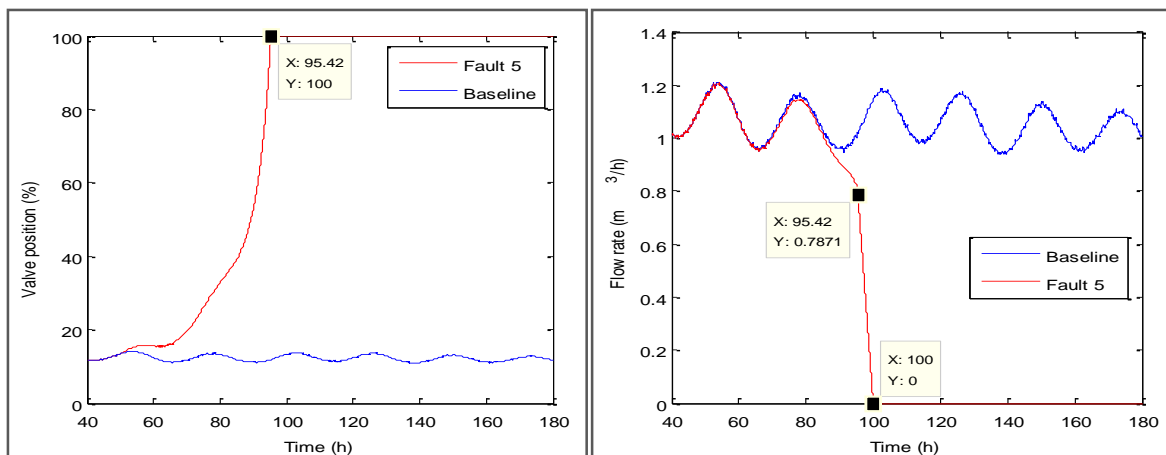


Figure 9.23: Verification of fault 5 occurrence: Compartment 2 temperature control valve (left) and flow rate (right)

The temperature control valve clearly deviates from the baseline from 50 simulation hours onward. Solid build-up in the cooling coil results in a reduced maximum flow rate attainable by the centrifugal pump due to the increase in pressure drop across the cooling coil. The valve position needs to increase in order to sustain a specific cooling water flow rate throughout the transition of the fault. The valve position increases and manages to keep the cooling water flow rate close to the expected baseline value. However, the solid builds up to such an extent that the valve saturates in an attempt to sustain the cooling water flow rate. This occurs at 95.42 hours. The cooling water flow rate at this point in time decreases dramatically since the saturated valve cannot move to compensate for the solid build-up. Figure 9.23 validates the occurrence of solid build-up within this simulation run.

Table 9.11 captures final KPI values that show significant variation from the baseline. The solid build-up in the cooling coil of the second autoclave compartment had a significant effect on many KPIs. The KPIs of the second compartment temperature controller shows the largest deviation (the fault originated at this location of process). This controller shows a significant average error, time not at set-point and travel distance, which is indicative of either major oscillatory behaviour or a combination of an offset and oscillatory behaviour. A similar conclusion can be drawn for the first compartment temperature controller. The fact that the travel distance for the pressure controller is unmistakably large suggests that this controller exhibits a definite form of oscillatory behaviour. Note that significant variation in a travel distance is uncommon due to the measurement noise which dominates this KPI, as discussed previously (this excluding valve travel distances since no noise were added to valve present-values). A significant variation in pressure would cause such a high pressure travel distance deviation.

Table 9.11: Significant KPIs for fault 5: Solid build-up in cooling coils

Controllers	TD (%)	AE (%)	MD (%)	TNASP (h)	SD (%)
Autoclave pressure control (bar)	425.7	34390	25550	75.70	37640
Compartment 1 temperature control (°C)	0.32	7033	3021	72.02	5591
Compartment 2 temperature control (°C)	3.26	39670	20570	85.96	27910
Compartment 3 temperature control (°C)	1.66	2196	1638	0.00	2621
Compartment 4 temperature control (°C)	0.71	2483	1555	3.32	2924

Valves	TD (%)	AE (%)	TNASP (h)	VR (%)	CS (#)	TS (h)	LTS (h)
Compartment 2 temperature control valve (%)	13.93	10.74	0.00	-78.24	1	84.74	84.74
Compartment 3 temperature control valve (%)	3936	3831	0.00	-60.00	0	0.00	0.00
Compartment 4 temperature control valve (%)	2620	2488	59.43	-54.95	30	0.83	0.04

Operational KPIs	Compartment 1	Compartment 2	Compartment 3	Compartment 4
Total PGMs in liquid (%)	105.1	91.12	127.3	97.10
Total BMs in solid (%)	15.45	16.88	14.81	14.70

Operational KPIs	
Decrease in total solid throughput (%)	-11.21
Total oxygen usage (%)	-14.07
Compartment 2 CW usage (%)	-59.75
Compartment 3 CW usage (%)	333.5

Consider the first and second compartment temperature profiles for both the fault and baseline runs.

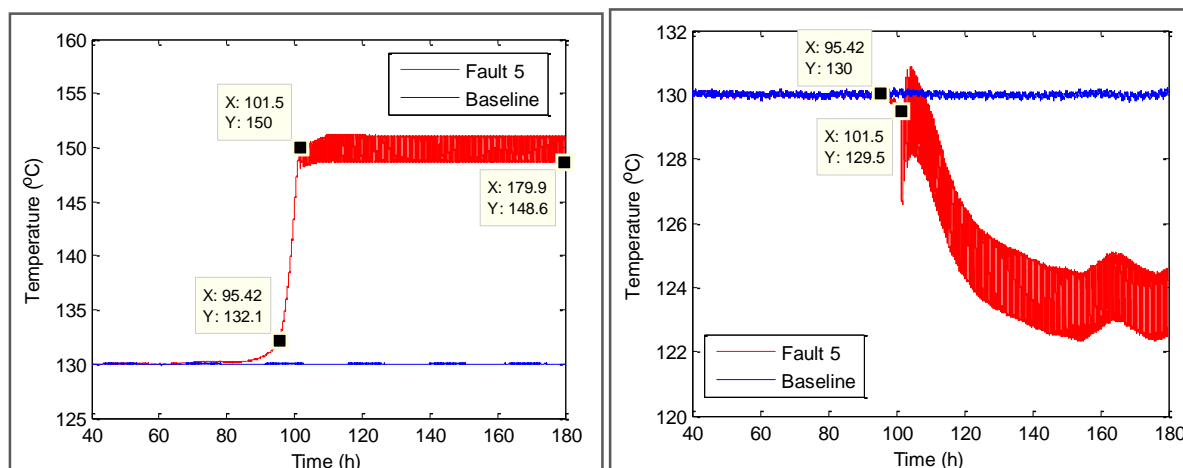


Figure 9.24: Temperature in compartment 2 (left) and compartment 1 (right) during fault 5 – solid build-up in cooling coils

The temperature in the second compartment starts to increase rapidly at the point where its corresponding temperature control valve saturates (refer to Figure 9.23 and Figure 9.24). This is expected since this is the point in time where the temperature controller is limited in its ability to change a manipulated variable to compensate for an offset. The significant increase in the second compartment temperature causes a reduction in the first

compartment temperature. This is attributed to the reduction in autoclave oxygen partial pressure which reduces the extent of base metal leaching and therefore the source of heat. The autoclave pressure interlinks all the compartments through their combined effect on the vapour temperature and vapour volume (refer to Equation 6.19 to Equation 6.21). This allows faults occurring in downstream compartments to affect upstream compartments. A reduction in oxygen partial pressure occurs due to the increase in water partial pressure associated with the increase in the second compartment temperature (i.e. less oxygen is available in the gas phase since the water vapour displaces the oxygen for a constant pressure set-point).

The rapid increase in the second compartment temperature plateaus at around 150 °C and 101.5 hours. The temperature in both the first and second compartments exhibit oscillatory behaviour after this point in time. Both the oscillatory behaviour and offset predicted from the KPIs for these controllers are therefore verified. The origin of this oscillatory behaviour is attributed to a safety interlock which continuously activates in an attempt to limit autoclave compartments from reaching temperatures above 150 °C (refer to Section 2.4.5 for a list of safety interlocks implemented at Western Platinum BMR). The oxygen to the autoclave is stopped when any autoclave compartment reaches a temperature above 150 °C in an attempt to prevent damage to the autoclave lead lining. This explains the reduction in pressure control performance and the significant pressure travel distance and average error. The temperature in the second compartment seems to increase above 150 °C which would result in autoclave damage. Operator intervention is expected at this point in time since the second compartment temperature interlock will not be able to entirely mitigate the fault effects but only prevent extensive damage.

The third and fourth compartment temperature controllers show significant travel distances and average errors but manage to stay within their set-point ranges. The fourth compartment temperature controller was unable to keep its controlled variable at its intended set-point for 3.32 hours. This could be partially attributed to the intermittent saturation of its corresponding temperature control valve, with a count of 30 saturations over a total of 0.83 saturation hours. The increase in travel distances and average errors for the third and fourth compartment temperature controllers are attributed to the effect that the reduced autoclave pressure performance has on the leaching of base metals and therefore the amount of heat released in these compartments.

A significant reduction in reversals is seen for the second, third and fourth compartment temperature control valves. The reduction in second compartment temperature control valve reversals is attributed to the fact that the valve becomes saturated at an early point in time

which reduces the amount of reversals when compared to the baseline. The same reason can be used to explain the small travel distance and average error performance decreases noticed for this valve. The reduction in the third and fourth compartment temperature control valve reversals is attributed to corresponding temperature controllers traveling larger distances in an attempt to mitigate the temperature oscillations caused by the variation in pressure. The third and fourth compartment temperature profiles are shown in Figure 9.25.

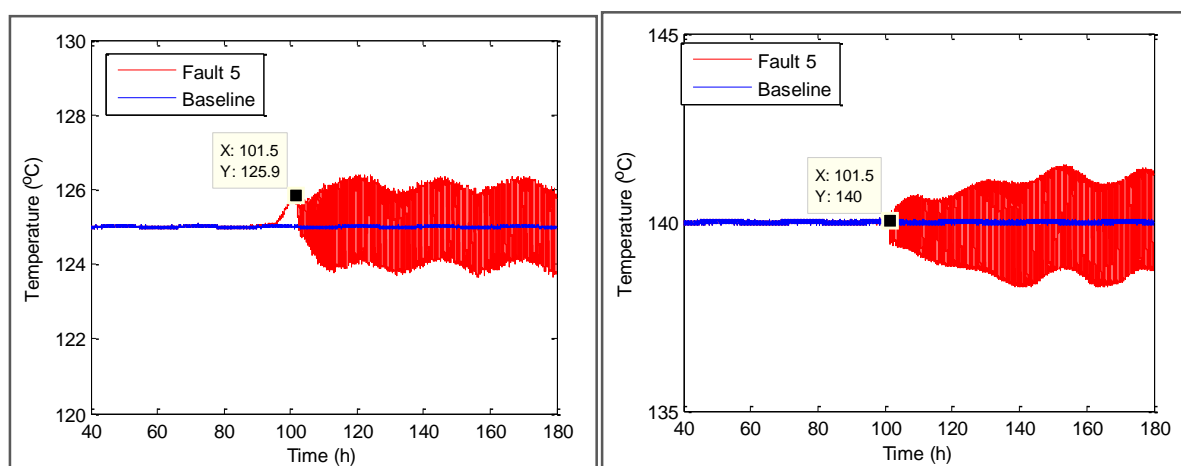


Figure 9.25: Temperature in compartment 3 (left) and compartment 4 (right) during fault 5 – solid build-up in cooling coils

The increase in valve travel distance caused by the mitigation effects of oscillatory behaviour results in less valve reversals when compared to a baseline. This is attributed to its comparison to a baseline with high valve reversals resulting from small scale controlled variable variation which ultimately causes the valve to change direction after moving very small distances (refer to Table 9.6). Notice the increase in the third compartment temperature prior to the oscillatory behaviour. This is in contrast with an initial decrease in the first compartment temperature. The initial increase in third compartment temperature is caused by the addition of high temperature slurry from the second compartment which overpowers the suppressing effects of base metal leaching caused by a decrease in oxygen partial pressure.

Figure 9.26 shows the total PGMs in the liquid and total base metals in the solid phase relative to the baseline.

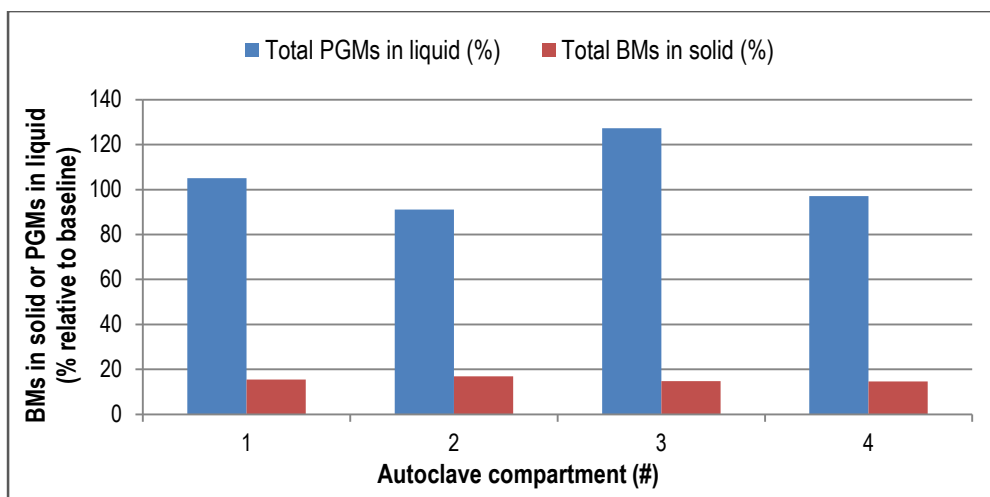


Figure 9.26: PGMs in liquid and BMs in solid for fault 5 – solid build-up in cooling coils

An increase in PGMs in the liquid phase and base metals in the solid phase is noticed for all autoclave compartments. The increase in base metals in the solid phase explains the increase in solid throughput for a constant solid input. These changes are solely caused by the extent of metal leaching since the total base metals and PGMs into the process are exactly the same as that of the baseline.

The variation of metals present in the respective phases is attributed to the effect that temperature has on the leaching kinetics. An increase in temperature increases the rate expression constant (refer to Equation 3.2) and therefore the rate of reactions. An increase in temperature also decreases the oxygen partial pressure as previously discussed. The increase in base metals present in the solid phase for each autoclave compartment is caused by the overall decrease in base metal reaction rates. This net decrease is caused by dominant effect that the reduced oxygen solubility has on the rate of base metal leaching. Temperature increases do not significantly increase the rate of most base metal leaching reactions due to their low associated activation energies. The increase in PGMs in the liquid phase, on the other hand, is attributed to the increase in PGM leaching rates which is caused by the increase in rate expression constants through their high associated activation energies (note that the rate of PGM precipitation also increases but to a lesser extent due to their relatively lower activation energies). Both the increase in PGMs in the liquid phase and base metals in the solid phase are undesirable. These increases result in the production of a lowered grade PGM residue while also possibly losing more PGMs when the high PGM-containing liquid phase is recycled to upstream processes.

Less cooling water is used in the second compartment, as expected. This decrease is caused by the solid build-up which prohibits the use of cooling water within this compartment. A significant increase cooling water usage is evident in the subsequent

compartment. This is understandable since the third compartment needs to remove additional heat which was not removed in the second compartment.

9.4.7. Peristaltic pump tube failure

Figure 9.27 shows the first stage leach residue flow rate over time.

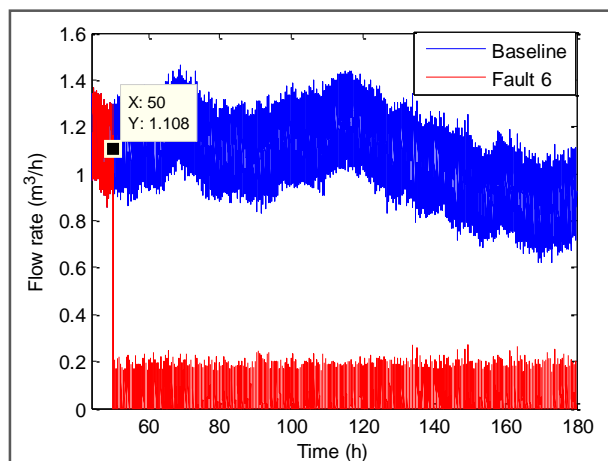


Figure 9.27: Verification of fault 6 occurrence: First stage leach residue flow rate

The flow rate of the first stage leach residue decreases abruptly at 50 hours in the case of the fault. This represents the point where the peristaltic pump tube failure causes a blockage in the first stage leach residue pipeline. Figure 9.27 verifies the occurrence of the peristaltic pump tube failure in this simulation run.

Table 9.12 captures final KPI values that show significant variation from the baseline. The total PGMs in liquid for the fourth compartment shows the largest deviation from that of the baseline. The fourth compartment is not close to the origin of the fault. The propagation of the fault needs to be considered in order to understand the major increase in PGMs present in the liquid phase of the fourth compartment.

Table 9.12: Significant KPIs for fault 6: Peristaltic pump tube failure

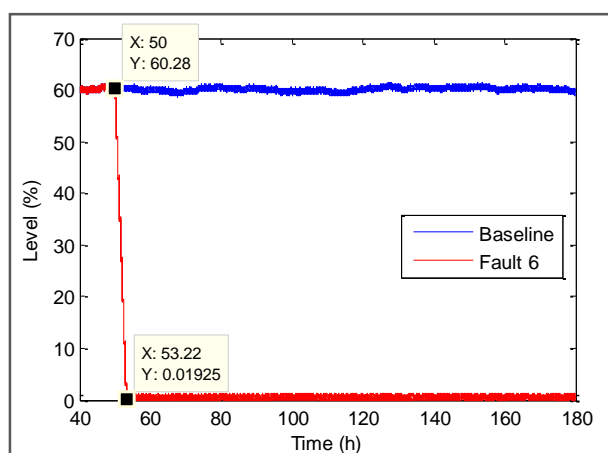
Controllers	TD (%)	AE (%)	MD (%)	TNASP (h)	SD (%)
Autoclave pressure control (bar)	1.29	2964	17570	26.83	4620
Compartment 1 temperature control (°C)	0.00	256.3	2341	3.27	904.0
Compartment 2 temperature control (°C)	0.01	59.75	2078	1.32	543.0
Compartment 3 temperature control (°C)	0.01	89.97	1342	0.00	392.0
Compartment 4 temperature control (°C)	0.00	10140	5725	61.97	8802
Second stage slurry preparation tank level control (%)	0.00	16480	3984	129.6	4217
Second stage slurry preparation tank density (kg/l)	0.00	2124	535.4	124.2	719.7

Valves	TD (%)	AE (%)	TNASP (h)	VR (%)	CS (#)	TS (h)	LTS (h)
Compartment 2 temperature control valve (%)	62.07	75.33	0.00	-12.13	0	0.00	0.00
Compartment 3 temperature control valve (%)	92.05	97.69	0.00	-36.44	0	0.00	0.00
Compartment 4 temperature control valve (%)	-55.53	-57.60	0.00	-62.43	21	86.54	37.18
Spent electrolyte flow control valve (%)	-34.92	-32.10	0.01	-3.51	0	0.00	0.00

Operational KPIs	Compartment 1	Compartment 2	Compartment 3	Compartment 4
Total PGMs in liquid (%)	14.81	31.09	21.11	128300
Total BMs in solid (%)	-1.15	1.67	1.20	31.68

Operational KPIs	
Decrease in total BM input (%)	89.53
Decrease in total PGM input (%)	89.92
Decrease in total solid throughput (%)	85.35
Total oxygen usage (%)	-64.25
Total steam usage (%)	34.72
Compartment 2 CW usage (%)	-87.20
Compartment 3 CW usage (%)	-81.97

The second stage slurry preparation tank level profile is shown in Figure 9.28.


Figure 9.28: Level of second stage slurry preparation tank during fault 6 – Peristaltic pump tube failure

The first stage leach residue flow rate is used as a secondary loop within the second stage slurry preparation tank level controller. The first stage leach residue pipeline blockage results

in a loss of level controllability. Figure 9.28 substantiates the major decrease in second stage slurry preparation tank level control performance, and notably the large time not at level set-point. The level decreases to such an extent that the second stage slurry preparation tank level interlock activates which stops the outlet flow (i.e. the feed to the flash recycle tank). The abrupt decrease in the first stage leach residue flow rate should cause the spent electrolyte and formic filtrate flow rates into this vessel to decrease in a similar way (i.e. through the solid percentage feedforward controller which reduces these flow rates in order to upkeep the solid percentage set-point). However, the spent electrolyte and formic filtrate flow rates do not decrease to an absolute zero. This is attributed to the first stage leach residue flow rate measurement which is not exactly zero (the first stage leach residue flow rate sensor noise causes small spent electrolyte and formic filtrate flow rate set-points - a similar feature seen and discussed in Section 9.4.5). The level safety interlock therefore activates and deactivates numerous times since the vessel is fed by the non-zero spent electrolyte and formic filtrate flow rates which do not match the outlet flow rate requirement of 3 m³/h. The following figure shows the second stage slurry preparation tank density profile.

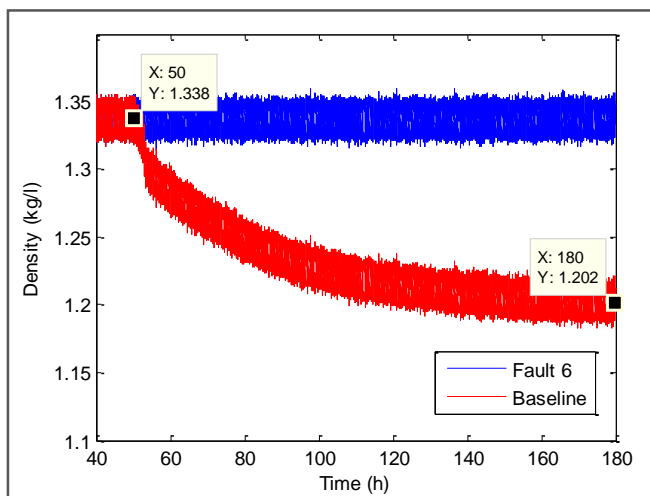


Figure 9.29: Density of second stage slurry preparation tank during fault 6 – Peristaltic pump tube failure

The non-zero spent electrolyte and formic filtrate flow rates causes a decrease in the second stage slurry preparation tank density. This is understandable since the only material entering this vessel is of low density (i.e. having a solid fraction of zero) which replaces the higher density slurry present in the vessel (i.e. having a non-zero solid fraction). This explains the decrease in second stage slurry preparation tank density control performance seen in Table 9.12. The decrease in density plateaus at a density of 1.2 kg/l which corresponds with the density of the spent electrolyte and formic filtrate material (i.e. the point where the solids are entirely replaced by liquid).

The abrupt decrease and subsequent low feed rate to the flash recycle tank causes a significant increase in the first, second and third compartment residence times. The increased residence time causes a variation in heat released within each compartment. This explains the high maximum deviation of these compartment temperatures. Notice that these three compartment temperatures have relatively low time not at set-point KPI values when considering the fact that the solids fed to the process was abruptly terminated (i.e. the source of heat). Figure 9.30 shows the solid fraction of the first three autoclave compartments.

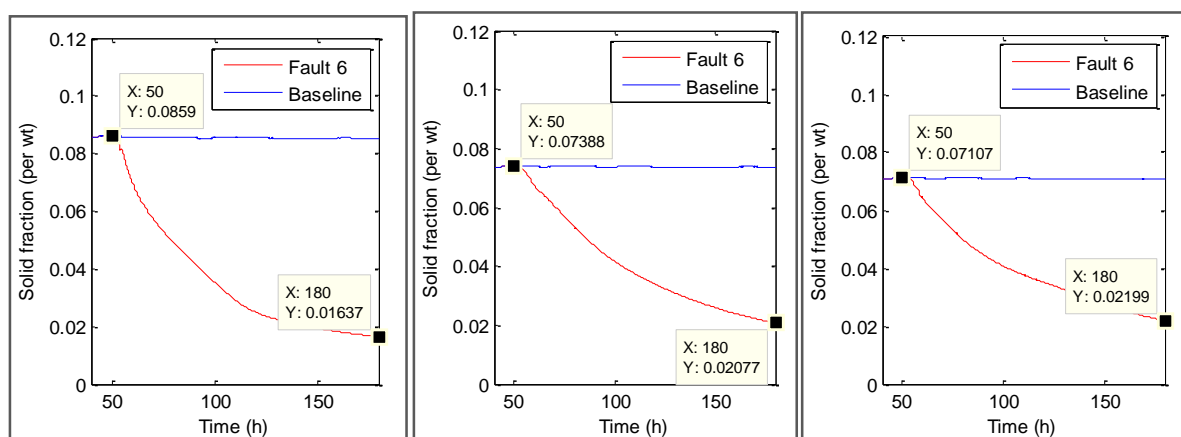


Figure 9.30: Solid fraction of compartment 1 (left), 2 (middle) and 3 (right) during fault 6 – Peristaltic pump tube failure

The solid fraction of the slurry in the compartments decrease over time as the base metals are leached and as small amounts of material is replaced by the overflow stream. Trends in Figure 9.30 and the low corresponding time not at temperature set-point values in Table 9.12 together suggest that the solids present in the first three compartments are sufficient in sustaining the required temperature even after the termination of the solids fed. That said, the inventory available in both the second stage slurry preparation flash recycle tanks also contribute to the extended solid loading in the autoclave. The temperature control performance in these three compartments will decrease if the simulation had to be continued. The solid fraction trends shown in Figure 9.30 are expected to decrease quicker in the actual process due to the increased rate of base metal leaching. The temperatures in these compartments are therefore also suspected to start to deviate from the set-point at an earlier stage in the actual process.

The fourth compartment temperature controller shows a large time not at set-point KPI value which suggests that the solids present in this compartment were insufficient in sustaining the required temperature. Figure 9.31 shows the solid fraction of the stream exiting the fourth autoclave compartment.

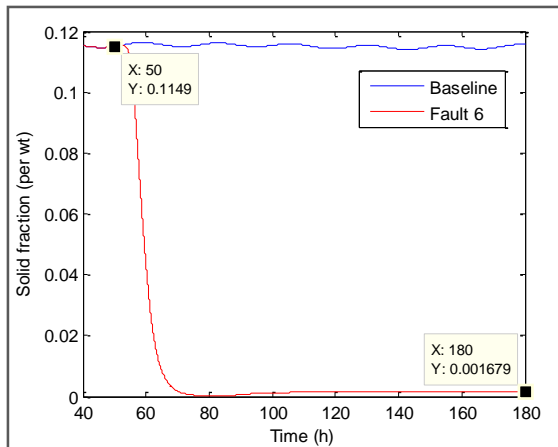


Figure 9.31: Solid fraction of compartment 4 during fault 6 – Peristaltic pump tube failure

Notice that the solid fraction trend for the fourth compartment decreases much more rapidly than that of the first three compartments. This is attributed to the constant fourth compartment feed of $1.42 \text{ m}^3/\text{h}$ while the third compartment outlet flow reduced significantly. The reduced third compartment outlet flow rate is ultimately compensated for by mostly water prior to entering the fourth compartment (i.e. water is used to control the level in the third stage slurry preparation tank). The reduced solid loading causes less heat to be released per unit of fourth compartment volume, which results in an increase in steam usage and fourth compartment temperature control valve saturation. Similar behaviour was noticed during the impeller wear fault, which makes sense since both these faults result in a reduced third compartment outlet flow rate.

The fact that the fourth compartment temperature control valve saturated explains the reduction in its travel distance, average error and valve reversals. A significant reduction in the travel distance and average error of the spent electrolyte flow control valve is noticed. This is attributed to the lower valve actuation due to the lowered variation in spent electrolyte flow rate set-point (remember that the set-point of this flow rate is calculated from the first stage leach residue flow rate which is in this case zero with some measurement noise). Notice that the average error and travel distance of both the second and third compartment temperature control valves increase while their valve reversals decrease. This is attributed to its comparison to a baseline with valve reversals resulting from small scale controlled variable variation which ultimately causes the valve to change direction after moving very small distances.

Figure 9.32 shows the total PGMs in the liquid and total base metals in the solid phase relative to the baseline.

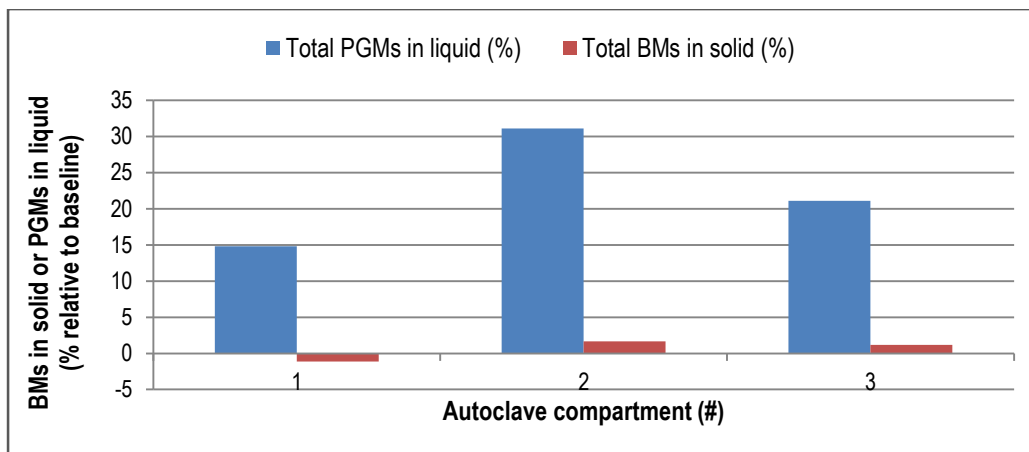


Figure 9.32: PGMs in liquid and BMs in solid for fault 6 – Peristaltic pump tube failure

An increase in PGMs present in the liquid phase is noticed for the first three autoclave compartments. This is attributed to a combination of the reduced rate of PGM precipitation due to a reduced available base metal surface area, and the increased extent of PGM leaching due to the increased residence time. Only a small variation is seen in the solid phase base metals. This could be attributed to a contest between a reduced rate of base metal leaching for those reactions which are dependent on base metal concentrations, and the increase in residence time which increases the base metal holding time. The fourth compartment was excluded from Figure 9.32 due the significant PGM value (it would conceal the trends in the other compartments). This significant value is attributed to the reduced rate of PGM precipitation in the fourth compartment due to the small ratio between the solid base metals and liquid PGMs.

The significant decrease in base metals and PGMs fed to the process is caused by the inability to feed new solids to the process. This also explains the significant reduction in solid throughput. Less solid base metals are available to react and produce heat which describes the significant reduction in cooling water requirements.

9.4.8. Sulphuric acid controller misuse

Figure 9.33 shows the profiles of the flash recycle tank acid concentration and acid flow rate for both the baseline and fault runs. The baseline acid concentration in the flash recycle tank varies around its 20 g/l set-point as the operator switches the acid flow controller on and off in a timely manner. Significant acid concentration spikes are evident after 50 simulation hours in the case of the fault run.

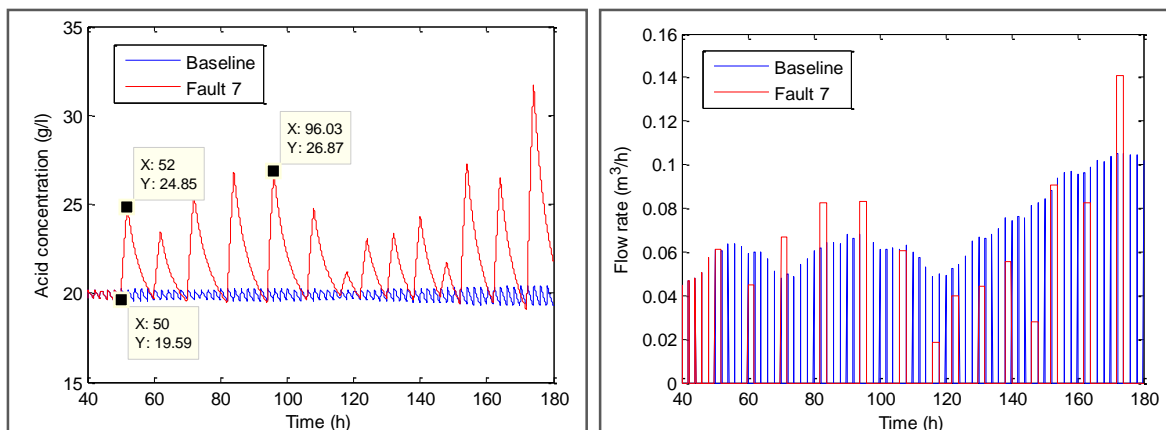


Figure 9.33: Verification of fault 7 occurrence: Flash recycle tank acid concentration (left) and acid flow rate (right)

The operator forgets to timeously switch off the acid flow controller which ultimately causes major acid concentration increases in the flash recycle tank and subsequently the autoclave. The set-point of the acid flow controller is held for 2 hours instead of the standard 10 minutes evident in the baseline. Figure 9.33 verifies the occurrence of the acid controller misuse in this simulation run.

Table 9.13 captures final KPI values that show significant variation from the baseline.

Table 9.13: Significant KPIs for fault 7: Sulphuric acid controller misuse

Controllers	TD (%)	AE (%)	MD (%)	TNASP (h)	SD (%)
Autoclave pressure control (bar)	0.00	94.13	116.5	0.00	99.98
Compartment 1 temperature control (°C)	0.00	52.02	102.7	0.00	65.63
Compartment 2 temperature control (°C)	0.00	37.01	67.60	0.00	45.13
Compartment 3 temperature control (°C)	0.00	7.08	8.33	0.00	7.40
Compartment 4 temperature control (°C)	0.00	-0.01	-0.03	0.00	-0.01

Valves	TD (%)	AE (%)	TNASP (h)	VR (%)	CS (#)	TS (h)	LTS (h)
Compartment 2 temperature control valve (%)	8.44	8.62	0.00	-8.80	0	0.00	0.00

Operational KPIs	Compartment 1	Compartment 2	Compartment 3	Compartment 4
Total PGMs in liquid (%)	2.20	5.22	8.20	2.91
Total BMs in solid (%)	-0.41	-2.26	-2.68	-2.78

Operational KPIs	
Decrease in total BM input (%)	0.00
Decrease in total PGM input (%)	0.00
Decrease in total solid throughput (%)	1.90
Total oxygen usage (%)	1.22
Compartment 2 CW usage (%)	14.97
Compartment 3 CW usage (%)	4.02

The largest KPI performance variations are that of the autoclave pressure controller. The autoclave pressure controller is however not at the location of fault origin. The fault propagation needs to be considered in order to understand the effects on this controller.

A significant average error, maximum deviation and standard deviation with an insignificant time not at set-point are noticed for the pressure controller. This suggests oscillation or variation around its set-point without any significant offset. A similar conclusion can be drawn for the temperature in the first and second compartments. Figure 9.34 shows the first and second compartment temperature profiles for both the baseline and fault runs. The acid concentration spikes shown in Figure 9.33 affect the compartment temperatures through its effect on the oxygen solubility and its natural association with the rate of base metal leaching. An increase in acid concentration reduces the oxygen solubility which ultimately reduces the rate of oxygen-dependent base metal leaching and therefore heat released (refer to Equation D.5 to Equation D.7). However, the rate of certain base metal reactions including that of millerite and digenite leaching (refer to Reaction 1, Reaction 3 and their associated rate expressions presented in Table D.1) are increased to some extent due to the acid concentration being present in their rate expressions (i.e. an increase in acid concentration increases the rate of these reactions).

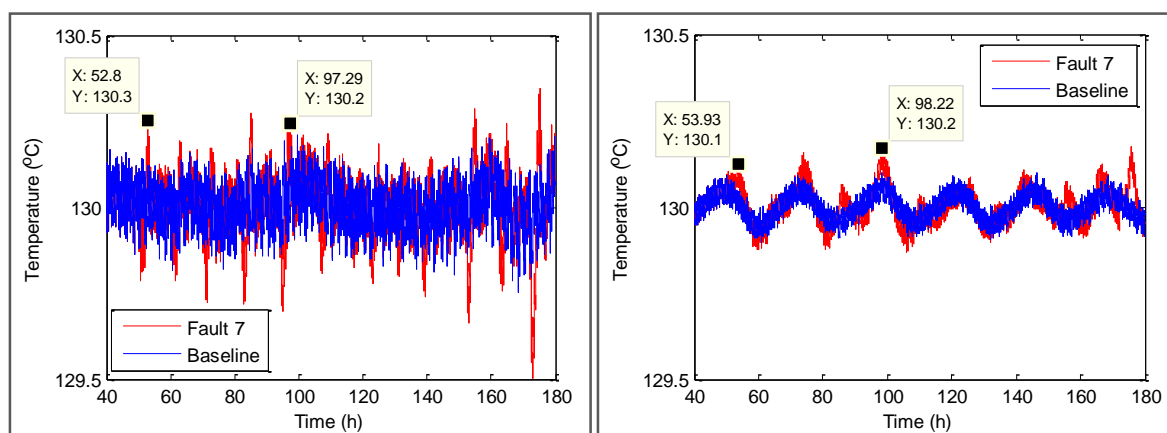


Figure 9.34: Temperature in compartment 1 (left) and compartment 2 (right) during fault 7 – H₂SO₄ controller misuse

A clear increase in temperature error and deviation exists. This error and deviation occurs not far from the temperature set-points of 130 °C as predicted by the KPIs. The frequency of these temperature deviations correlates somewhat with that of the acid concentration spikes depicted in Figure 9.33. Exact time correlation is not evident since the acid concentration spikes present in the flash recycle tank disturbs the downstream compartments over a significant period of time. The extent to which the compartment temperatures are affected by the acid concentration spikes reduce with an increasing compartment number (consider the colour scale for temperature controllers in Table 9.13). This is attributed to the inherent

disturbance attenuation ability of process volumes. The acid spikes reduce in size since the acid dilutes when moving through downstream process units. The acid concentration spikes are undetectable when reaching the fourth compartment. This is attributed to the fact that the solids entering the fourth compartment are mixed with a new liquid phase after being thickened.

The detrimental effects of pressure variation on compartment temperatures were highlighted in Section 9.4.6. Pressure variation exists in this fault run, but the fourth compartment shows no symptoms. Consider the pressure profile for this run.

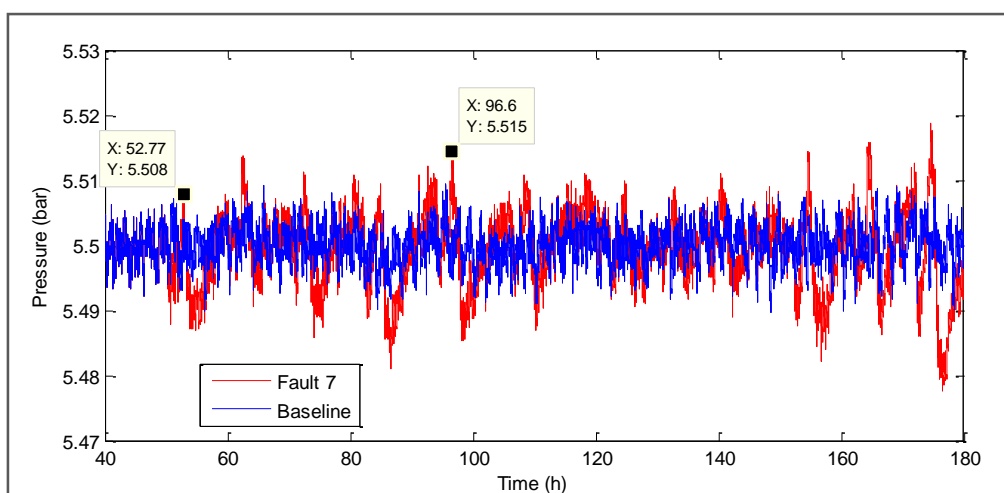


Figure 9.35: Autoclave pressure during fault 7 – H₂SO₄ controller misuse

The average error, maximum deviation and standard deviation of the autoclave pressure increases to 0.0042 bar, 0.022 bar and 0.005 bar, respectively. The oxygen partial pressure is unaffected by the small absolute reduction in autoclave pressure and upstream compartment temperature control performance, which leaves the fourth compartment temperature control performance unaffected.

Figure 9.36 shows the total PGMs in the liquid and total base metals in the solid phase relative to the baseline.

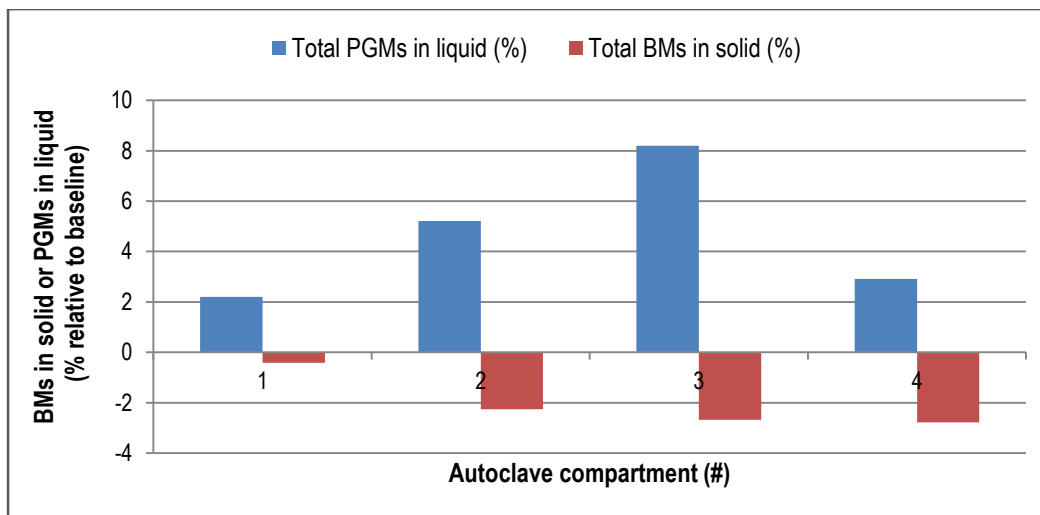


Figure 9.36: PGMs in liquid and BMs in solid for fault 7 – H₂SO₄ controller misuse

The decrease in base metals present in the solid phase suggests that the base metals leached further than that of the baseline when acid concentrations are increased. This corresponds with the decrease in solid throughput and increase in both the cooling water and oxygen usage. It also suggests that the inhibiting effect on base metal leaching via the reduction in oxygen solubility is overpowered by the increase in rate of millerite and digenite leaching (these two reactions contain the acid concentration in their rate expression, as previously stated). It has been shown that the dynamic process model underpredicts the extent of base metal leaching. It is also known that the higher ratio base metal-sulphide minerals (i.e. digenite and millerite) tend to leach first. It makes sense by this logic that the extent of base metal leaching increases since the extent of base metal leaching in the baseline is dominated by digenite and millerite leaching. This notion is substantiated by the fact that an increase in PGM leaching is evident. The digenite leaches faster at higher acid concentration which initiates the start of PGM leaching at an earlier stage. The earlier initiation of PGM leaching reactions effectively causes more PGMs to be leached, even though the rate of PGM leaching is reduced by the reduction in oxygen solubility (most of the PGM leaching reactions are oxygen-dependent, refer to the rate expressions presented in Table D.1). The rate of PGM cementation via digenite leaching is also reduced since these reactions (Reaction 7 to Reaction 9) depend on the availability of digenite surface area. This also contributes to the increase in PGMs present in the liquid phase (refer to Rate expression 7 to Rate expression 9 in Table D.1).

9.4.9. Bubbler level sensor blockage

Figure 9.37 shows the third compartment level profile for both the baseline and fault runs.

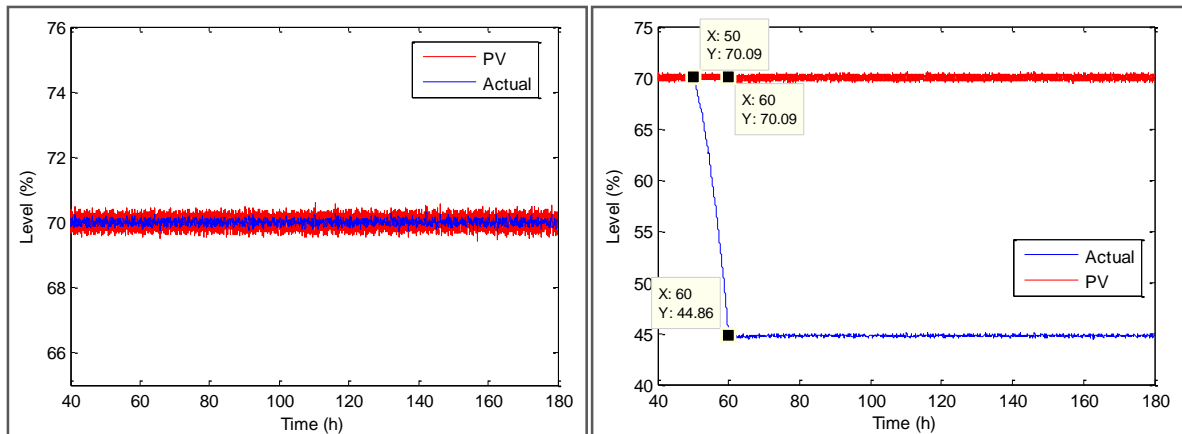


Figure 9.37: Verification of fault 15 occurrence: Compartment 3 level for the baseline (left) and fault (right)

The actual level shown in Figure 9.37 refers to the noiseless real level. The actual level and present-value level (i.e. the measured level) corresponds in the case of the baseline (differs only with a normally distributed measurement noise). The actual level clearly deviates from the measured level at 50 simulation hours in the case of the fault run. The third compartment level controller at 50 hours attempts to reduce the measured level from 70.09 % to its intended 70 % set-point by increasing the outlet flow rate. However, the level sensor is blocked and reports a constant level which corresponds with the level at the initiation of the fault (i.e. 70.09 %). This causes the actual level to decrease as the level controller continues in attempting to decrease the measured level. The level sense tube is blocked for a total of 10 hours (refer to Table 9.4). The level controller manages to mitigate the measured level offset when the measured level starts to move again (i.e. when the solids in the level sensor is unblocked at 60 hours). A clear offset between the actual and measured level exists at this point in time which signifies the solids that are still present in the sense tube. Figure 9.37 verifies the occurrence of the level sensor blockage in this simulation run.

Table 9.14 captures final KPI values that show significant variation from the baseline. The third compartment level controller shows the largest variation in KPIs after the occurrence of level sensor blockage. The third compartment level is exactly the location at which the fault occurs. A small travel distance with a large average error and time not at set-point is evident for the level controller, which suggests the occurrence of an offset. This statement is verified when Figure 9.37 is considered.

Table 9.14: Significant KPIs for fault 15: Level sensor blockage

Controllers	TD (%)	AE (%)	MD (%)	TNASP (h)	SD (%)
Compartment 3 temperature control (°C)	0.00	-3.36	12.28	0.00	-0.66
Compartment 3 level control (%)	5.25	36150	8034	127.0	9634

Operational KPIs	Compartment 1	Compartment 2	Compartment 3	Compartment 4
Total PGMs in liquid (%)	0.00	-0.01	26.52	-1.62
Total BMs in solid (%)	-0.01	0.00	1.79	1.72

Operational KPIs	
Decrease in total BM input (%)	0.00
Decrease in total PGM input (%)	0.00
Decrease in total solid throughput (%)	-1.29
Total oxygen usage (%)	-0.61
Compartment 2 CW usage (%)	-0.01
Compartment 3 CW usage (%)	-18.24

Consider the open-loop steady-state gain achieved for a step change in the cooling water flow rate:

$$K_{CW,T} = \frac{\Delta T_{comp\ 3}}{\Delta F_{CW}} \quad \text{Equation 9.3}$$

A significant increase in the steady-state gain shown in Equation 9.3 is expected when the level is operated at a lower percentage (not only a larger steady-state gain but also a quicker transfer response). This causes a slight improvement in the third compartment temperature control (i.e. a reduced average error). A temperature controller which is tuned too control aggressively could in a similar situation reduce the temperature controllability. A significant change in this process steady-state gain could cause an aggressive temperature controller to overshoot or undershoot in the case of disturbances, and reduce temperature controllability.

Figure 9.38 shows the total PGMs in the liquid and total base metals in the solid phase relative to the baseline.

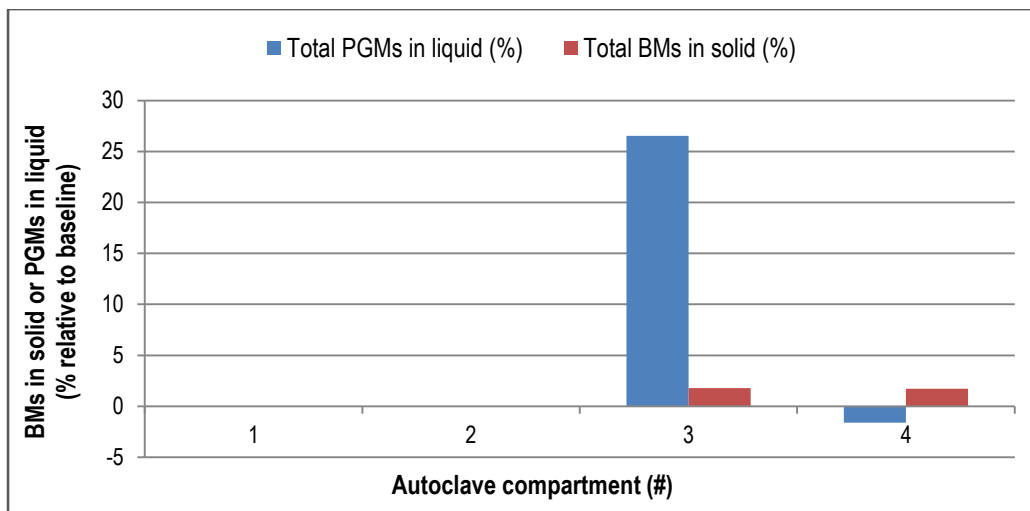


Figure 9.38: PGMs in liquid and BMs in solid for fault 15 – Level sensor blockage

The metal leaching upstream of the third compartment is clearly unaffected. This makes sense since the fault occurs at the third compartment. In addition, the fault does not affect the vapour conditions (i.e. vapour temperature and autoclave pressure) and therefore not the upstream compartment behaviour.

An increase in PGMs present in the third compartment liquid phase is evident. Reconsider Figure 9.4 which shows the extent of total PGMs leached during the baseline run. Figure 9.4 indicates that the PGMs are precipitated from the liquid phase as the compartment number increases. The significant increase in PGMs present in the third compartment liquid phase during the level sensor blockage is attributed to the reduced residence time caused by the smaller third compartment operating volume. The reduced residence time reduces the time in which PGMs can be precipitated. An increase in base metals present in the solid phase is also expected when following this logic, which is in fact what happens when Figure 9.38 is considered. The increase in base metals in the solid phase carries through to the fourth and final compartment, as expected.

The PGMs present in the liquid phase shows a significant drop from the third to fourth compartment. This is explained when considering the mechanism of the thickener. The thickener passes only solids through to the fourth compartment. The slight reduction in PGMs present in the fourth compartment liquid phase could be attributed to the reduced PGMs in the third compartment solid phase which reduces the rate at which PGMs are leached in the fourth compartment (since the PGM-mineral concentrations are present in the PGM leaching rate expressions - refer to Rate expression 13 to Rate expression 21 in Table D.1).

The increase in base metals present in the fourth compartment solid phase corresponds with the increase in solid throughput and the decrease in oxygen usage. The reduction in specifically the third compartment cooling water requirement also corresponds with the reduced extent of base metal leaching seen in this compartment (caused by the reduction in third compartment residence time).

9.5. Summary

The dynamic process model control performance was tested during the occurrence of eight independent medium-to-high priority faults seen Western Platinum BMR. The performance of 14 controllers, 8 valves, and 18 operational measurements strategically placed around the process served as a way to quantify the overall process performance. The control performance was expressed in terms of several key performance indicators and evaluated against a faultless baseline run. The key performance indicators in the case of faults were reported as percentage deviation from the baseline.

Figure 9.39 orders the faults based on their impact on the process performance (i.e. the hierarchy for mitigating control performance issues shown in Figure 9.1, related to important control loops such as pressure and temperature within the autoclave) and the extent to which the faults show significant propagation through the process.

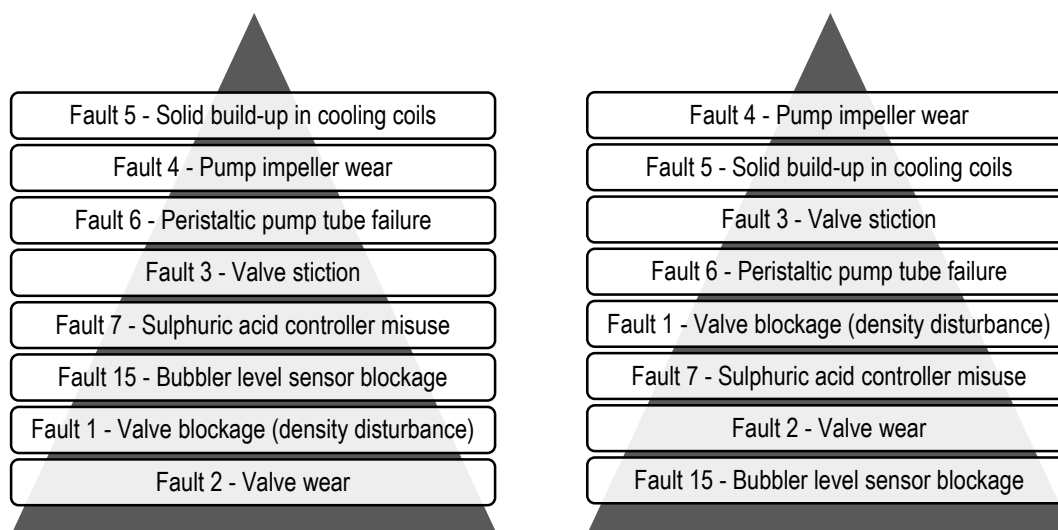


Figure 9.39: Hierarchy of faults based on performance impact (left) and least localised (right)

The solid build-up and pump impeller wear faults caused the largest process performance degradation while also propagating through most of the measured key performance indicators. These faults are the least localised since they have a major effect early in the

process which results in a propagation of symptoms. The large performance impact seen for both these faults correspond with experts from Western Platinum BMR which classifies their mitigation priority as high (shown in the fault database - refer to Table F.11). A high priority for mitigation suggests significant process performance degradation. Achieving control objectives such as smooth plant operation and production rate; product quality; and optimisation of profit were restricted during pump impeller wear (refer to Section 2.4.1 for generic control objectives). The solid build-up fault limited the protection of equipment and the safety of personnel, in addition to reducing product quality and producing unsmooth operation. Operators are expected to intervene after serious and obvious fault occurrences (i.e. visible through controlled variable deviation), but this would ultimately result in process downtime and therefore a reduced profit due to a reduced throughput.

The valve wear and level sensor blockage faults caused minimal deviation in process performance while also propagating through only a few of the measured key performance indicators. These faults occur in the latter part of the process and do not affect the autoclave temperature and pressure, which explains their localised symptoms. The symptoms of the worn valve fault are expected to be underpredicted as expert knowledge classified this fault as having a high priority for mitigation. The smaller performance impact of the level sensor blockage corresponds with the fault database which indicates only a medium priority for mitigation.

The density disturbance in the first stage leach residue proved to have minimal effects on process performance. However, the fault database indicates that the density disturbance has a high priority for mitigation. The first stage leach residue density disturbance is however the fault that occurs the most often at Western Platinum BMR. The cumulative effects of this disturbance might show a significant increase in process degradation if its frequency were comparable to other faults.

The modelled valve stiction and sulphuric acid controller misuse faults have a medium impact on process performance according to Figure 9.39. This corresponds with expert knowledge from Western Platinum which classifies it with a medium priority for mitigation.

The peristaltic pump tube failure caused the solids fed to the process to be terminated. This was therefore naturally classified by experts as a high priority, and corresponds to the performance impact hierarchy shown in Figure 9.39.

It has been shown that different faults exhibit different variable symptoms and also influence the KPIs in different manners. The fault signatures produced in this chapter could possibly

be used as a baseline at Western platinum BMR in an attempt to detect and identify fault occurrences via operators.

CHAPTER 10: CONCLUSIONS AND RECOMMENDATIONS

The conclusions are summarised in accordance with the specific objectives and tasks outlined in Chapter 5.

10.1. Model Verification and Validation

The open-loop dynamic process model developed by Dorfling (2012) and subsequently improved by Haasbroek and Linder (2015) was validated in order to build trust in the model predictability. Also, the validation process also provided an indication of necessary dynamic process model improvements required prior to undertaking other project objectives.

The dynamic process model cannot currently predict the extent of metal leaching. This is expected to be caused by batch experimental (i.e. used to develop reaction kinetics) conditions which did not correspond to that of Western Platinum BMR as the experimental acid concentrations were significantly higher.

Global tests conducted on flow rates from plant data at steady-state were indicative of significant biases and therefore limits the ability to quantitatively validate the model operation by using plant data as inputs. Extreme condition testing, static testing and face validation was however used to qualitatively validate and improve the model robustness, while dynamic testing was used to prove consistent mass balances. The updated dynamic process model was therefore able to handle extreme situations which are expected to occur during fault occurrences.

10.2. Control Implementation

Control strategies within the dynamic process model are required in order to assess control performance during the occurrence of abnormal events. More specifically, control strategies similar to that of Western Platinum BMR is required in order to mimic the actual operation.

A closed-loop dynamic process model was developed which mimics the operation and control seen at Western Platinum BMR. The closed-loop model comprise of 35 sensors; 21 actuators; 30 regulatory controllers; 33 alarms systems; 37 safety interlocks; and 4 supervisory controllers. A site visit provided control layer information which is currently

implemented at Western Platinum BMR (McCulloch et al., 2014). Each control layer was simulated and its behaviour validated.

The developed closed-loop dynamic process model can be used as a tool in operator training which is expected to assist in developing operator decision making.

10.3. Fault Database Creation and Simulation

A fault database was developed which is composed of 17 faults found at Western Platinum BMR. These faults include structural failures, actuator failures, sensor failures, process disturbances, operator interventions and controller malfunctions. Each fault entry contains valuable information such as fault transition rate, frequency of occurrence, priority for mitigation, type and symptoms. The fault database can also be used as a means of information transfer between several Western Platinum BMR operators and personnel.

A total of 12 faults were modelled using process knowledge and data-driven empirical correlations. The behaviour of each fault was validated using artificial inputs. The modelled faults have mitigation priorities of either medium or high. The modelled faults are therefore useful since finding ways to timely mitigate their occurrence will prove to be beneficial. The modelled faults together with the closed-loop dynamic process model allow the development and testing of fault detection and diagnostic algorithms for Western Platinum BMR.

10.4. Control Performance Assessment

A total of 8 modelled faults were individually used to assess the control performance of the closed-loop model in order to establish what effects faults have on process performance.

A wide range process performance impacts were noticed for the variety of faults. The mitigation priority hierarchy established by experts from Western Platinum BMR correlate well with the performance impact predicted by the dynamic process model. The localisation of faults proved to be dependent on both the fault origin and the extent to which it disturbs the process.

Several KPIs decreased during the occurrence of certain faults. The fact that a KPI decreases does not necessarily indicate improved process performance. A decrease in a KPI might prove to be beneficial in the short-term, but could easily lead to significant process

degradation when process conditions change. Any KPI variation, irrespective of direction, is indicative of a process regime shift and should be further investigated.

10.5. Recommendations

It is recommended that additional batch experiments are done at a lower solid loading and acid concentration. This will ensure that comparable conditions are obtained in the batch reactor, and will provide data so as to refit the current reaction kinetics. Additional batch experiments could also allow one to quantify and redefine the available surface area and therefore avoid rate expression issues such as defining initial concentrations.

The dynamic behaviour of the model needs to be quantitatively compared to plant data in order to conclude on model operational validity. Data sets need to be identified which do not contain significant biases. Dynamic data reconciliation can then be applied to these data sets so as to produce consistent and accurate plant data (possibly only after addressing sensor issues). These reconciled data sets can be used to confidently validate the dynamic process model behaviour. More compositional data points will also be required so as to confidently validate the base metal and PGM leaching.

Several other issues still exist in the dynamic process model, but the extents to which they reduce the model accuracy are unknown. It is recommended that these issues are classified based on the extent to which they reduce the model accuracy, and that they are addressed accordingly.

The behaviour of the control layers have been validated using mostly artificial inputs. It is recommended that the control strategy used in the dynamic process model is compared and validated to that of Western Platinum BMR (i.e. that the dynamic process model control behaviour is similar to that of the actual process). This will require the dynamic data reconciliation as previously discussed.

One of the major outcomes of this project is a closed-loop dynamic process model that mimics the Western Platinum BMR. This model can be used together with the modelled faults to develop and test fault detection and diagnostic algorithms for Western Platinum BMR. Moreover, fault signatures produced in this this project could possibly be used as a baseline at Western platinum BMR in an attempt to detect and identify fault occurrences through expert interpretation.

CHAPTER 11: FUTURE WORK

This chapter provides brief methodologies which could be followed as to address recommendations. Completing such a methodology should provide a novel contribution to the field of study.

11.1. Model Predictability

The following condensed procedure is expected to improve the model composition predictability:

1. Re-do batch experimentation
 - a. Lower solid loading and initial acid concentration
 - b. Varying factors: Pressure, initial acid concentration, particle size⁷, temperature⁷
 - c. Number of levels: 3
 - d. Ion species to measure⁸: [Cu²⁺], [Ni²⁺], [Fe³⁺], [H⁺], [Rh³⁺], [Ru³⁺], [Ir³⁺]
 - e. Additional measurements: Precipitation mass and composition (if precipitation occurs), available surface area or particle size
2. Improve the method used to quantify the available surface area in the reaction kinetics (link the improved method to available surface area or particle size measurements)
3. Fit the updated reaction kinetics to the new experimental data using MATLAB™ global optimisation
4. Implement the improved reaction kinetics into the Simulink™ dynamic process model
5. Implement population balances into the dynamic process model which produce available surface area information used in the improved reaction kinetics

This methodology can be completed over a period of 1 - 2 years.

⁷ Possible factors to vary (temperature included here since activation energies of each reaction was already determined).

⁸ Investigate the possibility of distinguishing between ion species.

11.2. Fault Detection and Diagnosis

The following condensed procedure can be used to develop fault detection and diagnosis techniques which can ultimately be used at Western Platinum BMR:

1. Identify feature extraction models which can be used in the fault detection investigation (i.e. techniques such as principal component analysis or kernel principal component analysis)
2. Generate faultless baseline dynamic process model data
3. Train the feature extraction models with the generated data
4. Generate faulty dynamic process model data
5. Project the faulty dynamic process model data onto the feature extraction models
6. Compare the ability of feature extraction models to detect fault occurrences, and select the best candidate
7. Use the best candidate and repeat step 3 – 5 on Western Platinum BMR plant data
8. Investigate the possibility of fault identification techniques

This methodology can be completed over a period of 1 year.

REFERENCES

- AEG, 2015. *Evans Analytical Group*. [Online] Available at: <http://www.eag.com/mc/icp-oes-vs-icp-ms.html> [Accessed 19 October 2015].
- Ahmad, A., 2008. *Process Control Strategy*. [Document] Available at: http://www.cheme.utm.my/staff/arshad/images/lecture/POT/2.2_singleloopcontrol.pdf [Accessed 10 June 2015].
- Almasy, G. & Szatno, T., 1975. Checking and Correction of Measurements on the Basis of Linear System Model. In *Problems of Control and Information Theory*. pp.57-69.
- Anon., 1979. *Process instrumentation terminology*. Technical report. Instrument Society of America.
- Anyakora, S.N., 1971. *Malfunction of Process Instruments and Its Detection Using a Process Control Computer*. PhD Thesis. Loughborough: Loughborough University of Technology.
- Bagajewicz, M., 1996. On the probability distribution and reconciliation of process plant data. *Computers Chemical Engineering*, 20, pp.813-19.
- Bainbridge, L., 1983. Ironies of Automation. *Automatica*, 19(6), pp.775-79.
- Balci, O., 1997. Verification, Validation and Accreditation of Simulation Models. *Proceedings of the Winter Simulation Conference*, pp.135-41.
- Banks, J., Gerstein, D. & Searles, S., 1987. Modeling processes, validation, and verification of complex simulations: a survey. In *1987 SCS Simulators Conference*, pp.13-18.
- Bartelt, T., 2007. *Instrumentation and process control*. Thomson Delmar Learning.
- Bartys, M. & de las Heras, S., 2003. Actuator Simulation of the DAMADICS Benchmark Actuator System. In *SafeProcess*. Washington DC, 2003.
- Bartys, M. et al., 2006. Introduction to the DAMADICS actuator FDI benchmark study. *Control Engineering Practice*, 14, pp.577-96.
- Bauer, M. & Craig, I.K., 2008. Economic assessment of advanced process control – A survey and framework. *Journal of Process Control*, 1(18), pp.2-18.

- Beall, J., n.d. *Emerson Process Experts*. [Online] Emerson Available at: <http://www.emersonprocessxperts.com> [Accessed 24 July 2015].
- Bernardis, F.L., Grant, R.A. & Sherrington, D.C., 2005. A review of methods of separation of the platinum-group metals through their chloro-complexes. *Reactive & Functional Polymers*, 65, pp.205-17.
- Bialkowski, W., 1993. Dreams vs reality. A view from both sides of the gap. *Pulp & Paper Canada*, 94, pp.19-27.
- Buchanan, D.L., 2012. *Platinum Group Element Exploration*. Chicago: Elsevier.
- Buchanan, D.A. & Bessant, J., 1985. Failure, Uncertainty and Control: The Role of Operators in a Computer Integrated Production System. *Journal of Management Studies*, 22(3), pp.292-308.
- Buranathiti, T. et al., 2006. Approaches for Model Validation: Methodology and Illustration on a Sheet Metal Flanging Process. *Manufacturing Science and Engineering*, 128, pp.588-97.
- Burkin, A., 2001. *Chemical hydrometallurgy: theory and principles*. London: Imperial College Press.
- Burks, S., 2013. Case studies of simultaneous mining and mineral processing optimization applied to platinum and nickel operations. *The Journal of The Southern African Institute of Mining and Metallurgy*, 113, pp.221-33.
- Burt, C. & Feist, K., 2012. Pump performance with sand wear. In *ITRC*. Reno, 2012.
- Carson, J.S., 2002. Model Verification and Validation. *Winter Simulation Conference*, 1, pp.52-58.
- Center for Chemical Process Safety, 1992. Guidelines for hazard evaluation procedures. *American Institute of Chemical Engineering*, 11(2), pp.50-52.
- Chen, D. et al., 2007. *Handbook of Hyphenated ICP-MS Applications*. 1st ed. USA: Agilent Technologies.
- Choo, W., Jeffrey, M. & Robertson, S., 2006. Analysis of leaching and cementation reaction kinetics: Correcting for volume changes in laboratory studies. *Hydrometallurgy*, 82, pp.110-16.
- Choudhury, M., Thornhill, N. & Shah, S., 2005. Modelling valve stiction. *Control Engineering Practice*, 13, pp.641-58.

Cramer, L.A., 2001. The Extractive Metallurgy of South Africa's platinum ores. *Journal of Metals*, 53(10), pp.14-18.

de Kock, M., 2013. *Simulation, control and fault detection for a base metal refinery high pressure leaching system*. Final Year Project. Stellenbosch: Stellenbosch University.

Desborough, L. & Miller, R., 2002. Increasing customer value of industrial control performance monitoring - Honeywell's experience. *AIChE symposium series*, 98(326), pp.169-89.

DMR, 2009. *Department of Mineral Resources*. [PDF] Available at: <http://www.dmr.gov.za/publications/south-africas-mineral-industry-sami.html>.

Dorfling, C., 2012. *Characterisation and dynamic modelling of the behaviour of platinum group metals in high pressure sulphuric acid/oxygen leaching systems*. PhD Thesis. Stellenbosch: Stellenbosch University.

Dorfling, C., Akdogan, G., Bradshaw, S. & Eksteen, J., 2013. Modelling of an autoclave used for high pressure sulphuric acid/oxygen leaching of first stage leach residue. Part 1: Model development. *Minerals Engineering*, 53, pp.220-27.

Dorfling, C. & Miskin, J., 2015. *Private meeting: Cupric ion decrease discussion*. Stellenbosch.

Downs, J. & Vogel, E., 1993. A plant-wide industrial process control problem. *Computers Chemical Engineering*, 17(3), pp.245-55.

Dutrillac, J. & Chen, T., 1987. A Mineralogical Study of the Phases formed during the CuSO₄-H₂SO₄-O₂ Leaching of Nickel-copper matte. *Canadian Metallurgical Quarterly*, 26, pp.265-76.

Dzvinamurungu, T., 2012. *Geometallurgical characterisation of Merensky Reef and UG2 at the Lonmin Marikana mine, Bushveld Complex, South Africa*. Johannesburg: University of Johannesburg.

Ender, D.B., 1993. Process control performance: Not as good as you think. *Control Engineering*, 40(10), pp.180-90.

Fairley, R., 1976. Dynamic Testing of Simulation Software. *Summer Computer Simulation Conference*, pp.40-46.

- Finch, F., Oyeleye, O. & Kramer, M., 1990. A robust event-oriented methodology for diagnosis of dynamic process systems. *Computers Chemical Engineering*, 14(12), pp.1379-96.
- Gerry, J., 2005. Real-Time Performance Assessment. In B.G. Lipták, ed. *Instrument Engineers' Handbook*. 4th ed. Boca Raton: Butterworth-Heinemann. pp.311-17.
- Glaister, B.J. & Mudd, G.M., 2010. The environmental costs of platinum–PGM mining and sustainability: Is the glass half-full or half-empty? *Minerals Engineering*, 23, pp.438-50.
- Grewal, I. et al., 1992. Total oxidative leaching of Cu₂S-containing residue at INCO Ltd. copper refinery: laboratory studies on the reaction pathways. *Hydrometallurgy*, 29(1-3), pp.319-33.
- Haasbroek, A. & Lindner, B., 2015. *Reconstruction of a BMR MATLAB model into Simulink*. Stellenbosch University.
- Haight, J.M. & Kecojevic, V., 2005. Automation vs. Human Intervention: What is the best fit for best performance? *Process Safety Progress*, 24(1), pp.45-51.
- Harris, T., 1989. Assessment of Control Loop Performance. *The Canadian Journal of Chemical Engineering*, 67, pp.856-61.
- Henning, A., 2014. *Model Validation, Improvement and Development for a Base Metal Refinery High Pressure Leaching System*. Final year project. Stellenbosch: Stellenbosch University.
- Hespanha, J.P., 2015. *Switched Supervisory Control*. [Slideshow] University of California Santa Barbara Available at: <http://www.ece.ucsb.edu/> [Accessed 10 June 2015].
- Himmelblau, D., 1978. *Fault Detection and Diagnosis in Chemical and Petrochemical Processes*. Amsterdam: Elsevier press.
- Hofirek, Z. & Kerfoot, D., 1992. The chemistry of the nickel-copper matte leach and its application to process control and optimisation. *Hydrometallurgy*, 29, pp.357-81.
- Hutchinson, J., ed., 1992. *ISA Handbook of Control Valves*. 2nd ed. NC.
- Incropera, F. & De Witt, D., 1996. *Fundamentals of heat and mass transfer*. 4th ed. New York: John Wiley and Sons.
- Isermann, R., 2005. Model-based fault-detection and diagnosis – status and applications. *Annual Reviews in Control*, 29, pp.71-85.

ITA, 2009. *Instrument Testing Association*. [Online] Available at: <http://www.instrument.org/> [Accessed 17 August 2015].

Jelali, M., 2006. An Overview of Control Performance Assessment technology and Industrial Application. *Control Engineering Practice*, 14, pp.441-66.

Johnson Matthey, 2008. *Johnson Matthey Precious Metal Management*. [Online] Available at: <http://www.platinum.matthey.com/documents/market-review/2008/special-chapter-downloads/south-african-pgm-production.pdf> [Accessed 24 September 2015].

Kanome, O., Abe, H., Okuwaki, A. & Okabe, T., 1987. Sulfuric Acid Oxygen-Pressure Leaching of Ni₃S₂ Prepared by a Wet Process. *Hydrometallurgy*, 19, pp.1-9.

Karlsson, C., 2004. *Tools for reconciliation of measurement data for processes at steady-state*. Sweden: Malardalen University Press Malardalen University.

Kletz, T., 1986. HAZOP & HAZAN notes on the identification and assessment of hazards. *The Institution of Chemical Engineers*.

Kletz, T., 1988. *What went wrong? — case histories of process plant disasters*. 2nd ed. Houston: Gulf Publishing.

Kletz, T., 1991. Incidents that could have been prevented by HAZOP. *Loss Prevention in the Process Industries*, 4, pp.238-129.

Knoblauch, N., 2012. *Preliminary Implementation and Analysis of Control Strategies for Second and Third Stage Leach*. Final Year Project. Stellenbosch: Stellenbosch University Stellenbosch University.

Knoblauch, N., 2014. *Advanced Process Control Development for BMR Pressure Leach*. MEng Thesis in progress. Stellenbosch: Stellenbosch University.

Koscielny, J. & Bartys, M., 2000. Application of information theory for actuators diagnosis. *Fourth IFAC symposium on fault detection, supervision and safety for technical processes*, 2, pp.949-54.

Kuehn, D. & Davidson, H., 1961. Computer control II: mathematics of control. *Chemical Engineering Progress*, 57, pp.44-47.

Lamya, R.M., 2007. *A Fundamental Evaluation of the Atmospheric pre-leaching section of the nickel-copper matte Treatment Process*. Stellenbosch: University of Stellenbosch.

- Lamya, R. & Lorenzen, L., 2006. Atmospheric acid leaching of nickel-copper matte from Impala Platinum Refineries. *Journal of SAIMM*, 106, pp.385-96.
- Landry, M., Malouin, J. & Oral, M., 1983. Model Validation in Operations Research: Review. *European Journal of Operational Research*, 14, pp.207-20.
- Lawler, G. & Vlada, L., 2010. *Random Walk: A Modern Introduction*. Cambridge University Press.
- Lees, F., 1976. The reliability of Instrumentation. *Chemical and Industry*, pp.195-205.
- Liddell, K., McRae, L. & Dunne, R., 1986. Process routes for beneficiation of noble metals from Merensky and UG-2 ores. *Extraction Metallurgy*, 85, p.795.
- Lindner, B., 2014. *Exploiting Process Topology for Optimal Process Monitoring*. MEng Thesis in progress. Stellenbosch: Stellenbosch University.
- Lindsay, N., 1988. *The processing and recovery of the Platinum-group elements*. Johannesburg: University of Witwatersrand.
- Lipták, B.G., 2006. *Process Control: Instrument Engineers' Handbook*. 4th ed. Boca Raton: Butterworth-Heinemann.
- Ljung, L., 2009. *System identification: Theory for the user*. 2nd ed. New Jersey: Prentice-Hall.
- Loferski, P., 2007. *Platinum-group metals, 2007 Minerals Yearbook*. [Online] Available at: minerals.usgs.gov/minerals/pubs/commodity/platinum [Accessed 4 April 2014].
- Madron, T. & Veverka, V.V.V., 1977. Statistical Analysis of Material Balance of a Chemical Reactor. *The American Institute of Chemical Engineers Journal*, 23, pp.482-86.
- Mah, R. & Tamhane, A., 1982. Detection of Gross Errors in Process Data. *The American Institute of Chemical Engineers Journal*, 28, pp.828-30.
- Mainza, A., Powell, M. & Knopjes, B., 2005. A comparison of different cyclones in addressing challenges in the classification of the dual density UG2 platinum ore. *Journal of the South African Institute of Mining and Metallurgy*, 105, pp.341-48.
- Marlin, T.E., 1995. *Process Control: Designing Processes and Control Systems for Dynamic Performance*. 2nd ed. New York: McGraw-Hill.

MathWorks, 2015. *MathWorks*. [Online] Available at: <http://www.mathworks.com> [Accessed 29 June 2015].

Matzopoulos, M., 2011. Dynamic Process Modelling: Combining Models and Experimental Data to Solve Industrial Problems. In M. Georgiadis, J. Banga & N. Pistikopoulos, eds. *Process Systems Engineering: Dynamic Process Modeling*. Weinheim: Wiley. pp.3-33.

Mayer, D. & Butler, D., 1993. Statistical validation. *Ecological Modelling*, 68, pp.21-32.

McCulloch, N., Steenekamp, N. & Mrubata, Z., 2014. *Site visit at Western Platinum BMR*. Marikana, North West, South Africa.

Merrick, C. & Ponton, J., 1995. *University of Edinburgh*. [Online] Available at: <http://www.see.ed.ac.uk> [Accessed 24 July 2015].

Mirsha, P., Kumar, V. & Rana, K., 2014. A novel intelligent controller for combating stiction in pneumatic control valves. *Control Engineering Practice*, 33, pp.94-104.

NCSA, 2003. *Introduction to data reconciliation*. [Online] North Carolina State University Available at: http://www.polymtl.ca/namp/docweb/Modules_Web/ [Accessed 04 September 2015].

Nicol, M., 2014. Mike Nicol Workshop. Cape Town, 2014.

Nordlund, K., 2006. *Monte Carlo simulations*. [PDF] University of Helsinki Available at: www.acclab.helsinki.fi/~knordlun/mc/ [Accessed 16 July 2015].

Patton, R.J., Frank, P.M. & Clark, R.N.(.), 2013. *Issues of Fault Diagnosis for Dynamic Systems*. Springer Science & Business Media.

PID Function Block, 2012. *Washington University in St. Louis*. [PDF] Washington University Available at: <http://classes.engineering.wustl.edu/> [Accessed 24 July 2015].

Provis, J., JSJ, v.D., Rademan, J. & Lorenzen, L., 2003. A kinetic model for the acid-oxygen pressure leaching of Ni–Cu matte. *Hydrometallurgy*, 70, pp.83-99.

Rademan, J.A., 1995. *The Simulation of a Transient Leaching Circuit*. Stellenbosch: Stellenbosch University.

Rademan, J., Lorenzen, L. & van Deventer, J., 1999. The leaching characteristics of Ni–Cu matte in the acid–oxygen pressure leach process at Impala Platinum. *Hydrometallurgy*, 52, pp.231-52.

- Rao, C. & Reddi, G., 2000. Platinum group metals (PGM); occurrence, use and recent trends in their determination. *Trends in analytical chemistry*, 19(9), pp.565-86.
- Rard, J., 1985. Chemistry and Thermodynamics of Ruthenium and Some of Its Inorganic Compounds and Aqueous Species. *Chemical Reviews*, 85(1), pp.1-39.
- Raza, J. & Liyanage, J., 2009. An integrated qualitative trend analysis approach to identify process abnormalities: a case of oil export pumps in an offshore oil and gas production facility. *Proc. IMechE*, 223, pp.251-58.
- Renner, H., 1992. *Ullmann's Encyclopedia of Industrial Chemistry*. 5th ed. Weinstein: Wiley.
- Richmond, G., 2004. The Mount Gordon Copper Process. In *International Colloquium on Hydrometallurgical Processing of Copper Sulfides*. Santiago, 2004.
- Ripps, D., 1965. Adjustment of Experimental Data. In *Chemical Engineering Progress Symposium Series.*, 1965.
- Romagnoli, J.A. & Palazoglu, A., 2012. *Introduction to Process Control*. Boca Raton: CRC Press.
- Ruiz, M., Gallardo, E. & Padilla, R., 2009. Copper extraction from white metal by pressure leaching in H₂SO₄-FeSO₄-O₂. *Hydrometallurgy*, 100, pp.50-55.
- Salmi, T. et al., 2010. Mechanistic modelling of kinetics and mass transfer for a solid-liquid system: leaching of zinc with ferric iron. *Chemical Engineering Science*, 65, pp.4460-71.
- Sargent, R., 2005. Verification and Validation of Simulation Models. *Proceedings of the 37th Winter Simulation Conference*, pp.130-42.
- Schlesinger, S. et al., 1979. Terminology for model credibility. *Simulation*, 32(3), pp.103-04.
- Scholkopf, B., 2015. *Regression Part II*. [PDF] University of Minnesota Available at: <http://gandalf.psych.umn.edu> [Accessed 7 July 2015].
- Seborg, D., Edgard, T. & Mellichamp, D., 2004. *Process Dynamics and Control*. 2nd ed. Wiley.
- Sheridan, T., 1992. *Telerobotics, automation, and human supervisory control*. 1st ed. United States of America: MIT press.
- Steenekamp, N. & Dunn, G., 1999. Operations of and improvements to the Lonrho Platinum Base Metal Refinery. *The Minerals, Metals & Materials Society*, pp.365-78.

- Steenekamp, N., Eksteen, J. & Esbach, A., 2009. *Draft Operating Philosophy: Autoclaves*. Lonmin Group.
- Symens, R., Queneau, P., Chou, E. & Clark, F., 1979. Leaching of Iron-containing Copper-nickel matte at Atmospheric Pressure. *Canadian Metallurgical Quarterly*, 18, pp.145-53.
- Tamhane, A. & Mah, R., 1985. Data Reconciliation and Gross Error Detection in Chemical Process Networks. *Technometrics*, 27(4), pp.409-22.
- Tano, K., 2005. *Continuous Monitoring of Mineral Processes with Special Focus on Tumbling Mills*. PhD Thesis. Luleå, Sweden: Luleå University of Technology.
- Thornhill, N., Huang, B. & Zhang, H., 2003. Detection of multiple oscillations in control loops. *Journal of Process Control*, (13), pp.91-100.
- Tromans, D., 1998. Oxygen solubility modelling in inorganic solutions: concentration, temperature and pressure effects. *Hydrometallurgy*, 50, pp.279-96.
- USGS, 2009. *Mineral Commodity Summaries 2009*. [Online] Available at: <http://minerals.usgs.gov/minerals/pubs/mcs/> [Accessed 4 April 2014].
- USGS, 2015. *Platinum-group metals*. [PDF] Available at: <http://minerals.usgs.gov/minerals/pubs/commodity/platinum/mcs-2015-plati.pdf> [Accessed 5 August 2015].
- van der Merwe, A., 2014. *Base Metal Refinery - Operating Guide*. Western Platinum BMR.
- van der Merwe, A. & Mrubata, Z., 2014. *Western Platinum BMR Operating Guide*.
- van Schalkwyk, R., 2011. *Leaching of Ni-Cu-Fe-S Pierce Smith converter matte: Effects of the Fe-endpoint and leaching conditions on kinetics and mineralogy*. Masters Thesis. Stellenbosch: Stellenbosch University.
- van Schalkwyk, R., Eksteen, J., Petersen, J. & Akdogan, G., 2011. An experimental evaluation of the leaching kinetics of PGM-containing Ni-Cu-Fe-S Peirce Smith converter matte, under atmospheric leach conditions. *Minerals Engineering*, 24, pp.524-34.
- Venkatasubramanian, V., Rengaswamy, R. & Kavuri, S., 2003a. A review of process fault detection and diagnosis Part II: Qualitative models and search strategies. *Computers and Chemical Engineering*, 27, pp.313-26.

- Venkatasubramanian, V., Rengaswamy, R., Kavuri, S. & Yin, K., 2003b. A review of process fault detection and diagnosis Part III: Process history based methods. *Computers and Chemical Engineering*, 27, pp.327-46.
- Venkatasubramanian, V., Rengaswamy, R., Yin, K. & Kavuri, S., 2003. A review of process fault detection and diagnosis. Part I: Quantitative model-based methods. *Computers and Chemical Engineering*, 27, pp.293-311.
- Venkatasubramanian, V. & Rich, S., 1988. An Object-oriented two-tier Architecture for Integrating Compiled and Deep-level Knowledge for Process Diagnosis. *Computer Chemical Engineering*, 12(9), pp.903-21.
- Vermaak, C., 1995. The platinum-group metals – a global perspective. Randburg, South Africa, 1995. Mintek.
- Von Gruenewaldt, G., 1977. The mineral resources of the Bushveld complex. *Minerals Science Engineering*, 9(2), pp.83-95.
- Webster, J., Halit, E. & eds., 2014. *Measurement, Instrumentation, and Sensors Handbook: Spatial, Mechanical, Thermal, and Radiation Measurement*. CRC press.
- Wilmot, J., Smith, J. & Brewer, R., 2004. Start up and operation of the Phelps Dodge concentrate leach facility at the Bagdad Mine. In *International Colloquium on Hydrometallurgical Processing of Copper Sulfides*. Santiago, 2004.
- Xiao, Z. & Laplante, A., 2004. Characterizing and recovering the platinum group minerals—a review. *Minerals Engineering*, 17, pp.961-79.
- Zevenbergen, J., Gerry, J. & Buckbee, G., 2006. Automation KPIs Critical for Improvements of Enterprise KPIs. In *7th Journées Scientifiques et Techniques*. Oran, Algeria, 2006.
- Zhang, Y. & Jiang, J., 2003. Fault Tolerant Control System Design with Explicit Consideration of Performance Degradation. *Institute of Electrical and Electronics Engineers*, 39(3), pp.838-48.
- Zisserman, A., 2015. *Regression ctd and multiple classes*. [PDF] University of Oxford Available at: <http://www.robots.ox.ac.uk> [Accessed 7 July 2015].

Appendix A: NOMENCLATURE

<u>Abbreviation</u>	<u>Description</u>
A1	Assumption number 1
AC	Autoclave
AE	Average absolute Error
Al ₂ O ₃	Alumina
As	Arsenide
BEP	Best Efficient Point
BMR	Base Metal Refinery
BM	Base Metal
BPCS	Basic Process Control Strategy
Calc.	Calculated
CaO	Quicklime
Cu	Copper
CPA	Control Performance Assessment
Cr ₂ O ₃	Chromium(II) Oxide
CS	Count (number of times) valve is Saturated
CSTR	Continuous Stirred Tank Reactor
Cu ²⁺	Cupric Ion
CuS	Covellite
Cu _{1.8} S	Digenite
Cu _{1.96} S	Djurleite
Cu ₂ S	Chalcocite
CV	Controlled Variable
CW	Cooling Water
DAMADICS	Development and Application of Methods for Actuator Diagnosis in Industrial Controls Systems

FDI	Fault Detection and Isolation
DE	Density Element
DOF	Degrees of Freedom
FCE	Final Control Element
fcn	Function
FCV	Flow Control Valve
Fe ²⁺	Ferrous ion
Fe ³⁺	Ferric ion
FeO	Iron(II) Oxide
FIC	Flow Indicator and Control
FMEA	Failure Modes and Effects Analysis
FO	First Order
FTA	Fault Tree Analysis
GA	Genetic Algorithm
GS	Global Search
HAZOP	Hazard and Operability
IAE	Integral of Absolute Error
ICP	Inductively Coupled Plasma
IE	Integral of Error
ISE	Integral of Square Error
Ir	Iridium
K	Steady-state gain
KPI	Key Performance Indicator
KPI%	Key Performance Indicator relative to baseline
LIC	Level Indicator and Control
Ltd.	Limited Company
LTS	Longest Time valve is Saturated
nO	n th Order

MD	Maximum Deviation
MgO	Magnesia
MIDAS	Model-Integrated Diagnostic Analysis System
MODEX2	Model Oriented Diagnostic Expert
MPC	Model Predictive Control
MS	Mass Spectrometry
MT	Measurement Test
MV	Manipulated Variable
NaN	Not a Number
NASP	Not At Set-Point
Ni	Nickel
NiS	Millerite
Ni ₃ S ₂	Heazlewoodite
Ni ₃ S ₄	Polydymite
Ni ₇ S ₆	Godlevskite
NPSH	Net Positive Suction Head
ODE	Ordinary Differential Equations
OES	Optical Emission Spectrometry
OPM	Other Precious Metal
Os	Osmium
P	Proportional
Pd	Palladium
PFD	Process Flow Diagram
PGE	Platinum Group Element
PGM	Platinum Group Metal
PHA	Process Hazard Analysis
PI	Proportional-Integral
PIC	Pressure Indicator and Control

PID	Proportional- Integral- Derivative
PLC	Public Limited Company
PS	Pattern Search
Pt	Platinum
PV	Present-Value
P&ID	Piping and Instrumentation Diagram
R	Ramp
Rh	Rhodium
RPM	Rotations per Minute
Ru	Ruthenium
Sb	Antimonide
S	Sulphur
SD	Standard Deviation
Se	Selenium
SG	Specific Gravity
SiO ₂	Silica
SP	Set-Point
TCV	Temperature Control Valve
TD	Travel Distance
Te	Telluride
TIC	Temperature Indicator and Control
TK	Tank
TNASP	Time Not At Set-Point
TS	Total time valve is Saturated
UG2	Upper Group 2
VR	Valve Reversal
V&V	Verification and Validation

<u>Symbol</u>	<u>Description</u>	<u>Units</u>
A	Surface area of solids	m^2
A_0	Initial surface area	m^2
$A_{liq,i}$	Liquid surface area of compartment i	m^2
C_E	Experimentally determined concentration	<i>mole/L</i>
C_i	Concentration of component i	<i>mole/L</i>
$C_{i,j}^*$	Adjusted concentration of species i for sample number j	<i>mole/L</i>
C_M	Model predicted concentration	<i>mole/L</i>
$C_{E,i,r}^{Max}$	Maximum concentration of component i for run r	<i>mole/L</i>
$c_{p,i}$	Specific heat capacity of component i	$J/(kg.K)$
f	Fault size	<i>Situation dependent</i>
f_{sh}	Shape factor	m^3/m^3
$\hat{H}_{i,k}$	Specific enthalpy of component i within stream k	J/kg
$\Delta\hat{H}_{rxn,j}^o$	Specific standard heat of reaction of reaction j	$J/mole$
J	Deadband and stickband	<i>Percentage</i>
$k_{0,j}$	Rate expression constant of reaction j	<i>Situation dependent</i>
$k'_{0,j}$	Adjusted rate expression constant of reaction j	<i>Situation dependent</i>
$k''_{0,j}$	Lumped rate expression constant of reaction j	<i>Situation dependent</i>
K_v	Valve characteristic	m^3/h
L_0	Initial length	m
l	Expected time related gradient	<i>Situation dependent</i>
m_{fin}	Mass flow in	kg/hr
m_0	Initial mass	kg
m_{tot}	Total mass	kg
$\dot{m}_{i,k}$	Mass flow rate of component i within stream k	kg/h
$M_{w,i}$	Molecular weight of component i	$kg/mole$

N	Number of data points used within statistics	-
N	Filter coefficient	<i>Dimensionless</i>
N_{DV}	Number of defined variables	-
N_{Eq}	Number of equations	-
N_V	Number of variables	-
n_0	Initial mole amount	<i>mole</i>
\dot{n}_i	Molar flow rate of stream i	<i>mole/h</i>
$ObjFunc$	Objective Function	<i>Situation dependent</i>
ρ_L	Density of liquid	<i>kg/m³</i>
ρ_m	Measured density	<i>kg/m³</i>
ρ_S	Density of solids	<i>kg/m³</i>
P_{tot}	Total autoclave pressure	<i>bar</i>
P_{O_2}	Partial pressure of oxygen	<i>bar</i>
P_{H_2O}	Partial pressure of water	<i>bar</i>
\dot{Q}	Rate of heat added to the system	<i>W</i>
r_j	Reaction rate of reaction j	<i>mole/(m³.min)</i>
R	Universal gas constant	<i>J/(kg.K)</i>
s_i	Random walk gradient of variable i	<i>Situation dependent</i>
S	Slipjump	<i>Percentage</i>
S_1	Maximum error (residual)	<i>Situation dependent</i>
S_2^2	Variance	<i>Situation dependent</i>
t	Time	<i>min</i>
T_r	Reset time	<i>h</i>
T_d	Derivative time	
U	Controller output	<i>Situation dependent</i>
$v_{i,j}$	Stoichiometric coefficient of component i participating in reaction j	<i>Dimensionless</i>
v_0	Variable starting point	<i>Situation dependent</i>
V	Volume	<i>m³</i>

V_0	Initial volume	m^3
\dot{V}_{sample}	Volumetric flow rate of a sample	ml/min
V_{vap}	Vapour space	m^3
\dot{W}_{shaft}	Shaft work	W
$wt\%$	Weight percentage	kg/kg
x_{jSin}	Solid mass fraction of components j in	kg/kg
x_{jLout}	Liquid mass fraction of components j out	kg/kg
$x_{new}^{(j)}$	New initial guessed value	<i>Situation dependent</i>
Y	Model output	<i>Situation dependent</i>
y	Process data	<i>Situation dependent</i>
$\hat{y}(t \hat{\theta}_N)$	Model predicted data at time t for N $\hat{\theta}$ inputs	<i>Situation dependent</i>
$\alpha_{r,j}$	Order of reactant r participating in reaction j	<i>Dimensionless</i>
$\alpha(t)$	Extent of valve degradation	<i>Dimensionless</i>
ε	Error (model predicted- and process data)	<i>Situation dependent</i>
σ	Original specific surface area	m^2/kg
$\sigma_{m,i}$	Standard deviation of sensor measurements for component i	<i>Situation dependent</i>
ζ	Measurement test statistic	<i>Dimensionless</i>
ζ	Damping factor	<i>Dimensionless</i>
φ	Process Parameter	<i>Situation dependent</i>
$\Delta\varphi$	Process parameter with certain size	<i>Situation dependent</i>
α_{MT}^*	Normal distribution significance boundaries (measurement test)	<i>Dimensionless</i>
θ	Dead time	h

Appendix B: DATA

Western Platinum BMR

Table B.1: Dynamic process model input data (Dorfling, 2012)

Stream Number	Flow rate (kg/h)	Temperature (°C)	Liquid mass fraction	Liquid composition by mass							Solid mass fraction	Solid composition by mass													
				Ni ²⁺	Cu ²⁺	Fe ³⁺	Rh ³⁺	Ru ³⁺	Ir ³⁺	H ⁺		NiS	Ni ₃ S ₄	Cu _{1.8} S	CuS	Fe(OH)SO ₄	Rh ₂ S ₃	Rh	RhO ₂	RuS ₂	Ru	RuO ₂	Ir ₂ S ₃	Ir	IrO ₂
1	1324	25	0.713	0.02	0.02	7.25E-04	4.24E-05	1.78E-04	3.81E-05	0.03	0.287	0.15	0.06	0.45	0.22	3.02E-03	6.46E-04	4.40E-04	0	2.33E-03	6.12E-04	0	2.25E-04	1.20E-04	0
2	472	25	1	0.02	0.02	7.25E-04	4.24E-05	1.78E-04	3.81E-05	0.03	0	-	-	-	-	-	-	-	-	-	-	-	-	-	-
3	600	25	1	0	0	0	0	0	0	0	0	-	-	-	-	-	-	-	-	-	-	-	-	-	-
4	51.4	25	1	0	0	0	0	0	0	0.96	0	-	-	-	-	-	-	-	-	-	-	-	-	-	-
10	118.9	25	0	-	-	-	-	-	-	-	0	-	-	-	-	-	-	-	-	-	-	-	-	-	-
11	43.3	25	0	-	-	-	-	-	-	-	0	-	-	-	-	-	-	-	-	-	-	-	-	-	-
12	54.1	25	0	-	-	-	-	-	-	-	0	-	-	-	-	-	-	-	-	-	-	-	-	-	-
13	24.2	180	0	-	-	-	-	-	-	-	0	-	-	-	-	-	-	-	-	-	-	-	-	-	-
18	472	25	1	0.02	0.02	7.25E-04	4.24E-05	1.78E-04	3.81E-05	0.03	0	-	-	-	-	-	-	-	-	-	-	-	-	-	-
19	50	25	1	0	0	0	0	0	0	0	0	-	-	-	-	-	-	-	-	-	-	-	-	-	-
20	12.8	25	1	0	0	0	0	0	0	0.96	0	-	-	-	-	-	-	-	-	-	-	-	-	-	-

Table B.2: Western Platinum BMR controller data obtained during a site visit (McCulloch et al., 2014)

Tags	Set-points				Tuning				Filters	
	Units	SP	H	L	P	I (hr ⁻¹)	D (hr)	N (hr ⁻¹)	PV filter (hr)	SP filter (hr)
FIC-0106	m ³ /h	LIC-0101	6	0	1.2	40	-	-	8.33E-05	-
FIC-1102	m ³ /h	Flow ratio	7	0	0.2	360.0	-	-	4.17E-03	6.94E-03
					0.1	72.0	-	-	4.17E-03	6.94E-03
					0.7	36.0	-	-	4.17E-03	6.94E-03
LIC-0101	%	60	100	0	3	7.2	-	-	4.17E-03	-
FIC-0101	m ³ /h	FF control	12	-0.3	2.11	336.4	-	-	5.56E-03	-
FIC-0201	m ³ /h	6	12	0	0.5	90.0	-	-	2.22E-03	8.33E-03
FIC-0202	l/min	0	5	0	0.2	90.5	-	-	2.78E-03	-
FIC-0203	m ³ /h	LIC-0201	45	0	0.8	60.0	-	-	2.78E-03	-
LIC-0201	%	55	100	0	-1	72.0	-	-	4.17E-03	-
FIC-0205	m ³ /h	TIC-3001	24.4	0	0.6	72.0	-	-	6.94E-03	-
TIC-3001	°C	130	144	0	-0.8	45.0	-	-	5.56E-04	2.78E-03
TIC-3003	°C	130	200	0	-3	240.0	2.78E-05	1.04E+09	-	-
TIC-3004	°C	125	200	0	-0.5	240.0	-	-	-	-
TIC-3005	°C	140	150	0	1.5	-	-	-	-	-
FIC-3001A	Nm ³ /h	PIC-3001	200	0	1	211.8	-	-	1.39E-03	-
FIC-3001B	Nm ³ /h	PIC-3001	200	0	1.29	211.8	-	-	6.94E-03	-
FIC-3001C	Nm ³ /h	PIC-3001	200	0	1	211.8	2.78E-04	1.04E+08	1.39E-03	-
LIC-3003	%	80	75	0	-1.5	102.9	-	-	1.39E-03	-
LIC-3002	%	70	80	0	-1.5	120.0	-	-	5.56E-03	-
FIC-3002	m ³ /h	LIC-3002	12	0	1.8	90.0	-	-	4.17E-03	1.39E-03
TIC-0401	°C	75	200	0	-3	720.0	-	-	-	-
LIC-0401	%	45	100	0	-0.6	12.0	2.78E-03	10368000	1.39E-03	-
FIC-0401	m ³ /h	LIC-0401	14.4	0	1.5	283.5	-	-	2.78E-03	-
FIC-0150-09	m ³ /h	0	6	0	0.5	36.0	-	-	5.56E-03	-
LIC-151	%	60	100	0	2	72.0	2.78E-01	103680	2.78E-03	-
FIC0150-4	l/h	Flow ratio	600	-5	2	120.0	-	-	4.17E-03	-
FIC-0150-5	m ³ /h	6	6	0	0.5	36.0	-	-	5.56E-03	-
FIC-0150-3	m ³ /h	LIC-151	6	0	0.5	60.0	-	-	1.67E-03	-
FIC-3003	m ³ /h	LIC-3003	18	0	1.47	91.8	-	-	1.39E-02	-
PIC-3001	kPa	550	1000	0	3.5	65.5	-	-	-	-

Appendix C: SAMPLE CALCULATIONS

Derivation of Equation 2.1

The solid percentage exiting the second stage slurry preparation tank is shown below.

$$solid\% = \frac{\dot{m}_{0101}x_s}{\dot{m}_{0106} + \dot{m}_{0101} + \dot{m}_{1102}} \times 100$$

The fractions above are that of mass. Each mass flow rate can be substituted with volumetric flow rates and densities. The solid fraction is substituted with Equation 7.12.

$$solid\% = \frac{\dot{V}_{0106} \left(\frac{\frac{1}{\rho_{0106}} - \frac{1}{\rho_{0106,L}}}{\frac{1}{\rho_{0106,S}} - \frac{1}{\rho_{0106,L}}} \right)}{\dot{V}_{0106}\rho_{0106} + \dot{V}_{0101}\rho_{0101} + \dot{V}_{1102}\rho_{1102}} \times 100$$

The definition of the spent% is given in Equation 2.2, and is used to substitute \dot{V}_{1102} .

$$solid\% = \frac{\dot{V}_{0106} \left(\frac{\frac{1}{\rho_{0106}} - \frac{1}{\rho_{0106,L}}}{\frac{1}{\rho_{0106,S}} - \frac{1}{\rho_{0106,L}}} \right)}{\dot{V}_{0106}\rho_{0106} + \dot{V}_{0101}\rho_{0101} + \left(\frac{100}{spent\%} - 1 \right) \dot{V}_{0101}\rho_{1102}} \times 100$$

The equation is now arranged so that the spent electrolyte volumetric flow rate is alone.

$$\dot{V}_{0101} = \frac{\dot{V}_{0106} \left(\frac{\frac{1}{\rho_{0106}} - \frac{1}{\rho_{0106,L}}}{\frac{1}{\rho_{0106,S}} - \frac{1}{\rho_{0106,L}}} \right) \times 100 - solid\% \dot{V}_{0106}\rho_{0106}}{solid\% (\rho_{0101} + \left(\frac{100}{spent\%} - 1 \right) \rho_{1102})}$$

Extent of valve degradation estimation

A fourth compartment outlet valve degradation rate of 0.0018 is evident from Figure 8.8. The extent of valve degradation is calculated by simply multiplying the rate of valve degradation with the time in which the valve is in operation:

$$\alpha = 0.0018 \times 9 \times 31 = 0.5022$$

Appendix D: EQUATIONS AND PROCEDURES

Rate Expressions

Table D.1: Rate expressions for Reaction 1 to Reaction 21 developed by Dorfling (2012)

$r_1 = \left(k_{0,1} e^{-\frac{E_{a,1}}{RT}}\right) C_{H^+} C'_{O_2,eq} \left(n_0^{\frac{1}{f_{sh}}} \times n^{1-\frac{1}{f_{sh}}}\right)_{NiS}$	Rate expression 1
$r_2 = \left(k_{0,2} e^{-\frac{E_{a,2}}{RT}}\right) C'_{O_2,eq} \left(n_0^{\frac{1}{f_{sh}}} \times n^{1-\frac{1}{f_{sh}}}\right)_{Ni_3S_4}$	Rate expression 2
$r_3 = \left(k_{0,3} e^{-\frac{E_{a,3}}{RT}}\right) C_{H^+} C'_{O_2,eq}$	Rate expression 3
$r_4 = \left(k_{0,4} e^{-\frac{E_{a,4}}{RT}}\right) C_{H^+} \left(n_0^{\frac{1}{f_{sh}}} \times n^{1-\frac{1}{f_{sh}}}\right)_{Fe(OH)SO_4}$	Rate expression 4
$r_5 = \left(k_{0,5} e^{-\frac{E_{a,5}}{RT}}\right) C'_{O_2,eq}{}^2 \left(n_0^{\frac{1}{f_{sh}}} \times n^{1-\frac{1}{f_{sh}}}\right)_{NiS}$	Rate expression 5
$r_6 = \left(k_{0,6} e^{-\frac{E_{a,6}}{RT}}\right) C'_{O_2,eq}{}^2$	Rate expression 6
$r_7 = \left(k_{0,7} e^{-\frac{E_{a,7}}{RT}}\right) C_{Rh^{3+}} C'_{O_2,eq} \left(n_0^{\frac{1}{f_{sh}}} \times n^{1-\frac{1}{f_{sh}}}\right)_{Cu_9S_5}$	Rate expression 7
$r_8 = \left(k_{0,8} e^{-\frac{E_{a,8}}{RT}}\right) C_{Ru^{3+}} C'_{O_2,eq} \left(n_0^{\frac{1}{f_{sh}}} \times n^{1-\frac{1}{f_{sh}}}\right)_{Cu_9S_5}$	Rate expression 8
$r_9 = \left(k_{0,9} e^{-\frac{E_{a,9}}{RT}}\right) C_{Ir^{3+}} C'_{O_2,eq} \left(n_0^{\frac{1}{f_{sh}}} \times n^{1-\frac{1}{f_{sh}}}\right)_{Cu_9S_5}$	Rate expression 9
$r_{10} = \left(k_{0,10} e^{-\frac{E_{a,10}}{RT}}\right) C_{Rh^{3+}} C'_{O_2,eq} \left(n_0^{\frac{1}{f_{sh}}} \times n^{1-\frac{1}{f_{sh}}}\right)_{Ni_3S_4}$	Rate expression 10
$r_{11} = \left(k_{0,11} e^{-\frac{E_{a,11}}{RT}}\right) C_{Ru^{3+}} C'_{O_2,eq} \left(n_0^{\frac{1}{f_{sh}}} \times n^{1-\frac{1}{f_{sh}}}\right)_{Ni_3S_4}$	Rate expression 11
$r_{12} = \left(k_{0,12} e^{-\frac{E_{a,12}}{RT}}\right) C_{Ir^{3+}} C'_{O_2,eq} \left(n_0^{\frac{1}{f_{sh}}} \times n^{1-\frac{1}{f_{sh}}}\right)_{Ni_3S_4}$	Rate expression 12

$r_{13} = \left(k_{0,13} e^{-\frac{E_{a,13}}{RT}} \right) C'_{O_2,eq} \left(n_0^{\frac{1}{f_{sh}}} \times n^{1-\frac{1}{f_{sh}}} \right)_{Rh_2S_3}$	Rate expression 13
$r_{14} = \left(k_{0,14} e^{-\frac{E_{a,14}}{RT}} \right) C'_{O_2,eq} \left(n_0^{\frac{1}{f_{sh}}} \times n^{1-\frac{1}{f_{sh}}} \right)_{RuS_2}$	Rate expression 14
$r_{15} = \left(k_{0,15} e^{-\frac{E_{a,15}}{RT}} \right) C'_{O_2,eq} \left(n_0^{\frac{1}{f_{sh}}} \times n^{1-\frac{1}{f_{sh}}} \right)_{Ir_2S_3}$	Rate expression 15
$r_{16} = \left(k_{0,16} e^{-\frac{E_{a,16}}{RT}} \right) C'_{O_2,eq} \left(n_0^{\frac{1}{f_{sh}}} \times n^{1-\frac{1}{f_{sh}}} \right)_{Rh}$	Rate expression 16
$r_{17} = \left(k_{0,17} e^{-\frac{E_{a,17}}{RT}} \right) C'_{O_2,eq} \left(n_0^{\frac{1}{f_{sh}}} \times n^{1-\frac{1}{f_{sh}}} \right)_{Ru}$	Rate expression 17
$r_{18} = \left(k_{0,18} e^{-\frac{E_{a,18}}{RT}} \right) C'_{O_2,eq} \left(n_0^{\frac{1}{f_{sh}}} \times n^{1-\frac{1}{f_{sh}}} \right)_{Ir}$	Rate expression 18
$r_{19} = \left(k_{0,19} e^{-\frac{E_{a,19}}{RT}} \right) \left(n_0^{\frac{1}{f_{sh}}} \times n^{1-\frac{1}{f_{sh}}} \right)_{RhO_2}$	Rate expression 19
$r_{20} = \left(k_{0,20} e^{-\frac{E_{a,20}}{RT}} \right) \left(n_0^{\frac{1}{f_{sh}}} \times n^{1-\frac{1}{f_{sh}}} \right)_{RuO_2}$	Rate expression 20
$r_{21} = \left(k_{0,21} e^{-\frac{E_{a,21}}{RT}} \right) \left(n_0^{\frac{1}{f_{sh}}} \times n^{1-\frac{1}{f_{sh}}} \right)_{IrO_2}$	Rate expression 21

Constitutive Equations used in dynamic process model

Specific heat capacities of respective streams were estimated by Dorfling (2012) using Kopp's law:

$$c_p = \sum_i c_{p,i} \times x_{i,l} \times x_l \quad \text{Equation D.1}$$

where $x_{i,l}$ refers to the mass fraction of component i in phase l . The specific heat capacities were estimated by only using the main components namely water, sulphuric acid, covellite, digenite, millerite and polydymite. Dorfling (2012) normalised the mass fractions by the sum of these main components. Dorfling (2012) calculated the specific enthalpy of stream k using a reference temperature (T_{ref}) of 25°C:

$$\hat{H}_k = c_{p,k} \times (T - T_{ref}) \quad \text{Equation D.2}$$

The rate at which heat is lost to the surroundings for a specific vessel was calculated by Dorfling (2012) using a correlation described by Incropera and De Witt (1996):

$$\dot{Q} = (Nu \times k_{Air} \times \pi \times (T_{outer} - T_{\infty}) + \varepsilon_{outer} \times \pi \times D_{outer} \times K_{SB} \times (T_{outer}^4 - T_{surr}^4)) \times L \quad \text{Equation D.3}$$

where T_{surr} , T_{outer} and T_{∞} refer to the surrounding temperature; outer temperature of the vessel; and the ambient temperature; respectively. k_{Air} , D_{outer} , L , ε_{outer} , and K_{SB} represent the thermal conductivity of air; outer vessel diameter; vessel length; surface emissivity; and Stefan-Boltzmann constant; respectively. The Nusselt number was approximated using the following correlation:

$$Nu = \left(0.6 + \frac{0.387 \times \left(\frac{g \times \beta_{Air} \times (T_{outer} - T_{\infty}) \times D_{outer}^3}{\mu_{Air} \times \alpha_{Air}} \right)^{\frac{1}{6}}}{\left(1 + \left(\frac{0.559}{Pr_{Air}} \right)^{\frac{9}{16}} \right)^{\frac{8}{27}}} \right)^2 \quad \text{Equation D.4}$$

where β_{Air} , μ_{Air} , α_{Air} and Pr_{Air} are the volumetric thermal expansion coefficient; kinematic viscosity; thermal diffusivity; and the Prandtl number of air; respectively.

Dorfling (2012) approximated the oxygen concentration in the liquid phase with a thermodynamic equation developed by Tromans (1998):

$$C'_{O_2,eq} = \phi_{eff} \times P_{O_2} \times f(T) \quad \text{Equation D.5}$$

Equation D.5 relates the partial pressure, effect of temperature, and effect of inorganic dissolved components to the oxygen solubility. The effective water fraction (ϕ_{eff}) was calculated using Equation D.6.

$$\phi_{eff} = \phi_1 \left(\prod_2^z \phi_i \right)^q \quad \text{Equation D.6}$$

where ϕ_1 is the lowest individual water fraction of all components in solution. Individual water fractions were calculated as follows:

$$\phi_i = \left(\frac{1}{1 + \chi_i \times (C'_i)^\vartheta} \right)^\delta \quad \text{Equation D.7}$$

values for χ , δ , and ϑ are defined based on the specific dissolved component i . The molalities of different ions were calculated by the conversion of mass fractions:

$$C'_i = \frac{\left(\frac{x_{i,l}}{M_{w,i}} \right)}{\left(1 - x_{Cu^{2+},liq} \times \frac{M_{w,CuSO_4}}{M_{w,Cu^{2+}}} - x_{Ni^{2+},liq} \times \frac{M_{w,NiSO_4}}{M_{w,Ni^{2+}}} - x_{H_2SO_4,liq} \right)} \quad \text{Equation D.8}$$

The denominator in Equation D.8 was used to calculate the mass fraction of water by subtracting all components that form a significant portion of the liquid phase. This not only included copper and nickel ions, but their corresponding sulphate anions as well.

The temperature function in Equation D.5 is given as follow:

$$f(T) = e^{\frac{(0.046T^2 + 203.35T \times \ln(\frac{T}{298}) - (299.378 + 0.092T) \times (T - 298) - 20591)}{8.3144T}} \quad \text{Equation D.9}$$

Equation D.9 is valid for temperatures between 273 K and 616 K and for pressures up to 60 atm.

Rate expressions developed by Dorfling (2012) require the molarity of species. Dorfling (2012) altered mass fractions of streams (readily available within the process model) into molarities using Equation D.10.

$$C_i = \frac{\left(\frac{x_{i,l} \times x_l \times \dot{m}_{tot}}{M_{w,i}} \right)}{\left(\frac{x_{solids} \times \dot{m}_{tot}}{\rho_{solids}} + \frac{(1 - x_{solids}) \times \dot{m}_{tot}}{\rho_{liquids}} \right)} \quad \text{Equation D.10}$$

Mass flow rates exiting most process units were assumed by Dorfling (2012) to be free flowing:

$$\dot{m}_{free-flow} = K'_i \sqrt{\dot{m}_{tot}} \quad \text{Equation D.11}$$

Proportionality constants (K'_i) relating the free-flow rates to the total mass in a vessel were estimated at steady-state.

Dorfling (2012) calculated the partial pressure of oxygen by simply subtracting the partial pressure of water from the total pressure:

$$P_{O_2} = P_{tot} - P_{H_2O} \quad \text{Equation D.12}$$

Dorfling (2012) assumed that the total pressure was constant. The partial pressure of water was estimated using Antoine's equation:

$$\log(P_{H_2O}) = A - \frac{B}{C + t} \quad \text{Equation D.13}$$

t represents the temperature in degrees Celsius. Two sets of values for A , B and C was used by Dorfling (2012) for temperatures above and below 60°C, respectively.

Control key performance indicator simulation procedure

Controlled variables

The following controlled variable KPIs were used to quantify controlled variable performance:

1. Travel distance (TD)
2. Integral absolute error (IAE)
3. Average absolute error (AE)
4. Maximum deviation (MD)
5. Time not at set-point (TNASP)
6. Standard deviation (SD)

The simulation procedure used to implement each KPI in Simulink™ will now be discussed.

Figure D.1 shows the travel distance KPI simulated in Simulink™.

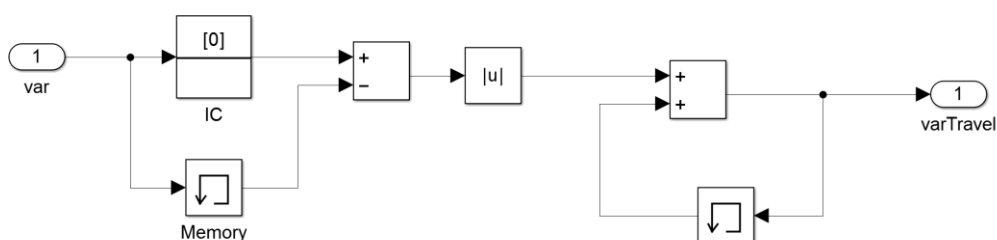


Figure D.1: Mechanism of the travel distance KPI implemented in Simulink™

The absolute difference between the controlled variable value at a specific and a preceding time step is calculated and accumulated. The behaviour of the travel distance KPI for an artificial sinusoidal temperature input is shown in Figure D.2.

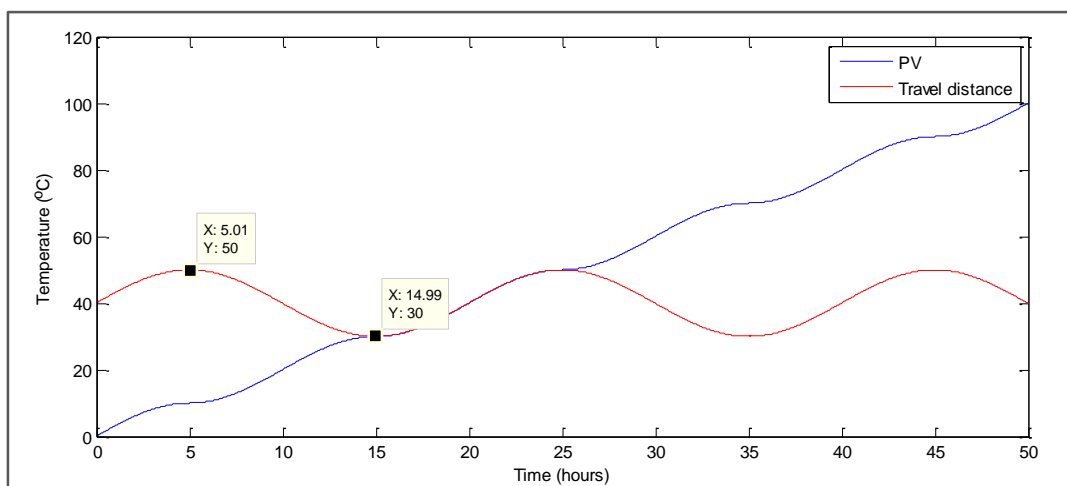


Figure D.2: Behaviour of the travel distance KPI for an artificial sinusoidal temperature

The input has amplitude of 10 °C. The total distance travelled between the first peak and trough is therefore equal to 30 °C; which is at 15 hours. The present-value and travel distance meet at this point, as expected. The behaviour of the travel distance is verified in this manner.

Figure D.3 shows the integral absolute error KPI simulated in Simulink™.

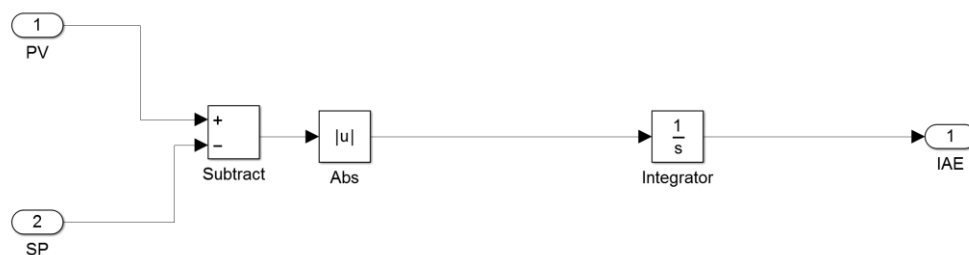


Figure D.3: Mechanism of the integral absolute error KPI implemented in Simulink™

The absolute difference between the present-value and set-point is simply integrated. The behaviour of the integral absolute error KPI for an artificial sinusoidal temperature present-value and set-point is shown in Figure D.4.

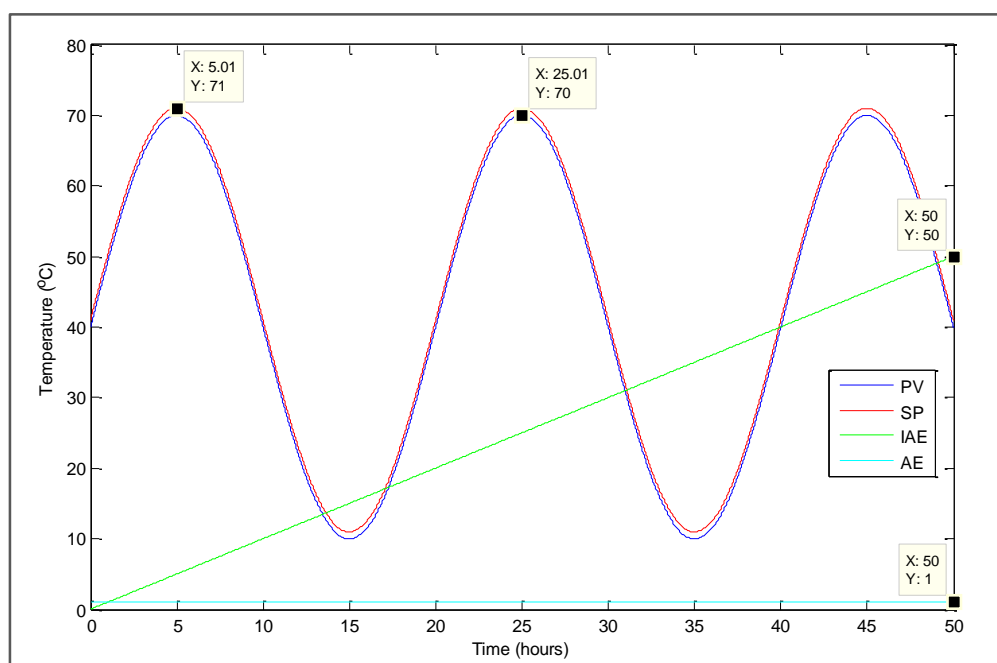


Figure D.4: Behaviour of the integral absolute error KPI for an artificial sinusoidal temperature

The present-value and set-point are identical sinusoidal signals, except for having a bias difference of 1 °C. The integral absolute error (IAE) at any time is therefore equal to the time multiplied by the bias difference of one. This validates the IAE KPI. The average absolute error (AE) is simply the IAE divided by the total time IAE is measured. An AE value of 1 °C is shown in Figure D.4 which is the size of the bias difference, as expected.

Figure D.5 shows the maximum deviation KPI simulated in Simulink™.

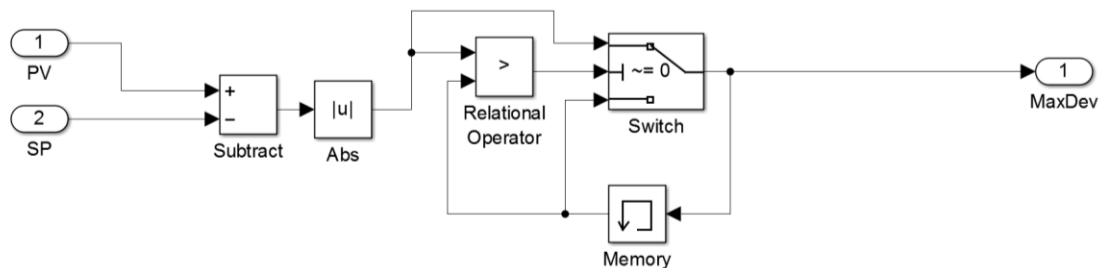


Figure D.5: Mechanism of the maximum deviation KPI implemented in Simulink™

The variable deviation is calculated and compared to a value from memory (initially at zero). The newly calculated deviation passes through the switch block and replaces the current value in the memory, if it is larger than the current value in memory. The behaviour of the maximum deviation KPI is shown in Figure D.6 for a set-point of zero and a random number generator on the present-value.

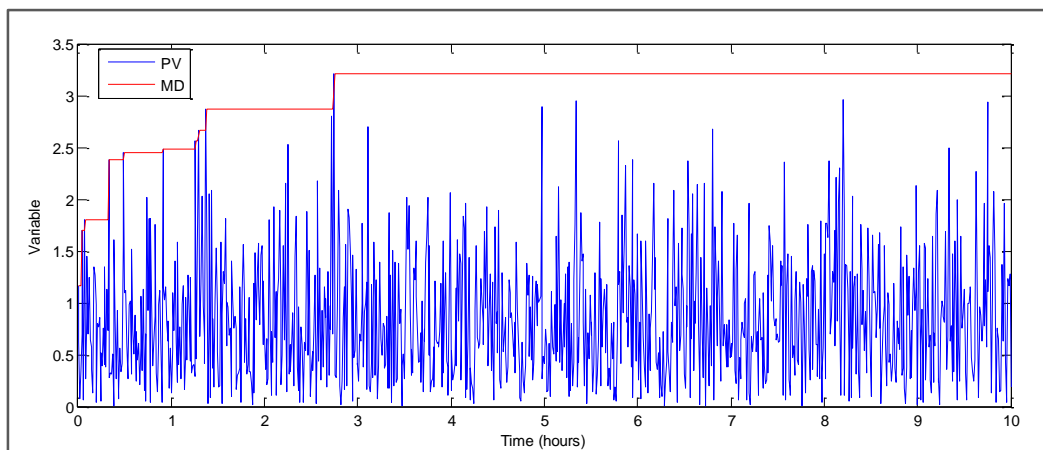


Figure D.6: Behaviour of the maximum deviation KPI for an artificial random number generator input

The variable maximum deviation (MD) increases as the present-value moves further away from zero. The MD is constant after 3 hours since the variable never assumed a value larger than the latest value in memory.

Figure D.7 shows the time not at set-point KPI simulated in Simulink™. Time not at set-point is defined as the time which a variable spends outside a user-defined margin around the set-point (i.e. when the controller error is larger than a user-defined NASP value). A relation block is used to activate rising and falling triggered subsystems which report the time at which the variable is outside and within the set-point margin, respectively.

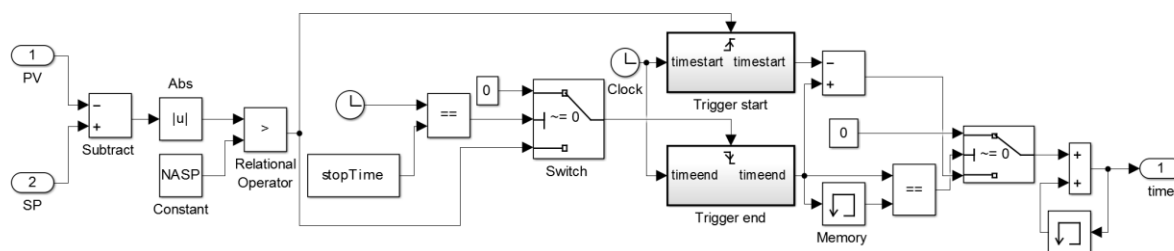


Figure D.7: Mechanism of the time not at set-point KPI implemented in Simulink™

The triggered subsystems are subtracted from one another, which represents interim time not at set-points. These interim values are accumulated in such a way that duplicate adding is avoided. The relation operator prior to the end time triggered subsystem ensures that the final interim value (if one exists) is added to the total at the end of the simulation. Figure D.8 shows the behaviour of the time not at set-point KPI for an NASP value of 0.01.

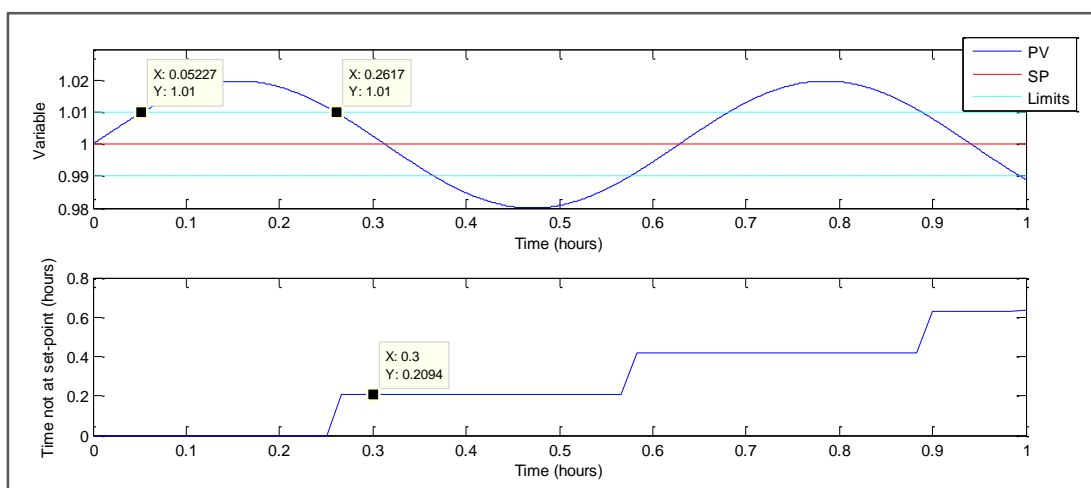


Figure D.8: Behaviour of the time not at set-point KPI for an artificial sinusoidal variable

The time not at set-point increases each time the present-value of the variable moves into the variable limits. The size of these increases is equal to the preceding time the variable was outside the limits. The total time not at set-point can be derived from the data tips in the upper graph. The total time not at set-point corresponds with what is given in the Figure D.8. NASP values for flow, temperature and pressure controllers were defined to be 1 % of the controller set-point range added to four standard deviations of their measurement noise, during the dynamic process model control performance assessment. A similar calculation was used for density and level NASP values but with a 5 % set-point range.

Figure D.9 captures the standard deviation KPI simulated in Simulink™.

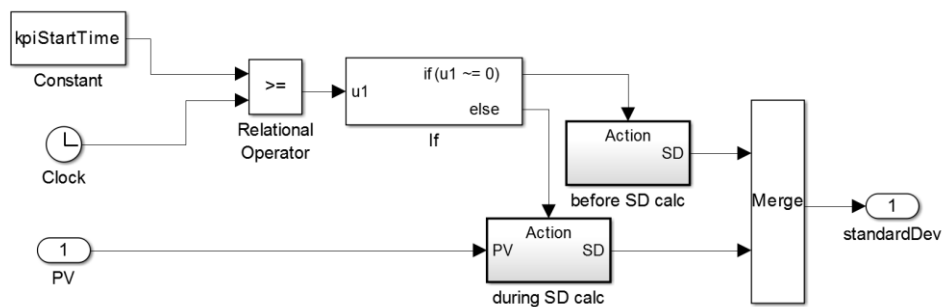


Figure D.9: Mechanism of the standard deviation KPI implemented in Simulink™

A running standard deviation calculator (i.e. continually calculating a standard deviation from an input signal) from the DSP System Toolbox™ in Simulink™ was used, and is present in the during SD calculation block. A switch block is used to activate the standard deviation calculator at the applicable point in time (i.e. at the start of all KPI measurements). The behaviour of the standard deviation KPI is validated in Figure D.10 by using a random number generator input with an arbitrary variance of 10.

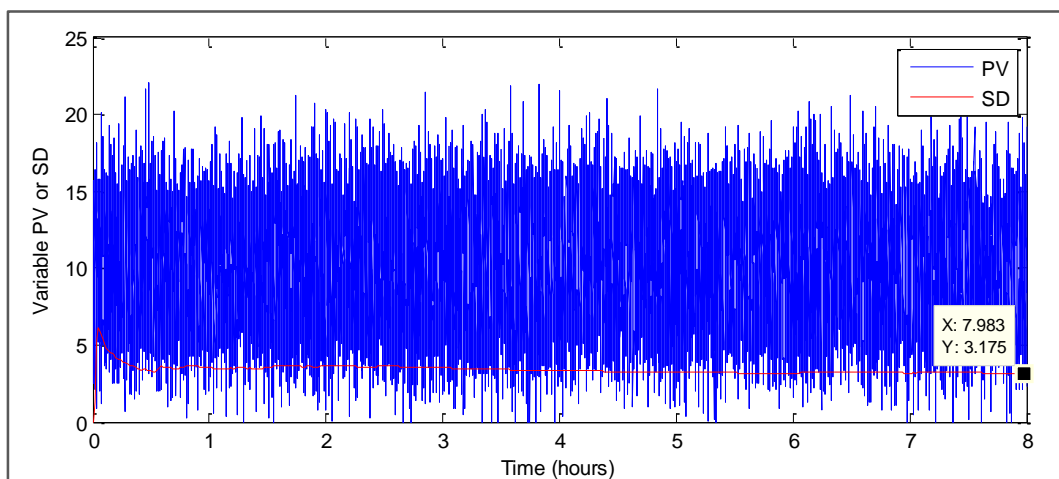


Figure D.10: Behaviour of the standard deviation KPI

The standard deviation is equal to the square root of the variance, calculated to be 3.162 in this scenario. The standard deviation (SD) in Figure D.10 tends toward this value, which validates the behaviour of this KPI in Simulink™.

Valves

The following valve KPIs were used to quantify valve performance:

1. Valve travel distance (TD)
2. Average absolute error (AE)
3. Integral absolute error (IAE)

4. Time not at valve set-point (TNASP)
5. Standard deviation (SD)
6. Valve at a limit (CS, TS, LTS)
7. Valve reversals (VR)

The simulation procedures of many valve KPIs were considered in the controlled variable KPI section. The simulation procedure used to implement other valve KPIs in Simulink™ will now be discussed.

Figure D.11 captures the valve at a limit KPIs that are simulated in Simulink™.

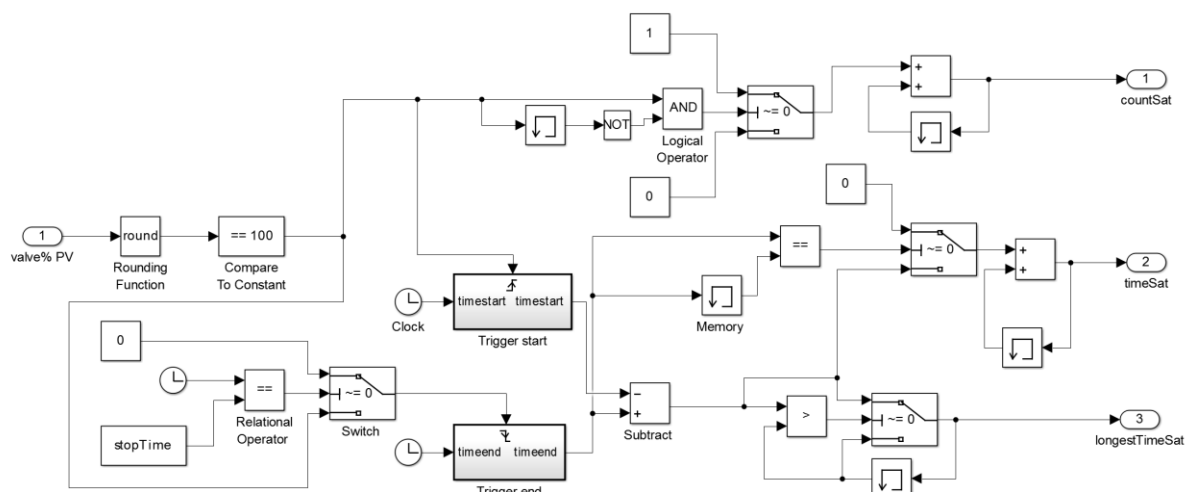


Figure D.11: Mechanism of the valve at a limit KPI implemented in Simulink™

The total time which the valve is saturated at 100 % (refer to port 2 in Figure D.11) is calculated in a similar way as the time not at set-point KPI, while the longest time which the valve is saturated (refer to port 3) is calculated similar to the maximum deviation KPI. The number of times the valve is saturated is calculated by simply comparing the current saturation state to that of the previous, and accumulating the total. The behaviour of the valve at a limit KPI is validated using an artificially built signal. Refer to Figure D.12.

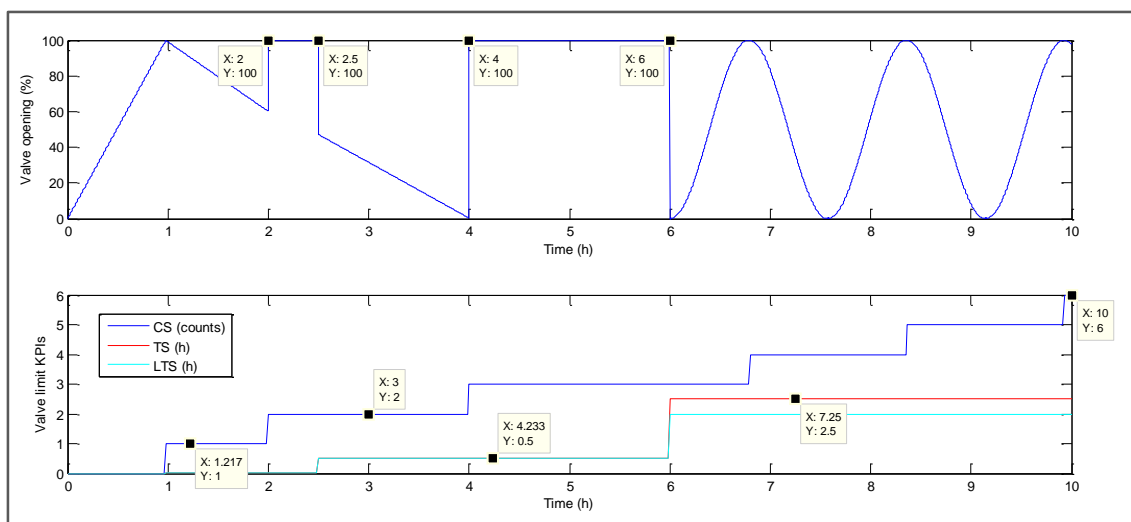


Figure D.12: Behaviour of the valve at a limit KPI for an artificial signal

The valve is saturated at 100 % in six different occasions, which corresponds with the count saturated (CS) KPI. The total time (TS) and longest time (LTS) the valve is saturated are almost identical up until 6 hours, which makes sense since the valve has only been saturated once with a significant timespan. The LTS increase after 6 hours with a value that represents the cumulative time the valve has been saturated. The LTS accepts the next highest saturation time of 2 hours.

Figure D.13 shows the valve reversal KPI implemented in Simulink™.

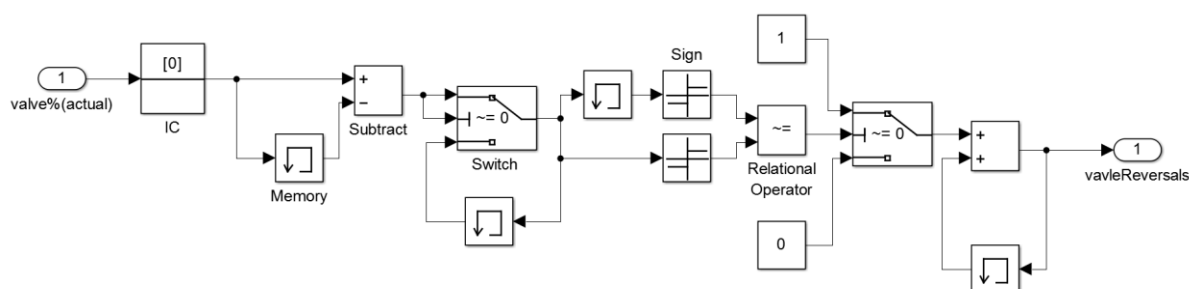


Figure D.13: Mechanism of the valve reversal KPI implemented in Simulink™

The difference between a current and preceding signal sample is determined. The sign of this difference is compared to the preceding sign. A count is made when the sign changes. The sign blocks can assume values of -1, 1 and 0. The latter case occurs when a value of zero passes through the sign block. The first switch block exists in order to avoid valve reversal counts when the valve merely moves to a stationary position. The behaviour of the valve reversal KPI for a sinusoidal valve input is captured in Figure D.14.

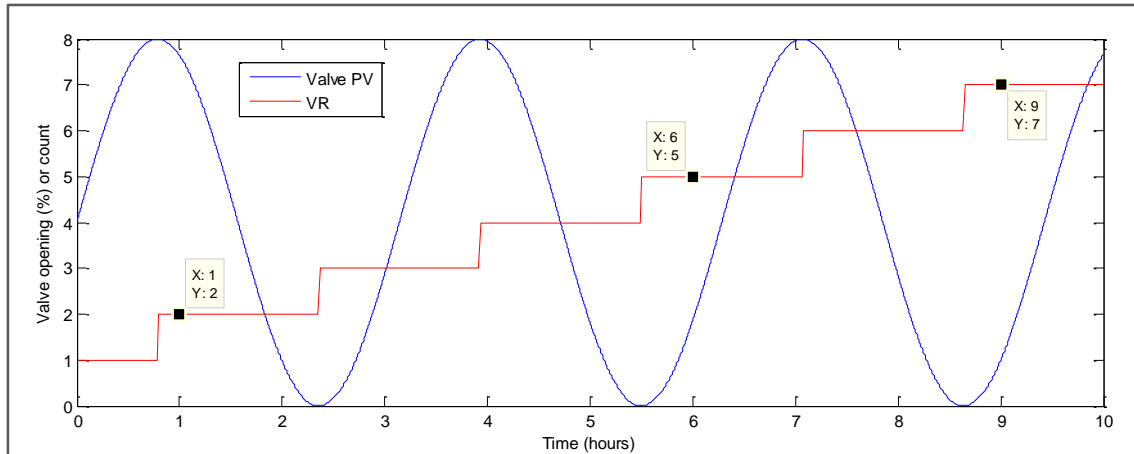


Figure D.14: Behaviour of the valve reversal KPI for an artificial sinusoidal signal

The valve reversal KPI (VR) starts with a value of one, which represents the initial movement of the valve. The valve reversal increases by one each time the sinusoidal signal changes direction, as expected.

Operational key performance indicators

The following operational KPIs were identified at Western Platinum BMR and used to quantify operational performance (McCulloch et al., 2014):

1. Extent of base metal leaching
2. Extent of PGM leaching
3. Utility usage
4. Throughput
5. Spillage

The extent of base metal leaching was expressed as the mass percentage of base metals which is left in the solid phase relative to the total amount of base metals that enter the process:

$$KPI_{Total\ BMs\ in\ solid} = \frac{\int_{t_0}^t \dot{m}_{BMs\ in\ solid, compartment\ i}}{\int_{t_0}^t \dot{m}_{BMs\ in\ stream\ 5}} \times 100 \quad \text{Equation D.14}$$

The KPI calculation shown in Equation D.14 dynamically quantifies the extent of base metal leaching throughout the entire simulation. A disadvantage of using Equation D.14 would be that it can be affected during the occurrence of spillage in-between stream 5 and compartment i . The extent of PGM leaching was expressed in a similar manner:

$$KPI_{Total\ PGMs\ in\ liquid} = \frac{\int_{t_0}^t \dot{m}_{PGMs\ in\ liquid, compartment\ i}}{\int_{t_0}^t \dot{m}_{PGMs\ in\ stream\ 5}} \times 100 \quad \text{Equation D.15}$$

The extent of PGM leaching was expressed as the mass percentage of PGMs which entered the solid phase relative to the total amount of PGMs that enter the process.

The utility usage was calculated by integrating the applicable utility mass flow rates over time. The throughput and spillages are calculated in a similar way:

$$KPI_{utility\ j} = \int_{t_0}^t \dot{m}_{utility\ j} \quad \text{Equation D.16}$$

$$KPI_{spillage\ j} = \int_{t_0}^t \dot{m}_{spillage\ j} \quad \text{Equation D.17}$$

$$KPI_{throughput} = \int_{t_0}^t \dot{m}_{solid, stream\ 22} \quad \text{Equation D.18}$$

Appendix E: FLOW DIAGRAMS

Western Platinum BMR

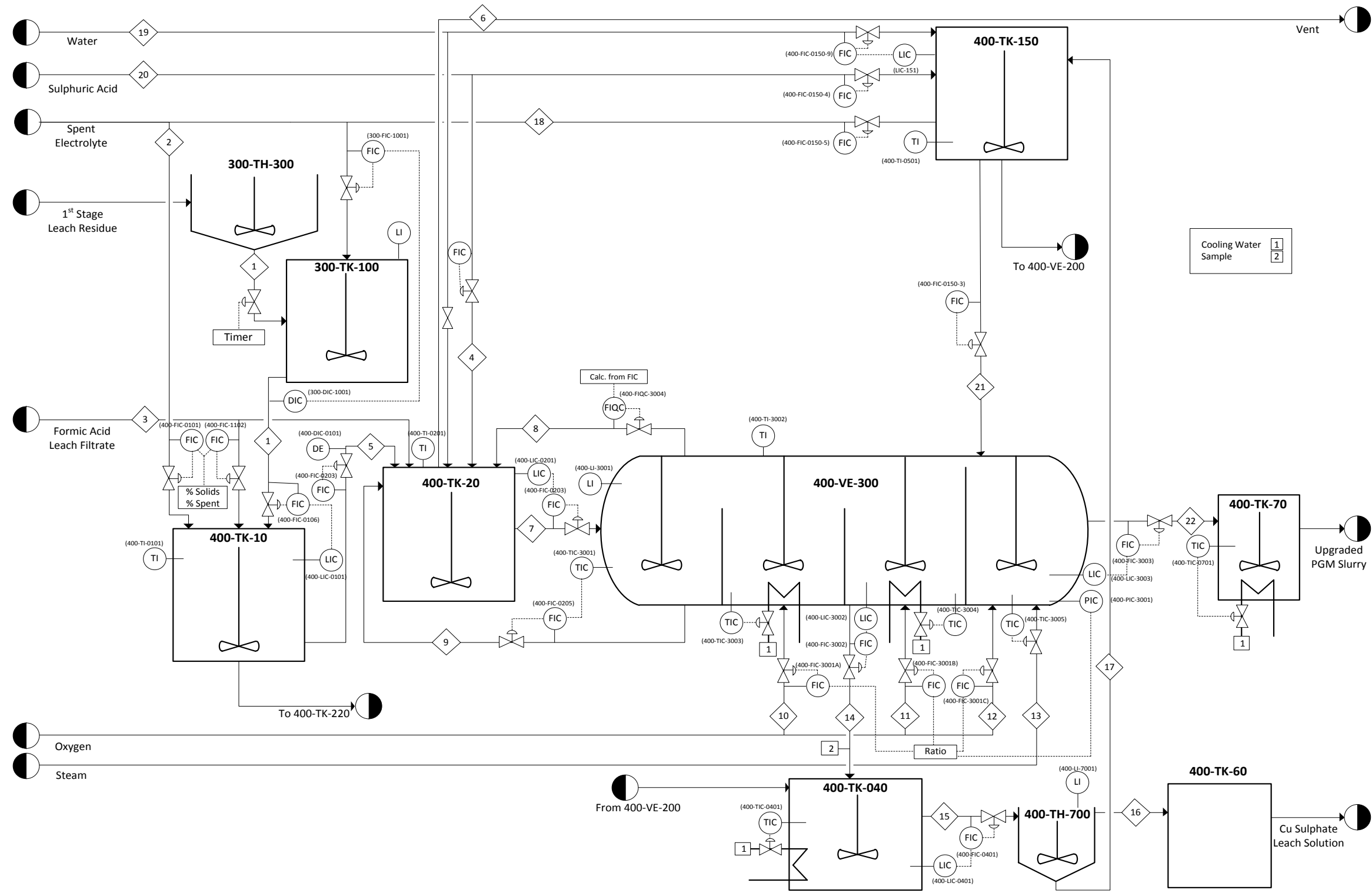


Figure E.1: P&ID of Leaching Process: Western Platinum Ltd. BMR autoclave 300

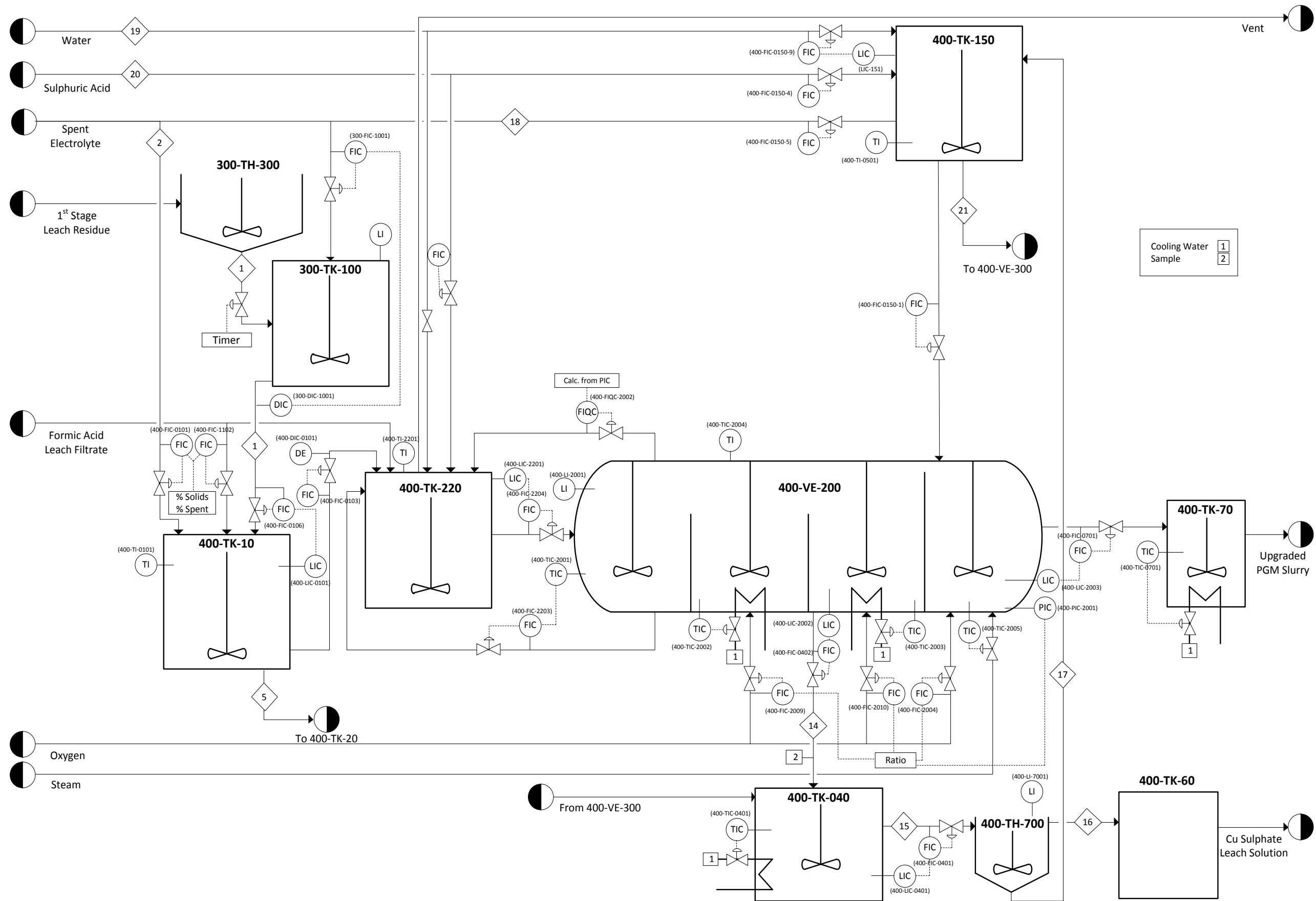


Figure E.2: P&ID of Leaching Process: Western Platinum Ltd. BMR autoclave 200

Dynamic process model

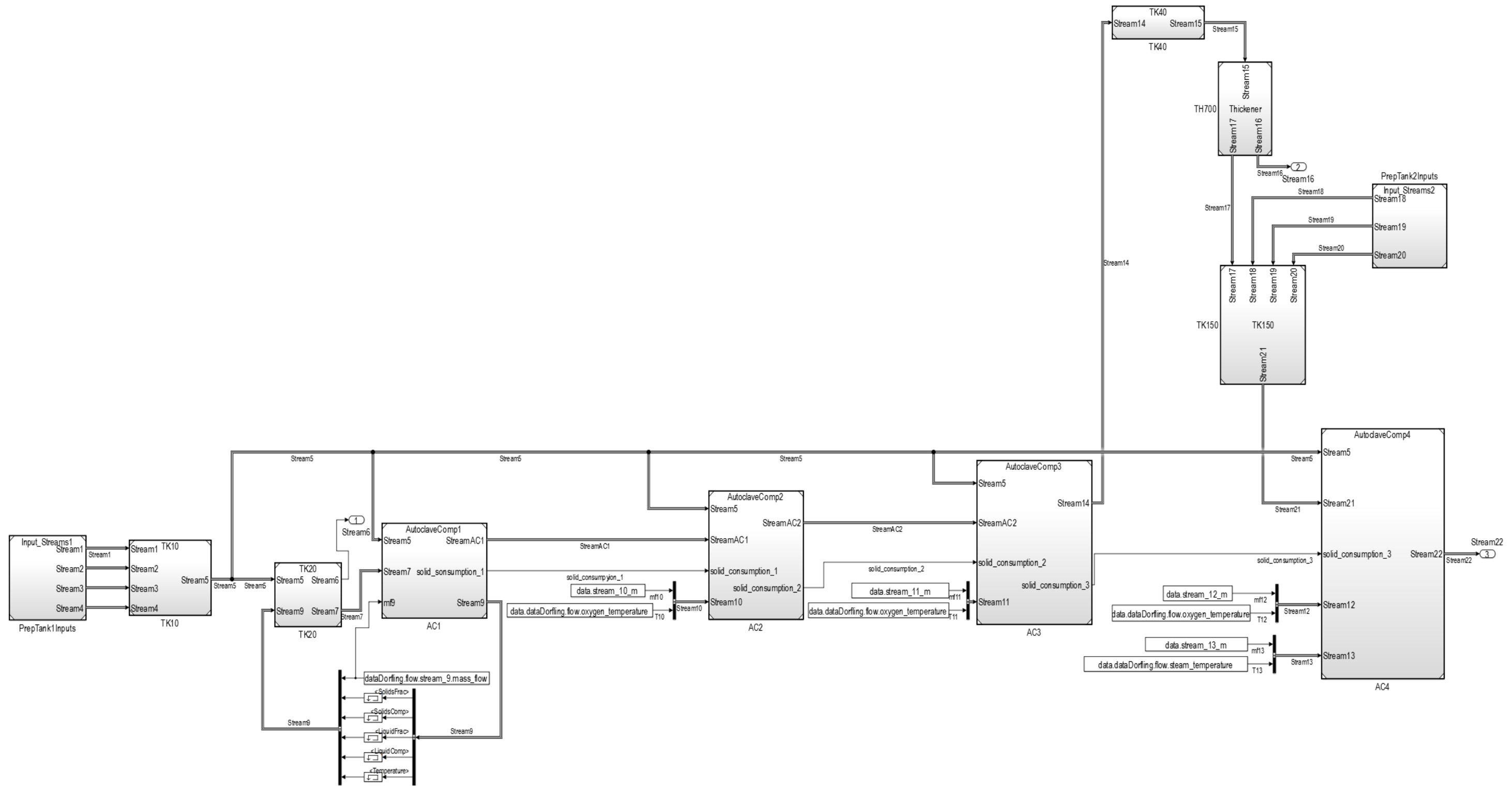


Figure E.3: Baseline Simulink™ model flow diagram of Leaching Process: Western Platinum Ltd. BMR

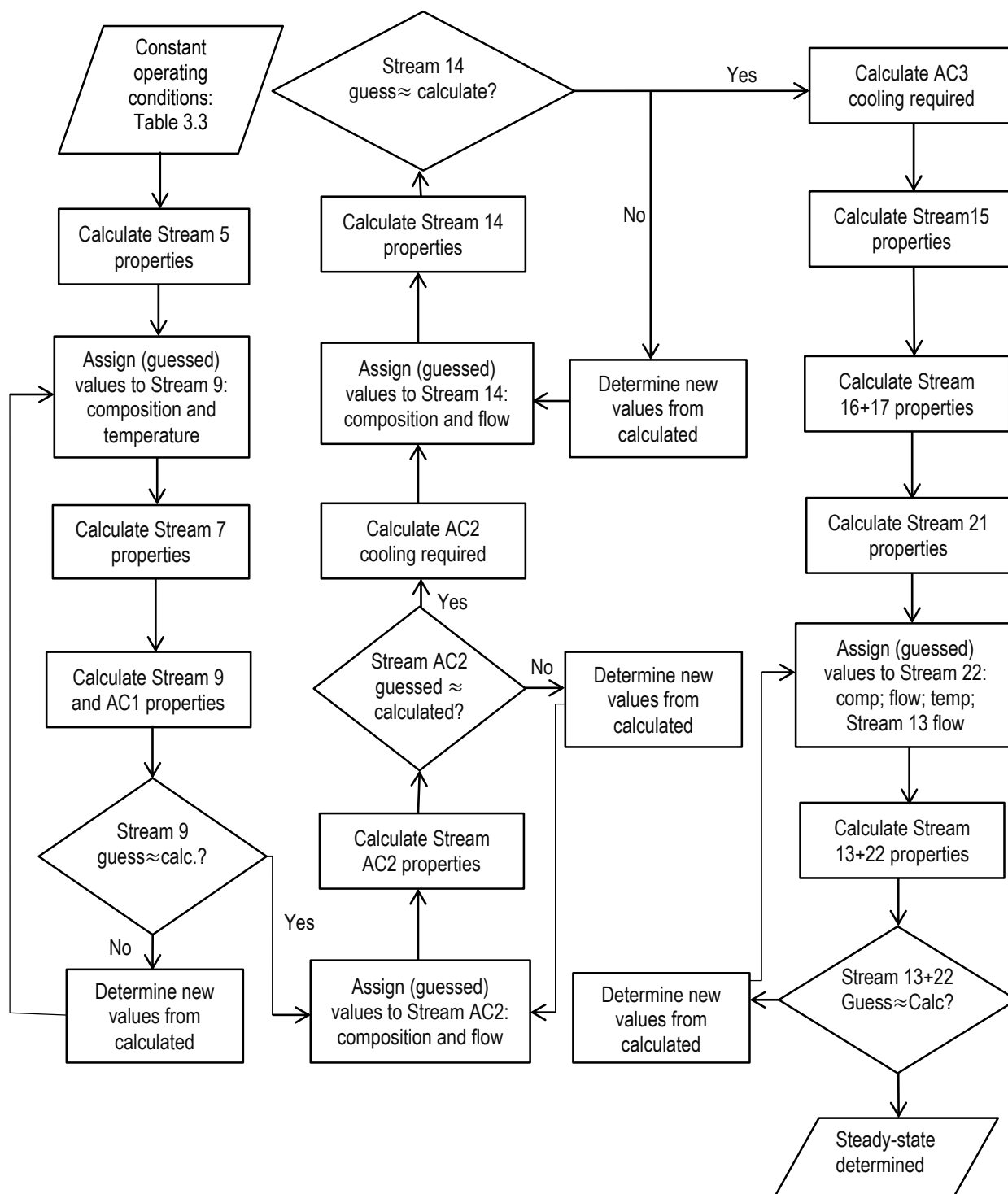


Figure E.4: Flow diagram to determine steady-state operating conditions

The method used by Dorfling (2012) to determine steady-state conditions firstly involves the calculation of stream 5 properties including liquid composition; solid composition; temperature; and flow rate using input data. A composition and temperature is guessed for stream 9 which is used in stream 7 property calculations by solving the flash recycle tank.

The resulting stream 7 properties are used in first compartment calculations to produce a new estimation of stream 9 properties. The new stream 9 properties, if not corresponding to guessed properties, are then used in new stream 7 property estimations:

$$p_{new}^{(\epsilon)} = p^{(\epsilon)} + f \times (p^{(\epsilon+1)} - p^{(\epsilon)}) \quad \text{Equation E.1}$$

where $p^{(\epsilon)}$, and f represent a specific property p at iteration ϵ and multiplication factor, respectively. Once the flash recycle tank and first compartment are solved, the properties of the next compartment is guessed and re-estimated in a similar manner described previously.

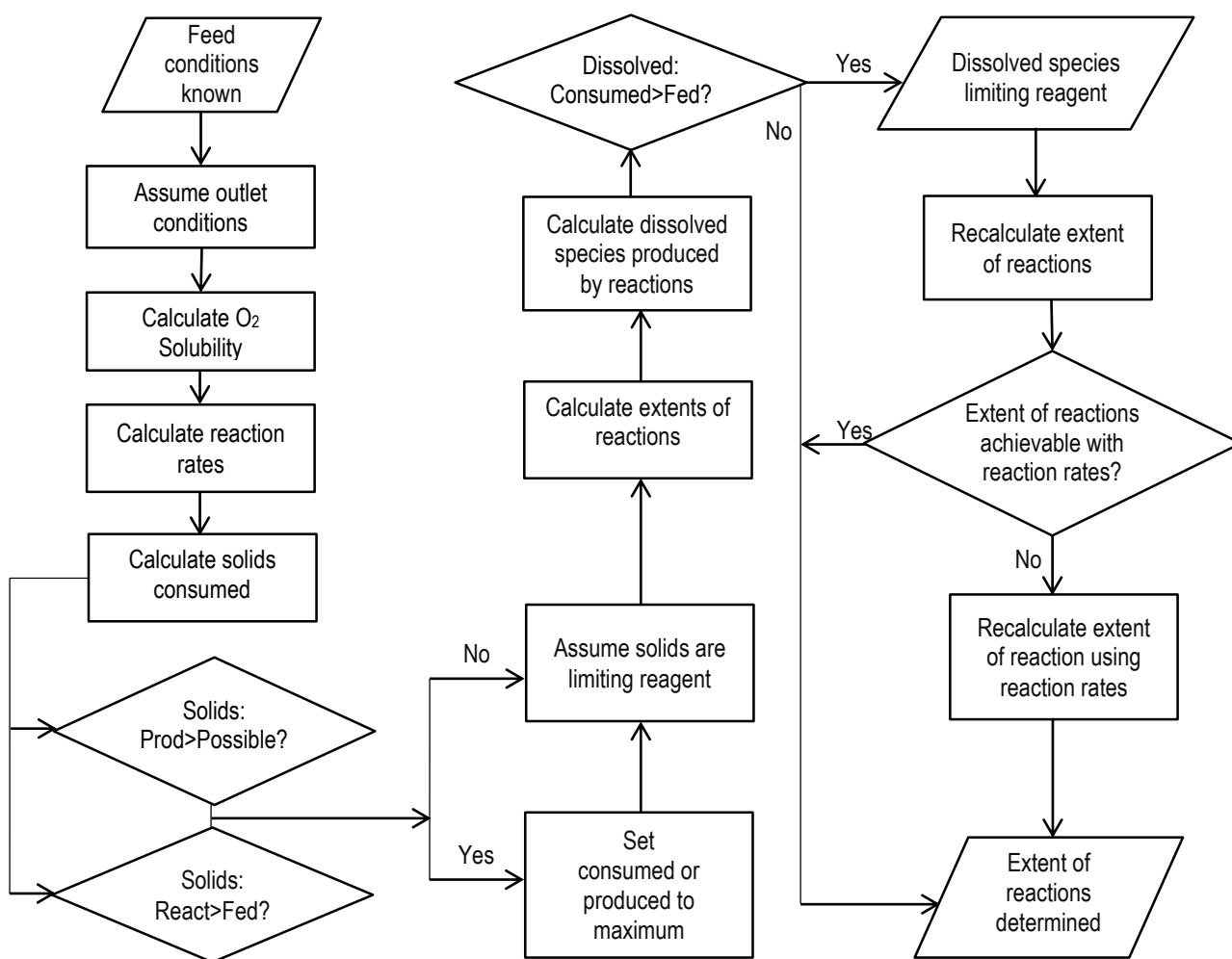


Figure E.5: Flow diagram to determine steady-state extent of reactions

Table F.2: KPIs at the end of simulation: Baseline

Controllers	TD (variable units)	AE (variable units)	IAE (variable units.h)	MD (variable units)	TNASP (h)	SD (variable units)
Autoclave pressure control (bar)	332.54	0.00	0.31	0.01	0.00	0.00
Compartment 1 temperature control (°C)	12857.30	0.04	5.73	0.25	0.00	0.05
Compartment 2 temperature control (°C)	4806.20	0.03	4.09	0.10	0.00	0.03
Compartment 3 temperature control (°C)	6136.79	0.02	2.36	0.08	0.00	0.02
Compartment 4 temperature control (°C)	10952.07	0.02	2.43	0.10	0.00	0.02
Second stage slurry preparation tank level control (%)	110409.38	0.33	46.07	1.48	0.00	0.37
Flash recycle tank level control (%)	178788.95	0.25	35.12	1.45	0.00	0.31
Compartment 3 level control (%)	48739.01	0.09	12.91	0.59	0.00	0.12
Compartment 4 level control (%)	187406.15	0.26	37.02	1.49	0.00	0.33
Second stage slurry preparation tank density (kg/l)	2817.36	0.00	0.65	0.02	0.00	0.00
Spent electrolyte flow control (m³/h)	67927.10	0.10	14.02	0.60	0.00	0.13
Flash recycle tank outlet flow control (m³/h)	125515.93	0.36	50.38	2.07	0.44	0.24
Compartment 3 outlet flow control (m³/h)	86490.90	0.13	17.53	0.78	0.00	0.16
Compartment 4 outlet flow control (m³/h)	98466.57	0.18	25.51	1.09	0.15	0.17

Valves	TD (variable units)	AE (variable units)	IAE (variable units.h)	TNASP (h)	VR (#)	CS (#)	TS (h)	LTS (h)
Compartment 2 temperature control valve (%)	99.38	0.02	3.09	0.00	71317.00	0	0.00	0.00
Compartment 3 temperature control valve (%)	94.98	0.02	3.25	0.00	89817.00	0	0.00	0.00
Compartment 4 temperature control valve (%)	1266.21	0.32	44.33	0.00	102594.00	0	0.00	0.00
Spent electrolyte flow control valve (%)	2186.23	0.58	80.98	0.00	103107.00	0	0.00	0.00
Flash recycle tank outlet flow control valve (%)	3530.70	0.87	121.57	0.00	67409.00	0	0.00	0.00
Compartment 1 outlet flow control valve (%)	443.10	0.12	16.24	0.00	100381.00	0	0.00	0.00
Compartment 3 outlet flow control valve (%)	2290.00	0.59	83.11	0.00	97618.00	0	0.00	0.00
Compartment 4 outlet flow control valve (%)	5470.00	1.45	202.69	0.82	104111.00	0	0.00	0.00

Operational KPIs	Compartment 1	Compartment 2	Compartment 3	Compartment 4
Total PGMs in liquid (wt%)	1.66	0.34	0.12	0.01
Total BMs in solid (wt%)	45.92	38.79	36.84	30.36

Operational KPIs	
Total BM input (kg)	62195.53
Total PGM input (kg)	265.29
Total solid throughput (kg)	34615.26
Total oxygen usage (kg)	34247.88
Total steam usage (kg)	31500.85
Compartment 2 CW usage (kg)	148247.43
Compartment 3 CW usage (kg)	54994.68
Second stage slurry preparation tank spillage (kg)	0.00
Flash recycle tank spillage (kg)	0.00
Third stage slurry preparation tank spillage (kg)	0.00
Compartment 3 spillage (kg)	0.00
Compartment 4 spillage (kg)	0.00

Table F.3: Equivalence of baseline KPIs and fault 1 KPIs at t = 50 hours

Controllers	TD	AE	IAE	MD	TNASP	SD
Autoclave pressure control (bar)	TRUE	TRUE	TRUE	TRUE	TRUE	TRUE
Compartment 1 temperature control (°C)	TRUE	TRUE	TRUE	TRUE	TRUE	TRUE
Compartment 2 temperature control (°C)	TRUE	TRUE	TRUE	TRUE	TRUE	TRUE
Compartment 3 temperature control (°C)	TRUE	TRUE	TRUE	TRUE	TRUE	TRUE
Compartment 4 temperature control (°C)	TRUE	TRUE	TRUE	TRUE	TRUE	TRUE
Second stage slurry preparation tank level control (%)	TRUE	TRUE	TRUE	TRUE	TRUE	TRUE
Flash recycle tank level control (%)	TRUE	TRUE	TRUE	TRUE	TRUE	TRUE
Compartment 3 level control (%)	TRUE	TRUE	TRUE	TRUE	TRUE	TRUE
Compartment 4 level control (%)	TRUE	TRUE	TRUE	TRUE	TRUE	TRUE
Second stage slurry preparation tank density (kg/l)	TRUE	TRUE	TRUE	TRUE	TRUE	TRUE
Spent electrolyte flow control (m ³ /h)	TRUE	TRUE	TRUE	TRUE	TRUE	TRUE
Flash recycle tank outlet flow control (m ³ /h)	TRUE	TRUE	TRUE	TRUE	TRUE	TRUE
Compartment 3 outlet flow control (m ³ /h)	TRUE	TRUE	TRUE	TRUE	TRUE	TRUE
Compartment 4 outlet flow control (m ³ /h)	TRUE	TRUE	TRUE	TRUE	TRUE	TRUE

Valves	TD	AE	IAE	TNASP	VR	CS	TS	LTS
Compartment 2 temperature control valve (%)	TRUE	TRUE	TRUE	TRUE	TRUE	TRUE	TRUE	TRUE
Compartment 3 temperature control valve (%)	TRUE	TRUE	TRUE	TRUE	TRUE	TRUE	TRUE	TRUE
Compartment 4 temperature control valve (%)	TRUE	TRUE	TRUE	TRUE	TRUE	TRUE	TRUE	TRUE
Spent electrolyte flow control valve (%)	TRUE	TRUE	TRUE	TRUE	TRUE	TRUE	TRUE	TRUE
Flash recycle tank outlet flow control valve (%)	TRUE	TRUE	TRUE	TRUE	TRUE	TRUE	TRUE	TRUE
Compartment 1 outlet flow control valve (%)	TRUE	TRUE	TRUE	TRUE	TRUE	TRUE	TRUE	TRUE
Compartment 3 outlet flow control valve (%)	TRUE	TRUE	TRUE	TRUE	TRUE	TRUE	TRUE	TRUE
Compartment 4 outlet flow control valve (%)	TRUE	TRUE	TRUE	TRUE	TRUE	TRUE	TRUE	TRUE

Operational KPIs	Compartment 1	Compartment 2	Compartment 3	Compartment 4
Total PGMs in liquid (wt%)	TRUE	TRUE	TRUE	TRUE
Total BMs in solid (wt%)	TRUE	TRUE	TRUE	TRUE

Operational KPIs	
Total BM input (kg)	TRUE
Total PGM input (kg)	TRUE
Total solid throughput (kg)	TRUE
Total oxygen usage (kg)	TRUE
Total steam usage (kg)	TRUE
Compartment 2 CW usage (kg)	TRUE
Compartment 3 CW usage (kg)	TRUE
Second stage slurry preparation tank spillage (kg)	TRUE
Flash recycle tank spillage (kg)	TRUE
Third stage slurry preparation tank spillage (kg)	TRUE
Compartment 3 spillage (kg)	TRUE
Compartment 4 spillage (kg)	TRUE

Table F.4: KPIs at the end of simulation: Fault 1 – Valve blockage

Controllers	TD (%)	AE (%)	IAE (%)	MD (%)	TNASP	SD (%)
Autoclave pressure control (bar)	0.00	32.74	32.74	123.56	0.00	47.11
Compartment 1 temperature control (°C)	0.00	2.19	2.19	0.41	0.00	1.90
Compartment 2 temperature control (°C)	0.00	13.34	13.34	44.92	0.00	18.36
Compartment 3 temperature control (°C)	0.00	0.48	0.48	-3.96	0.00	0.29
Compartment 4 temperature control (°C)	0.00	-0.14	-0.14	-0.04	0.00	-0.13
Second stage slurry preparation tank level control (%)	0.00	49.48	49.48	180.07	0.00	75.77
Flash recycle tank level control (%)	0.00	0.01	0.01	0.00	0.00	0.01
Compartment 3 level control (%)	0.00	-0.35	-0.35	-2.44	0.00	-0.33
Compartment 4 level control (%)	0.00	0.00	0.00	-0.04	0.00	0.00
Second stage slurry preparation tank density (kg/l)	0.00	4.18	4.18	58.15	0.00	14.39
Spent electrolyte flow control (m ³ /h)	0.00	-0.07	-0.07	0.69	0.00	4.98
Flash recycle tank outlet flow control (m ³ /h)	0.00	0.00	0.00	0.00	0.44	0.16
Compartment 3 outlet flow control (m ³ /h)	0.00	-0.01	-0.01	0.01	0.00	-0.04
Compartment 4 outlet flow control (m ³ /h)	0.00	0.00	0.00	0.00	0.15	0.00

Valves	TD (%)	AE (%)	IAE (%)	TNASP (h)	VR (%)	CS (#)	TS (h)	LTS (h)
Compartment 2 temperature control valve (%)	2.79	2.86	2.86	0.00	-2.86	0	0.00	0.00
Compartment 3 temperature control valve (%)	-0.06	-0.06	-0.06	0.00	0.05	0	0.00	0.00
Compartment 4 temperature control valve (%)	0.00	0.00	0.00	0.00	-0.02	0	0.00	0.00
Spent electrolyte flow control valve (%)	0.00	-0.03	-0.03	0.00	-0.05	0	0.00	0.00
Flash recycle tank outlet flow control valve (%)	0.00	0.00	0.00	0.00	0.01	0	0.00	0.00
Compartment 1 outlet flow control valve (%)	0.00	0.00	0.00	0.00	0.01	0	0.00	0.00
Compartment 3 outlet flow control valve (%)	-0.01	-0.01	-0.01	0.00	-0.01	0	0.00	0.00
Compartment 4 outlet flow control valve (%)	0.00	0.00	0.00	0.82	0.00	0	0.00	0.00

Operational KPIs	Compartment 1	Compartment 2	Compartment 3	Compartment 4
Total PGMs in liquid (%)	0.35	0.05	-0.21	-1.34
Total BMs in solid (%)	0.25	0.03	0.06	0.14

Operational KPIs	
Decrease in total BM input (%)	-0.55
Decrease in total PGM input (%)	-0.64
Decrease in total solid throughput (%)	-0.61
Total oxygen usage (%)	0.23
Total steam usage (%)	-0.16
Compartment 2 CW usage (%)	3.35
Compartment 3 CW usage (%)	0.09
Second stage slurry preparation tank spillage (kg)	0.00
Flash recycle tank spillage (kg)	0.00
Third stage slurry preparation tank spillage (kg)	0.00
Compartment 3 spillage (kg)	0.00
Compartment 4 spillage (kg)	0.00

Table F.5: KPIs at the end of simulation: Fault 2 – Valve wear

Controllers	TD (%)	AE (%)	IAE (%)	MD (%)	TNASP	SD (%)
Autoclave pressure control (bar)	0.00	0.28	0.28	1.99	0.00	0.25
Compartment 1 temperature control (°C)	0.00	-0.01	-0.01	-0.19	0.00	0.00
Compartment 2 temperature control (°C)	0.00	0.00	0.00	0.00	0.00	0.00
Compartment 3 temperature control (°C)	0.00	0.00	0.00	0.00	0.00	0.00
Compartment 4 temperature control (°C)	0.00	-0.01	-0.01	0.06	0.00	-0.01
Second stage slurry preparation tank level control (%)	0.00	0.00	0.00	0.00	0.00	0.00
Flash recycle tank level control (%)	0.00	0.00	0.00	0.00	0.00	0.00
Compartment 3 level control (%)	0.00	0.00	0.00	-0.01	0.00	0.00
Compartment 4 level control (%)	0.00	0.34	0.34	1.27	0.00	0.31
Second stage slurry preparation tank density (kg/l)	0.00	0.00	0.00	0.00	0.00	0.00
Spent electrolyte flow control (m ³ /h)	0.00	0.00	0.00	0.00	0.00	0.00
Flash recycle tank outlet flow control (m ³ /h)	0.00	0.00	0.00	0.00	0.44	0.00
Compartment 3 outlet flow control (m ³ /h)	0.00	0.00	0.00	0.00	0.00	0.00
Compartment 4 outlet flow control (m ³ /h)	0.02	2.92	2.92	6.84	0.20	1.47

Valves	TD (%)	AE (%)	IAE (%)	TNASP (h)	VR (%)	CS (#)	TS (h)	LTS (h)
Compartment 2 temperature control valve (%)	0.00	0.00	0.00	0.00	-0.03	0	0.00	0.00
Compartment 3 temperature control valve (%)	0.00	0.00	0.00	0.00	-0.02	0	0.00	0.00
Compartment 4 temperature control valve (%)	0.00	0.00	0.00	0.00	-0.01	0	0.00	0.00
Spent electrolyte flow control valve (%)	0.00	0.00	0.00	0.00	0.00	0	0.00	0.00
Flash recycle tank outlet flow control valve (%)	0.00	0.00	0.00	0.00	0.00	0	0.00	0.00
Compartment 1 outlet flow control valve (%)	0.00	0.00	0.00	0.00	0.00	0	0.00	0.00
Compartment 3 outlet flow control valve (%)	0.00	0.00	0.00	0.00	-0.01	0	0.00	0.00
Compartment 4 outlet flow control valve (%)	-35.17	-35.24	-35.24	0.32	-10.60	0	0.00	0.00

Operational KPIs	Compartment 1	Compartment 2	Compartment 3	Compartment 4
Total PGMs in liquid (%)	0.00	0.00	0.00	0.01
Total BMs in solid (%)	0.00	0.00	0.00	0.00

Operational KPIs	
Decrease in total BM input (%)	0.00
Decrease in total PGM input (%)	0.00
Decrease in total solid throughput (%)	0.00
Total oxygen usage (%)	0.00
Total steam usage (%)	0.00
Compartment 2 CW usage (%)	0.00
Compartment 3 CW usage (%)	0.00
Second stage slurry preparation tank spillage (kg)	0.00
Flash recycle tank spillage (kg)	0.00
Third stage slurry preparation tank spillage (kg)	0.00
Compartment 3 spillage (kg)	0.00
Compartment 4 spillage (kg)	0.00

Table F.6: KPIs at the end of simulation: Fault 3 – Valve stiction

Controllers	TD (%)	AE (%)	IAE (%)	MD (%)	TNASP	SD (%)
Autoclave pressure control (bar)	0.05	203.98	203.98	599.97	0.00	314.38
Compartment 1 temperature control (°C)	0.00	22.91	22.91	89.86	0.00	50.36
Compartment 2 temperature control (°C)	0.00	-4.34	-4.34	112.73	0.00	26.80
Compartment 3 temperature control (°C)	0.00	-4.20	-4.20	-0.40	0.00	-4.47
Compartment 4 temperature control (°C)	0.00	0.51	0.51	0.02	0.00	0.52
Second stage slurry preparation tank level control (%)	0.00	7.41	7.41	99.86	0.00	21.55
Flash recycle tank level control (%)	0.00	0.22	0.22	0.94	0.00	0.21
Compartment 3 level control (%)	0.00	-1.73	-1.73	-7.98	0.00	-1.83
Compartment 4 level control (%)	0.00	0.04	0.04	0.11	0.00	0.05
Second stage slurry preparation tank density (kg/l)	0.00	436.22	436.22	155.17	14.98	276.24
Spent electrolyte flow control (m ³ /h)	0.01	422.46	422.46	132.66	79.66	183.77
Flash recycle tank outlet flow control (m ³ /h)	0.01	0.96	0.96	6.36	0.53	61.42
Compartment 3 outlet flow control (m ³ /h)	0.01	0.08	0.08	-0.36	0.00	0.29
Compartment 4 outlet flow control (m ³ /h)	0.01	-0.02	-0.02	0.00	0.15	0.05

Valves	TD (%)	AE (%)	IAE (%)	TNASP (h)	VR (%)	CS (#)	TS (h)	LTS (h)
Compartment 2 temperature control valve (%)	1.66	-7.66	-7.66	0.00	15.32	0	0.00	0.00
Compartment 3 temperature control valve (%)	11.38	0.30	0.30	0.00	0.48	0	0.00	0.00
Compartment 4 temperature control valve (%)	13.26	1.46	1.46	0.00	-1.71	0	0.00	0.00
Spent electrolyte flow control valve (%)	125.71	1436.62	1436.62	89.66	-88.76	0	0.00	0.00
Flash recycle tank outlet flow control valve (%)	13.57	2.48	2.48	0.00	-1.92	0	0.00	0.00
Compartment 1 outlet flow control valve (%)	13.55	1.26	1.26	0.00	-1.28	0	0.00	0.00
Compartment 3 outlet flow control valve (%)	13.40	1.36	1.36	0.00	-1.31	0	0.00	0.00
Compartment 4 outlet flow control valve (%)	16.09	2.79	2.79	1.15	-2.64	0	0.00	0.00

Operational KPIs	Compartment 1	Compartment 2	Compartment 3	Compartment 4
Total PGMs in liquid (%)	48.31	82.95	122.42	63.86
Total BMs in solid (%)	-11.15	-9.05	-9.78	-9.26

Operational KPIs	
Decrease in total BM input (%)	10.45
Decrease in total PGM input (%)	8.35
Decrease in total solid throughput (%)	16.37
Total oxygen usage (%)	-7.81
Total steam usage (%)	3.28
Compartment 2 CW usage (%)	-38.71
Compartment 3 CW usage (%)	-2.09
Second stage slurry preparation tank spillage (kg)	0.00
Flash recycle tank spillage (kg)	0.00
Third stage slurry preparation tank spillage (kg)	0.00
Compartment 3 spillage (kg)	0.00
Compartment 4 spillage (kg)	0.00

Table F.7: KPIs at the end of simulation: Fault 4 – Pump impeller wear

Controllers	TD (%)	AE (%)	IAE (%)	MD (%)	TNASP	SD (%)
Autoclave pressure control (bar)	0.41	3607.36	3607.36	8829.67	42.87	4770.85
Compartment 1 temperature control (°C)	0.04	6847.09	6847.09	8327.90	68.84	8215.09
Compartment 2 temperature control (°C)	0.00	206.31	206.31	1524.96	2.96	726.04
Compartment 3 temperature control (°C)	0.00	85.18	85.18	912.69	0.00	365.37
Compartment 4 temperature control (°C)	0.00	13501.56	13501.56	7733.68	63.65	13205.61
Second stage slurry preparation tank level control (%)	0.00	2627.72	2627.72	1710.95	75.35	2232.88
Flash recycle tank level control (%)	0.00	12245.16	12245.16	4488.95	84.84	8045.82
Compartment 3 level control (%)	0.00	20773.89	20773.89	10515.19	84.18	17733.98
Compartment 4 level control (%)	0.00	-0.09	-0.09	0.00	0.00	-0.12
Second stage slurry preparation tank density (kg/l)	0.00	462.59	462.59	227.63	41.46	361.03
Spent electrolyte flow control (m ³ /h)	0.00	1.48	1.48	4.24	0.00	151.30
Flash recycle tank outlet flow control (m ³ /h)	0.00	7338.35	7338.35	2081.85	86.20	708.96
Compartment 3 outlet flow control (m ³ /h)	0.00	-0.50	-0.50	0.60	0.00	883.46
Compartment 4 outlet flow control (m ³ /h)	0.00	0.00	0.00	0.01	0.15	0.52

Valves	TD (%)	AE (%)	IAE (%)	TNASP (h)	VR (%)	CS (#)	TS (h)	LTS (h)
Compartment 2 temperature control valve (%)	-3.38	-2.97	-2.97	0.00	19.50	0	0.00	0.00
Compartment 3 temperature control valve (%)	4.13	4.31	4.31	0.00	5.18	0	0.00	0.00
Compartment 4 temperature control valve (%)	-46.42	-49.46	-49.46	0.00	-51.88	1	71.06	71.06
Spent electrolyte flow control valve (%)	-16.75	-17.13	-17.13	0.00	-1.92	0	0.00	0.00
Flash recycle tank outlet flow control valve (%)	-61.33	-61.60	-61.60	0.00	-61.78	1	86.37	86.37
Compartment 1 outlet flow control valve (%)	-1.64	-3.50	-3.50	0.00	-9.15	0	0.00	0.00
Compartment 3 outlet flow control valve (%)	-28.91	-28.83	-28.83	0.00	-2.35	0	0.00	0.00
Compartment 4 outlet flow control valve (%)	0.07	0.01	0.01	0.82	-0.04	0	0.00	0.00

Operational KPIs	Compartment 1	Compartment 2	Compartment 3	Compartment 4
Total PGMs in liquid (%)	-7.61	-7.36	-7.40	2792.04
Total BMs in solid (%)	-9.85	-9.44	-9.12	-1.23

Operational KPIs	
Decrease in total BM input (%)	56.37
Decrease in total PGM input (%)	57.01
Decrease in total solid throughput (%)	56.68
Total oxygen usage (%)	-41.71
Total steam usage (%)	23.24
Compartment 2 CW usage (%)	-59.92
Compartment 3 CW usage (%)	-58.67
Second stage slurry preparation tank spillage (kg)	0.00
Flash recycle tank spillage (kg)	10822.32
Third stage slurry preparation tank spillage (kg)	0.00
Compartment 3 spillage (kg)	0.00
Compartment 4 spillage (kg)	0.00

Table F.8: KPIs at the end of simulation: Fault 5 – Solid build-up in cooling coils

Controllers	TD (%)	AE (%)	IAE (%)	MD (%)	TNASP	SD (%)
Autoclave pressure control (bar)	425.67	34385.18	34385.18	25554.70	75.70	37635.94
Compartment 1 temperature control (°C)	0.32	7032.70	7032.70	3020.82	72.02	5591.44
Compartment 2 temperature control (°C)	3.26	39669.53	39669.53	20573.82	85.96	27909.90
Compartment 3 temperature control (°C)	1.66	2196.02	2196.02	1637.95	0.00	2620.62
Compartment 4 temperature control (°C)	0.71	2483.47	2483.47	1554.91	3.32	2924.05
Second stage slurry preparation tank level control (%)	0.00	0.00	0.00	0.00	0.00	0.00
Flash recycle tank level control (%)	0.00	1.71	1.71	11.73	0.00	1.67
Compartment 3 level control (%)	0.00	53.79	53.79	91.67	0.00	62.29
Compartment 4 level control (%)	0.00	2.21	2.21	2.69	0.00	2.21
Second stage slurry preparation tank density (kg/l)	0.00	0.00	0.00	0.00	0.00	0.00
Spent electrolyte flow control (m ³ /h)	0.00	0.00	0.00	0.00	0.00	0.00
Flash recycle tank outlet flow control (m ³ /h)	0.00	0.01	0.01	-0.06	0.44	310.17
Compartment 3 outlet flow control (m ³ /h)	0.00	5.16	5.16	3.17	0.00	9.14
Compartment 4 outlet flow control (m ³ /h)	0.00	0.08	0.08	0.15	0.15	0.33

Valves	TD (%)	AE (%)	IAE (%)	TNASP (h)	VR (%)	CS (#)	TS (h)	LTS (h)
Compartment 2 temperature control valve (%)	13.93	10.74	10.74	0.00	-78.24	1	84.74	84.74
Compartment 3 temperature control valve (%)	3935.67	3831.15	3831.15	0.00	-60.00	0	0.00	0.00
Compartment 4 temperature control valve (%)	2619.78	2487.98	2487.98	59.43	-54.95	30	0.83	0.04
Spent electrolyte flow control valve (%)	0.00	0.00	0.00	0.00	0.00	0	0.00	0.00
Flash recycle tank outlet flow control valve (%)	0.05	0.05	0.05	0.00	-0.01	0	0.00	0.00
Compartment 1 outlet flow control valve (%)	-19.64	-20.35	-20.35	0.00	-7.42	0	0.00	0.00
Compartment 3 outlet flow control valve (%)	9.30	7.84	7.84	0.00	-8.59	0	0.00	0.00
Compartment 4 outlet flow control valve (%)	0.12	0.10	0.10	0.84	-0.13	0	0.00	0.00

Operational KPIs	Compartment 1	Compartment 2	Compartment 3	Compartment 4
Total PGMs in liquid (%)	105.11	91.12	127.29	97.10
Total BMs in solid (%)	15.45	16.88	14.81	14.70

Operational KPIs	
Decrease in total BM input (%)	0.00
Decrease in total PGM input (%)	0.00
Decrease in total solid throughput (%)	-11.21
Total oxygen usage (%)	-14.07
Total steam usage (%)	-3.76
Compartment 2 CW usage (%)	-59.75
Compartment 3 CW usage (%)	333.54
Second stage slurry preparation tank spillage (kg)	0.00
Flash recycle tank spillage (kg)	0.00
Third stage slurry preparation tank spillage (kg)	0.00
Compartment 3 spillage (kg)	0.00
Compartment 4 spillage (kg)	0.00

Table F.9: KPIs at the end of simulation: Fault 6 – Peristaltic pump tube failure

Controllers	TD (%)	AE (%)	IAE (%)	MD (%)	TNASP	SD (%)
Autoclave pressure control (bar)	1.29	2964.43	2964.43	17573.81	26.83	4619.60
Compartment 1 temperature control (°C)	0.00	256.26	256.26	2341.05	3.27	903.98
Compartment 2 temperature control (°C)	0.01	59.75	59.75	2077.78	1.32	542.99
Compartment 3 temperature control (°C)	0.01	89.97	89.97	1341.53	0.00	392.02
Compartment 4 temperature control (°C)	0.00	10144.00	10144.00	5724.93	61.97	8802.21
Second stage slurry preparation tank level control (%)	0.00	16476.18	16476.18	3983.57	129.64	4216.94
Flash recycle tank level control (%)	0.00	5.47	5.47	34.94	0.00	5.08
Compartment 3 level control (%)	0.00	296.79	296.79	1133.00	2.42	743.90
Compartment 4 level control (%)	0.00	0.02	0.02	-1.01	0.00	-0.01
Second stage slurry preparation tank density (kg/l)	0.00	2123.60	2123.60	535.45	124.23	719.67
Spent electrolyte flow control (m ³ /h)	0.00	3.55	3.55	35.40	0.01	55.52
Flash recycle tank outlet flow control (m ³ /h)	0.00	-2.89	-2.89	-1.93	0.29	485.76
Compartment 3 outlet flow control (m ³ /h)	0.00	0.75	0.75	56.29	0.09	486.53
Compartment 4 outlet flow control (m ³ /h)	0.00	0.00	0.00	-0.18	0.15	0.28

Valves	TD (%)	AE (%)	IAE (%)	TNASP (h)	VR (%)	CS (#)	TS (h)	LTS (h)
Compartment 2 temperature control valve (%)	62.07	75.33	75.33	0.00	-12.13	0	0.00	0.00
Compartment 3 temperature control valve (%)	92.05	97.69	97.69	0.00	-36.44	0	0.00	0.00
Compartment 4 temperature control valve (%)	-55.53	-57.60	-57.60	0.00	-62.43	21	86.54	37.18
Spent electrolyte flow control valve (%)	-34.92	-32.10	-32.10	0.01	-3.51	0	0.00	0.00
Flash recycle tank outlet flow control valve (%)	-9.15	-4.05	-4.05	0.00	0.08	0	0.00	0.00
Compartment 1 outlet flow control valve (%)	-4.40	0.39	0.39	0.00	-0.11	0	0.00	0.00
Compartment 3 outlet flow control valve (%)	-14.07	-10.33	-10.33	0.01	0.34	0	0.00	0.00
Compartment 4 outlet flow control valve (%)	-4.31	0.45	0.45	0.90	-0.56	0	0.00	0.00

Operational KPIs	Compartment 1	Compartment 2	Compartment 3	Compartment 4
Total PGMs in liquid (%)	14.81	31.09	21.11	128319.80
Total BMs in solid (%)	-1.14	1.67	1.20	31.68

Operational KPIs	
Decrease in total BM input (%)	89.53
Decrease in total PGM input (%)	89.92
Decrease in total solid throughput (%)	85.35
Total oxygen usage (%)	-64.25
Total steam usage (%)	34.72
Compartment 2 CW usage (%)	-87.20
Compartment 3 CW usage (%)	-81.97
Second stage slurry preparation tank spillage (kg)	0.00
Flash recycle tank spillage (kg)	0.00
Third stage slurry preparation tank spillage (kg)	0.00
Compartment 3 spillage (kg)	0.00
Compartment 4 spillage (kg)	0.00

Table F.10: KPIs at the end of simulation: Fault 15 – Level sensor blockage

Controllers	TD (%)	AE (%)	IAE (%)	MD (%)	TNASP	SD (%)			
Autoclave pressure control (bar)	0.00	2.16	2.16	22.47	0.00	2.53			
Compartment 1 temperature control (°C)	0.00	-0.07	-0.07	0.10	0.00	-0.17			
Compartment 2 temperature control (°C)	0.00	0.32	0.32	-0.09	0.00	0.35			
Compartment 3 temperature control (°C)	0.00	-3.36	-3.36	12.28	0.00	-0.66			
Compartment 4 temperature control (°C)	0.00	-0.04	-0.04	-0.01	0.00	-0.04			
Second stage slurry preparation tank level control (%)	0.00	0.00	0.00	0.00	0.00	0.00			
Flash recycle tank level control (%)	0.00	0.00	0.00	-0.01	0.00	0.00			
Compartment 3 level control (%)	5.25	36149.22	36149.22	8034.30	127.05	9633.72			
Compartment 4 level control (%)	0.00	0.00	0.00	0.01	0.00	0.00			
Second stage slurry preparation tank density (kg/l)	0.00	0.00	0.00	0.00	0.00	0.00			
Spent electrolyte flow control (m ³ /h)	0.00	0.00	0.00	0.00	0.00	0.00			
Flash recycle tank outlet flow control (m ³ /h)	0.00	0.00	0.00	0.00	0.44	-0.01			
Compartment 3 outlet flow control (m ³ /h)	0.00	-0.08	-0.08	0.00	0.00	1.97			
Compartment 4 outlet flow control (m ³ /h)	0.00	0.00	0.00	0.00	0.15	0.00			

Valves	TD (%)	AE (%)	IAE (%)	TNASP (h)	VR (%)	CS (#)	TS (h)	LTS (h)
Compartment 2 temperature control valve (%)	0.08	0.09	0.09	0.00	-0.09	0	0.00	0.00
Compartment 3 temperature control valve (%)	12.23	11.06	11.06	0.00	-11.36	0	0.00	0.00
Compartment 4 temperature control valve (%)	0.00	0.00	0.00	0.00	-0.02	0	0.00	0.00
Spent electrolyte flow control valve (%)	0.00	0.00	0.00	0.00	0.00	0	0.00	0.00
Flash recycle tank outlet flow control valve (%)	0.00	0.00	0.00	0.00	0.00	0	0.00	0.00
Compartment 1 outlet flow control valve (%)	0.00	0.00	0.00	0.00	0.01	0	0.00	0.00
Compartment 3 outlet flow control valve (%)	-0.22	-0.19	-0.19	0.00	0.15	0	0.00	0.00
Compartment 4 outlet flow control valve (%)	0.00	0.00	0.00	0.82	0.00	0	0.00	0.00

Operational KPIs	Compartment 1	Compartment 2	Compartment 3	Compartment 4
Total PGMs in liquid (%)	0.00	-0.01	26.52	-1.62
Total BMs in solid (%)	-0.01	0.00	1.79	1.72

Operational KPIs	
Decrease in total BM input (%)	0.00
Decrease in total PGM input (%)	0.00
Decrease in total solid throughput (%)	-1.29
Total oxygen usage (%)	-0.61
Total steam usage (%)	-1.06
Compartment 2 CW usage (%)	-0.01
Compartment 3 CW usage (%)	-18.24
Second stage slurry preparation tank spillage (kg)	0.00
Flash recycle tank spillage (kg)	0.00
Third stage slurry preparation tank spillage (kg)	0.00
Compartment 3 spillage (kg)	0.00
Compartment 4 spillage (kg)	0.00

Western Platinum BMR

Table F.11: Fault database (McCulloch et al., 2014)

#	Classification	Fault name	Symptom identification method	Symptom dynamics	Fault location	Fault type	Rate of fault transition	Frequency of fault occurrence	Priority for fault mitigation	Possibility of fault modelling
1	Actuator failure	Valve blockage	Frequently measured: Second stage slurry preparation tank density	Density and solid% spikes out second stage slurry preparation tank	Stream 1	Additive	Intermittent	Once a day	High	Yes
2	Actuator failure	Valve wear	Qualitative: Internal valve abrasion	Valve characteristics changes	Autoclave compartment 3 discharge valve and flash recycle valve	Multiplicative	Incipient	Once every nine months replacement is required	High	Yes
3	Actuator failure	Valve stiction	Qualitative: Reduced valve movement	Slow valve movement with sticking effects that proceed valve reversals. SP of valve position% \neq PV of valve position%	Spent electrolyte control valve prior to second stage slurry preparation tank	Additive	Incipient	Once every three months	Medium	Yes
4	Structural failure	Pump impeller wear	Qualitative: Pump impeller abrasion	Pump cannot obtain necessary flow rates. Temperature control within autoclave becomes difficult.	Flash recycle tank outlet stream into autoclaves	Multiplicative	Incipient	Once every six months replacement is required	High	Yes
5	Structural failure	Solid build-up in cooling coils	Qualitative: Fouling in cooling coils	Hard water causing build-up of solids in cooling water pipes. Blockages occur and results in reduced heat removal	Autoclave compartment 2 and 3	Multiplicative	Incipient	Once every year	High	Yes
6	Structural failure	Peristaltic pump tube failure	Frequently measured: Flow stops	Lines block if flow stops for more than 5 minutes	Stream 1	Multiplicative	Abrupt	Once every three months	High	Yes
7	Operator intervention	Sulphuric acid controller misuse	Frequently measured: Manual acid concentration measurement	Adding excess amounts of H ₂ SO ₄ due to negligence, resulting in a very high acid concentrations	Stream 4	Additive	Abrupt	Four times a week	Medium	Yes
8	Operator intervention	Excessive steam addition by bypassing control valve	Frequently measured: Compartment 4 temperature	Temperature increase to 170 °C and pressure increase to 7.5 bar	Autoclave compartment 4	Additive	Abrupt	Two times a year	High	Yes
9	Process disturbance	Excessive water addition using manual valve	Frequently measured: Compartment 1 temperature	Disturbs control	Flow into flash recycle tank	Additive	Abrupt	Four times a week	Medium	Yes
10	Process disturbance	Crystallisation of metals due to high total metals in solution combined with a cold day	Frequently measured: Flow stops	Pipe blockages	Second stage discharge thickener overflow	Multiplicative	Incipient	Once every year	High	No
11	Process disturbance	Excess amounts of flocculent addition	Qualitative: Fouling of filter cloths	Binding of cloths in filters - blocking of filters	Filters downstream of autoclave compartment 4	Additive	Abrupt	Four times a year	High	No
12	Process disturbance	Addition of wrong flocculent	Qualitative: Fouling of filter cloths	Blocking of filters	Filters downstream of autoclave compartment 4	Additive	Abrupt	Four times a year	High	No
13	Process disturbance	Sudden addition of caustic leach slurry into formic filtrate tank	Frequently measured: Second stage slurry preparation tank density	Density and solid% spikes out second stage slurry preparation tank	Stream 3	Additive	Abrupt	Once every month	High	Yes
14	Sensor failure	Flow sensor scaling due to inadequate flushing of the line	Frequently measured: Flow seems to stop	No flow is indicated, even though there is flow	Upstream of second stage slurry preparation tank	Multiplicative	Abrupt	Once every month	Low	No
15	Sensor failure	Bubbler level sensor blockage	Frequently measured: Online level measurement \neq gauge level measurement	Indicating a bias level%	Autoclave compartment 1, 3 and 4	Additive	Abrupt	Twice every year	Medium	Yes
16	Controller malfunction	Incorrect valve sizing	Frequently measured: Flow controller instability	Control becomes difficult. The controller struggles to obtain zero flow	Stream 3	Multiplicative	Abrupt	Once every second month	Medium	Yes
17	Controller malfunction	Excess vibration results in malfunctioning of on/off valve control	Frequently measured: Flow control on/off abnormality	On/off valves indicated as "open" when closed (and vice versa). This affects sequencing on/off control valves.	Upstream of second stage slurry preparation tank	Multiplicative	Intermittent	Once every week	Low	No

Legend
Modelled and used in control performance assessment
Modelled but not used in control performance assessment
Not modelled

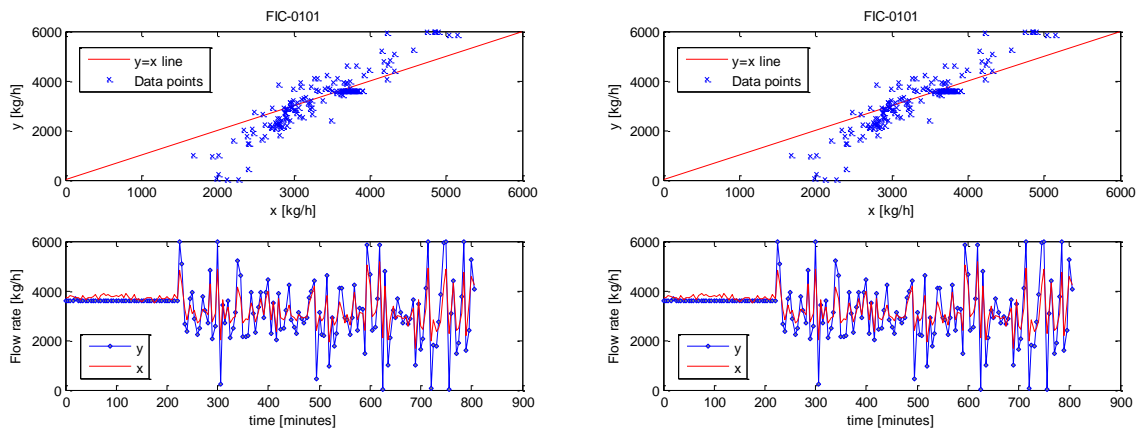


Figure F.1: Data reconciliation results: FIC-0101 (left) and FIC-1102 (right)

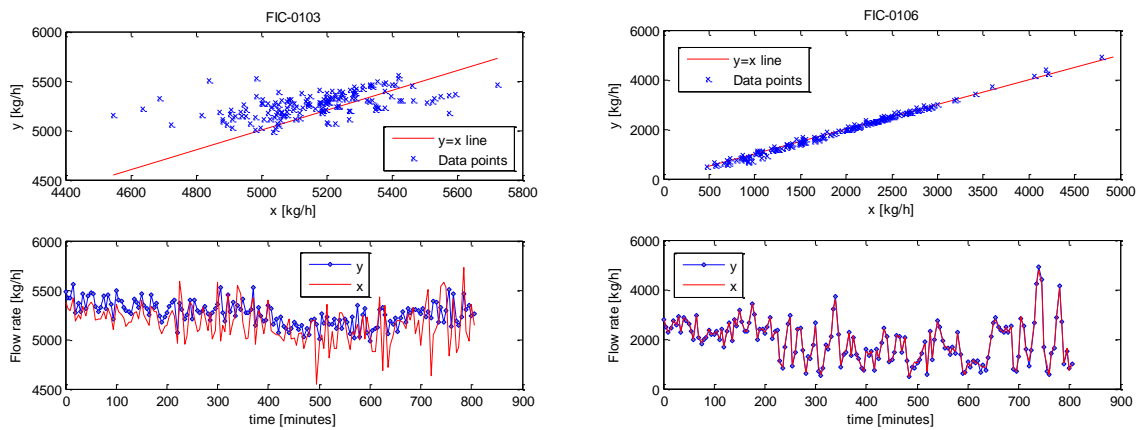


Figure F.2: Data reconciliation results: FIC-0103 (left) and FIC-0106 (right)

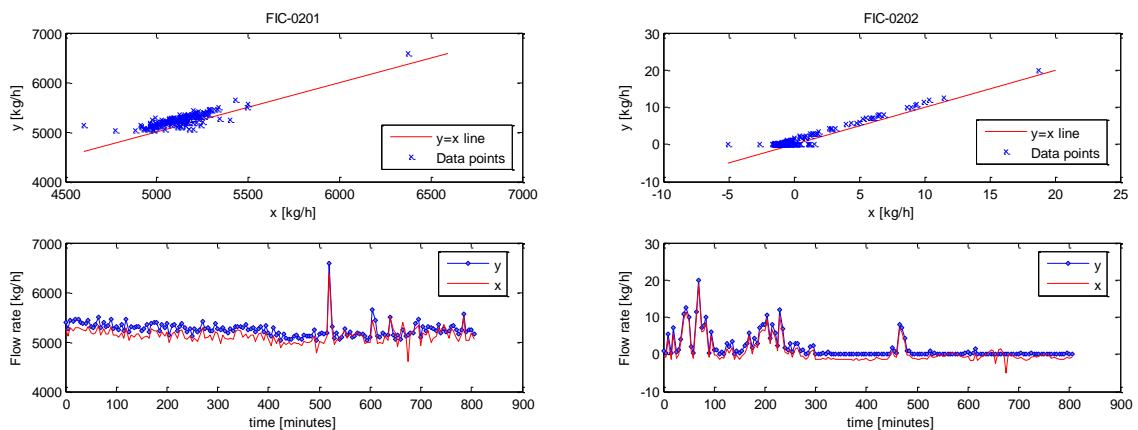


Figure F.3: Data reconciliation results: FIC-0201 (left) and FIC-0202 (right)

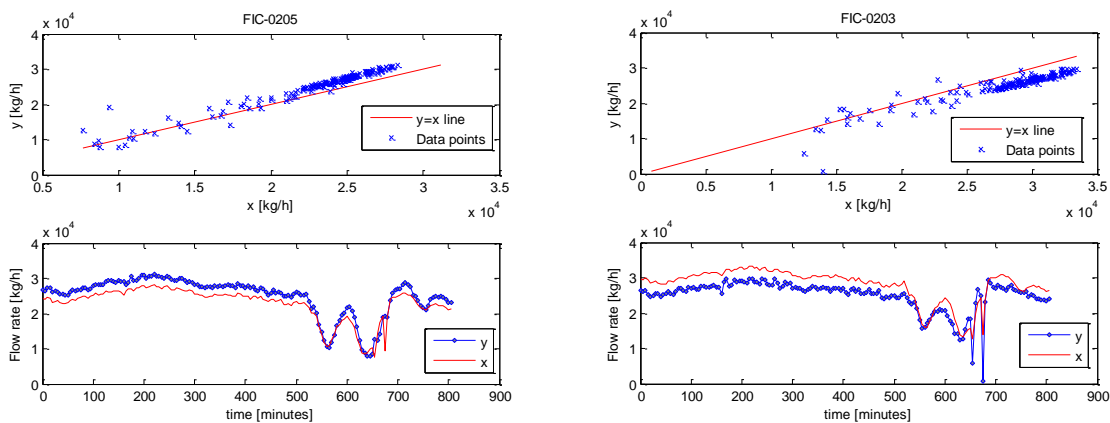


Figure F.4: Data reconciliation results: FIC-0205 (left) and FIC-0203 (right)

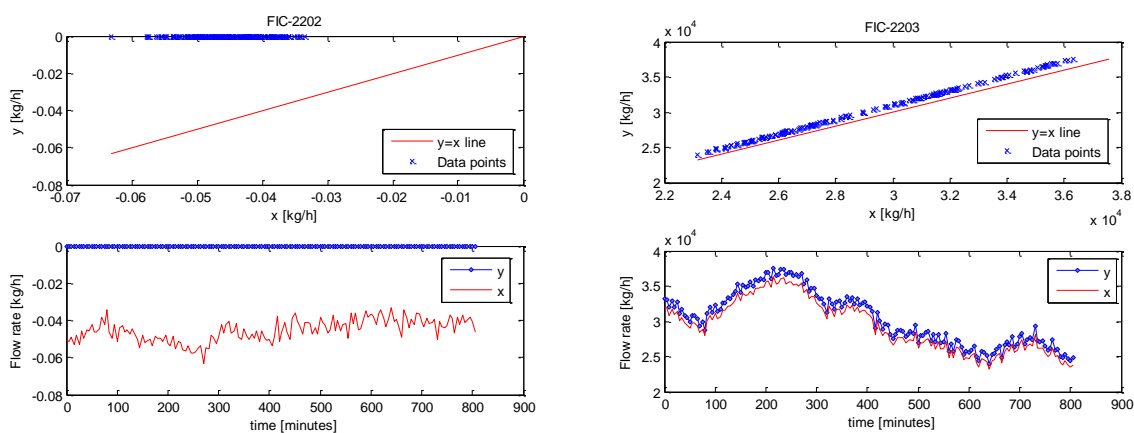


Figure F.5: Data reconciliation results: FIC-2202 (left) and FIC-2203 (right)

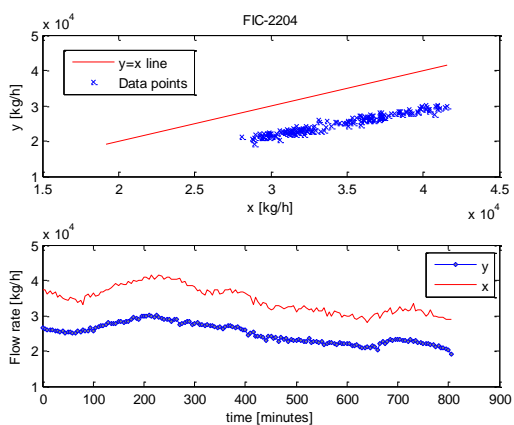


Figure F.6: Data reconciliation results: FIC-2204

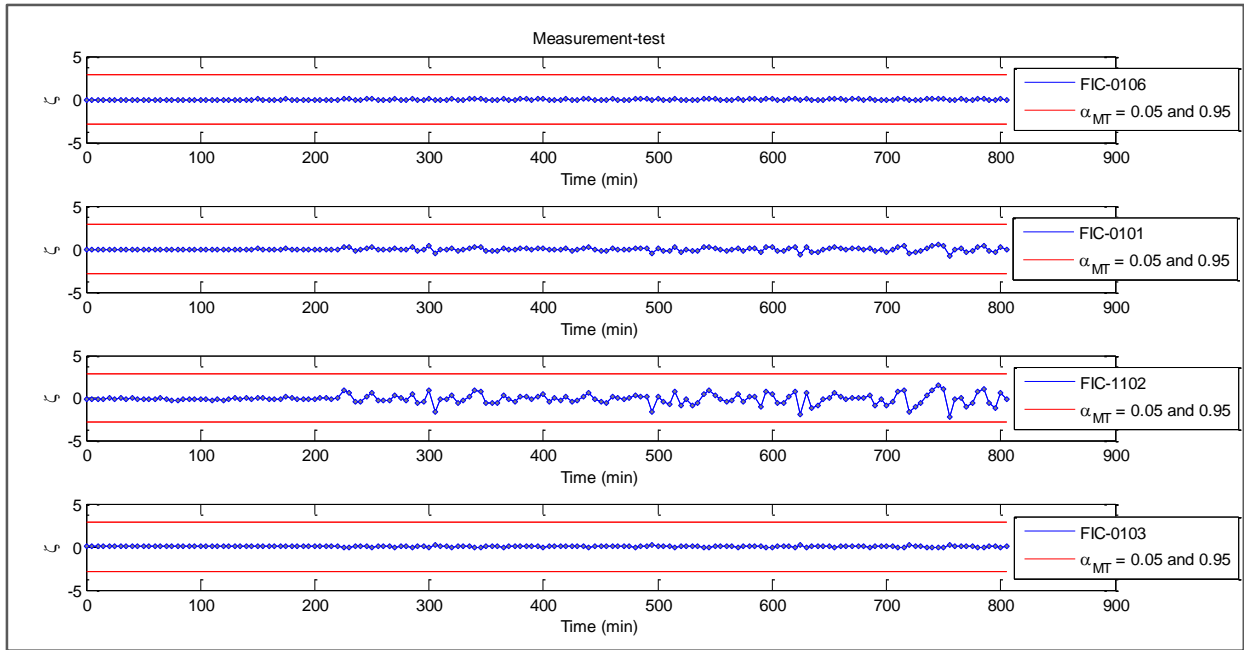


Figure F.7: Measurement test results: FIC-0106, FIC-0101, FIC-1102 and FIC-0103

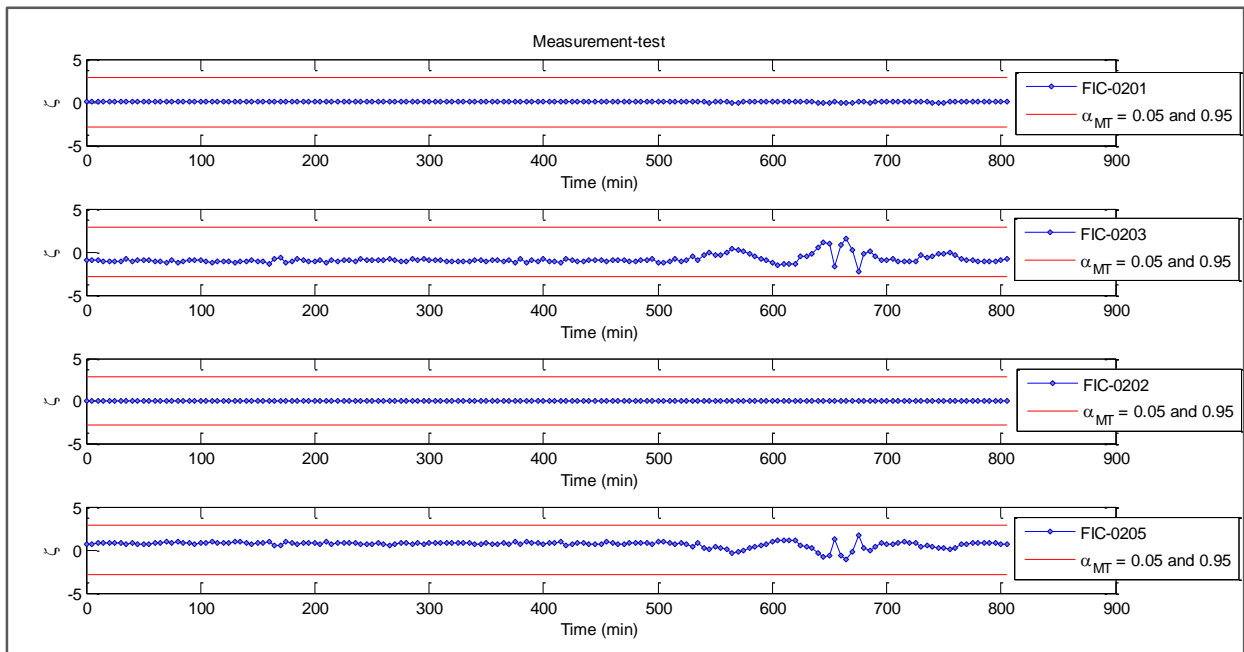


Figure F.8: Measurement test results: FIC-0201, FIC-0203, FIC-0202 and FIC-0205

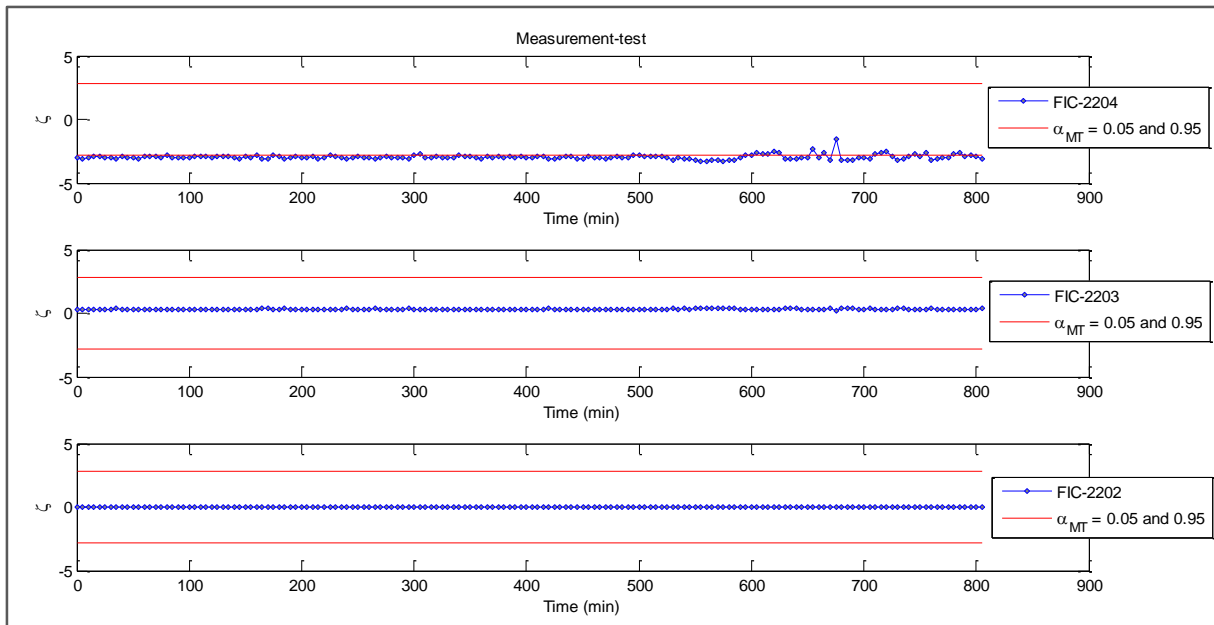


Figure F.9: Measurement test results: FIC-2204, FIC-2203 and FIC-2202

Table F.12: Reaction kinetic optimisation results: Parameters for GS and GS with PS

	GS				GS with PS			
	No updates	Shape factor changes	Initial concentration lumping	All updates	No updates	Shape factor changes	Initial concentration lumping	All updates
k ₀₁	2.33E+09	2.33E+09	2.33E+06	2.33E+06	2.33E+09	2.47E+09	1.17E+24	6.44E+10
k ₀₂	4.76E+08	4.76E+08	4.76E+05	4.76E+05	4.94E+08	4.77E+08	9.45E+22	4.30E+09
k ₀₃	1.68E+10	1.68E+10	1.68E+08	1.68E+08	1.58E+10	2.95E+10	1.73E+10	1.68E+08
k ₀₄	7.51E-05	1.07E-04	4.75E-03	2.46E-03	7.51E-05	1.07E-04	2.25E+16	2.46E-03
k ₀₅	5.41E+00	7.06E+00	4.72E+00	4.07E+00	5.41E+00	7.06E+00	4.72E+00	4.07E+00
k ₀₆	1.43E+03	1.43E+03	2.55E+02	4.29E+00	1.43E+03	1.43E+03	1.54E+23	2.37E+21
k ₀₇	4.66E+09	4.66E+09	4.66E+05	4.66E+05	5.70E+09	6.20E+09	7.93E+28	4.66E+05
k ₀₈	1.89E+08	1.89E+08	1.89E+06	1.89E+06	1.89E+08	1.89E+08	1.89E+06	1.89E+06
k ₀₉	7.34E+08	7.34E+08	7.34E+04	7.34E+04	7.34E+08	7.34E+08	1.06E+14	2.37E+21
k ₁₀	1.20E+05	1.20E+05	1.20E+03	1.20E+03	1.20E+05	1.20E+05	1.20E+03	1.20E+03
k ₁₁	2.18E+17	2.18E+17	2.18E+13	2.18E+13	2.34E+17	2.20E+17	4.96E+36	1.45E+18
k ₁₂	2.38E+06	2.38E+06	2.38E+04	2.38E+04	2.38E+06	2.38E+06	2.38E+04	2.38E+04
k ₁₃	7.10E+08	7.10E+08	7.10E+03	7.10E+03	7.10E+08	7.10E+08	1.53E+04	7.10E+03
k ₁₄	2.99E+17	2.99E+17	2.99E+13	2.99E+13	3.25E+17	3.29E+17	3.47E+14	2.45E+14
k ₁₅	1.25E+12	1.25E+12	1.25E+07	1.25E+07	1.23E+12	1.13E+12	5.19E+33	3.63E+19
k ₁₆	9.16E+06	9.16E+06	4.32E+01	1.18E-01	9.16E+06	9.16E+06	5.24E+05	1.18E-01
k ₁₇	1.44E+16	1.44E+16	1.44E+09	1.44E+09	1.56E+16	1.25E+16	1.23E+24	3.52E+13
k ₁₈	9.29E+14	9.29E+14	9.29E+10	9.29E+10	9.23E+14	9.47E+14	1.95E+22	2.79E+20
k ₁₉	1.20E+10	1.20E+10	1.20E+05	1.20E+05	1.31E+10	1.15E+10	1.20E+05	1.20E+05
k ₂₀	2.47E+22	2.47E+22	2.47E+17	2.47E+17	2.32E+22	3.05E+22	8.24E+17	2.14E+18
k ₂₁	3.09E+24	3.09E+24	3.09E+19	3.09E+19	3.00E+24	2.59E+24	2.50E+24	5.16E+21
E _{a1}	7.85E+04	7.85E+04	7.85E+04	7.85E+04	7.85E+04	7.85E+04	7.85E+04	7.85E+04
E _{a2}	4.11E+04	4.11E+04	4.11E+04	4.11E+04	4.11E+04	4.11E+04	4.11E+04	4.11E+04
E _{a3}	8.74E+04	8.74E+04	8.74E+04	8.74E+04	8.74E+04	8.74E+04	8.74E+04	8.74E+04
E _{a4}	-2.62E+04	-2.62E+04	-2.62E+04	-2.62E+04	-2.62E+04	-2.62E+04	-2.62E+04	-2.62E+04
E _{a5}	-5.94E+03	-5.94E+03	-5.94E+03	-5.94E+03	-5.94E+03	-5.94E+03	-5.94E+03	-5.94E+03
E _{a6}	3.43E+04	3.43E+04	3.43E+04	3.43E+04	3.43E+04	3.43E+04	3.43E+04	3.43E+04
E _{a7}	5.95E+04	5.95E+04	5.95E+04	5.95E+04	5.95E+04	5.95E+04	5.95E+04	5.95E+04
E _{a8}	6.46E+04	6.46E+04	6.46E+04	6.46E+04	6.46E+04	6.46E+04	6.46E+04	6.46E+04
E _{a9}	5.61E+04	5.61E+04	5.61E+04	5.61E+04	5.61E+04	5.61E+04	5.61E+04	5.61E+04
E _{a10}	5.21E+04	5.21E+04	5.21E+04	5.21E+04	5.21E+04	5.21E+04	5.21E+04	5.21E+04
E _{a11}	1.21E+05	1.21E+05	1.21E+05	1.21E+05	1.21E+05	1.21E+05	1.21E+05	1.21E+05
E _{a12}	4.85E+04	4.85E+04	4.85E+04	4.85E+04	4.85E+04	4.85E+04	4.85E+04	4.85E+04
E _{a13}	6.42E+04	6.42E+04	6.42E+04	6.42E+04	6.42E+04	6.42E+04	6.42E+04	6.42E+04
E _{a14}	1.38E+05	1.38E+05	1.38E+05	1.38E+05	1.38E+05	1.38E+05	1.38E+05	1.38E+05
E _{a15}	1.16E+05	1.16E+05	1.16E+05	1.16E+05	1.16E+05	1.16E+05	1.16E+05	1.16E+05
E _{a16}	5.28E+04	5.28E+04	5.28E+04	5.28E+04	5.28E+04	5.28E+04	5.28E+04	5.28E+04
E _{a17}	1.24E+05	1.24E+05	1.24E+05	1.24E+05	1.24E+05	1.24E+05	1.24E+05	1.24E+05
E _{a18}	1.34E+05	1.34E+05	1.34E+05	1.34E+05	1.34E+05	1.34E+05	1.34E+05	1.34E+05
E _{a19}	7.24E+04	7.24E+04	7.24E+04	7.24E+04	7.24E+04	7.24E+04	7.24E+04	7.24E+04
E _{a20}	1.75E+05	1.75E+05	1.75E+05	1.75E+05	1.75E+05	1.75E+05	1.75E+05	1.75E+05
E _{a21}	2.09E+05	2.09E+05	2.09E+05	2.09E+05	2.09E+05	2.09E+05	2.09E+05	2.09E+05
f _{sh1}	1.00E+00	1.00E+00	8.89E+01	1.00E+00	1.00E+00	1.00E+00	8.89E+01	1.00E+00
f _{sh2}	1.98E+00	2.74E+00	2.01E+01	1.79E+00	1.98E+00	2.74E+00	2.01E+01	1.79E+00
f _{sh3}	4.78E+00	1.00E+00	2.93E+01	4.65E+00	4.78E+00	1.00E+00	2.93E+01	4.65E+00
f _{sh4}	1.54E+00	2.90E+00	7.27E+00	1.41E+00	1.54E+00	2.90E+00	7.27E+00	1.41E+00
f _{sh5}	1.43E+00	2.52E+00	1.00E+00	1.00E+00	1.43E+00	2.52E+00	1.00E+00	1.00E+00
f _{sh6}	1.31E+00	1.57E+00	1.00E+00	1.00E+00	1.31E+00	1.57E+00	1.00E+00	1.00E+00
f _{sh7}	1.96E+00	4.75E+00	2.25E+01	1.72E+00	1.96E+00	4.75E+00	2.25E+01	1.72E+00
f _{sh8}	2.92E+00	8.12E+00	2.89E+01	5.63E+00	2.92E+00	8.12E+00	2.89E+01	5.63E+00
f _{sh9}	1.00E+00	1.04E+00	7.47E+01	1.00E+00	1.00E+00	1.04E+00	7.47E+01	1.00E+00
f _{sh10}	1.96E+00	4.23E+00	2.25E+01	1.68E+00	1.96E+00	4.23E+00	2.25E+01	1.68E+00
f _{sh11}	1.95E+00	1.60E+00	1.00E+00	1.00E+00	1.95E+00	1.60E+00	1.00E+00	1.00E+00
f _{sh12}	1.00E+00	2.79E+00	1.00E+00	1.00E+00	1.00E+00	2.79E+00	1.00E+00	1.00E+00
f _{sh13}	1.96E+00	3.63E+00	2.25E+01	1.72E+00	1.96E+00	3.63E+00	2.25E+01	1.72E+00
f _{sh14}	-	3.68E+00	-	1.00E+00	-	3.68E+00	-	1.00E+00

Table F.13: Reaction kinetic optimisation results: Parameters for GA and GA with PS

	GA					GA with PS			
	No updates	Shape factor changes	Initial concentration lumping	All updates		No updates	Shape factor changes	Initial concentration lumping	All updates
k ₀₁	4.54E+00	8.30E+26	5.33E+26	9.56E+26	5.75E+00	8.30E+26	5.33E+26	9.56E+26	
k ₀₂	1.70E+02	9.98E+26	8.82E+25	8.20E+26	5.77E+02	1.34E+27	8.82E+25	8.20E+26	
k ₀₃	1.00E+00	1.12E+26	2.79E+26	5.28E+26	1.00E+00	1.12E+26	2.79E+26	5.28E+26	
k ₀₄	1.28E-01	3.00E+26	1.41E+26	7.07E+26	2.42E-01	3.00E+26	1.41E+26	7.07E+26	
k ₀₅	4.11E+01	5.77E+26	9.84E+26	7.95E+26	4.02E+01	5.77E+26	9.84E+26	7.95E+26	
k ₀₆	7.50E-01	4.19E+26	8.10E+26	4.18E+25	6.48E+01	4.19E+26	8.10E+26	4.18E+25	
k ₀₇	6.25E-01	7.26E+26	2.65E+26	3.08E+26	4.25E+01	7.26E+26	2.65E+26	3.08E+26	
k ₀₈	3.70E+02	2.88E+26	3.87E+26	8.30E+25	2.83E+02	2.88E+26	3.87E+26	8.30E+25	
k ₀₉	2.25E+01	5.24E+26	5.52E+26	8.01E+26	2.30E+01	5.24E+26	5.52E+26	8.01E+26	
k ₁₀	1.94E-02	6.52E+26	3.69E+26	8.35E+26	4.84E+01	6.52E+26	3.69E+26	8.35E+26	
k ₁₁	1.88E+01	7.75E+26	8.69E+26	9.59E+26	1.54E+01	7.75E+26	8.69E+26	9.59E+26	
k ₁₂	3.49E-02	3.06E+25	2.15E+26	8.21E+26	5.33E+01	3.06E+25	2.15E+26	8.21E+26	
k ₁₃	7.35E+00	5.42E+25	7.74E+26	1.37E+26	2.25E+00	5.42E+25	7.74E+26	1.37E+26	
k ₁₄	2.50E-01	9.88E+26	1.22E+26	4.98E+26	2.03E-01	9.88E+26	1.22E+26	4.98E+26	
k ₁₅	8.97E-02	6.80E+26	9.68E+26	5.64E+26	9.23E-02	6.80E+26	9.68E+26	5.64E+26	
k ₁₆	5.63E-01	5.68E+26	8.06E+26	5.43E+26	5.00E-01	5.68E+26	8.06E+26	5.43E+26	
k ₁₇	1.06E+00	4.75E+26	9.51E+26	7.06E+26	1.00E+00	4.75E+26	9.51E+26	7.06E+26	
k ₁₈	1.15E-01	7.67E+26	5.28E+26	2.34E+26	2.38E-02	7.67E+26	5.28E+26	2.34E+26	
k ₁₉	3.52E+01	9.09E+26	4.15E+26	4.00E+26	1.94E+00	9.09E+26	4.15E+26	4.00E+26	
k ₂₀	6.67E-01	9.04E+26	6.62E+26	3.97E+26	7.81E-02	9.04E+26	6.62E+26	3.97E+26	
k ₂₁	1.80E+00	9.87E+26	1.10E+25	9.78E+26	2.15E-02	9.87E+26	1.10E+25	9.78E+26	
E _{a1}	1.55E+02	3.00E+07	7.39E+06	1.99E+05	1.70E+01	3.00E+07	7.39E+06	2.19E+05	
E _{a2}	2.62E+01	2.02E+05	2.13E+07	2.64E+05	1.03E+01	1.79E+05	2.13E+07	1.84E+05	
E _{a3}	1.77E+02	1.74E+07	9.57E+06	4.67E+07	8.23E+01	1.74E+07	9.57E+06	4.67E+07	
E _{a4}	7.49E+02	1.20E+07	8.85E+07	9.49E+07	8.72E+00	1.20E+07	8.85E+07	9.49E+07	
E _{a5}	6.13E+01	8.17E+07	2.07E+05	7.24E+06	1.19E+01	8.17E+07	2.07E+05	7.24E+06	
E _{a6}	1.50E+02	4.54E+07	7.94E+07	1.33E+07	9.58E+00	4.54E+07	7.94E+07	1.33E+07	
E _{a7}	7.05E+01	7.07E+06	1.12E+07	2.26E+07	1.43E+01	7.07E+06	1.12E+07	2.26E+07	
E _{a8}	-5.60E+01	1.68E+07	2.45E+07	2.09E+07	5.21E+00	1.68E+07	2.45E+07	2.09E+07	
E _{a9}	6.27E+01	5.12E+07	4.36E+07	9.42E+07	8.69E+00	5.12E+07	4.36E+07	9.42E+07	
E _{a10}	4.94E+01	9.89E+07	6.72E+07	3.96E+07	1.12E+00	9.89E+07	6.72E+07	3.96E+07	
E _{a11}	2.73E+01	1.21E+07	7.22E+07	6.02E+07	1.85E+01	1.21E+07	7.22E+07	6.02E+07	
E _{a12}	7.59E+01	7.50E+07	7.46E+06	1.54E+07	2.36E+00	7.50E+07	7.46E+06	1.54E+07	
E _{a13}	1.13E+02	8.19E+06	7.00E+07	6.99E+07	5.14E+00	8.19E+06	7.00E+07	6.99E+07	
E _{a14}	1.98E+02	2.94E+07	6.61E+07	4.42E+07	1.66E+01	2.94E+07	6.61E+07	4.42E+07	
E _{a15}	3.72E+02	3.10E+07	8.55E+07	9.48E+07	3.80E+01	3.10E+07	8.55E+07	9.48E+07	
E _{a16}	1.58E+00	5.34E+07	5.73E+07	1.52E+07	5.50E+01	5.34E+07	5.73E+07	1.52E+07	
E _{a17}	3.05E+01	3.19E+07	1.62E+07	8.19E+07	1.38E+01	3.19E+07	1.62E+07	8.19E+07	
E _{a18}	1.23E+02	1.13E+07	3.42E+07	3.83E+07	3.08E+01	1.13E+07	3.42E+07	3.83E+07	
E _{a19}	2.94E+07	7.25E+07	3.81E+07	-6.69E+06	1.33E-01	7.25E+07	3.81E+07	-6.69E+06	
E _{a20}	2.98E+02	8.88E+07	9.20E+07	3.99E+07	7.07E-01	8.88E+07	9.20E+07	3.99E+07	
E _{a21}	1.08E+02	7.25E+07	9.47E+07	8.97E+06	5.63E+01	7.25E+07	9.47E+07	8.97E+06	
f _{sh1}	9.15E+01	1.00E+00	6.50E+01	1.00E+00	4.68E+01	9.34E+00	6.50E+01	1.00E+00	
f _{sh2}	9.99E+01	5.55E+01	6.38E+01	1.35E+01	1.00E+02	5.55E+01	6.38E+01	1.35E+01	
f _{sh3}	9.99E+01	1.95E+01	8.72E+01	4.77E+01	4.23E+01	1.95E+01	8.72E+01	4.77E+01	
f _{sh4}	9.98E+01	6.88E+00	2.74E+01	9.81E+01	1.74E+01	6.88E+00	2.74E+01	9.81E+01	
f _{sh5}	2.63E+01	2.27E+01	9.39E+01	6.60E+01	1.75E+00	2.27E+01	9.39E+01	6.60E+01	
f _{sh6}	8.73E+01	3.72E+01	1.03E+00	8.32E+01	1.00E+02	3.72E+01	1.03E+00	8.32E+01	
f _{sh7}	4.36E+01	6.00E+01	8.05E+01	3.42E+01	8.50E+00	6.00E+01	8.05E+01	3.42E+01	
f _{sh8}	4.23E+00	8.49E+01	9.40E+01	7.98E+01	1.19E+00	8.49E+01	9.40E+01	7.98E+01	
f _{sh9}	1.00E+00	3.55E+01	2.84E+01	9.92E+01	1.19E+00	3.55E+01	2.84E+01	9.92E+01	
f _{sh10}	2.78E+01	8.24E+01	4.95E+01	4.64E+01	1.64E+01	8.24E+01	4.95E+01	4.64E+01	
f _{sh11}	4.71E+01	3.78E+01	8.36E+01	5.30E+01	1.00E+00	3.78E+01	8.36E+01	5.30E+01	
f _{sh12}	1.31E+00	4.17E+01	7.48E+01	6.01E+01	3.02E+00	4.17E+01	7.48E+01	6.01E+01	
f _{sh13}	5.08E+01	1.93E+01	6.27E+01	6.89E+01	1.10E+01	1.93E+01	6.27E+01	6.89E+01	
f _{sh14}	-	2.67E+01	-	5.56E+01	-	2.67E+01	-	5.56E+01	

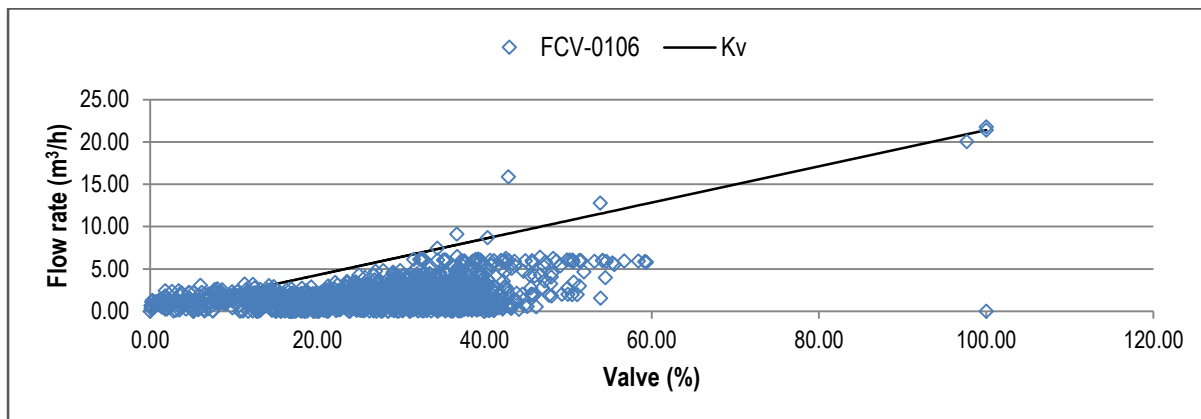


Figure F.10: Kv relationship for FCV-0106

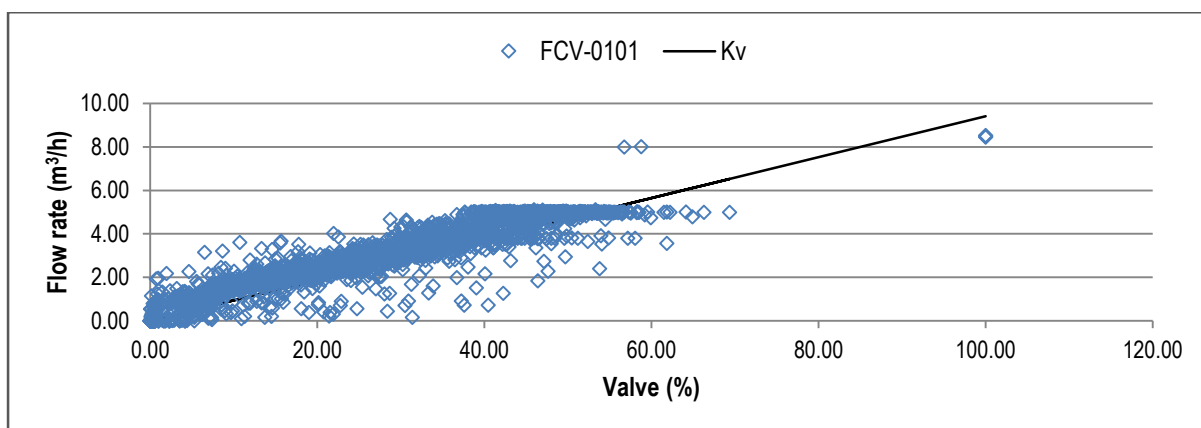


Figure F.11: Kv relationship for FCV-0101

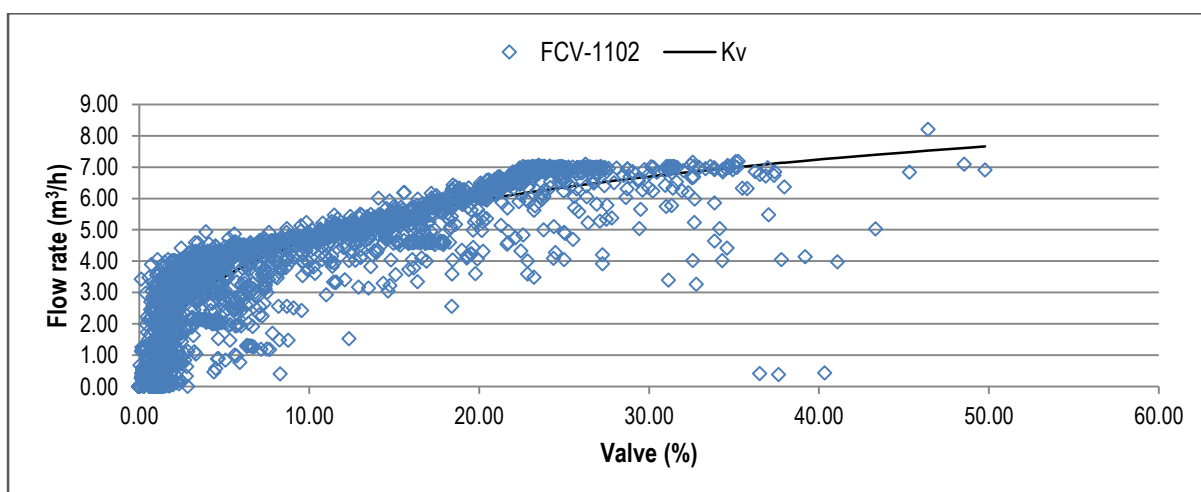


Figure F.12: Kv relationship for FCV-1102

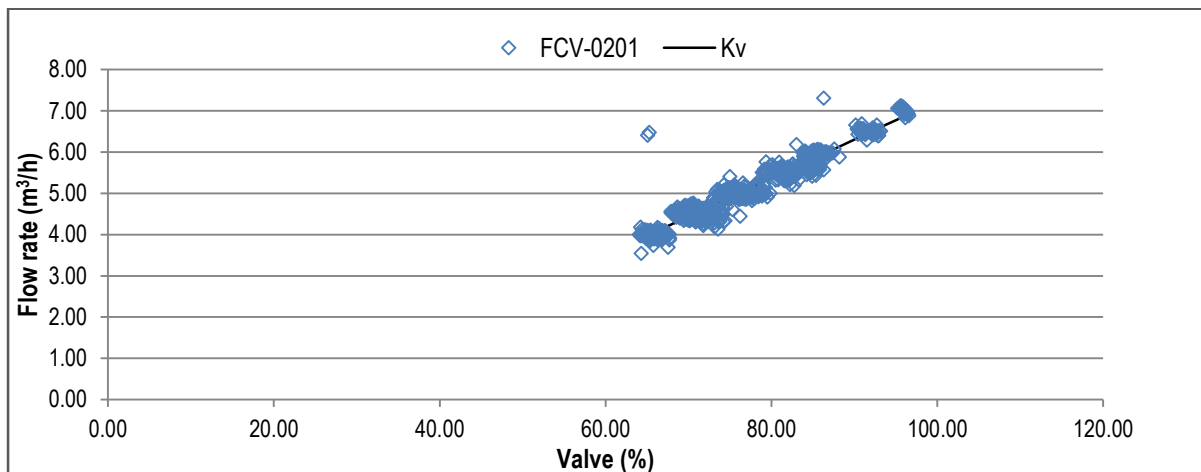


Figure F.13: K_v relationship for FCV-0201

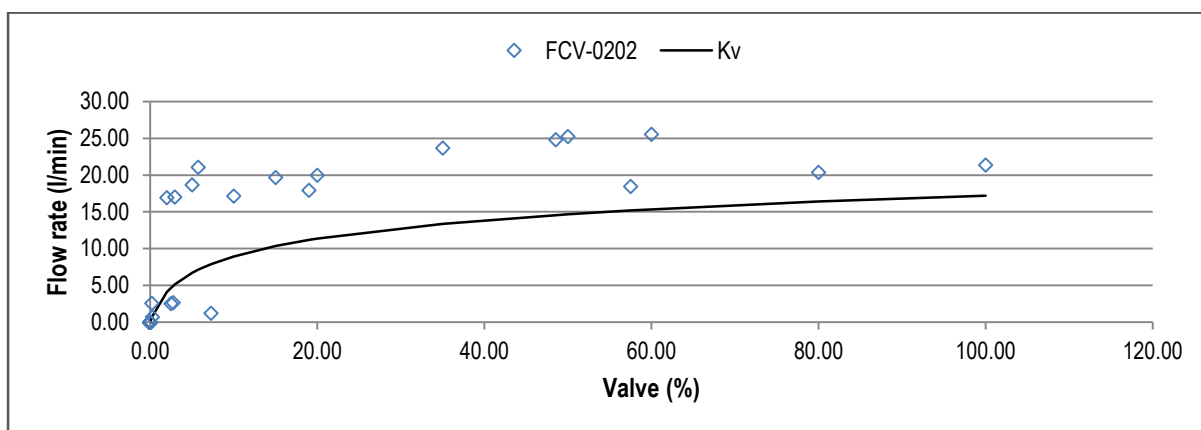


Figure F.14: K_v relationship for FCV-0202

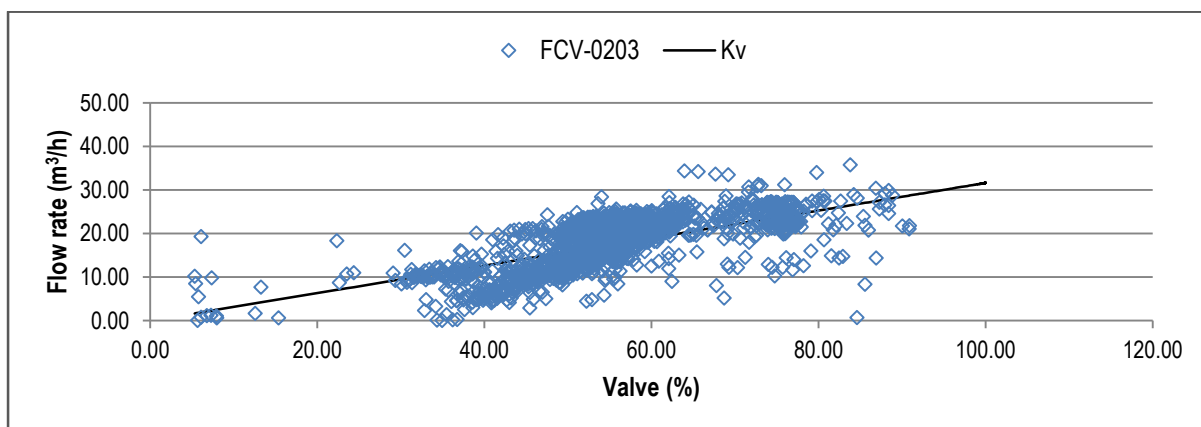


Figure F.15: K_v relationship for FCV-0203

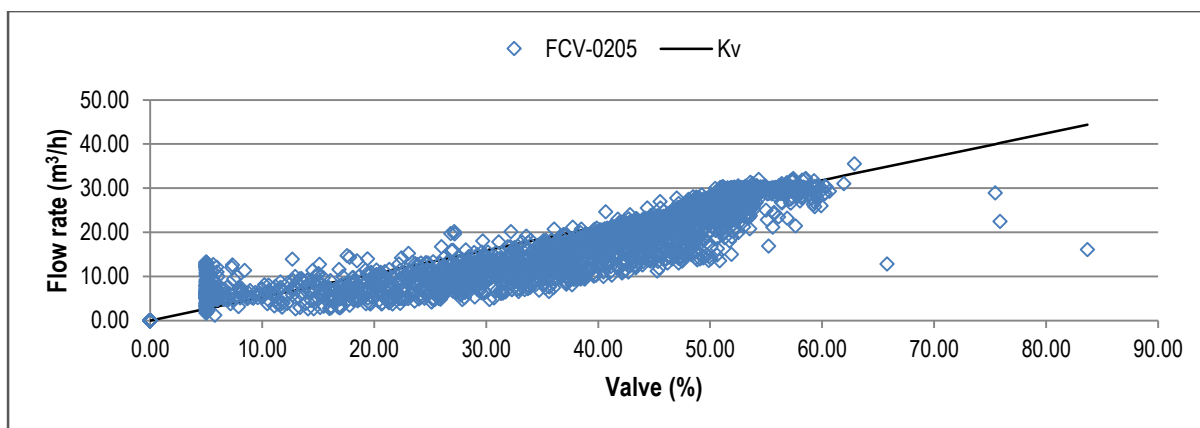


Figure F.16: Kv relationship for FCV-0205

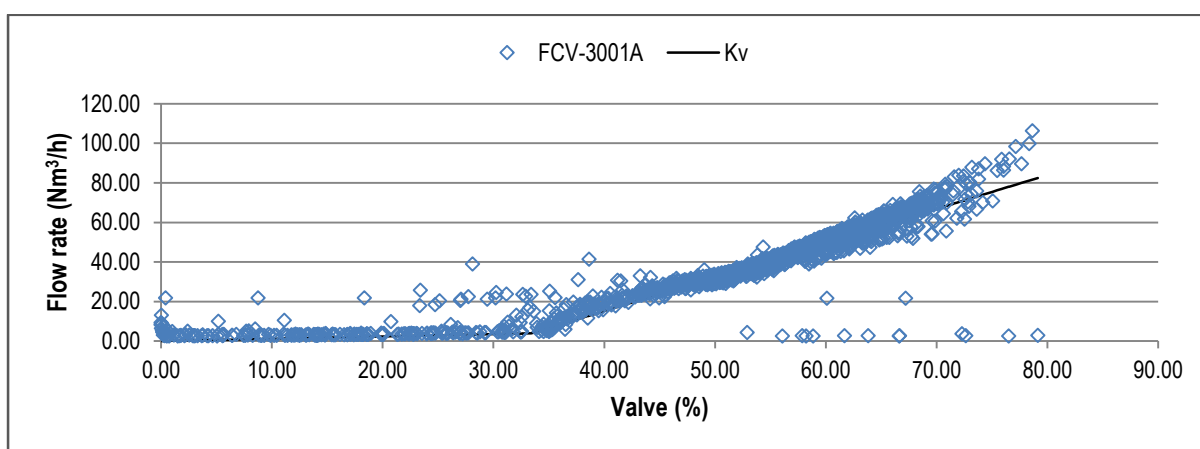


Figure F.17: Kv relationship for FCV-3001A

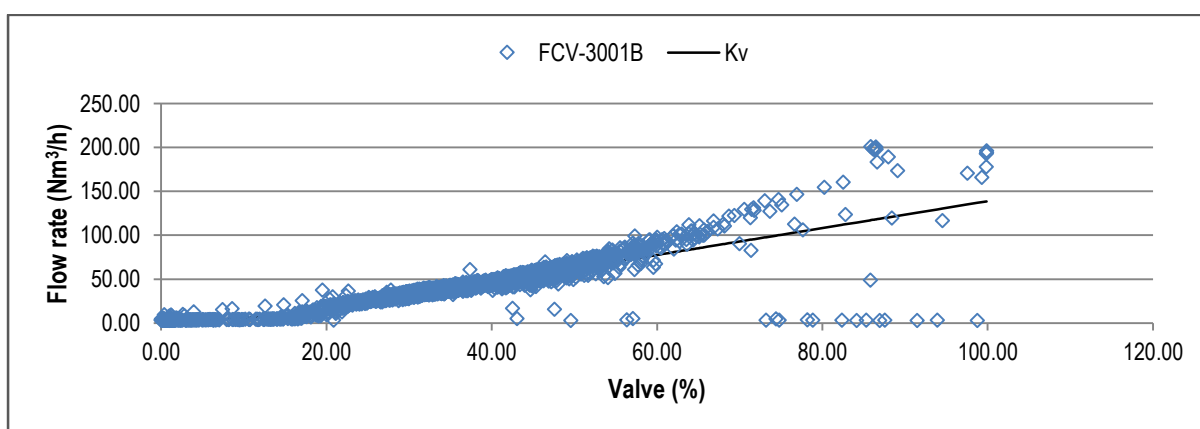


Figure F.18: Kv relationship for FCV-3001B

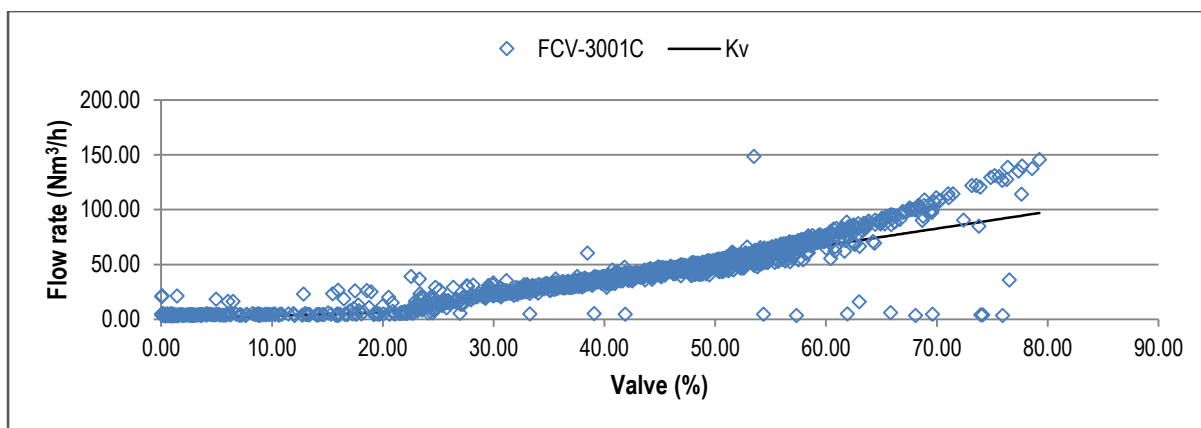


Figure F.19: K_v relationship for FCV-3001C

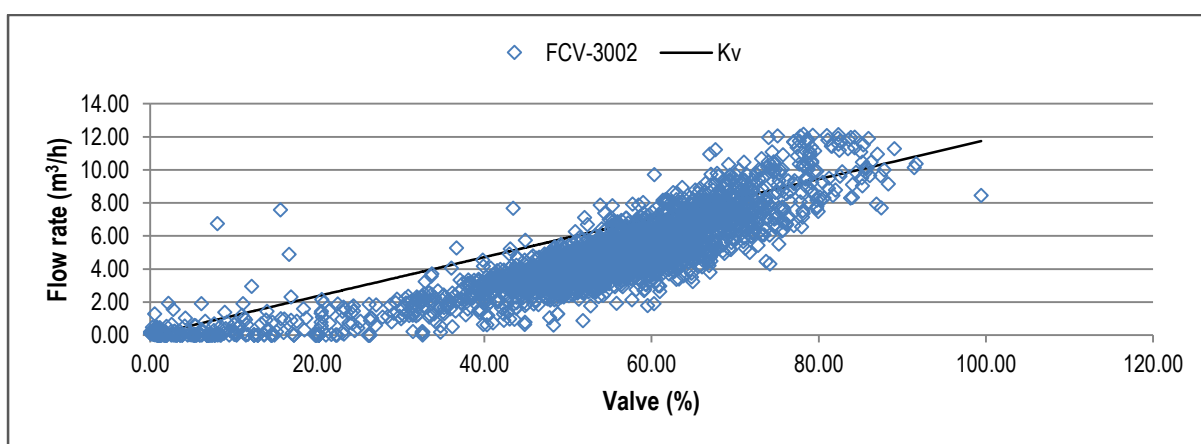


Figure F.20: K_v relationship for FCV-3002

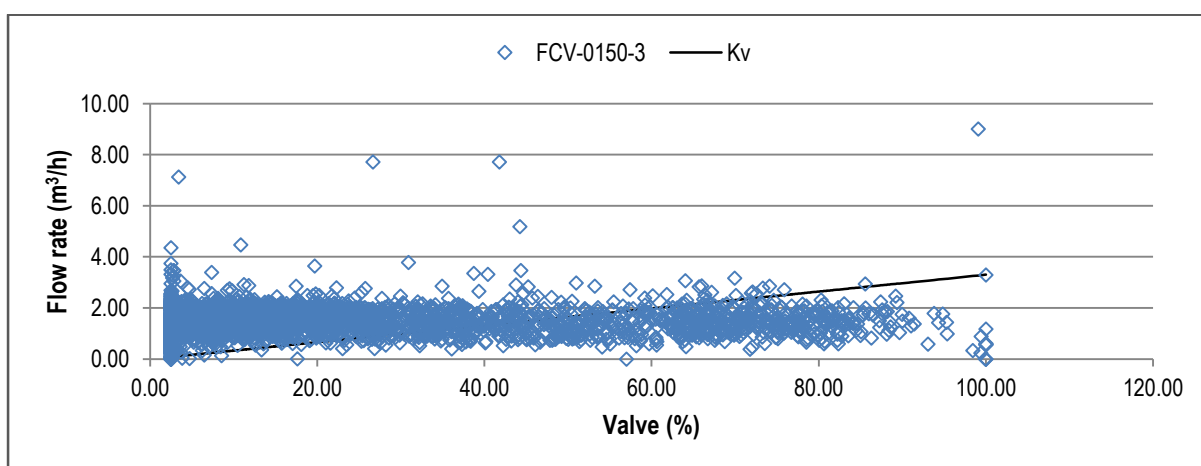


Figure F.21: K_v relationship for FCV-0150-3

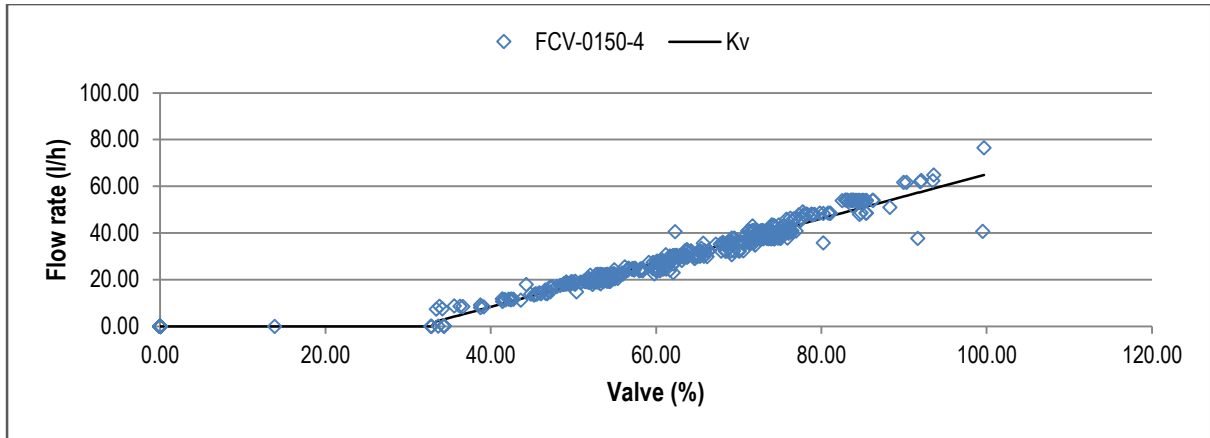


Figure F.22: K_v relationship for FCV-0150-4

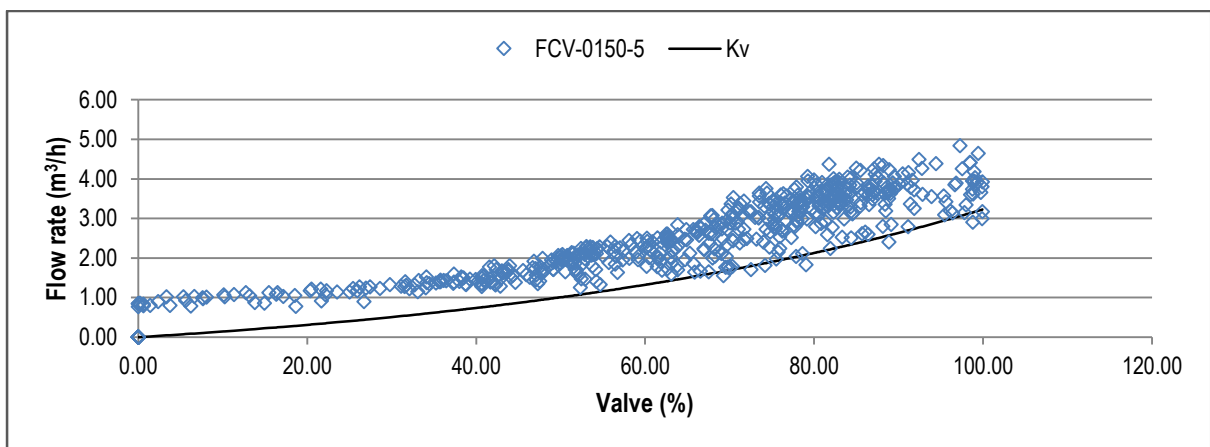


Figure F.23: K_v relationship for FCV-0150-5

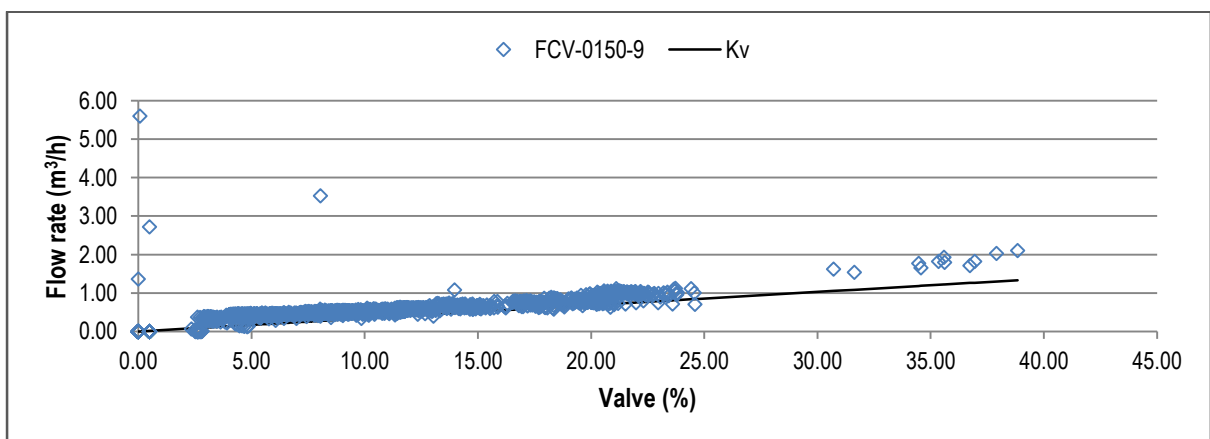


Figure F.24: K_v relationship for FCV-0150-9

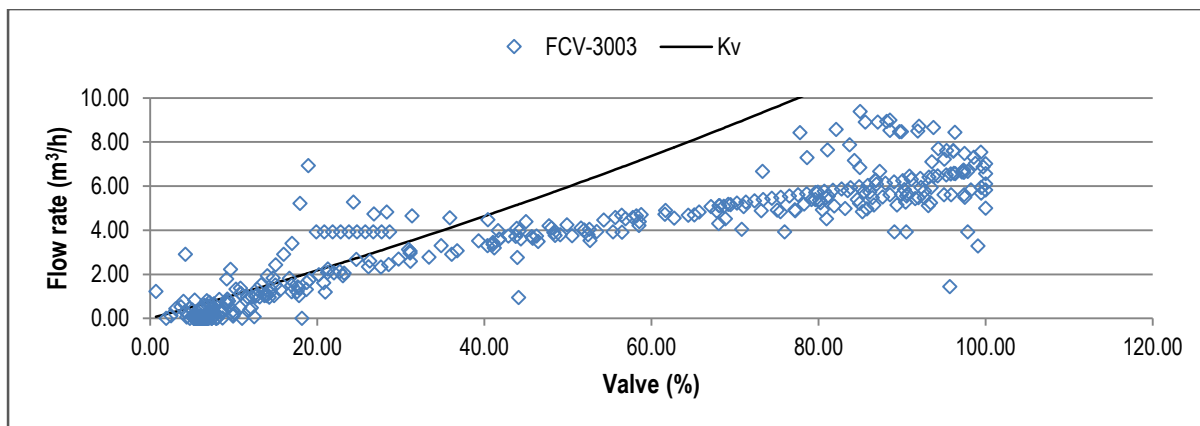


Figure F.25: Kv relationship for FCV-3003